# THE GEOLOGICAL INTERPRETATION OF WELL LOGS

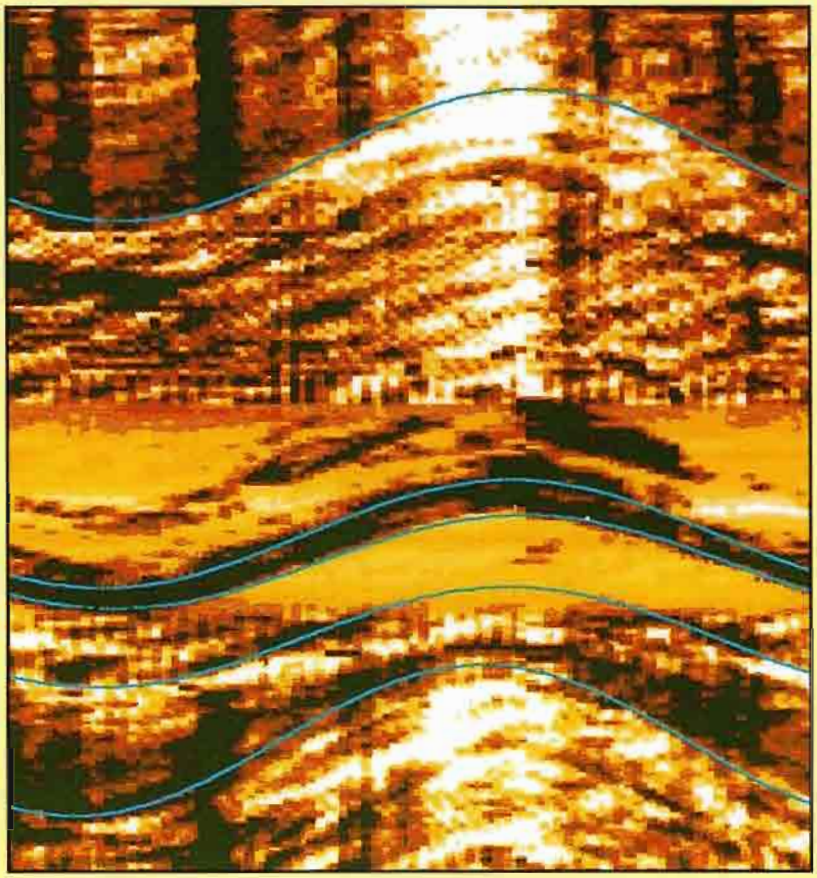

Second Edition

Malcolm Rider

# THE GEOLOGICAL INTERPRETATION OF WELL LOGS

## Second Edition

**Malcolm Rider**
Petroleum Exploration Consultant

RIDER FRENCH

Rider-French Consulting Ltd

Published by
Rider-French Consulting Ltd.,
P.O. Box 1,
Sutherland,
1V28 3XL
Scotland

email: rider_french@ compuserve.com
www.riderfrench.co.uk

2nd edition, Whittles Publishing 1996, reprinted 2000


ISBN: 0-9541906-0-2

Designed and typeset in 10/12pt Times by
Janet Watson

Printed by
Interprint Ltd., Malta

# PREFACE

This second edition of a book originally written ten years ago has a great deal of new material, new chapters and previous chapters much modified. But the philosophy and format and approximately half the text are the same. The book describes, discusses and illustrates with many *real* examples, the interpretation of well logs for geological ends. Basic tool design is an essential inclusion, but petrophysics, that is the use of logs for quantifying hydrocarbons, is only very briefly considered. This was the case in the first, widely sold edition.

In the intervening years there have been many significant changes. The PC has replaced the mainframe and the personal use of a computer for log analysis is now assumed: in the previous edition it was not even considered. There has been a revolution in logging tool design. Tools today incorporate downhole processing, and logging signals are digital. This has sourced new tools, which are described, as also are new versions of old tools. For this, the straightforward descriptive format used originally has been used again. Not only has logging advanced, so have geological ideas, notably with the advent of sequence stratigraphy. Using both the old and the newer logs for sub-surface sequence stratigraphy is discussed: the possibilities are exciting.

Although the new is attention grabbing, the old basic logs still form the foundation to a routine geological well evaluation. This edition, therefore, combines the well established with the newer and more experimental. But throughout, it is the geological content of the logs that is important: lithology, facies, depositional environment, sequence stratigraphy, correlation and more. Judging from the past, the book best serves the purpose of those beginning to acquaint themselves with logs, in industry or academia, and those who do not use logs all the time and like to use the book as an occasional reference.

I still feel that I owe an early debt to my old colleagues from CFP (Total) and to Oberto Serra, then Elf but recently retired from Schlumberger. Newer ideas have come from industry colleagues, many in the consulting world, and the feedback from many industry courses given. Especial ackowledgement must go to Gavin Cameron for his contributions in the dipmeter field. These feature in the dedicated dipmeter chapter, new in this edition, which leads naturally to a chapter on the exciting, new, image logs.

The manuscript has been significantly improved by suggestions and criticisms by specialists in a number of fields: dipmeter and image logging, Robert Trice; logging mechanics, Peter Elkington; sequence stratigraphy, John Underhill; and Tertiary geology, Robert Knox. Data and discussion have been provided by Amerada Hess UK Ltd, Western Atlas, Halliburton, Schlumberger, BPB and the Universities of London and Liverpool: they all receive my grateful thanks and recognition. But this new edition would not have been possible without the huge efforts made by the team at Whittles Publishing. They have achieved what I consider to be a superb presentation which makes the book both practical and agreeable to look at: for this my considerable thanks.

Journalists who write books are generally unsuccessful; their style is too obviously self-conscious. Most scientists who write suffer from the opposite; content is the only consideration (there are, of course, obvious exceptions). To most scientists, prose is like make up: it is there to embellish (hide, exaggerate, enhance) the truth. Since science prefers the truthful truth, prose is neglected. But most women will willingly admit that embellishing the truth has its benefits. And I would agree. In no way will there be an attempt to embellish the truth in this book but I do admit to an admiration for those who write well. I have done my conscious best to be clear; with jargon to the minimum.

Many books are dedicated to wives or mothers or children or even cats. This is a queer habit. And quite silly. I love my children but they have nothing to do with this book: they did their unconscious best to impede it. The best introduction to a book I have ever read is a quote (Barrow, 1992) from Groucho Marx: '*From the moment I picked up your book until I laid it down, I was convulsed with laughter. Some day I intend reading it*'.

# ACKNOWLEDGEMENTS

Permission to adapt and redraw the following material is gratefully acknowledged.

Figure 2.11: from Theys, Ph., Log data acquisition and quality control, in Éditions Technip, pp. 330, Figure 4.15, by permission of Éditions Technip.

Figure 2.14: from Dewar, (1983) in Essentials of Modern Open Hole Log Interpretation, Figure 3.14, by permission of Penn Well Books.

Figure 3.10: from Hill, A.D. (1990) Production logging – theoretical and interpretative elements. Monograph (14), Figure 4.10, from McKinley, R.M. Production Logging, paper SPE 10035 presented at the 1982 SPE Intl. Petroleum Exhibition and Technical Symposium, Beijing, March 18-26, by permission of Society of Petroleum Engineers.

Figure 3.11: from Hill, A.D. (1990) Production logging – theoretical and interpretative elements. Monograph (14), Figure 4.33, from Dobkins, T.A. Improved Methods to Determine Hydraulic Fracture Height, JPT (April, 1981) pp. 719-26, by permission of Society of Petroleum Engineers.

Figure 4.11: from Yassir and Dusseault., Stress trajectory determinations in S.W. Ontario from borehole logs, Figure 2. Geological Applications of Wireline Logs II. Sp. Pub. no. 65, pp 169-177 by permission of the Geological Society.

Figure 6.5: from Jackson, P.P., Taylor-Smith, D. and Stanford, P.N., 1978, in Geophysics 43(6), pp. 1250-1268, Figure 8, by permission of the Society of Exploration Geophysicists.

Figure 6.19: from Ellis, D.V. (1987) Well Logging for Earth Scientists, pp. 532, Figure 6.5, by permission of Elsevier Science Pub. Co. Inc.

Figure 6.29: from Theys, Ph., Log data acquisition and quality control, in Éditions Technip, pp. 330, Figure 22.18, by permission of Éditions Technip.

Figure 6.38: from Passey, Q.R., Creaney, S., Kulla, J.B., Moretti, F.J. and Stroud, J.D. (1990) in AAPG 74(12) pp.1777-1794, Figure 6, by permission of the American Association of Petroleum Geologists.

Figure 6.39: from Hillis, R.R., Quantification of Tertiary Exhumation in the UK southern North Sea using Sonic Velocity Data, in AAPG 79(1) pp. 130-152, Figure 1, by permission of the American Association of Petroleum Geologists.

Figure 7.5: from Serra, O. (1979), Diagraphies différées – bases de l'interprétation. Tome 1: Acquisition des données diagraphiques. Bull. Cent. Rech. Explor.-Prod. Elf- Aquitaine, Mém. 1, Figure 138, by permission of Éditions Technip.

Figure 7.15: from Dresser Atlas (1982), Well Logging and Interpretation Techniques, Figure 7.13, by permission of Dresser Atlas.

Figure 7.26: from Scherer (1980) AAPG Memoir 30, pp. 436 by permission of the American Association of Petroleum Geologists.

Figure 7.27: from Quirein *et al.*, (1982) in 1982 Annual Technical Conference and Exhibition, paper SPE 11143, Figure 2, pp. 2, by permission of Society of Petroleum Engineers.

Figure 8.2: from Ellis, D.V. (1987), Well Logging for Earth Scientists, Figure 16.12, pp. 371, after Schlumberger, by permission of Elsevier Science Publishing Co. Inc.

Figure 8.19: from Hillis, R.R., Quantification of Tertiary Exhumation in the UK southern North Sea using Sonic Velocity Data, in AAPG 79(1) pp. 130-152, Figure 2, by permission of the American Association of Petroleum Geologists.

Figure 8.23: from Passey, Q.R., Creaney, S., Kulla, J.B., Moretti, F.J., and Stroud, J.D. A practical model for Organic Richness from Porosity and Resistivity Logs. AAPG 74(12), Figure 12, pp.1789, by permission of the American Association of Petroleum Geologists.

Figure 8.30: from DSI Dipole Shear Sonic Imager, Figure 10, by permission of Schlumberger.

Figure 8.29: from Zemanek, J., Williams, D.M., Schmitt, D.P., Shear-Wave Logging using Multipole Sources. Log Analyst, 32(3), Figures 1 and 2, pp. 234, by permission of the American Association of Petroleum Geologists.

Figure 8.31: from Smith, M.L., Sondergeld, C.H., Norris, J.O., The Amoco Array Sonic Logger, Log Analyst, 32(3), Figure 1, pp. 202, by permission of the American Association of Petroleum Geologists.

Figure 8.32: from Hsuk and Chang Shu-Kong, 1987. Multiple short processing of array sonic waveforms, in Geophysics 52(10), pp. 1376-1390, Figures 1 and 3, by permission of the Society of Exploration Geophysicists.

Figure 8.34: from Smith, M.L., Sondergeld, C.H., Norris, J.O., The Amoco Array Sonic Logger, Log Analyst, 32(3), Figure 9 pp. 208, by permission of the American Association of Petroleum Geologists.

Figure 8.36: by permission of the Compagnie Générale de Geophysique.

Figure 8.37: from Bunch, A.W.H. and Dromgoole, P.W. Lithology and fluid prediction from seismic and well data, I, 1995, pp. 49-57, by permission of the Society of Exploration Geophysicists.

Figure 9.3: Ellis, D., Flaum, C., Roulet, C., Marienbach, E. and Seeman, B. The Litho-Density Tool Calibration, Paper SPE 12048, SPE Ann. Tech. Conf. and Exhibition, 1983, Figure 10.12 pp. 214, by permission of Elsevier Science Publishing Co. Inc.

Figure 9.4: Ellis, D., Flaum, C., Roulet, C., Marienbach, E. and Seeman, B. The Litho-Density Tool Calibration, Paper SPE 12048, SPE Ann. Tech. Conf. and Exhibition, 1983, Figure 10.3 pp. 206, by permission of Elsevier Science Publishing Co. Inc.

Figure 9.11: from Jackson, M.P.A., and Talbot, C.J. (1986), pp. 305-323. Bull. Geol. Soc. of America by permission of the Geological Society of America.

Figure 9.29: from Log Interpretation Principles/Applications, (1989), Figure 6.4, by permission of Schlumberger.

Figure 9.30: from Humphreys B. and Lott, G.K. An investigation into nuclear log responses of North Sea Jurassic sandstones using mineralogical analysis. Geological Applications of Wireline Logs, eds. Hurst, A., Lovell, M.A. and Morton, A.C., 1990 by permission of the Geological Society.

Figure 10.3: from Ellis, D.V. (1987) Well Logging for Earth Scientists, Figure 11.11, pp. 238, by permission of Elsevier Science Publishing Co. Inc.

Figure 12.1: from Cameron, G.J.F., Collinson, J.D., Rider, M.H., and Li Xu. Analogue dipmeter logs through a prograding deltaic sandbody from Advances in Reservoir Geology, ed., Ashton, M. Figure A2, pp. 215, by permission of the Geological Society.

Figure 12.9: from Cameron, G.J.F., Collinson, J.D., Rider, M.H., and Li Xu. Analogue dipmeter logs through a prograding deltaic sandbody from Advances in Reservoir Geology, ed., Ashton, M. Figure A2, pp. 215, by permission of the Geological Society.

Figure 12.21: from Cameron, G.J.F., Collinson, J.D., Rider, M.H., and Li Xu. Analogue dipmeter logs through a prograding deltaic sandbody from Advances in Reservoir Geology, ed., Ashton, M. Special publication 69, Figure 4, pp. 199, Figure 6, pp. 201 and Figure 7, pp. 202 all combined, by permission of the Geological Society.

Figure 12.27: from Phillips, S., Dipmeter Interpretation of Turbidite-Channel Reservoir Sandstones, Indian Draw Field, New Mexico from Reservoir Sedimentology, eds. Tillman, R.W. and Weber, K.J., special publication 40, Figure 14, pp. 123 by permission of Society of Economic Paleontologists and Mineralogists.

Figure 12.36: from Adams, J.T., Ayodele, J.K., Beedford, J., Kaars-Sijpesteijn, C.H., and Watts, N.L. Application of dipeter data in structural interpretation, Niger Delta from Geological Applications of Wireline Logs II, eds. Hurst *et al.*, special publication 65, Figure 10, pp. 256, by permission of the Geological Society.

Figure 13.6: from Serra, O. Formation MicroScanner Image Interpretation, Figure 6, page 6, by permission of Schlumberger.

Figure 13.13: from FMI Fullbore Formation MicroImager, page 8 (tool diagram), by permission of Schlumberger.

Figure 13.25: from Zemanek, J., Caldwell, R.L., Glenn, E.E., Holcomb, S.V., Norton, L.J., and Strauss, A.J.D. (1969). The borehole televiewer – a new logging concept for fracture location and other types of borehole inspection. JPT, 21, 762-774, Figure 1, page 255, by permission of Society of Petroleum Engineers.

Figure 13.26: from Atlas Wireline Services (1992) in Digital Circumferential Borehole Imaging Log (CBIL) tool brochure, by permission of Dresser Atlas.

Figure 13.29: from Trouiller et al., Thin-Bed Reservoir Analysis from Borehole Electrical Images. SPE 19578, pp. 61-72, Figure 9, by permission of Society of Petroleum Engineers.

Figure 14.6: from Finley, R.J. and Tyler, N. Geological Characterization of Sandstone Reeservoirs from Reservoir Characterization, eds. Lake, L.W. and Carroll, Jr., Figure 4, by permission of the Bureau of Economic Geology.

Figure 14.7: from Van Wagoner *et al.*, (1990), Siliclastic Sequence Stratigraphy in Well Logs, Cores, and Outcrops: Concepts for High-Resolution Correlation of Time and Facies, Figure 8, by permission of the American Association of Petroleum Geologists.

Figure 14.12: from Slatt *et al.*, (1992), Outcrop gamma-ray logging to improve understanding of subsurface well log correlations, from Geological Applications of Wireline Logs II, ed. Hurst et al., special publication 65, pp. 3-19, Figure 8 by permission of the Geological Society.

Figure 15.8: from Loutit et al., (1988) Condensed Sections: The Key to Age Determination and Correlation of Continental Margin Sequences from Sea-Level Changes: An Integrated Approach, ed. Wilgus et al., Figure 20, by permission of Society of Economic Paleontologists and Mineralogists.

Figure 15.10: from Ineson, J.R., The Lower Cretaceous chalk play in the Danish Central Trough from Petroleum Geology of Northwest Europe: Proceedings of the 4th Conference, I, ed., Parker, J.R., Figures 1 and 3, by permission of the Geological Society.

Figure 15.13: from Vail, P.R. and Wornardt, W.W., Well Log-Seismic Sequence Stratigraphy: an Integrated Tool for the 90s from Sequence Stratigraphy as an Exploration Tool, eds. Armentrout, J.M. and Perkins, B.F., Figures 3, 5, 7, 9, 11, by permission of Society of Economic Paleontologists and Mineralogists.

# CONTENTS

# Key

## LITHOLOGICAL SYMBOLS


Shale


Shale (alt.)


Organic shale


Silt

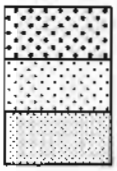
cse
med.
fine
Sandstone

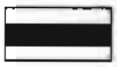
coal


coal debris


Limestone

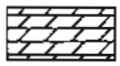
Dolomite

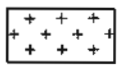
Salt (halite)

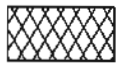
Anhydrite


Gypsum


Volcanic


carbonate cement

## SEDIMENTOLOGICAL FORMAT


## SEDIMENTARY STRUCTURES


cross-beds


current ripples
wave ripples


horizontal laminae


irregular laminae


concretion


horizontal burrows


vertical burrows


roots


shells


oolites

# 1
# INTRODUCTION

## 1.1 Well logs – a definition

The continuous recording of a geophysical parameter along a borehole produces a geophysical well log. The value of the measurement is plotted continuously against depth in the well (Figure 1.1). For example, the resistivity log is a continuous plot of a formation's resistivity from the bottom of the well to the top and may represent over 4 kilometres (2½ miles) of readings.

The most appropriate name for this continuous depth-related record is a wireline geophysical well log, conveniently shortened to well log or log. It has often been called an 'electrical log' because historically the first logs were electrical measurements of electrical properties. However, the measurements are no longer simply electrical, and modern methods of data transmission do not necessarily need a wire line so the name above is recommended. This book therefore concerns wireline geophysical well logs.

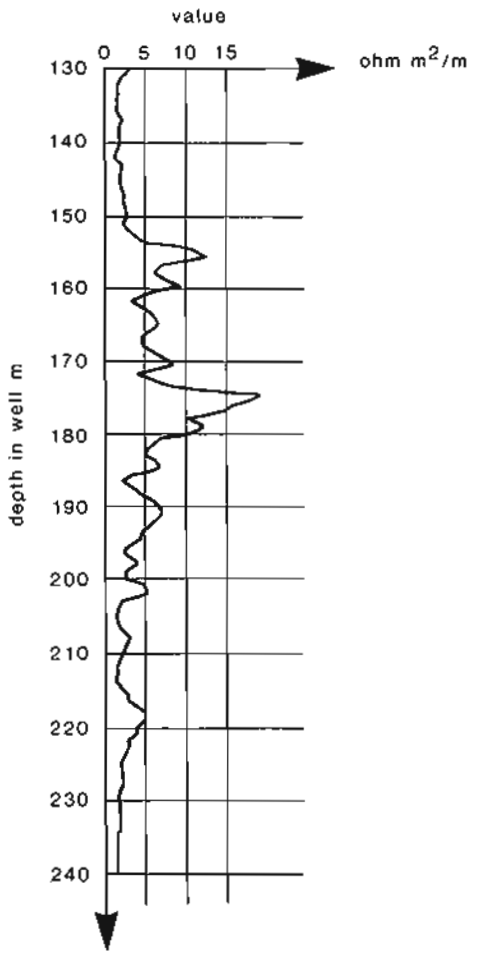


**Figure 1.1** A well log. Representation of the first 'log' made at Pechelbronn, Alsace, France, in 1927 by H. Doll. (From Allaud and Martin, 1976).

In France, where well logging was first invented by Conrad Schlumberger and Henri Doll, the original name was 'Carottage Électrique' (electrical coring) as opposed to mechanical coring. Today the name *diagraphies différées* (literally, 'deferred diagrams') is applied to distinguish wireline geophysical well logs, which are made after drilling, from the drill logs (*diagraphies immédiates*, i.e. immediate diagrams) made during the drilling. In English no such distinction is made – the word 'log' is universally used.

## 1.2 Well logs – the necessity

Many different modern geophysical well logs exist. They are records of sophisticated geophysical measurements along a borehole. These may be measurements of spontaneous phenomena, such as natural radioactivity (the gamma ray log), which requires a tool consisting simply of a very sensitive radiation detector; or they may be induced, as with the formation velocity log (sonic log), in which a tool emits sound into the formation and measures the time taken for the sound to reach a receiver at a set distance along the tool (Table 1.1).

Geophysical well logging is necessary because geological sampling during drilling ('cuttings sampling') leaves a very imprecise record of the formations encountered. Entire formation samples can be brought to the surface by mechanical coring, but this is both slow and expensive. The results of coring, of course, are unequivocal. Logging is precise, but equivocal, in that it needs interpretation to bring a log to the level of geological or petrophysical experience. However, logs fill the gap between 'cuttings' and 'cores', and with experience, calibration and computers, they can almost replace cores, as they certainly contain enough information to put outcrop reality into the subsurface.

## 1.3 Wireline logs – the making

Wireline geophysical well logs are recorded when the drilling tools are no longer in the hole. 'Open-hole' logs, (open-hole indicates that the formation forms the wall of a well, as opposed to 'cased-hole, in which a tube of metal casing lines the well), the subject of this book, are recorded immediately after drilling. MWD

**Table 1.1** Classification of the common wireline geophysical well measurements (in 'open hole').

| | Log Type | Formation parameter measured |
|---|---|---|
| Mechanical measurements | Caliper | Hole diameter |
| Spontaneous measurements | Temperature | Borehole temperature |
| | SP (self-potential) | Spontaneous electrical currents |
| | Gamma ray | Natural radioactivity |
| Induced measurements | Resistivity | Resistance to electrical current |
| | Induction | Conductivity of electrical current |
| | Sonic | Velocity of sound propagation |
| | Density | Reaction to gamma ray bombardment |
| | Photoelectric | Reaction to gamma ray bombardment |
| | Neutron | Reaction to neutron bombardment |

(measurement while drilling) or LWD (logging while drilling) logs, by contrast, are made as a formation is drilled. Quite different techniques are made to record MWD and LWD logs but the results are comparable to the open hole wireline logs (*see* Section 1.6).

Wireline logs are made using highly specialized equipment entirely separate from that used for drilling. Onshore, a motorized logging truck is used which brings its array of surface recorders, computers and a logging drum and cable to the drill site. Offshore, the same equipment is installed in a small cabin left permanently on the rig. Both truck and cabin use a variety of interchangeable logging tools, which are lowered into the well on the logging cable (Figure 1.2).

Most modern logs are recorded digitally. The sampling rate will normally be once every 15 cm (6 in), although for some specialized logs it will be as low as 2.5 mm (0.1 in). An average well of say 2000 m will therefore be sampled over 12,000 times for each individual log, and for a suite of 8 or so typical logs, it will be sampled over 100,000 times (although for some new, specialised tools, this can be the sampling rate per metre!). At typical logging speeds, data transmission rates will vary from 0.05 kilobits per second for simpler logs to over 200 kilobits per second for the new complex logs. The huge amount of data representing each logging run is fed into the computer of the surface unit. There is generally an instantaneous display for quality control and a full print-out immediately the log is finished, but the raw data are stored on magnetic tape for future processing and editing.

To run wireline logs, the hole is cleaned and stabilized and the drilling equipment extracted The first logging tool is then attached to the logging cable (wireline) and lowered into the hole to its maximum drilled depth. Most logs are run while pulling the tool up from the bottom of the hole. The cable attached to the tool acts both as a support for the tool and as a canal for data transmission. The outside consists of galvanized steel, while the electrical conductors are insulated in the interior (Figure 1.3). The cable is wound around a motorized drum on to which it is guided manually during logging. The drum will pull

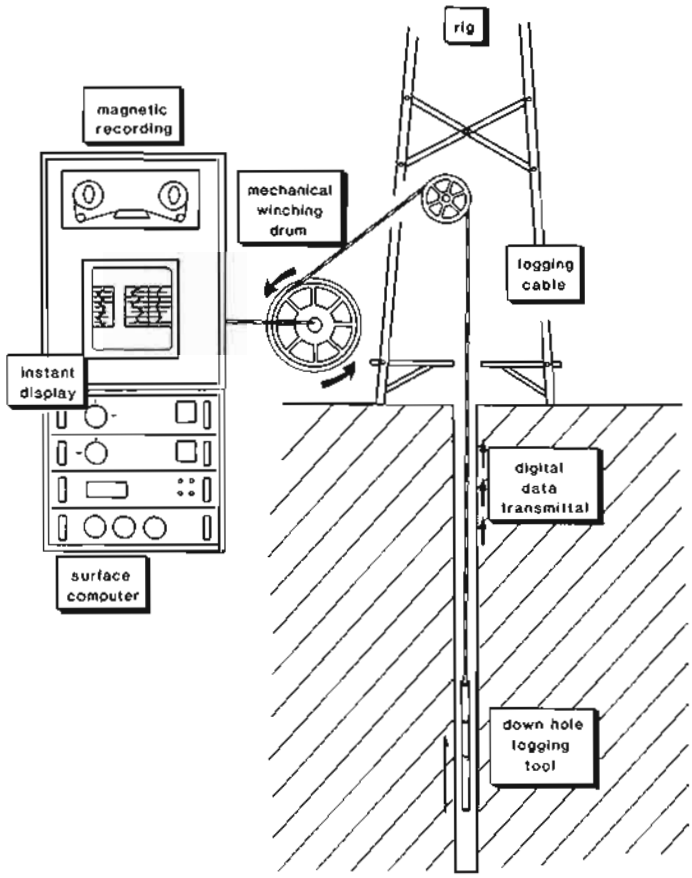


**Figure 1.2** Schematic diagram of a modern wireline logging set-up. The surface computer and electronic equipment are housed in a logging truck (on land) or cabin (offshore). The logging tool is winched up the hole by the logging cable which also transmits the tool readings. The transmittal is digital and recorded on magnetic tape. The surface computer allows instant display.

the cable at speeds of between 300 m/h (1000 ft/h) and 1800 m/h (6000 ft/h), i.e. 0.3 to 1.8 km/h, depending on the tool used. As the cable is pulled in, so the depth of the working tool is checked. Logging cables have magnetic markers set at regular intervals (e.g. 100 ft or 25m) along their length and depths are checked mechanically, but apparent depths must be corrected for cable tension and elasticity.

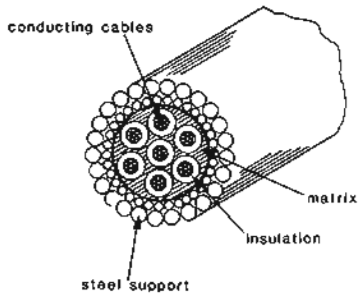


**Figure 1.3** Schematic diagram of a 7 core logging cable. (Modified from Moran and Attali, 1971.)

Because rig time is expensive and holes must be logged immediately, modern logging tools are multi-function (Figure 1.4). They may be up to 28 m (90 ft) in length, but still have an overall diameter of only 3–4 in (although new, shorter tools are being prepared). The Schlumberger ISF sonic tool, for example, of 3⅜ in diameter, is 55.5 ft (16.9 m) long and gives a simultaneous measurement of gamma ray or caliper, SP, deep resistivity (conductivity), shallow resistivity and sonic velocity. The complexity of such tools requires the use of the surface computer, not only to record but also to memorize and to depth-match the various readings. The gamma-ray sensor, for example, is not at the same depth as the resistivity sensors (Figure 1.4), so at any one instant, different formations are being sampled along the tool. The surface computer therefore memorizes the readings, compensates for depth or time lag and gives a depth-matched output.

Despite the use of the combined tools, the recording of a full set of logs still requires several different tool descents. While a quick, shallow logging job may only take 3–4 hours, a deep-hole, full set may take 2–3 days, each tool taking perhaps 4–5 hours to complete.

## 1.4 Log runs

When a log is made it is said to be 'run'. A log run is typically made at the end of each drilling phase, i.e. at the end of the drilling and before casing is put in the hole (Figure 1.5). Each specific log run is numbered, being counted from the first time that the particular log is recorded. Run 2 of the ISF Sonic, for example, may cover the same depth interval as a Formation Density Log Run 1. In this case it means that over the first interval of the ISF Sonic, (i.e. Run 1), there was no Formation Density log recorded (Figure 1.5).

Typically, through any well, more logs are run over intervals containing reservoirs or with shows, than over apparently uninteresting zones. The choice of logs depends on what it is hoped to find. Logging costing

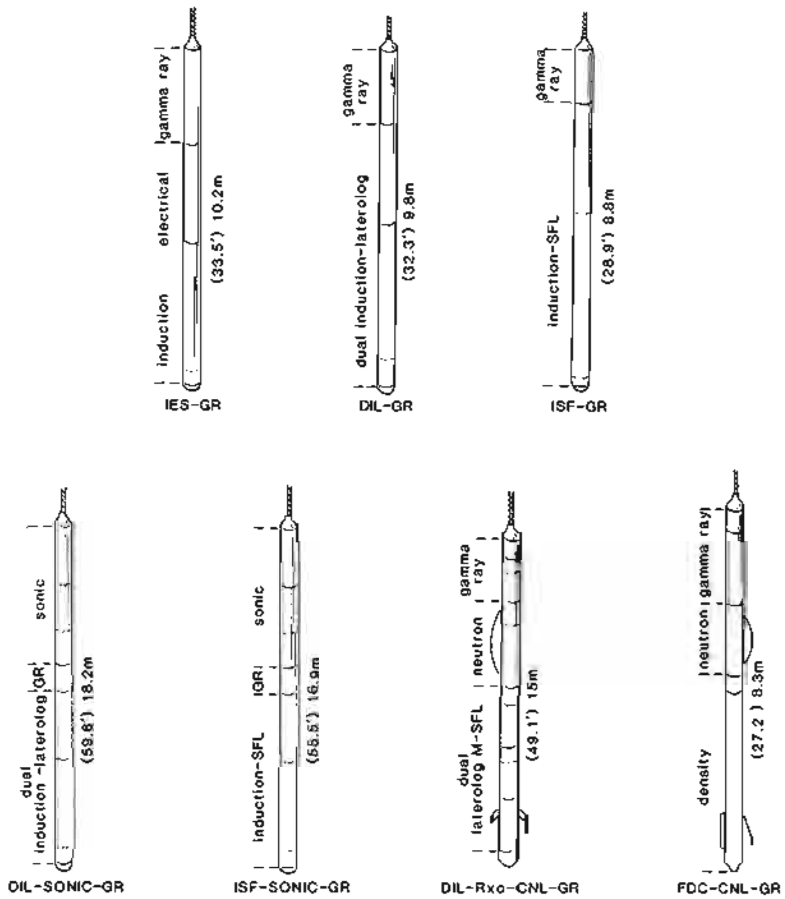


**Figure 1.4** Some typical modern combination logging tools. Lengths are as marked; diameters are mainly 3 in. (Modified from Schlumberger, 1974). For tool mnemonics *see* Appendix.

5–10% of total well costs is expensive, so that in cheap, onshore wells, in known terrain, a minimum set is run. Offshore, where everything is expensive, full sets of logs are generally run, even if hydrocarbons are not found, as each well represents hard-gained information. Cutting down on well logs is probably a false economy, but it can be forgiven when prices are considered.

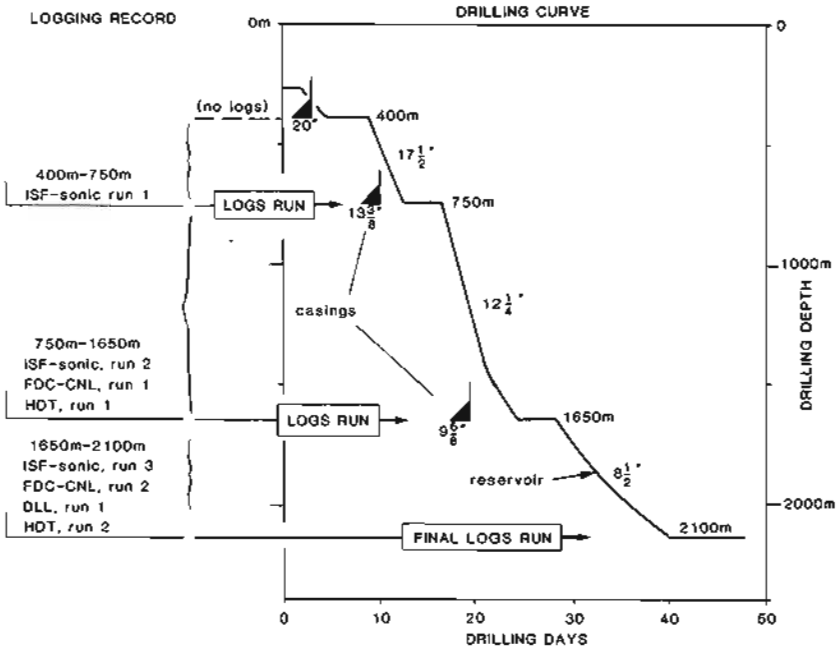


**Figure 1.5** Logging record. Log runs are indicated on a typical offshore drilling curve. Horizontal lines indicate no drilling, when logs are run. Casing follows logging. Note log run numbers. (Tool mnemonics – Schlumberger, *see* Appendix).

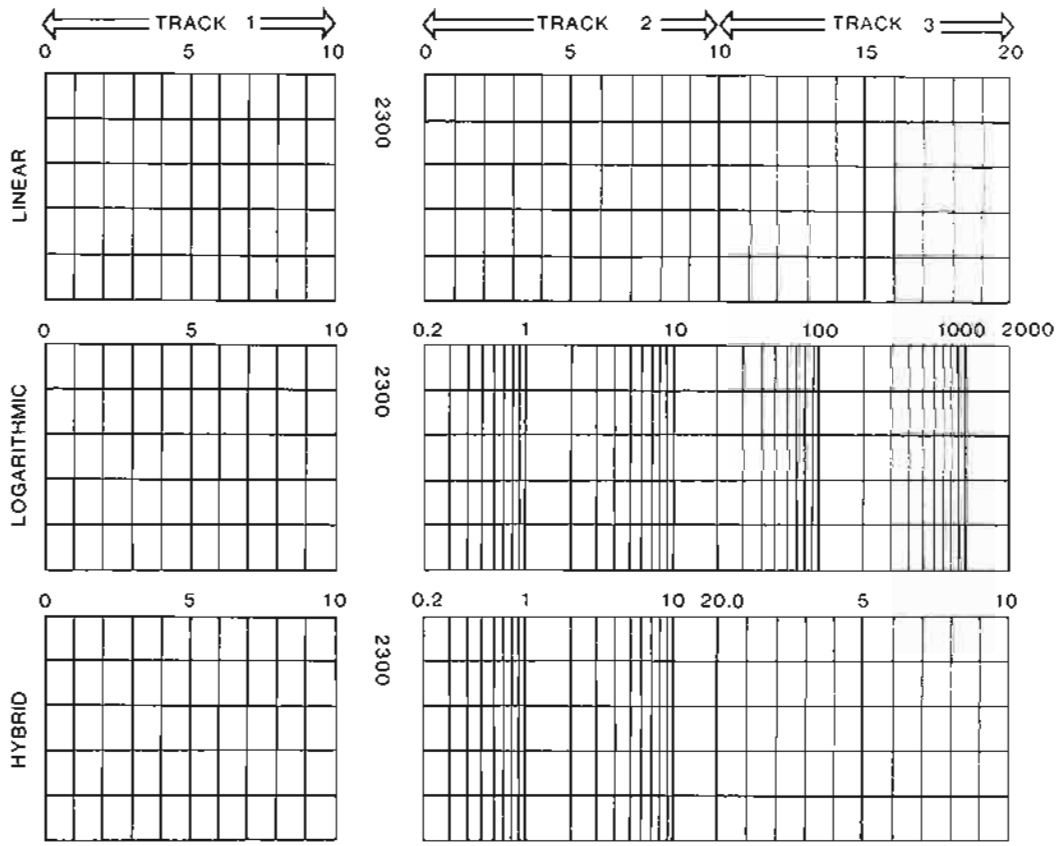


**Figure 1.6** Three typical API log formats. Tracks are 2.5in wide with a central 0.75in depth column. Overall width is 8.25in. Vertical scales are variable (*see text*).

## 1.5 Log presentations

A standard API (American Petroleum Institute) log format exists (Figure 1.6). The overall log width is 8.25 in (21 cm), with three tracks of 2.5 in (6.4 cm), tracks 1 and 2 being separated by a column of 0.75 in (1.9 cm) in which the depths are printed. There are various combinations of grid. Track 1 is always linear, with ten standard divisions of 0.25 in (0.64 cm). Tracks 2 and 3 may have a 4-cycle logarithmic scale, a linear scale of 20 standard divisions, or a hybrid of logarithmic scale in track 2 and linear scale in track 3 (Figure 1.6).

These are the classic presentations which, in the past, usually prevailed. With the advent of digitized logs, non-standard formats are becoming more common, especially on computer playbacks.

On the old analog logging systems, the choice of vertical or depth scales was limited to two of 1:1000, 1:500, 1:200, 1:100, 1:40 and 1:20. From these, the most frequent scale combinations were 1:500 (1cm≡ 5 m) for résumé or correlation logs and 1:200 (1cm ≡ 2 m) for detailed reservoir presentation.

The American area was an exception, where the available scales were 1:1200, 1:600, 1:240 and 1:48. From these the commonly-chosen scales were 1:600 (1 in≡100 feet) for résumé and correlation logs, and 1:240 (5 in ≡ 100 feet) for detail.

These scales still dominate industry documents, but as a result of modern computer storage other scales are becoming more common. Especially useful to the geologist are the reduced scales of 1:2000 (1 cm ≡ 20 m) and 1:5000 (1 cm ≡ 50 m). In fact any convenient scale can now be produced easily by the computer, whereas in the past scale changes could only be made by unsatisfactory photographic methods.

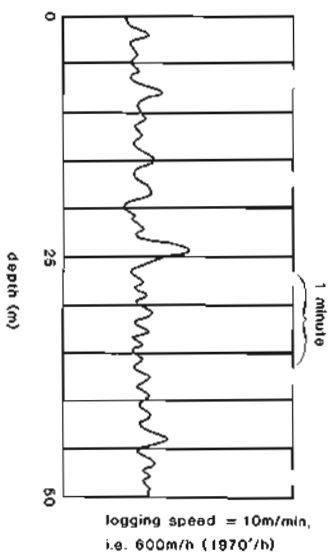


**Figure 1.7** Dashed log margin representing minute intervals (Schlumberger). The logging speed can be checked from these dashes.

One final aspect of the log grid to note are markers which indicate real time during logging. On Schlumberger logs, time is indicated by the dashed grid margins on the field prints. Each dash represents one minute, regardless of log scale (Figure 1.7). Other companies use ticks or spikes on the grid for the same purpose. Time markers allow a direct control of logging speed and, indirectly, log quality.

Every log grid is preceded by a comprehensive log heading. It covers all aspects which allow the proper interpretation of the log and, in addition, identification of the well, rig, logger and logging unit. The log heading illustrated (Figure 1.8) is but one example, each company having its own format.

On the log tail is found a repetition of some of the log-head data, simply for convenience. Calibration data are also added to the log tail, as are short, doubled-up or repeat sections which act as samples for empirical quality control.

## 1.6 LWD Logs (*Logging while drilling)

(*MWD, Measurement While Drilling, is generally taken to refer to simpler, drilling-type measurements such as hole deviation, while LWD, Logging While Drilling, is taken to refer to log-type measurements such as resistivity, density and so on. However, there is still some confusion.)

Wireline logs are made, as has been described (Section 1.3) on a single pass of each specialized tool once drilling ceases and the bit is taken out of the hole. LWD logs, on the contrary, are built up, metre by metre, as drilling actually takes place. The technique is quite different.

An LWD tool consists of three elements: downhole logging sensors, a data transmission system and a surface interface. The logging sensors are placed just behind the drill bit in specialised drill collars (lengths of reinforced drill string) and are active in the hole during drilling. The sensor signals are transmitted to the surface, generally in digital format, by pulse telemetry through the drilling mud and collected by surface receivers. The signals are converted and a continuous log slowly built up as drilling progresses. The formation is therefore logged very soon after drilling, a matter of minutes to several hours, depending on drilling rates and the distance between the bit and the downhole sensors.

Services now offered by the LWD companies include gamma ray, resistivity, density, neutron and a continuous directional survey (a sonic is imminent). The log types are similar (but not identical) to the wireline log types of similar category. Thus a gamma ray LWD log is comparable to a wireline gamma ray log, and an LWD resistivity log is comparable to a 'shallow' wireline resistivity log. In general, the LWD logs are as accurate as the wireline logs and can be interpreted in a similar way. However, the characteristics of the readings and data quality problems are rather different.

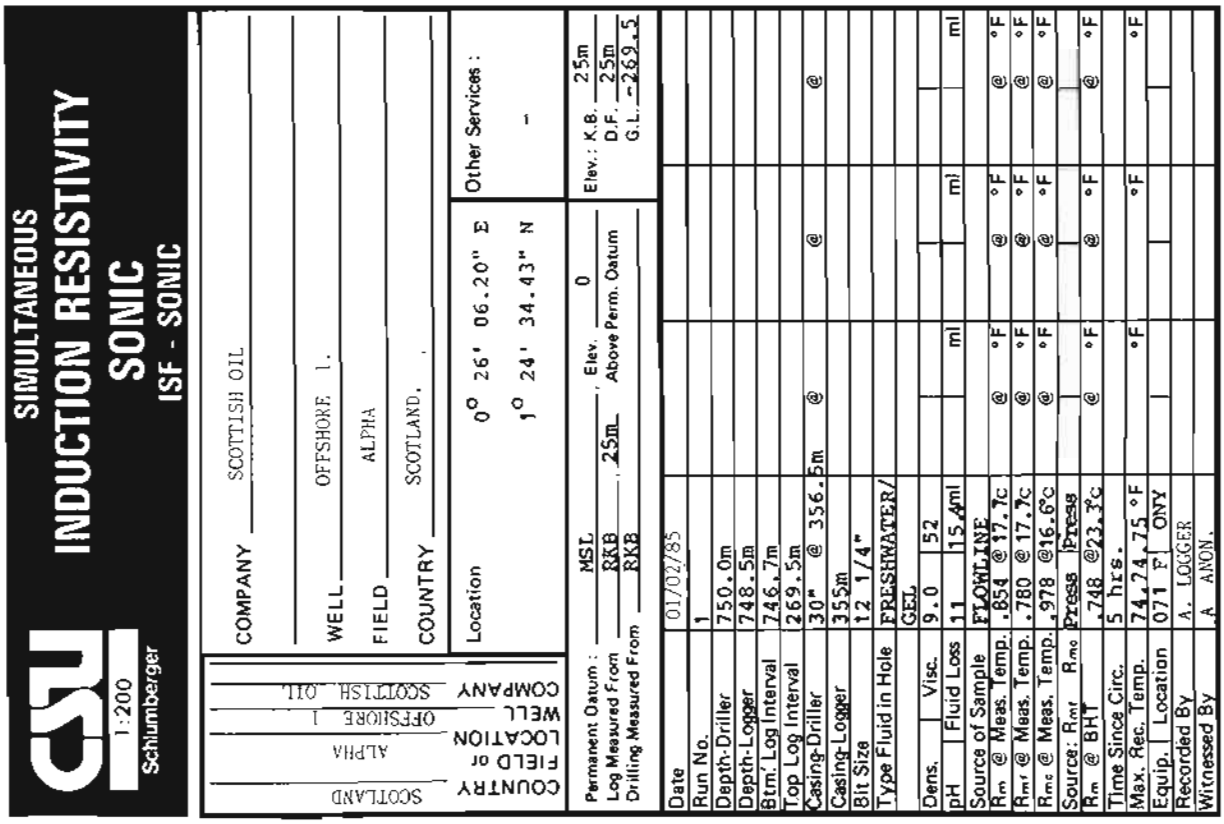


EQUIPMENT DATA

| Run N° | Induction Cartridge | Induction Sonde | Sonic Cartridge | Sonic Sonde | GR Cartridge | Caliper | CSU equipment Module | CSU equipment GEU | Program Name | Program Version |
|---|---|---|---|---|---|---|---|---|---|---|
| 1 | QB941 | VA945 | KB975 | RC231 | JAA498 | - | IEMBC869 | | ISN | 20.22 |
| | | | | | | | NSM 926 | | | |
| | | | | | | | SLMDA124 | | | |

LOGGING DATA

| Run N° | Gamma Ray Depth constant | Gamma Ray Speed | Stand-off inches | Centering Device | Zero cond. adjusted at Surface | Zero cond. adjusted at Depth | Max. hole deviation |
|---|---|---|---|---|---|---|---|
| 1 | | | 1 1/2" | Ex-centered | | | ° @ |
| | | | | | | | ° @ |
| | | | | | | | ° @ |
| | | | | | | | ° @ |

REMARKS GR logged to seabed.

PEH-A used.

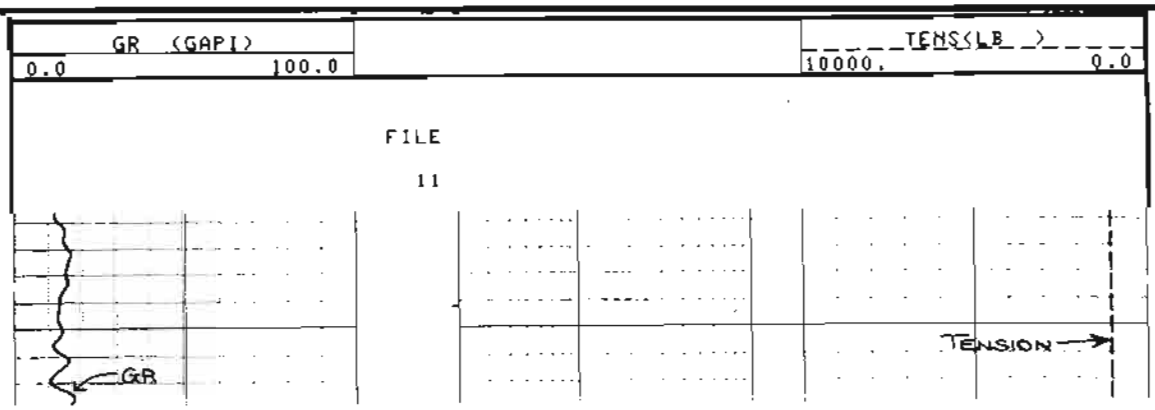


Figure 1.8 A typical log heading.

LWD tools are much used in highly deviated and horizontal wells where they help to direct the drilling and function in conditions very difficult for standard wireline tools. Also, it is found that multiple passes with the LWD tools, combined with the wireline log results, give a very accurate picture of fluid movement in the period following drilling (Chapter 6). Case studies suggest that often wireline logs are not run at the best time in terms of borehole conditions (Cunningham *et al.*, 1991).

LWD logs are clearly going to be used more and more, partly as a replacement to the open hole logs and partly as an addition, especially in horizontal or highly deviated wells (Walsgrove *et al.*, 1992). However, the interpretation of LWD logs involves problems rather specific to the LWD technique and tool types involved. At present we are still at the stage of comparing LWD with wireline logs, expecting the latter to be the 'standard'. Very soon the reverse will be true since the slower logging speed of the LWD technique offers the potential for a better reading. But, in order to keep this book at a relatively straightforward level, the LWD logs are used occasionally as examples, but are not considered further, *per se*.

## 1.7 The logging companies

The wireline well-logging world is dominated by one, extremely successful, giant international company – Schlumberger. In America a number of other companies exist but in many parts of the world Schlumberger has a quasi-monopoly. The reasons for this domination are partly historical: it was the frères Schlumberger, Conrad and Marcel, who created the original SPE (Société de Prospection Électrique) in 1926, the precursor of the modern Schlumberger. The brothers, along with H.G. Doll, were the creators of the well-logging technique.

The international forum is becoming more competitive, and in America smaller companies are active. However, two names stand out in the general logging field apart from Schlumberger: Western Atlas Logging Services, which was called Atlas Wireline Services (ex-Dresser Atlas) and Halliburton Logging Services (ex-Gearhart and incorporating Welex). B.P.B. Wireline, originally the logging arm of British Plaster Board, is an additional, small player.

**Table 1.2** Principal uses of open-hole wireline logs.

| Chapter | Uses | General geology | | | | | | Reservoir geology | | Geochemistry | | Petrophysics | | | | | | Seismic | |
|---|---|---|---|---|---|---|---|---|---|---|---|---|---|---|---|---|---|---|---|
| | | Lithology – general | Volcanics Unusual } Evaporites Lithology | | Mineral identification | Correlation: stratigraphy | Facies depositional env. | Fracture identification | Over-pressure identification | Source rock identification | Maturity | Porosity | Permeability | Shale volume | Fm. water salinity | Hydrocarbon saturation | Gas identification | Interval velocity | Acoustic impedance |
| 3 | Temperature | | | | | | | | – | | + | | | | | | – | | |
| 4 | Caliper | | | | | | | – | | | | | – | | | | | | |
| 5 | SP | | | | | – | – | | | | | | – | + | * | | | | |
| 6 | Resistivity | – | | – | | – | – | | + | + | + | + | – | | – | * | – | | |
| 7 | Gamma ray | – | – | + | – | – | – | | | + | | | | + | | | | | |
| 7 | Spectral GR | – | – | + | + | – | – | – | | + | | | | + | | | | | |
| 8 | Sonic | + | | – | | – | | + | + | + | | * | | | | | – | * | * |
| 9 | Density | + | – | – | – | | – | + | – | + | | * | | | | | – | | * |
| 9 | Photoelectric | + | – | – | + | | | | | | | | | | | | | | |
| 10 | Neutron | + | – | – | – | | – | | | – | | * | | – | | | – | | |
| 12 | Dipmeter | | | | | – | – | | | | | | | | | | | dip | |
| 13 | Image logs | – | | | – | – | – | + | | | | | + | | | + | | dip | |

- (Essentially) qualitative use
+ Semi-quantitative and quantitative uses
* Strictly quantitative

## 1.8 Well-log interpretation and uses

The accepted user of the well log is the petrophysicist. His interest is strictly quantitative. From the logs, a petrophysicist will calculate porosity, water saturation, moveable hydrocarbons, hydrocarbon density and so on, all the factors related to quantifying the amount of hydrocarbons in a reservoir for estimates of reserves. The Society of Professional Well Log Analysts (SPWLA), the principal society of log interpreters, is mainly composed of petrophysicists.

Reservoir rocks, however, comprise perhaps only 15% of a typical well, and of this 15% only a small percentage actually contains hydrocarbons. The petrophysicist is therefore not interested in 85% or more of the well logs recorded. The exploration geologist, in contrast, should be interested in 100% of well logs, as the amount of geological information they contain is enormous.

The geophysical measurements made during logging are sensitive, accurate and characteristic of the formation logged. However, to those familiar with the aspect of rocks as seen at outcrop, the geophysical signatures of this selfsame rock in the subsurface are impossible to imagine. To an experienced geological analyst of well logs, the reverse is true. A formation that he can instantly identify on the logs, down to the nearest metre, he is hard put to find, even tentatively, at outcrop.

In the following pages it is intended to relate the outcrop more closely to the wireline, geophysical well log. Logs can and should be interpreted in terms meaningful at outcrop. They contain as much information, even sometimes more, than the outcrop, but can be studied conveniently on a small desktop or computer screen.

## 1.9 This book – content and aims

Table 1.2 shows the logs considered in this book and their principal applications, both geological and geophysical. The applications have been divided into qualitative, semi-quantitative and strictly quantitative. Seismic and petrophysical applications are generally, by necessity, quantitative or semi-quantitative: geological applications, by default, usually qualitative. This should not be. A log sample set of over 100,000 values for a typical well of 2000 m represents an enormous *quantitative database*. Statistical, quasi-quantitative and of course purely quantitative methods applied to this digital log database bring precision to *geological* interpretation. So this book is concerned with qualitative and, wherever possible, the more quantitative methods of *geological log interpretation.*

# 2
# THE LOGGING ENVIRONMENT

## 2.1 Introduction

Treated simply as an instrument of measurement, a logging tool is required to do two things: to give a true, repeatable reading, and to make the reading of a representative, undisturbed sample of the subsurface formation. For the following reasons, neither of these ideals can be realized.

The first is that the undisturbed formation environment is irrevocably disturbed by drilling a well. The new drill-created conditions are those in which the logging tools work. A tool can only 'guess' at the original states. This chapter examines what is involved in this guess, in terms of drilling pressure, drilling temperature and invasion.

The second reason is that the ideal conditions for a perfect geophysical measurement cannot be met in borehole logging methods. Ideal conditions would require a logging tool to be motionless for each individual measurement, and to have a sensor of zero dimensions measuring a point sample. Sensors have dimensions and tools move. Tool design acknowledges this, and a compromise is made between a practical and practicable measurement and one that is perfect. This chapter will also examine, in general terms, the effects of the logging method on the measurements made. The notions of depths of investigation, minimum bed resolution and bed-boundary definition will be discussed.

## 2.2 The pressure environments of borehole logging and invasion

The pressure environment during drilling and, inevitably, during logging, is made up of an interplay between two elements; formation pressure and drilling-mud column pressure.

The formation pressure is the pressure under which the subsurface formation fluids, and gases are confined. The pressure of the drilling mud is hydrostatic and depends only on the depth of a well, that is the height of the mud column, and the mud density. Maintaining the pressure exerted by the column of drilling mud at just a little above the pressure of the subsurface formations encountered is one of the necessities for equilibrium drilling: it is a delicate balance. The two pressure environments are examined below.

***Hydrostatic pressure***

Fluids transmit pressure perfectly so that the pressure exerted by the column of fluid is dependent simply on the height of the fluid column and the density of the fluid. The pressure in kg in a column of water can be calculated thus:

$$\frac{\text{height of water column (m)} \times \text{density (g/cm}^3\text{)}}{10} = \text{pressure (kg) per sq. cm} \quad (1)$$

For a column of pure water of 2500 m (density of pure water = 1.00 g/cm$^3$)

$$\frac{2500 \times 1}{10} = 250 \text{kg/cm}^2 \quad (2)$$

In oilfield terms, the pressure of a column of fluid may be expressed by its pressure gradient. Thus pure water has a gradient of 1.00 g/cm$^3$. That is, a column of pure water will show a pressure increase of 1 kg/cm$^2$ per 10 m of column (or 1 g/cm$^2$ per cm of column) (Figure 2.1). The term 'column of water' is used as applicable to wells: 'depth' is equally applicable and more understandable when talking about water masses, such as the oceans.

As water becomes more saline, its density increases (Figure 2.2). Water which has a salinity of 140,000 ppm (parts per million) of solids (mainly NaCl), has a density

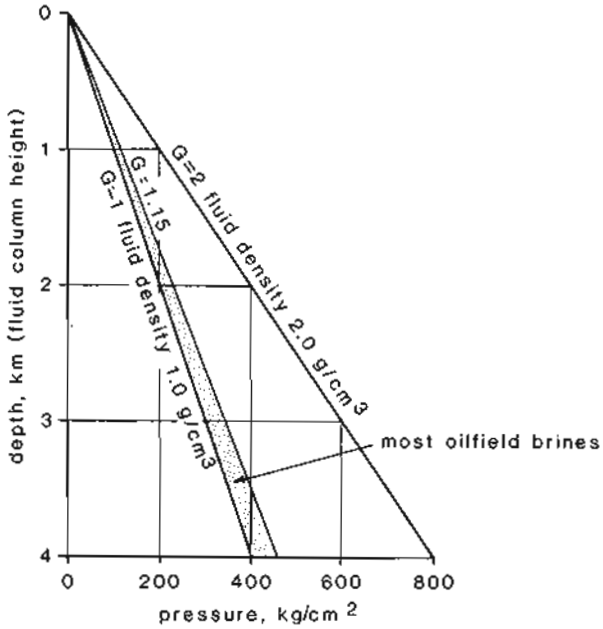


**Figure 2.1** Fluid pressure gradients related to depth, or height of fluid column.

of 1.09 g/cm³ (at 15.5°C). A column of water of this salinity will have a gradient of 1.09 g/cm³ and at 2500 m will exert a pressure of

$$\frac{2500 \times 1.09}{10} = 272.5 \text{kg/cm}^2 \quad (3)$$

Figure 2.1 shows the various gradients for fluids of different densities and the increases with depth. All gradients are shown as linear.

***Formation pressures***

In most geological basins the pressure at which pore fluids are found increases from the 'normal' to moderately over-pressured. Normal pressure is defined as hydrostatic pressure: it is due only to the weight of the fluid column above the formation. To calculate normal pressure it is sufficient to know only the depth of the formation and the density of the fluids in the formation. If a formation water has the same salinity as sea water, then the pressure at 1000 m in a formation with normal pressure is the same as the pressure at the sea floor below 1000 m of sea water. The graph (Figure 2.1) therefore shows normal pressure gradients for various salinities.

Overpressure is simply defined as any pressure above the hydrostatic (or normal) for a particular depth. Thus, if the formation fluids are salty with a density of 1.09 g/cm³ and the measured formation pressure is 350 kg/cm² at 2500 m, there is an over-pressure, calculated as follows.

Normal pressure at 2500 m, fluid density 1.09 g/cm³, from (3)

$$\frac{2500 \times 1.09}{10} = 272.5 \text{kg/cm}^2$$

Measured pressure at 2500 m = 350 kg/cm²
Overpressure = 350–272.5 = 77.5 kg/cm²

Overpressure exists for a number of reasons, but in all cases it means that the formation fluids are being squeezed by the surrounding rocks. It is similar to the pressure regime in car brakes. When the brakes are at rest, the brake fluid is at normal pressure. Putting the foot on the brake puts the fluid under overpressure: it is being squeezed by the extra pressure of the foot.

Generally, most wells drilled show a typical subsurface pressure development. Shallow formations have 'normal' or hydrostatic formation pressures: there is no rock squeezing, no overpressure. Deeper into the subsurface slight overpressures are encountered so there is slight squeezing. As the depths increase, so the overpressure increases and the formation fluids support more of the rock overburden pressure (Figure 2.3).

Overpressures can increase up to an empirical maximum called the lithostatic gradient. This gradient, also called the geostatic or overburden gradient, is taken as a convenient gradient representing the probable maximum pressure likely to be encountered in a well at any depth. The average gradient frequently used comes from the Gulf Coast of North America, and in American oilfield units is a gradient of 1 psi/ft (i.e. in metric 2.3 g/cm³) and corresponds to an average rock density of 2.3 g/cm³ (Figure 2.3) (cf. Levorsen, 1967). The true lithostatic gradient will in fact vary from well to well and will depend on the densities of the formations encountered. In the example given (Figure 2.4), which is from a well in Germany, the average formation density is 2.4 g/cm³ (Meyer-Gürr, 1976).

The average well, therefore, encounters formation pressures somewhere between the normal hydrostatic gradient and the lithostatic gradient (Figure 2.3). In absolute terms this will give usual logging pressures of between about 150 kg/cm² and 1000 kg/cm² (2000 psi

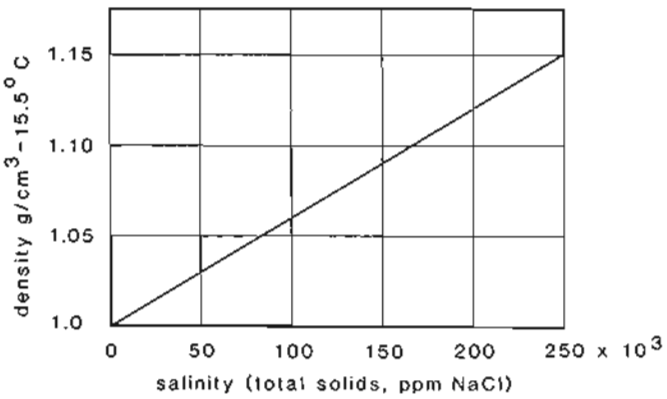


**Figure 2.2** Graph showing the increase in water density with increase in salinity (NaCl). (From Pirson, 1963.)

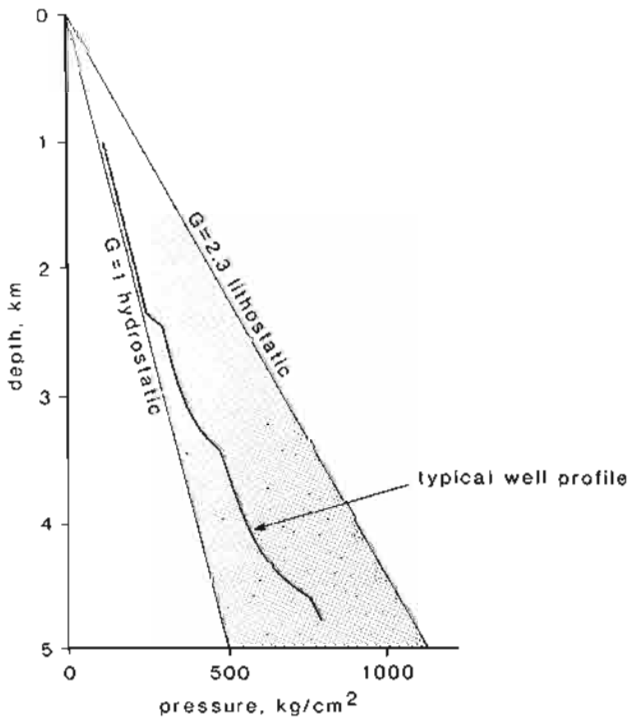


**Figure 2.3** Formation fluid pressure increases with depth in a typical oilfield well. The pressure varies between the hydrostatic (fluid) and the lithostatic (rock) gradients.

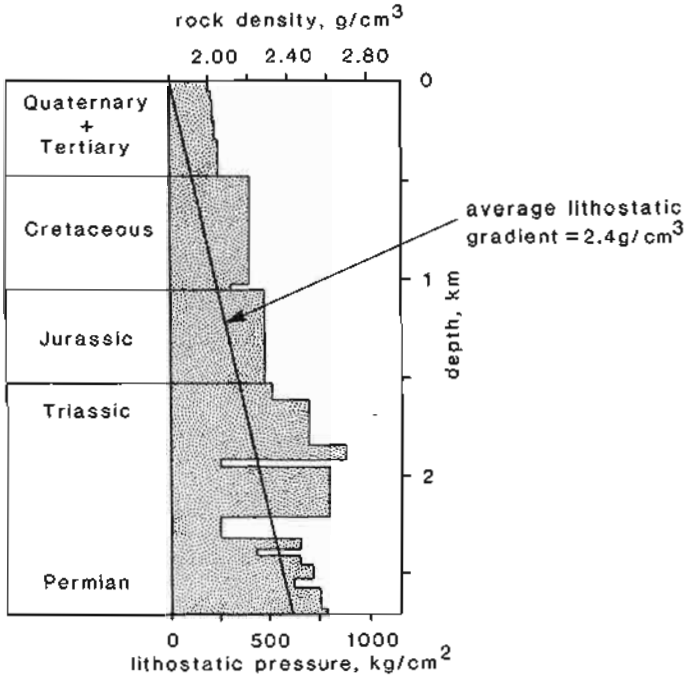


**Figure 2.4** True rock density profile and average lithostatic gradient from a North German well. (Redrawn from Meyer-Gürr, 1976).

–15,000 psi). Most oilfield logging tools are designed to withstand pressures up to a maximum of 1050–1750 kg/cm² (15,000–20,000 psi), significantly above the highest pressure usually encountered.

***Invasion-drilling pressures***

Under ideal conditions, the pressure exerted by the column of drilling mud will be such that when a porous and permeable formation is encountered, as the drill enters the formation, mud will be forced into it (Figure 2.5). The porous rock will then begin to act as a filter, separating the mud into its liquid and solid constituents. The mud filtrate (the water used to mix the mud) will flow into the formation, while the solids (the mud) will form a deposit around the borehole wall once the bit has passed. In the hole just drilled, the solid deposit around the borehole wall, the *mud cake*, will gradually build up to form a skin over the porous interval.

Initially, as the bit enters the porous formation there is complete disequilibrium and dynamic filtration takes place (Figure 2.6). That is, below and around the bit there is a continuous flow of filtrate into the formation, provided of course that the mud pressure is sufficient. Gradually, as the mud cake builds up, it creates a barrier and the movement of fluids diminishes, until finally the mud cake becomes impermeable and filtration practically ceases (Figure 2.6). A cross-section through the borehole at this stage would show mud in the hole, mud cake on the borehole wall and then the porous formation now filled almost entirely by mud filtrate. The original formation fluids have been pushed away from the hole (Figure 2.7). This is usually the situation when the open-hole well logs are run.

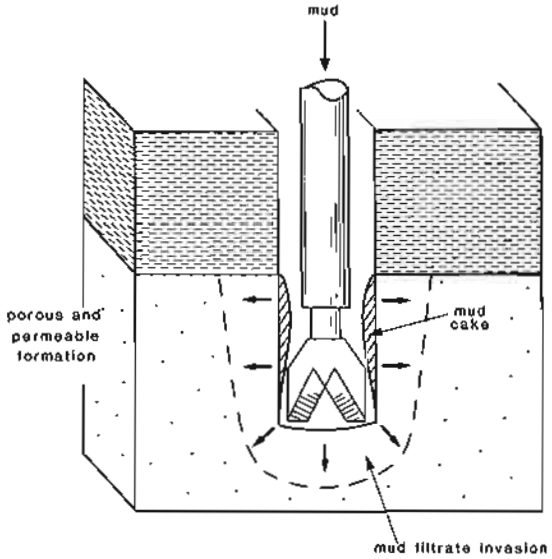


**Figure 2.5** Schematic representation of dynamic filtration as a bit enters a porous formation. Note the progressive mud-cake build-up.

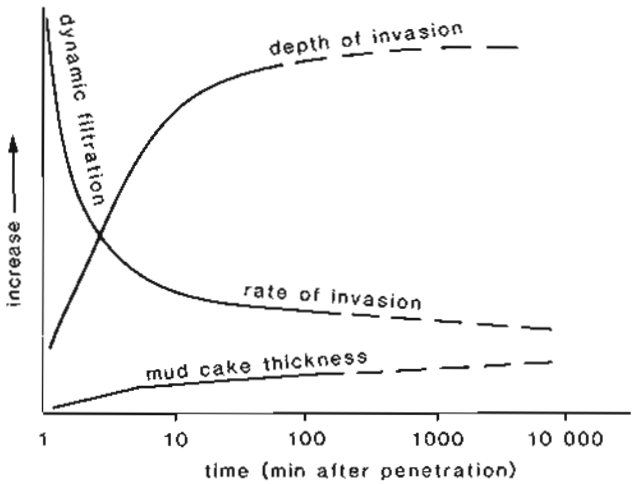


**Figure 2.6** Graphic representation (schematic) of invasion and mud-cake build-up as a porous formation is penetrated (modified from Dewan, 1983).

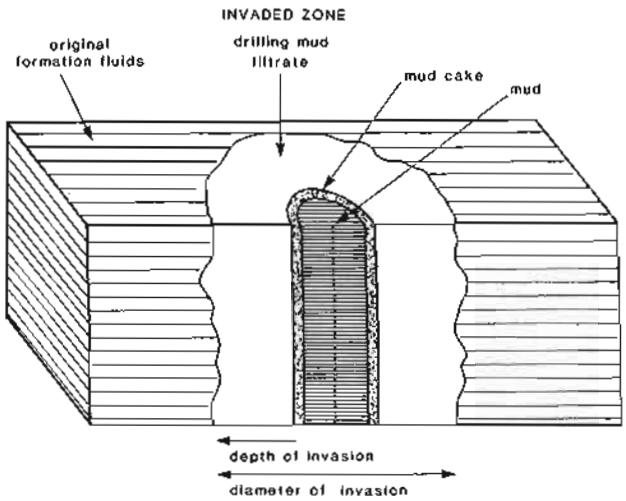


**Figure 2.7** Invasion: simple representation of the effect of drilling on fluids in a porous and permeable formation.

The phenomenon of the replacement of formation fluids by drilling mud filtrate is called *invasion*. Invasion affects porous and permeable formations in the immediate vicinity of a borehole. It is described by 'depth' or 'diameter' of invasion, that is the distance reached by the invading filtrate with respect to the borehole (Figure 2.7). In general, invasion is small in very porous and permeable formations, the mud cake building up rapidly to block dynamic filtration (Table 2.1). The contrary is the case in poorly permeable zones, vuggy carbonates or fractured formations, where mud cake formation is slow and invasion may be very deep, up to several metres.

Since excessive invasion is the worst-situation for logging and takes the real formation fluids too far away from the borehole to be detected, chemicals are added to the drilling mud to reduce water loss creating a protective mud cake as quickly as possible. Products such as lignosulphonates and starch are used.

**Table 2.1** Depth of invasion (distance from borehole wall) vs. porosity (approximate) from Miesch and Albright, 1967).

| Hole size (in) | 17½ | 12¼ | 8½ | |
|---|---|---|---|---|
| Porosity % | Depth of invasion | | | Ratio invasion diameter: hole diameter |
| 1-8 | 200.0cm | 140.0cm | 97.0cm | 10 |
| 8-20 | 90.0cm | 62.0cm | 43.0cm | 5 |
| 20-30 | 22.5cm | 15.5cm | 11.0cm | 2 |
| 30+ | ≃ 3.0cm | ≃ 2.0cm | ≃ 1.7cm | <2 |

## 2.3 Temperature environment of borehole logging

***Formation temperatures***

Normal sedimentary basins show a more or less regular increase in temperature with depth (Figure 2.8). The increase is not linear as frequently depicted; it varies according to lithology depending principally on the latter's thermal conductivity (*see* Figure 3.1). However, despite the irregularities there is an overall, persistent increase in temperature with depth (Figure 2.8). This increase is often expressed as a gradient, the geothermal gradient (the increase in temperature with depth). The metric values are usually °C per 100 m or °C per km.

Typical gradients for sedimentary basins are between 20°C per km and 35°C per km (*see* Chapter 3 and Table 3.2).

***Temperatures in boreholes***

Just as the geopressure regime is disturbed by drilling, so is the subsurface temperature. A well drilled into a subsurface formation introduces relatively cold mud and mud filtrate into a hot formation. While drilling continues

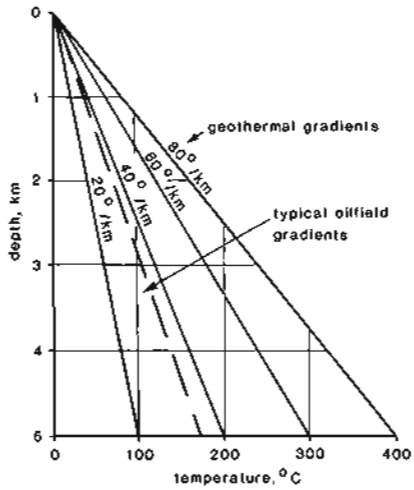


**Figure 2.8** Graph of geothermal gradients. The zone of typical oilfield gradients is indicated.

and mud is circulating, the formation is cooled slightly and the mud heated. But, the mud remains undisturbed in the borehole when circulation ceases and it gradually heats up to reach, or at least approach, the temperature of the surrounding formation. The two, however, are rarely in equilibrium. Logging temperatures taken in the mud are usually measured after only 5–10 hours of mud immobility: equilibrium is probably approached only after 5–10 days! (Temperature is considered at greater length in Chapter 3.)

Typical borehole tools are generally designed to withstand temperatures up to around 200°C (400°F): this gives a guide to maxima expected during drilling.

## 2.4 Logging tool capabilities

It was suggested earlier that logging tools should be able to sense the undisturbed formation and to make a true measurement of it. As indicated, the undisturbed formation environment is forced away from the borehole by drilling, to be replaced by the invaded zone. Logging tools are therefore designed either to 'by-pass' the invaded zone to reach the undisturbed formation, or to deliberately measure just the invaded zone itself. That is, they are designed with various capabilities of penetration, called the 'depth of investigation' (*see below*). Inevitably, such demands on tool design create secondary effects. Logging is comparable to photography with its close-up lenses and long-distance lenses. Close-up logging tools give great resolution but little depth of investigation: long-distance logging tools give great depth of investigation but blurred resolution.

Three inter-related phenomena of logging and logging tools are examined below; depth of investigation, minimum bed resolution and bed boundary definition. Geometry of investigation will also be briefly considered.

***Depth of investigation***

Most geophysical logs have an extremely shallow *depth of investigation*. By 'depth of investigation' we mean the

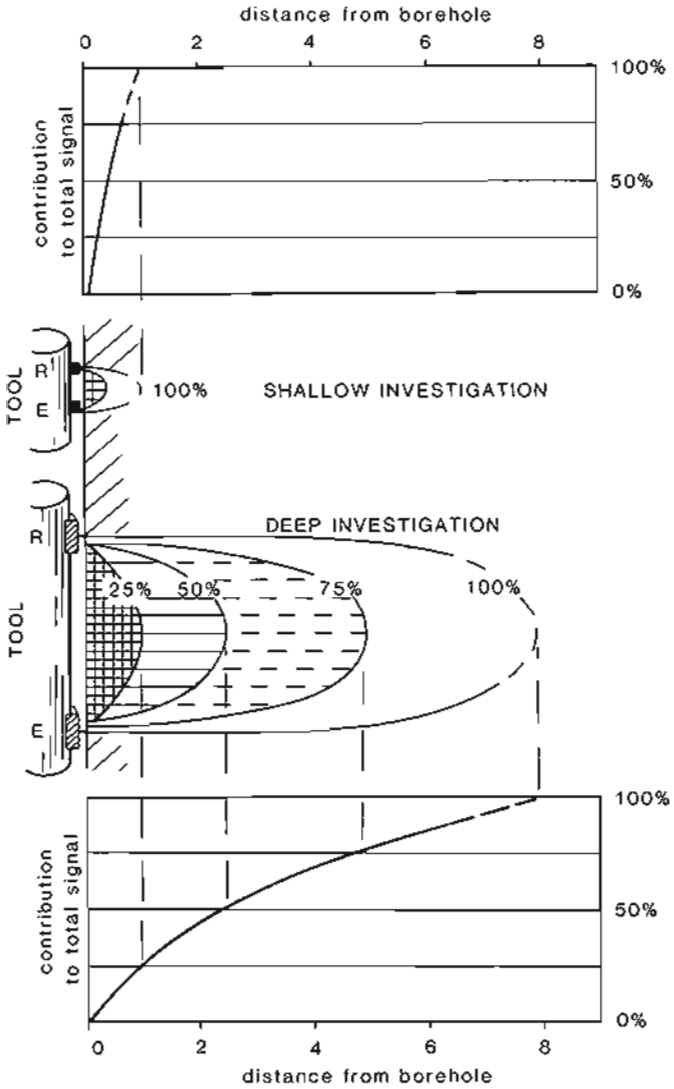


**Figure 2.9** Illustration of the notion of depth of investigation. Two tools are shown schematically, along with a graphic representation of formation contribution to their overall signal. E, emitter; R, receiver.

distance away from the borehole to which the formation is having an effect on a tool reading. So-called 'deep' investigation is only a matter of 2–5 m away from the borehole and into the formation. The environment of logging tools is therefore from the borehole itself (shallow investigation) to a distance of 5 m from the borehole wall (deep investigation).

In general, with tools that subject the formation to a bombarding signal (Table 1.1), the depth of investigation of the tool depends on the separation distance between the emitter and receiver. For example, with the resistivity tools (Chapter 6), when the emitting and receiving electrodes are very close, the depth of investigation is very small (Figure 2.9). The Micro-Inverse Resistivity Tool, with electrodes 2.54 cm (1 in) apart, has such a shallow depth of investigation that it reads only the resistivity of the mud cake (when present). Conversely, the Induction Conductivity Tool with emitter and receiver

**Table 2.2** Depth of investigation of the neutron tool (modified from Serra, 1979, after Schlumberger).

| **Porosity** (%) | **Depth* of Investigation** (cm) |
|---|---|
| 0 | 60.0 |
| 10 | 34.0 |
| 20 | 23.0 |
| 30 | 16.5 |

*90% of the signal

1 m (40 in) apart, has a depth of investigation which may reach about 5 m. The Induction Tool is considered to be the most likely to give the resistivity (in fact, conductivity) of the untouched formation ($R_t$).

The emitter-receiver separation is not the only factor affecting depth of investigation. Necessarily it varies with the character being measured. Thus for the sonic tools which measure the speed of sound waves in the formation, the waves take the quickest path from emitter to receiver: this is generally along the borehole wall (Chapter 8). For nuclear tools, the emitter-receiver separation is fixed as a function of the average penetration of gamma rays, neutrons, etc., the field being more or less spherical around the emitter. These characteristics are considered in general below (geometry of investigation) and in more detail when each tool is described.

Finally, depth of investigation also depends on the formation, whether it is susceptible to penetration or not. In the case of the neutron tools, for example, a non-porous bed is 'seen' to a far greater depth than a porous bed, due to variations in the absorbency of the signal (Table 2.2).

In reality, depth of investigation is a very difficult term to fully understand. It is not precise; a bed is not investigated to a particular point and no further. It is a progressive character, like the radiant heat from a fire. We feel the heat near to the fire, but not at some distance away. Can we say exactly at what distance the fire has no more effect?

With logging tools, the depth of investigation is more realistically defined as the zone from which *x%* of the tool reading is derived (Figure 2.9). For instance, the neutron tool figures given above (Table 2.2) are defined on 90% of the tool signal. This is called the *geometric factor*, and the principle is true for all tools.

### *Minimum bed resolution*

*Minimum bed resolution* and depth of investigation are intimately related. A tool is only capable of making a true measurement of a bed if the bed is thicker than the emitter-receiver distance of the tool (Figure 2.10). Thus, a tool with an emitter-receiver distance of 2.54 cm (1 in) can resolve beds down to about 10 cm, providing some idea of their true resistivity. An induction log with an emitter to receiver distance of 1 m (40 in) can resolve beds to give true tool resistivities only down to 1.2 m, and then only under ideal conditions.

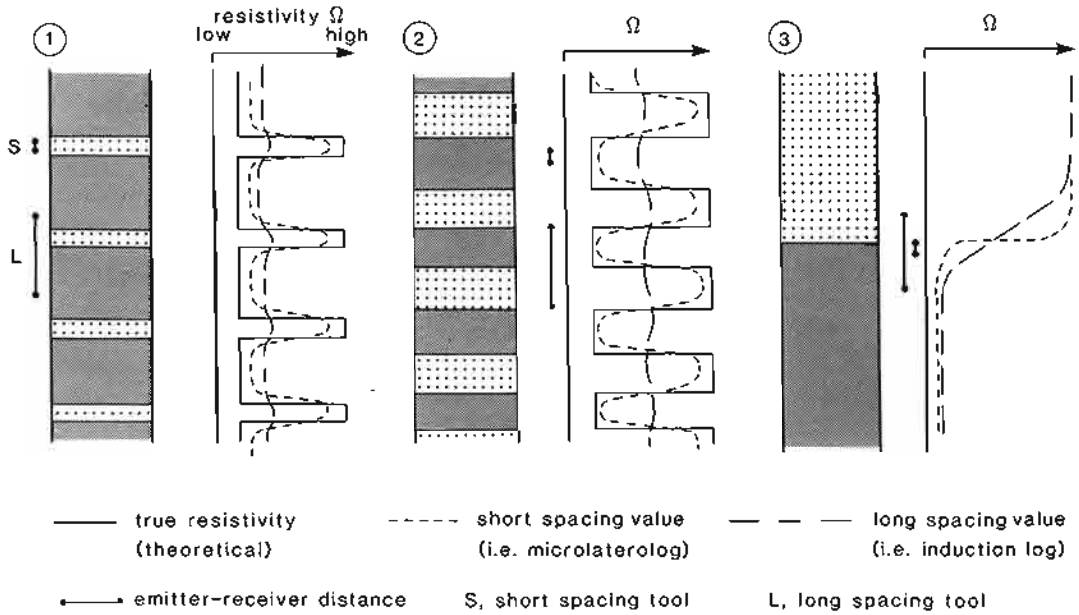


**Figure 2.10** The effect of minimum bed resolution on logging-tool values in various scales of interbedding. (1) Fine interbeds; (2) coarse interbedding; (3) single bed boundary (schematic).

Table 2.3 shows some common tools, their emitter-to-receiver spacings and minimum bed resolution for true values under the best conditions.

A bed which is much thinner than a tool's emitter-to-receiver distance may still be identifiable. However, the value indicated on the log for this bed will only be a percentage of the real reading it should give. The tool takes a global measurement of the formation between the emitter and the receiver, the thin bed forming only a small percentage of this (Figure 2.10, *1*). The value on the log will depend on the percentage contribution that this thin bed makes to the global measurement. An induction log opposite a thin, resistive, limestone bed in a shale sequence will show a subdued 'blip'. On a microlog this becomes a fully developed peak (Figure 2.10, *1*). In reality, where lithologies vary rapidly and individual beds are thin, it is only average values that appear on the log, especially the logs derived from long spacing tools. The averaged value will tend to approach that of the dominant lithology. When the mixture is 50/50, logs will even give a constant value, but it will be somewhere between the two 'real' values (Figure 2.10, 2) (*see* Hartmann, 1975).

**Table 2.3** Minimum bed resolution of some common tools under best conditions (modified from Hartmann, 1975).

| | **Emitter-to-receiver spacing** | | **Minimum bed resolution for 'true' values*** |
|---|---|---|---|
| **Tool** | (in) | (cm) | (cm) |
| Microlog | 1-2 | 2.5 5.0 | 15.0 |
| Microlaterolog proximity | 1 | 2.5 | 10.0 |
| SFL | 12 | 30.5 | 30.0 |
| Laterolog 3 | 12 | 30.5 | 60.0 |
| Laterlog 8 | 14 | 35.6 | 60.0 |
| Sonic | 24 | 60.0 | 60.0 |
| Density | 18 | 46.6 | 60.0 |
| SNP-CNL | 19 | 48.0 | 60.0 |
| Laterlog 7 | 32 | 81.0 | 75.0 |
| Laterlog S | 32 | 81.0 | 75.0 |
| Laterlog D | 32 | 81.0 | 75.0 |
| GR | | | 90.0 |
| Induction M | | | |
| Induction D | 40 | 100.0 | 120.0 |

*For 'true' log reading

Equating bed resolution to emitter-to-receiver spacing, as in the previous paragraphs, is not always correct. For the resistivity logs it is generally true, but for the nuclear logs especially, the concept may be misleading. Rather than use tool design, an alternative is to use a tool's performance in laboratory conditions. In this context, tool *vertical resolution* may be examined. Vertical resolution is defined as: *the full width, at half maximum, of the response to the measurement of an infinitesimally short event* (Theys, 1991). This definition is shown graphically (Figure 2.11) and some values based on it for some common tools are shown in the table (Table 2.4). These can be compared to the bed resolution table (Table 2.3): differences are obvious.

The differences between the tables (Tables 2.3 and 2.4) show how difficult it is to define consistently what a tool is capable of resolving. A single tool, in fact, has variable resolution. A thin, very dense bed in a low density formation will be better resolved by a density tool than a similar thin bed of low density in a high density formation. A resistivity tool can resolve thin beds in the salt water leg of a reservoir that it cannot detect effectively at high background resistivities in the hydrocarbon leg of the reservoir. The laboratory definition of vertical resolution

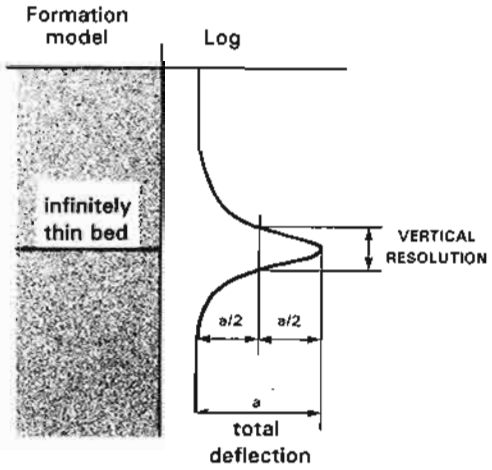


**Figure 2.11** Graphical representation of the theoretical definition of tool vertical resolution (re-drawn, modified, from Theys, 1991).

can therefore be hard to apply in many field situations. It is obvious that tools have different bed resolution, but being precise about it is very difficult. From a geological point of view, rather than be precise, it is probably more useful to indicate qualitatively the expected capabilities of the tools in relation to typical sedimentary and structural features (Figure 2.12). This enables the correct tool to be selected for identifying particular features. It is the qualitative indications that become clear, for example, when logs and cores are compared.

**Table 2.4** *Vertical resolution of some logging tools (from Theys, 1991).
*see Figure 2.11

| Logging tool measurement | Vertical Resolution inches | cm |
|---|---|---|
| FMS/FMI (individual electrodes) | 0.2" | 0.5cm |
| SHDT dipmeter curves | 0.4" | 1.0cm |
| HDT dipmeter curves | 0.5" | 1.3cm |
| Microlog | 2"-4" | 5cm-10cm |
| Micro Spherically Focused Resistivity | 2"-3" | 5cm-7.6cm |
| Phasor Induction SFL: | | |
| deep | 84"-96" (7'-8') | 2.0m |
| medium | 60"-72" (5'-6') | 1.5m |
| Spherically Focused Resistivity | 30" (2'6") | 76cm |
| Laterolog | 24" (2') | 61cm |
| Litho-Density tool | 15" (1'3") | 38cm |
| Litho-Density Pef | 2" | 5cm |
| Compensation Neutron tool | 15" (1'3") | 38cm |
| Gamma ray | 8"-12" | 20cm-31cm |
| Array sonic: | | |
| standard mode | 48" (4') | 1.2m |
| six inch mode | 6" | 15cm |
| Borehole Compensated Sonic | 24" (2') | 61cm |

***Bed boundary definition***

A bed, in geology, is generally thought of as a distinctive, planar unit (lithology, composition, facies etc.), limited by significant differences (in lithology, composition, facies etc.). The limits tend to be abrupt. On well logs, sharp boundaries are inevitably seen as gradations. The way in which a sharp boundary is seen on the logs, termed *bed boundary definition*, is influenced by several effects, the principal being the tool's vertical resolution (as defined above). The effects of logging speed and sensor size will also be examined.

The principal influence on bed boundary definition, a tool's vertical resolution, has been discussed above in terms of depth of investigation and bed resolution.

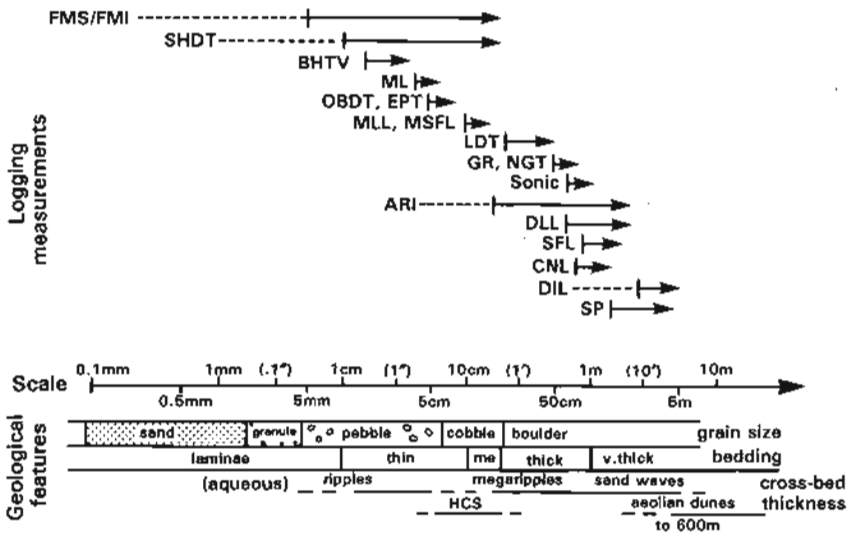


**Figure 2.12** Qualitative indications of (Schlumberger) logging tool resolutions compared to the geological features of grain size, bedding thickness and typical sedimentary structure, cross-bed thickness. Dashed line = higher sensitivity than resolution (tool resolution from Serra *et al*, 1993). For tool mnemonics *see* Appendix.

However, vertical resolution characteristics also influence tool response at any sharp bed boundary. A tool with a large vertical resolution will show a very gradual response, even at a sharp boundary, while a tool with a small vertical resolution will show a much more rapid response (Figure 2.10, *3*). If, for example, a tool has a vertical resolution of 2 m, then over a minimum of 1 m (Figure 2.11), the signals from the bed above and from the bed below will be totally mixed. This will produce a progressive response over 1 m, typically called a *shoulder effect*, a name which covers the special, sometimes predictable tool effects at sharp surfaces between different beds (i.e. lithologies). In the present example, over the 1m of log which shows shoulder effects, the contributions of the two lithologies are being mixed in constantly varying proportions, the actual log values being more indicative of the tool position relative to the bed boundary, than to the values of the beds themselves. These shoulder effects are obviously much reduced in vertical thickness in tools with small vertical resolution: in these, bed boundary definition is good (Figure 2.10, *3*).

Another influence on bed boundary definition, that of logging speed, is well illustrated using the gamma ray log. This is because the tool actually 'counts' discrete events, namely gamma rays. In practice, the tool counts the gamma rays during a certain time period called a time constant, which may be for example, four seconds, so that the tool converts the counts made over four seconds into a log value. By experience, for the gamma ray tool, no more than 30 cm of formation should be logged during one time constant, giving a maximum logging speed, using a four second count, of 270 m/hr (Chapter 7, Table 7.5). A tool travelling too fast will sample, for example, 1m of formation during the four second time constant (i.e. logging at 900 m/hr). In this case the count will come from the entire 1 m of formation travelled in the time constant. Over a sharp bed boundary, some of the count will be from the bed below and some from the bed above, so that the actual limit will be diffuse. The count obtained in the diffuse zone gives no indication of real formation values.

The illustration of this effect (Figure 2.13) shows the changing shape of a gamma ray curve, opposite a sharply defined bed, as logging speed is increased. At a properly selected logging speed and time constant (log 1, Figure 2.13), the log gives a reasonable resolution of the bed boundaries and the shoulder effects are moderate, about 25 cm either side of the sharp bed boundaries (for the example). Within the bed, true bed values are observed. When the logging speed is increased, the bed appears to be located higher than the reality and the shoulder effects are significantly increased, albeit asymmetrically (log 2, Figure 2.13). At higher speeds still, the bed appears to be located even higher than is the case and true bed values are not reached, the true bed response being saturated by the even greater, asymmetric shoulder effects (log 3, Figure 2.13).

For the gamma ray, the averaging effects of a moving

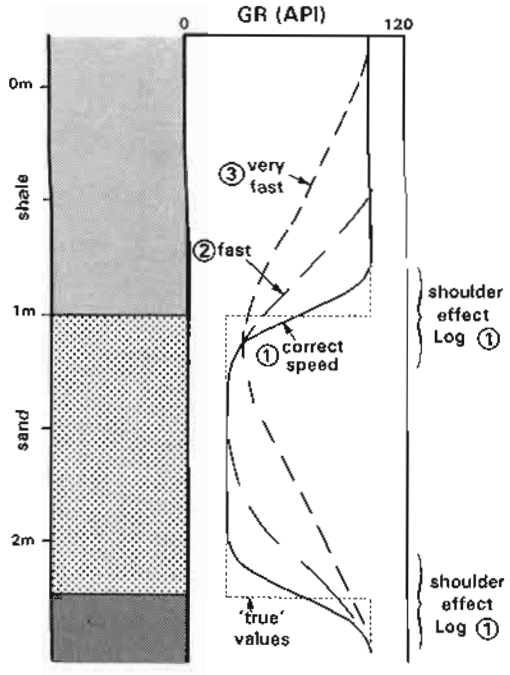


**Figure 2.13** The effect of logging speed on the bed boundary definition of a gamma ray log (modified from Dewan 1983).

tool are compounded by another aspect of boundary resolution, that of sensor size. A log sample is seldom a point: sensors have their own volume. For example, a gamma ray sensor with a window 3 cm long in the direction of the tool axis, will receive radiations from a formation volume with a radius of 30 cm around the sensor (Desbrandes, 1968). At bed boundaries, the radiations detected will be coming from both beds simultaneously. Even at very low logging speeds, a gamma ray tool will still detect a sharp boundary as a gradual change because of sensor size.

Log interpretation always requires bed boundaries to be drawn. From the discussions above it is clear that placing a precise boundary involves interpretation: there are a number of possible positions. There is a general tendency to assume that the boundary is at the point of maximum change of value or maximum slope. This may not represent the reality but is a good guide and is consistent (this is discussed further in Chapter 11, Section 11.4).

In an effort to deal scientifically with the bed boundary problem, logs may be squared or blocked by computer. That is, the computer is programmed to eliminate the shoulder effects which occur on the logs between beds of differing values. Log curves are resolved into zones of constant value, separated by horizontal 'boundaries': they become more 'bed-like' in appearance (Figure 2.14). The usual method requires the squared log to be a true reflection of the raw log, but with transition zones or ramps eliminated. The exercise is one of reassignment of the transition zone values to pre-designated blocks of real, non-transition values (Griffiths, 1982) (Figure 2.14). The algorithm applied assumes that the original log values are adequate.

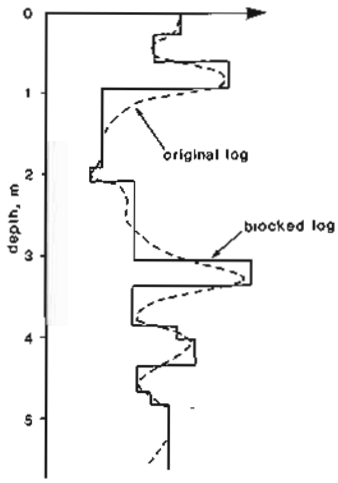


**Figure 2.14** The effect of blocking on log data. Note the reallocation of 'transition' values.

The method can be applied to several logs simultaneously so that they all become perfectly comparable (Serra and Abott, 1980) and the problems of comparing logs of differing depths of investigation and bed-resolving capabilities are eliminated.

A more complex method (Kerzner and Frost, 1984) does not assume that the raw log values are adequate, and tries to compensate for assumed tool deficiencies. For instance, it is well known that the SP will only reach its full value and real deflection in very thick beds (Chapter 5). The more complex blocking method tries to approach this full value from the raw log values using the known tool limitations.

The squaring of logs certainly gives a nearer approach to real formation values and formation aspects and can be a great aid to geological interpretation. Additionally, with the increasing use of logs on the computer, squaring is essential to bring all logs to comparable sensitivities so as to allow valid comparisons and cross-plotting: this is not always done.

***Geometry of investigation***

It would be natural to assume that a tool generally investigates a spherical volume of formation. However, this is rarely the case. There are two reasons; tool design and formation interaction.

Tool design and tool type are very variable, each tool having a characteristic volume of investigation. Through the book, in the chapters where each tool is described, these characteristics will be discussed for the tool in question. In this section it will simply be pointed out that these differences in investigating characteristics exist (Figure 2.15). There is an inherent difference between the volumes investigated by resistivity logs, acoustic logs and by nuclear logs because of the geophysical differences in the measurements. The behaviour of an ion in a formation is quite different from the behaviour of a gamma ray.

When the volume of investigation of a tool is measured in the laboratory, it is generally for a pure, homogeneous

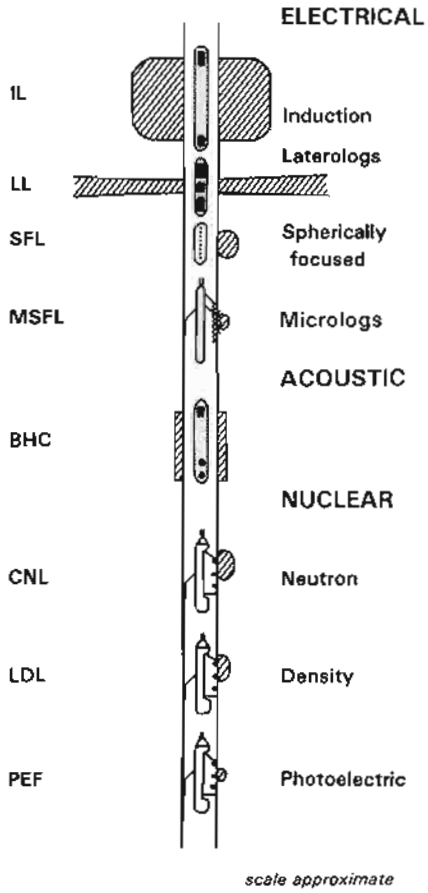


**Figure 2.15** Investigation geometry of various logging tools (modified from Desbrandes, 1968 and Serra, 1979).

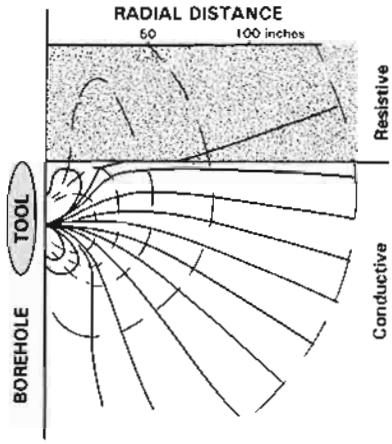


**Figure 2.16** Formation influence on electrical tool response (SFL) at a resistive to conductive bed boundary (from Anderson and Chew, 1985).

medium. The formation influence is consistent and predictable. In the subsurface, unfortunately, it is neither. This was touched upon when depth of investigation was considered previously, the neutron tool being shown to have a greater depth of investigation in the absence of porosity, the volume of investigation therefore varying with porosity (Table 2.2). In other words, formation response is dynamic rather than passive and especially

complex in the presence of heterogeneities and often unpredictable. For example, for the resistivity logs, when a resistive bed and a conductive bed are in contact, the conductive bed tends to act as a sink for the electrical current which flows preferentially into it. Current fields around the boundary are distorted and the precise tool response difficult to define (Figure 2.16).

These effects will be discussed more fully in the chapters describing the individual tools.

## 2.5 Borehole depth measurement

All log measurements are recorded against depth: it is the fundamental measurement. Generally depth is assumed to be accurate and it is a surprise to find that it is not. But like any measurement, borehole log depth has limits of accuracy.

In boreholes, two sets of independent depth measurement exist side by side; '*loggers depth*' and '*drillers depth*'. Driller's depth, considered to be the least accurate, is constructed by measuring with a tape measure the lengths or stands of drill pipe as they are run into the hole and simply adding up the lengths. Corrections are seldom applied to these measurements and human error not unusual. Lengths of drill-pipe are easily 'forgotten'. Logger's depth, generally the more accurate, is measured with the wireline cable. There are two ways, by using magnetic markers on the cable and by direct measurement with an odometer. The direct measurement generally supplies the primary depth. The two wireline measurement methods are briefly described.

Magnetic markers are placed on a cable by the logging company every 100 feet or 25 m, under a standard tension of 1000 lbs. The system is reasonably accurate (error 1 part in 5000; Søllie and Rodgers, 1994). During logging, the marks are detected at surface as the cable is spooled (in or out). Because of tension, the real depth between the marks will change as the cable length increases. These differences are corrected for, generally by using charts which account for tension and temperature effects. These may work in opposing directions, tension extending the cable, temperature and mud pressure causing it to contract, so that for accurate corrections, all effects should be considered.

The direct measurement of depth is made by measuring wheels which turn as the cable is spooled in or out. The equipment consists of two wheels, tangential to the cable, which turn in opposite directions, each wheel supplying a separate depth measurement. This measurement is considered very accurate but it too must be corrected. This is done by comparing the running-in depth to the pulling-out depth and correcting for the stretch due to the friction induced tension difference between running-in and pulling-out (Søllie and Rodgers, 1994). For Schlumberger, the primary depth measurement is from their IDW (Integrated Dual Wheel spooler) (Theys, 1991). The influences on the accuracy of the direct measurement method are shown in the table (Table 2.5).

**Table 2.5** *Factors affecting wireline depth measurements. *figures for heptacable at 3000m (from Theys, 1991 and Søllie and Rodgers, 1994).

| Factor | Potential error (metres) | Remarks |
|---|---|---|
| Elastic stretch | 3.0m | incudes cable twisting |
| Inelastic stretch | 2.0m | first runs only |
| Temperature | -1.5m | temperature change from ref. |
| Mud radial pressure | -0.75m | |
| Measuring wheels (a) | 1-3m | more recent wheels |
| (b) | 1.5-3m | previous wheels |
| Surface set-up changes | 1.0m | cable sag, sheave movement |
| Tidal effects | ± 1.5m | offshore (North Sea) |
| Zeroing | -0.25m | not if zero in mud |
| Tool sticking | up to 12m | |
| Yoyo | 0.6m | |

In practice, the depth in any single well is tied to a particular log, often the density. If there is a depth mismatch, the other logs can be shifted to match the 'master log'. Problems in a single well only come when very detailed, centimetre scale calibration is necessary between, for example, core and an image log (Chapter 13). When such calibrations are attempted, it is clear that at this level cable stretch has a significant effect (*see* Chapter 13). These are relative depth problems, that is between one log and another or between log and core.

Absolute depth problems clearly also exist. These become important when comparing two wells or, more importantly, comparing depth sensitive measurements such as fluid pressures and hydrocarbon contacts in different wells. Differences of up to 6 m are reported using fluid contacts as absolute, horizontal markers (Søllie and Rodgers, 1994).

As logging tools become capable of more and more detailed geophysical measurements, a very accurate measurement of depth is becoming an absolute necessity.

## 2.6 Conclusion

It is suggested in this chapter that, for a proper interpretation, a logging tool is required to make a true, repeatable geophysical measurement of a formation. This was shown in fact to be impossible because of drill-created disturbances (invasion), and because of the logging method itself. However, with a knowledge of typical formation behaviour, typical tool capabilities, log characteristics and depth accuracies, it is possible, using the right methodology, to reconstruct the specific formation characteristics being shown on the log.

A projection of this approach will be used in the following chapters. Each type of individual open-hole log will be considered and described in terms of the corresponding logging tool's capabilities, log characteristics, their significance in terms of the real formation and interpretation in common geological terms – in short, the geological interpretation of the individual well logs.

# 3
# TEMPERATURE LOGGING

A knowledge of borehole temperatures is important. It is required for accurate log evaluation and is effective in the detection of fluid movement and subsurface pressures. Also, with the development of geochemical modelling and more precise quantitative geochemistry, a knowledge of geotemperature is a pre-requisite for geothermal and source maturity studies.

## 3.1 Geotemperatures

The temperature of the earth usually increases with depth, and, as a result, we can conclude that thermal energy flows from the earth's interior to the surface. A well drilled into the earth, therefore, shows a persistent rise in temperature with depth. This persistent rise is usually expressed in terms of a temperature gradient, that is in °C increase per kilometre of depth (*F*/100 ft) as has been discussed previously (Chapter 2 and Figure 2.8).

$$\text{Geothermal gradient, } G = \frac{T^\circ_{\text{formation}} - T^\circ_{\text{surface}}}{\text{Depth}}$$

where $T^\circ_{\text{formation}}$ = formation temperature;
$T^\circ_{\text{surface}}$ = average, mean, surface (or sea bottom) temperature (i.e. -5°C permafrost; +5°C cold zones; 15°C temperate zones; 25°C tropical zones)

Thus, for a well in a temperate zone ($T_s$ = 15°C) which has a maximum bottom hole temperature (BHT) of 80°C at 3000 m, the geothermal gradient is

$$G = \frac{80 - 15}{3} = 21.6^\circ\text{C/km (or } 2.16^\circ\text{C/100m)}$$

This is an average gradient and assumes a linear increase in temperature with depth. This is true in a homogeneous medium. However, in detail, the geothermal gradient depends on a formation's thermal conductivity (the efficiency with which that formation transmits heat or, in the case of the earth, permits heat loss). Shale, like a blanket, is inefficient; it keeps heat in and has a low thermal conductivity. Salt, conversely is very efficient, lets heat escape rapidly and therefore has a high thermal conductivity. Table 3.1 gives some ranges of thermal conductivities for typical lithologies.

When a rock with high thermal conductivity is encountered, it will show a low thermal gradient. That is, the rate of temperature increase (or rather decrease upwards if we think in terms of cooling) will be low. In shales, where the passage of heat is slow, the gradient will be higher. In other words a blanket of shale would keep us warm at night while a blanket of salt would not! Thus, the real temperature gradient in a well is not a straight line but a series of gradients related to the thermal conductivities of the various strata, the gradient varying inversely to the thermal conductivity (Figure 3.1).

**Table 3.1** Ranges of thermal conductivity values for some typical lithologies (from Serra, 1979 and Gearhart, 1983).

| Rock type | Thermal conductivities (CGS × $10^3$) | |
|---|---|---|
| Coal, lignite | 0.33-1 | poor conductivity |
| Shale | 2-4 | |
| Chalk | 2-3 | |
| Porous limestone | 2.4-5 | |
| Compact limestone | 5-8 | |
| Sand | 3-12.2 | good conductivity |
| Salt | 3-15(14.3) | |
| Basalt | 4-7 | |
| Granite | 5-8.4 | |

In oilfields, temperature gradients vary from the extremes of 0.05°C/km (0.3°F/100ft) to 85°C/km (4.7°F/100ft) although typical figures are 20°–35°C/km (Table 3.2, Figure 3.2).

Variations in thermal gradient are not just a result of different thermal conductivities, they are also a result of differences in heat flow, or the amount of heat that enters the strata from the earth's interior and flows out again. Thermal gradient, because of variations in thermal conductivity, varies independently of heat flow. The actual temperature in a well, therefore, depends not only on lithology but also on the heat-flow value for the area.

Notions of temperature variations with depth and with position in a basin may be expressed in map form, using contours of equal geothermal gradients (Figure 3.2). The temperature differences in a basin may also be expressed by isotherms (lines of constant temperature) plotted for a constant depth or, conversely, lines of depth for a constant temperature. Isotherms may also be used on geological sections (Figure 3.3).

## 3.2 Borehole temperature measurement

Every individual logging run should be accompanied by a reading of at least the maximum temperature in

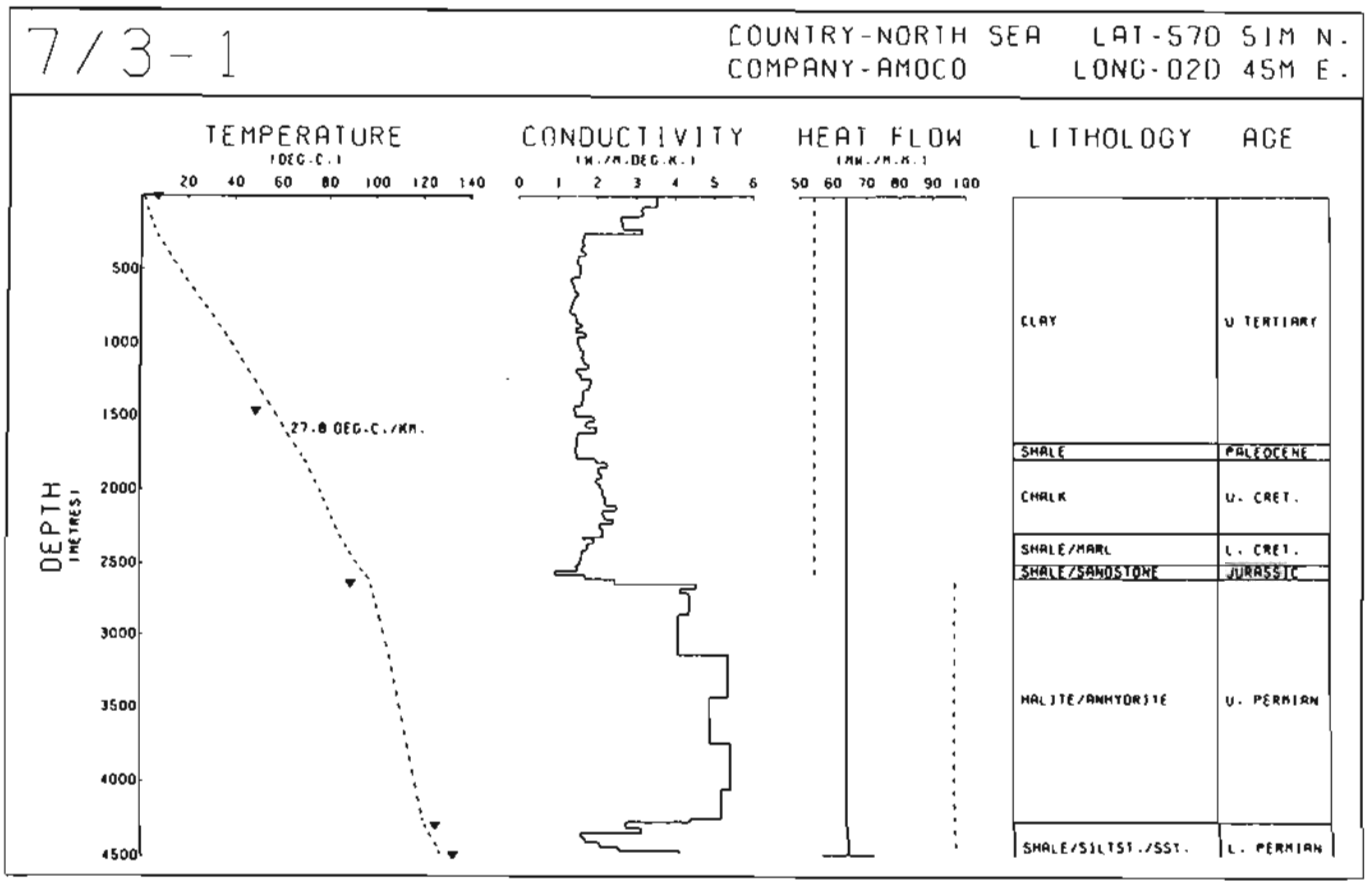


**Figure 3.1** Temperature gradient, thermal conductivity and heat flow compared in North Sea well 7/3-1. Lithology and age are indicated. (From Evans, 1977).

**Table 3.2** Some typical geothermal gradients in sedimentary basins.

| | Gradient | |
|---|---|---|
| | °C/km | °F/100ft |
| Rhine Valley | 66 | 3.6 |
| Red Sea | 45 | 2.5 |
| Central Ruhr basin | 40 | 2.2 |
| Madagascar | 38 | 2.1 |
| Western Canada, Alberta* | 31.8 | 1.8 |
| Mississippi (typical)* | 29 | 1.6 |
| Louisiana (typical)* | 24 | 1.3 |
| Eastern Canada* | 22 | 1.2 |

*typical oil regions

the borehole. Up until the mid 1980s, bottom hole temperature (BHT) was most commonly measured by strapping to the tool, usually three, pressure resistant, maximum thermometers. The three temperatures (maxima) were noted on the log-head, and an average or the most reliable temperature used as the bottom hole temperature (BHT). Although this habit is still generally continued, in every tool string (at least from Schlumberger), a small, special sonde is included which measures temperature continuously along with mud resistivity and cable tension. With this sonde (AMS), a continuous temperature may be read either going into the hole or coming out.

When more detail is needed, a special thermometer tool may be used to give continuous temperature readings. The tool uses a thermistor, or metal whose resistance is sensitive to temperature changes, fitted into the circuit of a Wheatstone bridge. Typically the tool will give not just the absolute temperature but also, using two separate thermistors, a temperature differential. Such is the case, for instance, in the Temperature Survey of Atlas Wireline (Figure 3.4).

The absolute accuracy of temperature logs is generally not good and is in the region of ±2.5°C (±5°F), although the resolution is good, around 0.025°C (0.05°F) (Hill, 1990).

## 3.3 True formation temperatures (BHT corrections)

The temperature measured in boreholes is not the formation temperature, it is the temperature of the mud in the borehole. Borehole mud is cooler than the formations being drilled (apart from the immediate surface strata). Thus, the invasion of mud filtrate into a formation will cool it down immediately by convection. As a result of the infinite mass around the borehole, the true formation

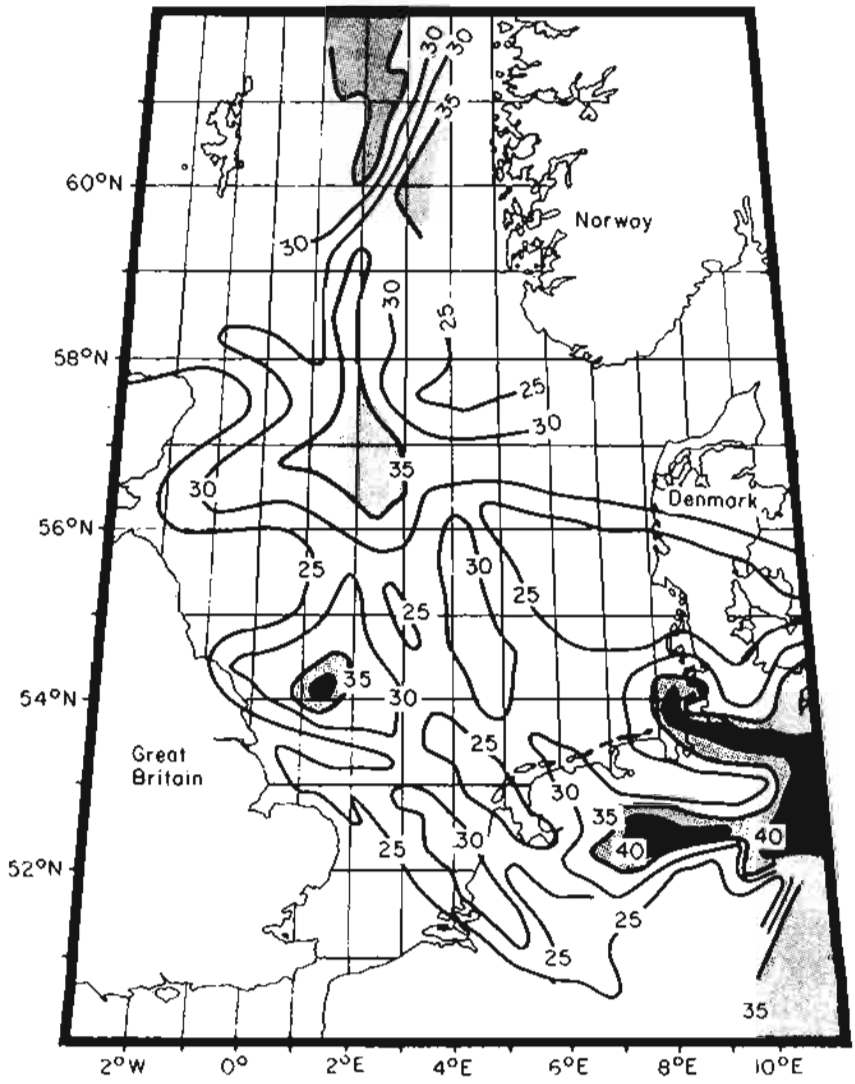


**Figure 3.2** Present-day North Sea geothermal gradients. (After Cornelius, 1975; Carstens and Finstad, 1981; Harper, 1971). Taken from Cornford (1984).

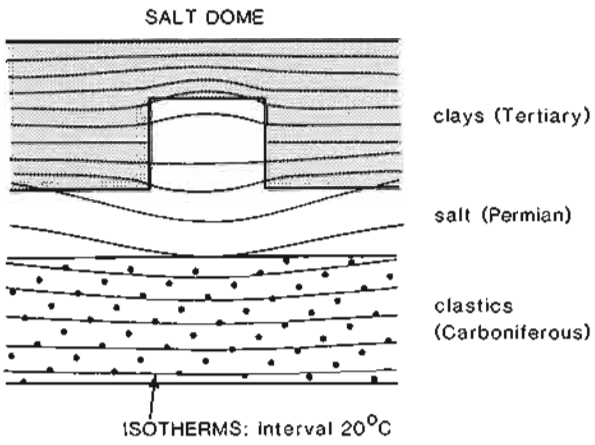


**Figure 3.3** The theoretical distribution of isotherms around a salt dome indicated on a geological section: change in gradient is shown by isotherm spacing. (Redrawn from Evans, 1977).

temperature will be that at the eventual equilibrium: the mud and filtrate will be heated up to formation temperature. This process can begin only when mud circulation stops. Moreover, the process occurs through conduction and is very slow. Examination of several temperature logging runs made at increasing time intervals after drilling shows that equilibrium may be established only after months (Figure 3.5). Temperatures taken in boreholes during drilling (as is usually the case) are therefore consistently well below the real formation temperature.

To correct BHT values, numerous methods have been devised (cf. Hermanrud and Shen, 1989). The modern tendency is to model the thermal recovery of a well from the available data but a generally accepted way of doing this does not exist and the results from presently available methods show considerable variation (Hermanrud and Shen, 1989). One of the older and still frequently applied methods uses the Horner plot (Fertl and Timko, 1972). This method appears to be about as accurate as the modelling methods.

The Horner plot method relies on the concept of a straight-line relationship between BHT and the log of $\Delta t/\Delta t + t$, where $\Delta t$ = time in hours since circulation

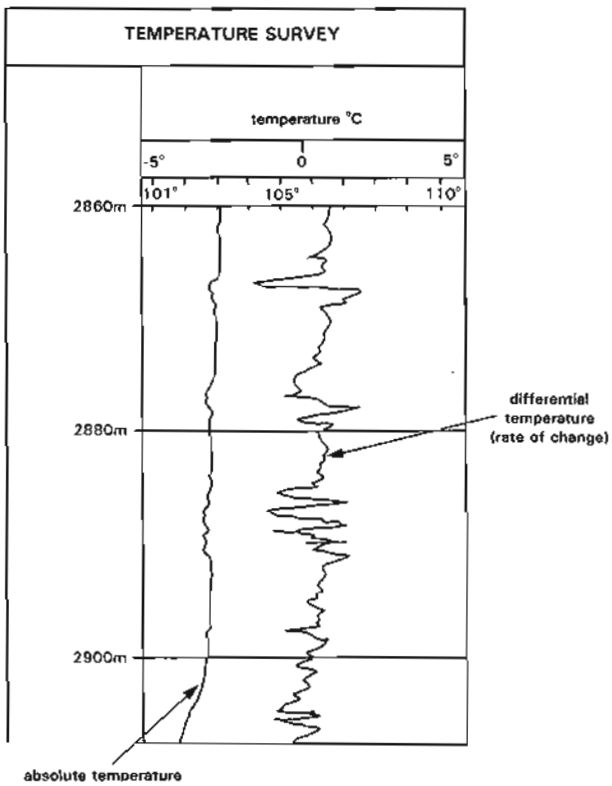


**Figure 3.4** Presentation of the detailed borehole temperature survey. A temperature gradient of absolute values is recorded alongside temperature changes or differential temperature. The log should be recorded going into the hole.

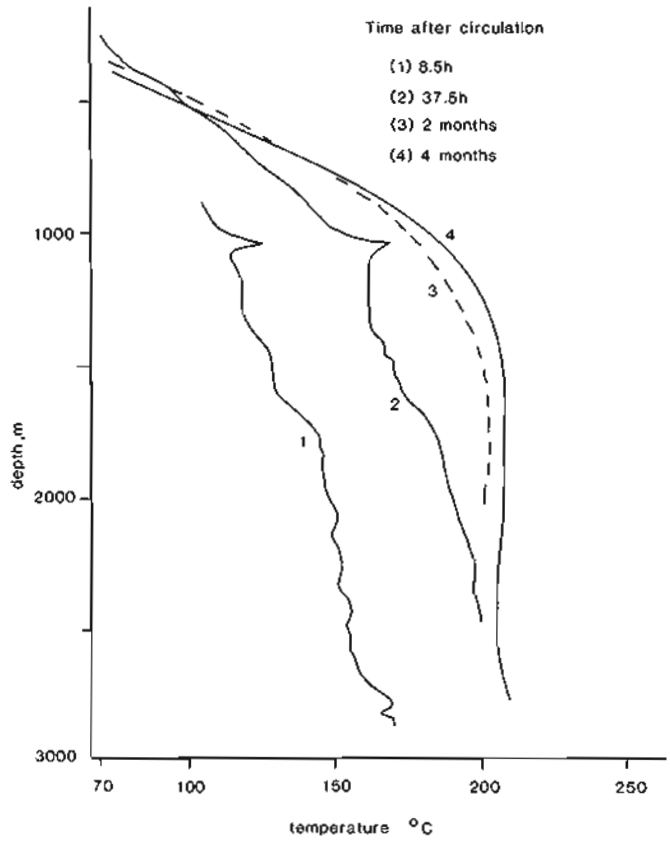


**Figure 3.5** Change in borehole temperature with time (in a geothermal well). Equilibrium is only being re-established 4 months after circulation (i.e. drilling) stopped. (Redrawn from Benoit *et al.*, 1980).

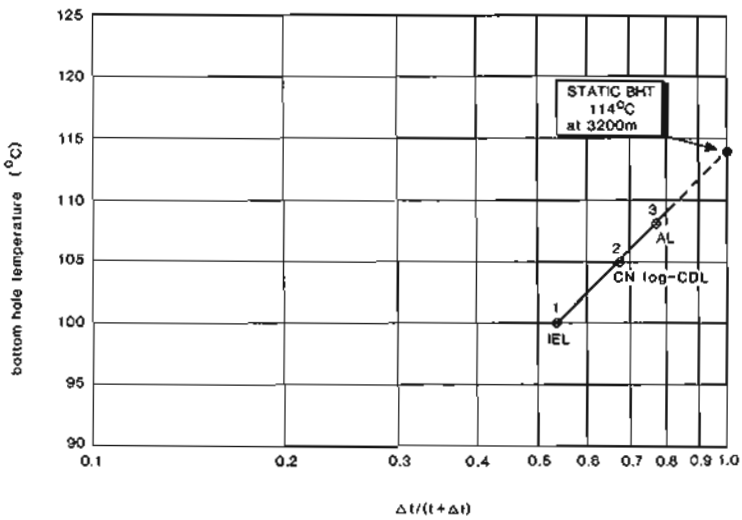


**Figure 3.6** Bottom hole temperature correction example.
$\Delta t$, time since circulation stopped (hours); $t$, circulation time (6 hours).

| Log | $\Delta t$ | Temperature recorded | $\Delta t/(t + \Delta t)$ |
|---|---|---|---|
| IEL | 7 | 100°C | $7/(6 + 7) = 0.538$ |
| CN-CDL | 11.5 | 105°C | $11.5/(6 + 11.5) = 0.671$ |
| AL | 19.5 | 108°C | $19.5/(6 + 19.5) = 0.765$ |

(From Fertl and Wichmann, 1977).

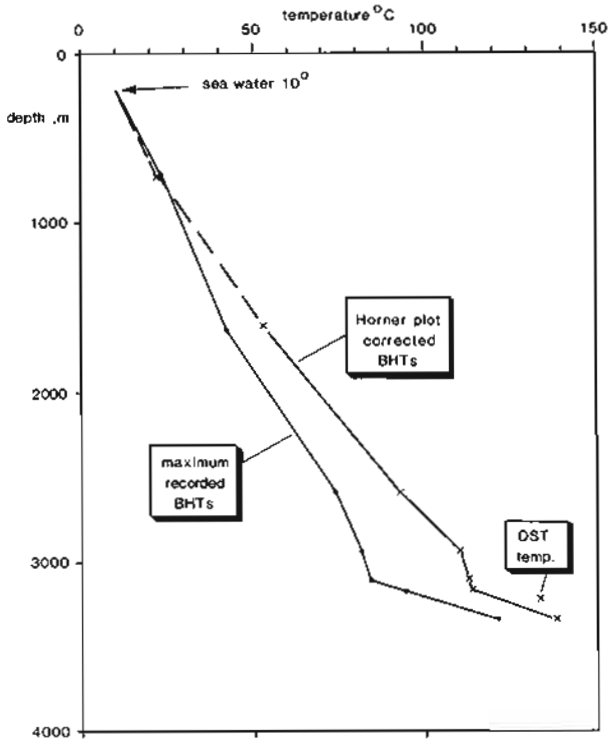


**Figure 3.7** Effect of correcting recorded temperature by the Horner plot method. The correction is negative at surface (cold surface temperature) but requires up to 30°C increase at 3000m. The Drill Stem Test (DST) temperature at 3200m is considered to be a good measure of formation temperature. (From stabilized build-up).

stopped, and $t$ = time of circulation at TD before logging (Figure 3.6). $\Delta t$ then represents the time available for an equilibrium temperature to be reached, while $t$ represents the time that the formation is exposed to cooling mud. In practice it is best to take $t$ as the time needed to drill the last metre of hole plus the circulating time at TD (Serra, 1979). Since a BHT is taken on each tool descent, several temperature readings are available at different times after circulation stopped ($\Delta t$). The true formation temperature is on the line through these points where it crosses the abscissa at 1 (Figure 3.6). This form of correction has a significant effect on measured temperatures and appears to make them more meaningful (Figure 3.7).

## 3.4 Temperature log uses

### Using BHT Measurements only

***Environmental correction***

Logging tool sensors and logging tool results are frequently sensitive to temperature. Nuclear tool detectors, for example, only operate effectively over certain temperature ranges. Corrections may have to be made for temperature effects if the range is exceeded. Also, the effects themselves being measured may be temperature dependent, as is the case with resistivity. Temperature log measurements, therefore, are used to calibrate resistivity logs to standard temperature conditions, typically 24°C (75°F).

Environmental correction is a basic but essential use for temperature measurements: generally BHT values suffice but continuous logs will give more accuracy.

***Thermal maturation of organic matter***

Perhaps the best known use of borehole temperature measurements, simply as BHT values, is for calculating organic matter maturity. Landes (1967) proposed that there was a fairly strict relationship between thermal gradient, depth and hydrocarbon type. The modern view is to interpret this relationship in terms of hydrocarbon generation and maturity. It is certain that simply plotting temperature against depth (and pressure), allows typical expected hydrocarbon depth ranges to be defined (Figure 3.8). However, these plots define an effect rather than a cause and anomalies often occur, hydrocarbons being found in deeper or hotter reservoirs than they 'should'.

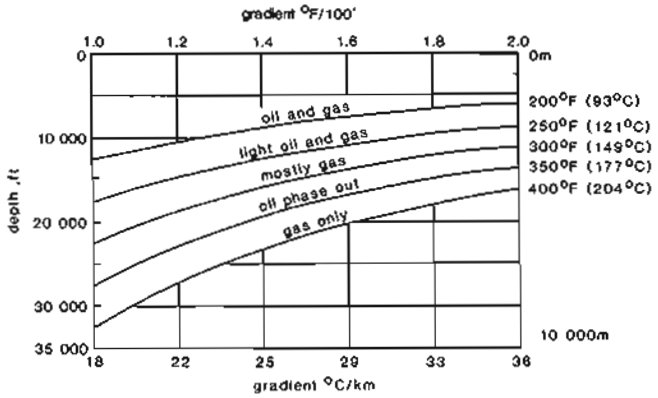


**Figure 3.8** An early proposal for the temperature control on oil and gas distribution (surface temperature = 24°C, 75°F). (Redrawn from Landes, 1967).

If however, the degree of maturity of organic matter is considered, that is the degree of conversion into hydrocarbons, hydrocarbon presence is found to be regulated by time, temperature and pressure. Temperature being considered the most important element but time being essential (Waples, 1980). A method using the combined influence of temperature and time for the quantification of hydrocarbon generation was proposed by Lopatin (Waples, 1980 *op cit*) based essentially on the time a source rock spends at a certain temperature range. Present day temperature gradients are effectively extended back in time and combined with burial curves to arrive at a generation curve (Figure 3.9). The temperature data used in this method generally come from simple BHT values, corrected to present day formation temperature (*see* Section 3.3) and presented as a temperature gradient. This gradient is either extended back in time un-modified or varied based on geological arguments. The BHT measurements and corrections should obviously be as accurate as possible for the method to be effective.

For detailed discussions on the use of temperature in organic matter studies and especially the use of time and temperature to predict maturity, specialist papers and books should be consulted (esp. Waples, 1980).

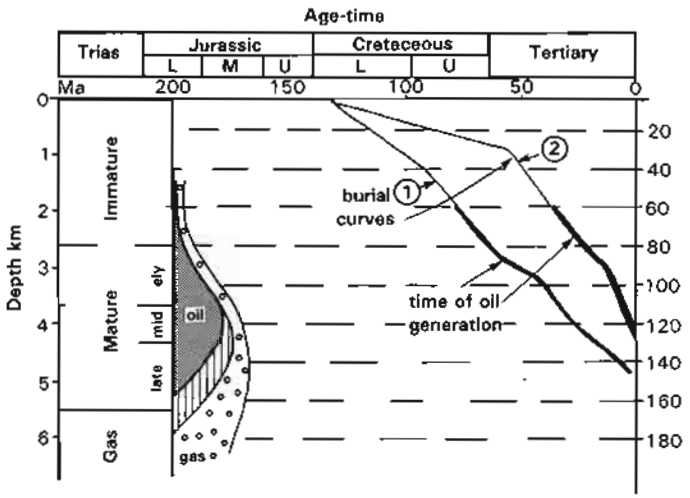


**Figure 3.9** Source rock maturation plotted against geologic time. Well 1 shows oil generation from a lower Cretaceous source rock beginning in the Upper Cretaceous and continuing to the present. Well 2 shows the same source rock only beginning oil generation in the Mid-Tertiary and continuing to the present. The period of oil generation has been calculated using the method of Lopatin (Waples, 1980) in which temperature is the major control through time. In this example the present day temperature gradient, derived from well logs, is extended back in time unchanged. The maturity scale to the left of the grid is schematic and based on temperature only.

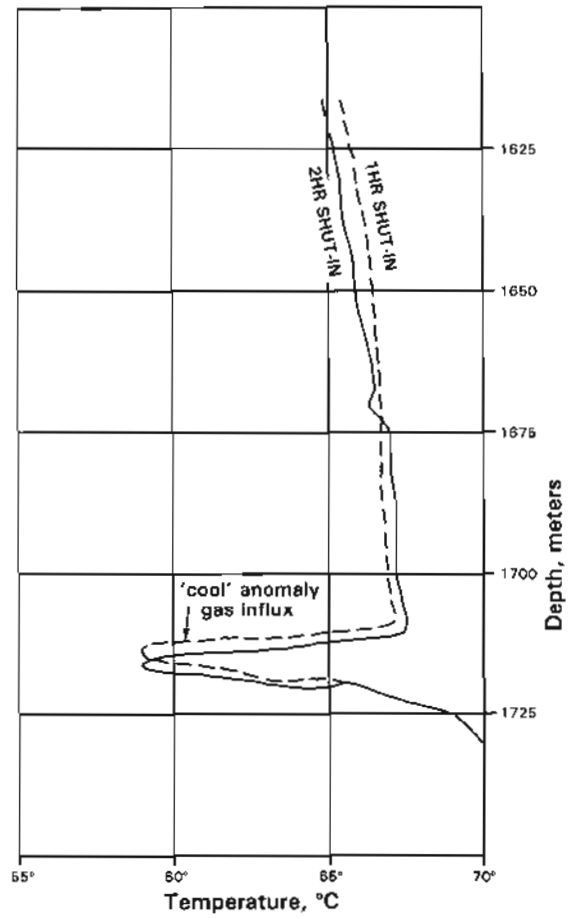


**Figure 3.10** A borehole temperature anomaly caused by the influx of gas. The gas expands and cools on entering the mud-filled borehole (re-drawn from Hill, 1990 after McKinley, 1981).

## Using Continuous Temperature Measurements

### *Correlation*

A postulated, but unusual use for continuous, high resolution temperature logs is in correlation. The proposal being that the high resolution logs are sensitive indicators of the thermal conductivity of a formation and that this bulk feature is distinctive and therefore correlatable (Reiter *et al.*, 1980). This use is dependent on having very good quality logs and consistent drilling conditions. It is not frequently used.

### *Overpressure identification and locating fluid movements*

The typical, gradually increasing geothermal gradient measured down a drilling mud column, can be disturbed by any inflow of formation fluids (flow into the borehole) or outflow of drilling fluids (into the formation). A temperature anomaly is caused which may be either an increase or a decrease, depending on conditions. This type of examination requires continuous temperature profiling logged running into the borehole.

For example, drilling into high pressure shales (under compacted) causes a sharp increase in temperature gradient downwards (Lewis and Rose, 1970). The increase is due to the high content of hot (i.e. at formation temperature) formation water in the overpressured shales. This formation water enters the borehole and causes the anomalous temperature rise in the mud.

Similarly, if there is a direct, continuous flow of formation water or hydrocarbon fluids into the borehole, then the logged temperature shows a marked increase at the inflow point (Hill, 1990). This is because the inflowing fluids are at formation temperature which, in a newly drilled well, is higher than the mud temperature (cf. Figure 3.5). If gaseous hydrocarbons enter the well, however, a cool anomaly is seen: the gas expands on entering the borehole, dropping rapidly in temperature (Figure 3.10).

In the same way as inflows to the borehole from the formation produce temperature anomalies, so also does an outflow or loss of drilling fluid (Hill, 1990). Typically, where the cooler drilling fluid enters into the formation, there will be a cool temperature anomaly. This effect is used to identify hydraulically fractured zones (i.e. purposely fractured for production) where a pre-fracturing gradient will contrast with the post-fracturing gradient which shows a cool anomaly opposite the fractures (Figure 3.11). Multiple, closely spaced (in time) passes of the temperature log are especially effective in these cases and allow continuous changes in convection effects (fluid movement) to be monitored, which are

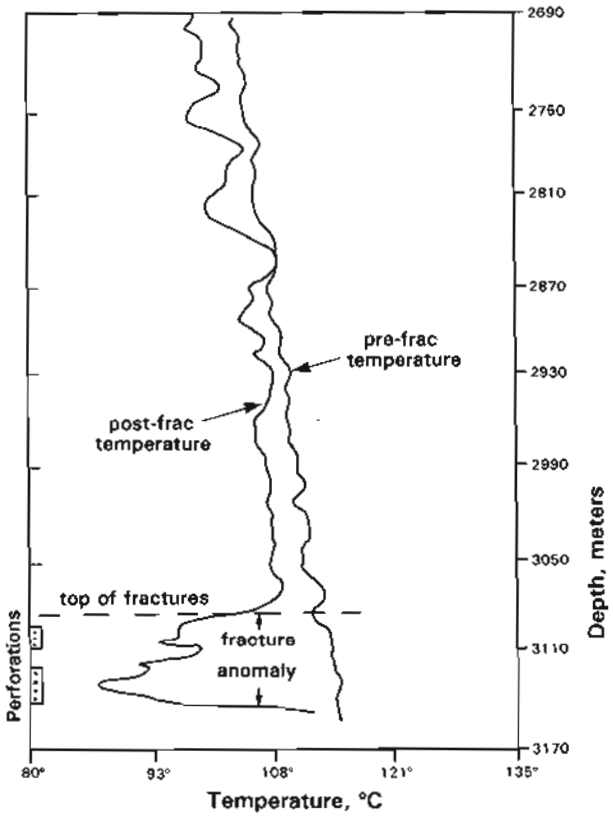


**Figure 3.11** A borehole temperature anomaly created by hydraulic fracturing. Borehole mud enters the created fractures causing a cool anomaly which did not exist before fracturing was done (re-drawn from Hill, 1990 after Dobkin, 1981).

rapid, as opposed to conduction effects which are slow (Alm, 1992).

The use of the continuous temperature log to detect fluid movement is most common in production logging (Hill, 1990) but the same principles can be used effectively in un-cased (open hole) exploration wells. This is not generally the case at present.

# 4
# CALIPER LOGS

Caliper tools measure hole size and shape. The simple mechanical caliper measures a vertical profile of hole diameter (Figure 4.1). The more sophisticated borehole geometry tools record two simultaneous calipers and give an accurate borehole shape and orientation.

## 4.1 Mechanical calipers – the tools

The mechanical caliper measures variations in borehole diameter with depth. The measurements are made by two articulated arms pushed against the borehole wall. The arms are linked to the cursor of a variable resistance (Figure 4.2). Lateral movement of the arms is translated into movements of the cursor along the resistance, and hence variations in electrical output. The variations in output are translated into diameter variations after a simple calibration. Frequently logging tools are automatically equipped with a caliper, such as the micrologs (Chapter 6) and the density-neutron tools (Chapters 9, 10) where the caliper arm is used to apply the measuring head of the tool to the borehole wall. Sophisticated, dual caliper tools, such as the Borehole Geometry Tool of Schlumberger, also exist specifically for measuring hole size and volume. However, today, such information is generally taken from dipmeter tools, which acquire geometry data in order to derive dip (Chapter 12). These tools have four pads fixed at right angles, opposite pairs being linked but independent of the perpendicular set. This, in terms of geometry, gives two independent calipers at 90°. The tool also contains gyroscopic orientation equipment so that the azimuth (bearing) of the two calipers is permanently defined.

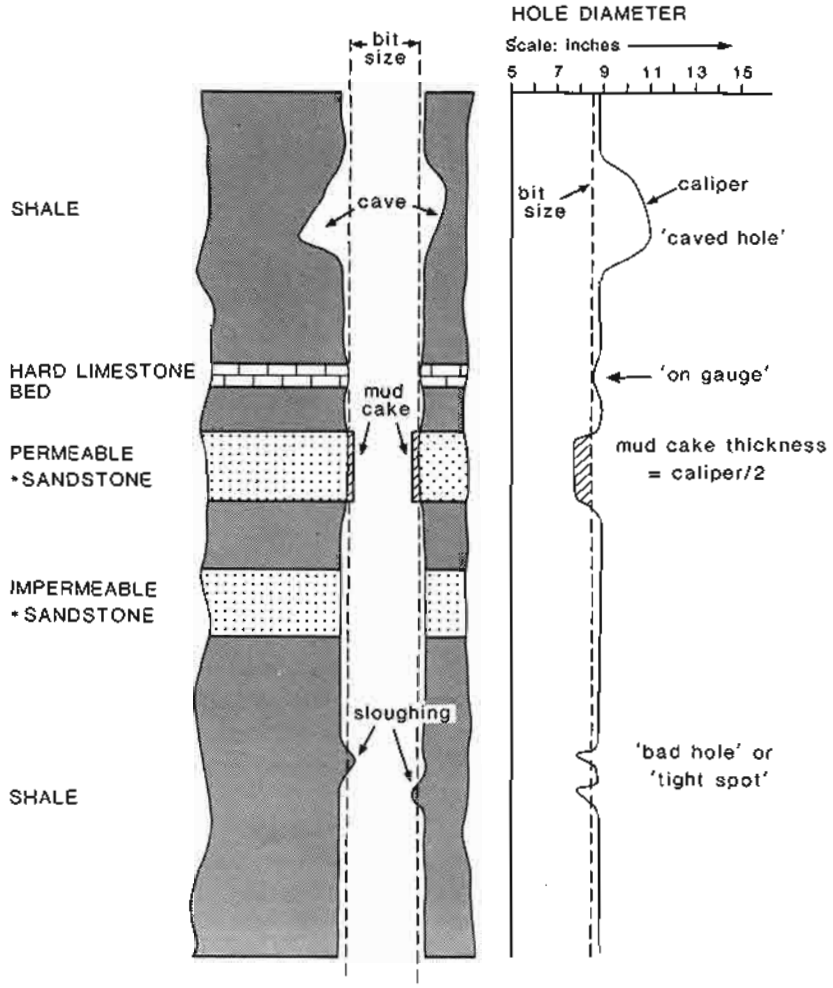


**Figure 4.1** The caliper log showing hole diameter: some typical responses. *Limestone, dolomite, etc. equally applicable.

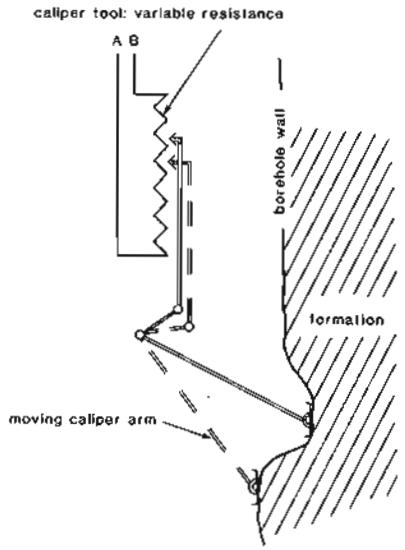


**Figure 4.2** Schematic caliper tool showing the conversion of a mechanical movement to an electrical signal using a variable resistance. (Adapted from Serra, 1979).

## 4.2. Log presentations

The caliper log is printed out simply as a continuous value of hole diameter with depth (Figure 4.3). The curve is traditionally a dashed line and usually plotted in track 1. The horizontal scale may be inches of diameter or, in the differential caliper, expressed as increase or decrease in hole diameter about a zero defined by the bit size (Figure 4.3). The ordinary caliper log is accompanied by a reference line indicating bit size.

The geometrical data from four-arm, dual-caliper tools such as the dipmeter are presented in various formats, only one of which is shown (Figure 4.4). The two hole diameters measured by the two calipers are combined with the directional elements of tool orientation (pad 1 azimuth), hole deviation and azimuth of the deviation. An integrated hole volume may be added as horizontal ticks on the depth column giving a continuous record of hole volume (not on the example).

The calipers of the example presented (Figure 4.4), show the geometry tool turning slowly as it moves upwards in a persistently oval hole with a small diameter of approximately 9" and a large diameter of approximately 11". The larger diameter is oriented nearly north to south as indicated by the pad 1 azimuth over the depth 0–15 m (calipers 1–3 in larger diameter). At depth 30 m, calipers 2–4 show the larger radius (approx. 11"), calipers 1–3 the smaller (approx. 9"). The rotation of the tool is indicated by the persistent change in the pad 1 azimuth and explains the caliper cross-over at depth 17 m (where both calipers show the same diameter but the hole is still oval). Above this, calipers 1–3 follow the larger diameter (approx. 11"), while calipers 2–4 follow the smaller (approx. 9").

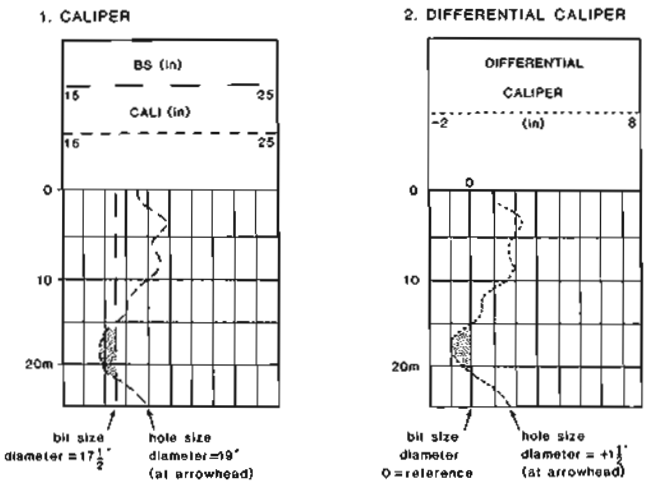


**Figure 4.3** Presentation of the caliper log: (1), in ordinary format; (2), in differential format.
BS = bit size

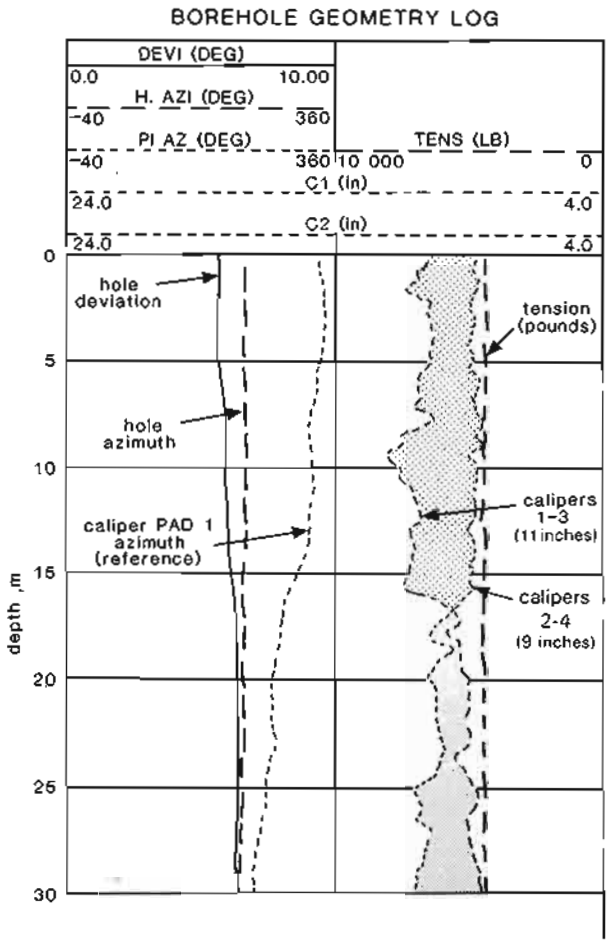


**Figure 4.4** Borehole geometry log presentation (*see* text for explanation).

## 4.3 Simple, two-arm, caliper interpretation

***Increase in borehole diameter***

The simple caliper log records the mechanical response of formations to drilling. A hole that has the same size (diameter) as the bit which drilled it, is called *on gauge* (Figure 4.1). On gauge holes are the target for all drilling and essentially indicate good drilling technique. Holes with a much larger diameter than the bit size are '*caved*' or '*washed out*'. That is, during deepening of the hole, the borehole walls cave in, are broken by the turning drill pipe, or are eroded away by the circulating borehole mud. This is typical of shales, especially when geologically young and unconsolidated, so that caving can have a general lithological significance (Figure 4.1).

However, caving is also typical of certain specific lithologies such as coals or even organic shales. In some fields, even with varied drilling fluids and drilling techniques, it is found that certain stratigraphic levels habitually cave – generally for mechanical (textural) reasons. The example (Figure 4.5) shows a section of Carboniferous shale from the UK East Midlands in which moderate caving occurs in the same organic rich interval, over a wide area. The shale is either very laminated or locally fractured.

***Decrease in borehole diameter***

Calipers may show a hole diameter smaller than the bit size (diameter). If the log has a smooth profile, a mud-cake build-up is indicated (Figure 4.6*a*). This is an extremely useful indicator of permeability: only permeable beds allow mud cake to form. The limits of mud-cake indicate clearly the limits of the potential reservoir. Mud cake thickness can be estimated from the caliper by dividing the decrease in hole size by two (the caliper giving the hole diameter), i.e.

$$\frac{\text{bit size (diam)} - \text{caliper reading (diam)}}{2} = \text{mud cake thickness}$$

It should be remembered that this thickness may vary between tools. The caliper of a density tool is applied harder to the formation than the caliper of a micro-log: the former probably causes a groove in the mud cake and therefore gives a thinner, log derived mud-cake thickness.

Boreholes with a smaller diameter than the bit size but rugose, are probably sloughed (Figure 4.6*b*). The zones of small holes will be the 'tight spots' encountered during drilling, trips or logging. That is, it will be at these points that tools stick or the bit gets stuck while being pulled out of the hole. A frequent cause of tight spots is abundant smectite in the clay mineral mixture. Smectite is a swelling clay which takes water from the drilling mud, expands, breaks from the formation and sloughs or collapses into the hole. The Gulf Coast 'gumbo', which often causes hole problems, is smectite rich.

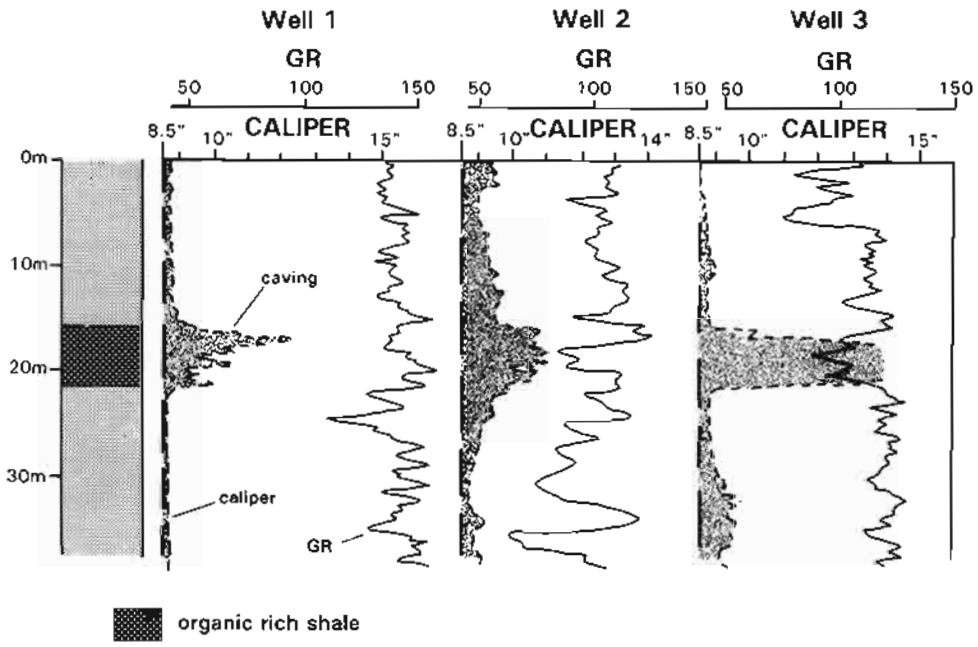


**Figure 4.5** Consistent caving, indicated on the caliper log, over the same, organic rich, stratigraphic level in three different wells. Upper Carboniferous, East Midlands, U.K.

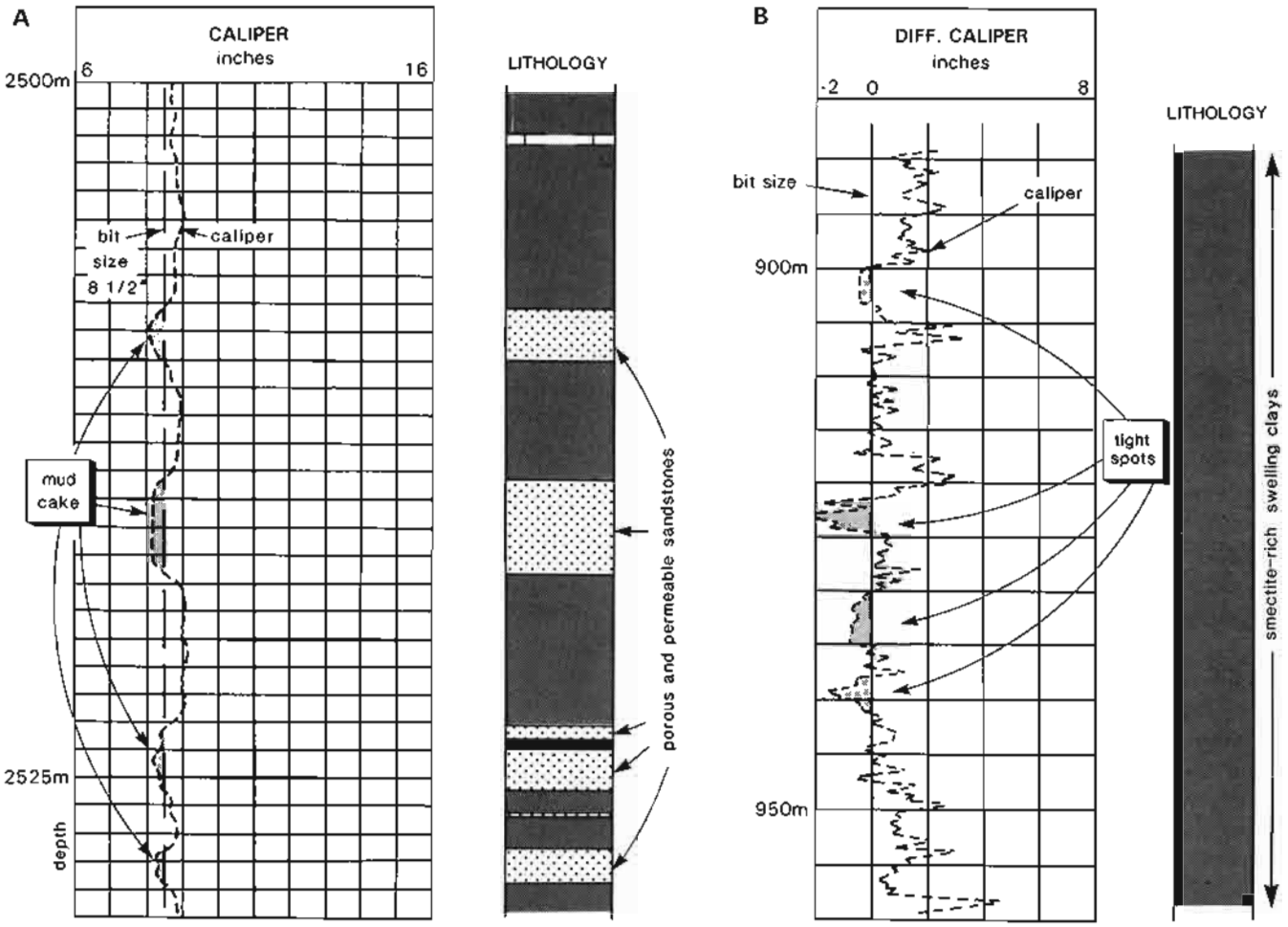


**Figure 4.6** Hole size diminution seen on the simple caliper. (A) Mud-cake build-up opposite porous and permeable sandstones. (B) Tight spots in a shale sequence caused by hole sloughing due to swelling clays.

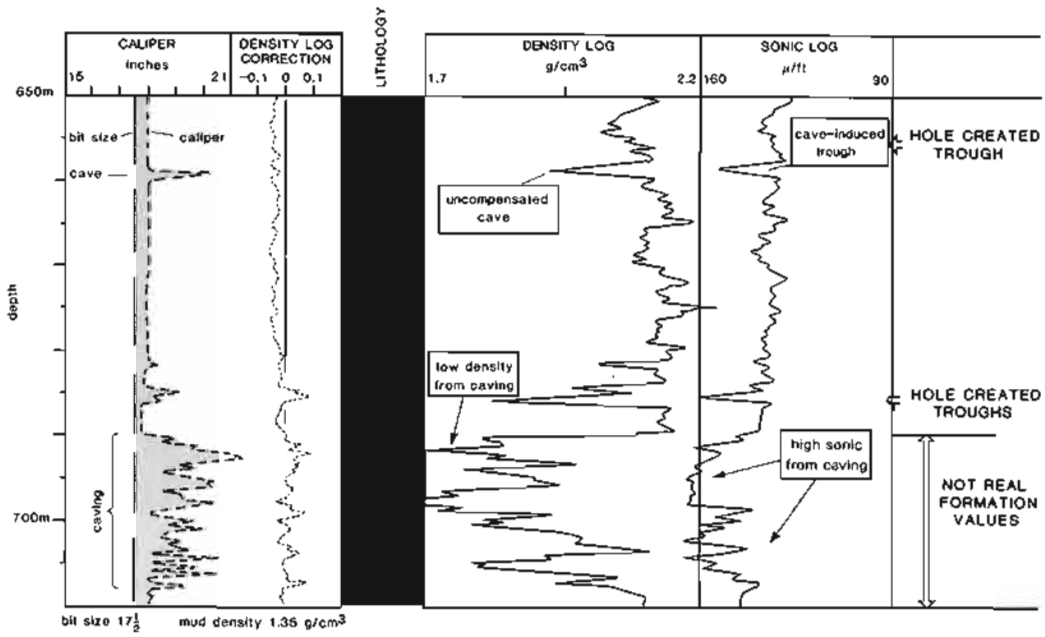


**Figure 4.7** Poor hole conditions and caving creating zones of poor data quality where log readings do not represent real formation values. The automatic density correction derived from the caliper is insufficient to compensate for the large caves at around 700m. The density and sonic logs suggest a formation change at 690m, but the interval is homogeneous from top to bottom, being poorly consolidated clay/shales.

*Quality control using the caliper*

With the simple, two arm caliper, one extremely important use is in the quality control of logs in general. When caving is serious, the quality of log readings is impaired. In some tools, such as the micrologs, a caliper is registered simply because the tool sensors are pad mounted. Lack of pad contact with the formation, a problem in rugose holes with pad-mounted tools, is quickly seen by using the caliper. In other tools, such as the formation density, the caliper reading is used for an automatic hole size and mud-cake thickness correction or compensation (Chapter 9). Caving will demand inordinately large corrections to many logs and the log values will be of little use. It is therefore essential to look at the caliper before using any logs (Figure 4.7).

However, it should be pointed out that the simple caliper attached to the open hole tools such as the micrologs and the formation density, will generally be pessimistic in terms of hole condition, because in oval holes a simple caliper will naturally open to the maximum diameter of the borehole (Figure 4.8). And although the log measurements recorded will be made across the larger diameter, the hole condition itself is not as bad as may first appear.

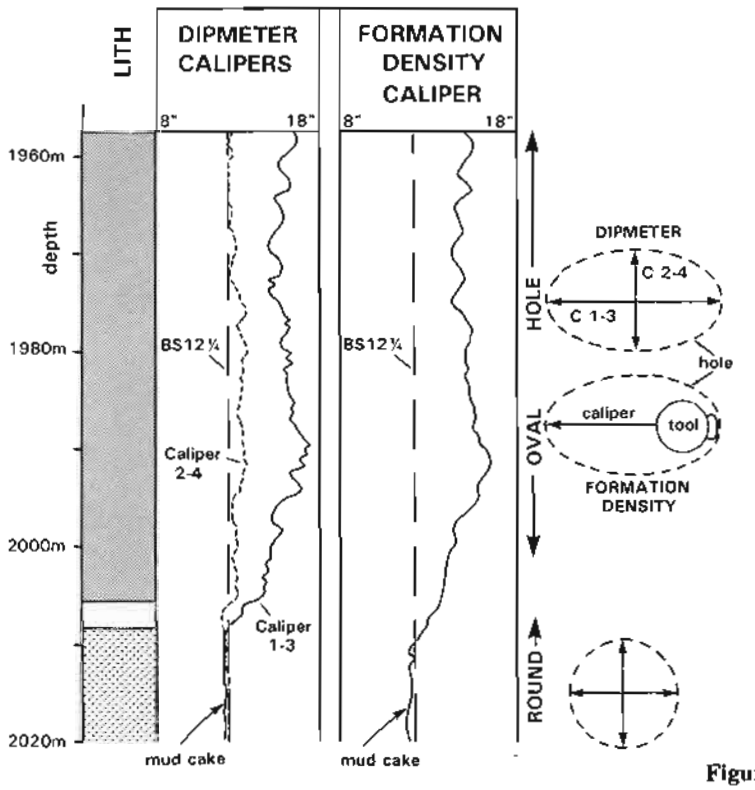


**Figure 4.8** Comparison between the simple caliper of the formation density tool and the two-arm caliper of the dipmeter tool in an oval hole. The simple caliper normally extends to the long axis in an oval hole.

## 4.4 Four-arm caliper interpretation

***Breakouts***

A great deal more information can be gained from dual caliper tools than from the simple caliper tool. As indicated above, dual caliper information is generally taken from the four-arm dipmeter tool.

Using just a single caliper, borehole shape cannot be interpreted. Data from a four arm caliper however, enables the shape of a hole to be much better defined. A hole can be seen to be 'on gauge' and round (Figure 4.9*a*) or oval and 'washed out' (Figure 4.9*c*) or enlarged by a 'key seat' (Figure 4.9*b*). When oval, the direction of enlargement can be given. However, much more can be interpreted from borehole shape.

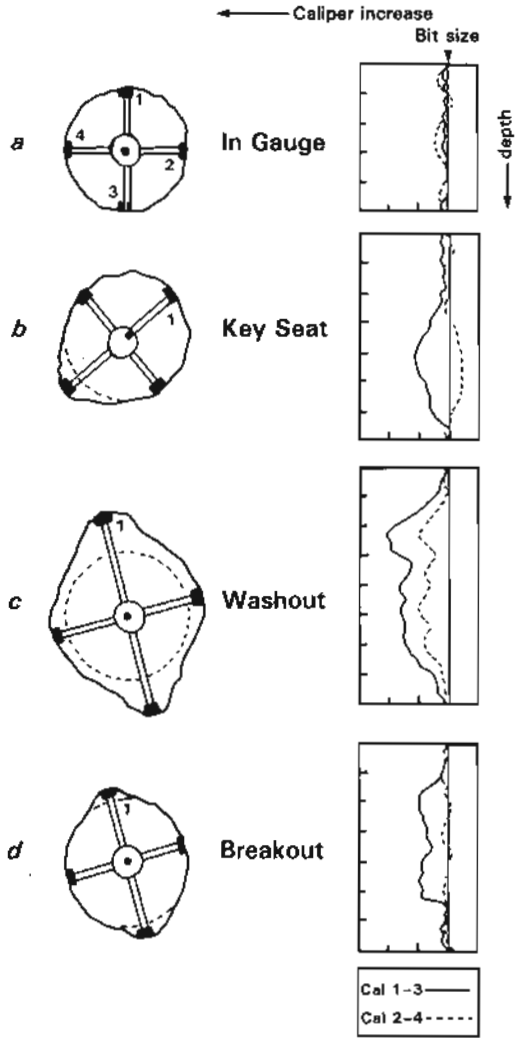


**Figure 4.9** Diagrammatic representation of types of borehole shape and profile as identified on the two-arm caliper. *a*. Round, in-gauge hole. *b*. Key seat hole enlargement at a dogleg. *c*. Washout hole enlargement due to general drilling wear. *d*. Breakout, showing characteristic oval hole with abrupt vertical limits (re-drawn, modified from Plumb and Hickman, 1985).

Three main types of elliptical borehole have been recognized, 'keyseats', 'washouts' and 'breakouts' (Figure 4.9). Washouts develop from general drilling wear, especially in shaly zones and dipping beds. On the geometry logs, a washout has a considerable vertical extent and both calipers are larger than the drill bit size with one caliper being much larger than the other. Shape changes are variable and gradual (Figures 4.9*c*; 4.10,*2*). Keyseats are asymmetric oval holes, formed by wear against the drill string at points where the borehole inclination changes (doglegs) (Figure 4.9*b*). Both washouts and keyseats are general drilling phenomena: breakouts, however, have a specific cause.

Breakouts are recognised using the following strict criteria (Figure 4.11) (i.e. Bell, 1990):

1. The tool must stop rotating (ideally the tool should rotate before and after a breakout zone).
2. The calipers must separate to indicate an oval hole. The larger caliper should exceed hole gauge: the smaller caliper should not be less than hole gauge and its trace should be straight (the caliper difference should be larger than 6 mm and the zone of elongation greater than 1.5 m). The limits of the breakout should normally be well marked.
3. The larger diameter of hole elongation and its direction should not consistently coincide with the azimuth of hole deviation.

Breakouts are considered to form as a the result of the interaction of stresses induced by drilling and the existing stress regime of the country rock (Bell and Gough, 1979). Small brittle fractures (spalling) occur in the borehole around a rotating bit which, if there is unequal horizontal stress in the formation, form in a preferential direction, that of the minimum horizontal stress, $Sh_{min}$ (Figure 4.12, *a*). In more precise terms, compressive shear fracturing of the borehole wall is localised in the direction of the minimum horizontal formation stress $Sh_{min}$, and is the cause of breakouts (Bell, 1990). Laboratory experiments and empirical observations seem to back up the theory (*see* Prensky, 1992b for a review and references). Hence, breakouts indicate the present day stress-field orientation and are independent of lithology, dip and existing fractures or joints.

Breakout studies to define in-situ stress fields are now being carried out on many scales from the local to the global. On the global scale, breakout derived stress-field orientations are similar to those derived from earthquake studies and tend to indicate intra-plate tectonic stresses (Zoback *et al.*, 1989). On a local scale, breakout studies have an importance for field development (Figure 4.13). Natural and artificial fractures are most likely to be oriented in the maximum horizontal stress direction $Sh_{max}$ (i.e. normal to breakouts) (Figure 4.12,*b*). Fracture connection between wells during field production is then more likely in this orientation (Bell, 1990). It is also possible that horizontal drilling will be more stable in the $Sh_{max}$ (maximum horizontal stress) direction (Hillis and Williams, 1992).

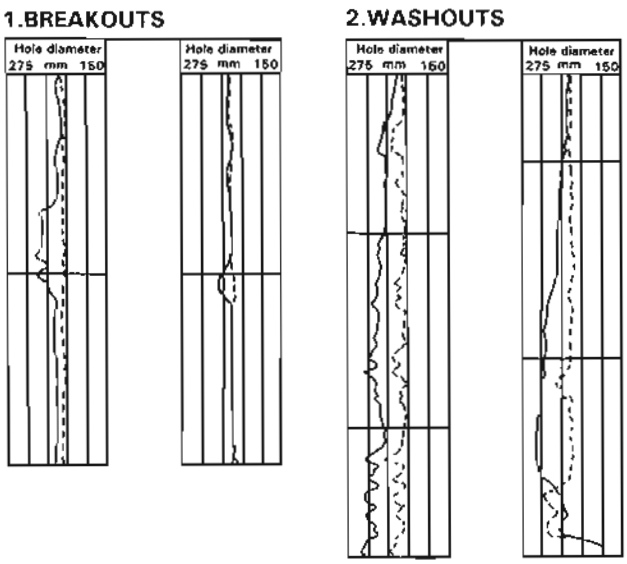


**Figure 4.10** Field examples of hole size enlargement seen on the two-arm, dual caliper. 1. Breakouts, seen as well-defined, oval hole developments. 2. Washouts, seen as generalised hole ovality. Hole diameter increases to the left (from Cox, 1983).

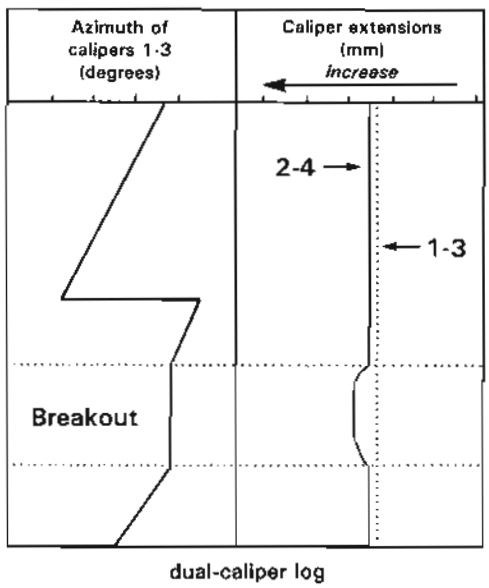


**Figure 4.11** Schematic representation of the characteristics used to identify breakouts on caliper logs (re-drawn from Yassir and Dusseault, 1992).

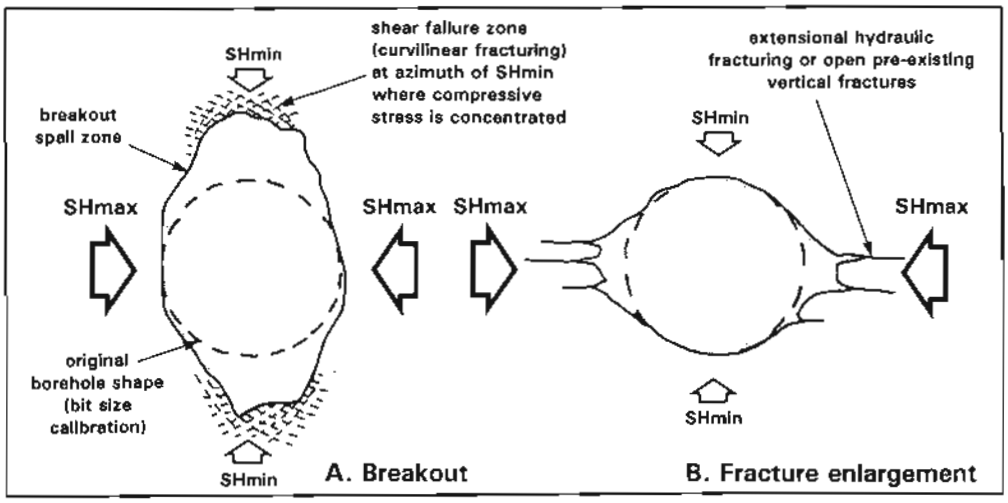


**Figure 4.12** Horizontal stress field relationship to borehole shape. a. Breakout formation due to spalling during drilling, in the direction of minimum horizontal stress ($Sh_{min}$). *b*. Hole enlargement along drilling induced extensional fractures oriented in the direction of maximum horizontal stress ($Sh_{max}$) (modified from Dart and Zoback, 1989 and Hillis and Williams, 1992).

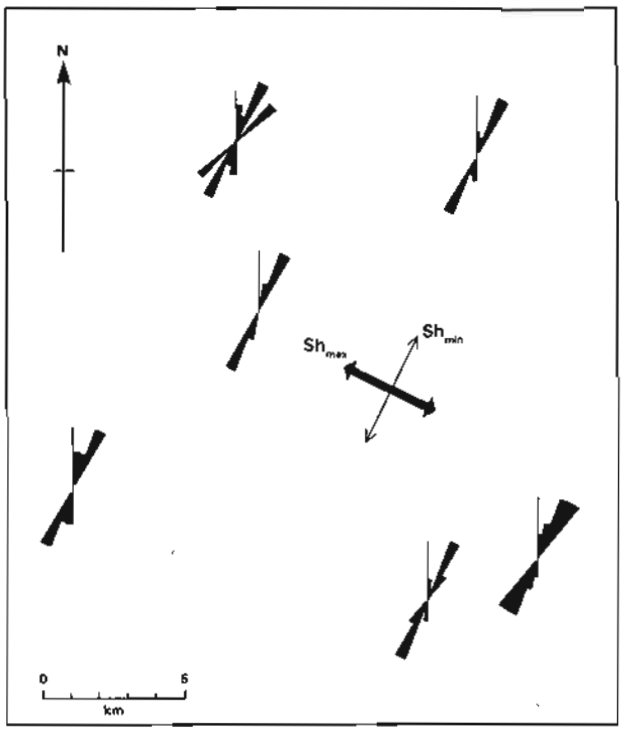


**Figure 4.13** Consistently oriented breakouts, identified from dipmeter caliper data in an offshore field, indicating the present day, horizontal stress field. Depth of analysed interval from 2.5 to 3.5 kilometres. $Sh_{min}$ = minimum horizontal stress, $Sh_{max}$ = maximum horizontal stress.

# 5
# SELF-POTENTIAL OR SP LOGS

## 5.1 Generalities

***The log***

The SP log is a measurement of the natural potential differences or self-potentials between an electrode in the borehole and a reference electrode at the surface: no artificial currents are applied (Figure 5.2). (The currents were actually called '*potentiels spontanés*', or 'spontaneous potentials', by Conrad Schlumberger and H.G. Doll who discovered them.) They originate from the electrical disequilibrium created by connecting formations vertically (in the electrical sense) when in nature they are isolated.

***Principal uses***

The principal uses of the SP log are to calculate formation-water resistivity and to indicate permeability. It can also be used to estimate shale volume, to indicate facies and, in some cases, for correlation (Table 5.1, Figure 5.1).

## 5.2 Principles of measurement

Three factors are necessary to provoke an SP current: a conductive fluid in the borehole; a porous and permeable bed surrounded by an impermeable formation; and a difference in salinity (or pressure) between the borehole fluid and the formation fluid. In oilfield wells, the two fluids concerned are the mud filtrate and (usually), formation water.

SP currents are created, when two solutions of different salinity concentrations are in contact, by two principal electrochemical effects; *diffusion or liquid junction potential and shale potential* (Figure 5.3). The diffusion potential (or liquid junction potential) arises when solutions of differing salinity are in contact through a porous medium. Sodium chloride, NaCl, is the most common cause of oilfield salinity, so that it is effectively two solutions of sodium chloride of different salinities that come into contact. Through the porous medium,

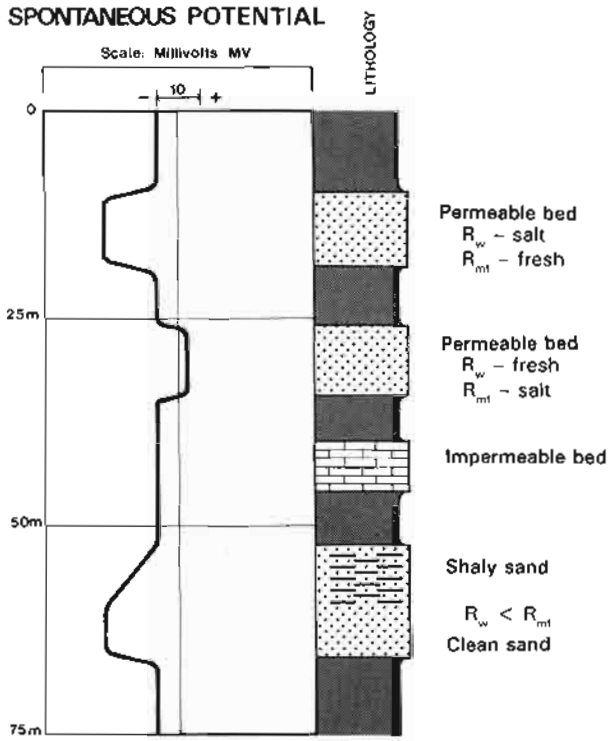


**Figure 5.1** The SP log: some typical responses. The SP log shows variations in natural potentials. $R_w$ = formation-water resistivity; $R_{mf}$ = mud filtrate resistivity.

**Table 5.1** The principal uses of the SP log.

| | Discipline | Used for | Knowing |
|---|---|---|---|
| Quantitative | Petrophysics | Formation-water resistivity | Mud filtrate resistivity and formation temperature |
| | | Shale volume | SSP and shale line |
| Qualitative | Petrophysics | To indicate permeability | Shale line |
| | Geology | Facies (shaliness) | Clay/Grain size relationships |
| | | Correlation | |

mixing of the two solutions takes place by ionic diffusion. The $Cl^-$ ion is both smaller and more mobile than the larger, slower $Na^+$ ion. The ions mix (diffuse), therefore, at unequal rates, creating a charge separation. The $Cl^-$ ion mixes the quickest, thus increasing its saturation in the more dilute solution. A potential is created between the negatively charged dilute solution with excess $Cl^-$ and the positively charged, concentrated solution with excess $Na^+$ (Figure 5.3,*1*).

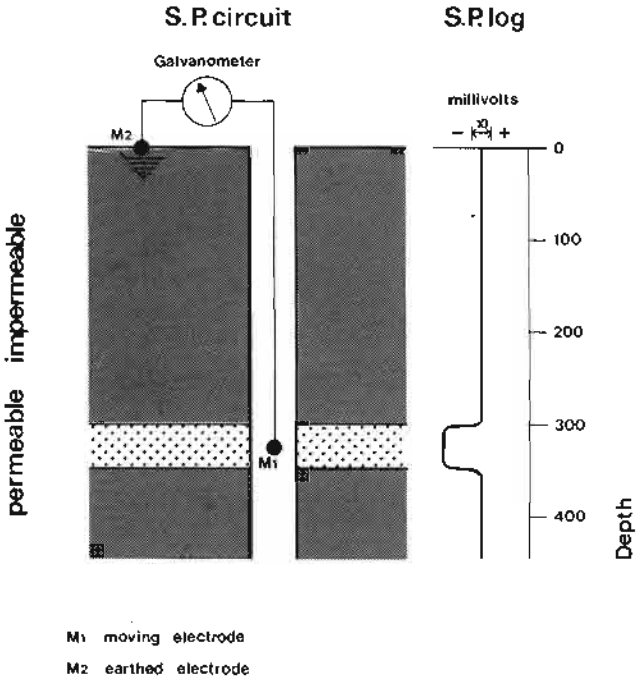


**Figure 5.2** Illustration of the principle of the SP log. A natural potential is measured between an electrode in the well and an earth at the surface.

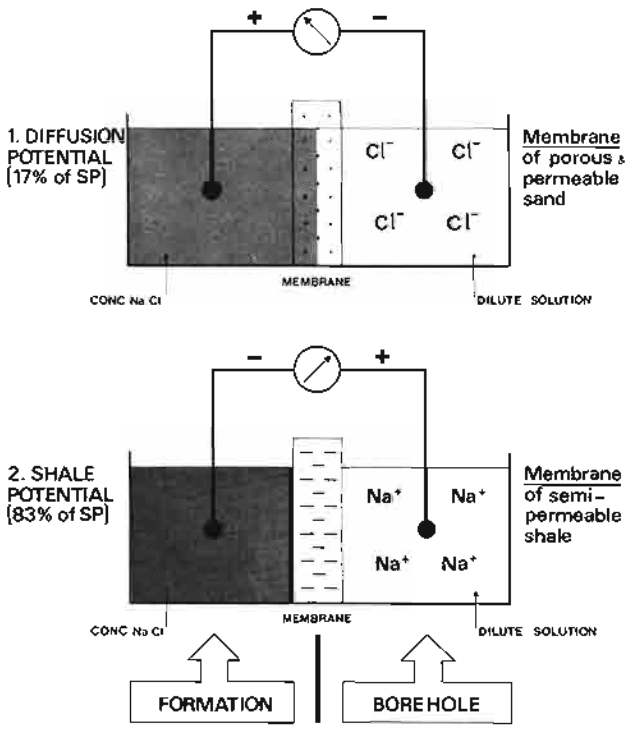


**Figure 5.3** Schematic illustration of the main electrochemical SP effects. (1) Diffusion potential across a porous and permeable membrane; (2) shale potential across a membrane of semi-permeable shale. (Modified from Desbrandes, 1968).

The shale potential arises when the same two solutions are in contact across a semi-permeable membrane. In the borehole, this, as the name suggests, is shale (Figure 5.3,*2*). Clay minerals which form shales, consist of layers with large negative surface charge. Because of charge similarity, the negative chloride ions effectively cannot pass through the negatively charged shale layers, while the positive sodium ions pass easily. The shale acts as a selective barrier. As $Na^+$ ions therefore diffuse preferentially across a shale membrane, an overbalance of $Na^+$ ions is created in the dilute solution, and hence a positive charge. A corresponding negative charge is produced in the concentrated solution (Figure 5.3,*2*). The shale potential is the larger of the two electrochemical effects.

The actual spontaneous potential currents which are measured in the borehole are, for the most part, a result of the combination of the two electrochemical effects described above. Consider a porous and permeable sandstone penetrated by a borehole; the mud filtrate (for the example) is less saline than the formation waters (Figure 5.4). Opposite the sandstone bed (permeable membrane) the less saline solution, the mud filtrate, will become negatively charged as a result of the diffusion potential (cf. Figure 5.3,*1*). But above the sand, opposite the shale (semi-permeable membrane), because of the shale potential the less saline solution, the mud filtrate, will become positively charged (cf. Figure 5.3,2). The excess charge is therefore negative opposite the sand and positive opposite the shale.

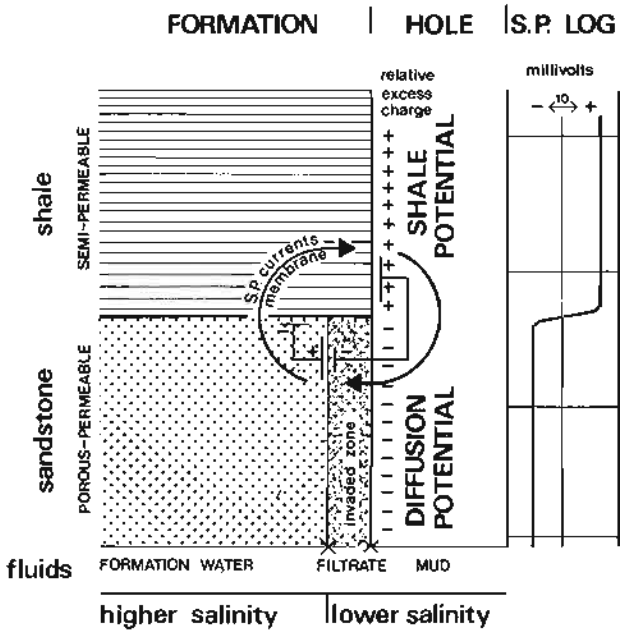


**Figure 5.4** SP currents in the borehole. The effects of the shale potential and the diffusion potential act together at bed boundaries causing an SP log deflection.

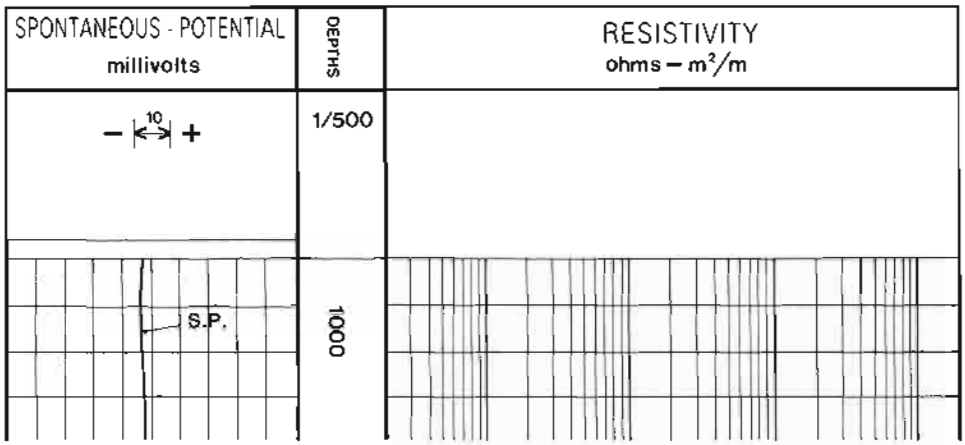


**Figure 5.5** SP log presentation. The SP is in track 1. There is no absolute scale, only relative deflection – negative or positive. 1 division equals 10 millivolts.

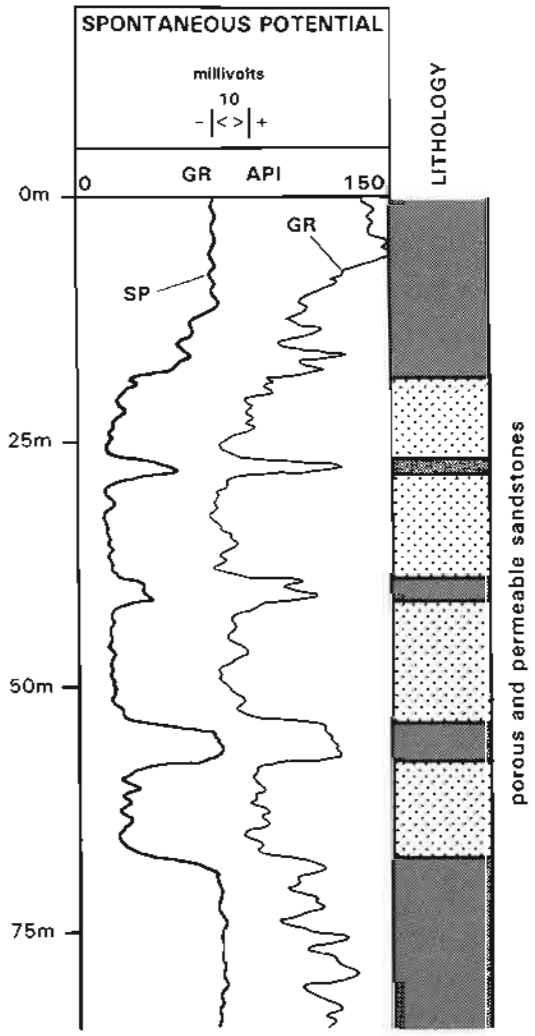


**Figure 5.6** The bed definition and 'character' of the SP log compared to the gamma ray log. In most cases the gamma ray log gives much more formation information and better bed boundary definition than the SP.

This couple works in a complementary sense and creates a spontaneous current flowing between the borehole (mud filtrate), the porous formation and the

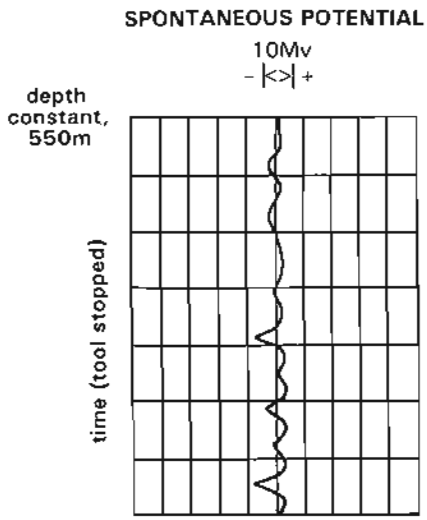


**Figure 5.7** The SP log indicating sea state! For this test, offshore Louisiana, the SP tool was grounded to the rig and stopped at 550m. The changes in SP potential occur with the passing waves, which were 2.5m – 3.0m (8' – 10') crest to trough. The hole was cased (from Wallace, 1968).

contiguous shale (Figure 5.4). The flow of current is focused at the bed junction. It is only here that there is a change in potential. This is important since SP measurements are made not of absolute values, but of changes in values. It is only at the bed junctions, then, that changes take place and will be recorded.

If a bed is not permeable, ions will not be able to move, there will be no current flow and thus no potential change: that means no SP. However, even the slightest permeability will permit current flow and an SP change will be recorded.

### *The SP tool*

The SP tool approaches the simplicity of the circuit described (Figure 5.2) and consists simply of an electrode (lead) mounted on an electrically isolated bridle on the downhole tool. A 1.5 volt battery is included in the circuit to give a bucking current to bring the SP to the required scale. The tool's galvanometer records only

changes in potential: it gives no absolute values. The surface electrode of the SP must be an effective earth (Wallace, 1968).

***Log presentation: units and scales***

SP currents are measured in millivolts ($1 \times 10^{-3}$ volts) and the scale is in + or – millivolts, negative deflections to the left, positive to the right (Figure 5.5). The log is usually run in track 1 with a gamma ray or caliper log (Figure 5.5).

***Unwanted logging effects***

As indicated above, for the SP tool to work effectively, it must be connected to a surface earth. For onland wells this causes no problem and an iron probe can be pushed directly into the soil. Offshore, however, no such possibility exists. Without an effective earth, the SP will not be recorded. The SP from many offshore wells, especially from floating rigs, is useless and mostly ignored. This is a pity. The SP is a cheap and useful log.

The search for an effective earth offshore is difficult. The one most commonly used for floating rigs is the riser, but this is usually in electrical connection to the rig and any rig is electrically noisy. Using the rig legs is not helpful either since these are given a potential themselves to stop rusting and as waves pass, this potential changes and causes a wavy SP – which is only indicative of sea state and not formation characteristics! (Wallace, 1968) (Figure 5.7).

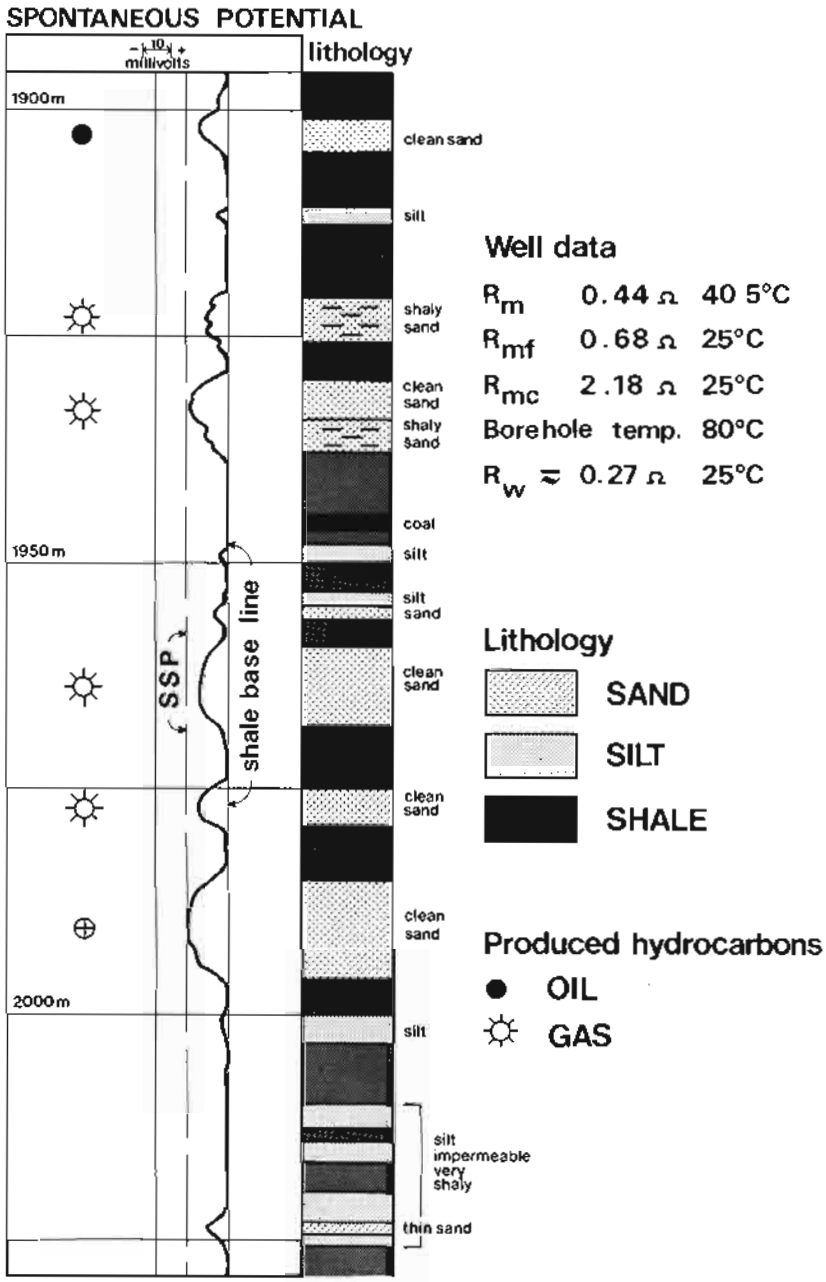


**Figure 5.8** Example of the shale baseline and the SSP defined on an SP log. The shale baseline is the maximum positive deflection (in this example) and occurs opposite shales. The SSP is a maximum negative deflection and occurs opposite clean, porous and permeable water-bearing sandstones.

Using the anchor chain produces a similar effect.

So far, the logging companies seem to have given little thought to the offshore SP problem, perhaps because the SP is not an expensive hi-tech tool. However it produces a cheap, useful log and should be requested.

## 5.3 Log characteristics

***Bed boundary definition and bed resolution***

The sharpness of a boundary will depend on the shape and extent of the SP current patterns. Generally when there is considerable difference between mud and formation resistivity, currents will be spread widely and the SP will deflect slowly: definition will be poor (Dewan, 1983). The contrary also applies. When resistivities are similar, boundaries are sharper. In general, boundaries should not be drawn using the SP. If the log has to be used, the boundary should be placed at the point of maximum curve slope (i.e., maximum rate of change of the SP – Figure 5.6).

SP bed resolution is also poor. For a full SP deflection (i.e. SSP or static SP, *see* Section 5.4) and proper bed resolution, as a rule of thumb, a bed should be thicker than 20 times the borehole diameter (Ellis, 1987). The exact minimum SP bed resolution will obviously depend on depth of invasion and salinity differences, in the same way as described above for bed boundary definition.

## 5.4 Quantitative uses

***Methodology***

Quantitatively, the SP log is used mainly for the evaluation of formation-water resistivities but it can also be used for shale-volume calculation The quantitative use of the SP requires a special methodology which is described briefly below.

***SP values for calculation – shale baseline and static SP***

With no absolute values, the SP is treated quantitatively and qualitatively in terms of deflection, that is, the amount the curve moves to the left or the right of a defined zero. The definition of the SP zero is made on thick shale intervals where the SP does not move: it is called the shale base line (Figure 5.8). All values are related to this line.

The theoretical maximum deflection of the SP opposite permeable beds is called the static SP or SSP. It represents the SP value that would be observed in an ideal case with the permeable bed isolated electrically. It is the maximum possible SP opposite a permeable, water-bearing formation with no shale (Figure 5.8). It is only the log-derived SSP that can be used for the quantitative evaluation of $R_w$ (the formation-water resistivity).

Frequently the SP does not show its full deflection, for a number of reasons: the bed is not thick enough, there is shale in the formation, the invasion is very deep, there are adverse lithological effects (junction beds with high resistivity) or hydrocarbons are present (Figure 5.9) (Pied *et al.*, 1966). These conditions must be considered when taking SP values for calculation.

**Figure 5.9** Some conditions causing aberrant SP values when the SSP is not attained.

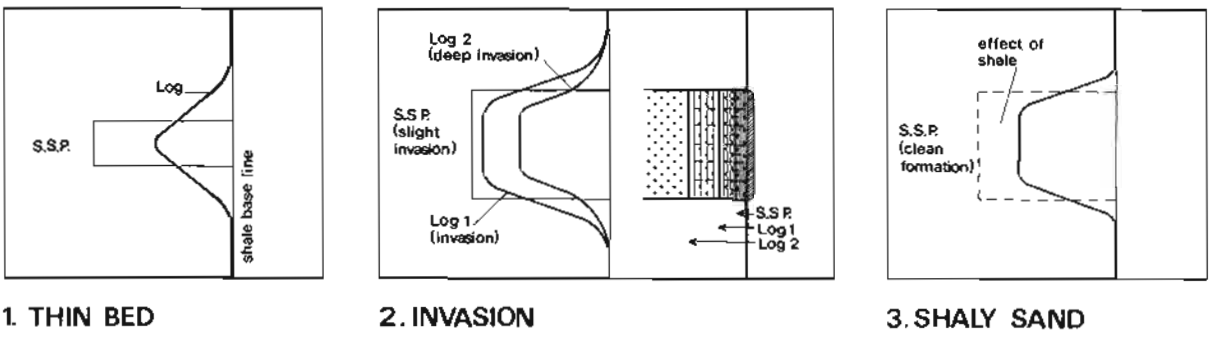

***Water resistivity ($R_w$), quick look and calculations***

Qualitatively, the greater the SP deflection, the greater the salinity contrast between the mud filtrate and the formation water. A rapid look at the SP over a certain series of beds in a sand-shale sequence will show water-salinity changes. Generally these will be negative deflections, the formation waters being more saline than the mud filtrate. Deflections to positive values however, occur with fresh formation waters, or at least those fresher than the mud filtrate (Figure 5.10). Typically, a positive SP deflection is much less marked than a negative one: the positive potential difference is much smaller (Taherian *et al.*, 1992).

Quantitatively, the SP is used to calculate formation-water resistivity using the relationship between resistivity and ionic activity. Ionic activity is the major contributing factor to the electrochemical SP, as explained previously. There is a direct relationship between ionic activity and the resistivity of a solution, at least for the most frequently-encountered values in logging (Gondouin *et al.*, 1957) (Figure 5.11).

This relationship allows a mathematical expression of the amplitude of the SP deflection to be expressed in terms of formation-water resistivity in the following way.

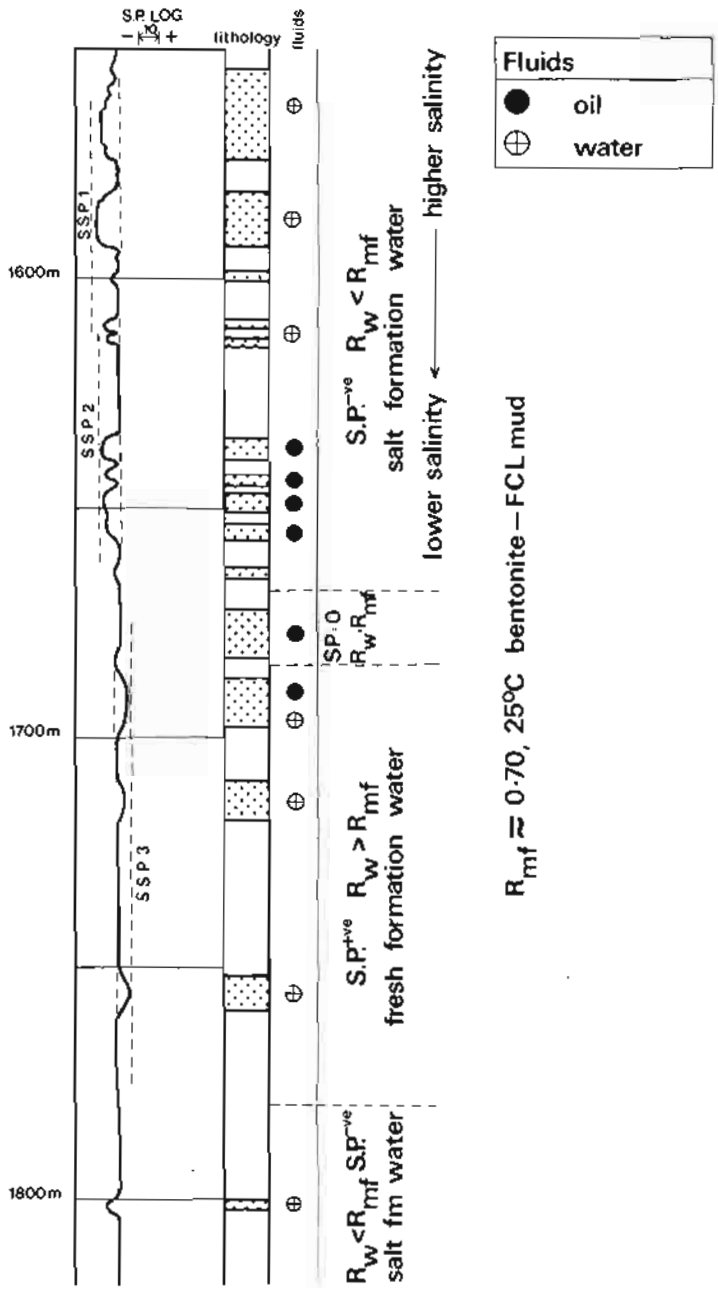


**Figure 5.10** Behaviour of the SP in a sand shale sequence with varying formation-water salinity. A zone of fresh formation water occurs between about 1680m and 1775m. Mud filtrate resistivity is constant.

$$(S)SP = -K \log \frac{(R_{mf})e}{(R_w)e} \qquad (1)$$

S(SP) = SP value: this should be the SSP (static SP)
$(R_{mf})e$ = equivalent mud filtrate resistivity (for the SSP equation) closely related to $R_{mf}$
$(R_w)e$ = equivalent formation water resistivity (for the SSP equation) closely related to $R_w$.
$K$ = temperature-dependent coefficient, as an average, 71 at 25°C (65 + 0.24 x T°C) (cf. Desbrandes, 1982).

The preceding method allows an approximation of the resistivity of formation water (*see* Figure 5.11). However, it is based on the ionic activity of NaCl solutions, although it is generally observed that salinities of both mud filtrates and of formation waters are due to ionic mixtures and that calcium and magnesium as well as sodium ions are present. The effects of calcium and magnesium are especially important at high resistivities in 'fresh' waters. Corrections must be made to the formulae shown above.

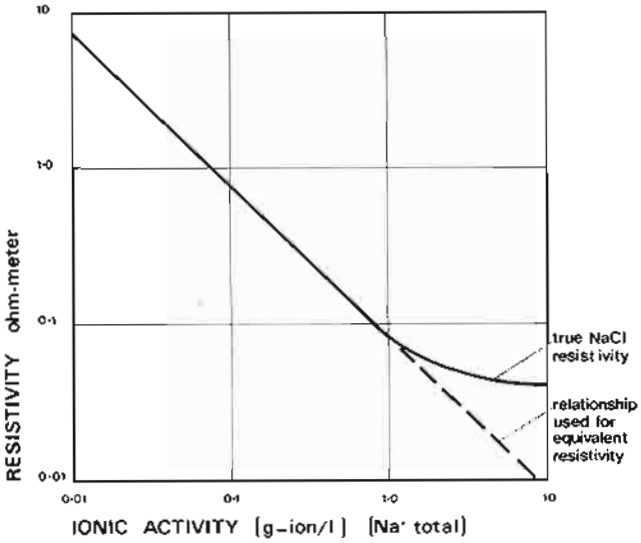


**Figure 5.11** Graph of the relationship between water resistivity and SP deflection (ionic activity) for salt solutions. This is the basis for using the SP to calculate formation water resistivity, $R_w$. (From Gondouin *et al.*, 1957).

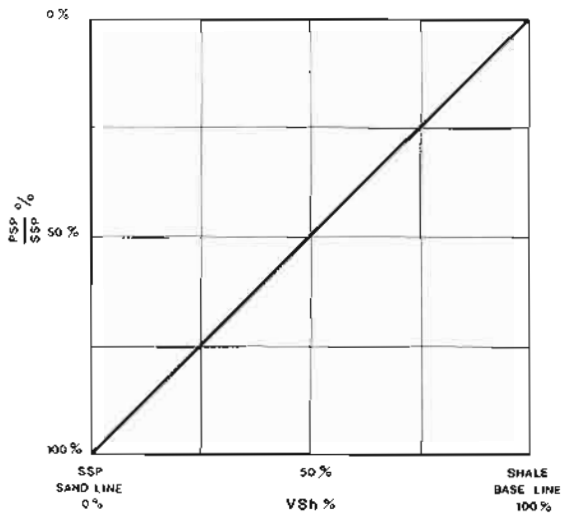


**Figure 5.12** Graph of the clay volume-SP relationship. The shale baseline represents 100% shale and the SSP 0% shale. The relative deflection then depends on the clay volume as shown by the graph.

*Shale volume from SP (Pseudo-static SP)*
It is considered that the volume of shale $V_{sh}$ in a water-wet, shaly sandstone can be simply calculated using the SP as follows:

$$VV_{sh}(\%) = \left(1 - \frac{PSP}{SSP}\right) \times 100$$

PSP = pseudo-static spontaneous potential = the SP read in the water-bearing *shaly sand* zone.
SSP = static spontaneous potential = maximum SP value in a *clean sand* zone.

This simply assumes that the SP deflection between the shale base line (100% shale) and the static SP in a clean sand (0% shale) is proportional to the shale volume (Figure 5.12). This relationship is certainly true qualitatively, but quantitatively there is no theoretical basis. The SP-derived $V_{sh}$ is probably over-estimated.

## 5.5 Qualitative uses

*Permeability recognition*
If there is even a slight deflection on the SP, the bed opposite the deflection is permeable. All deflections (with some rare exceptions) on the SP indicate, the *priori*, a permeable bed. The amount of deflection, however, does not indicate the amount of permeability: a very slightly permeable bed will give the same value as a permeable bed (other values being equal).

Naturally, the reverse is not true; not all permeable beds give an SP deflection, although these cases are rare (Figure 5.10).

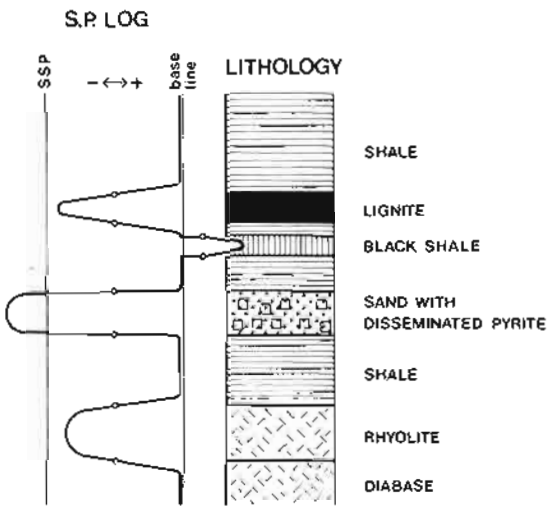


**Figure 5.13** Identification of some minerals and lithologies using the SP curve. The log is idealized. (Redrawn from Pirson, 1963).

***Mineral identification***

The rare exceptions when the SP will deflect and the formation is not permeable are due to mineralizations. Pyrite is an example (Figure 5.13). It is also possible that the SP reacts to excessively reduced and excessively oxidized beds (shales or sandstones) which are not in subsurface electrical equilibrium (Hallenburg, 1978). However, coals, which are extremely reduced, give a large negative SP deflection (Figure 5.13) or no deflection at all, although the reasons are obscure. The SP should be used with caution for mineral or redox identification – other logs are much more diagnostic.

***Facies***

When it was introduced the SP was to become one of the first logs to permit correlation in sand-shale sequences, principally because certain intervals had typical log shapes. This shape, in sand-shale sequences, is related to shale abundance, the full SP occurring over clean intervals, a diminished SP over shaly zones. The relationship is considered linear as discussed. In so far as shaliness is related to grain size, the SP is a good facies indicator. The example (Figure 5.14) shows a well-marked channel sand; the coarse-grained base is clean while the finer-grained top is shaly. The SP is, therefore, following grain-size change (*see also* Chapter 14).

The SP has now been largely replaced by the gamma ray log for facies identification: the gamma ray log has more character and is more repeatable (Figure 5.6).

***Correlation***

Previously, the SP log was one of those used for correlation but, for the reasons given above, has now been replaced especially by the gamma ray log. The SP is still useful for correlation, however, in areas of varied water salinities. If wells are quite close (and drilling mud fluids are similar), correlation should only be made between sands with similar salinity values (Figure 5.15). For this the SP is the only log that can be used as a guide.

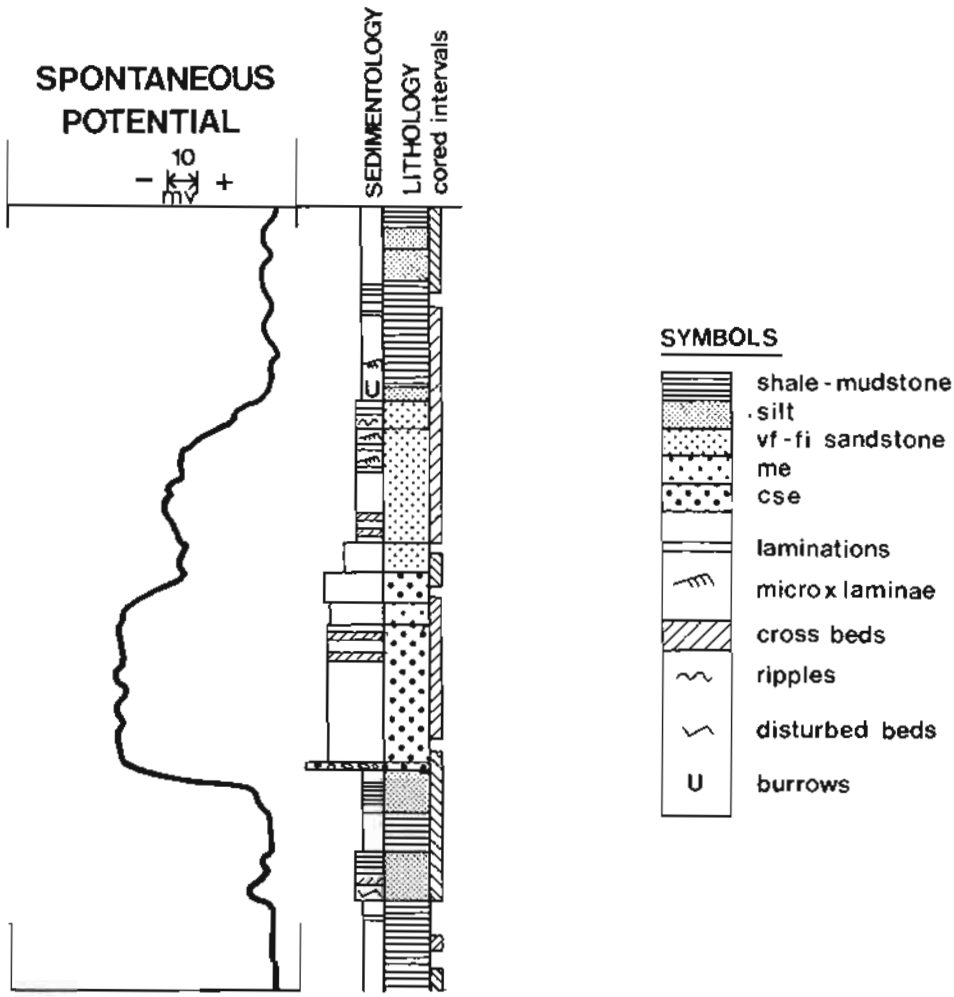


**Figure 5.14** Facies identification using the SP log. A typical fining-upwards, channel sandstone giving a bell-shaped SP curve. From the Carboniferous, UK. (After Hawkins, 1972).

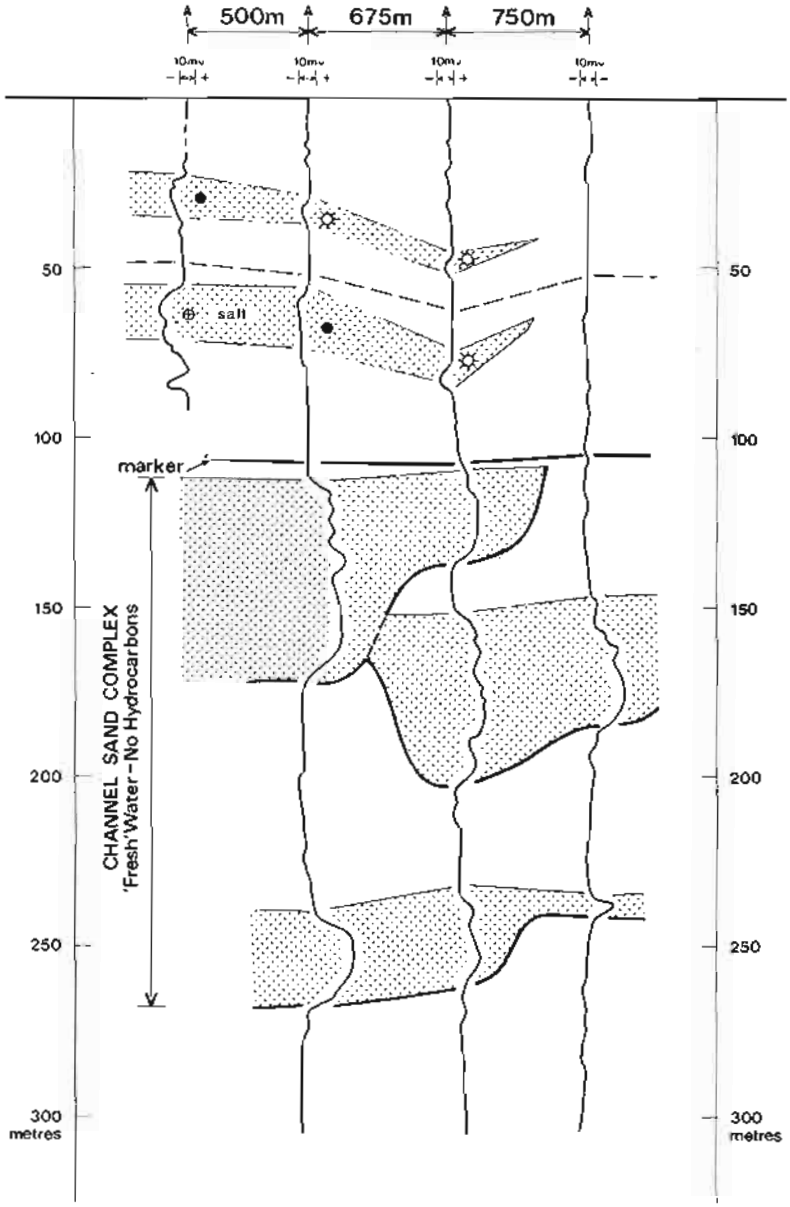


**Figure 5.15** Correlation using the SP log. Changes in water salinity indicate which sand bodies can be correlated. Drilling-mud filtrate is similar in all wells.

# 6
# RESISTIVITY AND CONDUCTIVITY LOGS

## 6.1 Generalities

***The log***

Of all the logging tools, those that measure resistivity are archetypal. It was with resistivity measurements that Conrad Schlumberger started his company in 1919.

The resistivity log is a measurement of a formation's *resistivity*, that is its resistance to the passage of an electric current. It is measured by *resistivity tools*. Conductivity tools measure a formation's *conductivity* or its ability to conduct an electric current. It is measured by the *induction tools*. Conductivity is generally converted directly and plotted as resistivity on log plots.

Most rock materials are essentially insulators, while their enclosed fluids are conductors. Hydrocarbons are the exception to fluid conductivity, and on the contrary, they are infinitely resistive. When a formation is porous and contains salty water the overall resistivity will be low. When this same formation contains hydrocarbons, its resistivity will be very high. It is this character that is exploited by the resistivity logs: high resistivity values may indicate a porous, hydrocarbon-bearing formation (Figure 6.1).

***Principal uses***

The resistivity logs were developed to find hydro-

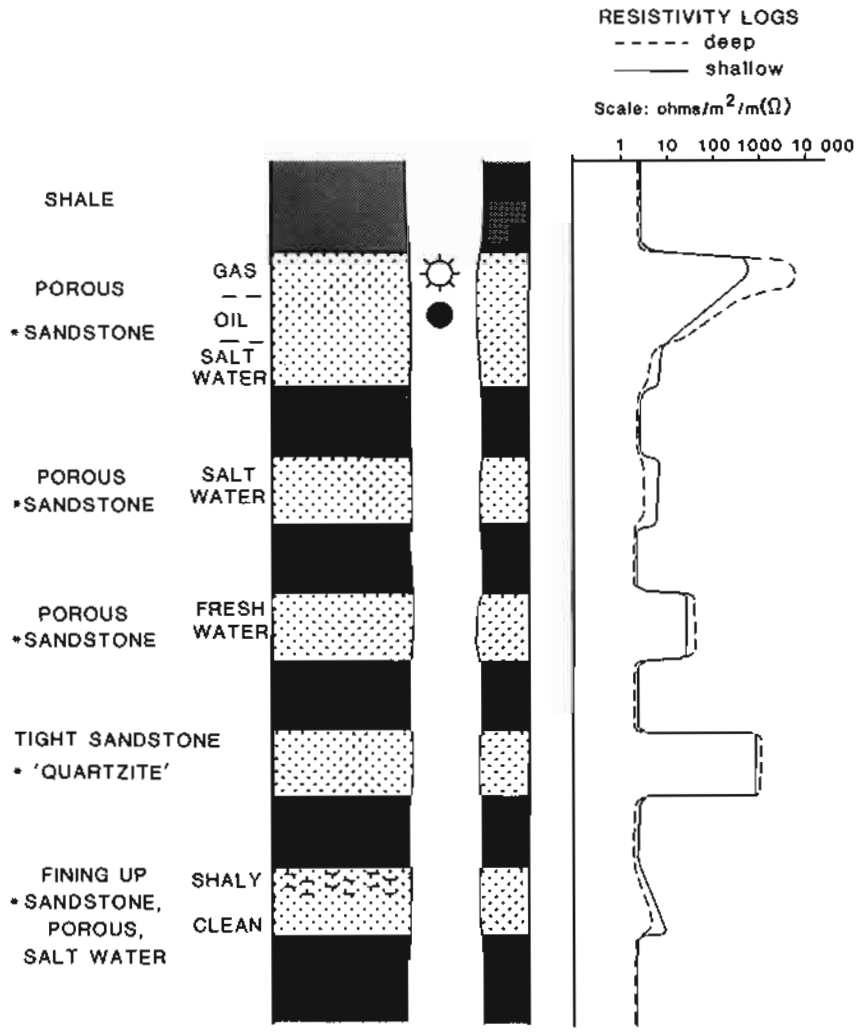


**Figure 6.1** The resistivity log: some typical responses. The resistivity log shows the effect of the formation and its contained fluids on the passage of an electric current. *Limestone, dolomite, etc., equally applicable.

carbons. This is still their principal quantitative use: resistivity logs furnish the basic numbers for petrophysical calculations. However, a formation's resistivity is one of its typical geophysical characteristics and as such can contribute information on lithology, texture, facies, overpressure and source rock aspects.

The log is used frequently for correlation (Table 6.1).

***Limitations***

Resistivity tools (Section 6.4) can only function in boreholes containing conductive muds, that is muds mixed with salt water. They cannot be run in oil-based muds or freshwater based muds. Induction logs (Section 6.5), on the contrary, are most effective with non-conductive muds, oil-based or fresh water based. However, induction logs are also run in salt water based muds and are reasonably effective, although corrections to the raw readings may be necessary for quantitative use (Table 6.8).

## 6.2 Theoretical considerations

***Earth resistivity and conductivity***

The laws which govern electrical resistance in a wired circuit apply also to currents flowing in the earth. Resistance (in ohms) is the electrical term, while *resistivity* is the logger's term. *Resistivity* is in units of ohms $m^2/m$, being the resistance with normalized dimensions.

Two tests can be applied under subsurface conditions to measure resistivity. The first test is a direct measurement. A current is passed between two electrodes on a logging tool and the potential drop between them provides the resistivity. The second test is indirect in that it measures conductivity. A current is induced in the formation around the borehole and the capacity to carry the current is observed. This carrying capacity is the conductivity. The resistivity is simply the reciprocal of the conductivity. Thus in oilfield units:

$$\text{resistivity (ohms m}^2\text{/ m)} = \frac{1 \times 1000}{\text{conductivity}} \text{(millimhos/ m)}$$

As previously stated, rock materials are essentially insulators (like all generalities this is a half-truth, and will be modified later). However, normal rocks consist not just of rock materials, but also voids or pores. The pore spaces are principally filled with water, in subsurface

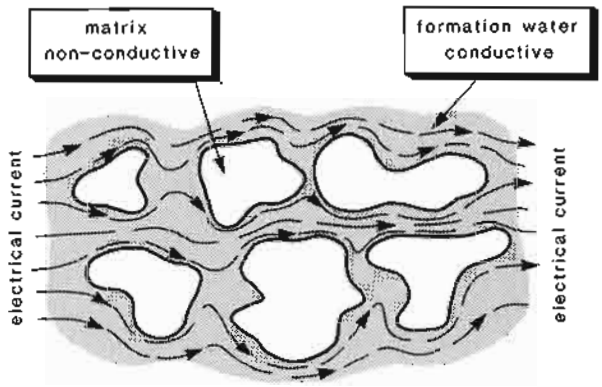


**Figure 6.2** Formation conductivity - schematic. The electrical current is restricted to the formation fluids (formation water): the matrix is non-conductive.

**Table 6.1** The principal uses of the resistivity and conductivity (induction) logs.

| | Discipline | Used for | Knowing |
|---|---|---|---|
| Quantitative | Petrophysics | Fluid saturations:<br>Formation ($S_w$)<br>Invaded zone ($S_{xo}$)<br>i.e. detect hydrocarbons | Formation water resistivity ($R_w$)<br>Mud-filtrate resistivity ($R_{mf}$)<br>Porosity (ø) (and F)<br>Temperature ($T_{fm}$) |
| Semi-quantitative and Qualitative | Geology | Textures | Calibration with laboratory samples |
| | | Lithology | Mineral resistivities |
| | | Correlation | |
| | Sedimentology | Facies,<br>Bedding characteristics | Gross lithologies |
| | Reservoir geology | Compaction,<br>overpressure and<br>shale porosity | Normal pressure trends |
| | Geochemistry | Source rock identification<br>Source rock maturation | Sonic and density log values<br>Formation temperature |

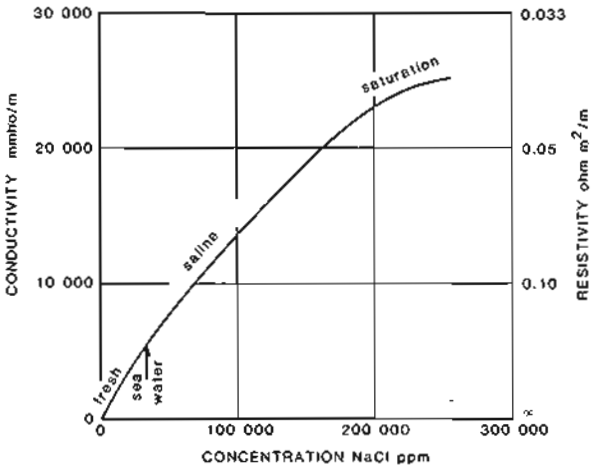


**Figure 6.3** Relationship between conductivity (resistivity) and concentration in a salt (NaCl) solution, at 24°C (75°F), modified from Serra, 1979).

**Table 6.2** Some typical formation-water salinities.

| Origin | Total salinity (ppm) | Type | $R_w$* ohm m²/m |
|---|---|---|---|
| Sea water | 35,000 | | 0.19 |
| Lagunillas, Venezuela | 7548† | Fresh | 0.77 |
| Woodbine, E. Texas | 68,964† | Saline | 0.10 |
| Burgan, Kuwait | 154,388 | Saline | 0.053 |
| Simpson sd., Oklahoma | 298,497† | Very Saline | (0.04)** |

†From Levorsen (1967)
*Approximate $R_w$ (formation-water resistivity) at 24°C (75°F).
**Near the saturation limit.

terms, formation water (pores, of course, may also be filled with oil and natural gas). Conductivity is essentially restricted to formation waters (Figure 6.2). They vary from fresh to very saline: usually they are saline, and the salinity increases with depth (e.g. Dickey, 1969). For oilfield purposes, salinity is usually quoted in NaCl equivalent salinity, although formation-water brines have a variety of dissolved solids. Sea water has an average salinity of 35,000 ppm (parts per million of dissolved solids) while a typical formation brine may have a salinity of 200,000 ppm (Table 6.2). Other factors remaining constant, the more saline a solution the greater the conductivity, the electric current being carried by dissociated ions, e.g., $Na^+$, $Cl^-$ in a salt solution. The same formation containing fresh water shows a far lower conductivity (higher resistivity) than if it contained salt water (Figure 6.3).

It is often necessary to consider the resistivity of a formation water *per se*, that is its resistivity as a solution. The symbol used is $R_w$ (resistivity of water) (Table 6.2).

***Rock resistivity – formation resistivity factor 'F'***

If, as suggested above, it is only the formation waters that are conductive, the conductivity of the rock in general should be that of the solution it contains. But it is not. Although the rock plays no active part, it plays an important passive one (Figure 6.2). This passive role is basically dependent on rock texture or more specifically on the geometry of the pores and pore connections (Figure 6.4). A good analogy is that of a comparison between conventional roads and motorways. Vehicles will travel far more quickly and in greater volume between two towns along a wide straight motorway than along a narrow twisting conventional road. Thus, in rocks, the easier the path through the pores the more current that passes. The expression of this passive behaviour of a rock is called the *Formation Resistivity Factor*, usually abbreviated to $F$ (sometimes $FF$). When the passive role of the rock is small, $F$ is small: when the rock has a large inhibiting effect, $F$ is large (Figure 6.4).

To understand $F$ better it is useful to examine the influence porosity has upon it. In any one rock formation, $F$ and porosity can show a consistent relationship (Figure 6.5). However, as indicated, porosity is not the only influence on $F$, and the $F$ to porosity relationship varies from one rock to another. Laboratory work with artificial mixtures shows that in any grain population with similarly shaped grains, the $F$ – porosity changes are mathematically

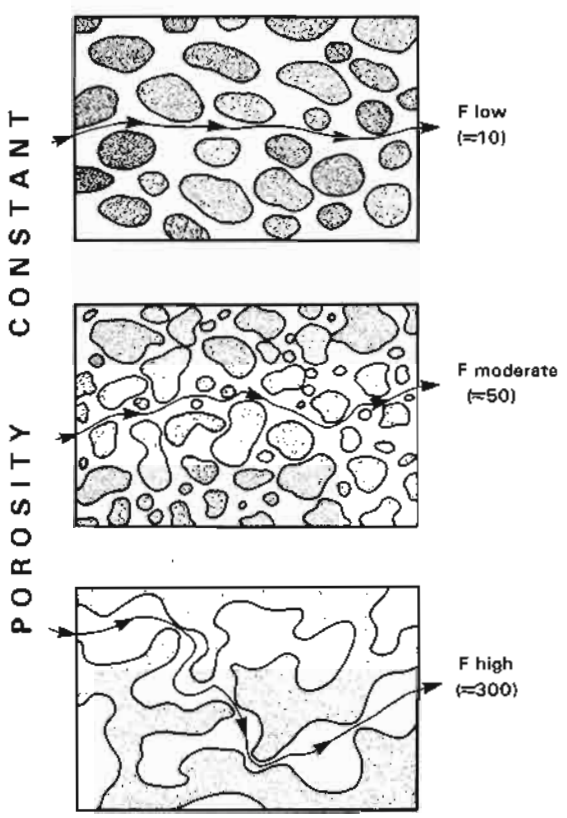


**Figure 6.4** Schematic illustration of three formations which have the same porosity but different values of formation resistivity factor, $F$. The role of the matrix is evident: less at low values of $F$ (top), greater at high values of $F$ (bottom).

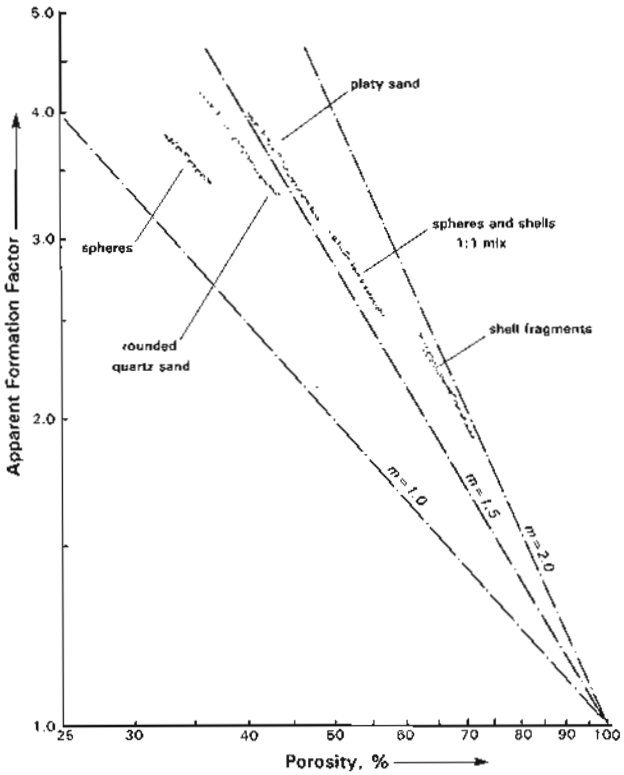


**Figure 6.5** Graph of formation resistivity factor, *F* and porosity showing their relationship to grain shape (texture) illustrated by analyses of laboratory samples. A predictable relationship between *F* and porosity only exists for one type of grain population m = cementation factor (re-drawn from Jackson *et al.*, 1978).

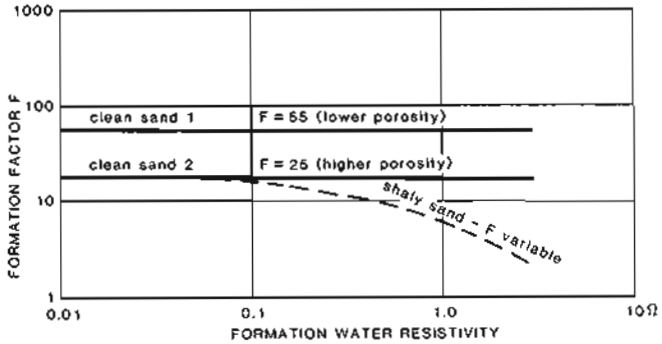


**Figure 6.6** The effect of changes in formation-water resistivity on *F* (formation resistivity factor). *F* will not change with different water salinities in a clean formation. In a shaly formation *F* will constantly change (schematic).

predictable (follow Archie's law, Section 6.7) (Jackson *et al.*, 1978). But, when grain shape is changed, the relationship changes, although still in a predictable way (Figure 6.5). *F* is therefore strongly influenced by grain shape, (theoretically because of changes in pore throat geometry). However, in geological terms, grain shape is an element of texture, along with other factors such as size and arrangement (sorting). Geologically then, *F* becomes a texturally related term, an aspect which will be considered in more detail when the geological applications of resistivity logs are considered (Section 6.8).

For petrophysical purposes, it is necessary to quantify the relationship between *F* and porosity (porosity being measurable by other logs). Fundamental work by Gus Archie established an empirical relationship (Archie, 1942), which has been confirmed by subsequent work (e.g. Figure 6.5). However, as indicated above, the relationship varies with each population of grains and to establish a universally applicable relationship has proved elusive (e.g., Winsauer and McCardell, 1953; Maute, 1992). Presently available formulae give only a good estimate (*see* 'Basic equations of petrophysics' Section 6.7).

*F* is usually between 5 and 500, the higher numbers indicating a greater effect due to the formation. Good porous sandstones will have an *F* value around 10, while a poorly permeable limestone may have a value around 300–400. *F* is dimensionless (Figure 6.4).

*F* is an independent element in the expression of rock resistivity. The F value of a particular rock reservoir will remain constant no matter what the resistivity of the fluid filling the pores. In other words, *F* will not vary with changes in formation-water salinity which entail overall rock resistivity changes (Figure 6.6). The *F* value is therefore constant between the reservoir containing oil and the same reservoir containing water. This behaviour can be expressed mathematically:

$$R_o = F \times R_w$$

That is, *F* is the ratio of the formation resistivity to the resistivity of the fluid which it contains. Hence when porosity is 100% (impossible) *F* is 1 (Figure 6.5). This is the basic relationship which is used in all calculations involving the resistivity measured by well logs (Section 6.7).

***Resistivity (conductivity) of clays***

Discussion thus far suggests that rock resistivity (or conductivity) is only a function of the active part played by a conductive formation water (resistivity $R_w$) and the apparently passive part played by the rock skeleton *(F)*. However, the part played by the rock skeleton is not always passive. When shale is present it plays an active role in conductivity and F is no longer constant (Figure 6.6).

Clays conduct electricity in two ways, through pore water and through the clay itself. The porosity in clay, like that in other rocks, encloses conductive formation water. This may be up to 80% in newly-deposited clays but diminishes rapidly through compaction (*see* 'Compaction, over-pressure and shale porosity', Section 6.8 ). Conductivity in the clay mass itself is more complex.

Clay consists of stacked silicate layers which, in the presence of water, become negatively charged. Clay may in fact be considered to act like a salt, dissociating into an immobile, negatively-charged framework and positive,

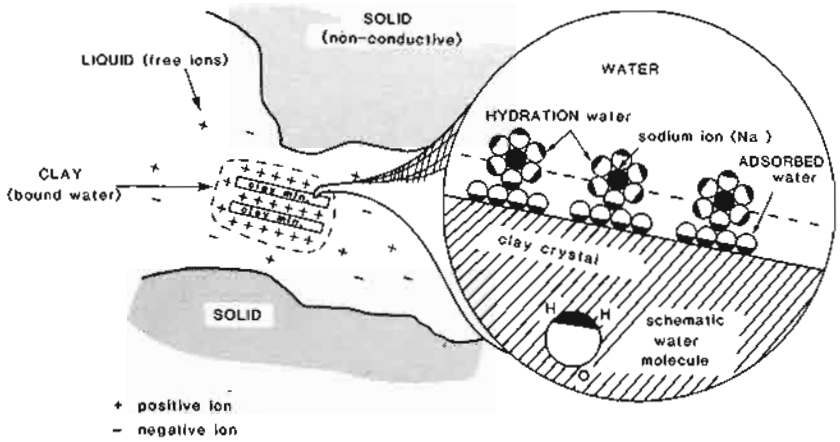


**Figure 6.7** Models of the conductivity capacity of clay minerals. (Modified from Wyllie, 1963; detail Clavier *et al.*, 1977).

current-conducting ions (Wyllie, 1963). However, it is only at the surface of clay-mineral layers that the dissociation occurs and a current is able to be carried (Figure 6.7). Clay is like an inverted electric cable; the inside is non-conductive while the outside conducts electricity. The outside conducting layer is complex; adsorbed water clings to the immediate clay layer and the positive ions ($Na^+$ in a salt solution) surrounded by hydration water form a further, outer layer (Clavier *et al.*, 1977) (Figure 6.7). The external water, called 'bound water', is chemically free but physically bound.

The capacity of clays to conduct electricity varies between clay species and seems to depend on the surface area available in the clay. An independent expression, but one related to the surface area (which is difficult to measure), is the cation exchange capacity or CEC (Patchett, 1975). This is simply the ability of the clay to exchange cations, expressed per unit weight of clay and is measured chemically. The surface area-CEC relation suggests that the number of exchangeable ions per unit surface remains constant whatever the type of clay (Patchett, *op. cit.*). This means, as indicated, that differences between the conductivity of clay species should be related to surface area. Geologically this is of interest, since montmorillonite has a far greater specific surface area than the other clays and is therefore more conductive (Table 6.3).

The conductivity behaviour of clays in clay-sand mixtures (shaly-sands) is complex. Because of the bound water, the conductivity of clays is to some extent dependent on the surrounding formation fluid. As a general rule, the higher the resistivity of the formation fluids, the greater the current carried by the shale: that is, the greater the shale effect on $F$ (it diminishes, Figure 6.6). Importantly, in oil zones where the formation fluids have very high resistivities, the clays are conductive: resistivities in oil-saturated shaly-sands may be quite low. This is the reason for the petrophysicists' interest in shaly-sands.

**Table 6.3** Clay mineral properties (from Dewan, 1983)

| Clay mineral | CEC (meq/g) | Av. CEC |
|---|---|---|
| Smectite | 0.8 -1.5 | 1.00 |
| Illite | 0.1 -0.4 | 0.25 |
| Chlorite | 0.0 -0.1 | 0.04 |
| Kaolinite | 0.03-0.06 | 0.04 |

Without entering into the details of the shaly-sand problem, it is worth concluding by quoting from a review article by an experienced petrophysicist from a major company; it sums up the industry view of the shaly-sand question at present and for the foreseeable future (Maute, 1992):

*'More than 50 different shaly-sand equations, frequently empirical variations of Archie's equation, exist. No equation is definitive or universally accepted. Some equations work well in local regions. Shaly-sand interpretation is an important unsolved problem in petrophysics. One point that has emerged in recent years, is that knowing the shale volume and shale conductivity is not enough; the distribution of shale in the formation is also important'.*

So that even for shaly-sands it comes back to a question of texture again. (For details on shaly-sands *see* SPWLA, 1982, or for a discussion, Dewan, 1983).

***Conclusions: earth resistivity***

The conductivity of a rock is due to interstitial pore waters (formation waters) which contain dissociated, current-carrying salts. The rock skeleton is a non-conductor but plays an inhibiting role expressed quantitatively by $R_o = F \times R_w$. In mixtures of clay and non-conducting materials, conductivity is afforded by the formation water but also by the clay itself.

## 6.3 Zones of invasion and resistivity

The notion of invasion has already been described (Chapter 2) and it is all-important to the understanding of borehole resistivity. The essential target of resistivity logging is that of the true resistivity of the formation ($R_t$) and, especially, its saturation in hydrocarbons. To this

**Table 6.4** Resistivity notation.

| Zone | Formation resistivity (tool measured) | Fluid resistivity (laboratory measured and/ or log calculated) | Fluid saturation |
|---|---|---|---|
| Hole | $R_m$ (m = mud) | $R_m$ | |
| Mud cake | $R_{mc}$ (mc = mud cake) | $R_{mc}$ | |
| Flushed zone | $R_{xo}$ | $R_{mf}$ (mf = mud filtrate) | $S_{xo}$ (saturation in mud filtrate) |
| Invaded zone (transition) | $R_i$ (i = invaded) | $R_z$ ($R_{mf}$ + $R_w$ mixed) | |
| Uninvaded zone | $*R_t$ (t = true) | $R_w$ (w = formation water)<br>$R_o$ (o = original) | $S_w$ (saturation in formation water |

$*R_t$ = true, uninvaded formation resistivity of rock which may contain hydrocarbons – *tool measured.*
$R_o$ = Original, uninvaded formation resistivity of rock with 100% formation water saturation. Cannot be tool measured. It is an ideal figure for calculations. In *clean 100% water-saturated zones* $R_t = R_o$ (or is very close).

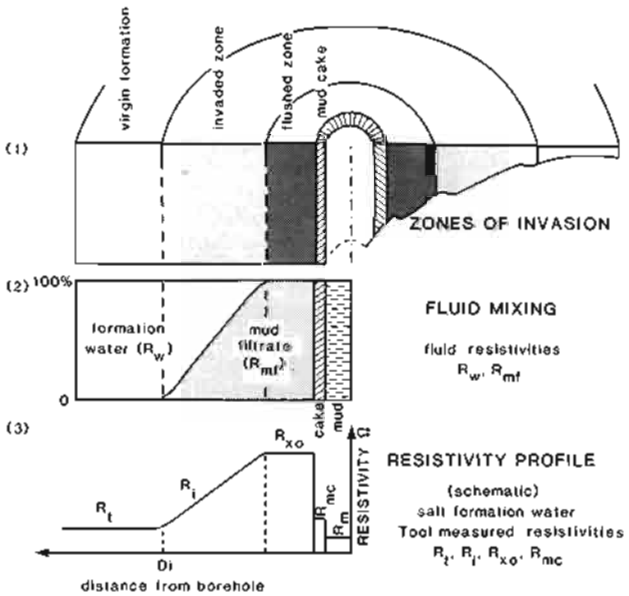


**Figure 6.8** (1) Zones of invasion about a borehole; (2) equivalent schematic representations of fluid mixing; (3) resistivity profile.

effect, it is necessary to consider the invasion of mud filtrate (with a certain salinity and hence resistivity, $R_{mf}$) into a formation containing either formation water (resistivity $R_w$) or hydrocarbons.

For convenience, the invasion of a porous and permeable bed by mud filtrate is divided into zones (Figure 6.8, *1*). In reality the zones grade one into the other. Closest to the borehole, behind the mud cake, is the flushed zone where the mud filtrate has replaced all but a small volume of the original, in-place fluids. Gradually, further and further away from the hole, the volume of invading mud filtrate becomes less and less until only original formation fluids are found (Figure 6.8,*2*). This is the transition or invaded zone which gives way to the uninvaded, virgin formation.

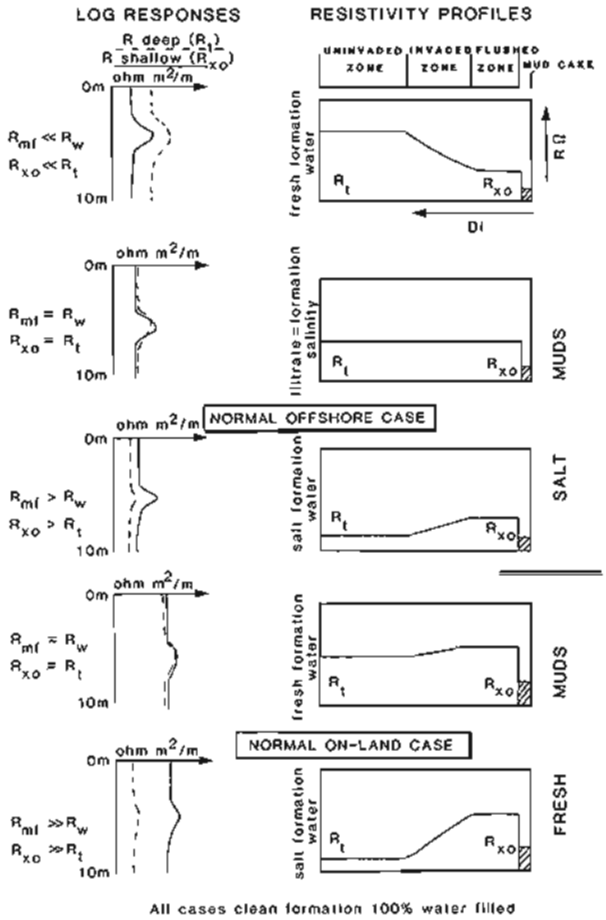


**Figure 6.9** Schematic log response and resistivity profiles for water-bearing reservoir considering various cases of mud resistivity and formation-water resistivity. For symbols *see* Table 6.4 (*see also* Table 6.5).

The regular change in fluids away from the borehole gives rise to a parallel change in the resistivity of the formation as a function of the distance away from the borehole. The resistivity variations can be conveniently

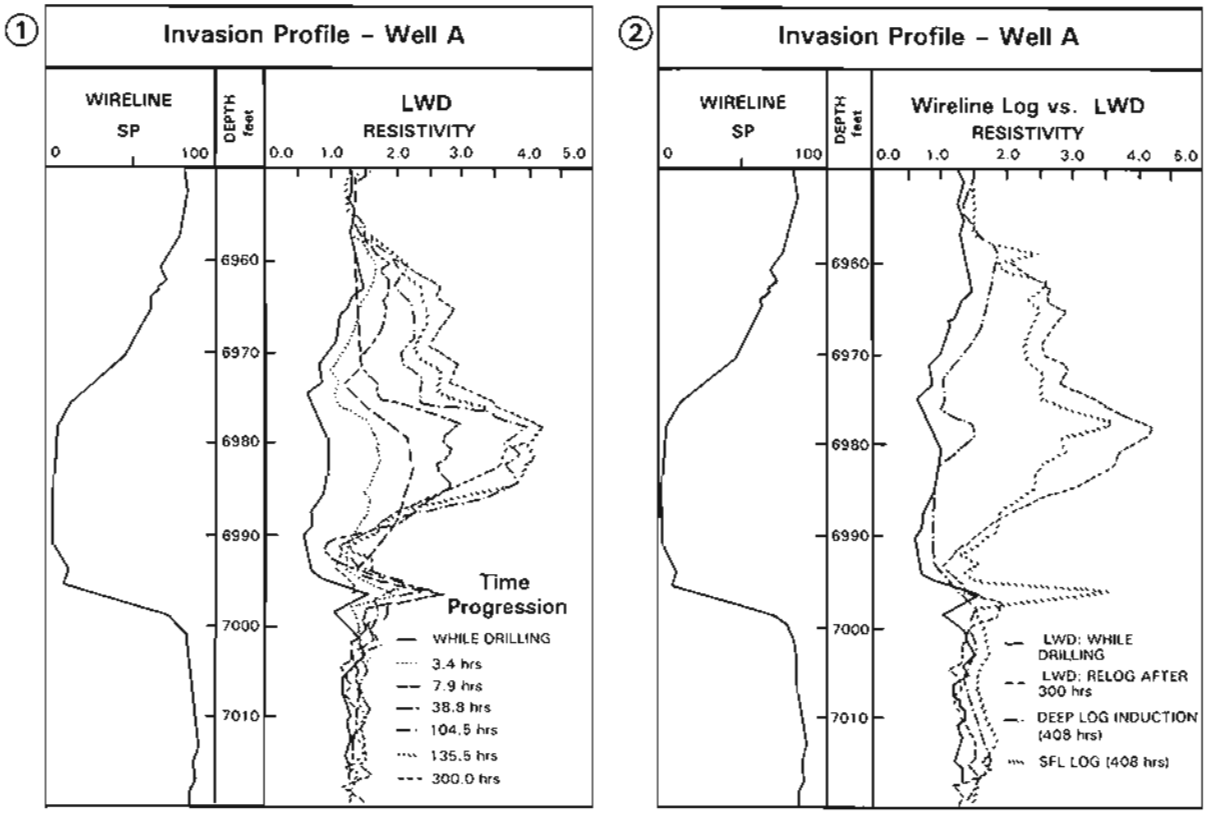


**Figure 6.10** Progressive formation invasion demonstrated by LWD and wireline resistivity logs run over a porous, salt water bearing sandstone interval.
*1.* LWD resistivity logs measured repeatedly over the interval from 3.4 hrs after drilling to 12.5 days (300 hrs). *2.* LWD logs (first and last) compared to wireline resistivity logs run 17 days (408 hrs) after drilling. The deep induction wireline measurement compares with the first LWD measurement (no invasion, Rt), the shallow wireline SFL measurement compares with the final LWD measurement (flushed zone, Rxo) (from Cobern and Nuckols, 1985).

depicted by a graph of resistivity against distance from the borehole at a constant depth (Figure 6.8,*3*). The variations are due entirely to changes in fluid content, it being the same rock formation (thus $F$ is constant).

This effect can be 'brought to life' by comparing LWD resistivity measurements, made before significant invasion takes place, with wireline resistivities made when invasion is near its maximum. The example, of a saltwater bearing sandstone (Figure 6.10, *1*), shows LWD measurements, one taken immediately during drilling and a series at intervals over the next 300 hours (12.5 days). The resistivity progressively increases for the first 104.5 hours (4.3 days) as invasion increases, the invading fluid having a higher resistivity than the in-place, salty formation water. After 4.3 days the invasion stabilises and logs taken over the next 8 days are similar (Figure 6.10, *1*) (Cobern and Nuckols, 1985). For comparison, wireline logging took place 17 days after drilling (407 hours). The wireline resistivity representing the flushed zone (the SFL) is similar to the stabilised LWD log (maximum invasion), while the wireline log representing the virgin formation (deep induction) is similar to the first LWD log measured before any invasion (i.e. when the reservoir contained salt water). It is truly with such a set of logs that invasion can be monitored (it takes a surprisingly long time in this case) and the depth of investigation characteristics of the resistivity tools empirically evaluated.

The zones of invasion, associated fluid resistivities and corresponding zone resistivities all have accepted notations (Table 6.4). These will be used henceforth.

***Resistivity profile variations***

Since the variations in resistivity about a borehole are due to the mixing of two fluids, mud filtrate and formation fluid, it is as well to know their average characteristics. Formation-water characteristics have already been described (Chapter 2). Essentially, three types of mud are used; saltwater mud, freshwater mud and, in certain cases, oil-based mud. The different resistivity regimes caused by the combinations of muds and formation waters are shown in Table 6.5 and Figure 6.9. When interpreting the resistivity logs, care should be taken to note the fluids used in the borehole and their characteristics. They appear on the log heading.

**Table 6.5** Variations in filtrate and formation-water resistivity values, as read by resistivity tools (*see also* Figure 6.9).

| | Formation-water salinity | | |
|---|---|---|---|
| | Fresh formation water | Formation-water salinity = filtrate salinity | Saline formation water |
| Saltwater mud (usual offshore) | $R_{mf} < R_w$ | $R_{mf} = R_w$ | $R_{mf} \geqslant R_w$ |
| Freshwater mud | $R_{mf} \geqslant R_w$ | $R_{mf} \gg R_w$ | $R_{mf} > R_w$ |
| Oil-based mud (special cases) | Oil filtrate contamination<br>Only $R_i$ induction is usable | | |

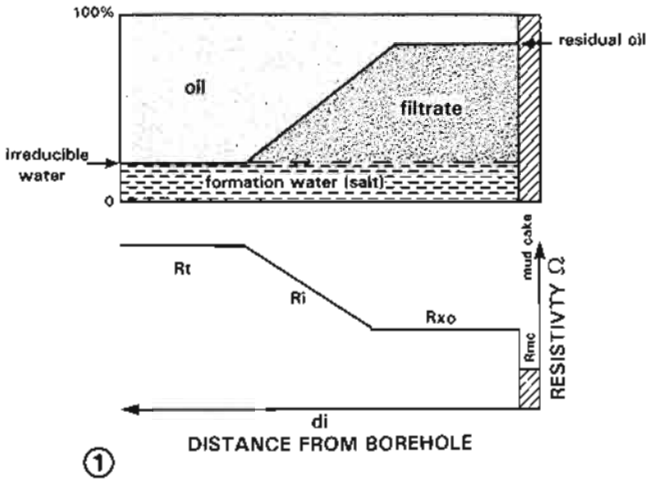


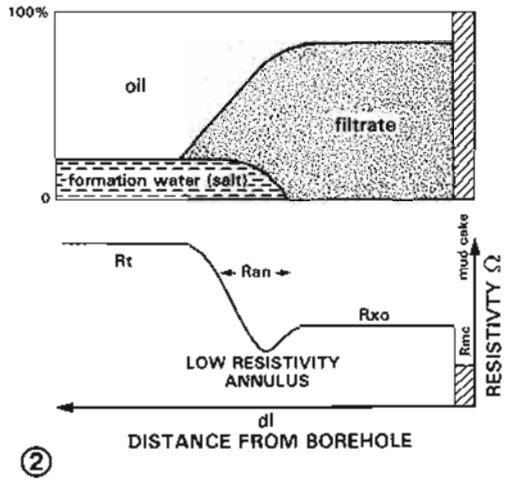


**Figure 6.11** Schematic oil zone resistivity profiles.
1. Simple invasion model. 2. Model with low resistivity annulus. $R_{an}$ = annulus resistivity. For symbols *see* Table 6.4.

### *Oil (hydrocarbon) zone resistivity profiles*

All previous examples have assumed 100% water saturation in the porous and permeable bed, the resistivity variations being due to mud filtrate and formation water mixing, a two phase system of miscible fluids. When hydrocarbons are present, the system becomes three phase and much more complex. The mud filtrate will replace the oil and gas immediately around the borehole, essentially replacing them through the flushed zone, while the original saturation in hydrocarbons is only found in the virgin formation (Figure 6.11,*1*). A resistivity profile across a hydrocarbon zone will show a flushed zone with a moderate to low resistivity, filled with mud filtrate (with resistivity depending on mud type) and the virgin formation with an extremely high resistivity because of the high saturation in hydrocarbons. Both oil and gas are infinitely resistive and show the same effect on resistivity logs. The resistivity profile then, shows a big increase away from the borehole, the exact reverse of a water zone. (Figure 6.11,*1*). This increase in resistivity deeper into the formation, away from the borehole, is expressed very distinctly on the logs. Shallow looking tools which read in the flushed zone show low (relatively) resistivity values, while deep reading tools show very high resistivities (Figure 6.12) The separation between the curves from the shallow and deep tools, plotted on the same resistivity scale, is diagnostic of hydrocarbons. It is sometimes called the *hydrocarbon separation* and is used in the 'quick look' technique for locating oil or gas. A quick look, however, must be verified by calculation since curve separation can be caused by fresh water and many hydrocarbon zones do not give any obvious separation.

In practice, the behaviour of fluids in a drill encountered hydrocarbon zone is not simple. Theoretically there is a differential rate of flushing of formation water and of oil or gas by the mud filtrate. This is supposed to create a zone where there is a high volume of formation water with only residual hydrocarbons, the so-called low

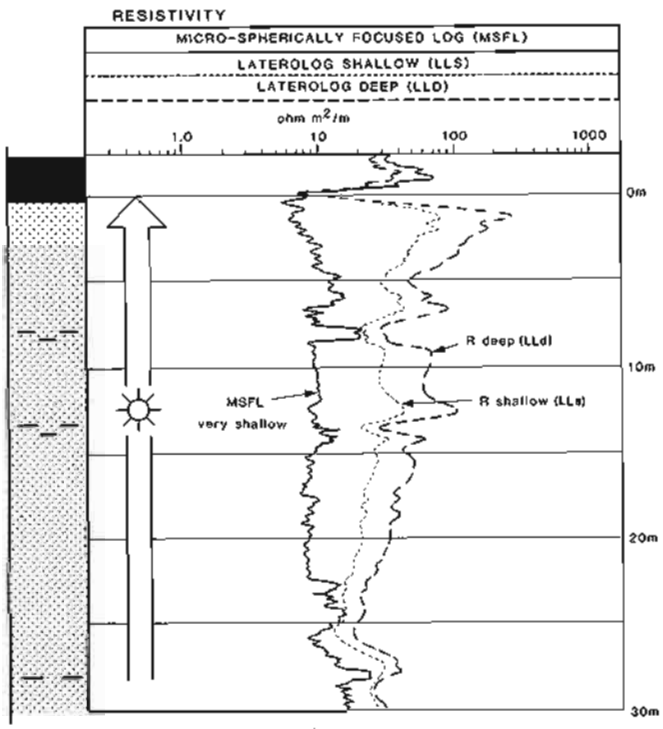


**Figure 6.12** Strong separation of resistivity logs in a gas zone. Porosity is around 15%.

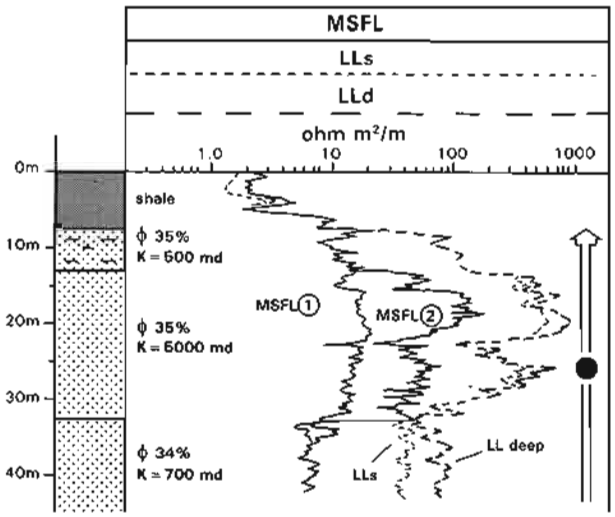


**Figure 6.13** Active fluid movement during logging shown by a comparison between a main run and 'repeat' section. MSFL 1, the 'repeat' section, was run 1.5 hours before MSFL 2, the main run. The comparison shows that hydrocarbons are re-migrating into the flushed zone, measured by the MSFL, over the extremely permeable section (*see* text for explanation).

resistivity annulus on the outer fringe of the flushed zone (Figure 6.11,2). Doubt was always cast on the stability of such a zone, even if it was created (Threadgold, 1971). From the data sets now accumulating from LWD measurements (i.e. Figure 6.10), it is clear that there is considerable fluid movement not only during drilling when invasion occurs, but also when drilling ceases. The fluid equilibrium which existed before drilling attempts to re-establish itself, especially in gas filled reservoirs or those with very high permeabilities. The example (Figure 6.13) shows a highly permeable reservoir containing oil found in an offshore well drilled with a saltwater mud and logged by a resistivity tool combination of shallow, medium and deep devices (DLL-MSFL of Schlumberger). A 'repeat' run of the tool was made and completed 1.5 hours before the same interval was logged during the main run. In that 1.5 hours, the re-migration of the hydrocarbons back towards the well was taking place. This is shown by the increasing flushed zone resistivity (MSFL) over the central part of the reservoir. The two deep logs (LLd and LLs) are unchanged as is the shallow reading (MSFL) in the upper and lower reservoir zones (Figure 6.13). In this case, no doubt, the re-migration of the hydrocarbons was helped by the huge permeability of 5000 mD in the affected reservoir. However, hydrocarbon movement after drilling is nicely demonstrated.

### *Oil-based mud resistivity profiles*

Many modern wells are now drilled with oil-based mud. It helps stop water loss, is a good lubricant and often reduces drilling time considerably. Clearly, the invasion behaviour of an oil filtrate is quite different from a water filtrate. The oil filtrate will mix with the hydrocarbons in a hydrocarbon zone while the water filtrate will be immiscible: the water filtrate will mix with the formation water

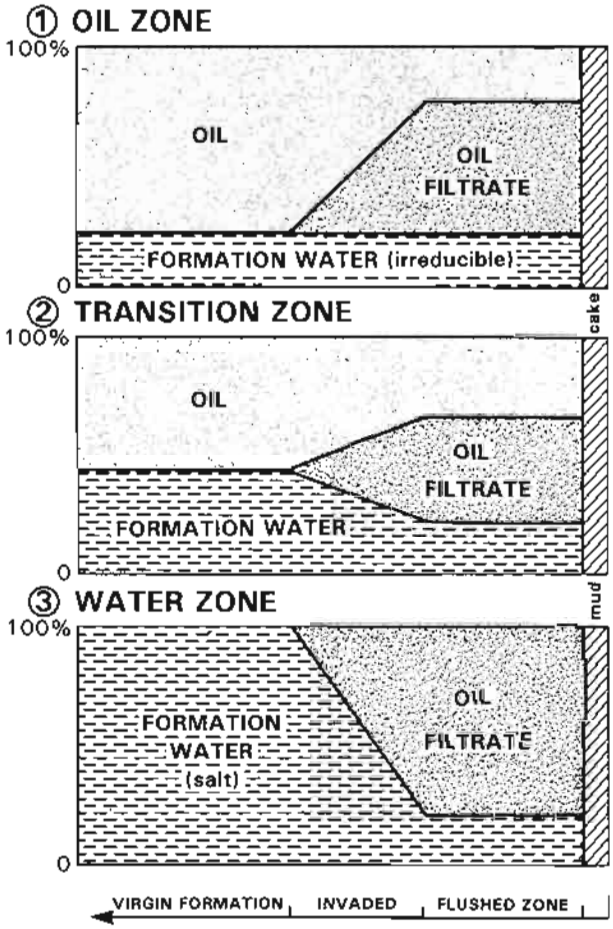


**Figure 6.14** Fluid mixing in a well drilled with oil-based mud. *1.* Oil zone. *2.* Transition zone. *3.* Water zone. (Modified after Boyeldieu *et al.*, 1984).

in a water zone while it is the oil filtrate which will be immiscible (Figure 6.14). Thus, in an oil zone the effects of invasion will be difficult to identify while high resistivities will be present close to the borehole in water zones.

As will be discussed below, boreholes in which oil-based muds are used cannot be logged with the standard resistivity tools: only induction devices are effective. It is only recently, with the modern array induction tools (*see* Section 6.5, Induction tools) that the invasion behaviour of oil-based muds can be monitored by logs.

## 6.4 Resistivity tools

### *Standard tools*

The basic circuitry of the resistivity tools was established by Conrad Schlumberger in 1927. He passed a current between two electrodes in the earth and measured the potential drop between two other electrodes. Modern tools are considerably more complex than this, especially because emitted currents are 'focused' by contiguous guard currents (Figures 6.15, 6.16). Focused currents are less prone to borehole effects and can be directed at required areas of the formation.

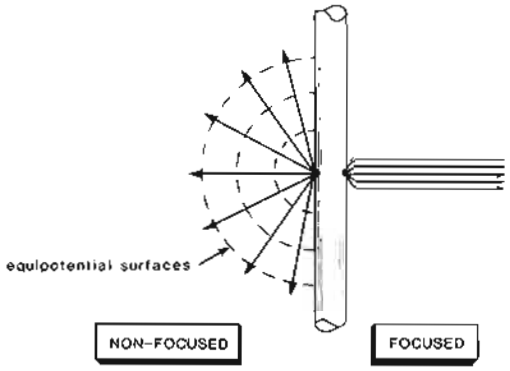


**Figure 6.15** Schematic drawing of focused and non-focused electrical current distribution about a logging tool. The old Electrical Survey tools were not focused: modern Laterologs are focused.

Resistivity tools exist with diverse capabilities as a result of the need to measure formation resistivity from anywhere between the immediate vicinity of the borehole wall and the flushed zone, to the distant, uninvaded formation (Figure 6.18). The deeper looking devices are hole-centred (Figure 6.16) while the shallow investigating devices, like the microlog, are mounted on a pad pressed against the borehole wall (Table 6.6, Figure 6.17). It should be noted here that in the literature, measured depth of investigation usually refers to the detection of 50% of the emitted signal.

In the modern logging suite, the focused laterologs are the deepest 'looking' and most likely to give the virgin formation resistivity, $R_t$. Slightly shallower, invaded zone resistivities, $R_i$, are measured by shallow focused laterologs and body mounted devices such as the SFL. All

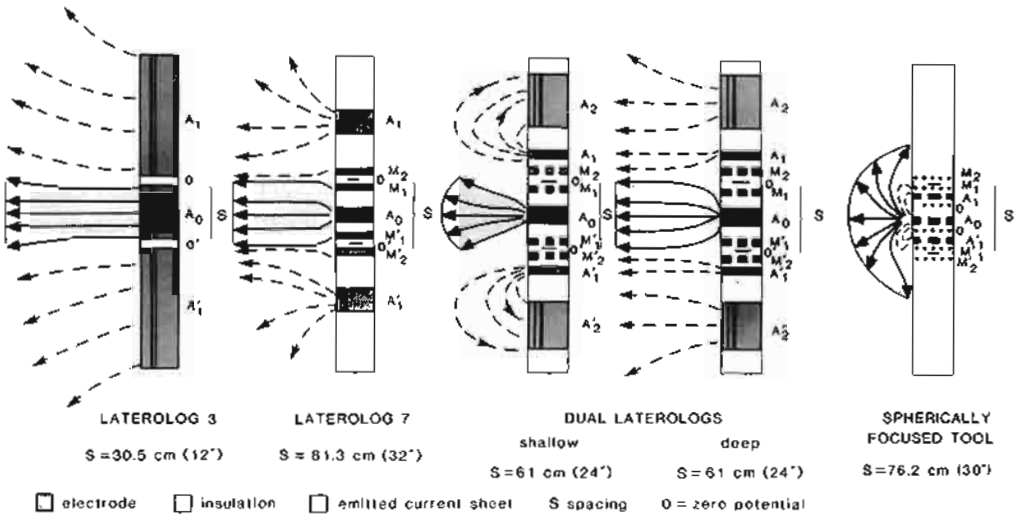


**Figure 6.16** Schematic electrode disposition in several body mounted, focused resistivity tools from Schlumberger. A = electrode, M = monitoring electrode. (From Schlumberger, re-drawn).

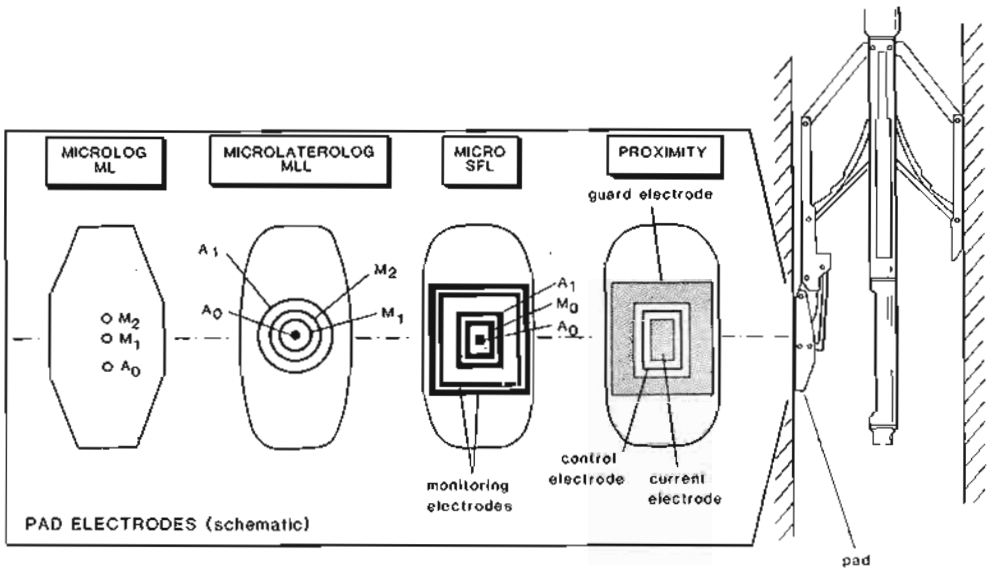


**Figure 6.17** Schematic drawings of electrode dispositions on pad-type resistivity tools. One tool (MSFL) is shown in the hole. SFL = spherically focused log. A, M, electrodes. (Modified from Schlumberger documents).

**Table 6.6** Resistivity (conductivity) measuring tools (*see also* Figures, 6.14, 6.17 and symbols in Table 6.4).

| | Tool | | Symbol | Resistivity |
|---|---|---|---|---|
| Pad tool | †Micro-log | normal | ML2" | $R_{mc} + R_{xo}$ |
| | | inverse | ML1" × 1" | |
| | Micro-laterolog | | MLL | $R_{xo}(+ R_{mc})$ |
| | Proximity log | | PL | $R_{xo} + R_i$ |
| | *Micro-spherically focused log | | MSFL | $R_{xo}$ |
| Hole centred | *Spherically focused log | | SFL | $R_t$ |
| | Laterolog | shallow | LLs | $R_i$ |
| | | deep | LLd | $R_t$ |
| | Induction log | medium | ILm | $R_i - R_t$ |
| | | deep | ILd | $R_t$ |
| | Array Induction | shallow to deep | | $R_i - R_t$ (profile) |

†Minilog – Dresser
*Schlumberger

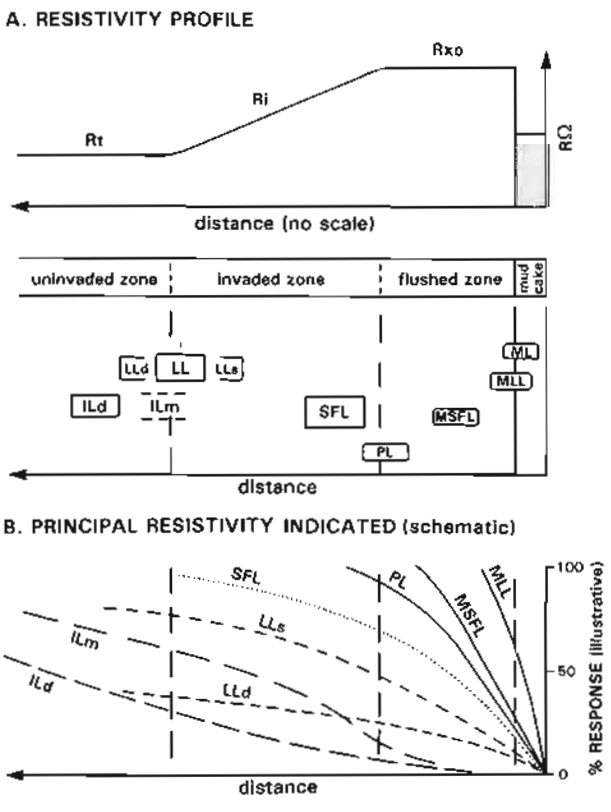


**Figure 6.18** The type of resistivity measured by the various tools (after Schlumberger). IL = induction log, deep-medium; LL = laterologs, deep-shallow; SFL = spherically focused log; MSFL = micro-spherically focused log; PL = proximity log; MLL = microlaterolog; ML = microlog.

these tools are best used in holes drilled with conductive (salt) muds. (*see* Section 6.6). Of the very shallow 'looking', pad mounted devices, the Micro-spherically focused log of Schlumberger (MSFL) or equivalent from other companies, is the one most frequently used for a good measurement of flushed zone resistivity, $R_{xo}$ (Table 6.6, Figure 6.18). The pad devices can only be run in holes with conductive muds.

***Recent developments***

There has been very little change in the basic, standard 'hardware' of resistivity logging over the last 20 years, such as the laterologs and the microlaterologs. Perhaps the only new departure in this area is the array laterolog of BPB which gives a pad micro-resistivity, intermediate resistivity and conventional shallow and deep resistivities. With four measurements an invasion profile can be built up. There has however been change in the way that the data are presented so that presently profile colour images, and even colour images of simple logs are available.

Considerable new development is occurring in the more specialist fields and the present effort in resistivity logging seems to be centred on such aspects as thin bed deep resistivity evaluation, oriented (directed) resistivity measurements for horizontal drilling (i.e. the Azimuthal Resistivity Imager, ARI of Schlumberger, *see* Chapter 16) and improved signal processing (cf. Maute, 1992). These efforts are directed at petrophysical problems and a geological evaluation of the new tools and processing techniques is continuing.

## 6.5 Induction tools

***Standard tools***

The induction tool was introduced to the industry by Henri Doll of Schlumberger in 1949. It was based on the design of a mine detector. A basic induction tool consists of an emitting coil and a receiving coil separated along the length of the tool by an electrically isolated section (mandrel). A constant amplitude sinusoidal current is applied to the transmitter coil. This creates a magnetic field around the tool which in turn induces eddy currents in the formation, flowing in a circular path around the tool (Figure 6.19). The eddy currents create their own magnetic field and induce an alternating current in the receiver coil. The eddy currents are 90° out of phase with the emitter current and the receiver current a further 90°: the emitter and receiver therefore, show a 180° phase shift. This measured current is the so called *R-signal*. There is also a much stronger current caused by a direct coupling of the emitter and receiver coils which is 90° out of phase with the emitting current: this is the *X-signal*.

The standard modern induction tool, such as the Dual Induction of Schlumberger, was introduced in 1963, although the technology had already existed in separate tools for some time. These dual induction tools consisted of emitting and receiving coils along with a series of paired, reverse wound coils, precisely placed to eliminate

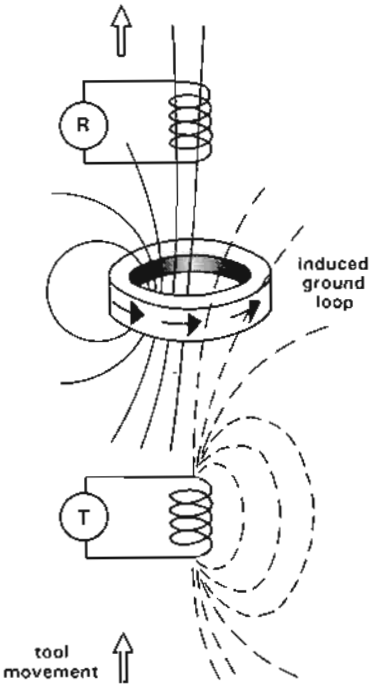


**Figure 6.19** The principle of the simple induction tool. The vertical component of the magnetic field from the transmitting coil, T, induces a ground loop in the formation which in turn is detected by the receiver coil, R (re-drawn, modified from Ellis, 1987).

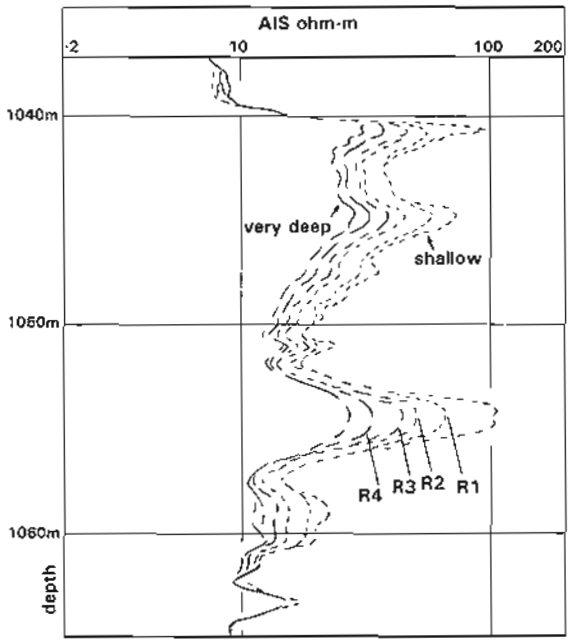


**Figure 6.20** Invasion profile indicated by the BPB AIS, array induction tool in a water-filled limestone drilled with oil-based mud. The 4 raw induction tool readings (R1 – R4) have been resolution matched and modelled to give the invasion profile. The results may be presented as a colour image (from Elkington, 1995).

or buck out the unwanted *X*-signal. The typical tool used today, the dual induction (combined with other modules) has been improved but has the same basic construction as the earlier ones. The principal coils are set 1 m (40") apart and it is considered that the induced current comes from the formation between 1 m and 5 m (Western Atlas, 1.6 m) away from the borehole, the exact depth of investigation depending on formation and mud conductivities. The corresponding average depth of investigation for the medium or shallow induction is 80 cm (i.e. detection depth of 50% of the tool signal).

***Recent developments, Array induction tools***

Advances have been made in recent years in induction logging. A significant new tool is the array induction. For example the Array Induction Tool (AIS) of BPB, who were the first to introduce such a tool in 1983 (Martin *et al.*, 1984), consists of one emitter coil and four receiver coils.The raw signals are processed mathematically using the laws of electromagnetics, to produce a log value or formation signal. The multiple investigation depths calculated from the tool response can be reconstructed into an invasion profile (Figure 6.20) impossible with 2 value tools, although the shallowest reading is probably not generally into the flushed zone (Head *et al.*, 1992).

A second advance in induction tool design is that modern tools measure both the *R*- and *X*-signals, principally because the *X*-signals are used in subsequent signal processing (*see below*). The modern tools also have the possibility of using different current frequencies. The older tools used a fixed frequency of 40 kHz while modern tools give a choice of 10, 20 and 40 kHz.

The other area of advance in induction logging is in signal processing. Induction tool responses can be very satisfactorily modelled mathematically. This means that the difference between tool derived values and real formation values can be 'modelled out'. It is, effectively, the *'reconstruction of a formation property profile consistent with the measured data'* (Dyos, 1987). This technique, inversion, can be applied in several ways, but essentially consists of predicting realistic formation values from the tool recorded values, by satisfying mathematically, the calculated distortion to the tool signal that the proposed formation would have. This is in fact forward modelling. The Phasor Induction tool of Schlumberger uses signal processing to improve the conventional induction tool measurements using one set of log values to correct the other (Maute, 1992).

The induction tools are important because they provide the only resistivity measurement in wells drilled with oil-based mud. With the older standard tools, signal distortion was common and it was not possible to have a flushed zone resistivity, only a deep reading. Inversion is diminishing signal distortion and with the new array tools a spectrum of resistivities can be presented (Figure 6.20).

## 6.6 Log characteristics

***Bed resolution***

The micro-resistivity tools are capable of very fine bed resolution, the finest of all the logging tools. It is this capability which is used in dipmeter and electrical imaging tools. On the opposite scale, induction tools give only a very much smoothed picture of individual beds, and bed boundaries are poorly defined. Bed resolution is intimately related to the depth of investigation of the various tools.

For petrophysical calculations it is important to know the minimum bed resolution for true formation resistivity measurements. The subject has already been mentioned

**Table 6.7** Minimum bed resolution of the resistivity tools (from Hartmann, 1975).

| Bed thickness | Logging tool | | Estimated bed resolution | | | | | | Resistivity measured |
|---|---|---|---|---|---|---|---|---|---|
| | Type | Spacing (in) | ratio of edge bed to zone | | | | | | |
| | | | 5:1 | 1:5 | 20:1 | 1:20 | 100:1 | 1:100 | |
| Less than 30cm | Microlog | 1 & 2 | 0.5 | 0.0 | 1.0 | 0.0 | 1.0 | 0.0 | |
| (1ft) | Micro-laterolog | | 0.3 | 0.0 | 0.5 | 0.0 | 1.0 | 0.0 | $R_{xo}$ |
| | Proximity | 1 | 0.3 | 0.0 | 0.5 | 0.0 | 1.0 | 0.0 | |
| 30cm–1m | SFL | | 1.0 | 0.0 | 2.0 | 0.0 | 3.0 | 0.0 | $R_i$ |
| (1ft–3ft) | Laterolog 3 | 12 | 2.0 | 2.0 | 2.0 | 3.0 | 2.5 | 4.0 | $R_i$ |
| | Laterolog 8 | 14 | 2.0 | 2.0 | 2.0 | 3.0 | 2.5 | 4.0 | $R_i$ |
| 1m–3m | Laterolog 7 | 32 | 2.5 | 3.5 | 3.0 | 4.0 | 3.5 | 5.0 | $R_i$ |
| (3ft–10ft) | Laterolog S | 32 | 2.5 | 3.0 | 3.0 | 3.5 | 3.0 | 5.0 | $R_{xo}$ |
| | Laterolog D | 32 | 2.5 | 3.0 | 3.0 | 3.5 | 3.0 | 4.0 | $R_i$ |
| | Induction M | 40 | 4.0 | 10.0 | 4.0 | 20.0 | 10.0 | 25.0 | $R_i$–$R_t$ |
| | Induction D | 40 | 4.0 | 10.0 | 4.0 | 20.0 | 10.0 | 25.0 | $R_t$ |
| Greater | 64in Normal | 64 | 6.0 | 0.0 | 8.0 | 0.0 | 1.0 | 0.0 | $R_i$–$R_t$ |
| than 3m | 18ft Lateral | 216 | 20.0 | 0.0 | 30.0 | 0.0 | 50.0 | 0.0 | $R_t$ |
| (10ft) | SN 16 | 16 | 10.0 | 6.0 | 20.0 | 10.0 | 0.0 | 0.0 | $R_i$ ($R_m = 0.1$) |

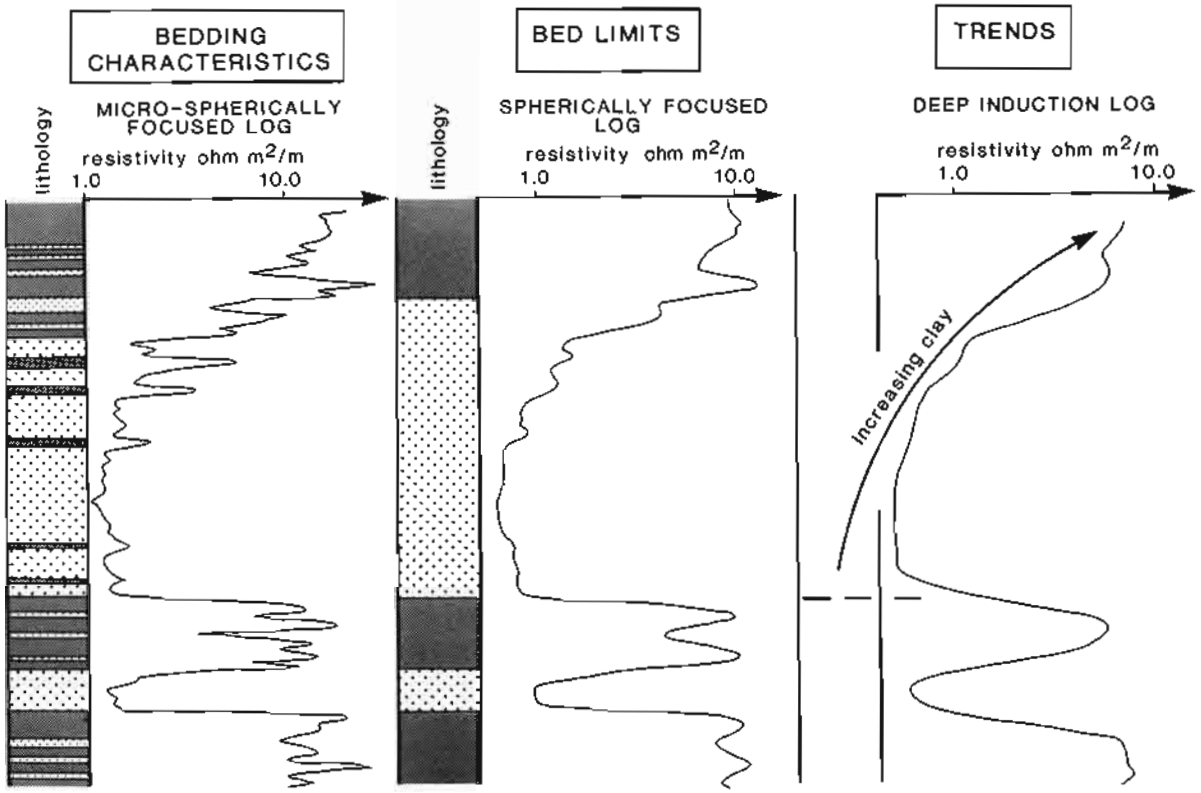


**Figure 6.21** Contrasting bed resolution characteristics of the resistivity tools and their geological application (*see* text).

in Chapter 2 (*see* Table 2.3). Table 6.7 gives the approximate bed resolutions for petrophysical purposes. For beds thinner than the minimum resolution, correction charts must be used to find real values (consult logging company bed-correction charts), or specialist tools used.

For geological purposes, the resistivity logs should be used knowing their resolution capabilities. The micro-tool logs give too fine a resolution for practical, usable, geological bed resolutions. The logs are best used for defining bedding characteristics (Figure 6.21: *see also* Chapter 14). The laterologs resolve beds at the right scale for bed-boundary indications (Figure 6.21), but they should be used in conjunction with the other logs. The induction logs give very poor bed-boundary resolution but, at the same time, they average all the bed effects in such a way as to make lithology trends stand out, and should be used for this purpose (Figure 6.21).

### *Depth of investigation*

The depth of investigation of the resistivity tools has been discussed previously as related to tool performance, the capabilities being created for petrophysical needs (Figure 6.18). Depth of investigation also has geological significance.

The logs from deep-reading devices, especially the induction logs, are best used for gross formation

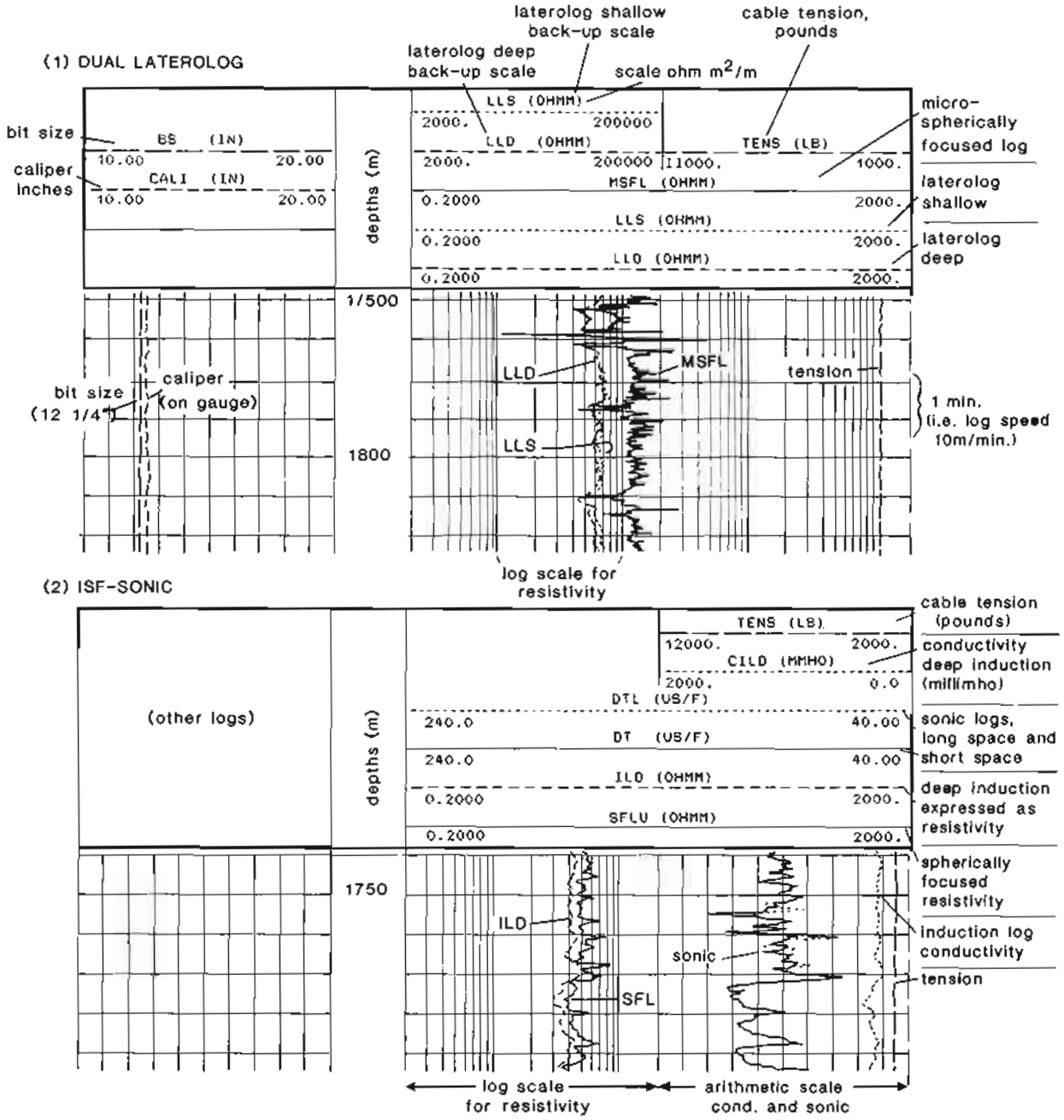


**Figure 6.22** Typical resistivity log formats. (1) Dual laterolog combination; (2) induction, spherically focused log combination. Both from Schlumberger.

characteristics in which individual beds are unimportant. Such is the case with shale porosity trends and correlation. The deep-reading logs should not be used for absolute bed values or characteristics which have rapid vertical changes (vertical anisotropy). Texture-related changes are best seen on the logs from tools mainly influenced by the invaded zone. There is a mixing of formation water and mud filtrate in the invaded zone and the way in which it takes place is very dependent on formation texture. Such changes cannot, in general, be seen on the logs from deep-reading devices. Rapid vertical anisotropy is best seen on the micro-logs. The identification of thin source beds, for example, is possible only with the logs from the micro-tools. This sort of rapid variation is generally associated with the structure of a formation.

The use of the resistivity logs for geological interpretation should thus make use of the general indications as follows: gross characteristics – deep logs; texture – intermediate logs; texture and structure – micro-logs.

***Log format and scales***

The unit of resistivity logs is ohms $m^2/m$; it is called the ohm metre for short.

Resistivity logs are plotted on a logarithmic scale, either in track 2 alone, or in tracks 2 and 3 (Figure 6.22). The values are usually 0.20-20.0 ohm $m^2/m$ for one track, or 0.20-2000 ohm $m^2/m$ when tracks 2 and 3 are used together.

Deep and shallow tool readings are plotted side by side on the same track to allow direct comparison. The actual logs plotted depends on the logging tool combination. The example (Figure 6.22) shows a dual laterolog from Schlumberger with the logs plotted from the deep and shallow laterologs and the micro-spherically focused device, and also an ISF log with curves from the deep induction tool (converted to resistivity) and the spherically-focused device.

The induction log, as the above example shows (Figure 6.22), can be plotted directly in resistivity units alongside the resistivity logs. However, the original conductivity values, in millimhos/m, can also be plotted. The scale is generally 0–2000 mmho. The micro-inverse and micro-normal combination of resistivities is generally plotted on track 1. The scales are identical for the two logs, generally 0–10 ohm $m^2/m$.

The presentation format of the new multi-value resistivity and conductivity tools is variable (Figure 6.20). As a final processing these logs can lead to the production of an invasion profile, generally presented as a colour scale plot of water saturation or invasion. The most effective method of presentation, in which the raw data can be assessed, is to plot the actual values in resistivity scale alongside the colour scale invasion profile. However, there is a tendency on the side of the service companies simply to present a colour plot, which inevitably looks impressive but cannot be judged for validity.

***Unwanted logging effects***

The resistivity and conductivity logs are especially affected by large resistivity contrasts between the logging environment and the formation. Table 6.8 gives a résumé of these effects and their importance.

## 6.7 Quantitative uses of the resistivity logs

The quantitative use of log resistivity measurements is at the heart of the whole domain of quantitative well-log interpretation – the domain of petrophysics. Rock resistivity was the parameter depicted on the first well log and it was also the first parameter to be used quantitatively. The principal use of well logs is to detect oil: the principal use of the resistivity log is to quantify oil (and of course, gas). That is, resistivity logs are used to give the volume of oil in a particular reservoir, or, in petrophysical terms, to define the water saturation, $S_w$. When $S_w$ is not 100% there are hydrocarbons present:

$1 - S_w = S_{hc}$ ($S_{hc}$ = saturation in hydrocarbons).

**Table 6.8** Factors affecting resistivity measurements (apart from invasion and bed thickness). More common effects are italicized. Sh, Shallow; D, Deep

| | Tool | Mud cake influence | Mud | Hole size | Other |
|---|---|---|---|---|---|
| Pad Electrodes | Microlog<br>Microlaterolog | Reads mud cake<br>> ½" cake<br>*strong influence* | Not applicable | Poor reading<br>in bad hole | |
| | Proximity | *Small influence* | | | |
| | Micro–SFL | *Influenced* | | (floating pad) | |
| Tool Electrodes | SFL<br>Laterlogs Sh<br>D | Mainly small | *Readings inhibited in resistive mud* | *Some correction – depends on resistivity contrasts* | Delaware effect and other anomalous resistivities |
| | Induction Sh<br>D | Small | *Poor readings in conductive mud* | Needs a stand off | Skin effect in conductive beds |

***The basic equations of petrophysics***

Below, the fundamental equations of petrophysics appear in a specific order, followed by explanation and comment on their computation. In fact, these equations have applications beyond resistivity measurement, but their use is not discussed here. Such information is found in logging company handbooks and specialist publications (*see* references).

$$R_o = F.R_w \tag{1}$$

*Overall rock resistivity* = the formation resistivity factor × resistivity of the formation fluid (*see* 'Rock resistivity', p.44). Rock resistivity consists of two elements, the passive but constricting formation and the conductive formation fluids. As Wyllie said in 1956 (Wyllie, 1963), *This is perhaps the most important single relationship in electric log interpretation and must be committed to memory.*

$$I = \frac{R_t}{R_o} \tag{2}$$

The *resistivity index* = the resistivity of a rock containing hydrocarbons divided by the resistivity of a rock with 100% water. The equation introduces the notion of the ratio (in one particular reservoir) of the resistivity when entirely water-saturated, as opposed to the resistivity in the presence of hydrocarbons.

***The Archie Equation***

$$S_w^{\,n} = \frac{F.R_w}{R_t} \tag{3}$$

where $S_w$ = water saturation;
$n$ = saturation exponent, usually 2.
$F \cdot R_w = R_o$ when the formation is 100% water-saturated (*see* equation 1). Thus, equation (3) is usually written

$$S_w^{\,2} = \frac{R_o}{R_t} \tag{3a}$$

The water saturation (squared) = the rock resistivity with 100% water saturation divided by the rock resistivity with possible hydrocarbons. The equation is more commonly written

$$S_w = \sqrt{\frac{R_o}{R_t}} \text{ or } \sqrt{\frac{F.R_w}{R_t}} \tag{3b,c}$$

This equation, due to G.E. Archie of Shell, makes use of the ratio of resistivities from equation (2).

***Invaded zone resistivities – movable hydrocarbons***

$$S_{xo} = \sqrt{\frac{R_{xo}(100\%\text{ mud filtrate})}{R_{xo}(\text{with residual hydrocarbons})}} \tag{4}$$

Flushed zone saturation = the square root of the flushed zone resistivity in a 100% water zone divided by the flushed zone resistivity with possible residual hydrocarbons. Residual hydrocarbon saturation, $S_{hr} = 1 - S_{xo}$. The equation gives the saturation in unmoved or residual hydrocarbons of the invaded zone. This is the same Archie Equation as above, but here uses the resistivity ratio in the flushed zone. Comparison of $S_w$ and $S_{xo}$ in a hydrocarbon zone is considered to give movable hydrocarbons. $S_{xo} - S_w$ is equal to the fraction of movable hydrocarbons in the formation. The percentage volume in terms of the reservoir is given by multiplying the term by the porosity, i.e. % volume of reservoir with movable hydrocarbons = $(S_{xo} - S_w) \times \phi$ (where $\phi$ = porosity).

***Formation resistivity factor-porosity relationships***

$$F = \frac{a}{\phi^m} \tag{5}$$

where $F$ = formation resistivity factor
$\phi$ = porosity
$m$ = so-called cementation factor, dependent on rock type, and more closely related to texture than to cementation (Figure 6.5), and
$a$ = a constant.

The equation indicates that the formation resistivity factor is a function of porosity and rock type ($m$). Archie discovered this relationship between $F$ and porosity (*see* Figure 6.5) and equation (5) is the result. Subsequent research and empirical correlations show that the global relationship varies; average figures used for the relationship are:

$$F = \frac{0.81}{\phi^2} \text{ in most sandstones} \tag{5a}$$

$$F = \frac{0.62}{\phi^{2.15}} \text{ (best average for sandstones)} \tag{5b}$$

– this is the *Humble Formula*

$$F = \frac{1}{\phi^2} \text{ compact formations, chalks} \tag{5c}$$

$$F = \frac{1}{\phi^m} \text{ where m = variable (usually 1.8 to 3)} \tag{5d}$$

The most frequently-used formula is (5*b*) which is applicable to sandstones. In limestones, the $F$-porosity relationships are quite variable.

***Practical average Archie Equation***

$$S_w = \sqrt{\frac{0.62 \times R_w}{\phi^{2.15} \times R_t}} \tag{6}$$

This is the general equation for finding the water saturation,

**Table 6.9** Construction of the average Archie Formula.

| | Symbol | Character | Derived from |
|---|---|---|---|
| $R_o$ | ø | Porosity | Sonic log, neutron log, density log, cross–plots, etc. |
| $R_o$ | $\frac{0.62}{ø^{2.15}}$ | $F$ (Humble Formula) | calculated using empirical formulae (e.g. Humble Formula) and porosity as above |
| $R_o$ | $R_w$ | Formation–water | SP or laboratory measurements resistivities of water samples |
| | $R_o$ | Rock resistivity saturated 100% with formation water | $R_o = F \times R_w$ (can only be calculated, cannot be measured with logs) |
| | $R_t$ | True formation resistivity | Induction logs Laterologs (deep resistivities) |
| | $S_w$ | Water saturation of pores | $\frac{S_w \text{ hydrocarbons}}{S_w \text{ 100\% water}} = \frac{R_o}{R_t}$ |

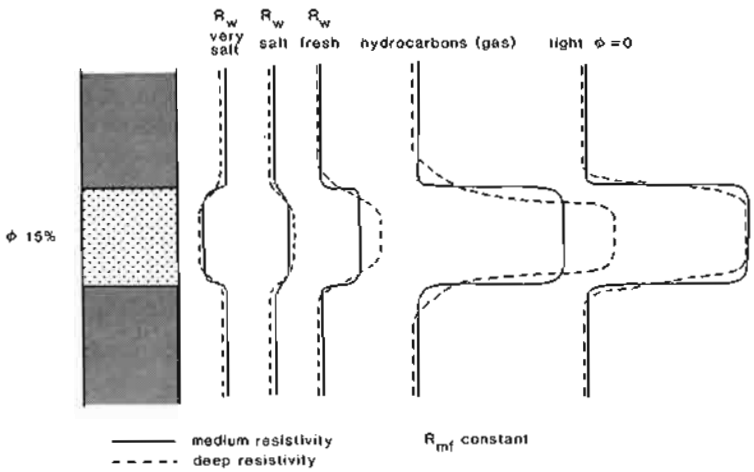


**Figure 6.23** Schematic illustration of the behaviour of resistivity logs over the same reservoir bed but with different fluids and, in the last case, no porosity.

and values for the unknowns may be obtained as shown in Table 6.9.

## 6.8 Qualitative uses

***General indications for resistivity log interpretation***

To interpret the geological significance of resistivity logs it is essential to realize that the same porous bed can have a multitude of resistivity responses, depending on fluid content (Figure 6.23). In petrophysical terms, $F$ will remain constant while $R_w$ varies (*see* Figure 6.6). No porous bed can be said to have a typical resistivity – this is a general principle for qualitative geological work.

General notions of depth of investigation and bed resolution as previously described (*see* 'Log characteristics') must also be considered. The indications for interpretation are: gross indications – deep logs; texture – intermediate logs; texture and structure – micro-logs.

***Textures***

The resistivity of a rock is intimately related to texture. The simplest expression of this is the variation of resistivity with porosity changes. When the porosity decreases, the resistivity increases other things being equal (Figure 6.24). This is in fact the basis of the porosity-resistivity cross-plots (Hingle and Pickett), in which a departure from a constant porosity to resistivity relationship indicates a change in water saturation and the presence of hydrocarbons (*see* Asquith, 1982).

However, as discussed previously (Section 6.2), the influence a rock (as opposed to fluids) has on resistivity can be expressed by $F$, the formation resistivity factor,

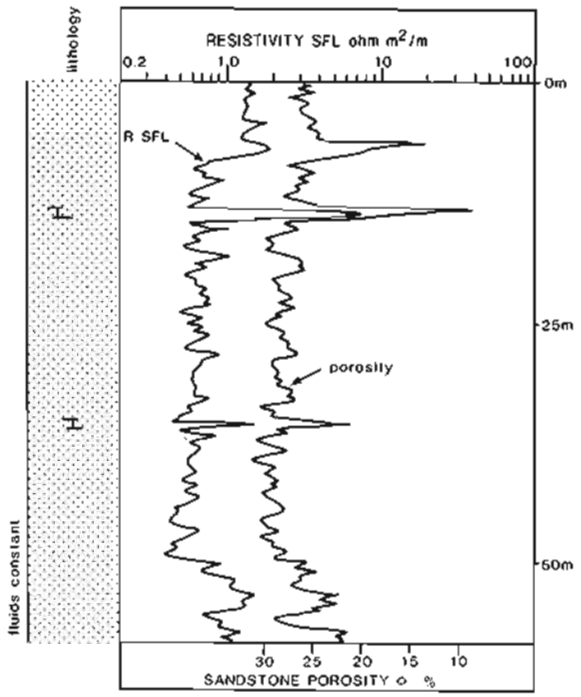


**Figure 6.24** The close relationship between resistivity and porosity in a water-bearing sandstone. Resistivity from spherically focused log, SFL: porosity is log-derived.

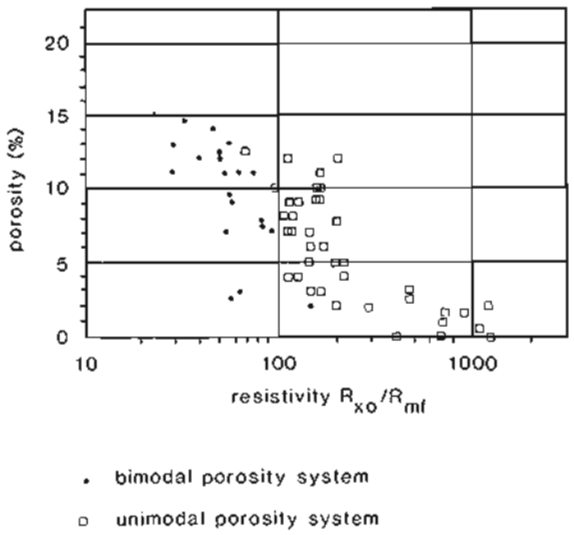


**Figure 6.26** Textural patterns indicated on the resistivity log in the Rodessa Limestone, East Texas. Porosity is density-log derived: resistivity is from the shallow laterolog. (From Keith and Pittman, 1983).

and porosity is only one element of it (Figure 6.5). The chosen example (Figure 6.5), illustrated $F$ as sensitive to grain shape, which it was suggested, showed $F$ to be texturally related (Section 6.2). But shape is just one element of texture. Others such as size, composition, orientation and arrangement (sorting) also have their influence on $F$, and hence – resistivity (Figure 6.25). In reality, every lamina has a different texture to the next, a different $F$ value. The changes in texture (and $F$) may be small in absolute terms, but are still sufficient to affect the high resolution resistivity tools such as the dipmeter and the electrical imaging tools. Indeed, they are the basis for the existence of such a thing as an electrical image (Chapter 13).

The geological importance of the link between $F$ and resistivity in terms of texture, and the way in which this may be exploited, is nicely shown by the following example.

The Rodessa limestone of the East Texas Basin shows different porosity characteristics in different sub-facies, depending on grain type. Ooid limestones tend to have bimodal porosity, skeletal limestones tend to have

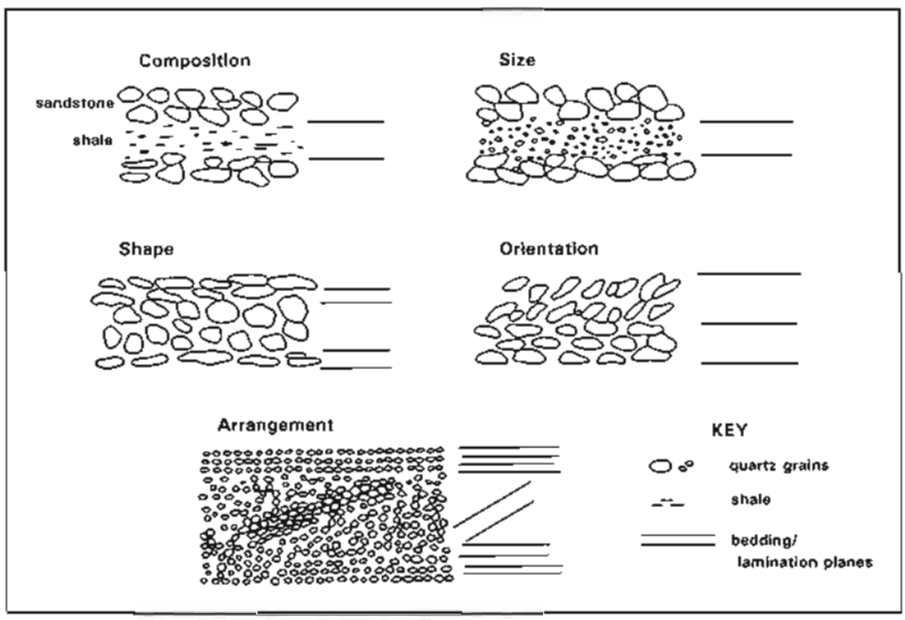


**Figure 6.25** The influence of texture on the formation resistivity factor, $F$. Each thin bed or lamina has a different $F$ value. This figure should be compared to Figures 6.4 and 6.5 (modified from Nurmi, 1984).

unimodal porosity (Keith and Pittman, 1983). The effect of each of these facies on the resistivity log is quite distinct. Thus, for the same porosity value, the unimodal porosity facies (skeletal) shows a higher resistivity than the bimodal (ooid). This is brought out by plotting density log porosities against resistivity from the shallow laterolog corrected for $R_{mf}$ (Figure 6.26). The textural difference between the facies is most distinctly shown by their behaviour to invasion–plotting corrected invasion-zone resistivities against $R_t$ (un-invaded formation) clearly separates the facies. The authors found that resistivity, especially from the invaded zone, was a better discriminator of facies than porosity.

The example of the Rodessa limestone simply shows that the two porosity populations have different $F$ values. If porosity is facies related, so is $F$, and the resistivity log becomes an excellent facies discriminator.

### *Gross lithology*

Resistivity logs cannot be used for a first recognition of the common lithologies. There are no characteristic resistivity limits for shale, or limestone or sandstone. The values depend on many variables such as compaction, composition, fluid content and so on. However, in any restricted zone, gross characteristics tend to be constant and the resistivity log may be used as a discriminator. For example, in sand shale sequences, shale characteristics may be constant and sands may be similar and with constant fluid salinities (Figure 6.27). The resistivity then becomes an excellent log for lithological distinction. Indeed, this is especially the case in younger, unconsolidated sediments and in the top sections of offshore boreholes where the quality of most logs is poor, but the deep resistivities can still be used.

In certain specific cases, however, the resistivity logs can be used to indicate a lithology. These cases are clearly where certain minerals have distinctive resistivity values. Salt, anhydrite, gypsum and coal all have unusually high, diagnostic resistivities (Figure 6.28, Table 6.10). High resistivities will also be associated with tight limestones and dolomites.

Unusually low resistivities may also be indicative. A low resistivity can be associated with electronic (metallic) conductivity as opposed to ionic conductivity (Table 6.10). This is the case for mineral concentrations. The effect is noted with pyrite, especially when concentrations are higher than around 7% (Figure 6.29) (Theys, 1991) and can be seen in detail on the electrical image logs (Chapter 13). Another example, not so far fully explained, is that of chamosite, a hydrated iron mineral. Quite thick beds of chamosite in the Lower Jurassic of the North Sea show very high densities (Figure 10.22) and low resistivities.

### *Subtle lithological variations*

Although resistivity logs do not allow the direct identification of common lithologies, they are nonetheless very sensitive lithology indicators. This is illustrated by a set of resistivity logs through a shale with numerous siderite-rich stringers and concretions (Figure 6.30). The lithology is known from cores and consists in general of bedded shales with very thin beds, bands and concretionary beds of sideritic shale. Even the thinnest siderite rich interval is recorded on the resistivity curves. Of the example logs (Figure 6.30), the SHDT curve, with a 2.5 mm sample spacing, shows the fine detail. This detail is slightly smoothed out by the MSFL log and greatly smoothed by the deep induction log (both sampled at 15 cm), nevertheless the sensitivity to the small variations in the shales is clear. The resistivity logs are in fact responding to two things, both quite subtle: changes in texture and changes in composition.

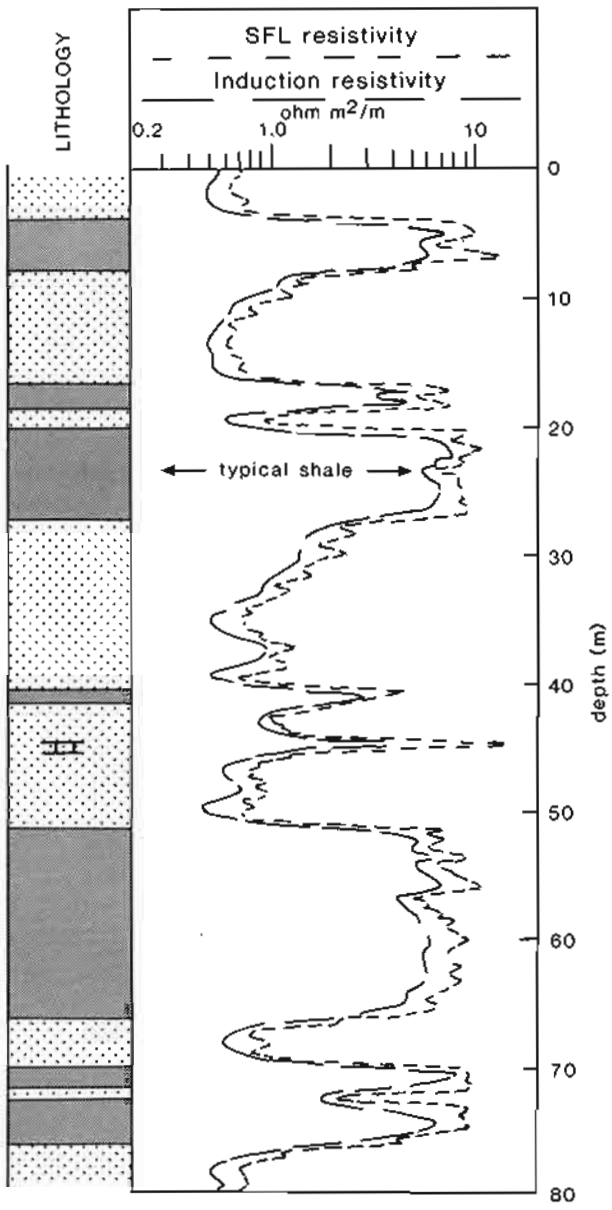


**Figure 6.27** Shale intervals shown on the resistivity logs. In most sand-shale sequences, shales tend to have a constant, typical value.

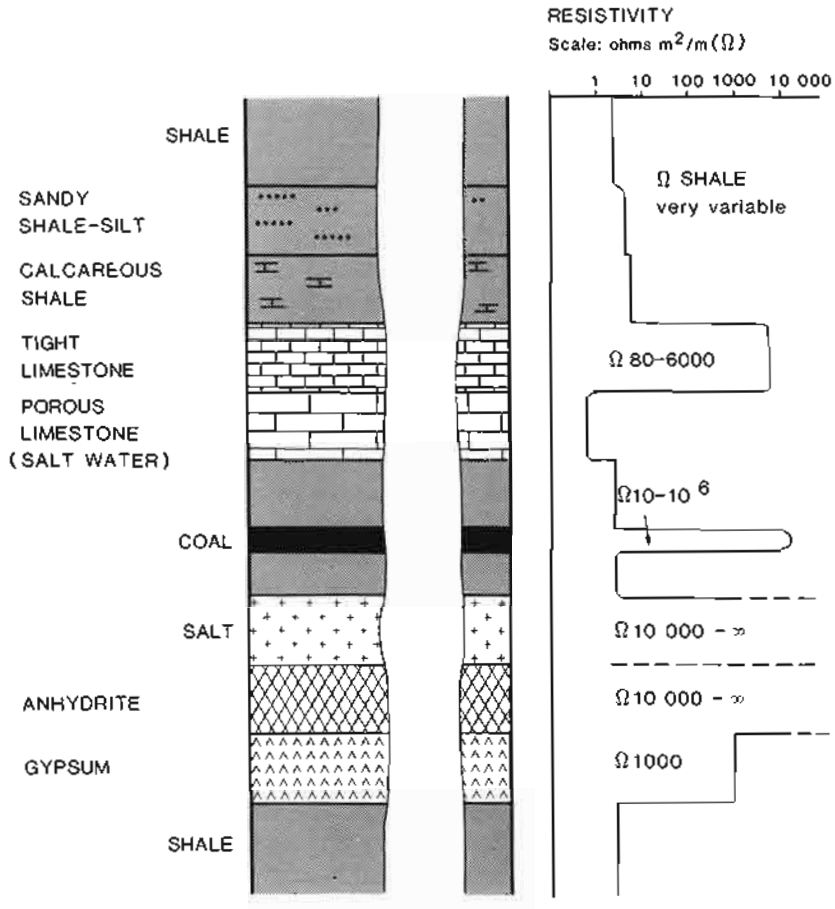


**Figure 6.28** Responses on a deep resistivity log of some minerals and some typical, distinctive lithologies. To these mineral values should be added the following fluid values: pure, fresh water (26.7°C) = α , salt-saturated water (26.7°C) = 0.032Ω , methane = α .

**Table 6.10** Some typical diagnostic resistivity values (mainly from Serra, 1972).

| **Lithology/ Mineral** | **Resistivity** | **Resistivity Range** ohm m²/m |
|---|---|---|
| Shale | Moderate | Extremely variable (0.5000–1000.0) |
| Limestone | Generally high | Variable – depends on porosity and formation water salinity |
| Dolomite | " | |
| Sandstone | Moderate–low | |
| Salt | Very high | 10,000 – infinity |
| Anhydrite | " | 10,000 – infinity |
| Gypsum | High | 1000 |
| Coal | High (variable) | 10 – 1,000,000 |
| Pyrite | Very low | 0.0001 – 0.1 |

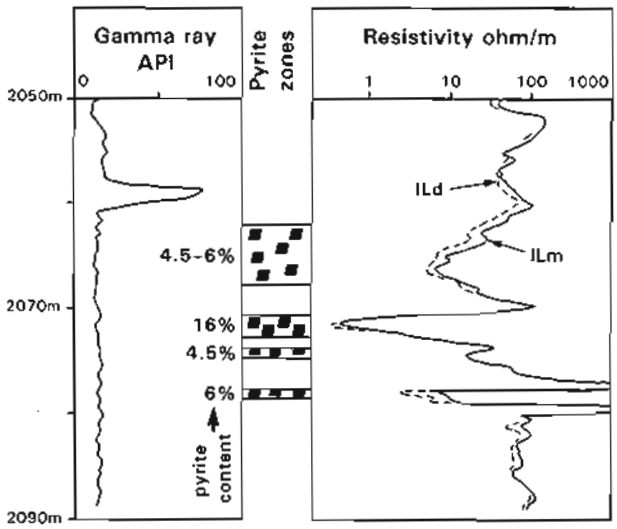


**Figure 6.29** The effect of pyrite on induction logs. At high concentrations the electrical conductivity of pyrite is seen and log resistivity values are significantly lowered (re-drawn, modified from Theys, 1991, attributed to Clavier *et al.*, 1976).

This sensitivity of the resistivity logs is brought out by a second example in which there are bulk changes in a shale, probably in texture as well as composition, brought about by a series of marine flooding events (Figure 6.31).

The shale rich in organic matter shows a low resistivity; it is probably well laminated (*see below*) and was deposited in deep water (actually condensed deposits). Analysis of palynodebris shows that most of the organic material is

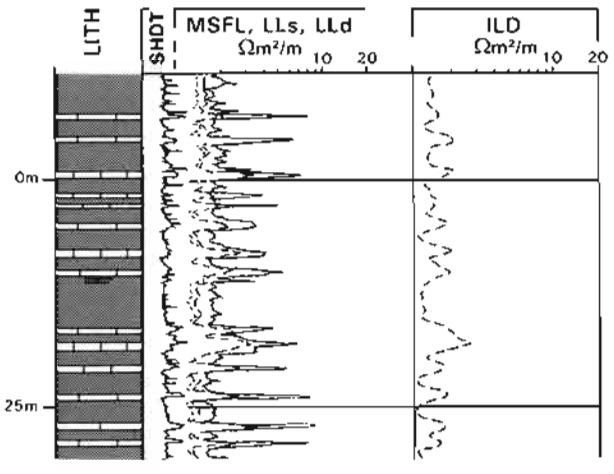


**Figure 6.30** Siderite stringers in a shale sequence as seen on resistivity logs. The SHDT dipmeter curve (2.5mm sampling) shows that these are very thin, often concretionary layers.

structureless, indicative of an anoxic environment. The overlying shales are slightly silty and also probably laminated. They contain woody organic matter, typical of more open, oxygenated waters. These then grade upwards into silty shale (Figure 6.31).

This example also illustrates how bedding characteristics can affect the resistivity logs. In normal circumstances, when there is no permeability, *shallow* and *deep* resistivity devices should show similar values related to the formation lithology (cf. Figure 6.23). It has been observed, however, that in certain fine grained (as in the example Figure 6.31) or crystalline formations, the resistivities show significant separation. Research has shown that the separation is due to the presence of microscopic permeability paths associated with bedding lamination or small scale vertical fractures. These have a selective effect on the electrical behaviour of the different tools (Pezard and Anderson, 1990). *Deep* reading devices have current fields which use horizontal permeability paths, such as bedding: *shallow* devices tend to use vertical permeability paths such as vertical fractures or joints. Thus, in well bedded shales, deep devices tend to be the lower, following the bedding permeability. When vertical joints or fractures are present the reverse is true, *shallow* devices are lower. The log values are similar in homogeneous formations. In the example (Figure 6.31), the *shallow* device (SFL) is consistently higher than the *deeper* device (ILD). This effect can be caused by persistent horizontal bedding.

### *Correlation*

The sensitivity of the resistivity logs to subtle lithological changes is the basis for their use in correlation. Ideally, logs which correlate well are those which are more sensitive to vertical changes than to lateral variations. Within a limited geographical extent, this is often the case with the resistivity logs, especially in shale or silt intervals. Distinctive shapes, trends or peaks over shale zones are related to subtle compositional changes reflecting original patterns of sedimentation, (i.e. Figure 6.31) and as such can be correlated. The best log for this purpose is usually the deep induction log (Figure 6.32).

Despite its frequent (and successful) use for correlation, mainly as a result of its availability, the resistivity log has drawbacks for this task. It is influenced by

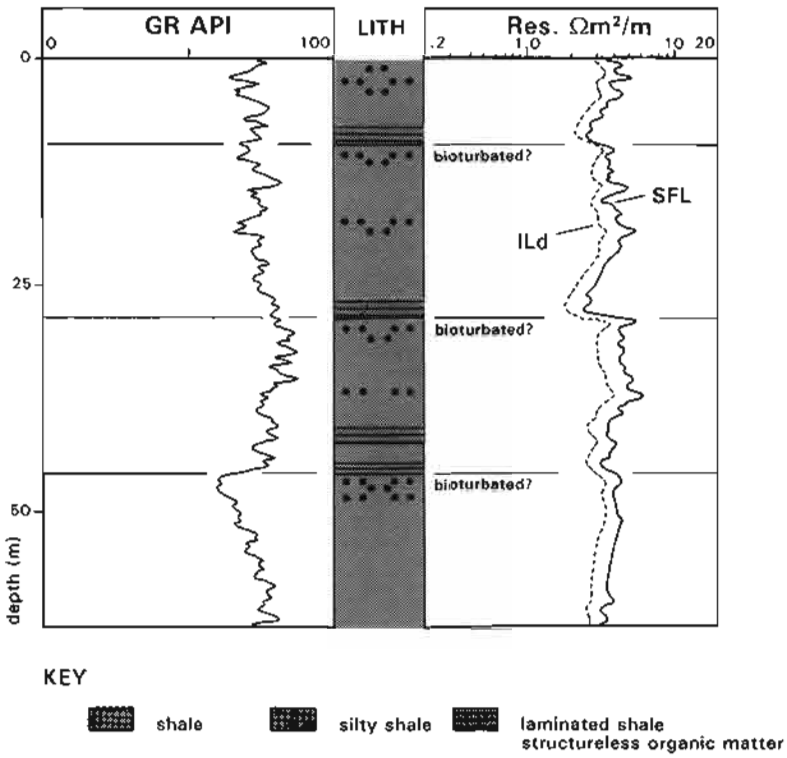


**Figure 6.31** Subtle textural and compositional variations in shallow marine shales indicated on the resistivity logs.

Compositional changes are noted in the organic matter content and in the amount of silt. Textural variation is seen in the fine lamination of the organic rich shales which causes distinctive, low resistivities. Note the separation between the shallow (SFL) and deep (ILd) devices (*see* text).

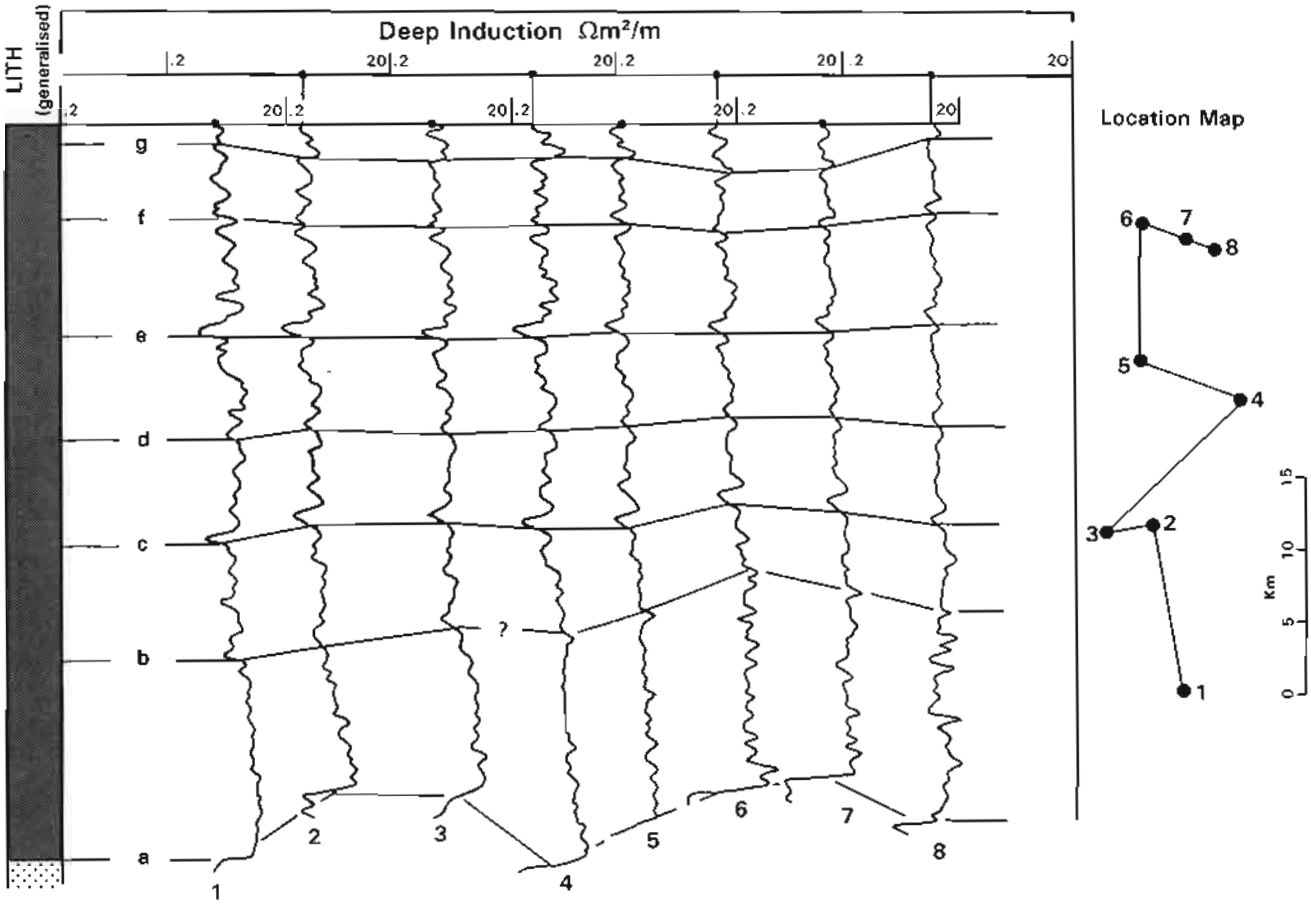


**Figure 6.32** Correlation using deep induction logs (resistivity plots). The interval is one of thick, seemingly characterless, marine shales. The logs show persistent, subtle changes which allow excellent correlation over a distance of 30km.

changes in formation pressure and interstitial water salinity which are non-stratigraphic, post-depositional elements that tend to obliterate the original depositional features (cf. Figure 6.37).

***Facies***

From the shale example illustrated previously (Figure 6.31), it is clear that facies and facies changes can be followed on the resistivity logs. Indeed, it can be argued that a subtle lithological change is in fact a facies change.

One of the principal uses of the resistivity log in facies analysis is its ability to register changes in quartz (sand)-shale mixtures. This is especially so in the fine-grained rocks, shales and silts, more so than in sandstones themselves. The example (Figure 6.33) shows small-scale deltaic cycles 15 m–20 m thick, picked out by resistivity trends. The increase in resistivity corresponds to an increase in the silt (quartz) content. Even slight, subcyclic events are visible on the logs.

Within sands themselves, it is suggested that in hydrocarbon-bearing zones, different resistivity values may be correlated with differences in grain size. A coarser-grained sand will generally have a low irreducible water saturation and hence higher resistivity, the saturation in hydrocarbons being higher (Figure 6.34). A fine-grained sand with higher irreducible water will show lower resistivity. A clean, fining-upwards sandstone filled with hydrocarbons should show a regular upwards decrease in resistivity.

A second, well-known example, comes from the Devonian of Canada (Figure 6.35; McCrossan, 1961). The interval of study contains reefs and deeper water shales. The reefs contain oil. Careful mapping of the resistivity values in the shales shows that a facies change occurs as the reefs are approached, reflected in an increase in resistivity. The effect is probably one of increasing carbonate content and decreasing shale porosity, although bedding characteristics also change. However, mapping the resistivity values enabled a more accurate localisation of the near-reef shale facies and the reefs themselves.

***Compaction, shale porosity and overpressure***

The normal compaction of shale seen along a borehole shows up in a plot of shale resistivity against depth: as compaction increases so the resistivity increases (in a homogeneous shale) (Figure 6.36). This trend is especially apparent in conductivities and a plot of shale conductivity (deep induction) on a log scale against depth shows a near-linear distribution (Macgregor, 1965)

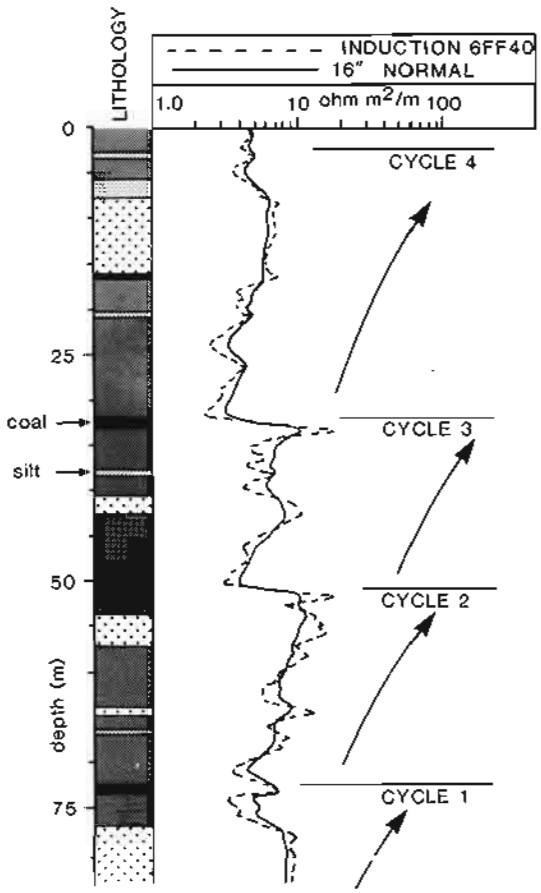


**Figure 6.33** Resistivity logs showing small-scale deltaic cycles. The resistivity varies with changes in the sand-shale percentages.

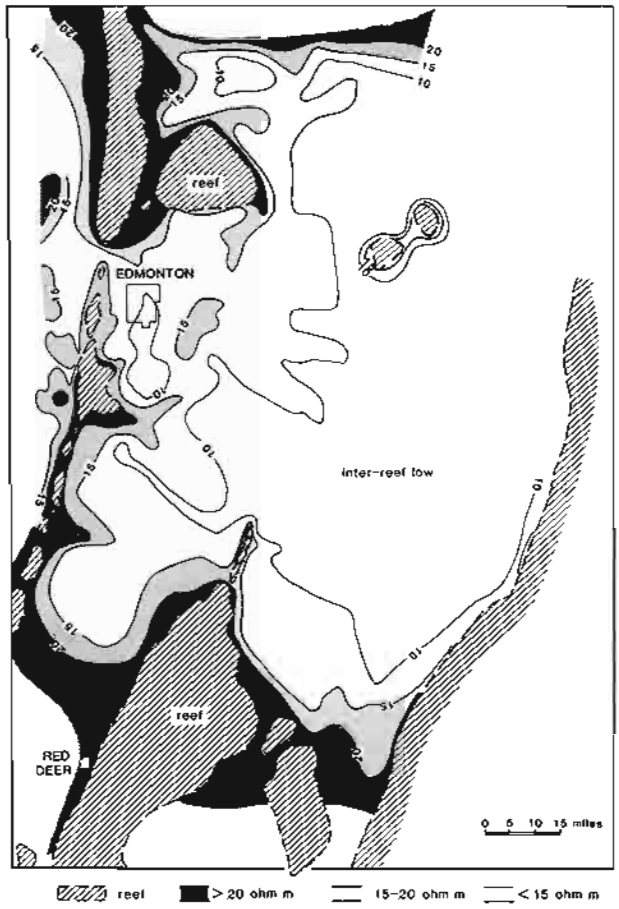


**Figure 6.35** A resistivity map of the middle and lower Ireton. Devonian reef complex, Canada. The reefs are surrounded by a 'resistivity gradient'. (Redrawn from McCrossan, 1961).

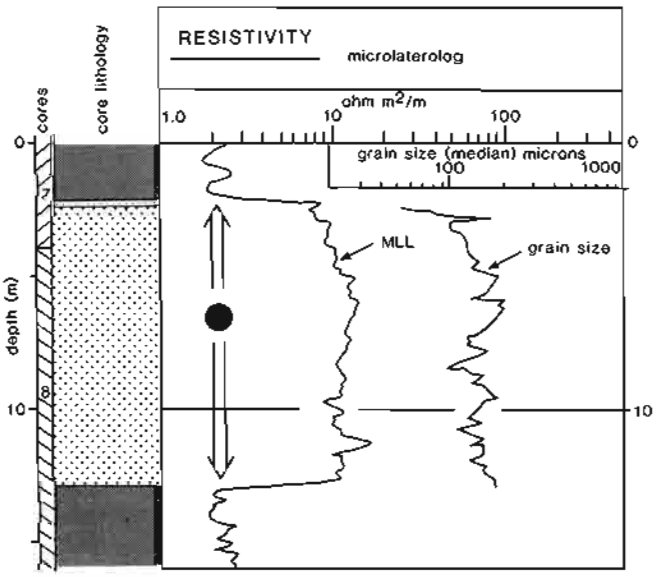


**Figure 6.34** Grain size-resistivity relationship in an oil zone. The resistivity variations are related to grain-size changes (*see* text).

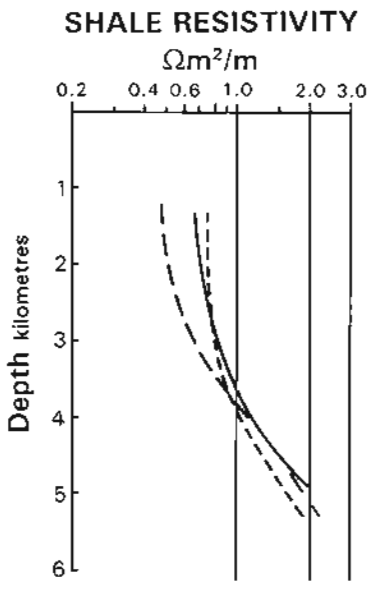


**Figure 6.36** Shale resistivity trends with depth. The example shows normal compaction trends from the Gulf Coast 1, Oligocene-Miocene; 2, 3, Miocene, Louisiana. (Redrawn from Magara, 1978, after Hottman and Johnson, 1965).

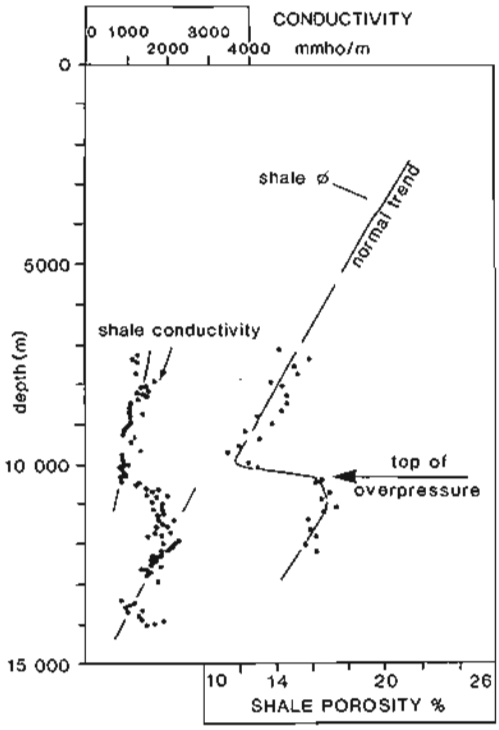


**Figure 6.37** Indication of overpressure on a conductivity plot. Conductivity changes correlate with changes in shale porosity. (Data source, Schmidt, 1973).

corresponding to persistent, normal compaction. The reason for this trend seems to be a relationship between conductivity and shale porosity (Figure 6.37). The same relationship to shale porosity is shown by the sonic log, which also gives persistent trends with shale compaction (Chapter 8).

In some wells, a reversal in shale conductivity with depth is encountered: in such cases overpressure is diagnosed. When a zone of overpressure is encountered, shale conductivity increases abruptly and considerably (Figure 6.37) although possibly taking on a new diminishing trend below. The abrupt increase is probably related to and caused by an increase in shale porosity which occurs as the overpressured zone is entered (Schmidt, 1973). Plotting shale conductivity with depth therefore brings out normal pressure and compaction trends, and abnormally pressured zones. Care must be taken with such plots to ensure that the changes are not due to variations in shale composition (cf. Figure 6.31). If enough data are available in a particular region, tables can be constructed to give quantitative estimates of over-pressure from resistivity values (Ichara and Avbovbo, 1985). This relationship has taken on considerable importance with the advent of LWD measurements since resistivity (conductivity) anomalies can now be detected during drilling (Rasmus and Voisin, 1990).

Normal conductivity depth trends may be used simply to indicate geological compaction. In rapidly-deposited or stratigraphically contiguous zones, compaction will be persistent and regular. When there is a break, either in sedimentation or, more importantly, an unconformity, compaction trends will be interrupted and hence so will resistivity trends. Breaks in resistivity trends can therefore be used to diagnose geological breaks (*see* Chapters 14, 15).

### *Source-rock investigation*

The resistivity log may be used both qualitatively and quantitatively to investigate source rocks.

The effect a source rock has on the resistivity log depends on the maturity of the organic matter: it has little effect when immature, but causes a large increase when it is mature (Figure 6.38). The reason seems to be that it is the pore fluid content that causes the increase and not the solid matter. A typical shale which is not a source-rock consists of a clay mineral matrix and a certain water filled porosity. A source shale also contains both matrix and porosity but typically 4%–12% of the matrix is organic matter (Figure 6.39). If the source is immature the pore

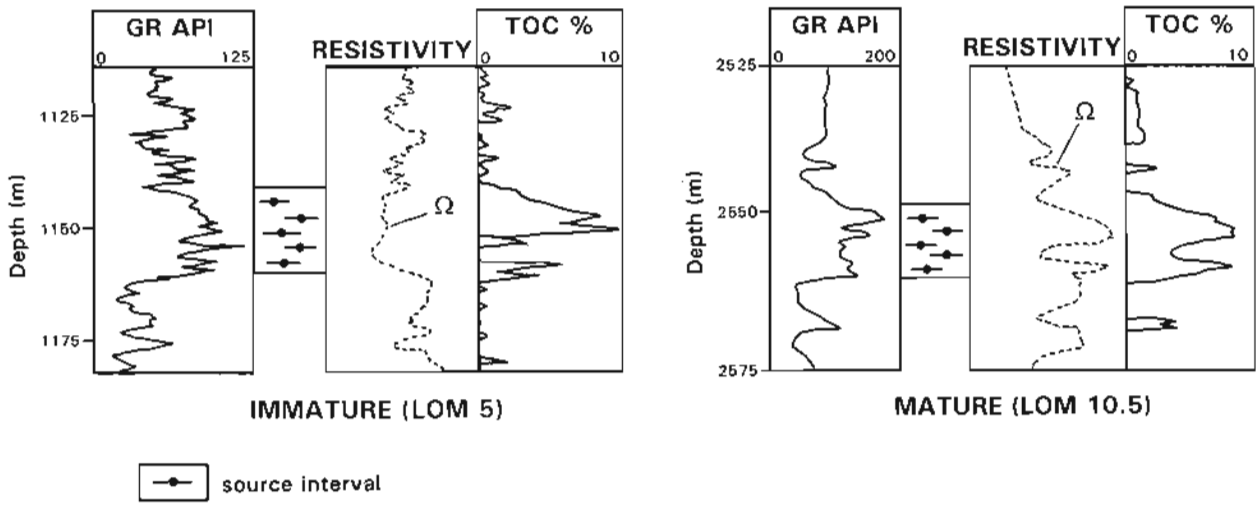


**Figure 6.38** Resistivity log characteristics in source rocks. When a source rock is immature, no resistivity anomaly is seen. When it is mature, high resistivities are measured. TOC = total organic carbon. LOM = level of maturity (re-drawn from Passey *et al.*, 1990).

space is filled with water, but if the source is mature, the pores contain both water and free hydrocarbons (Figure 6.39). The resistivity log responds to the free hydrocarbon fluids, the high resistivity is simply an indication that hydrocarbon fluids are present in the pores and not that a solid organic matter source is present. Some authors indicate that the numerical size of the resistivity anomaly is related to the degree of source maturity (Passey *et al.*, 1990), which implies that the amount of hydrocarbon in the pores is related to the maturity.

To investigate source-rocks, the resistivity log cannot be used alone: a high resistivity in a shale interval may be caused by other textural or compositional effects such as carbonate-rich zones or lack of porosity, and not just a mature source rock. If the hydrocarbon effect is to be highlighted, these compositional and textural effects must be subtracted. This is achieved by comparing the resistivity log to another log which is principally affected by texture and composition and not by pore fluid, logs such as the sonic and the density.

For example, a method based on the analysis of source-rocks from around the world, showed that if resistivity log values were cross-plotted with either sonic or density log values, then a sample could be reliably identified as either source or non-source (Meyer and Nederlof, 1984). (The quantitative application of this method is discussed in Chapter 8 on the sonic log, Section 8.6, Source-rock identification).

A second method suggests that it is even possible to calculate the amount of organic matter in a source-rock with the resistivity and the sonic. This method simply requires that the sonic log is plotted on a normalised scale with the resistivity log (the quantitative aspects of this method are also discussed in Chapter 8 on the sonic log, Section 8.6, Source-rock identification). When the normalized scales are correct, the sonic and resistivity logs 'track' one another but separate when a source rock is present (Passey *et al.*, 1990). The degree of separation is said to be related to both degree of maturity and source abundance (TOC%), so that if level of maturity (LOM) is known, the TOC% can be calculated (for details *see* Chapter 8, Section 8.6; methods using the density log are discussed in Chapter 9, Section 9.6).

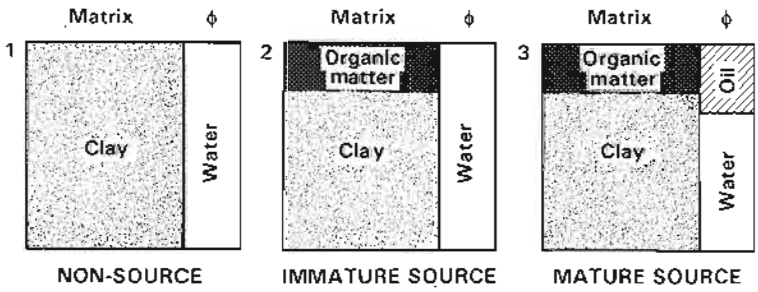


**Figure 6.39** Schematic volumetric content of an argillaceous, 1. non-source, 2. immature source and 3, mature source. The mature source contains oil in the pore space which causes high values on the resistivity log as illustrated in Figure 6.38 (re-drawn from Passey *et al.*, 1990).

# 7
# THE GAMMA RAY AND SPECTRAL GAMMA RAY LOG

## 7.1 Generalities

*The log*

The gamma ray log is a record of a formation's radioactivity. The radiation emanates from naturally-occurring uranium, thorium and potassium (*see below*). The simple gamma ray log gives the radioactivity of the three elements combined, while the spectral gamma ray log shows the amount of each individual element contributing to this radioactivity.

The geological significance of radioactivity lies in the distribution of these three elements. Most rocks are radioactive to some degree, igneous and metamorphic rocks more so than sediments. However, amongst the sediments, shales have by far the strongest radiation. It is

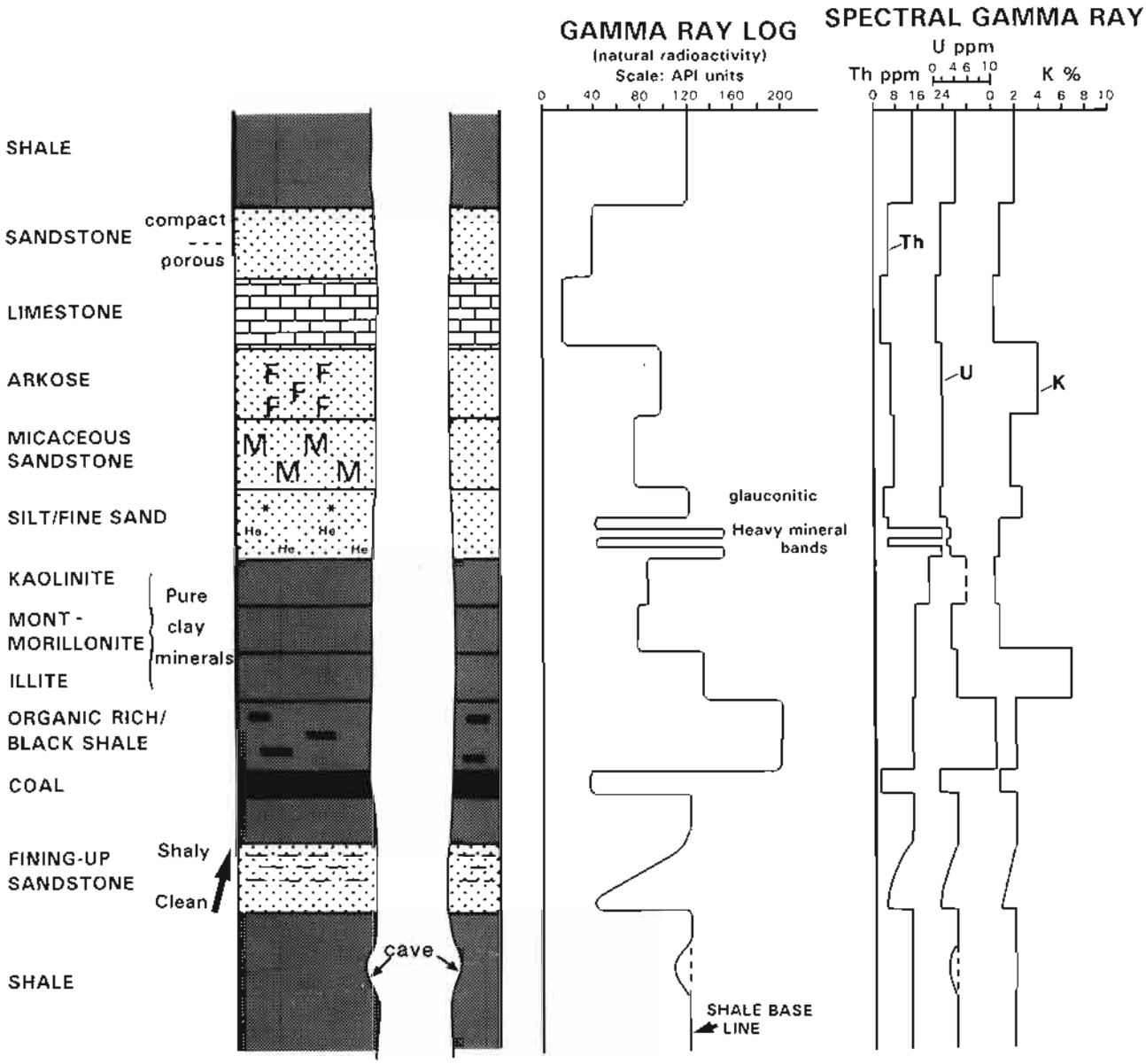


**Figure 7.1** The gamma ray log and spectral gamma ray log: some typical responses. The gamma ray log shows natural radioactivity. The spectral gamma ray log gives the abundances of the naturally radioactive elements, thorium, Th and uranium, U in parts per million (ppm) and potassium, K in %. F - feldspar, M = mica, * = glauconite.

for this reason that the simple gamma ray log has been called the 'shale log', although modern thinking shows that it is quite insufficient to equate gamma ray emission with shale occurrence. Not all shales are radioactive, and all that is radioactive is not necessarily shale (Figure 7.1) – *see* Section 7.6.

***Principal uses***

The gamma ray log is still principally used quantitatively to derive shale volume. Qualitatively, in its simple form, it can be used to correlate, to suggest facies and sequences and, of course, to identify lithology (shalyness). The spectral gamma ray can be used additionally to derive a quantitative radioactive mineral volume and a more accurate shale volume. Qualitatively it can indicate dominant clay mineral types, give indications of depositional environment, indicate fractures and help to localize source rocks (Table 7.1*a,b*).

**Table 7.1(a)** Principal uses of the gamma ray log.

| | Discipline | Used for | Knowing |
|---|---|---|---|
| Quantitative | Petrophysics | Shale volume (*Vsh*) | gamma ray (max)<br>gamma ray (min) |
| Qualitative | Geology | Shale (shaliness) | gamma ray (max)<br>gamma ray (min) |
| | | Lithology | typical radioactivity values |
| | | Mineral identification | Mineral radioactivity |
| | Sedimentology | Facies | Clay/grain size relationship |
| | Sequence Stratigraphy | Parasequence & condensed sequence identification | Clay/grain size & organic matter/radioactivity relationships |
| | Stratigraphy | correlation | – |
| | | Unconformity identification | – |

**Table 7.1(b)** Principal uses of the spectral gamma ray log.

| | Discipline | Used for | Knowing |
|---|---|---|---|
| Quantitative | Petrophysics | Shale volume ($V_{sh}$) | Th (max), Th (min) for pure shale |
| | | Radioactive mineral volume | $V_{sh}$ (Th), K (max), K (min) for shale |
| Semi-quantitative and qualitative | Geology | Dominant clay material | Th, K, U content of individual clay minerals |
| | | Detrital clay mineral suite | Radioactive content of individual clay minerals |
| | Sedimentology & Sequence Stratigraphy | Condensed section recognition from excess uranium | Normal U and Th content or Th/U ratio of shales |
| | | Climatic changes? | Th/K ratio changes in shale |
| | Reservoir geology | Fracture detection | Uranium contribution to radioactivity |
| | Geochemistry | Marine source rock identification | Uranium content of organic matter |

## 7.2 Natural gamma radiation

Natural radiation in rocks comes essentially from only three elemental sources: the radioactive elements of the thorium family, of the uranium-radium family and of the radioactive isotope of potassium $^{40}K$ (Adams and Weaver, 1958).

Quantitatively, potassium is by far the most abundant of the three elements (Table 7.2) but its contribution to the overall radioactivity in relation to its weight is small. In reality, the contribution to the overall radioactivity of the three elements is of the same order of magnitude, the abundance seeming to be the inverse of the contribution in energy: a small quantity of uranium has a large effect on the radioactivity, a large quantity of potassium a small effect.

Each of the three sources emits gamma rays spontaneously. That is, they emit photons with no mass and no charge but great energy (this being the definition of a gamma ray). The energy in the case of uranium, thorium and potassium emissions occurs in the spectrum from 0 – 3MeV (million electron volts).

**Table 7.2** Abundance and relative radiation activity of the natural radioactive elements.

| | K | Th | U |
|---|---|---|---|
| †Relative abundance in the earth's crust | 2.59% | ~12ppm | ~3ppm |
| *Gamma rays per unit weight | 1 | 1300 | 3600 |

†Serra (1979), Serra *et al.*, (1980)
*Adams and Weaver (1958)

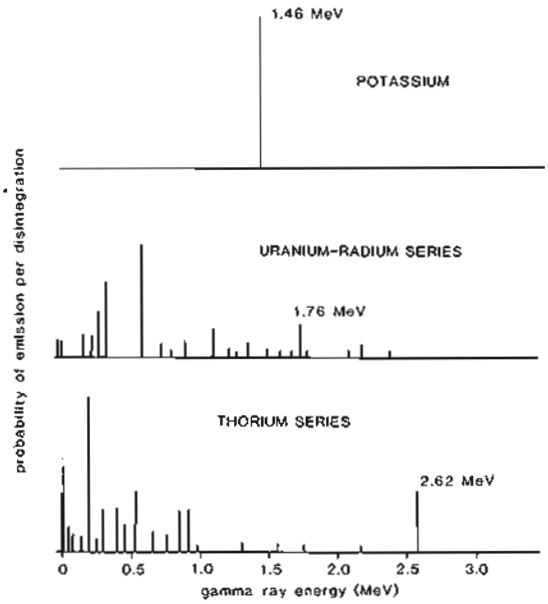


**Figure 7.2** The gamma ray emission spectra of naturally radioactive minerals. The principal peaks used to identify each source are indicated. (After Tittman *et al.*, 1965, re-drawn from Schlumberger, 1972).

The radiation from $^{40}K$ is distinct, with a single energy value of 1.46 MeV (Figure 7.2). Both thorium and uranium emit radiations with a whole range of energies, but with certain peak frequencies. These peaks are especially distinct at the higher energy levels of 2.62 MeV for thorium and 1.76 MeV for uranium (Figure 7.2).

The spectra and the energy levels illustrated are those at the point of emission. One of the characteristics of gamma rays is that when they pass through any material their energy is progressively absorbed. The effect is known as Compton scattering, and is due to the collision between gamma rays and electrons which produces a degrading (lowering) of energy (Figure 7.3). The higher the common density through which the gamma rays pass, the more rapid the degradation or loss of energy (in reality it depends on the material's electron density, which is very similar to common density).

In borehole logging, when radiations are observed by the tool, they have already passed through the formation and probably also the drilling mud, both of which cause Compton scattering. Thus, the discrete energy levels at which gamma rays are emitted become degraded, and a continuous spectrum of values is observed (Figure 7.4). When each of the radioactive minerals is present, their radiations become mixed and the resulting spectrum is very complex. However, a glance at the original spectra (Figure 7.2) will show that the final complex, mixed spectrum, even after Compton scattering, will still contain diagnostic peaks, especially in the 1-3 MeV region. The original distinct peaks of potassium at 1.46 MeV, uranium

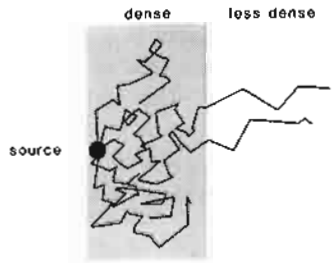


**Figure 7.3** Schematic drawing of the Compton scattering of gamma rays. The effect is more marked in denser matter (cf. Lavenda, 1985).

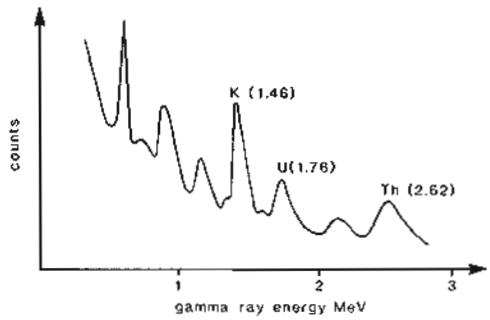


**Figure 7.4** Complex spectrum observed from a radioactive source containing potassium, thorium and uranium, after Compton scattering. (After Hassan *et al.*, 1976).

**Table 7.3** Typical modern gamma ray tools.

| Name | Symbol | Company |
|---|---|---|
| Gamma ray log | GR | all |
| Spectralog | SL | Western Atlas |
| Natural gamma ray spectrometry | NGS | Schlumberger |
| Spectral gamma ray | SGR, CSNG | Halliburton |
| Spectral gamma sonde | SGS | B.P.B. |

**Table 7.4** Ratios of radioactive to non-radioactive material in normal elemental mixtures (Serra *et al.*, 1980).

| | $^{40}K$ | $^{232}Th$ | $^{238}U$ | $^{235}U$ | $^{234}U$ |
|---|---|---|---|---|---|
| % radioactive isotopes in normal mixtures | 0.0199 | 100 | 99.27 | 0.72 | 0.0057 |
| | $\frac{^{40}K}{K_{total}}$ | All | $\frac{^{238}U}{U_{total}}$ | $\frac{^{235}U}{U_{total}}$ | $\frac{^{234}U}{U_{total}}$ |

at 1.76 MeV and thorium at 2.62 MeV still exist and can be used to identify the original source of radiations. This is the principle used in the spectral gamma ray tool (Section 7.3).

## 7.3 Tools

***Simple gamma ray tool***

The simple gamma ray tool is a sensitive gamma ray detector consisting of a scintillation counter and a photo-multiplier (Figure 7.5). The scintillation counter is typically a sodium iodide crystal, 2 cm in diameter and 5 cm long in the simple tool, with minor impurities of Thallium. When gamma rays pass through the crystal, they cause a flash. These are collected by the photo-multiplier and stored in the attached condenser over a set period of time, the time constant (Table 7.5). The energy accumulated during the time constant is the detector value at that depth for that time constant. The tool literally 'counts' the gamma rays.

***Spectral gamma ray tool***

The spectral gamma ray tool, like the simple tool, consists of a scintillation counter and photo-multiplier. However, in the spectral tool, the sodium iodide crystal has a much greater volume, typically 5 cm in diameter and 20 cm long and so gives the tool a much better 'counting' sensitivity. When a gamma ray passes through a scintillation crystal, it not only causes a flash, but the intensity of that flash depends on the energy of the incident gamma ray. This characteristic is used by the spectral gamma ray tool, with its large scintillator crystal, to identify the gamma radiations in several, pre-defined energy bins or windows. These windows are designed to separate the distinctive energy peaks of the individual radioactive elements discussed above (Figure 7.4), namely bracketing the energies of 2.62 MeV for thorium, 1.76 MeV for uranium and 1.46 MeV for potassium. In most tools the lower energy counts are also used and 'allocated' to each element.

**Table 7.5** Logging speed v. time-constant – simple gamma ray tool.

| Time-constant (seconds) | Logging speed (m/h) | Formation logged in time-constant (cm) |
|---|---|---|
| 1 | 1080 | 30.0 |
| 2 | 550 | 30.5 |
| 4 | 275 | 30.5 |
| 6 | 140 | 31.0 |

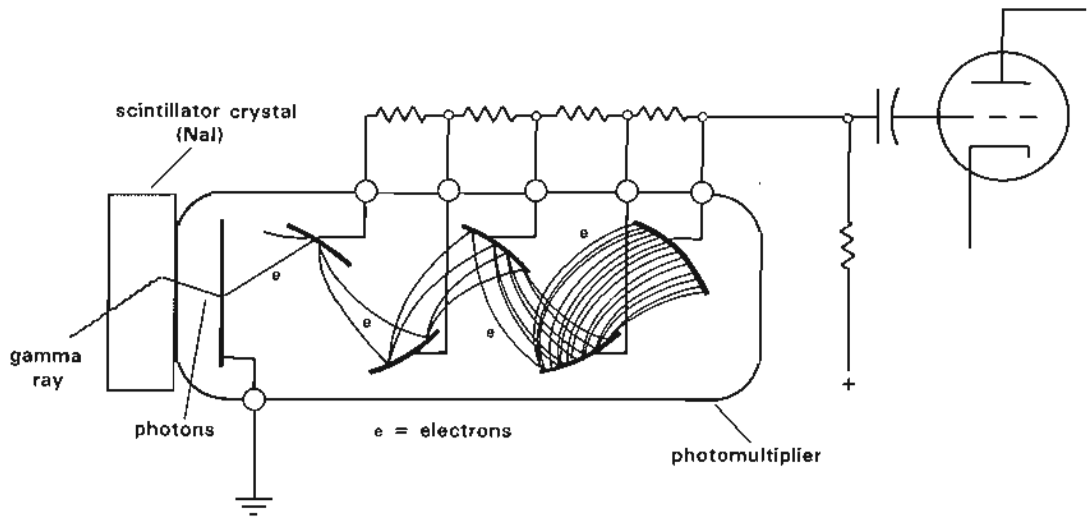


**Figure 7.5** Schema of a gamma ray tool (re-drawn from Serra, 1979 after a Lane Wells document).

The relative contributions of the three radioisotopes are therefore measured by the tool. These can be related to the abundance of each element by comparison with known spectra, since the measured, composite spectrum, is a simple addition of the spectra from the three different sources. Using the known abundances of the radioisotopes in normal elemental mixtures (Table 7.4), the actual abundances of each element can be derived. Thus, the log results from the spectral tool are the quantitative, elemental abundances of thorium, uranium and potassium (Section 7.4, Figure 7.6).

## 7.4 Log characteristics

***Calibration, log presentation, units and scales***

*Simple gamma ray log* – The accepted unit for radioactivity logging is the API (American Petroleum Institute) unit. The API unit is defined in a reference well in the grounds of the University of Houston, Texas. The well contains specially mixed, high-radioactivity concrete surrounded by equally special low-radioactivity concrete. An API unit is 1/200 of the difference between the two radioactivities (Belknap *et al.*, 1959). If a particular gamma ray tool is tested, the API unit for that tool is 1/200 of the difference between the low and high values. Thus, not only does the Houston pit serve as a standard for the API unit, it also serves to calibrate a tool.

The simple gamma ray log is usually recorded in track 1 along with the caliper. Scales are chosen locally, but 0–100 or 0–150 API are common (Figure 7.6a). The tool is small and can be combined with practically any other tool be it a resistivity or porosity device.

*Spectral gamma ray log* – The essential results of the spectral gamma ray tool are elemental abundances, derived as described above. The calibration facility for the spectral tools is the same pit in the University of Houston that is used for the simple gamma ray tool. This is because the high activity cement of this pit has known quantities of uranium (13.1 ppm), thorium (24.4 ppm) and potassium (4.07%) which contribute to the overall radioactivity (Belknap *et al.*, 1959). The individual channels of the spectral tool can be empirically calibrated.

There are several common presentation formats for the gamma ray spectral log. The simplest, and probably best, is a straightforward plot of elemental abundances across tracks 2 and 3 on arithmetic scales (Figure 7.6b). Thorium and uranium are given in ppm while potassium is given in per cent.

Track 1 of this (Schlumberger) presentation shows two curves, the CGR and SGR. The SGR, or standard gamma ray, is the total contribution of the three elements in API units. That is, it is the same as the simple gamma ray log, but re-constructed from the elemental values plotted on tracks 2 and 3. To arrive at this value (for the Schlumberger NGT-A) the following multipliers are used: 1ppm U = 8.09 API units, 1 ppm Th = 3.93 API units, 1% K = 16.32 API units. Thus, 3 ppm of uranium in

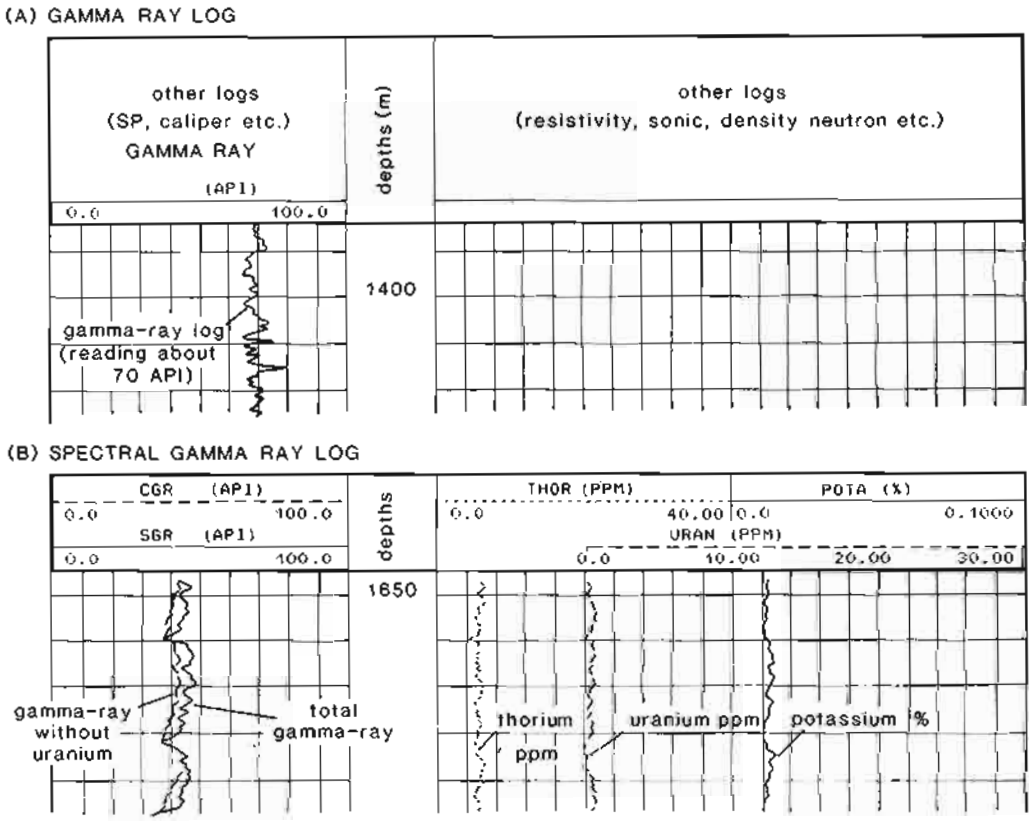


**Figure 7.6** Typical gamma ray and spectral gamma ray log headings.

a mix contributes 24.27 API units, and so on. The SGR is therefore the sum of these API contributions (and can be remembered as the *S*um *G*amma *R*ays). The CGR, or computed gamma ray curve, represents the contributions of only the thorium and potassium in API units. Hence, the difference between the SGR and the CGR is the contribution, in API units, of uranium. For reasons explained below (Section 7.10), the CGR is considered to be an improved clay volume indicator to the total (SGR) API count (and can be remembered as the *C*lay *G*amma *R*ay). In formats not described here, curves of the different elemental ratios can be displayed.

***Depth of investigation***

The depth from which radiations can be detected by the simple gamma ray tool is generally small but difficult to be precise about. One experiment found that 75% of radiations detected came from a 14 cm radius and 25 cm vertically above and below the detector. This was for gamma rays with a single energy of 1.76 MeV and the detector centralised in a 15 cm diameter hole filled with 1.2 cm$^3$ density mud (Rhodes and Mott, 1966). Clearly, natural conditions vary greatly from this specific case. However, as a rough guide the volume of investigation

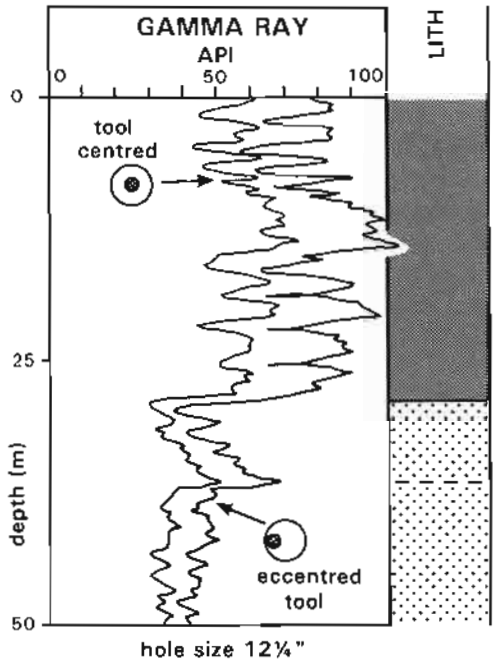


**Figure 7.8** Comparison of a gamma ray log from a hole centred tool (DLL-MSFL-GR logged at 10m/min) and an eccentred tool (LDL-CNL-GR logged at 4m/min). The eccentred tool shows higher values and greater sensitivity.

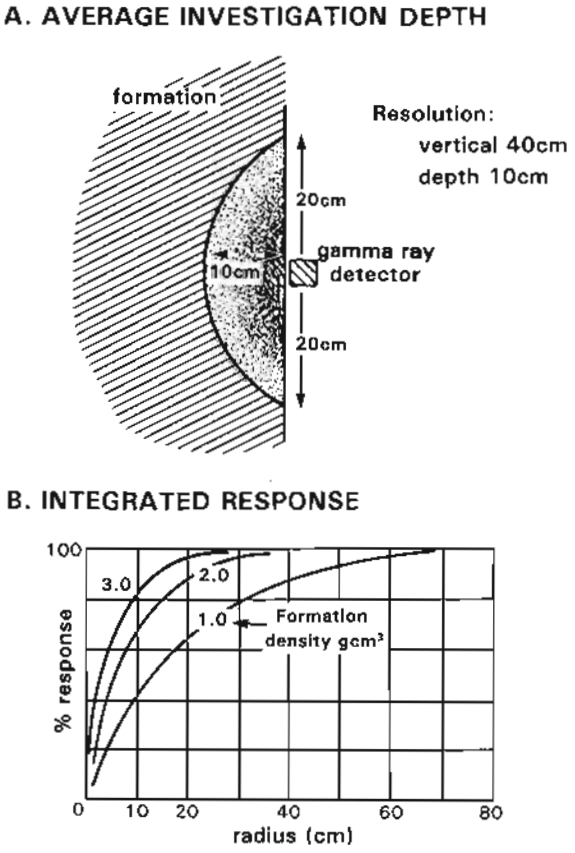


**Figure 7.7** Depth of investigation of the gamma ray tool. a. average volume from which radiations are detected. b. depth of investigation shown to be dependent on formation density. Investigation depth is less in dense formations (graph, B, re-drawn from Hallenberg, 1992).

can be considered to be approximately 20 cm vertically above and below the detector (along the borehole) and 10 cm radially (Figure 7.7*a*). Because of Compton scattering, this volume will vary with formation density: it will be smaller in dense formations (cf. Hallenburg, 1992) (Figure 7.7*b*). Moreover, readings will be commonly smeared, since the presented gamma ray log value is generally an average of three contiguous raw values.

The simple gamma ray sonde can be combined in many tools; it is run both centred in the borehole (sonic and resistivity tools) or against the borehole wall, that is eccentred (density and neutron tools). Because of Compton scattering in the drilling mud, the log made against the borehole wall with direct contact to the formation, will always show a higher reading and higher amplitude than the borehole centred version emersed in the mud (Figure 7.8).

***Logging speed***

Because gamma radiations are discrete events and, as described, are measured in the gamma ray tools by 'counting', there are restrictions on logging speeds. Radiations are 'counted' by the tool over a fixed period of time, called the *time constant*. Because the number of individual emissions is not high, to have as large a count as possible, the time constant should be long. However, since a borehole tool is constantly moving, too long a time-constant will blur bed boundaries and mix several lithologies (Figure 2.12). With a rapidly moving tool, the rock being 'counted' at the beginning of a long time-constant will not be the same as the rock being 'counted' at the end (for a discussion of this *see* 'Bed boundary definition' Chapter 2).

In practical terms, the compromise is that the simple gamma ray tool should not travel more than 30 cm in the time constant. Table 7.5 sets out the limitations of time-constants and logging speeds. However, even following these constraints, gamma ray log repeatability in the minor variations is poor. This is caused by a combination of the logging method, the computing method and the natural statistical variation of gamma ray emissions. A comparison between a main log and a repeat section or between separate runs of the gamma ray tool, gives an empirical indication of the extent of the problem. It only involves the small scale variations.

**Table 7.6** Spectral tool logging, time constants.

| **Time constant** (seconds) | **Logging speed** (m/h) | **Formation logged in time constant** (cm) | **Company** |
|---|---|---|---|
| 4 | 275 | 30.5 | Schlumberger |
| 6-8 | 183 | 30.5-40.6 | Western Atlas |
| depth related | 275 | n/a | B.P.B. |

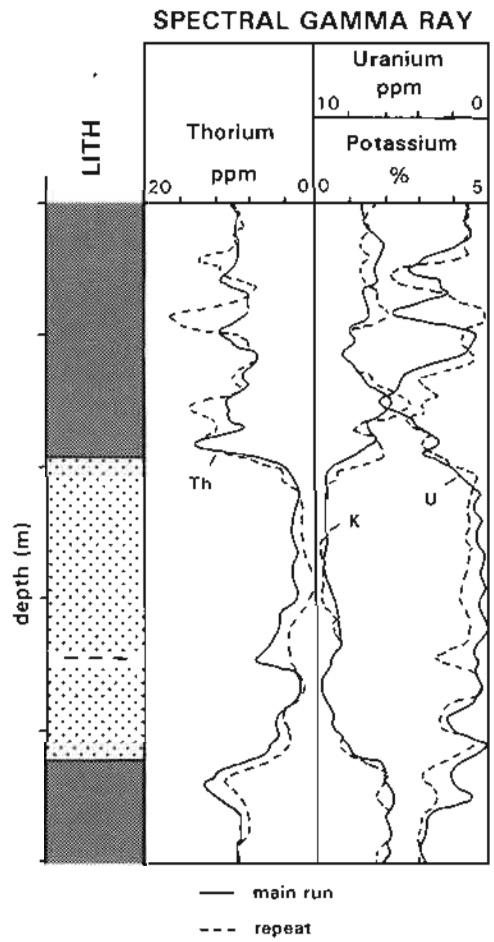


**Figure 7.9** Repeatability of the spectral gamma ray. Precise repeatability is generally poor but it should be noted that the quantities being detected are very small.

The spectral tool is sensitive to speed effects, essentially because the count rate of the individual detection windows is very small. Because the time constant is generally fixed, the significant variable is the logging speed. Lower speeds allow higher counts per formation interval. Tools in which the low energy spectrum is used are as a rule run faster than tools in which the low energy spectrum is not used. Table 7.6 gives recommended speeds. Despite these recommendations, many, if not most spectral logs have poor repeatability (Hurst, 1990 and Figure 7.9), which may be a result of logging speed rather than any inherent error. It is good practice to run a repeat section with every spectral log so that the variability can be judged. Moreover, interpretation methods must take the quantitative level of variability into account.

***Unwanted borehole effects***

*Simple gamma ray* – The simple gamma ray log is relatively unaffected by small-scale borehole irregularities, but is affected by large caves (Table 7.7). The effect is due to the increased volume of drilling mud between the formation and the gamma ray detector which causes increased Compton scattering and a consequent diminution in the gamma ray log value, as described previously. Most logging companies publish charts to correct for borehole size with mud weight consideration.

A quite different effect is caused by the use of the radioactive mud additive KCl. The potassium radioactivity of the KCl is detected by the gamma ray tool and the usual result is a marked increase in the absolute

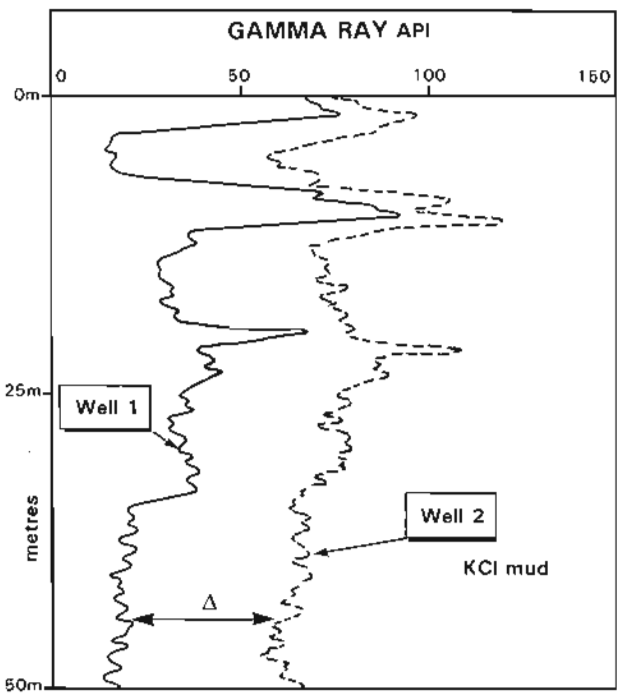


**Figure 7.10** The effect of KCl in the drilling mud on gamma ray values. Well 1, with ordinary mud, well 2 with KCl mud. The formation values should be the same. Δ, is the difference created by the KCl content. The wells are 3km apart.

**Table 7.7** Unwanted environmental effects – gamma ray logs.

| Factor | Effect on log | Severity |
|---|---|---|
| ***Simple Tool*** | | |
| caving | lowers values, bigger the cave, lower the value | common |
| barite in mud | lowering of value in thick mudcakes | common |
| KCl mud | significant increase in 'background' | present |
| ***Spectral Tool*** | | |
| caving | lowers value in caves: tool eccentred so effect much reduced | common |
| barite in mud | increase in calculated thorium and uranium | common |
| KCl mud | increase in calculated potassium and uranium | present |

values (Figure 7.10). It is sometimes proposed that this is simply a 'base line shift', because the mud volume through the hole is relatively constant so there will only be a constant increase in the background: relative amplitude changes will remain unaffected. This is not always the case, especially so when there is invasion and KCl-rich mud enters into the formation. Such a situation will cause an invaded reservoir to show too high a gamma ray reading (*see also* the spectral log below).

*Spectral gamma ray* – The spectral gamma ray log is run held near the borehole wall by a bowspring to reduce the borehole effects which occur when a tool is centred. However, this does not eliminate mud effects entirely and the spectral log is affected by the mud additives barite and KCl (Table 7.7). The effects vary depending on tool design (Company), and the algorithms used to derive abundances. If only the three energy windows around the high energy gamma ray emission peaks are used (Figure 7.4), barite does not affect the result while KCl will only affect the potassium result and can be corrected for. But when the low energy part of the gamma ray spectrum is used, the barite effect on this part of the spectrum causes an increase in thorium and decrease in uranium. KCl causes an increase in the potassium (as to be expected) but also a decrease in the uranium. Charts and computer algorithms are available to correct for these errors but are not entirely adequate since they are non-linear.

**Table 7.8** Potassium in clay minerals: chemical content. From Serra (1979), Dresser Atlas (1983).

| | †Potassium content | | |
|---|---|---|---|
| Mineral | % by weight | Average % | Construction |
| Illite | 3.51–8.31 | 5.20 | K, Al,Silicate |
| Glauconite | 3.20–5.80 | 4.50 | K, Mg, Fe, Al, Silicate |
| Kaolinite | 0.00–1.49 | 0.63 | Al, Silicate |
| Smectite | 0.00–0.60 | 0.22 | Ca, Na, Mg, Al Silicate |
| Chlorite | 0 | 0 | Mg, Fe, Al, Silicate |

†Average shale = 2% – 3.5% potassium

## 7.5 Geochemical behaviour of potassium, thorium and uranium and natural radioactivity

The old tenet that the gamma ray log is a 'shale log' was based on its use as a black box, not understanding what was inside. In modern interpretation an understanding of the mineralogy and geochemistry leading to radiation is used. Described below are the natural occurrences of the radioactive minerals and their geological significance.

***Potassium***

Potassium is both chemically active and volumetrically common in naturally occurring rocks. Because of its chemical activity it is generally chemically combined. In the clay minerals, for example, it (and invariably its radioactive isotope) occurs in the clay silicate structure. In evaporites it occurs chemically as a salt, and in rock-forming minerals, such as the feldspars, it is again chemically combined in the silicate structure. The behaviour of potassium can therefore be considered in terms of chemical composition, as can its contribution to radioactivity.

The potassium content of the clay mineral species varies considerably. Illites contain by far the greatest amount, while kaolinite has very little or none (Table 7.8). The consequence of this is that clay mixtures with a high kaolinite or high smectite content will have lower potassium radioactivity than clays made up essentially of illite (mica) (Figure 7.1). However, since most clays are mixtures of several clay minerals, the differences discussed above are muted. The average shale has a potassium content of about 2% – 3.5% (Table 7.8).

Potassium is present in many rock-forming minerals besides the micas, considered above as clay minerals. The most important of these are the feldspars. Microcline contains approximately 16% potassium by weight, and orthoclase approximately 14%; such percentages render the feldspars highly radioactive in geological terms (*see* Table 7.15). Feldspathic sediments may therefore be detected by their radioactivity.

Finally, potassium is found in some of the less commonly occurring evaporites but in sufficient quantities to have an

**Table 7.9** Potassium content of evaporites.

| Species | Formula % | Potassium by weight* | Typical gamma ray value API† |
|---|---|---|---|
| Sylvite | KCl | 52.5 | 500 |
| Carnallite | $KCl.MgCl_2(H_2O)_6$ | 14.1 | 200 |
| Polyhalite | $K_2SO_4.MgSO_4$ | 12.9 | 190 |

*Serra *et al.*, 1980
†Serra, 1979.

important effect on the radioactivity (Table 7.9). In these salts there is between 10% and 50% potassium by weight. When it is considered that the average shale contains only 2% – 3.5% potassium, the very strong radioactivity of these potassium evaporites is understandable (Table 7.9, Figure 7.21).

### *Uranium*

Acid igneous rocks on average contain 4.65ppm of uranium and are the principal original source for the element. It forms soluble salts, especially in the uranyle form ($U^{6+}$) being stable in oxidising conditions, and as the oxide $UO_2^{2+}$(the uranyle ion) is transported in river water (the uranous form $U^{4+}$ also exists and is stable in reducing conditions, but is less common) which contains on average 0.6 μg/ml of uranium in solution. However, it is suggested that most (around 90%) uranium in rivers is actually carried attached (loosely?) to clay particles and not in solution (Durrance, 1986). This is suggested because suspended river sediment contains approximately 3ppm of uranium, while the bedload sediments have much lower values. Sea water, on average contains about 3ppb of dissolved uranium.

From river or especially sea water, uranium passes into sediments in three principal ways (Serra, 1979): 1, chemical precipitation in acid (pH 2.5–4.0), reducing (rH 0–0.4) environments: 2, adsorption by organic matter, or living plants and animals: 3, chemical reaction in phosphorites (phosphate rich rocks).

The extremely acid, reducing conditions required for the direct chemical precipitation of uranium (pH 2.5–4.0, rH 0–0.4) are found in few natural environments. They do occur, however, in stagnant, anoxic waters with a relatively slow rate of sediment deposition, which typically produce black shales (Adams and Weaver, 1958). The high gamma radiation values of the North Sea Jurassic 'hot shales', typical black shales, come from a high uranium content, some of which was probably chemically precipitated (Figure 7.11, Table 7.10) (Bjørlykke *et al.*, 1975).

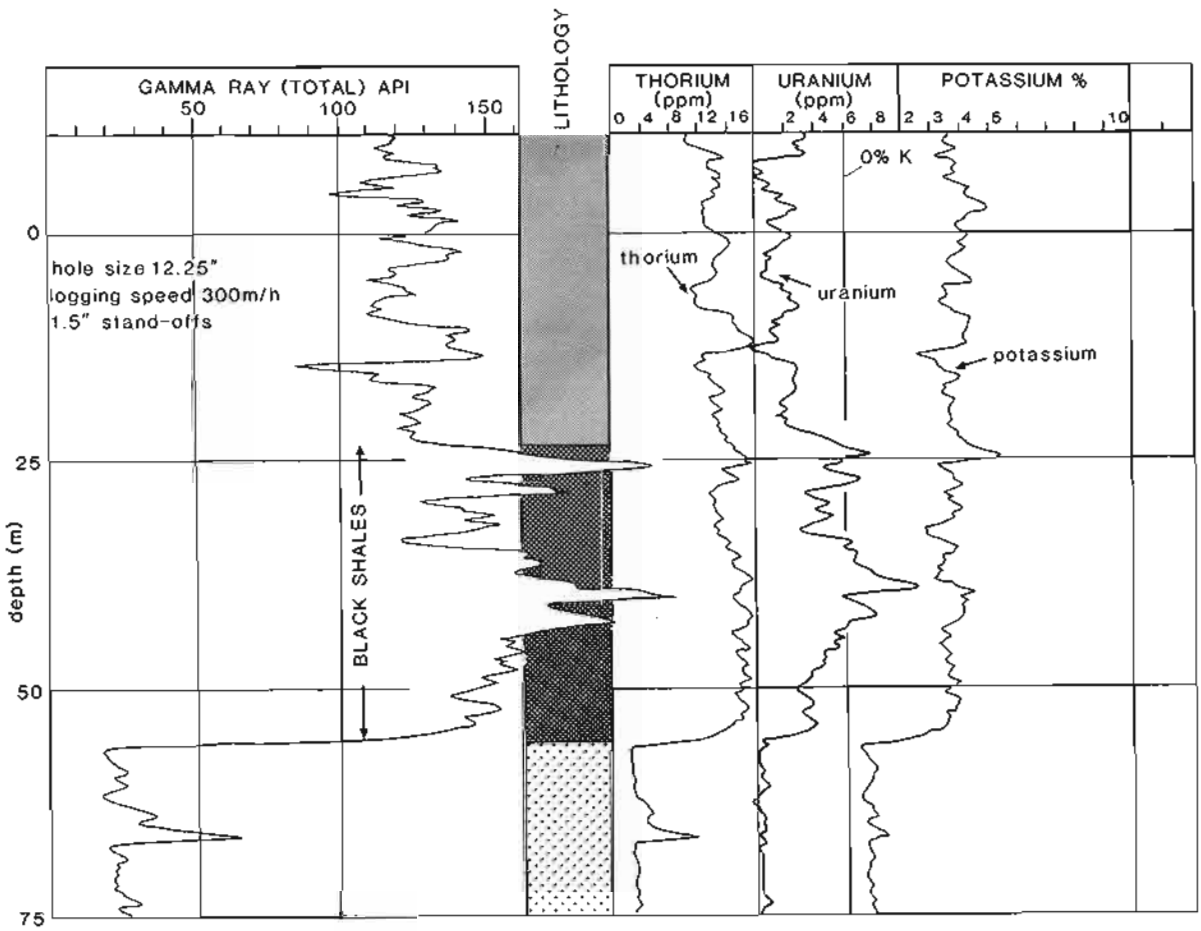


**Figure 7.11** 'Black shale' radioactivity. A spectral gamma ray log over the Upper Jurassic black shales of the North Sea showing the high uranium contribution.

**Table 7.10** The abundance of the radioactive elements and their relative contributions to the overall radioactivity of the black shale example of Figure 7.11 (values calculated for the peak at 40m).

| Element | Content | *gamma ray API equivalent | % gamma ray value |
|---|---|---|---|
| Uranium | 11 ppm | 89.0API | 41.0% |
| Thorium | 18 ppm | 70.7 API | 32.6% |
| Potassium | 3.5% | 57.1 API | 26.4% |

*using the multipliers given in the text (section 7.4)

Probably a more common way of introducing uranium into sediments is in association with organic matter. It has been established experimentally that carbonaceous material can extract uranium from solution very efficiently, especially over the range of pH 3.5–6.0 (acidic) (Durrance, 1986). Organic-rich shales often (but not always) contain large amounts of syngenetic uranium (i.e. extracted locally), in which case they are associated with high gamma ray log values (e.g. Schmoker and Hester, 1983) (Figures 7.1, 7.22). It is the large size and high charge density of the uranyle ion which allows this, and it is thought that the process eventually involves an ionic bonding. The urano-organic complexes produced may form coatings on organic or inorganic particles or be disseminated through the sediment mass. However, the exact relationship between organic matter and total uranium content is not easy to establish, since high organic matter content is not always related to high uranium content (cf. Meyer and Nederlof, 1984) (Figure 7.12). Empirically, the constant presence of organic matter in shales (Table 7.11) suggests that uranium adsorbed by organic matter is an important contributor to overall shale radioactivity (*see* Section 7.6).

The third way of introducing uranium into sediments concerns principally phosphates and associated deposits. The uranium present in phosphatic rocks is generally syngenetic and is found within the phosphates. Primary uranium minerals are absent. The very variable valence behaviour of uranium means that under the right conditions it forms complex ions with carbonate, phosphate, hydroxide and others and it is assumed that $U^{4+}$ substitutes for calcium in the carbonate-fluorapatite generally found in marine phosphorites (Durrance, 1986). The correct chemical conditions for this type of reaction may be very localised, such as exist in hardgrounds.

In general, uranium behaves as an independent constituent: it is not chemically combined in the principal molecules of rocks like potassium, but is loosely associated with secondary components. For this reason it has a very heterogeneous distribution in sediments. Moreover, its continued solubility even in the subsurface, which is a function of its loose attachments, renders it susceptible to leaching and redeposition, making its distribution even more irregular.

**Table 7.11** Average weight (%) of organic matter in sediments (from Shaw, 1980).

| Sediment | Average weight % |
|---|---|
| Shales | 2.90 |
| Carbonates | 0.29 |
| Sandstones | 0.05 |

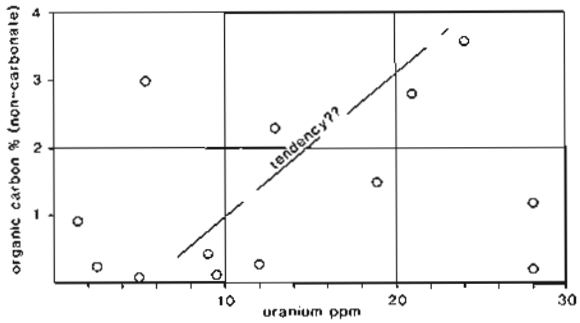


**Figure 7.12** Organic carbon content compared to uranium content: there is wide dispersion. (Source of data, Adams and Weaver, 1958).

Typically, on the logs, uranium is shown by irregular, high peaks corresponding to its uneven distribution. Due to the unusual requirements of its original deposition, these peaks are associated with unusual environments such as are found in condensed sequences or at unconformities (i.e. Figure 7.31).

***Thorium***

Like uranium, thorium has its origin principally in acid and intermediate igneous rocks. However, it is extremely stable and, unlike uranium, will not go into solution. For this reason it is found in bauxites (residual soils). Although there is a possibility that thorium is adsorbed onto clay minerals (Durrance, 1986), it is generally transported to sites of sediment deposition as clay fraction detrital grains. These are of heavy minerals such as zircon, thorite, monazite, epidote and sphene (Table 7.12) which are all very stable.

Because of its detrital nature and current transport in

**Table 7.12** Thorium-bearing heavy minerals (Serra *et al.*, 1980).

| | Composition | $ThO_2$ content (%) |
|---|---|---|
| Thorite | Th, Si, $O_4$ | 25–63 |
| Monazite | Ce, Y, La, $PO_4$ | 4–12 |
| Zircon | Zr, Si, $O_4$ | less than 1 |
| | **Uranium ppm** | **Thorium pm** |
| Zircon | 300–3000 | 100–2500 |
| Sphene | 100–700 | 100–600 |
| Epidote | 20–50 | 50–500 |
| Apatite | 5–150 | 2–150 |

**Table 7.13** Thorium abundance in clay minerals. (From Hassan *et al.*, 1976; Dresser Atlas, 1983).

| Mineral | Thorium ppm (approximate average) | |
|---|---|---|
| Bauxite | 8–132 (42) | More continental |
| Kaolinite | 18–26 | ↑ |
| Illite–muscovite | 6–22 | ↕ |
| Smectite | 10–24 | ↓ |
| Glauconite | 2–8 | More marine |

the clay-grain sized fraction, thorium shows an affinity for terrestrial clay minerals. For example, it shows higher concentrations in kaolinites (of terrestrial origin) than in glauconites (of marine origin) (Hassan *et al.*, 1976; Figure 7.1, Table 7.13). In the coarse grained sediments, thorium minerals may be found as silt-sized heavy mineral concentrations or placer deposits (see 'sandstone radioactivity' below).

Despite its lack of solubility, thorium is however, widely and relatively evenly distributed in sediments. So much so that in shales it is used as a base level from which the relative abundance of the other radioactive elements, especially uranium, is measured (Section 7.10).

## 7.6 Radioactivity of shales and clays

In petroleum borehole logging the commonest natural radioactivity (by volume) is found in shales (clays). A high gamma ray value frequently means shale. A typical shale analysed by a spectral gamma ray tool shows that each of the three elements, U, Th, and K, is contributing (Figure 7.13) and an analysis of shales in general shows

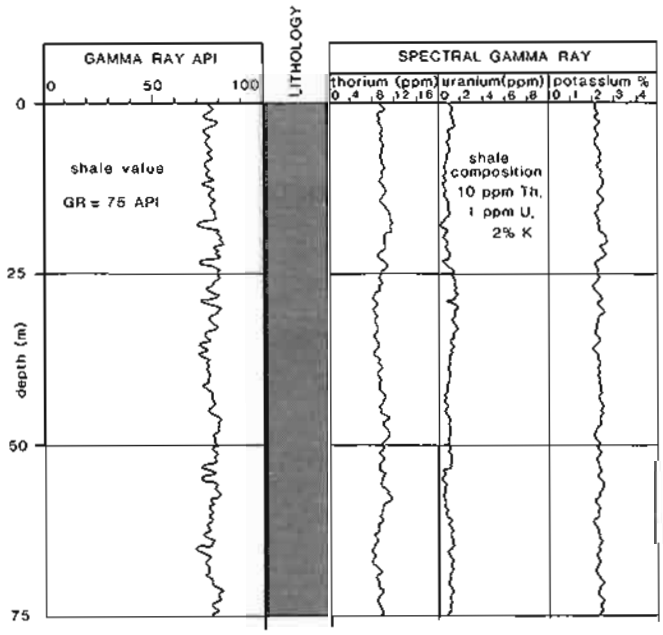


**Figure 7.13** A typical shale interval analysed by a spectral gamma ray tool. The log shows the individual contributions of thorium, potassium and uranium to the overall radioactivity.

**Table 7.14** Average radioactive mineral content and contribution to total shale radioactivity (this is only one set of figures among several).

| | †Average content | †Range | *contribution to total radioactivity % |
|---|---|---|---|
| Uranium | 4 ppm | 2 ppm – 6 ppm | 29% |
| Thorium | 12 ppm | 8 ppm – 18 ppm | 42% |
| Potassium | 2.0% | 2.0% – 3.5% | 29% |

†Myers, K. pers. comm.
*using the average figures (column 2)

the relative contribution of each element to the overall radioactivity (Table 7.14).

But the gamma ray log should not be used as a 'black box' shale indicator either qualitatively or quantitatively, as is commonly the case. The behaviour of the individual radioactive elements in clay minerals and clays in general is so different, as the preceding geochemical descriptions indicate, that there is a need for more detailed understanding.

Potassium is involved in the chemical make up of clay mineral structure and, despite the variations of this in specific clay mineral species (Table 7.8), has a fairly consistent content in most shales, of around 2% – 3.5%. This is the case since shales are generally a mix of several of the clay mineral types. Potassium therefore is a moderately good 'shale indicator'. However, potassium occurs in detrital minerals such as feldspars as well as in clay minerals, so that in sand-shale mixtures, potassium may occur in both the shales and the sands and cannot alone be used as a shale indicator and descriptor (see Section 7.9). Uranium distribution is very irregular as has been shown, because its affinity is to secondary components and not the main the rock forming minerals. Thus, in the average shale it may contribute only 10% – 30% of the total radioactivity (Table 7.14) but in certain cases this can increase dramatically (e.g. Table 7.10, Figure 7.31). Since its distribution is not related to clay volume, uranium is a poor 'shale indicator'. For this reason, on spectral gamma ray logs, a curve is plotted without the uranium content (the CGR) to give a better clay volume estimate (Section 7.4, Figure 7.6).

The behaviour of thorium in shales is not fully understood. Experience shows that despite its varying content in clay mineral species (Table 7.13), it has a constant value in almost all naturally occurring shales. The average value is about 12.0 ppm (range 8–18 ppm) for a typical shale, contributing between 40% – 50% of the overall shale radioactivity (Table 7.14 and ref.). Considering therefore the constant average value and the high percentage contribution to the overall radioactivity, thorium is a very good 'shale indicator'. In mixtures of sand and shale, thorium will occur only in the shale fraction (except in rare occurrences).

To summarise: as shale indicators, thorium, may be used in most cases, potassium may be used in many cases but uranium should not be used at all. This obviously has implications for the simple gamma ray log: it is not necessarily a good 'shale indicator'.

## 7.7 Quantitative use of the simple gamma ray log

The gamma ray log may often be used quantitatively, and although the gamma ray value for shales varies enormously, in any one area or well, the values for pure shale tend to be constant (Figure 7.14). Thus, if one considers the maximum average gamma ray log value to be pure 100% shale (i.e., shale line, Figure 7.14), and the lowest value to indicate no shale at all (i.e., sand line, Figure 7.14), a scale from 0 – 100% shale can be constructed. If the scale is considered to be linear, any value (GR) of the gamma ray log will give the volume of shale from the simple calculation

$$\text{volume of shale \%} = \frac{\text{GR value (log)} - \text{GR (min)}}{\text{GR (max)} - \text{GR (min)}} \quad (1)$$

GR (max) = 100% shale, GR (min) = 0% shale, i.e. clean formation.

Generally the value is not very accurate and tends to give an upper limit to the volume of shale (Vsh or Vclay). Moreover, there is no scientific basis for assuming that the relationship between gamma ray value and shale volume should be linear. Thus, a modification of the simple linear relationship used above has been proposed as a result of empirical correlation (Dresser Atlas, 1982). The relationship changes between younger (unconsolidated) rocks and older (consolidated) rocks (Figure 7.15):

for pre-Tertiary (consolidated) rocks,

$$V_{sh} = 0.33(2^{2V^*_{sh}} - 1) \quad (2)$$

for Tertiary (unconsolidated) rocks,

$$V_{sh} = 0.083(2^{3.7V^*_{sh}} - 1) \quad (3)$$

where Vsh = shale volume from these formulae (*see* Figure 7.15) and

$$V^*_{sh} = \frac{\text{GR} - \text{GR(min)}}{\text{GR(max)} - \text{GR(min)}}$$

as shown previously in (1).

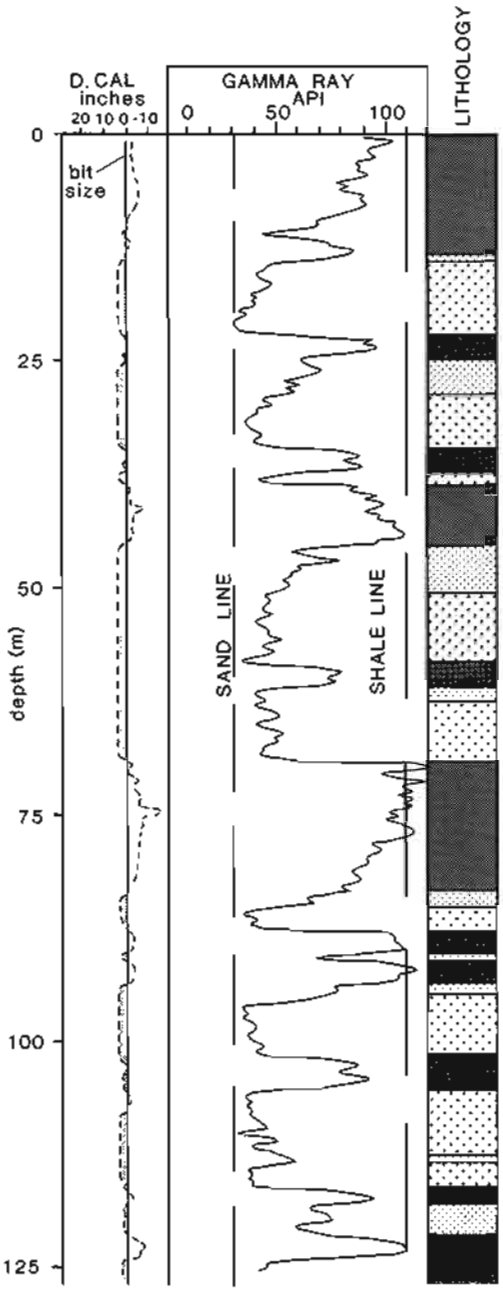


**Figure 7.14** Sand line and shale line defined on a gamma ray log. These 'baselines' are for the quantitative use of the log, and may be reasonably constant in any one zone.

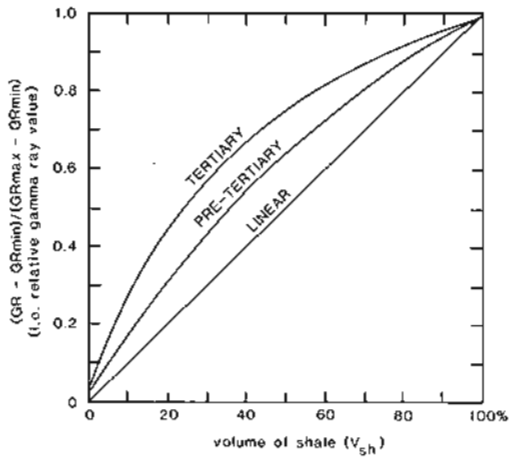


**Figure 7.15** Graphical representation of the relationship between relative gamma ray deflection and shale volume. (From Dresser Atlas, 1982).

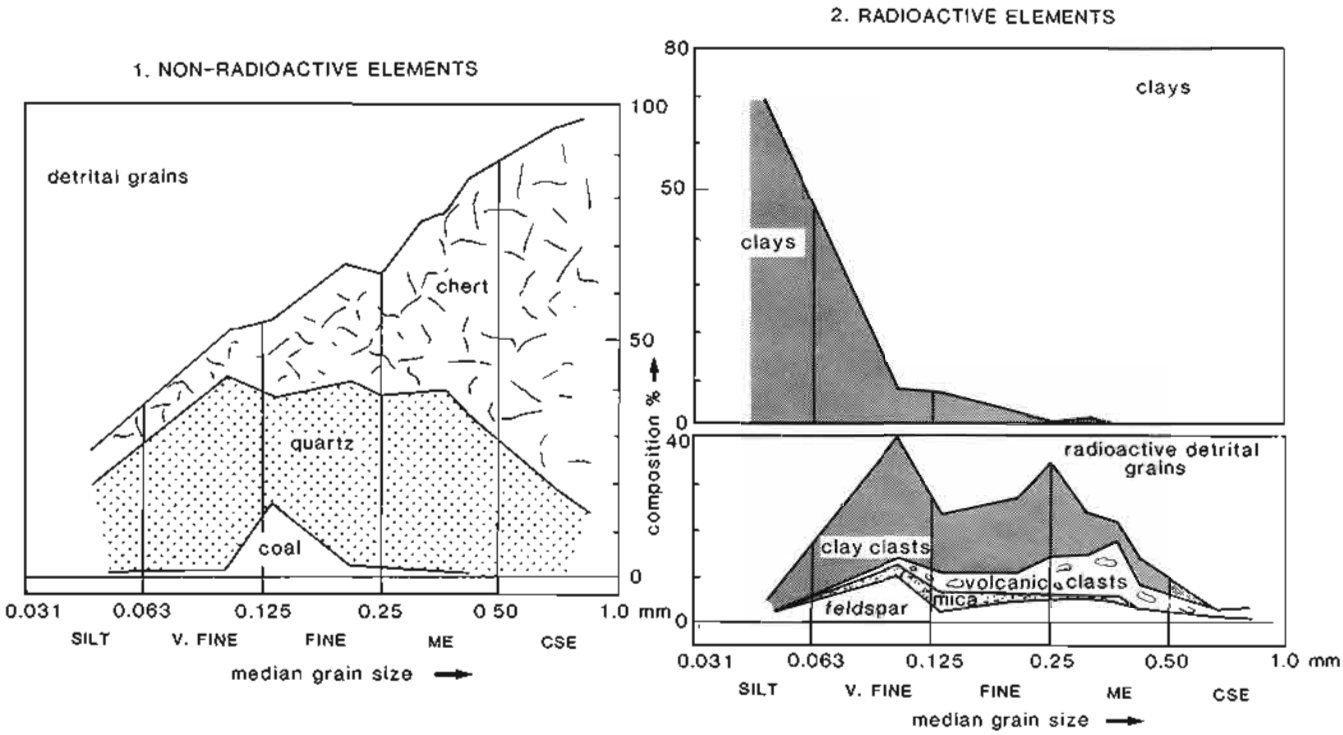


**Figure 7.16** Radioactive elements in detrital rocks. Typical sandstone composition shown against grain size for the Reindeer Formation, Mackenzie Delta, Beaufort Sea. Radioactive elements vary with grain size. It is a deltaic sand of Lower Tertiary age. (Redrawn from Nentwich and Yole, 1982).

**Table 7.15** Potassium content of some common detrital materials (from Serra, 1979; Edmundson *et al.*, 1979; Dresser Atlas, 1983; Schlumberger, 1985).

| | Mineral species | % potassium by weight | Average % | Gamma ray value (API) |
|---|---|---|---|---|
| Micas | Glauconite* | 3.2 –5.8 | 4.5 | 75† – 90† |
| | Muscovite | 7.9 – 9.8 | 9.8 | 140† – 270 |
| | Botite | 6.2 – 10.1 | 8.7 | 90† – 275 |
| Feldspars | Microline | 10.9 – 16 | 16 | 220 – 280† |
| | Orthoclase | 11.8 – 14 | 14 | 220 – 280† |

*Detrital or authigenic
†For 8in hole, 1.2g/cm³ mud, 3½in NaI scintillator

## 7.8 Qualitative use of the simple gamma ray log

### *Lithology*

As a first indicator of lithology, the gamma ray log is extremely useful as it suggests where shale may be expected (Figure 7.1). Moreover, as shown above, the higher the gamma ray value, the higher the percentage of shale (Figure 7.15). But the log is only a first indicator. The radioactivity of some typical lithologies other than shale is now considered. This shows that any lithology indicated by the simple gamma ray log must be confirmed by other logs.

### *Radioactivity of sandstones and other arenaceous rocks*

Quartz, the principal component of the coarse-grained detrital rocks, shows no radioactivity. Sandstones consequently usually show low gamma ray values (Figure 7.1). However, associated detrital minerals are radioactive. The most common of these are feldspars, micas, heavy minerals and lithic fragments (Figure 7.16). The first two groups contain potassium (Table 7.15), the third thorium (Table 7.12) and the last contains shale. These all cause sandstones with high to moderate gamma ray values.

There are many examples of radioactive sandstones that may be quoted. The fine-grained mica sands of the North Sea (Nyberg *et al.*, 1978) are a typical, well-known example (Figure 7.17). Some marine sands contain glauconite and, if the concentrations are sufficiently high, render the sands radioactive (Figure 7.18). In fact radioactive sandstones are far more common than realized. Arkoses are radioactive by definition (Table 7.16).

Thorium, as previously described, is present in heavy-mineral suites. Placer silts (concentrations of heavy minerals) are frequently radioactive, producing a spiky aspect to the gamma ray log (Figure 7.19). However, this is the only case, and in general detrital grain radioactivity is caused by potassium (Table 7.16).

For sandstone reservoir studies, identifying clay as opposed to non-clay radioactive elements is important. Neglecting radioactive sandstone intervals as being shales means missing essential reservoir. The fact that only potassium should be causing detrital mineral radioactivity in sandstones (e.g. Table 7.15) is used in the interpretation of the spectral gamma ray log to separate shale radioactivity from detrital grain radioactivity (*see below*, 'Quantitative uses of the spectral gamma ray').

***Radioactivity in carbonates***

Carbonates in their pure state are not radioactive and this aids their identification (Figure 7.1). Nonetheless, in certain facies, carbonates contain organic matter and this is frequently radioactive due to uranium. This is certainly the case in the example given (Figure 7.20) and it is proposed (Hassan, 1973) that pure carbonate radioactivity is due only to uranium. Shaly carbonates will show the presence of potassium and thorium.

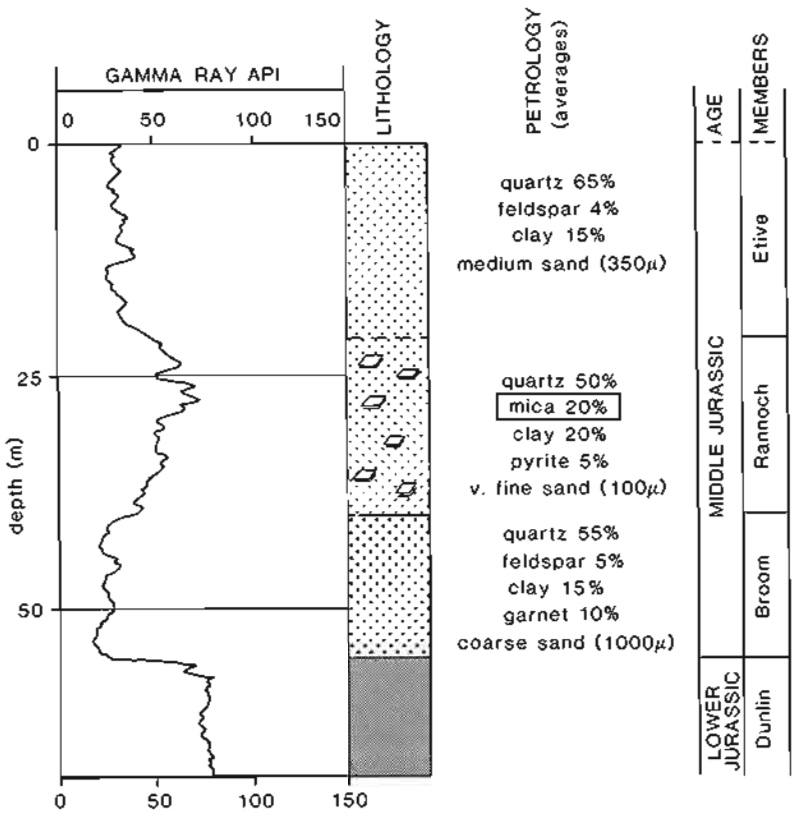


**Figure 7.17** Radioactive sand, the 'mica sands' of the North Sea Jurassic. They are fine-grained shallow marine sandstones with perhaps 20% clay but 15 – 30% mica, mainly muscovite, which causes the radioactivity.

**Table 7.16** Radioactivity in sandstones.

| Species | Mineral | Radioactive element |
|---|---|---|
| Mica sand | Muscovite/biotite | $^{40}K$ |
| Glauconitic sand | Glauconite | $^{40}K$ |
| Arkose | Potassic feldspar | $^{40}K$ |
| Placer silt | Heavy minerals | Th |

***Radioactivity in evaporites***

The most common evaporites, such as salt and anhydrite, give extremely and abnormally low values on the gamma ray log. However, the high radioactivity in some evaporites caused by potassium content has already been mentioned (Table 7.9). The log example shows a typical aspect of this evaporite radioactivity. Frequently there are extreme contrasts between the potassium and non-potassium-bearing zones (Figure 7.21). Volumetrically, potassium rich evaporites are rare.

It is considered that in logging potassium salts the percentage of $K_2O$ can be estimated from the gamma ray response. Thus, for a 6.25 inch, liquid-filled hole, Edwards *et al.* (1967) found a correlation of 12.6 API units per 1% $K_2O$. Obviously, the logs must always be calibrated before making generalizations of this kind.

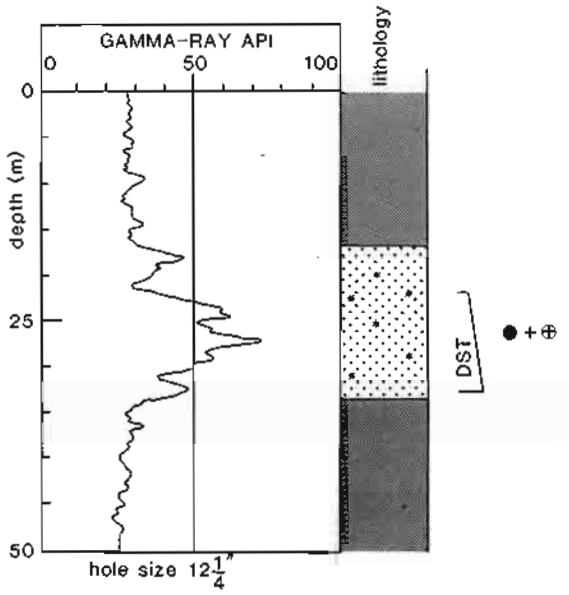


**Figure 7.18** Glauconite causing radioactivity in a sandstone interval. Silty sands envelop this marine, glauconite-rich sand giving the sands higher gamma ray log values than the shales. An oil flow confirms the reservoir characteristics. DST = Drill Stem Test. *Glauconite.

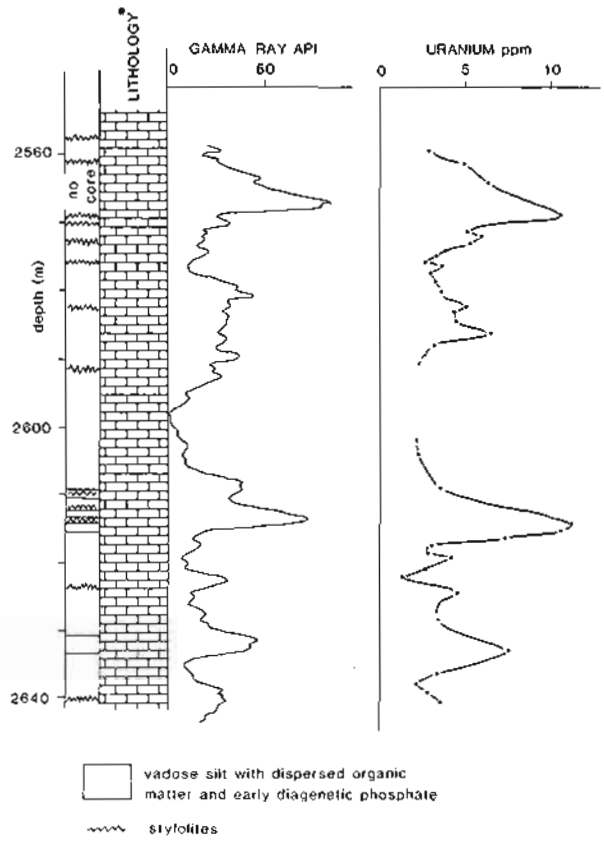


**Figure 7.20** Radioactivity of Ypresian (Eocene) Limestones, Tunisia, related to uranium concentrations. The uranium is associated with early diagenesis, organic matter and phosphatic concentrations. (Re-drawn from Hassan, 1973).

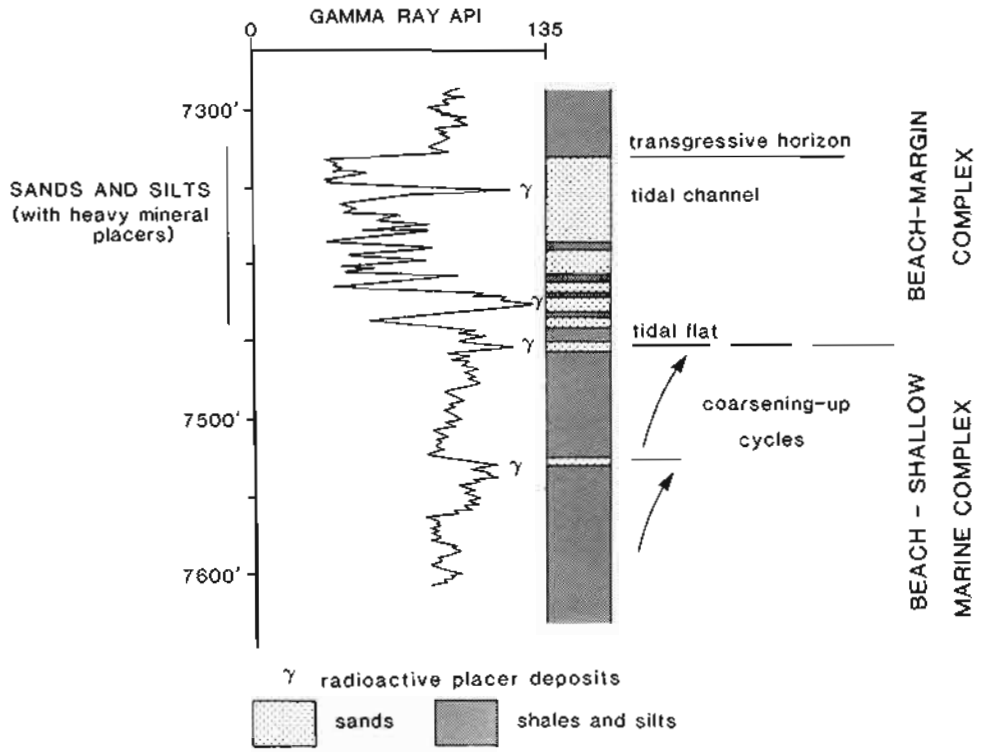


**Figure 7.19** Heavy mineral concentrations (placer deposits) causing a spiky gamma ray log. Shales have lower gamma ray values than the heavy mineral deposits (Nigeria). (Re-drawn from Serra, 1974).

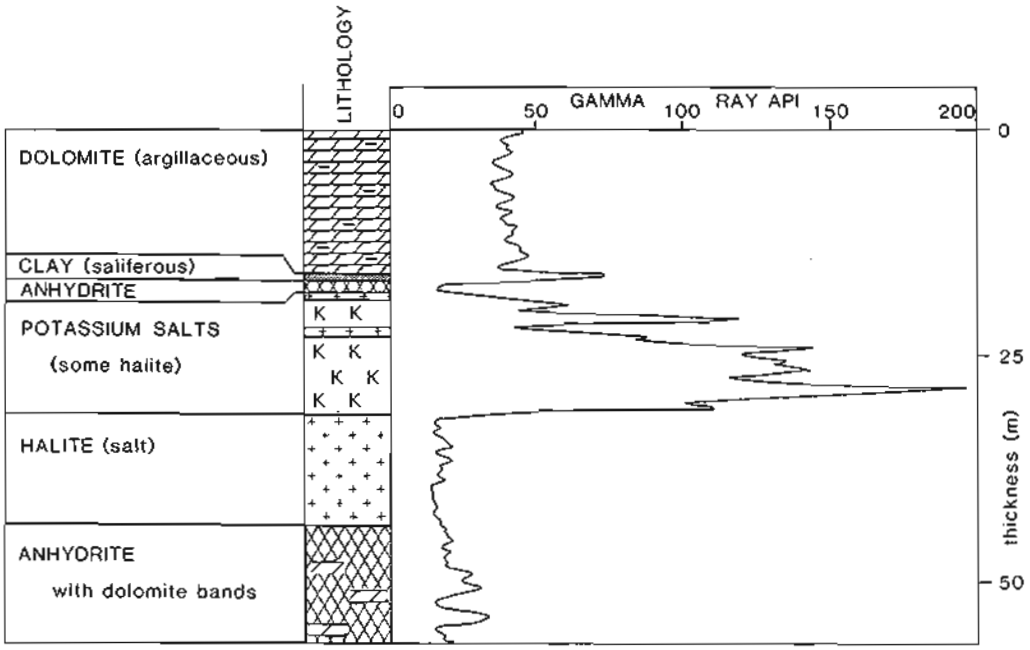


**Figure 7.21** Potassium salts giving very high peaks of radioactivity in an evaporite sequence. (The lithology comes from an interpretation of combined logs and cuttings). Permian, North Sea.

### *Coal and organic rich shale (source rock) radioactivity*

The relationship between organic matter and uranium enrichment is the basis for being able to identify organic rich shales (source-rocks) using the gamma ray log and is discussed under Section 7.10 (Organic matter and source rocks: uranium content). In practice, although high gamma ray values often correspond to organic matter rich, source-rock intervals (Figure 7.22), such intervals do not always have a high gamma ray value (i.e. Schmoker, 1981 and Section 7.10 below).

Coals have low gamma ray values (Figures 7.1, 7.23). The contrast in this response between pure coals and organic shales is remarkable, especially when, in typical cyclic deltaic sequences, a low gamma ray coal is immediately overlain by a high gamma ray, organic-rich shale (Figure 7.23). It appears that uranium, which is adsorbed by organic matter to cause the high gamma ray values in the organic rich shales, is not adsorbed by organic matter in terrestrial swamps where no clay is present. Clay seems to be a catalyst to the adsorption. Thus, pure coals have the typical low gamma ray response while shaly coals have a gamma ray value which depends on the shale (or ash) content (Kayal and Christoffel, 1989).

### *Igneous and volcanic rock radioactivity*

Igneous rocks are not volumetrically important in petroleum wells, but occur sufficiently frequently to be a

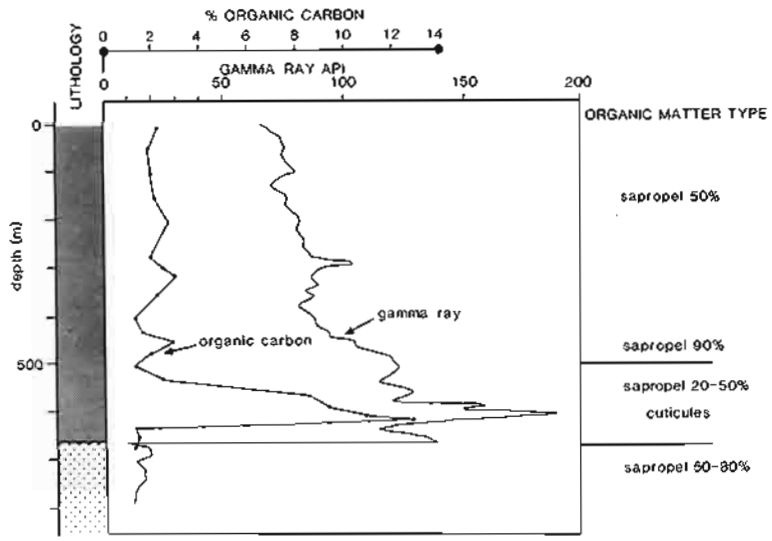


**Figure 7.22** High organic carbon values and the total gamma ray giving good correlation, in this case due to uranium associated with organic matter.

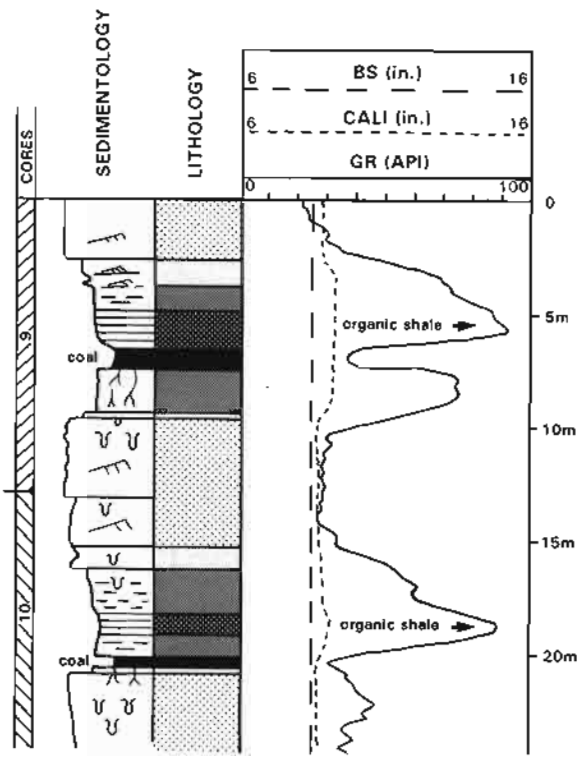


**Figure 7.23** Gamma ray characteristics of coal (very low values) and organic rich shale (very high values) in a deltaic sequence.

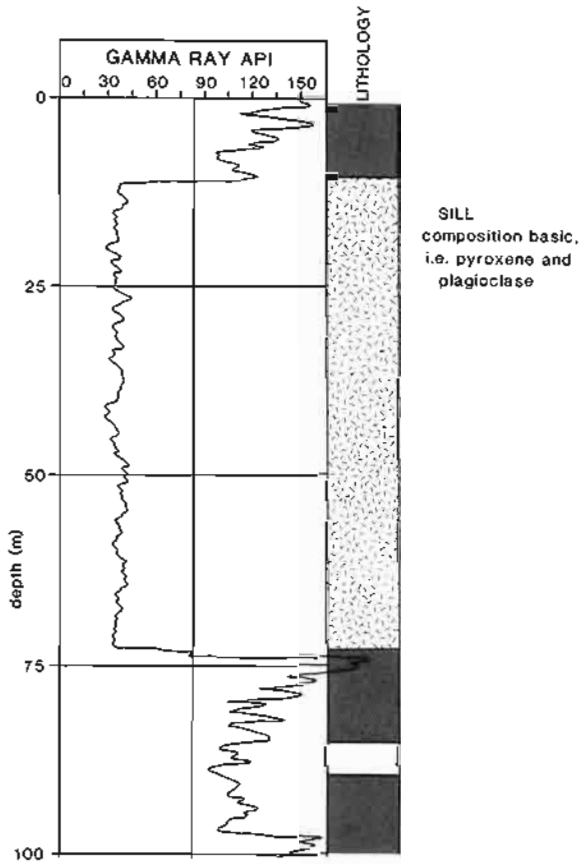


**Figure 7.24** Low gamma ray values through a basic sill. It may be confused with a sandstone interval.

necessary element in the lithologic vocabulary. Both uranium and thorium originate in the acid to intermediate igneous rocks, but their distribution is very irregular since they are associated with secondary minerals such as apatite. Potassium is present, especially in the acid igneous rocks, principally in the alkali (potassic) feldspars. The net result is that basic igneous rocks have low radioactivity, while the intermediate and acid types show progressively higher values (Keys, 1979; Sanyal *et al.*, 1980) (Table 7.17).

The example shows a typical basalt which may be confused with sand (Figure 7.24).

### *Unconformities*

Unusually high gamma ray values often occur as narrow, isolated peaks. Considering the geochemistry of the radioactive minerals, these peaks are generally associated with uranium concentrations. As discussed (*see 'Uranium'* above) uranium concentrations indicate extreme conditions of deposition. Experience has shown that these conditions frequently occur around unconformities where a long passage of time is represented by little deposition. The minerals associated may be uranium-enriched phosphates or uranium-enriched organic matter (*see also* Chapter 15, and Figure 14.19).

### *Facies and grain size*

An interesting and fairly comprehensive scheme for facies identification in detrital sediments (sand-shale) has been developed using gamma ray log shapes. The basis for the scheme is the relationship between grain size and shale content. It is shale content that the gamma ray log indicates, but it is interpreted in terms of grain size. For example, a coarse-grained sand will have a very low shale content, a medium-grained sand some shale, and a fine-grained sand may be very shaly. The changes in grain size will be followed by changes in gamma ray value (Figure 7.25).

**Table 7.17** Radioactive elements in igneous and volcanic rocks (from Serra, *et al.*, 1980; figures approximate).

| Rock type | Th (ppm) | U (ppm) | $K_2O$% | Typical radioactivity |
|---|---|---|---|---|
| Acid intrusive | 1–25 | 1–8 4. | 11–2.00 | High |
| Acid extrusive | 9–25 | 2–7 | 2.00–6.00 | |
| Basic intrusive | 0.5–5 | 0.3–2 | 0.90–2.20 | Low |
| Basic extrusive | 0.5–10 | 0.2–4 | 1.40–2.50 | |
| Ultrabasic | – | 0.0001–0.03 | 1.6 | Very low |

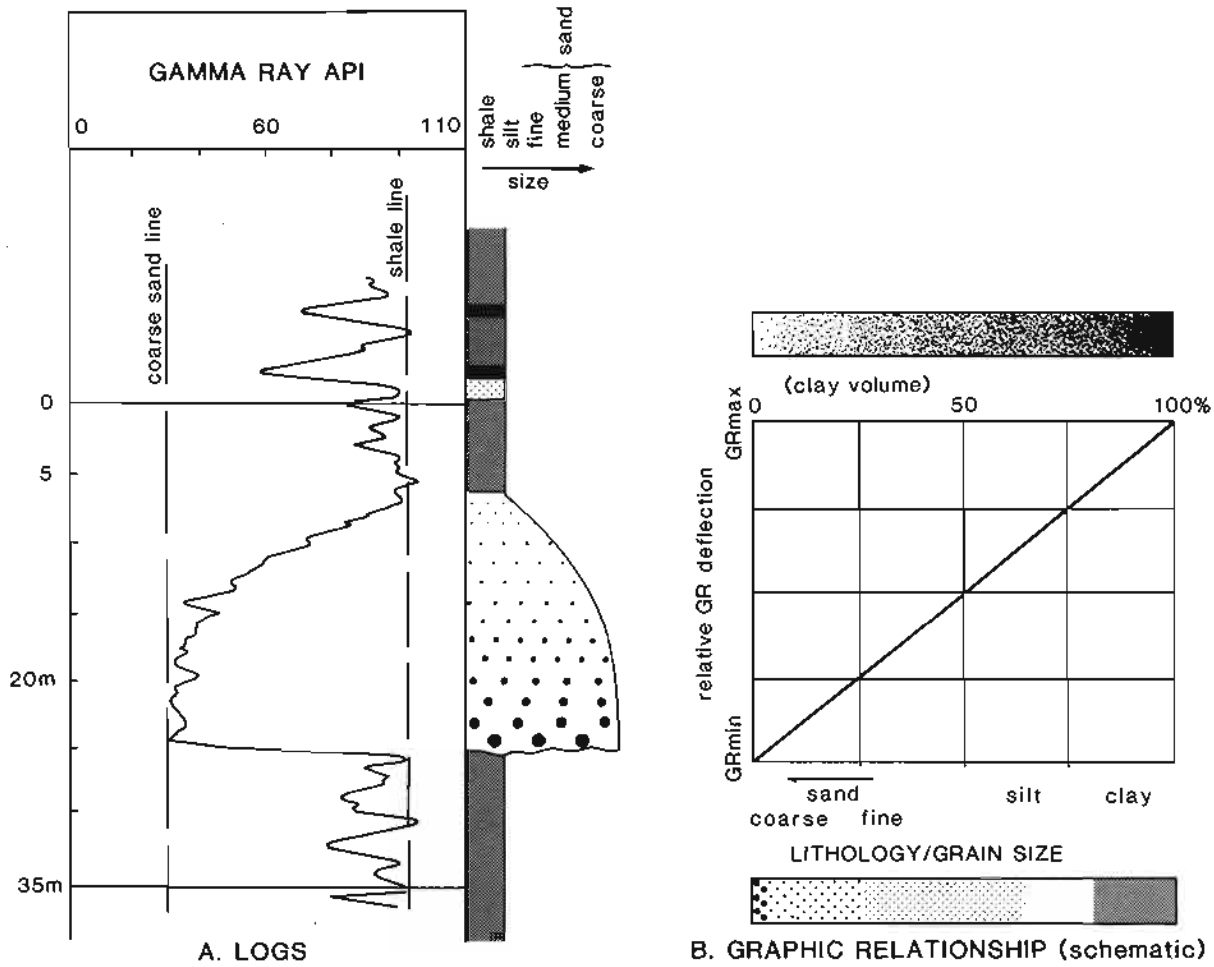


**Figure 7.25** Facies from the gamma ray log. (A) The changes in sandstone grain size are reflected in changes in the gamma ray value. This allows a facies to be suggested. (B) Graphic representation of the variation of grain size with gamma ray value. Here it is expressed as a straight line but the relationship is very variable. It should parallel the clay volume change.

This method of indicating facies with the gamma ray log, however, is not straightforward. The relationship between grain size and shale content is very variable, as is the relationship between shale volume and gamma ray value (*see* 'Shale volume'). Empirically, if the gamma ray log shows a typical shape it can be taken as indicating grain-size changes. A lack of shape is not evidence for lack of grain-size change since it cannot be interpreted (Rider, 1990).

The facies scheme derived from the gamma ray log is fully described in Chapter 14.

### *Correlation*

The gamma ray log is one of the most frequently-used logs for correlation. It has 'character', is repeatable, is not affected by depth, it gives some indication of lithology and is simple (Figure 7.26). Moreover, it is almost always run and the sensitivity scales are always relatively similar. Generally, because it is used for correlation, it is reproduced on the well completion log, the document used to reassemble the essential drilling and geological data at the end of a well (*see* Chapter 11).

Besides its availability, the gamma ray log has inherent advantages for correlation, especially when this concerns shales. The gamma ray value of shale formations is often variable, depending on the various amounts of clay, minerals, carbonate and organic matter present. Horizontally, at the same stratigraphic level, these various elements tend to show only slight variability in the complex mix, i.e., the depositional environment which controls the mix is laterally persistent.The complexity does not persist through time, as most abrupt changes are vertical. There are changes, amongst others, in source and age. Thus, the gamma ray log value in shales remains constant laterally but changes vertically. These are ideal characteristics for correlation.

Recently, correlation with the gamma ray log has taken on a new significance. It is suggested that gamma ray peaks in shale sequences represent condensed sections, (maximum flooding surfaces in sequence stratigraphic parlance) which are effective time lines and should be correlated. This subject is considered in detail later in the book (Chapter 15) and in more detail in terms of the gamma ray below (Section 7.10).

In sandstones, gamma ray log shapes are often used to correlate. However, the shape is a facies characteristic

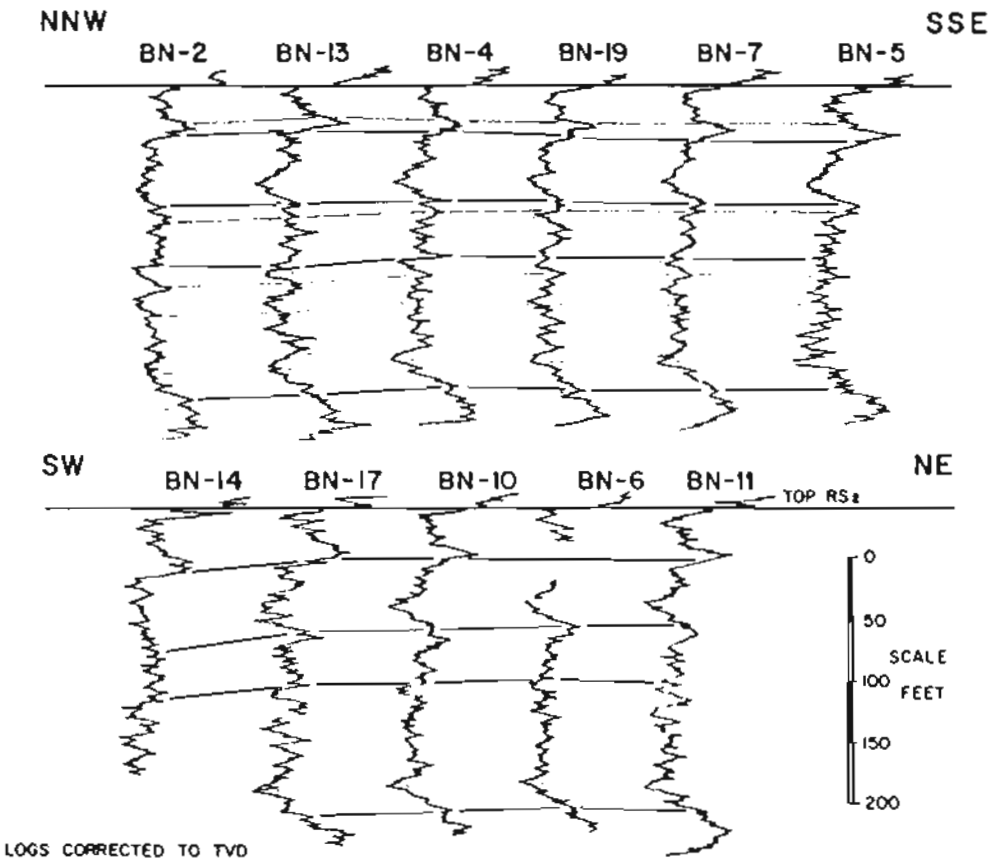


**Figure 7.26** Correlation using the gamma ray log. Baronia field, Sarawak. (From Scherer, 1980).

and often leads to false correlations (e.g., Figure 15.20). Log shapes in carbonates are generally related to shale distribution and as such are more reliable for correlation. However, the shapes must be sufficiently consistent to ensure that they are not related to uranium concentration, as discussed above (*see* 'Radioactivity in Carbonates' above).

Although it has many advantages for correlation, the gamma ray log also has disadvantages. The fine detail on the logs is generally noise and statistical variation (para 7.4). A comparison between any log and a repeat section shows to what extent this has an effect. Fine peaks therefore cannot be used for correlation. The second disadvantage is that the gamma ray cannot be calibrated (cf. Chapellier, 1992). Although absolute values are given on the logs they are relative both to hole size and tool, (Section 7.4, Figure 7.8). Logs, to be entirely comparable, must be 'normalized' (*see* Chapter 11).

## 7.9 Quantitative use of the spectral gamma ray log

The spectral gamma ray log, like the simple gamma ray, is used to calculate shale volume. It can also be used to calculate the volume of radioactive minerals.

***Shale volume***

In the description of shale radioactivity given previously (Section 7.6), it was shown that the three naturally radioactive elements are not distributed regularly in shales. Some spectral logs are therefore plotted with a computed potassium + thorium radioactivity curve as a better shale indicator (Figure 7.6). However, as described, potassium can occur in detrital minerals such as micas and feldspars so that thorium can be considered as the best shale indicator (Fertl, 1979; Schenewerk *et al.*, 1980). The shale volume calculated from the spectral gamma ray log therefore may be based entirely on the thorium values.

The mathematical relationship between thorium value (in ppm) and shale volume is taken as linear, the same relationship as between the simple gamma ray and shale volume. The equation becomes

$$V_{sh}(t) = \frac{\text{Th (log value)} - \text{Th (min)}}{\text{Th (max)} - \text{Th (min)}} \qquad (4)$$

Th (min) = thorium value in clean formation (ppm); Th (max) = thorium value in pure shale (ppm), and $V_{sh}(t)$ = shale volume from thorium values.

As with the simple gamma ray, an empirical, exponential relationship to clay volume may be used instead of the simple linear one shown above (Fertl, 1979), i.e. for consolidated and Mesozoic rocks

$$V_{sh} = 0.33(2^{2V_{sh}(t)} - 1.0) \qquad (5)$$

and for Tertiary clastics

$$V_{sh} = 0.083(2^{3.7V_{sh(t)}} - 1.0) \quad (6)$$

where $V_{sh}$ = shale volume.

***Radioactive mineral volume***

Attempts to quantify the presence of radioactive minerals such as feldspars or mica are based on two assumptions: (1) all thorium radioactivity is from shale, and (2) radioactive detrital minerals show only potassium radioactivity.

For the quantification, the potassium values are normalized for shale volume using the maximum and minimum method as for thorium. The normalized potassium value will give shale volume + radioactive minerals volume. Subtracting the shale volume derived from the thorium log will leave the volume of radioactive minerals (Schenewerk *et al.*, 1980).

Volume of radioactive minerals

$$= \frac{K(\text{log value}) - K(\text{min}) - V_{sh}[(K(\text{max}) - (\text{min}))]}{a} \quad (7)$$

where $K$(min) = potassium % in clean formation; $K$(max) = potassium % in pure shale and $a$ = empirical factor for the formation concerned.

The two strictly quantitative methods outlined above are essentially used in petrophysical applications. Other, geologically applicable, qualitative and semi-quantitative uses of the gamma ray spectral log are described below.

## 7.10 Qualitative and semi-quantitative uses of the spectral gamma ray log

***Shale and clay minerals***

A certain amount of literature exists on the possibility of identifying individual clay minerals using the spectral gamma ray log. Most results have local significance only, are inconclusive or unsuccessful. As was shown previously (Geochemical behaviour, Section 7.5) the potassium content of the clay minerals varies considerably between species but is moderately constant within species (Table 7.8). Thorium, too, varies with each species but with slightly less consistency (Table 7.13). The intent is to find if these variations enable the individual species to be identified qualitatively, and eventually quantitatively.

The interval of the Muddy 'J' formation of Eastern Wyoming has been studied by Donovan and Hilchie (1981). They found a fairly good correlation between potassium radioactivity and illite content. However, they also found that while there was no correlation between clay mineral content and total gamma radiation, there was a strong correlation between total counts and uranium content. The essential radiation was therefore coming from uranium. The evidence suggested that the uranium source was principally smectite, its presence being caused by the exchange of the uranyl ion from the formation waters. Uranium radioactivity was therefore related to the presence of smectite. Almost exactly the opposite was found in the analysis of shales around the North Sea (Dypvik and Eriksen, 1983). The authors found that potassium and thorium were the dominant contributors to gamma ray activity with uranium being of minor importance (cf. Table 7.14).

A complex quantitative approach to clay-mineral identification has been proposed (Quirein *et al.*, 1982). The authors suggest that clay mineral species, along with feldspar and evaporites, can all be identified relatively simply by their Th/K ratios (Figure 7.27). There is certainly a tendency for this behaviour (cf. Tables 7.8, 7.13) and it is the basis for using just thorium as a shale indicator (*see* 'Quantitative uses'). However, individual clay minerals do not fall into such a simple classification. Such a classification demands a strict chemical control for the distribution of the elements. As was indicated, potassium is chemically involved in the clay lattice, but the exact behaviour of thorium in terms of clay-mineral composition is not clear. This method has no experimental justification and the precision for the identification of specific clay minerals is not justified (Hurst, 1990).

Local variations, complexity of clay-mineral mixtures and many other contributory variables allow no convincingly clear picture as yet for precise clay-mineral identification. The use of the spectral gamma ray log for this purpose is not yet available. Qualitative uses are, however, available (*see below*).

***Dominant clay mineral and detrital mineral content: use of the Th/K ratio***

The method described previously for quantifying radioactive mineral volume (Section 7.9) was based on the proposition that thorium occurs effectively only in clays and is thus a clay volume indicator, while potassium occurs in both clays and radioactive minerals. The method was applied quantitatively to sandstones but may be used semi-quantitatively for both sandstones and mudstones: the lithologies should be interpreted separately. That is, the Th/K ratio will be largely a function of detrital mineral content in sands, but of clay mineral content in shales (in that these are potassium rich). In both lithologies, the usual value for the Th/K ratio is 4–6 (Myers, pers comm), deviations from this band will be the result of certain detrital mineral or clay mineral abundances. For instance, a sandstone with a low Th/K ratio (of less than 4), will generally be dominated by feldspars, micas or glauconite: with high ratios, (greater than 6), it is likely that heavy minerals dominate.

In mudstones, a low Th/K ratio (of less than 4), probably indicates that illites dominate the clay minerals, while high ratios (more than 6) probably indicate that kaolinite dominates. For example a study of the Permian

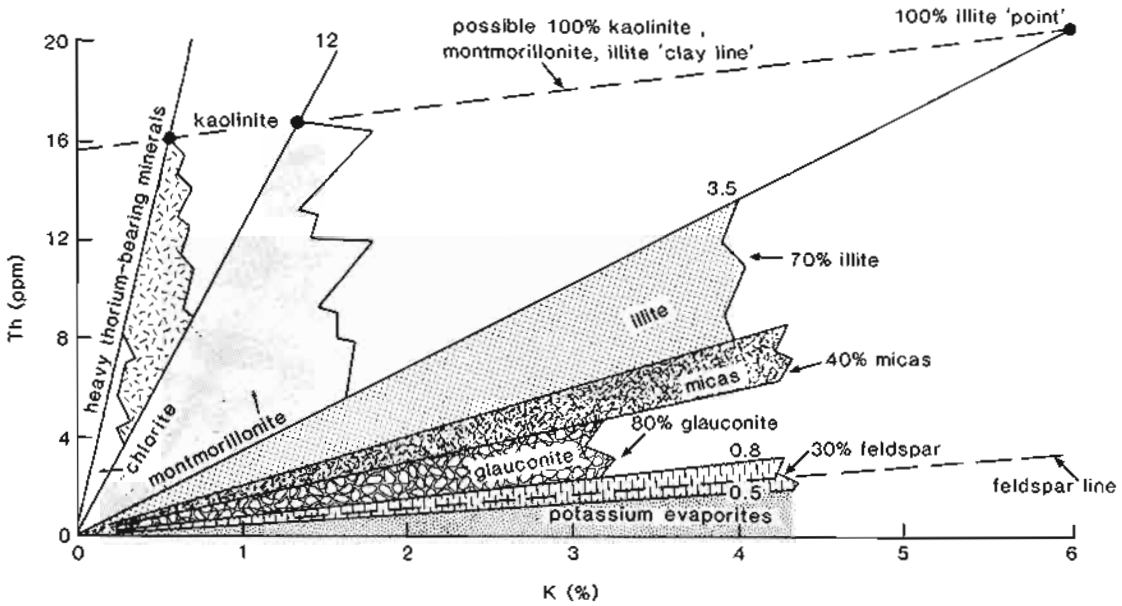


**Figure 7.27** Graph of the theoretical distribution of clay minerals, heavy minerals and evaporites, in terms of potassium and thorium content. (Re-drawn from Quirein *et al.*, 1982).

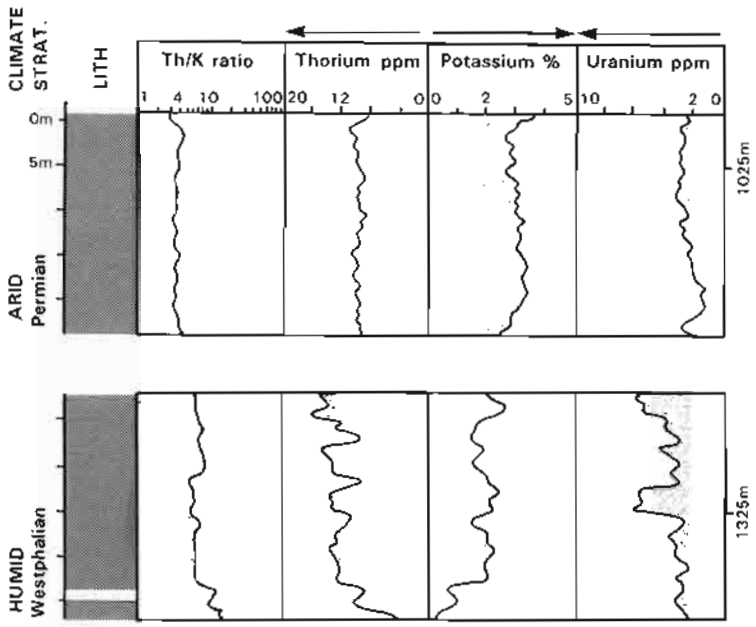


**Figure 7.28** Thorium/potassium, Th/K ratio changes in shales, associated with climatic variation. High ratios are associated with a humid climate (abundant kaolinite) low values with an arid climate (abundant illites). Westphalian and basal Permian, central UK.

to Cretaceous of central Kansas (Doveton, 1991), shows that low Th/K ratios (high potassium) are typical of the aeolian Permian shales and silts, where the high potassium content comes from feldspars, rock fragments and illites, while high Th/K ratios (low potassium) occur in the marine, Lower Cretaceous because the shales are dominated by kaolinite and illite with some chlorite, smectite and mixed layer clays, all generally low in potassium content.

This example contains an often observed aspect of Th/K ratios: when they change *progressively* in shale sections, it is an indication of climatic change (it is in effect a progressive change in clay mineralogy). The example (Figure 7.28) shows two sections from the same well over a 300 m interval. The Th/K ratio decreases progressively upwards in the shales. The lowest section is from the deltaic coal-bearing Westphalian which had a humid climate. The top section is from the Permian with an arid climate (Figure 7.28). Within a sandstone sequence, similar progressive changes are more likely to indicate mineralogical variations than climatic ones and for instance, channel lags often show a high Th/K ratio because of the heavy minerals they contain.

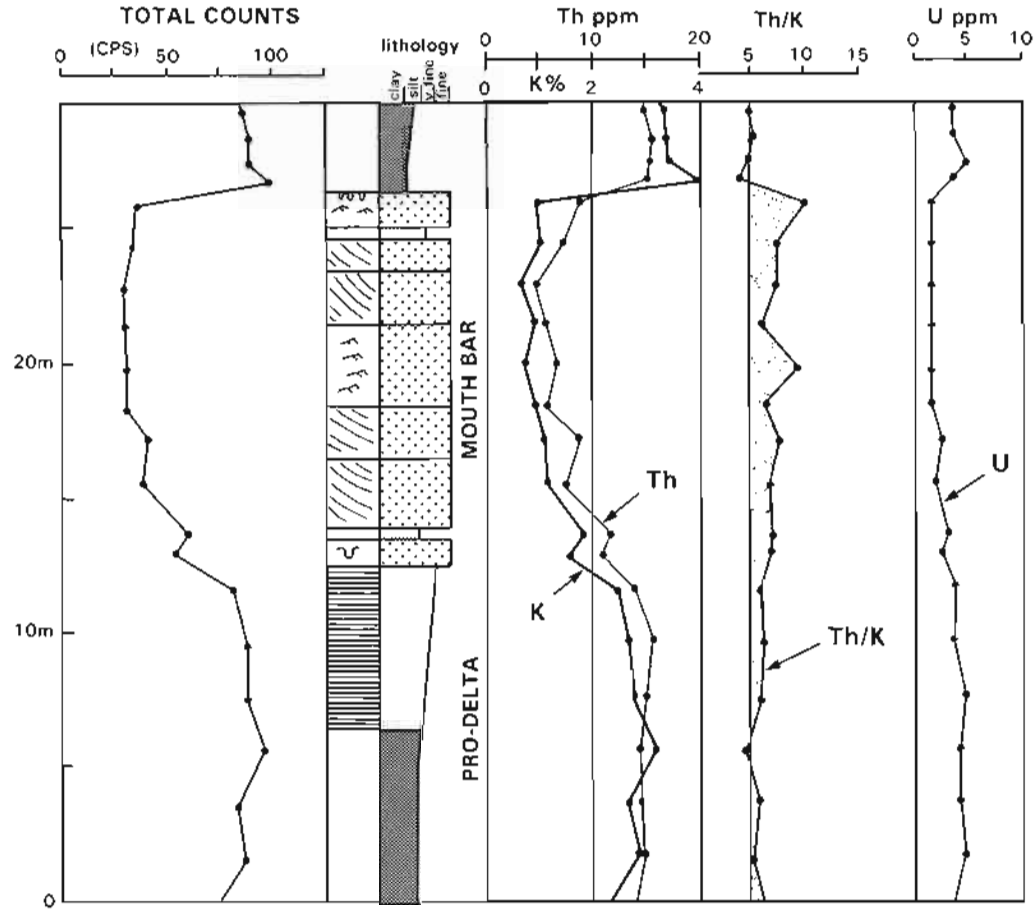


**Figure 7.29** Thorium/potassium, Th/K ratios in silts and sands associated with change in grain size. Thorium is relatively more abundant in coarser grained fractions when sediment source is constant (Namurian outcrop, Co. Clare, Ireland, from Myers, 1987).

The interpretation of the Th/K ratio must be carefully controlled and as a general rule, sandstones and shales should be studied separately. This is necessary because the ratio is often seen to be related to grain size. Thus, in coarsening-up sequences the Th/K ratio will change between the fine grained clays and silts and the coarser grained sandstones, generally increasing upwards into the sandstones (Figure 7.29). Another factor which must be considered is that potassium distribution changes during diagenesis. If there is dissolution of potassic feldspars and consequent redistribution of the potassium, the present-day Th/K ratio will not be related to original mineralogical content.

***Organic matter and source rocks: uranium content***

The theory of uranium adsorption by organic matter has already been discussed (*see* Uranium, Section 7.5) and illustrated (Figures 7.11, 7.12) and explains why source-rocks may be identified by their uranium content and consequent overall high gamma ray value. This is the case with the Upper Jurassic, Kimmeridgian of the North Sea area, where organic matter levels are high (TOC = 5%+) and so are gamma ray values as a result of uranium content (Bjørlykke *et al.*,1975; Figure 7.11, Table 7.10).

Although marine source-rocks, like the Kimmeridgian, generally have high gamma ray values (high uranium content), lacustrine source rocks have no gamma ray signature and are not uranium enriched (Meyer and Nederlof, 1983). This means that gamma ray response and uranium content are unreliable source-rock indicators (cf. Figure 7.12). It appears that lakes do not have reserves of dissolved uranium available to be adsorbed by organic matter, while oceans do. Using high gamma ray values to indicate source intervals should only be used in certain cases.

***Depositional environment and condensed sequences: use of the Th/U ratio***

Efforts to relate depositional environment to radioactive mineral content are generally based on thorium and uranium content and their inter-relationships. The affinity of uranium for shales of marine origin can be demonstrated (Koczy, 1956) as can the affinity of thorium for terrestrial sediments (Hassan *et al.*, 1976). Consequently, the contrast between thorium and uranium content should indicate the relative marine or relative continental influence (Adams and Weaver, 1958). Analysis of a wide range of mainly mudrocks, shows that the 'normal' Th/U ratio is 3–6 with higher ratios (higher thorium) in 'continental' environments and lower values (higher uranium) in more marine environments (Figure 7.30).

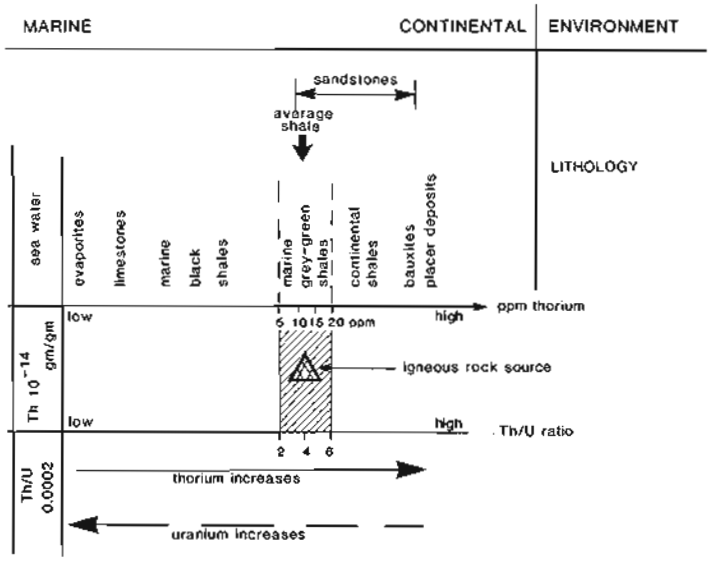


**Figure 7.30** Schematic representation of the use of the Th/U ratio to indicate environment of deposition. (Source of data, Adams and Weaver, 1958).

Using these ratios to define depositional environments across a broad range has not been successful, there are too many variables involved, although recent work in central Kansas does show that there can be a ratio contrast between generally transgressive and generally regressive intervals (Doveton, 1991). It is suggested however, as outlined below, that a less comprehensive, and selective application is more practical and practicable.

From a study of Upper Jurassic Kimmeridge clay outcrops in England, Myers and Wignall (1987) suggest that thorium content can be used as a quantitative reference level when studying variations in uranium content, as expressed by the Th/U ratio. Their analyses indicate that the typical Th/U ratio for shales is 3.9 ± 0.7, similar to the value of 3.8 ± 1.1 found by Adams and Weaver (1958) from analyses of American shales. If then, the expected, normal ratio is set at Th/U = 3 (i.e. slightly low), this can be used as a basis for an interpretation of abnormal ('excess') uranium content and eventually the identification of condensed sequences as explained below. In the method described below, high Th/U ratios, i.e. with high thorium content, are not interpreted, although Doveton, after Weaver, considers ratios above 7 as indicating 'leached uranium' (Doveton, 1991)

The Th/U ratio in 'normal' *shales* then, is set at 3 for the interpretation method. Variations away from this set value (effectively the 'norm') are essentially a result of variations in uranium and not thorium. Setting the ratio at 3 means that only significantly high amounts of uranium will be signalled (or significantly low amounts but see end of previous paragraph). A ratio of less than 3, less than the 'norm' (high uranium), can then be said to contain more uranium than expected, or *'excess'* uranium. For example, if a shale is found to contain 12ppm thorium and 10ppm uranium then:

U log = 10ppm  Th log = 12ppm

$$\frac{\text{Th log}}{\text{U norm}} = 3 \quad \text{general formula}$$

$$\text{U norm} = \frac{12}{3} = 4 \quad \text{example case}$$

$$\text{U xess} = \text{U log} - \text{U norm}$$

$$\text{U xess} = 10 - 4 = 6\text{ppm (excess)}$$

There is therefore 6ppm more of uranium than would be expected from the thorium content. Where:

U norm = 'normal' shale uranium
U xess = excess shale uranium
U log = uranium log reading in shale of interest
Th log = thorium log reading in shale of interest

(NB. The method outlined above, as proposed by Myers and Wignall (1987), uses the terms detrital uranium instead of 'normal' and authigenic uranium instead of 'excess'. To avoid suggesting that all sediments with high values of uranium (i.e. with a low Th/U ratio) contain authigenic uranium rather than any other form and that correspondingly low values are detrital, the terms 'excess' and 'normal' respectively are used in this book.)

Shale zones recognized as having 'excess' or higher than normal uranium will have a high organic matter content in most cases (*see* previous section). This in turn suggests an environment where the organic matter is preserved; typically this will be anoxic. This aspect is enlarged upon below. Zones with less than normal amounts of uranium (i.e. with a Th/U ratio of more than 3 or negative values from the formula above), are given no regular significance that is interpreted.

The method described above may be used to identify possible marine condensed sequences, important in themselves but doubly important in a sequence stratigraphic

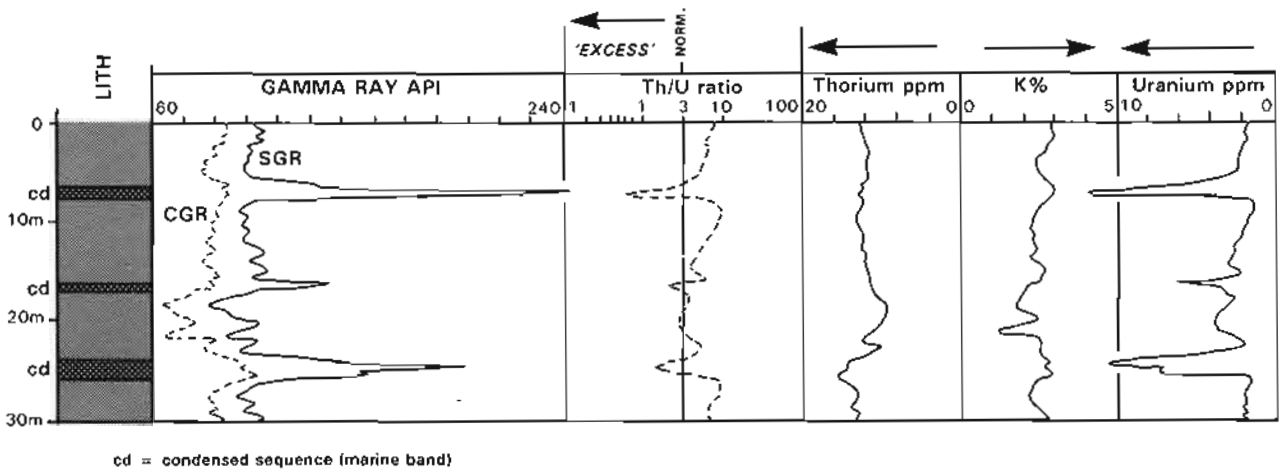


**Figure 7.31** Condensed shale sequences showing very low thorium/uranium, Th/U ratios due to 'excess' uranium content. Most shales have a Th/U ratio of 3-6, the 'norm'. In condensed sections, where organic matter is concentrated, uranium values are abnormally high and cause Th/U ratios of less than 3. The low ratio can be diagnostic.

analysis (Chapter 15). Condensed sequences in marine areas arise when the detrital influx into an environment is low. This causes a relative increase in the in-situ material over the externally derived detritus. In-place material typically consists of the shells of pelagic macro- and micro-fauna and locally derived organic material, all of which simply falls to the depositional surface to form a slowly accumulating (organic rich) sediment. Provided that there is a low rate of dissolution, (i.e. that the environment is oxygen depleted or deficient = anoxic) the amount of organic matter in the condensed sequence will be high, and in a marine environment, will have a high adsorbed uranium content. On the gamma ray spectral log, this high uranium content will show up as a low Th/U ratio. That is, using the methodology proposed above, condensed sequences will show 'excess' uranium (Figure 7.31). Using this ratio based method is more accurate and selective than simply using high overall gamma ray (i.e. gamma spike) or even high uranium values (Chapter 15).

***Fracture localization***

The mobility of uranium and its presence in formation waters is considered to be the cause of high uranium radioactivity in fractures and faults (Fertl, 1979; Fertl and Rieke, 1980). Using the spectral gamma ray log, zones of high uranium radiation can be detected, and other logs may be used to confirm that fractures are present.

***Comment***

Because a precise, quantitative, petrophysical use for the gamma ray spectral log has not been found, it is frequently not included in a logging suite. This is short-sighted. As methods are developed, such as those outlined above (but which only represent a start), spectral logs in old wells will be sought in vain. There is no doubt that geologically, a knowledge of the distribution of the three naturally radioactive elements leads to a much more refined interpretation of depositional environments, mineral content and fluid localisation. The use of these logs in sequence stratigraphy and all that it implies is particularly significant.

# 8
# SONIC OR ACOUSTIC LOGS

## 8.1 Generalities

***The log***

The sonic log provides a formation's *interval transit time*, designated Δt (delta-t, the reciprocal of the *velocity*). It is a measure of the formation's capacity to transmit sound waves. Geologically this capacity varies with lithology and rock texture, notably porosity (Figure 8.1).

*(The main text of this chapter on the sonic logs concerns the conventional, general purpose sonic tools that only measure* **compressional** *or* **P waves**, *the first arrival. A modern generation of tools is now able to measure the full wave train which includes the compressional wave, shear wave and Stoneley wave. These tools have more specialist applications and are considered in section* **8.8 Full waveform acoustic logs***).*

***Principal uses***

Quantitatively, the sonic log is used to evaluate porosity in liquid-filled holes. As an aid to seismic interpretation it can be used to give interval velocities and velocity profiles, and can be calibrated with the seismic section. Cross-multiplied with the density, the sonic is used to produce the acoustic impedance log, the first step in making a synthetic seismic trace.

Qualitatively, for the geologist, the sonic log is sensitive to subtle textural variations (of which porosity is only one) in both sands and shales. It can help to identify lithology and may help to indicate source rocks, normal

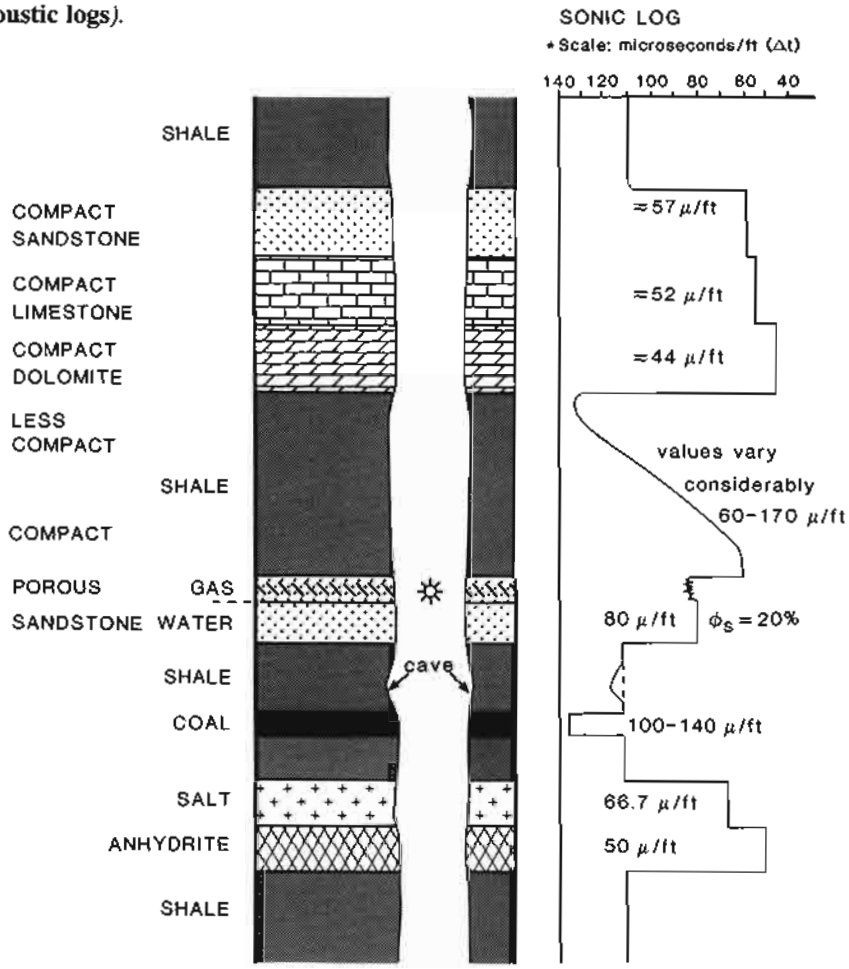


**Figure 8.1** The sonic log: some typical responses. The sonic log shows a formation's ability to transmit sound waves. It is expressed as Interval Transit Time, Δt. $*(1 \times 10^6) / \Delta t$ = sonic velocity, ft/sec.

**Table 8.1** The principal uses of the sonic log (conventional, compressional wave tools).

| | Discipline | Used for | Knowing |
|---|---|---|---|
| Quantitative | Petrophysics | Porosity | Matrix velocity |
| | | | Fluid velocity |
| | Seismic | Interval velocity | Integrated travel time |
| | | | Seismic markers |
| | | Seismic calibration | Check shots |
| | | Acoustic impedance | Direct use of sonic log |
| Qualitative and semi-quantitative | Geology | Lithology | Matrix and mineral velocities |
| | | Correlation | |
| | | Texture | |
| | | Fracture identification | Density log porosities |
| | | Compaction and overpressure | Normal compaction trends |
| | Geochemistry | Source rock evaluation | Resistivity log values |

compaction and overpressure and to some extent fractures. It is frequently used in correlation (Table 8.1).

## 8.2 Principles of measurement

The conventional, general purpose sonic tools measure the time it takes for a sound pulse to travel between a transmitter and a receiver, mounted a set distance away along the logging tool. The pulse measured is that of the compressional or 'P' wave (Figure 8.2) and tool design enables the velocity of this wave in the formation to be measured. The compressional wave is simply the fastest or 'first arrival', in which particles vibrate in the direction of the sense of movement. The compressional wave is followed by shear and Stoneley waves (Figure 8.2) which, in the conventional tools, are ignored but in the modern array acoustic tools, can be fully measured (Section 8.8).

Typical sonic tool transmitters (transducers) are either magnetostrictive or, more commonly, piezoelectric and translate an electrical signal into an ultrasonic vibration. Receivers are usually piezoelectric, and convert pressure waves into electromagnetic signals which can be amplified to provide the logging signal. Piezoelectric materials have a type of structure which, when a stress is applied, shows separation of centres of negative and positive charge, thus creating a polarisation charge. It is this, amplified, which gives an electrical signal. In piezoelectric transmitters, the application of an electrical charge causes a change in volume which can be translated into a pressure pulse. A common piezoelectric material used is lead zirconate titanate or PZT.

A sonic tool transmitter typically produces source frequencies of between 10–40kHz (kilohertz) or 10,000–40,000 cycles per second. At 10–20kHz, the acoustic wave has a wavelength of between 7.5cm (0.25ft) – 75cm (2.5ft) over the velocity range of 1500m/s (5000ft/sec) to 7500m/s (25,000ft/sec). This is clearly a huge contrast to the typical seismic signal (sonic and seismic velocities are routinely compared) which has a content in the 10–50 hertz range (i.e. 10–50 cycles per second) and with wavelengths of 30m–50m (*see* Section 8.7, Seismic applications).

## 8.3 Tools

Modern sonic tools do not consist of just a single emitter and a single receiver, but of a number of both transmitters and receivers, the actual arrangement depending on the tool type. Modern designs allow unwanted borehole and tool effects to be largely eliminated and give a reliable measure of formation values even in quite poor borehole conditions. Typical tool design and use of compensation can be illustrated by the borehole-compensated (BHC) sonic tool (Figure 8.4).

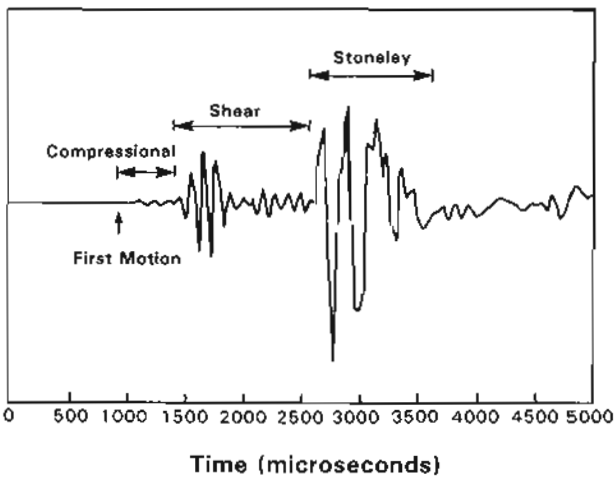


**Figure 8.2** The full acoustic waveform that may be recorded in a borehole. The standard sonic records only the first arrival of the compressional (P) wave. Array sonic tools record the full waveform (modified from Ellis, 1987, after Schlumberger).

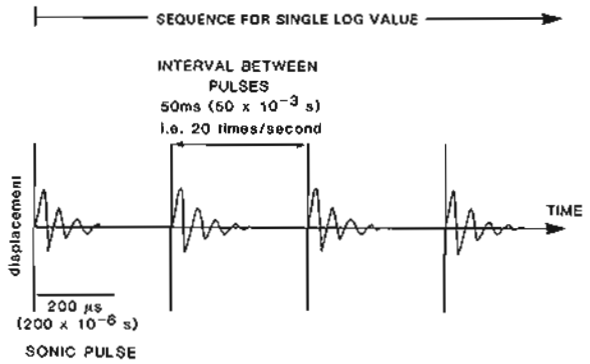


**Figure 8.3** Sonic tool emitter patterns (schematic). Typically a pulse lasting 200 microseconds is emitted every 50 milliseconds, i.e. 20 times a second. Four pulses are needed for a complete (BHC) log measurement. (Re-drawn from Serra, 1979).

The borehole-compensated sonic tool has two transmitter-receiver groups (one inverted), each group consisting of a transmitter coupled with a near receiver and a far receiver (Figure 8.4*a*). Because the sonic is generally run hole-centred, any pulse transmitted by the tool, passes first into the mud, it is then refracted at the borehole wall, travels through the formation close to the borehole wall and, at a critical (slower) velocity is refracted back into the mud, so to reach the tool again where it is detected. A significant part of the trajectory is in the borehole mud (Figure 8.4*a*). However, if this travel path is considered when one transmitter is used with two receivers (a near and a far), the mud effects can be eliminated. This is simply achieved by measuring the time it takes for the signal to reach the far receiver and from this subtracting the time it takes to reach the near receiver. The path from tool to borehole wall and back, in the mud, is effectively common to both trajectories, as is the section of the path between the transmitter and near receiver: all are eliminated on subtraction. What is not common to the two trajectories is the time taken between

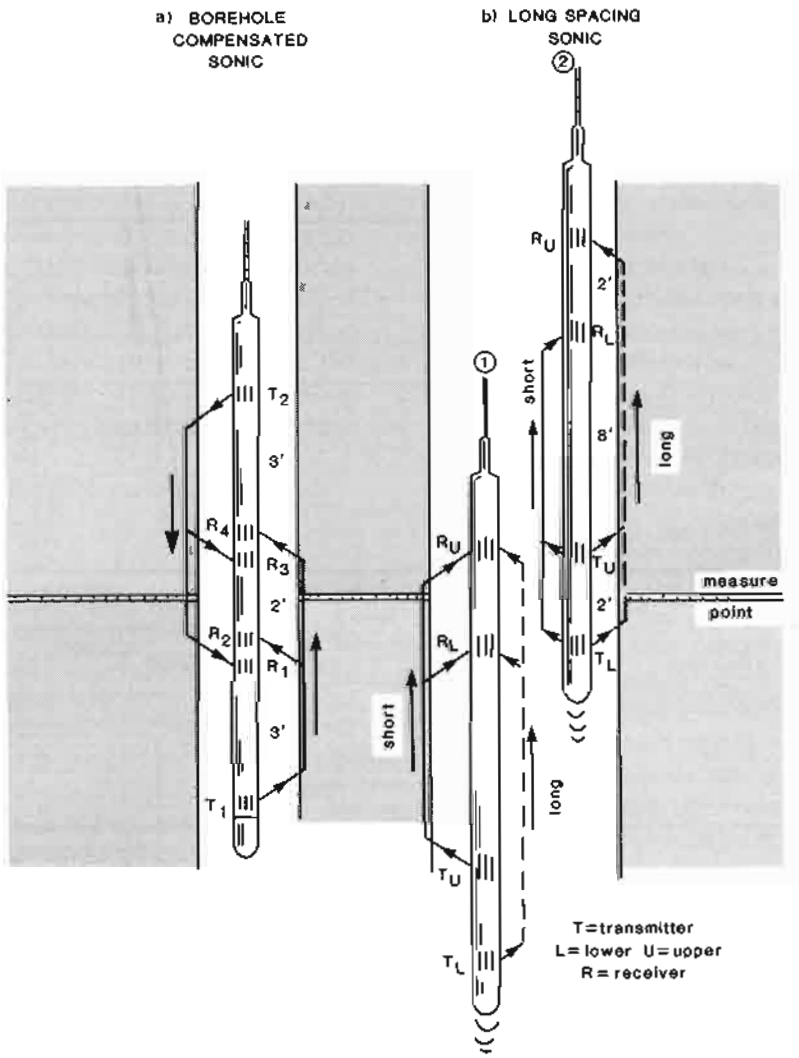


**Figure 8.4** Sonic tools. Representations of (*a*) a borehole-compensated sonic tool which gives instantaneous readings with an inverted receiver transmitter array and (*b*) the Long Spacing Sonic Tool (Schlumberger) which gives long and short-spaced readings using a time (i.e. position) delay system: positions (1) and (2) are both relative to the same measure point. (Modified from Thomas, 1977 and Purdy, 1982).

the two receivers (Figure 8.4*a*), and this time is the formation reading; the value required.

Since tool tilt and hole size may make the common parts of the trajectory unequal, a second, inverted array (with a downward moving signal), is averaged with the first (with the upward moving signal) to provide compensation. This means that each value recorded on the sonic log is the result of a sequence of four separate transmitter-receiver readings, two from the lower transmitter to its near and far receivers and two from the upper transmitter to its near and far receivers. The up and down receiver sets are offset vertically to allow for the tool moving (Figure 8.4*a*).

In terms of typical values for the BHC tool, a transmitter pulse lasts between 100μs – 200μs (microseconds), the gap between the pulses is 50ms (milliseconds) or 20 pulses per second, allowing five complete sequences of four individual transmitter-receiver readings per second (Figure 8.3). At a typical sonic tool logging speed of 1500m/h (5000ft/h), (i.e. approximately 40cm/sec or 16"/sec) each complete sequence of four readings will give one log reading for every 8cm (3") of borehole.

The borehole-compensated (BHC) sonic described above has a 'static' compensation and has been used commonly since the 1960s. It typically has transmitter-receiver distances of three feet and five feet with two feet between the two receivers (Figure 8.4*a*). In the late 1970s it was found that longer transmitter-receiver distances could help under certain borehole conditions and the long spaced sonic was designed with two receivers two feet apart separated by eight feet from two transmitters also two feet apart (i.e. the LSS of Schlumberger, Figure 8.4*b*, Table 8.2). This tool gives a near reading with 8–10 foot spacings and a far reading with 10–12 foot spacings (Figure 8.4*b*). Because of its length, the long spaced sonic has a 'dynamic' compensation system where depth

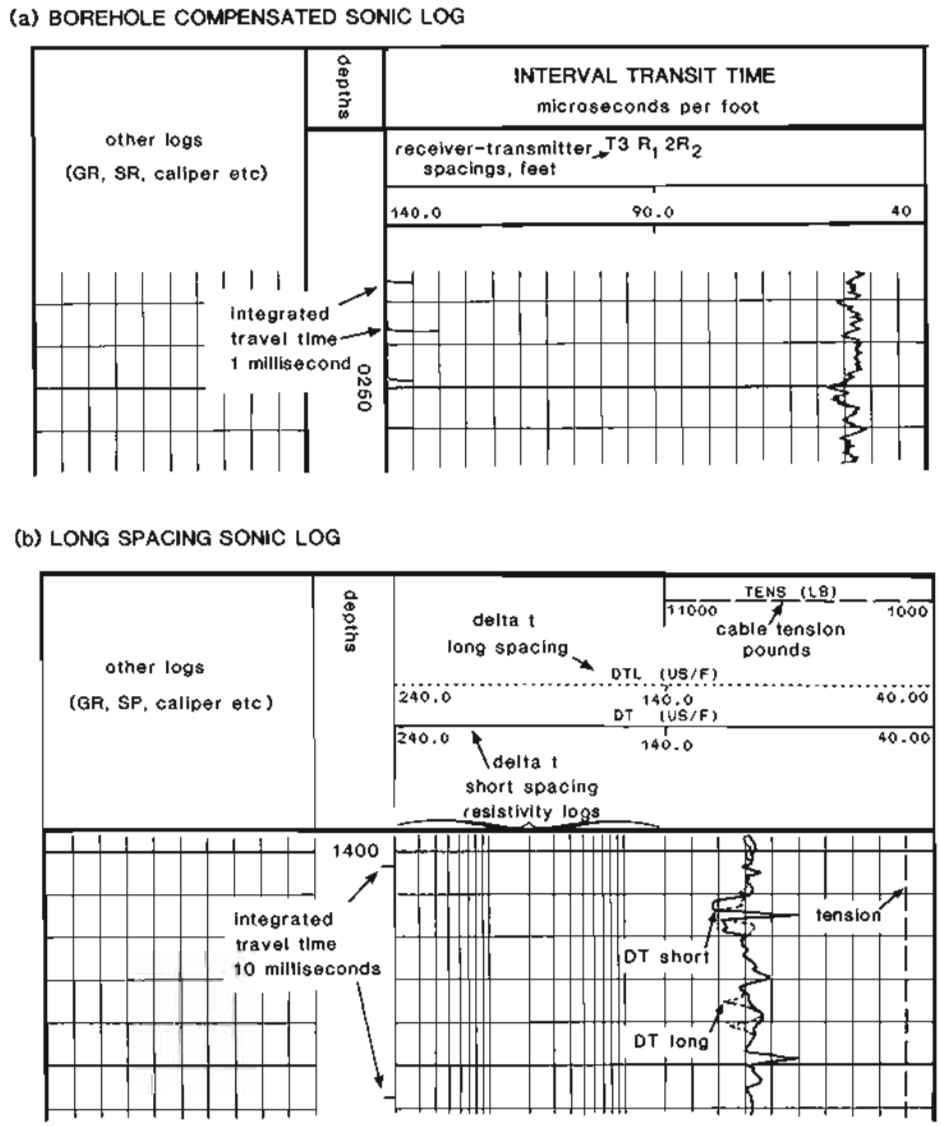


**Figure 8.5** Typical sonic log headings. (*a*) BHC tool; (*b*) long spacing tool (on the ISF-sonic combination of Schlumberger).

**Table 8.2** The principal standard sonic tools.

| Name | Mnemonic | Company |
|---|---|---|
| Borehole Compensated Sonic | BHC | Schlumberger |
| Long Spaced Sonic | LSS | |
| Array-Sonic (standard mode) | DTCO | |
| Borehole Compensated Acoustilog | AC | Western Atlas |
| Long Spaced BHC Acoustilog | ACL | |
| Compensated Sonic Sonde | CSS | BPB |
| Long Spaced Compensated Sonic | LCS | |
| Borehole Compensated Sonic | BCS | Halliburton |
| Long Spaced Sonic | LSS | |

memorisation is employed. To complete a full compensation sequence for both the near and far readings, the tool must record a full transmitter-receiver sequence at two depth positions separated by 10 feet, the tool's compensation shift. The system is diagrammatically illustrated (Figure 8.4b).

***Log presentation, scales and units***

Sonic values are given in microseconds (μs) per foot (1 microsecond = $1 \times 10^{-6}$ seconds). The value is called the *interval transit time* and is symbolized as $\Delta t$ (Figure 8.5). The most common interval transit times fall between 40μs and 140μs: this is the arithmetic sensitivity scale usually chosen for the log (Figure 8.5*a*). The velocity is the reciprocal of the sonic transit time, i.e., velocity ft/s = $1/\Delta t$ μs/ft. Even on logs with a metric depth scale, the transit time is mostly still given in μs/ft. The necessary conversions must be made to extract the metric velocity, thus:

$$\Delta t = 40\mu s \text{ from the sonic log.}$$

$$\text{Velocity} = \frac{1}{40 \times 10^{-6}} = 25{,}000 \text{ ft/sec} = 7{,}620 \text{ m/s}$$

When a sonic tool is run on its own it is presented in full-width track 2 and 3 (Figure 8.5a). If, as is often the case, the sonic log is combined with other tools, the log appears only on track 3, often with the sensitivity scale of 40μs – 140μs maintained (Figure 8.5*b*).

An *integrated travel time* (or TTI) is recorded simultaneously with most sonic logs. It represents a time derived from the average velocity of the formation logged and plotted over the vertical depth of the interval in milliseconds ($10^{-3}$ seconds) (Figure 8.5), each millisecond appearing on the inside depth column as a bar. Each 10ms is a longer bar (Figure 8.5). Adding the milliseconds and dividing by the thickness of the interval covered gives the velocity. The TTI milliseconds may be added together to correspond to the travel times on the seismic section: seismic sections are in two-way time, that is TTI × 2.

The sonic tool is frequently run in combination with the resistivity logs (e.g. Schlumberger ISF-Sonic tool; Atlas Wireline Acoustilog-Resistivity tool). It is best run hole-centred, although modern tools may be eccentred, especially in large holes.

## 8.4 Log characteristics

***Depth of investigation***

The path of the compressional waves detected by sonic tools is essentially along the borehole wall with very little penetration, generally between about 2.5cm to 25cm (1"–10") from the borehole wall (Dewan 1983; Chemali *et al.*, 1984). The penetration is independent of receiver separation and depends on the signal wavelength; the greater the wavelength the greater the penetration. For a particular frequency therefore, penetration is greater in higher velocity formations (i.e. λ=vel/freq).

This simple picture is complicated by the observation that mechanical and chemical damage at the borehole wall can have an effect on sonic response (Section 8.6, Figure 8.21) (Blakeman, 1982). Damage can create a low velocity zone around the borehole. When this occurs, increasing the transmitter-receiver distance on a sonic tool increases the compressional wave penetration, which was the reason for the introduction of the long spaced sonic sonde. The increase in investigation occurs because the compressional wave in the damaged zone is slower than the wave in the undamaged formation. If the transmitter-receiver distances are large enough, these two waves become separated and it is the faster, deeper penetrating wave which is detected as the first arrival. For example, with borehole damage, while the standard sonde has a depth of investigation of 15cm – 25cm (6"–10"), the long spaced tool has an investigation of 38cm – 50cm (15"–20"). Consequently, a long spaced sonic has a greater chance of detecting the compressional wave from undamaged formation. In the reverse physical situation, in gas zones where the invaded formation, with fluid saturation, has a faster velocity than the virgin formation saturated with gas, a difference in penetration is still said to exist. In this case the standard sonic will have a very small investigation, 5cm (2") or less while the long spaced tool may reach 25cm (10") (Chemali *et al.*, 1984).

Through experience, however, the effects of wall damage on the standard sonic appear to have been exaggerated and the effectiveness of the long spacing sonic not demonstrated, a meaningful separation of the long and short spaced readings seldom being observed. The standard tool remains effective in most cases. In short, although there are variations, the depth of investigation of all sonic tools is small and the detected wave is generally from the immediate borehole wall or the invaded zone in permeable intervals.

***Bed resolution***

The vertical resolution of the sonic is the span between receivers for the borehole compensated tools and should be similar for the long-spacing tools (Figure 8.4). This is frequently two feet (61cm). Beds of less than 60cm

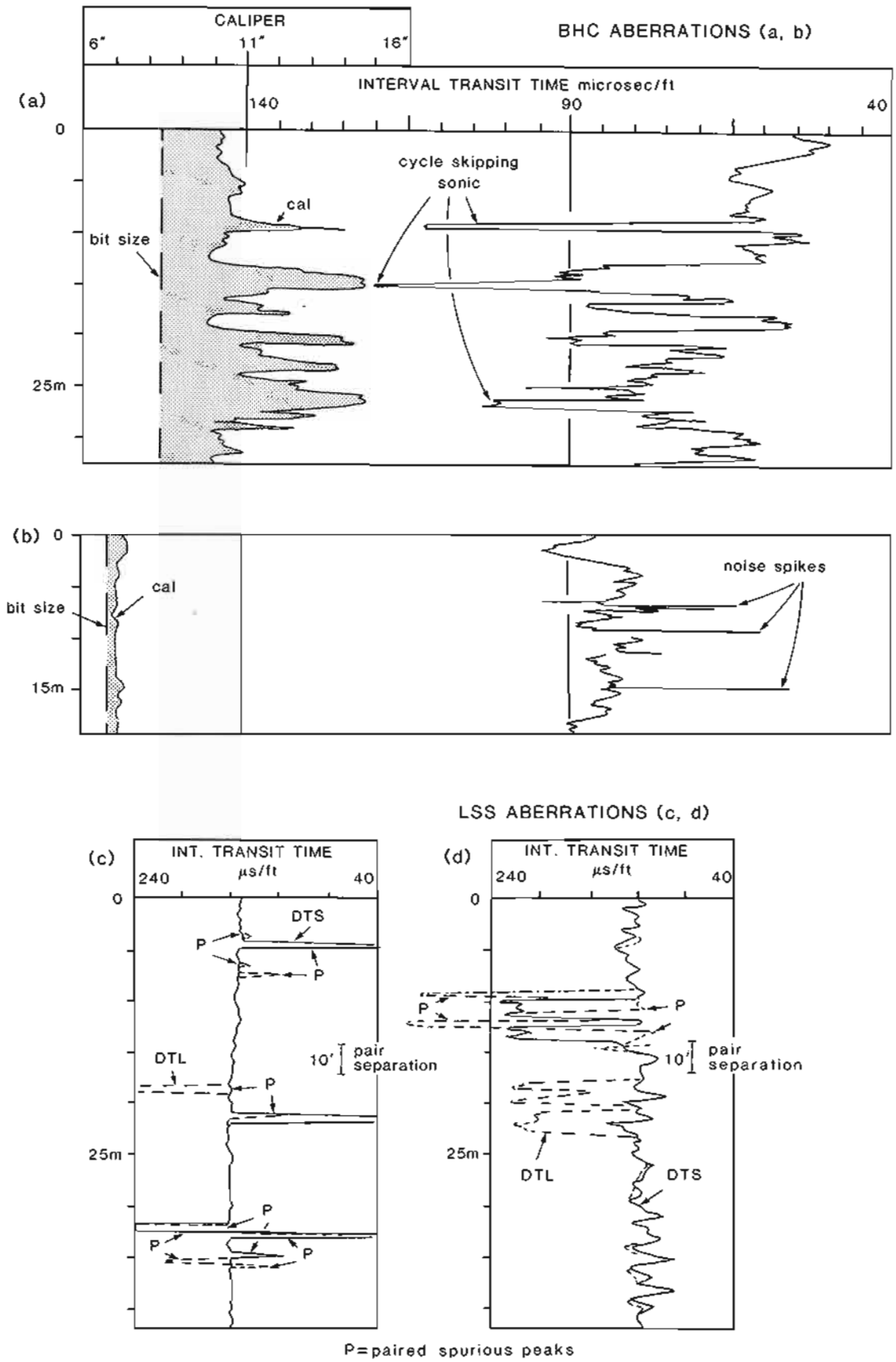


**Figure 8.6** Unwanted environmental effects on the sonic log. (*a*) BHC tool, cycle skipping; (*b*) BHC tool, noise spikes; (*c, d*) long-spacing tool, paired aberrations; DTS = short-spaced sonic, DTL = long-spaced sonic. The pairs are separated for the most part by 10ft, the compensation shift distance.

thickness will be registered on the sonic log, but a true velocity will not be recorded. Specialist tools now exist with much higher resolutions (i.e. the array sonic of Schlumberger in certain modes, the digital array acoustilog of Atlas Wireline, Section 8.8).

***Unwanted logging effects***

The conventional borehole-compensated sonic is very robust, even in poor and over-sized holes (cf. Ellis, 1987) due to the effectiveness of the compensation system (*see* 'tools' above). However, in extremely poor holes, cycle skipping occurs (Table 8.3). This is the effect when the first, compressional wave arrival is too attenuated (weak) to activate the receiver, which is only tripped by a subsequent arrival: the recorded time is therefore too long (interval transit time too large) (Figure 8.6*a*). The reverse situation occurs when noise signals trip a receiver. This causes noise spikes on the log and is found in hard formations such as limestones (Figure 8.6*b*).

While the conventional sonic is robust, the long spaced sonic is not. There are two weaknesses in the tool which are compounded, signal attenuation and the dynamic compensation system. Attenuation results in a signal too weak to trigger a receiver, and causes cycle skipping. In the dynamic compensation system, each transmitter-receiver reading is used twice (i.e. at two levels) and an error on any one of the eight readings comprising a full sequence, causes paired errors on the log (Figure 8.6*c*). Paired errors and serious cycle skipping are frequent on many long spaced sonic recordings despite computer 'smoothing' (Table 8.3) (Purdy, 1982).

**Table 8.3** Unwanted environmental effects – sonic log.

| Factor | Effect on log | Severity* |
|---|---|---|
| Caving | 'Cycle skipping' | Present |
| | Diminished $\Delta t$ troughs to a mud value (BHC) | |
| | High or low or alternate paired anomalous peaks (LSS) | Common |
| Hole rugosity | 'Noise triggering' | Rare |
| | Increased $\Delta t$ spikes (BHC) | |
| | High or low or alternate paired anomalous peaks (LSS) | Common |

*When the effect makes the log reading unusable.
Ratings: frequent, common, present, rare.
BHC = Borehole Compensated Sonic.
LSS = Long-Spaced Sonic.

## 8.5 Quantitative uses

The sonic log can be used to calculate porosities, although it is usually inferior to neutron or density-log calculated values.

To use the log it is necessary to propose that when a formation has, on average, a uniform distribution of small pores and is subjected to a heavy confining pressure, there is a simple relationship between velocity and porosity (Wyllie *et al.*, 1956).

$$\frac{1}{V} = \frac{\phi}{V_L} + \frac{1-\phi}{V_{ma}} \qquad (1)$$

which can be written, replacing $\Delta t$ for $V$, as

$$\Delta t = \phi \Delta t_L + (1-\phi)\Delta t_{ma} \qquad (2)$$

where $V$ = tool-measured velocity; $V_L$ = velocity of the interstitial fluid; $V_{ma}$ = velocity of the matrix material; $\phi$ = porosity; $\Delta t$ = tool measured interval transit time; $\Delta t_L$ = transit time of interstitial fluid; and $\Delta t_{ma}$ = transit time of matrix material.

Equation (2) simply states that the transit time measured by the tool is the sum of the time spent in the solid matrix and the time in the fluid: it is called the *time average relationship* (Wyllie *et al.*, 1956). This 'time' is a function of the matrix velocity and constituents volumes (i.e. wave path length) (Figure 8.7). The relationship is best translated into graphic form, where it becomes obvious that the measured interval transit time has a linear relationship with porosity (Figure 8.8). The relationship will vary depending on the velocity of the matrix material (*see* equation 2). Some of the more common matrix velocities are shown in Table 8.4.

The quantitative derivation of porosity using the time average relationship is usually imprecise and modifications are necessary (Raymer *et al.*, 1980) although these are often only effective very locally (Brereton and McCann,

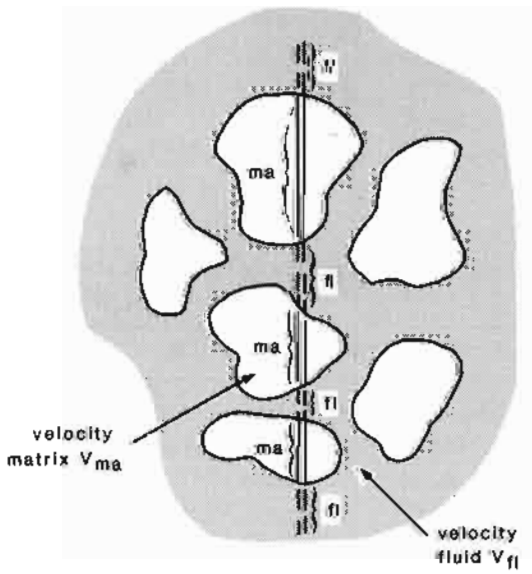


**Figure 8.7** Diagrammatic representation of the path of P waves through a rock, showing the relationship between time spent in the matrix ($V_{ma}$) and time in the fluid ($V_{fl}$) giving the basis for the calculation of porosity from sonic velocities.

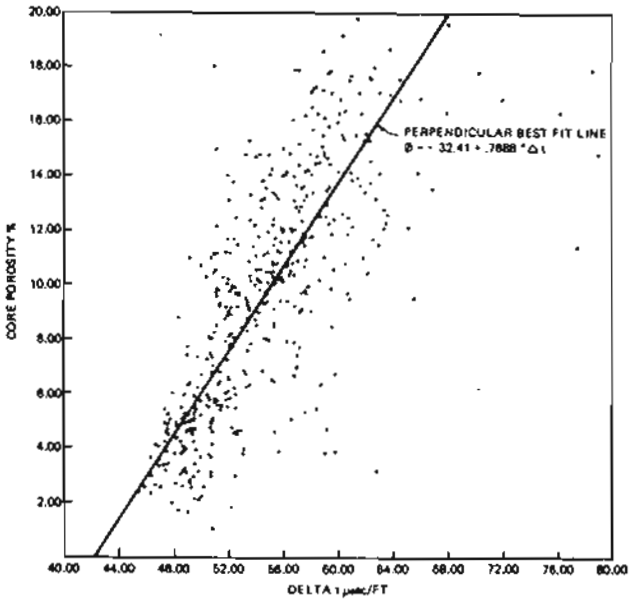


**Figure 8.8** Interval transit time compared to measured porosity in a dolomite. (From McFadzean, 1973).

1990). Clearly, the physical relationship between porosity and sonic velocity is still to be explained. From experience, the effect which causes most deviation from the simple law is lack of compaction (i.e. external pressure), when porosities are very high, especially in sandstones. However, recent work has shown that the failure of the time average equation in fact covers the whole range of porosities (Brereton and McCann, 1990) (Figure 8.9). For a particular set of known matrix velocities, the time average formula always over-estimates the porosity. The simple schematic representation illustrated (Figure 8.7) of a straight wave path through a sediment is, not surprisingly, incorrect. If an incorrect ray path is the cause of the general error, then the path through the fluid is longer than expected (or shorter through the matrix), hence the overestimation of porosity. This is only one possibility.

For unconsolidated sediments, most logging companies provide compaction correction coefficients, based on cross-plotting sonic porosities and density- or neutron-log porosities. It is, however, best to avoid using the sonic log to calculate porosity in unconsolidated formations (Sarmiento, 1961).

When gas replaces liquid in the formation, the time-average graph no longer applies (i.e., $V_L$ is replaced by $V_L$ and $V_{gas}$). Even though the sonic pulse does not penetrate deeply into the formation, there is often sufficient gas in the invaded zone to affect the velocity. Indeed, the effect can be used to identify gaseous hydrocarbons when a gas/water contact is present (Figure 8.10). To estimate the real porosity in the presence of gas, the porosity calculated from the raw log should be multiplied by between about 0.7–0.8, but this is only an estimate.

To calculate porosity in the presence of shale the sonic log must be corrected for a shale volume derived from other logs.

## 8.6 Qualitative uses

***Lithology identification***

The velocity of the common sedimentary rock types is rarely diagnostic of lithology: there is too much variation within each type and too much overlap between types

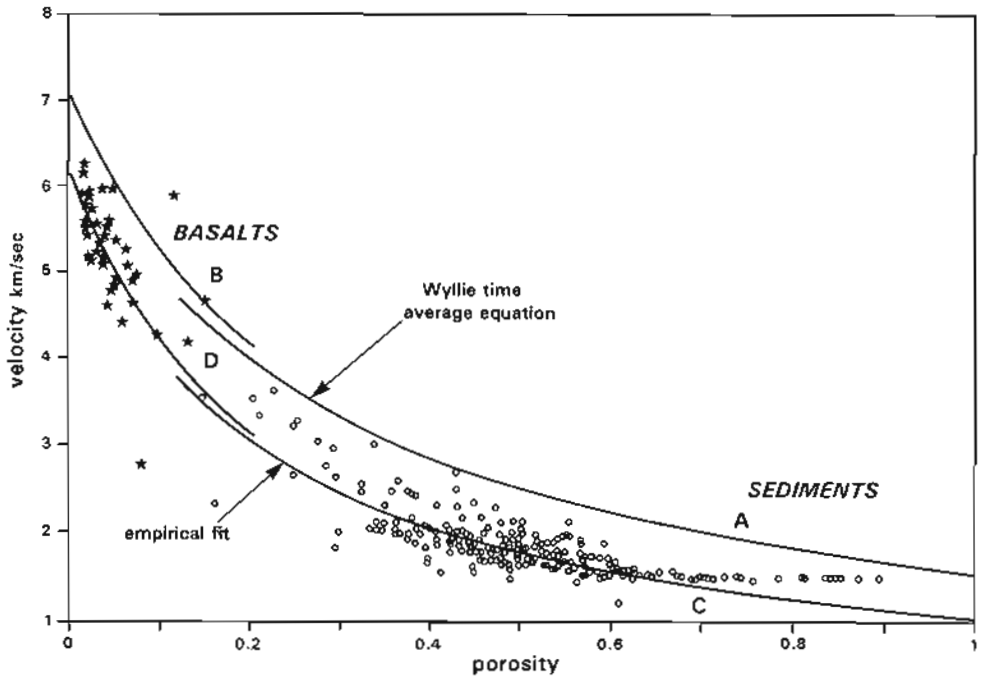


**Figure 8.9** Porosity predictions from the Wyllie 'time average equation' in (A) sediments (calcareous oozes), (B) oceanic basalts. Empirical curve fit for (C) sediments and (D) oceanic basalts. The indication is that the Wyllie equation overestimates porosity across a wide range of values (from Brereton and McCann, 1990).

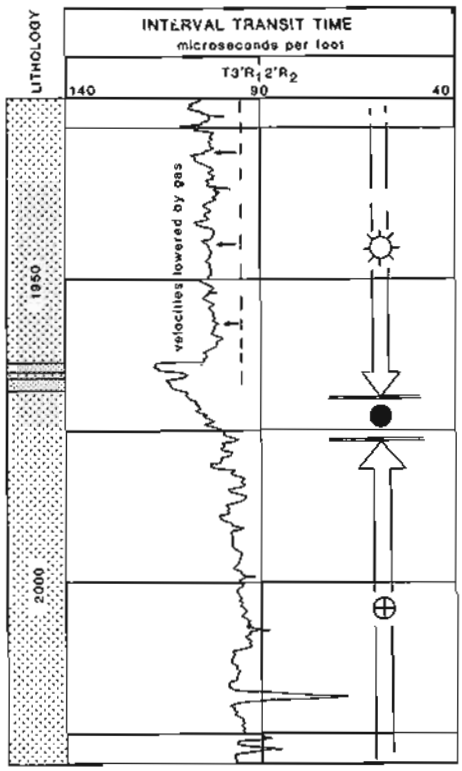


**Figure 8.10** The effect of gas on the sonic log. The sonic velocity in this porous sandstone is lowered by about 8%.

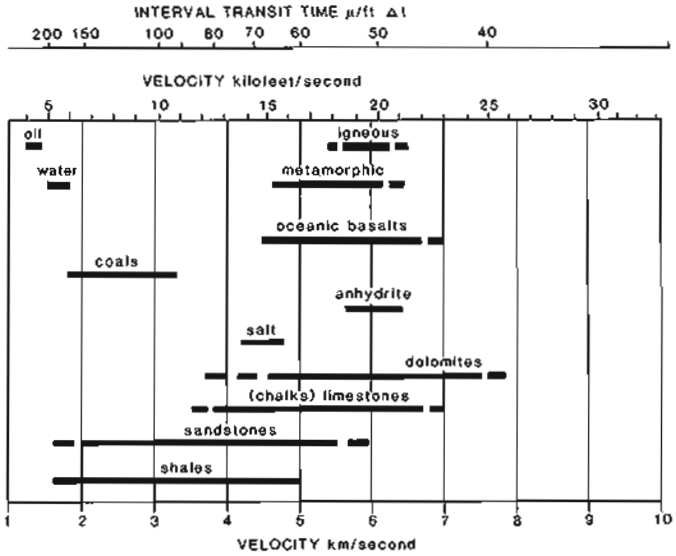


**Figure 8.11** The average velocity ranges of common lithologies compared. The considerable amount of overlap indicates that velocity alone is seldom diagnostic of lithology (values are for depths typical of oil exploration wells). *See* Table 8.4 for matrix velocities and Table 8.5 for mineral velocities.

(Table 8.4, Figures 8.11, 8.12). However, such is the natural occurrence that high velocities are more likely to be associated with carbonates, middle velocities with sands and shales and low velocities with shales (Figure 8.11).

Velocity, nonetheless, is diagnostic of coals, which have unusually low values (high interval transit times) (Figure 8.13). It is also diagnostic of the evaporites, which are essentially chemically pure substances with predictable physical properties, such as halite (rock salt), gypsum and anhydrite (Table 8.5). Moreover, halite velocities do not vary with depth.

### *Texture*

Although sonic response may not be diagnostic in terms of lithology, it is very sensitive to rock texture, even subtle changes. The way in which sound travels through a formation is intimately associated with 'matrix, matrix materials, grain size distribution and shape, and cementation' (Wyllie *et al.*, 1956), in other words texture (Figure 8.7). This is true for most lithologies and in fact extends upwards in scale to include also structural characteristics such as bedding. For example, the sonic has a very distinctive response to slumped, debris flow intervals in the Upper Cretaceous chalks of the North Sea. Over a cored interval where the chalk bedding characteristics can be detailed, intervals of debris flow, which have chaotic textures and no bedding, show distinctly higher interval transit times (lower velocity) than normal chalk which is generally thin-bedded (Hatton, 1986).

**Table 8.4** Some typical sonic matrix velocities (*see also* Figure 8.11) (from Schlumberger, 1972; Serra, 1979; Gearhart, 1983).

| | $\Delta t_{ma}$(μ/ft) | $V$(m/s) | $V$(ft/s) |
|---|---|---|---|
| Sandstones (compacted) | 55.5–51 | 5490–5950 | 18,000–19,500 |
| Quartz | 55.1 | 5530 | 18,150 |
| Limestones | 53–47.6 | 5800–7000 | 19,000–23,000 |
| Calcite | 46.5 | 6555 | 21,500 |
| Dolomites | 45–38.5 | 6770–7925 | 22,200–26,000 |
| Dolomite | 40 | 7620 | 25,000 |
| Shale | 167–62.5 | 1600–5000 | 5000–16,000 |

**Table 8.5** Some diagnostic (mineral) velocities (from Serra, 1979; Gearhart, 1983; Schlumberger, 1985).

| | Δ$t$(μs/ft) | Velocity*(m/s) | Velocity*(ft/s) |
|---|---|---|---|
| Water (saline) | 189–200 | 1610–1525 | 5290–5000 |
| Halite | 66.7–67 | 4550 | 15,000 |
| Anhydrite | 50 | 6100 | 20,000 |
| Gypsum | 52–53 | 5860 | 19,000 |
| Anthracite | 90–120 | 3050 | ≃ 10,000 |
| Lignite | 140–180 | 2000 | ≃ 6500 |
| casing (steel) | 57.8 | 5270 | 17,300 |

*Averages

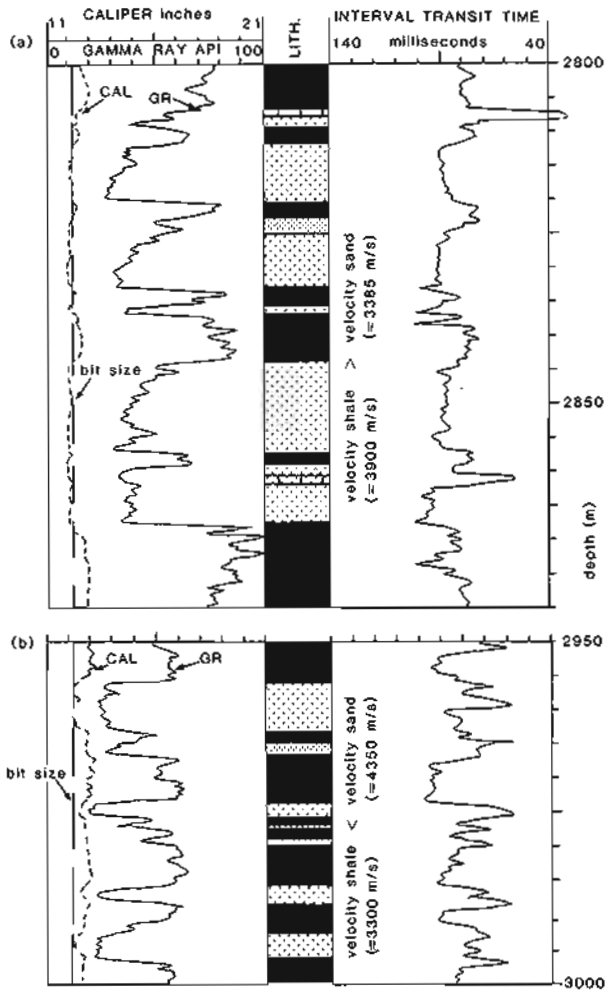


**Figure 8.12** Sonic log in sand-shale sequences. (*a*) The sands have a lower sonic velocity (about 3385m/s) than the shales (3900m/s). (*b*) The reverse, where the sands have higher velocity (about 4350m/s) than the shales (3300m/s). Sonic velocities are therefore not diagnostic of lithology.

It is probable that the sensitivity of the sonic to bedding, as well as to texture at a smaller scale, is because the detected signals physically travel up (and down) through the formation. Any horizontal feature, such as bedding, must be crossed and will affect the response. This is well illustrated in shales where finely laminated intervals have a different response to massive intervals. The example (Figure 8.14) shows a shallow marine shale cycle in which the laminated section at the base shows higher interval transit times (lower velocity) than the more massive, upper section.

In many cases the exact textural effects causing the sonic log response may not be known and the difficulty in calculating porosity from the sonic is a demonstration of this. An example of textural changes in turbidites is an illustration (Figure 8.15). The consistently low gamma ray response suggests that there are no compositional changes and yet the sonic shows distinct variations. Undoubtedly porosity change occurs, but there are also changes in grain size and bedding (sedimentary structures). It is not possible to extract, separate and identify each individual influence.

### *Correlation – sonic log character*

The sonic transit time of a formation is a very distinctive characteristic although, as indicated, the precise textural and lithological (compositional) causes are difficult to define. Rather like colour, it is not diagnostic of a particular lithology but in some formations it is very typical and slight changes indicate subtle formation changes. The sequence illustrated (Figure 8.16) is entirely shaly: cuttings and side-wall cores find only shale. The sonic log, however, picks out small variations, probably in texture, carbonate content and quartz content, to show a very distinct stratigraphic interval despite the depth differences. It is this characteristic which makes the sonic log excellent for correlation, and even for identifying

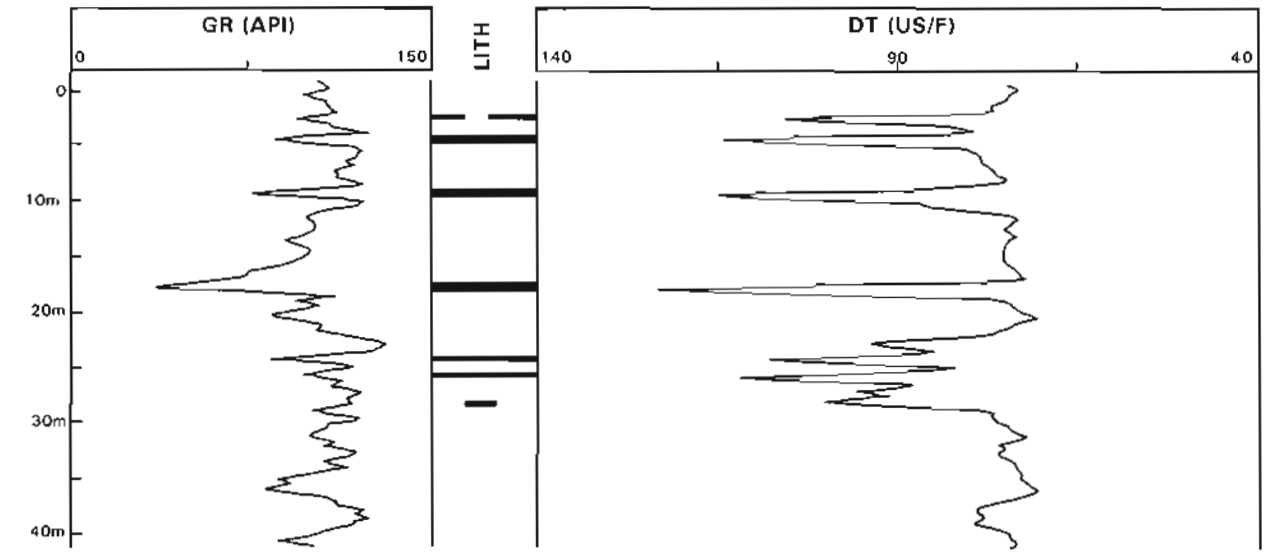


**Figure 8.13** Distinctive sonic log response in coals. The interval transit time is characteristically very high (low velocity) (cf. Figure 8.11).

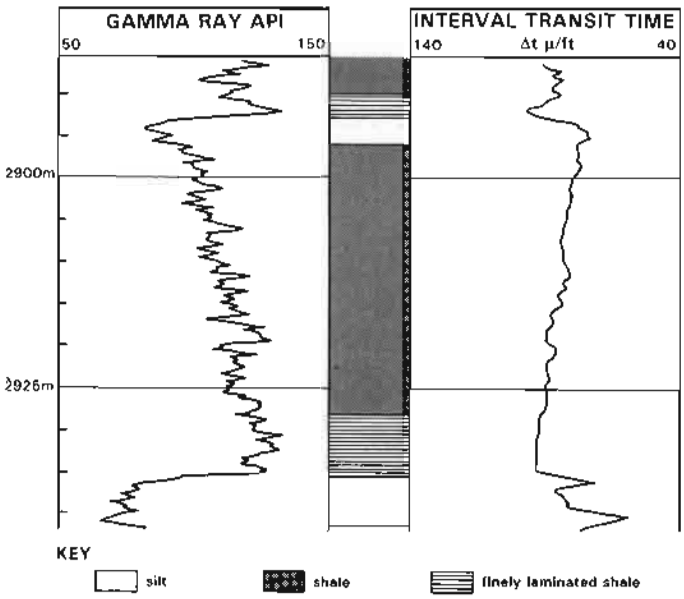


**Figure 8.14** Sonic response to shale structure in a shallow marine, coarsening-up sequence. The finely laminated shales at the base of the sequence show a high interval transit time (low velocity), while in the more massive, bioturbated, silty upper parts of the sequence, interval transit times are lower (velocity higher).

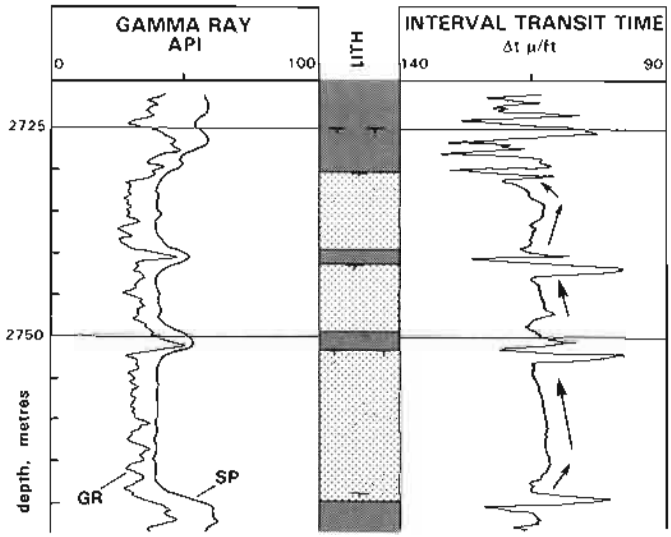


**Figure 8.15** Subtle textural and structural variations in deep sea, turbidite sands, shown on the sonic log. The log changes indicate variations in grain-size, texture and structure but which dominates in this example is not known.

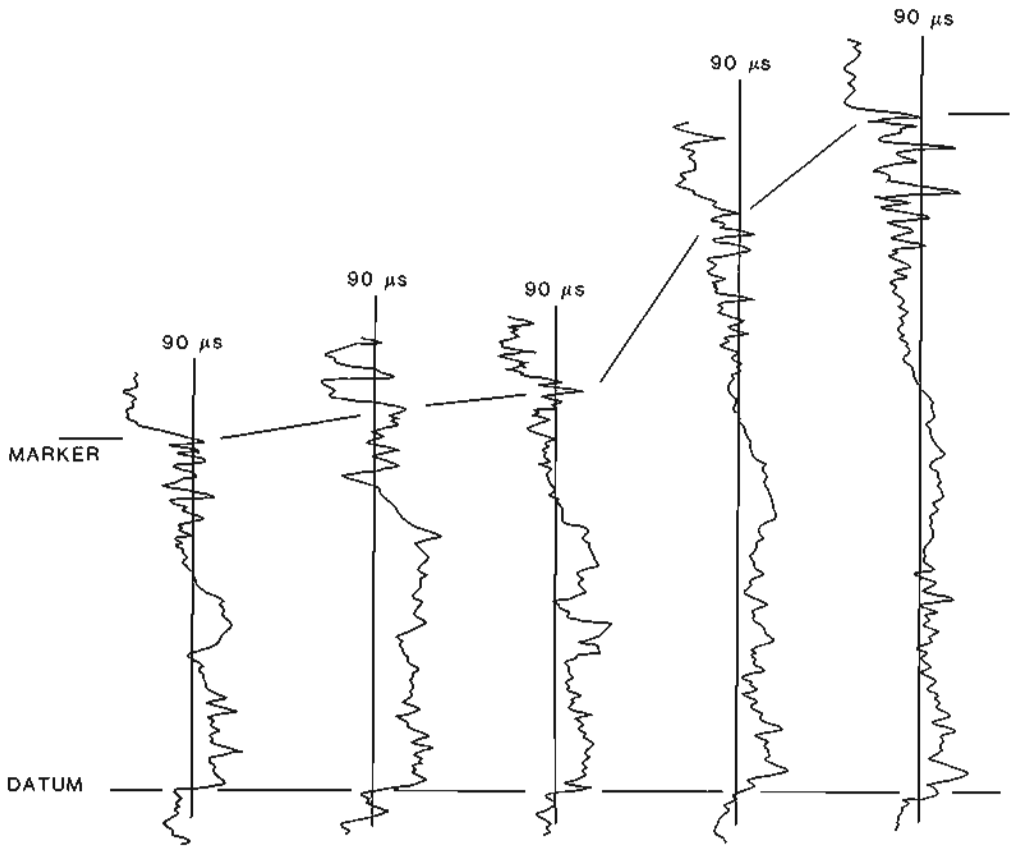


**Figure 8.16** The 'character' of the sonic log used for correlation. The log is sensitive to lithological changes (texture and composition) as indicated by the logs in this shale sequence. The outside wells are 40km apart, the zone between 40m and 75m thick.

specific stratigraphic intervals, especially in fine grained sequences. There are many examples in the literature (i.e. Michelsen, 1989; Whittaker *et al.*, 1985).

***Fracture identification***

A knowledge of the presumed travel paths of the sonic signals (Figure 8.7) suggests that the log may be used for fracture identification. The sonic log porosity is probably only that due to the matrix, and does not include fracture porosity. This is because the sonic pulse will follow the fastest path to the receiver and this will avoid fractures. Comparing sonic porosity to global porosity should indicate zones of fracture. The subject is fully described under the Density Log (*see* Chapter 9, 'Fracture identification'). The use of the full waveform acoustic log in fracture analysis is discussed below (Section 8.8).

***Compaction***

As a sediment becomes compact, so its velocity increases. The effect is most obvious on reduced-scale sonic logs where, over thick shale intervals, there is a regular increase in velocity downwards due to compaction (Figure 8.17). In extremely homogeneous intervals when interval transit time is plotted on a logarithmic scale and depth on an arithmetic scale, there may be a straight-line relationship which represents a very regular compaction (Hottman and Johnson, 1965). Such regular relationships are especially visible in Tertiary sediments in many parts of the world (e.g. Herring, 1973; Magara, 1968; Issler, 1992).

But graphical methods have limitations and compaction is better studied quantitatively by measuring changes in shale porosity with depth. In turn, shale porosities can be calibrated with log derived interval transit times (Magara, 1978; Issler, 1992) (Figure 8.18). Using data from Japan and Eastern Canada, Magara (1978) proposed an empirical relationship:

$$\phi = 0.466\Delta t - 31.7$$

where $\phi$ = shale porosity and $\Delta t$ = sonic transit time.

But both the Wyllie time average equation (i.e. Bulat and Stoker, 1987, *see above* for the formula) and the 'acoustic formation factor' approach (Raiga-Clemenceau *et al.*, 1988) have been used. The latter, when used in the Beaufort-Mackenzie Basin gives the following results (Issler, 1992):

$$\phi = 1 - \left(\frac{\Delta tma}{\Delta t}\right)\frac{1}{x}$$

where $\phi$ = porosity, $\Delta t$ = sonic log value, $\Delta t_{ma}$ = matrix transit time (67μs/ft) and $x$ = acoustic formation factor (2.19), (the figures are applicable to the Beaufort-Mackenzie Basin).

However, the Wyllie 'time average' and the 'acoustic formation factor' formulae were intended for sandstones. The compaction characteristics of shales and sandstones are different, shales responding essentially to physical forces, sandstones more to chemical and mineralogical agents (Magara, 1980). Thus, applying either the Wyllie formula or the acoustic formation factor is theoretically incorrect. According to Magara (1980) shales tend to compact under the general formula:

$$\phi = \phi_0 \exp\frac{(-Z)}{C}$$

where $\phi$ = shale porosity, $\phi_0$ = initial porosity (i.e. $Z = 0$), $Z$ = depth of burial and $C$ = decay constant.

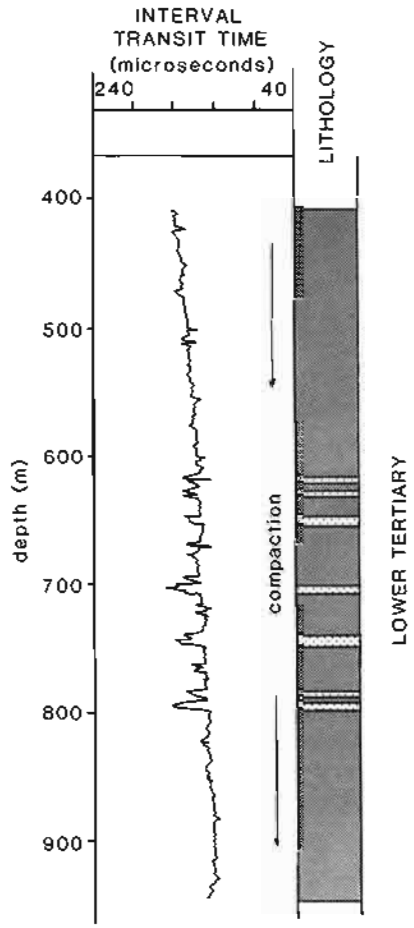


**Figure 8.17** Compaction in a shale sequence shown by a regular decrease in interval transit time with depth. The velocity decreases from approximately 160μ/ft to 140μ/ft over 500m.

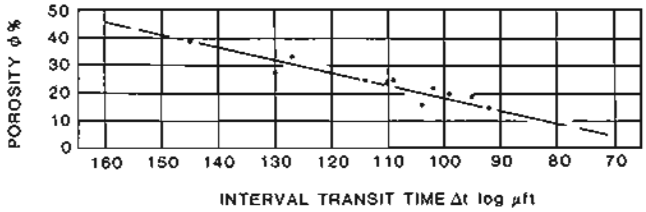


**Figure 8.18** The relationship between mudstone porosity ( $\phi$%) and interval transit time in Miocene mudstones, Japan. (From Magara, 1968).

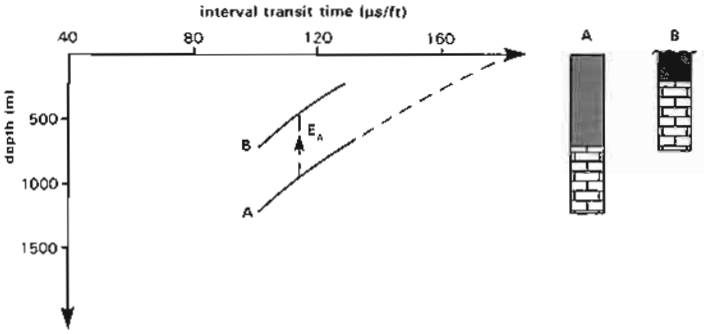


**Figure 8.19** The sonic used to estimate uplift. Well A shows normal compaction (curve A). Well B shows 'over-compaction' relative to well A at the same depth, because of uplift and subsequent erosion (curve B). The amount of uplift and erosion (Ea) is the vertical (depth) distance between curve A and curve B. Curves represent chalk compaction (re-drawn from Hillis, 1995).

Whatever relationship between shale porosity and transit time is preferred, it may be substituted in this relationship (cf. Bulat and Stoker, 1987).

Using general compaction trends it is possible to estimate erosion at unconformities or the relative amount of uplift (Lang, 1978; Magara, 1978; Vorren *et al.*, 1991; Hillis, 1995). Compaction is generally accompanied by diagenetic effects which are irreversible (e.g. Schmidt, 1973) and stay 'frozen' during uplift. The compaction of a sediment, therefore, represents its deepest burial. Using the general compaction curve for a particular interval, any 'over-compaction' can be explained by uplift. Tracking back to the general curve gives the amount of uplift (Figure 8.19). Similarly, any 'jumps' in compaction as at unconformities or faults, when compared to general well trends can give some idea of the amount of missing section. However, it should be stressed that such generalities should only be applied to one stratigraphic interval at a time and then in a relatively consistent facies (cf. Hillis, 1995). The method has many irregularities and should be used with circumspection, but in general the sonic is the best log for compaction and uplift studies.

***High-pressure identification***

Acoustic velocity can be used to identify overpressure. Other things remaining constant, an increase in pore-pressure or overpressure is indicated by a drop in sonic velocity. A plot of shale interval transit times through an overpressured zone shows a distinct break in the average compaction line (Figure 8.20). The principal reason for this drop is probably the increase in shale porosity, although several factors are probably compounded. It is considered possible to calculate the amount of overpressure from the extent of deviation of the sonic velocity from the normal compaction trend (Table 8.6) (Hottman and Johnson, 1965). Overpressure may also be calculated by an equivalent depth method, the simplest of which gives the following formula (Magara, 1978):

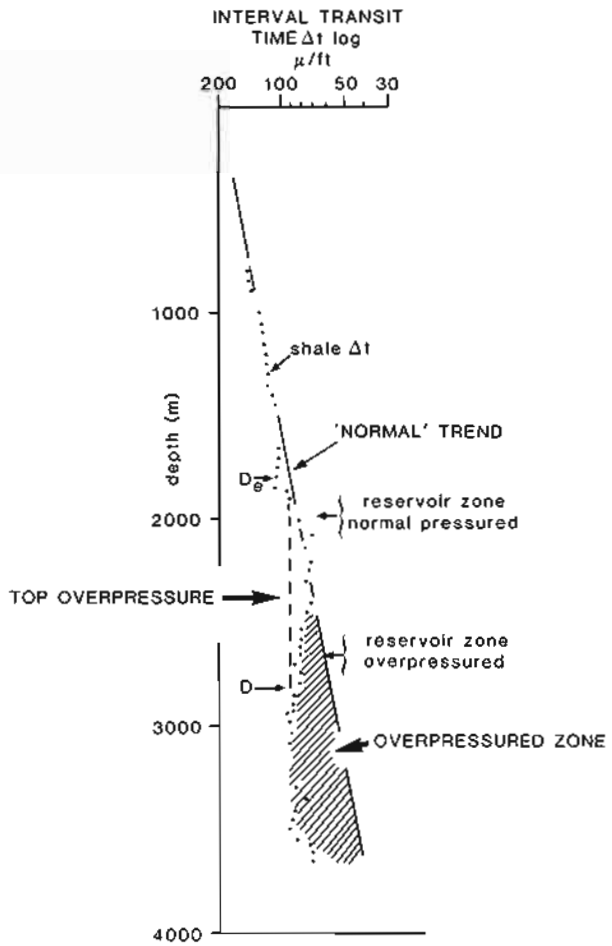


**Figure 8.20** Overpressure indicated by a plot of shale interval transmit times against depth. A decrease from the normal compaction trend indicates overpressure. (*D* and $D_e$ are for overpressure calculations, *see text*).

**Table 8.6** Overpressure estimates (after Hottman and Johnson, 1965).

| Dt decreases from average trends (μs) | 0 | 20 | 40 | 60? |
|---|---|---|---|---|
| Reservoir fliud pressure gradient (g/cm²) | 1.07 | 1.84 | 2.16 | 2.3? |
| Gradient (psi/ft) | 0.465 | 0.800 | .935 | ≃1.00 |

$$P = (\delta_w \times D_e) + \delta_r(D - D_e)$$

where $P$ = formation fluid pressure at depth $D$ (psi); $\delta_w$ = formation-water gradient (psi/ft); $\delta_r$ = lithostatic gradient (psi/ft); $D$ = depth of calculation point (ft); $D_e$ = equivalent depth (ft) with same sonic transit time (*see below*).

$D_e$ is a point in the section at normal pressure which has the same interval transit time as the point being measured. An example of $D$ and $D_e$ equivalence is marked on the sonic-log depth plot (Figure 8.20). The above calculation suggests that the pressure at $D$ is the

sum of the hydrostatic pressure to $D_e$ and the lithostatic pressure from $D_e$ to $D$.

Although the sonic log can be used to identify overpressure, it can only do so once drilling and logging are completed, by which time it may be too late!

***Borehole damage***

The frequent comparison between seismic and sonic velocities has shown that there are often differences between the two which cannot be accounted for by frequency difference (Figure 8.25). The differences are thought to exist, at least partly, because sonic velocities can be affected by mechanical or chemical damage immediately around the borehole. The very shallow depth of penetration of the sonic pulse has been discussed (Section 8.4) which means that it is susceptible to immediate borehole conditions. Drilling can cause damage at the borehole wall, especially to shales either mechanically, by fracturing and spalling (Section 4.4), or chemically by the (chemical) reaction of the drilling mud with the formation. Figure 8.21 shows the effect on the sonic measurements of progressive chemical reaction between the mud filtrate and swelling clays in a well in Colombia (Blakeman, 1982). The example is extreme since holes are not normally left uncased (i.e. open) for 30–40 days. However, it does demonstrate that the phenomenon exists and that it dramatically increases the interval transit time (lowers the velocity). It means that sonic logs recorded as soon as possible after drilling will be the most representative (Blakeman, 1982).

***Source-rock identification***

By itself, the sonic log cannot be used to indicate source-rock potential. However, the presence of organic matter, especially in shales, lowers sonic velocities, apparently in direct relation to abundance and when combined with the resistivity log value the velocity is a good qualitative and possibly quantitative source indicator (*see also* Section 6.8, Source-rock identification). Several methods of quantification exist: two are described below.

Based on an analysis of source rocks from around the world, a general formula has been derived for simply separating source from non-source rocks using a sonic-resistivity combination (Meyer and Nederlof, 1984). A regression line on a sonic-resistivity cross-plot is said to separate source rocks from the non-source, both shale and limestone (Figure 8.22). The linear equation for this discriminant D, is:

$$D = -6.906 + 3.186 \log_{10} \Delta t + 0.487 \log_{10} R75°$$

where $\Delta t$ = sonic log value, μs/ft; $R75°$ = log resistivity corrected to 75° F (24° C).

A second, rather unusual, empirical method, is considered to enable actual values of TOC (total organic carbon) to be derived (Passey *et al.*, 1990). The sonic and a resistivity log are used in a standard depth plot format but the method requires two essential steps to make them 'compatible', before they can be interpreted. First, both logs are 'scale normalized' by plotting the sonic log on a scale where 50μs/ft = 1 logarithmic cycle on the resistivity log (for example 50μs = .01 to 0.1 ohm/m). Second, a non-source shale interval is located (in the stratigraphic interval being considered) and the two logs made to plot one on the other over that interval (Figure 8.23). The authors call this a Δ log $R$ plot (Passey *et al.*, 1990). When the two logs are plotted like this, they will track each other over all non-source shales, regardless of compaction and compositional changes. In source intervals, there will be a marked separation (Figure 8.23). There will also be a separation in hydrocarbon reservoirs and in coals but these can be eliminated on lithological grounds using, for example, the gamma ray (Figure 8.23). If the level of maturity is known, then the TOC% can be derived. The empirical equation for this is:

$$\text{TOC\%} = (\Delta \log R) \times 10^{(2.297 - 0.1688 \times \text{LOM})}$$

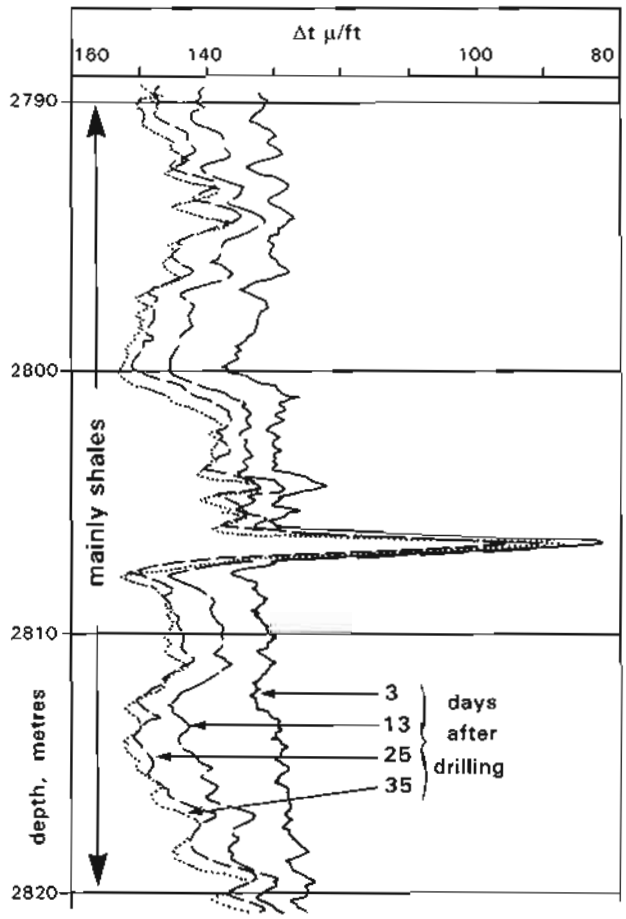


**Figure 8.21** Shale alteration affecting interval transit times in a well offshore Columbia (No. 1-1 Punta Gallinas). Successive passes of the sonic were made over 35 days and show a persistent increase in interval transit time (decreasing velocity) indicating shale alteration and deterioration. Note there is little change in the hard band at 2807m (re-drawn from Blakeman, 1982).

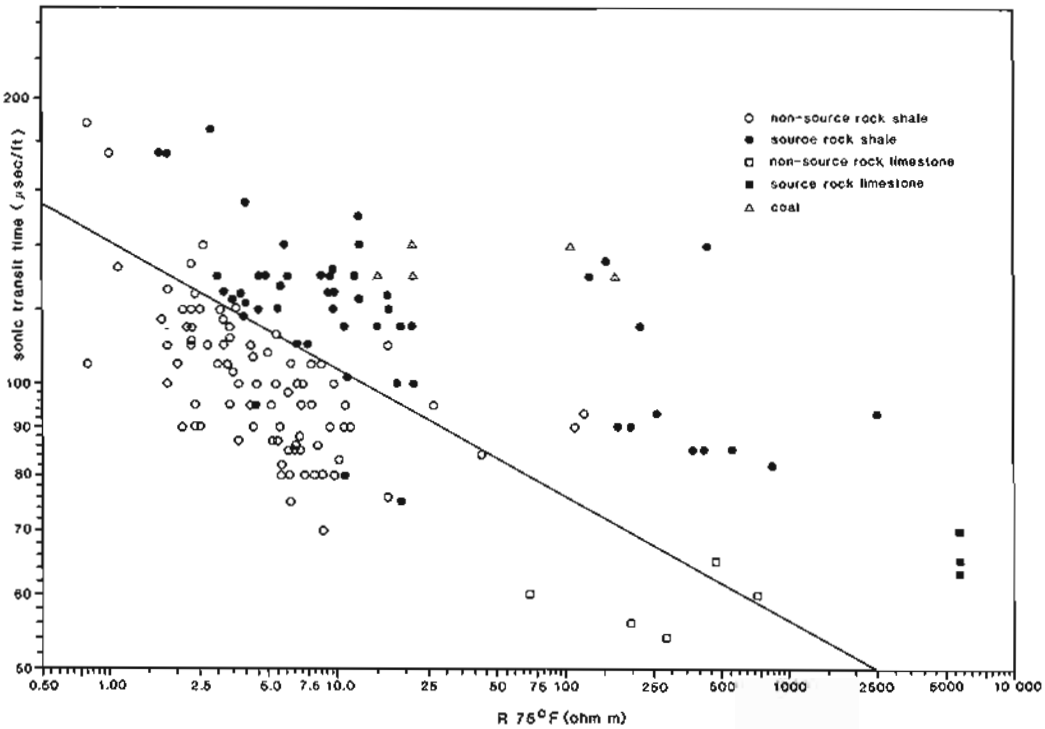


**Figure 8.22** The identification of source-rock intervals on a cross-plot of resistivity against sonic transit time. The oblique line is D = 0, from discriminant analysis using points of known source-rock potential. (From Meyer and Nederlof, 1984).

where TOC% = total organic carbon in %; LOM = level of maturity (Hood *et al.*, 1975) and $\Delta$ log $R$ = curve separation in resistivity units.

The level of maturity must be known for the quantification since the resistivity log responds to the amount of liquid hydrocarbons in the shale pores, not the amount of solid hydrocarbon, as discussed in the chapter on the resistivity log (Section 6.8). For example, a mature source rock is marked by a sonic low and resistivity rise; an immature source has an equally low sonic but no change in resistivity (Figure 8.23). However, that the amount of free hydrocarbon fluid in the pores of a shale is quantitatively related to the degree of maturation of the organic matter, as this method implies, remains to be proven.

This method seems to be useful qualitatively but quantitatively cumbersome and doubtful. Moreover, as the authors point out, with just the sonic log, it is impossible to separate low sonic values due to organic matter and low sonic values due to porosity changes (such as overpressure). This is a frequent dilemma in much log interpretation: separating the compositional effects from the textural effects. For log-based source-rock quantification, the density log appears to be simpler to use (*see* Section 9.6).

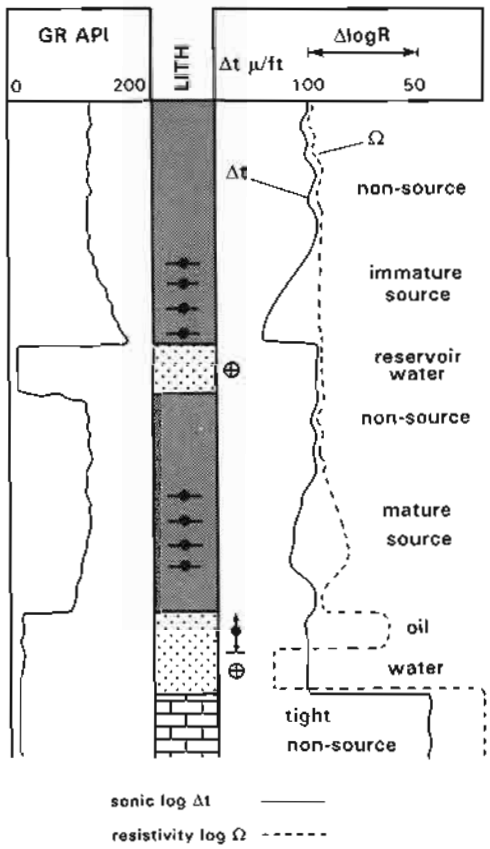


**Figure 8.23** Schematic representation of sonic and resistivity log responses in source, non-source and reservoir intervals using a delta log R overlay (compare Figure 6.38) (modified from Passey *et al.*, 1990).

RÉPUBLIQUE FRANÇAISE.

MINISTÈRE DU COMMERCE ET DE L'INDUSTRIE.

DIRECTION DE LA PROPRIÉTÉ INDUSTRIELLE.

# BREVET D'INVENTION.

**Gr. 8. — Cl. 1.** **N° 786.863**

**Procédé et appareillage pour la reconnaissance des terrains traversés par un sondage.**

Société dite : SOCIÉTÉ DE PROSPECTION ÉLECTRIQUE (Procédés SCHLUMBERGER) résidant en France (Seine).

**Demandé le 1er juin 1934, à 16 heures, à Paris.**
Délivré le 17 juin 1935. — Publié le 11 septembre 1935.

[Brevet d'invention dont la délivrance a été ajournée en exécution de l'art. 11 § 7 de la loi du 5 juillet 1844 modifiée par la loi du 7 avril 1902.]

N° 786.863 Société dite : Société de Prospection Électrique (Procédés Schlumberger) Pl. unique

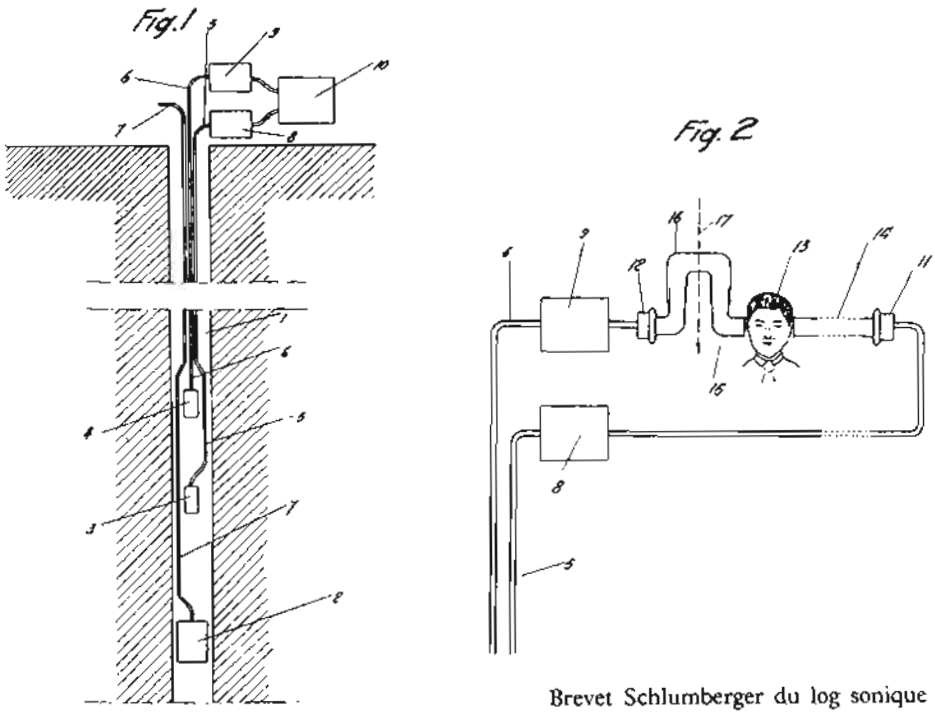


Brevet Schlumberger du log sonique

**Figure 8.24** The *brevet d'invention* for the sonic log deposited by Schlumberger in Paris, June 1934. (From Allaud and Martin, 1976).

## 8.7 Seismic applications of the sonic log

Acoustic velocity is the essence of the seismic section and the sonic log. Indeed, the sonic log was originally invented as an aid to seismic prospection as is seen by Schlumberger's *brevet d'invention* registered in Paris in June 1934 (Figure 8.24) (Allaud and Martin, 1976). After its invention the sonic log became a tool for petrophysicists and geologists, but today it is reverting to its origins and is increasingly becoming a supplementary tool in seismic prospection.

***Seismic v. sonic velocities***

The frequency of the sound pulse used in sonic logging is in the range 10–40kHz; the equivalent pulse in seismic work is 10–50Hz. The sonic tool can detect beds down to about 60cm or even thinner. The seismic wave can resolve, typically, down to about 10 m in shallow section but only 50m, in deeper section; it depends on velocity and wavelength. Seismic resolution, then, is approximately 1/100 that of the sonic log (Sheriff, 1980). The difference is well illustrated when seismic and sonic traces are directly compared (Figure 8.25)

Sonic log data, if it is to be compared to seismic data, must be brought up to the same scale and must be averaged.

***Interval velocities***

The results of sonic logging may be presented in several ways so that they may be used in seismic interpretation. Two presentations, which are complementary, are the interval velocity and the time-depth curve.

To find interval velocities, the sonic velocity is averaged over important stratigraphic intervals, or intervals likely to be indicated on the seismic section (Figure 8.26). The velocity is found by counting the integrated travel-time marks (Figure 8.5) over the interval concerned, and then dividing by the depth covered by the time. For instance, if 200 marks are counted (i.e., 200 milliseconds) between 2400m and 3400m (thickness 1000m), the interval velocity is $1000/200 \times 10^{-3}$ m/s = 5000m/s. Interval velocities are usually presented in histogram form against depth (Figure 8.26).

The time-depth curve represents the accumulated interval velocities. That is, the accumulated milliseconds are plotted against depth (Figure 8.26). The first cross on the time-depth curve (Figure 8.26) is 150 milliseconds (0.15sec) from zero and at 200 metres depth (an interval velocity of 200/0.15 = 1333m/sec). The coordinates of the next cross are 250 milliseconds (+100 millisecs) from zero at 450 metres (+ 250m) depth (an interval velocity of 250/0.1 = 2500m/s). The presentation on the time axis

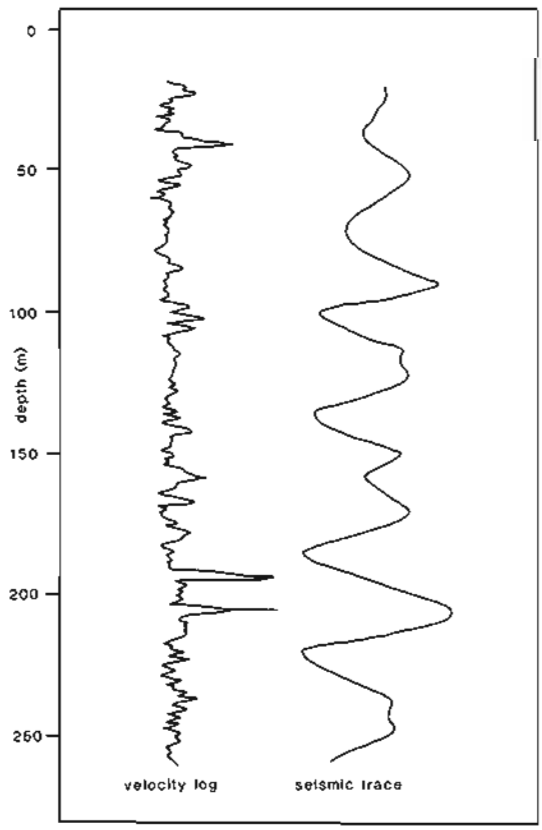


**Figure 8.25** The contrasting frequency content of the sonic log and a seismic trace. (Re-drawn from Sheriff, 1980).

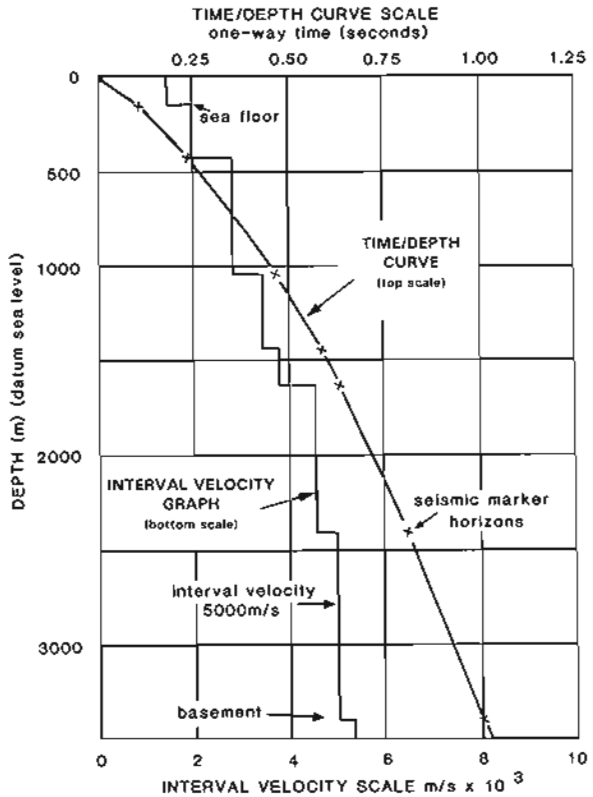


**Figure 8.26** The presentation of sonic velocity data to match the scale of seismic data: the time-depth curve and the interval velocity graph. The two horizontal scales are independent: the depth scale is common to both curves.

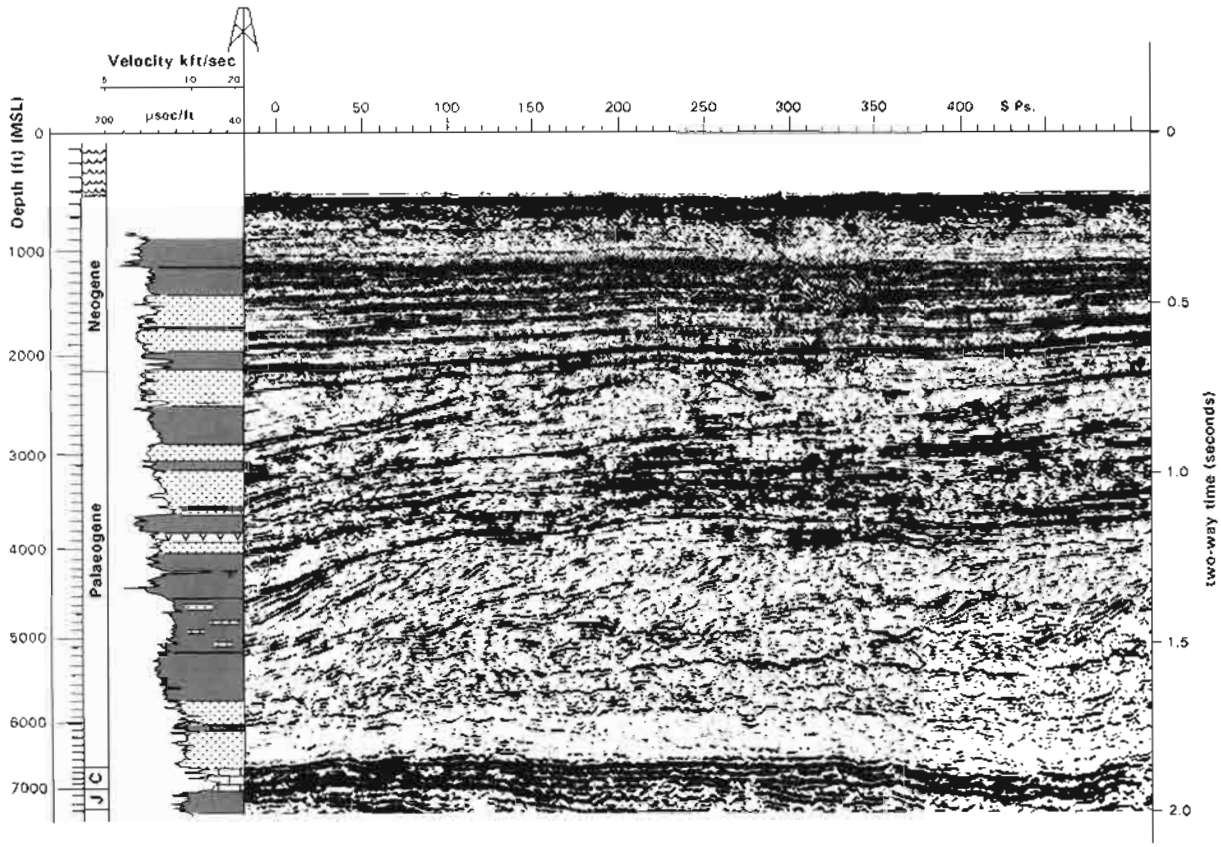


**Figure 8.27** A sonic log re-played on a time scale furnished with a lithology and stratigraphy, gives an accurate visual geology to the seismic section.

(top horizontal scale) then becomes compatible with the seismic section. A normal time-depth curve is taken from zero time and zero depth (i.e. corrected from well KB to a surface datum which is mean sea level offshore) to the well TD. From this can be read the average time to any particular depth or stratigraphic horizon, and this value can then be used to convert seismic time maps (isochron maps) to depth maps (isobath maps). But it should be remembered that time-depth curves are in *one-way time* and seismic sections and isochron maps are in *two-way time* (the time it takes for a seismic signal to go from the surface to the reflector and back).

In practice, when a well is completed a series of 'check shots' is run to calibrate the sonic log. That is, a geophone is lowered into the well and a shot is fired at the surface. The time taken by the sound pulse from the surface to reach the geophone is recorded. The precise depth of the geophone is known and therefore also the precise time to this depth. The shots are made throughout the borehole either with the geophone at strategic stratigraphic and seismic levels (just above a probable reflector) or, more commonly nowadays at regular close intervals such as every 25m or 50m. A time-depth curve can be made from the check shots which is independent of the sonic-derived time-depth curve. Alternatively, the check-shot depths may be used by relating them to the sonic log, the latter then being squeezed or stretched from shot to shot so that the average velocities between check shots correspond to the average velocities on the sonic log (Goetz *et al.*, 1979). With the achieved precision, the sonic log may now be replotted by the computer on a linear time scale similar to that of a seismic section (say 10cm = 1 second) rather than a linear depth scale as in a well (Figure 8.27). A geological and stratigraphic representation on a time-scale log is a powerful tool for both geophysicist and geologist. The seismic section takes on a direct geological significance (Figure 8.27).

### *Synthetic seismic logs*

A synthetic seismic log is a presentation of the data contained in a sonic log in the form of a seismic trace. In a computer-derived calculation, the high frequency data of the sonic log is replayed at the low frequency of seismic data.

A seismic section is the result of acoustic reflections from subsurface strata. The reflections depend on the contrasts of the acoustic impedances (i.e. velocity × density) of the adjacent layers, that is the reflection coefficient ($R$):

$$R = \frac{\text{acoustic impedance below} - \text{acoustic impedance above}}{\text{acoustic impedance above} + \text{acoustic impedance below}}$$

$$\text{i.e.} \quad \frac{D_2V_2 - D_1V_1}{D_2V_2 + D_1V_1}$$

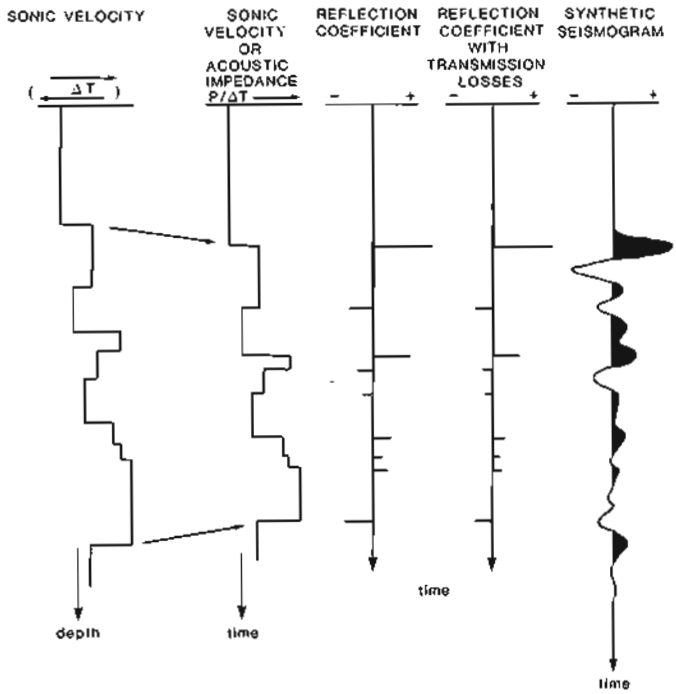


**Figure 8.28** Diagrammatic representation of the construction of a synthetic seismic trace from the sonic log. (From Thomas, 1977).

When both a sonic log and a density log are run in a well, the acoustic impedances of the layers logged can be calculated (Figure 8.28). The acoustic impedance log represents the logged section as it would be sensed by the seismic pulse.

With the aid of a computer, a synthetic seismic signal is formulated and passed through the acoustic impedance log. The seismic signal is distorted just as it would be if it were going through these layers in the subsurface. Recording the signal distortions, the computer constructs a synthetic seismic response (Figure 8.28). The original sonic data have been converted into a seismic trace. The synthetic seismic log is invaluable for 'tying' wells to the seismic, and demonstrating the effective resolution on the section.

## 8.8 Full waveform acoustic logs (array sonic)

### *Generalities*

The standard sonic logging tools, available for the last 40 years and described previously, measure only the first or compressional (P) wave arrival (Section 8.2). A new generation of tools with a great deal more sophistication measure a full waveform. They tend to be called array sonic tools through the use of an array of receivers which under the right conditions, allow the identification of compressional (P), shear (S) and Stoneley (St) wave arrivals (Figure 8.2). For reasons, which will be briefly explained (*see* Full waveform tools), two types of full waveform tool exist, those with standard monopole or multi-directional transmitters and those with dipole (polarised) transmitters which are better adapted to shear wave detection.

The desired output from the full waveform sonic is either some form of waveform plot against depth or a continuous log of discrete values of the slowness of the compressional (P), shear (S) and Stoneley (St) waves. Slowness (the reciprocal of velocity) is the average wave lag between two consecutive receivers (or transmitters) corresponding to the difference in wave arrival times at each of the receivers and given in μ/ft or μ/m. From these and their inter-relationships such as Poisson's ratio, information can be extracted on fractures, permeability, lithology, porosity and fluid content.

### *Full waveform tools*

One of the difficulties in full waveform sonic logging is the identification of the shear wave arrival. Typical transmitters and receivers in the standard sonic are multi-directional (monopole), emitting sound waves equally in all directions around the tool (Figure 8.29*a*). With this transmission mode, in certain so called 'slow' formations (that is when the shear wave velocity, refracted from the formation, is the same or less than the borehole fluid velocity), the shear and fluid arrivals cannot be separated. Using monopole or multi-directional transmitters, therefore, may not allow a direct detection of shear waves. For this reason, tools exist with dipole transmitters able to provide a direct shear wave detection in both 'slow' and 'fast' formations. Dipole transmitters are non-axisymmetric and produce sound waves which are directed, the transmitted pulse giving a positive displacement to the borehole fluid (push) in one direction and an equal, negative displacement (pull) in the opposite direction (Figure 8.29*b*). Monopole and dipole transmitters are used in different tools (Table 8.7) although they may also be combined in one tool.

Full waveform tool design differs between companies and is evolving. A common feature, however, is the need for an array of receivers, 12 in the Atlas tool, 8 in the Schlumberger tool (Figure 8.30) and four in the Haliburton tool (Table 8.7). At least 8 receivers seem to be preferable (Smith *et al.*,1991). The Schlumberger Dipole Shear Sonic Imager (DSI) can be used as an example. This tool has an array of eight receivers. It has two dipole transmitters at right angles to each other, 3.35m and 3.5m (11ft and 11.5ft) from the nearest receiver and one monopole transmitter 2.7m (9ft) from the receivers (Figure 8.30). The monopole transmitter is used with a low frequency pulse for Stoneley wave detection and a high frequency pulse for P and S wave detection. The dipole transmitters use a low frequency pulse (Table 8.7). The array of 8 receivers spans 1.07m (3.5ft), with a 15.24cm (6") spacing between each one. For full waveform acquisition, the tool may operate in a number of different modes: using one dipole transmitter

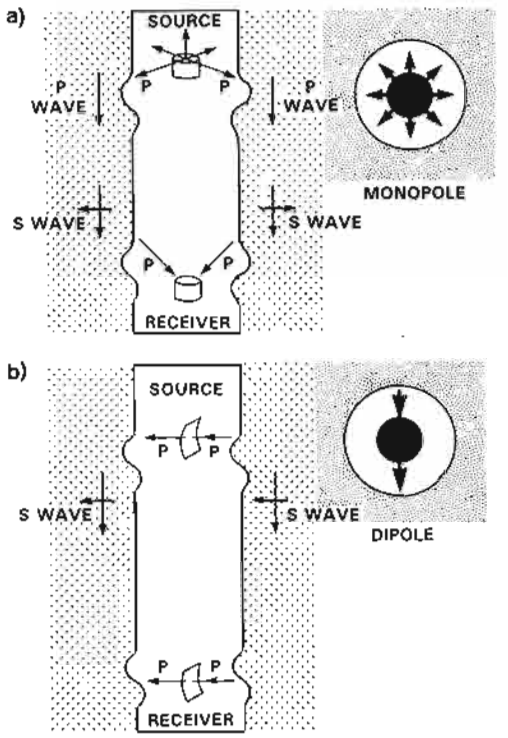


**Figure 8.29** Array sonic transmitter types. a) monopole transmitter giving a multi-directional pulse; b) dipole transmitter giving a directed pulse (modified from Zemanek *et al.*, 1991).

for 8, or two for 32 waveforms and using one monopole transmitter for 8 waveforms using either a high frequency signal for P and S waves or a low frequency signal for Stoneley wave detection. The tool acquires digital waveform data with 512 samples per waveform. Logging speed varies but can be at a maximum of 1100m/hr (3600 ft/hr) which is similar to the standard nuclear tools.

All tools using an array of receivers acquire a number of receiver (or transmitter) common measurements at each depth station (Figure 8.31), the number of common datapoints depending on the number of receivers and/or transmitters used. Receiver threshold detection, as used in the standard tools, is inadequate and inappropriate for the full waveform tool. Instead, a full, digital waveform is recorded and gathering techniques are used to collect the common datapoints from a single depth (or selected interval). The gathering may be made using one transmitter position and a full receiver array (Smith *et al.*, 1991) (Figure 8.31), or a sub-array as used by Schlumberger, when several consecutive transmitter and receiver points are used (Hsu & Chang, 1987) (Figure 8.32). Sampling depths are normally the same as the separation between the receivers of the array, typically 15.24cm (6"). However, since gathering may be over an interval covering several receivers as described, the effective interval being measured depends on the gathering process (Figure 8.32), as discussed below.

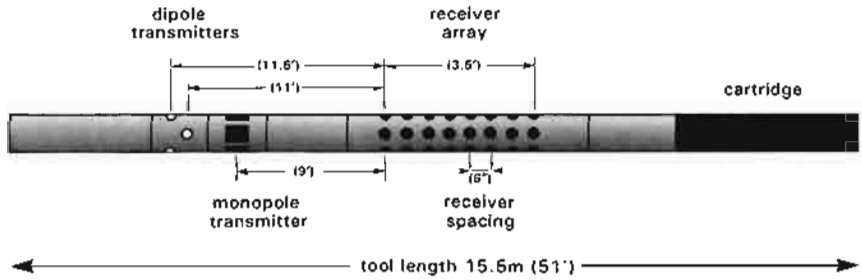


**Figure 8.30** The Dipole Shear Imager Tool of Schlumberger (re-drawn from Schlumberger document).

**Table 8.7** Full waveform acoustic tools.

| Company | Tool | Receiver Array | Transmitters & Frequency (Fq) |
|---|---|---|---|
| Schlumberger | Array Sonic ASL | 8 receivers | 2 transmitters, monopole, Fq = 10–15 kHz |
| | Dipole Shear Imager DSI | 8 receivers | 3 transmitters, 1 monopole, 2 dipole Fq = 1 kHz (diopole), Fq = variable (mononpole) |
| Atlas Wireline | Digital Array Acoustilog DAC | 12 receivers | 2 transmitters, monopole, Fq = 9 kHz |
| | Multipole Acoustic Tool MAC | 8 receivers | 4 transmitters, 2 monopole, 2 dipole Fq = 1–3 Hz (dip), Fq = 8 kHz (mono) |
| Halliburton | Full Wave Sonic Log FWS | 4 receivers | 1 transmitter, monopole, Fq = 13 kHz |

***Data output, velocity picking***

With a full, digital waveform from all of the receivers in an array at each sampling depth, separating the various wave arrival times and slowness values requires special processing. For example, the output from an eight receiver array provides 8 waveforms with different offsets (Figures 8.31, 8.33*a*). To derive the separate P, S and St wave velocities (slowness) various methods are used comparable to stacking in seismic processing (Block *et al.*, 1991). Effectively, the data from the individual traces are combined in such a way as to enhance individual wave information and diminish noise or other unwanted effects. Typically, at each depth, a map in a time-velocity domain is produced (Figure 8.33*b*) from which individual wave slowness values can be picked and a log of slowness against depth produced.

A complication arises using tools with only *monopole* transmitters in 'slow' formations where the shear energy and the Stoneley energy cannot be separated. In order to have shear velocity with this data, it is modelled from the Stoneley information and an *interpreted* shear arrival is given. With the *dipole* transmitters, direct detection of the shear arrival is possible in both 'fast' and 'slow' formations, as indicated above.

The resolution of the array tools is related to the array size used in the processing gather or the gather technique. This will be the vertical height of the array or 1.07m (3.5ft) for the DSI of Schlumberger (Figure 8.32). A bed thinner than the array gather will still be indicated and in its real depth position, but it will not be fully resolved (Hsu and Chang, 1987). Generally, all the receiver information will be included in one gather and borehole compensation may be applied by using transmitter stations through the receiver array section (Figure 8.32*a*).

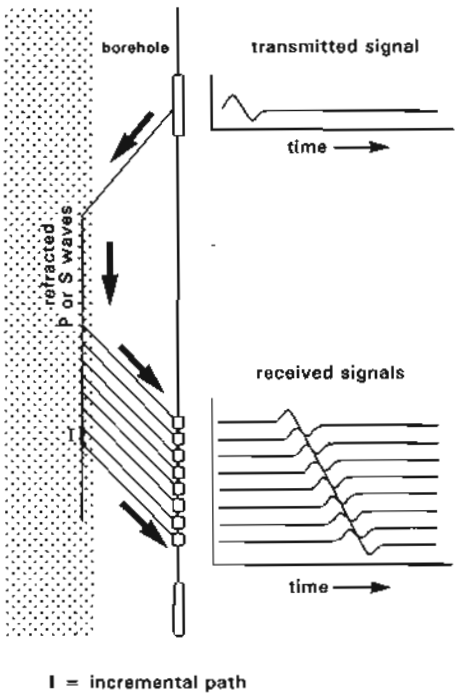


**Figure 8.31** Array sonic sampling system. At any depth, a series of transmitter common readings are made, with different offsets. Sequences of readings are gathered in various ways (*see* text and Figure 8.32) (from Smith *et al.*, 1991).

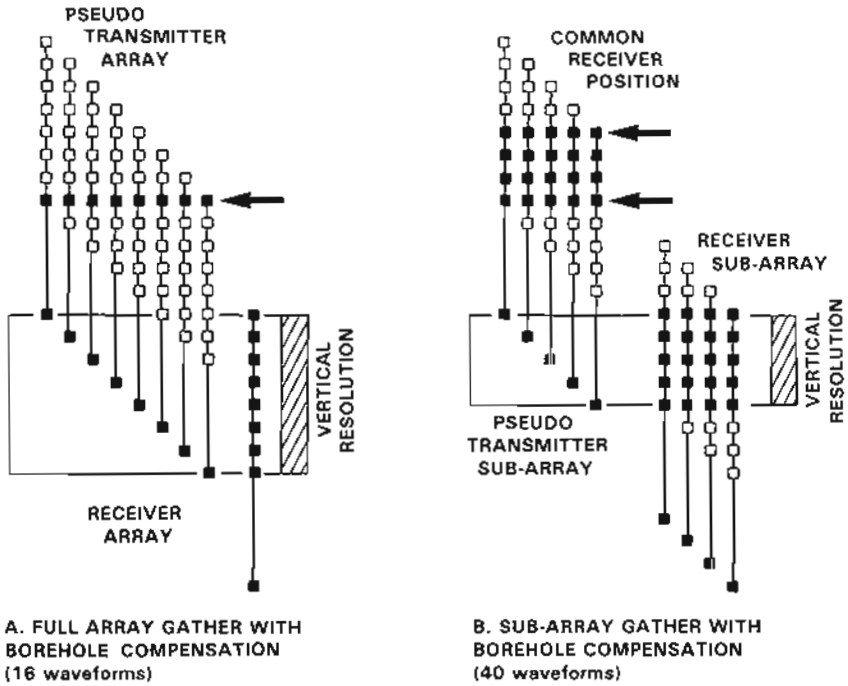


**Figure 8.32** Data gathering methods for the array sonic used by Schlumberger. A) gather using one transmitter position and an array of 8 receivers. B) gather using 4 transmitter positions and an array of 5 receivers. The vertical resolution of the measurements will be the vertical height of the array or sub-array (re-drawn modified from Hsu and Chang, 1987).

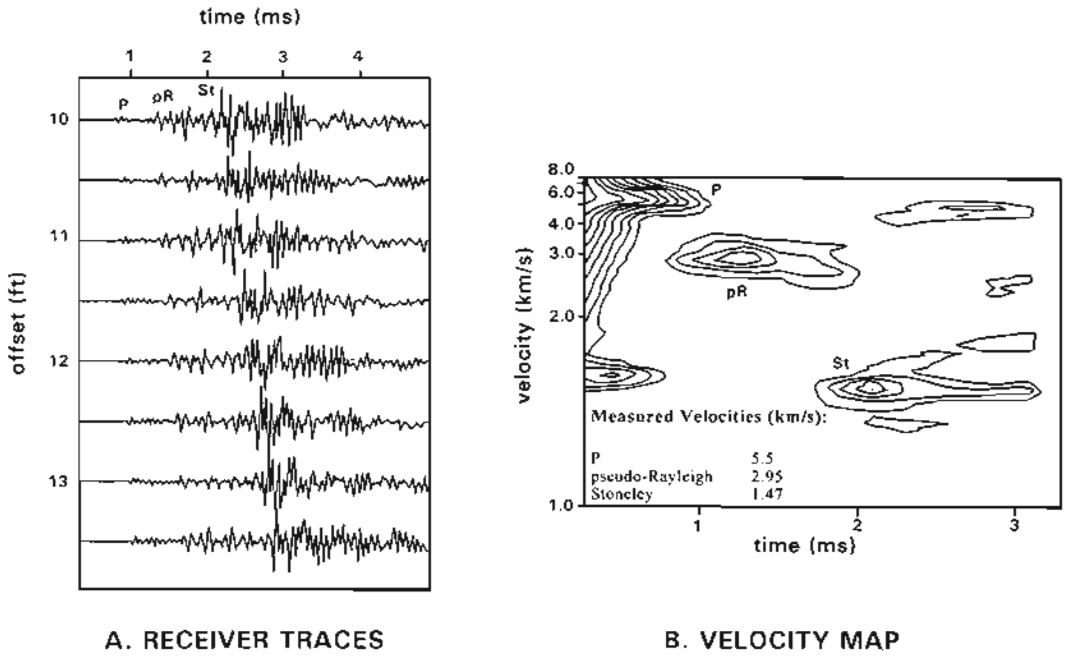


**Figure 8.33** Data gathering from an array sonic at one position. A) individual, full-wave receiver traces with different offsets (i.e. positions). B) dataset combined into a map of velocity vs. time, showing the positions of the compressional (P), shear (pseudo-Rayleigh, pR) and Stoneley (St) arrivals (from Block *et al.*, 1991).

However, Schlumberger also use a technique (called the multishot slowness-time-coherence method) in which a sub-array of receivers is used as a common gather in combination with a sub-array of transmitter positions (Figure 8.32*b*). In this case, when a 5-fold receiver sub-array is used, there is an increased vertical resolution to approximately 0.6m (2ft) (Schlumberger, 1994a).

*Displays*

A typical output from a full waveform sonic tool is a plot against depth of the individual slownesses for each of the compressional (P), shear (S) and Stoneley (St) waves, in the same way as standard logs are plotted (Figure 8.34*a*). The velocity analysis processing provides the information for this type of plot as described. Having a discrete set of slowness values for each depth point allows further analysis of the data in terms of rock properties such as Poisson's ratio or other mathematical inter-relationships, but a lot of information is not used.

Information on the full waveform can be shown in constant-offset sections or seismic-like variable density waveform plots or such as the 'waterfall display' of Amoco (Figure 8.34*b*). This type of plot allows the analysis of secondary as well as primary wave behaviour (*see* fractures and permeability *below*)

*Applications*

Generally the full waveform sonic tool produces data for specialist applications: the tools are not run as part of the standard log set. Moreover, the applications at present tend to have more to do with seismic interpretation than

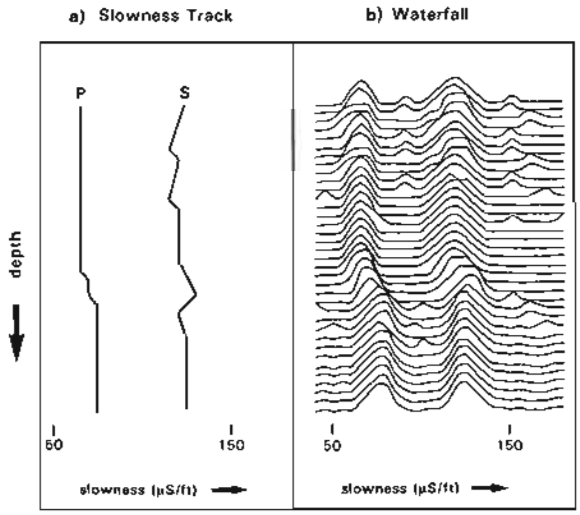


**Figure 8.34** Data display for the array sonic. *a*) individual slowness logs of discrete, picked values against depth. *b*) 'waterfall' waveform display of illustrative waveforms at selected depths (re-drawn from Smith *et al.*, 1991).

standard borehole log analysis. But more and more studies are being reported in which the tool's measurements are being used to advantage at the borehole scale (cf. Paillet, 1992). Probably the one application which will develop in this respect is that of detecting open fractures. Some examples of applications are given on page 113 (Table 8.8)

*-fractures and permeability*

The consistent association of tube-wave attenuation with

**Table 8.8** Acoustic information used to discriminate reservoir characteristics.

| Characteristic | Compressional Slowness | Shear Slowness | Stoneley Slowness |
|---|---|---|---|
| Fractures | – | + | *** |
| Permeability | + | + | *** |
| Lithology | *** | *** | – |
| Porosity | *** | + | – |
| Fluids | *** | *** | – |

*** required, + often useful, – not neeeded
after Paillet *et al.*, 1992

permeability in both porous sediments and fractured crystalline rocks is well established in the literature (Paillet *et al.*, 1991). Full waveform measurements, in fact, give one of the few opportunities to estimate *in situ* permeability in boreholes. The Stoneley (or tube) wave can be looked on as a pressure pulse moving along the borehole. When this pulse encounters an open fracture, pressure is released into it and the pulse is attenuated (Figure 8.35*b*). It is especially important to note that it is only *open fractures* that will be detected: surface studies do not allow differentiation between fractures which are closed and fractures which are open in the subsurface. With open fractures a reflected, secondary Stoneley wave is produced with a strength related to the amount of pressure released. Thus, under the right conditions, not only can open fractures be detected but also their permeability (Hornby *et al.*, 1992). Unfortunately not only *open fractures* create these effects but also hole washouts and significant formation boundaries.

Although research has tended to concentrate on fractures in crystalline rocks and hard formations (i.e. Paillet 1991; Hornby *et al.*, 1992), some work suggests that the experience gained in these formations can also be used in sedimentary successions (e.g. Mari *et al.*, 1994). It is clear that information from array sonic analysis must be combined with information from borehole imaging tools (Figure 8.35), core analysis and, where available, test flow rate information (Paillet, 1991). Borehole imaging tools supply information on the immediate borehole environment which includes drilling induced fractures. The array sonic data provides information on fractures penetrating up to metres away from the borehole, and more likely to be providing flow, although as indicated, there may be confusion with effects not caused by fracturing.

In the same way as Stoneley wave attenuation occurs with open fractures, attenuation may also be caused by any permeability. Typically, such attenuation will be more marked in hard formations, such as limestones, where the acoustic contrast between formation and mud-filled aperture is greatest.

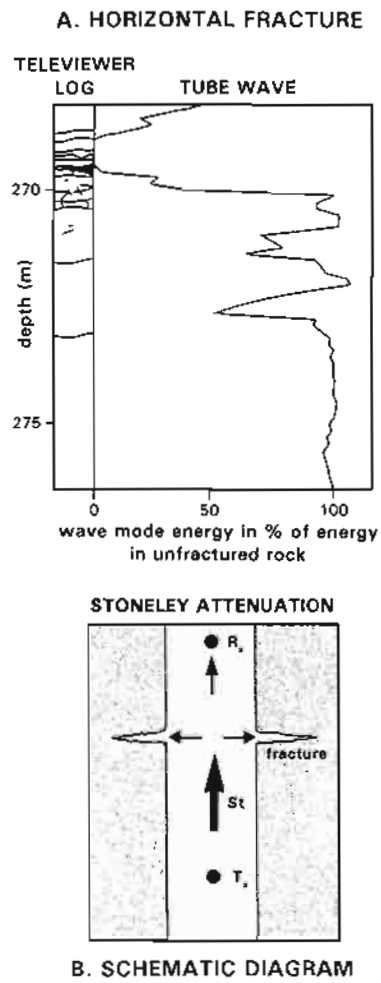


**Figure 8.35** The effect of an open fracture on Stoneley (tube) waves. A) energy loss shown on a log compared to open, horizontal fractures interpreted from a borehole televiewer. B) schematic illustration of Stoneley waves attenuated across an open fracture (modified from Paillet, 1991).

*-lithology (and porosity)*

Neither the detail nor the resolution of lithological information from the full waveform sonic are as good for borehole work as the information supplied by the standard open hole tools (Chapter 11). However, there is considerable need to try to define the lithological content of seismic sections and the information for this can be extracted from the full waveform sonic. The determination depends on the variations of elastic parameters between rock types. A simple way of characterising lithologies is to plot compressional slowness against shear slowness (Pickett 1963; Leslie and Mons 1982). With these plots, sandstones generally show ratios of 1.6 to 1.75 while limestones show a ratio of approximately 1.9 (Figure 8.36). Unfortunately, in detail such relationships are generally only valid for one set of data (*see also* Section 8.5) and cannot be used in a general application (Paillet *et al.*, 1992). None the less, full waveform sonic data are invaluable as input to seismic interpretation and processing.

*-fluid content*

Free gas or light (compressible) oil will tend to sharply decrease the compressional wave velocity in sands (Figure 8.10), especially loosely consolidated sands, but there will be little effect on shear wave velocity. This fluid content effect is noted in Poisson's ratio (the ratio of lateral strain to longitudinal strain which is derived from the P and S wave velocities). An example from a North Sea, Palaeocene sand-shale sequence (Bunch and Dromgoole, 1995), shows that shale, water sands and gas sands can be reasonably differentiated using Poisson's ratio but no such separation can be made based on acoustic impedance (i.e. compressional wave × density) (Figure 8.37). Observations such as these can be used to refine seismic analysis.

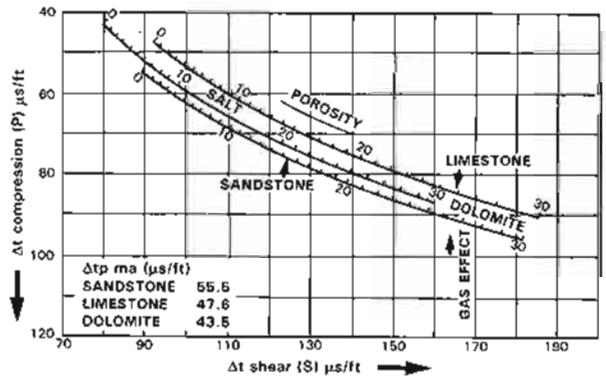


**Figure 8.36** Graph of compressional against shear slowness derived from the array sonic. The graph shows sandstone, limestone and dolomite fields over porosity ranges to 30%. (From CGG document).

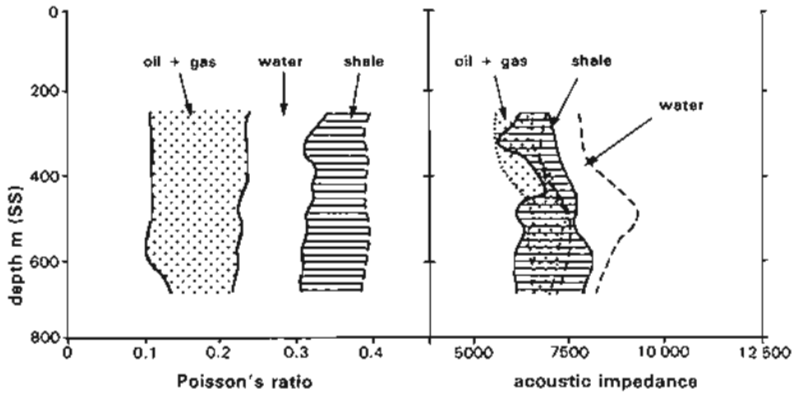


**Figure 8.37** Example of the use of Poisson's ratio. Shale, water-bearing sandstone and gas sands showing markedly different values of Poisson's ratio (left) but similar acoustic impedance; (right) North Sea Palaeocene (modified from Bunch and Dromgoole, 1995).

# 9
# THE DENSITY AND PHOTOELECTRIC FACTOR LOGS

## 9.1 The density log, generalities

***The log***

The density log is a continuous record of a formation's *bulk density* (Figure 9.1). This is the overall density of a rock including solid matrix and the fluid enclosed in the pores. Geologically, bulk density is a function of the density of the minerals forming a rock (i.e. matrix) and the volume of free fluids which it encloses (i.e. porosity). For example, a sandstone with no porosity will have a bulk density of 2.65g/cm³, the density of pure quartz. At 10% porosity the bulk density is only 2.49g/cm³, being the sum of 90% quartz grains (density 2.65g/cm³) and 10% water (density 1.0g/cm³).

***Principal uses***

Quantitatively, the density log is used to calculate porosity and indirectly, hydrocarbon density. It is also used to calculate acoustic impedance. Qualitatively, it is a useful lithology indicator, can be used to identify certain minerals, can help to assess source rock organic matter content (even quantitatively) and may help to identify overpressure and fracture porosity (Table 9.1).

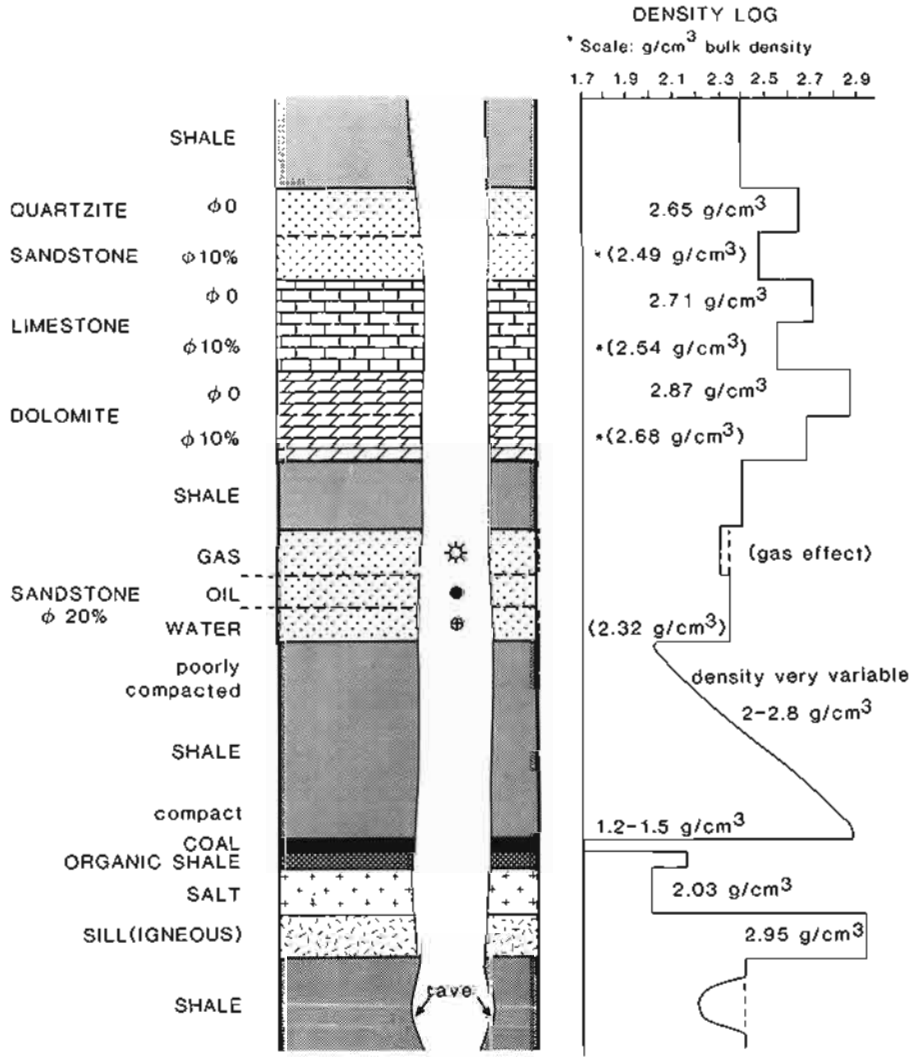


**Figure 9.1** The density log: some typical responses. The density log shows *bulk density*. *Density and porosity with fresh formation-water density 1.0g/cm³ (cf. Figure 10.1, which is on a compatible scale of neutron porosity).

**Table 9.1** The principal uses of the density log.

| | Discipline | Used for | Knowing |
|---|---|---|---|
| Quantitative | Petrophysics | Porosity | Matrix density<br>Fluid density |
| | Seismic | Acoustic impedance | (Use raw log) |
| Qualitative and semi-quantitative | Geology | General Lithology<br>Shale textural changes<br>Mineral identification | Combined with neutron*<br>Average trends<br>Mineral densities |
| | Reservoir geology | Overpressure identification<br>Fracture recognition | Average trends<br>Sonic porosities |
| | Geochemistry | Source rock evaluation | Density – O.M. calibration |

*using density log combined with neutron log on compatible scale

## 9.2 Principles of measurement

The logging technique of the density tool is to subject the formation to a bombardment of medium-high energy (0.2–2.0 MeV) collimated (focused) gamma rays and to measure their attenuation between the tool source and detectors. Such is the physical relationship that the attenuation (Compton scattering, *see* Section 7.2) is a function of the number of electrons that the formation contains – its electron density (electrons/cm$^3$) – which in turn is very closely related to its common density (g/cm$^3$) (Table 9.2). In dense formations, Compton scattering attenuation is extreme and few detectable gamma rays reach the tool's detectors, while in a lesser density the number is much higher. The change in counts with change in density is exponential over the average logging density range from about 2.0–3.0 g/cm$^3$ (Figure 9.2). Detector counts in modern tools are converted directly to bulk density for the log printout (Figure 9.5). However, although electron density, as detected by the tool, and real density are almost identical, there are differences when water (hydrogen) is involved. For this reason, the actual values presented on the density log are transformed to give actual values of calcite (2.71g/cm$^3$) and pure water (1.00g/cm$^3$) (Table 9.2). (There are still slight differences between log density and real density, especially when chlorine is involved.)

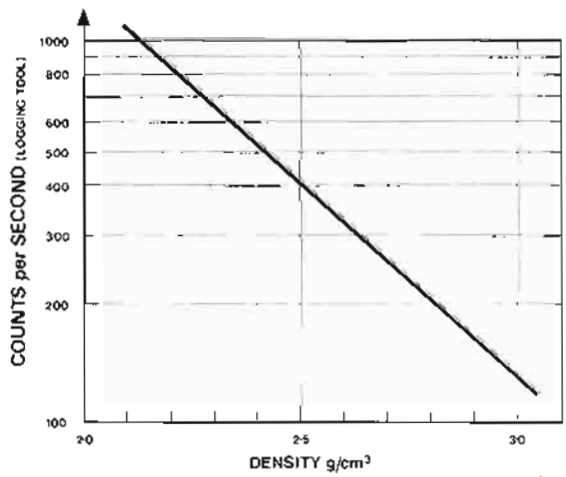


**Figure 9.2** Correlation between the density-tool radiation count (counts per second) and bulk density. A high density gives a low count. (Re-drawn from Desbrandes, 1968).

## 9.3 Tools

The standard density tools have a collimated gamma ray source (usually radiocaesium which emits gamma rays at 662 keV, but radiocobalt is also used) and two detectors (near and far) which allow compensation for borehole effects when their readings are combined and compared in calculated ratios. The near detector response is essentially due to borehole influences which, when removed from the

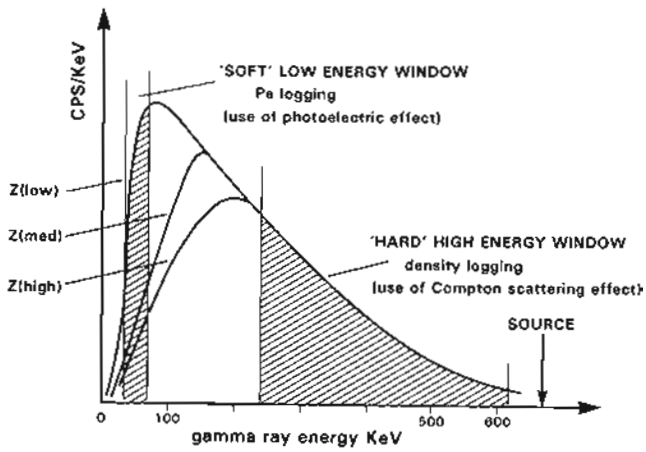


**Figure 9.3** Density and lithodensity (photoelectric) logging in relation to gamma ray energy. Density logging uses the high energy regions where Compton scattering occurs. Photoelectric logging uses the low energy region where the photoelectric effect is dominant. CPS = counts per second. KeV – kilo electron volts. Z = atomic number. (Modified from Ellis, 1987).

**Table 9.2** Density, electron density and tool given density for some common compounds (from Schlumberger, 1989a).

| Compound | Formula | Actual density $\rho_b$, g/cm$^3$ | Tool density based on electron density ($\rho e$), g/cm$^3$ | *Density given on log g/cm$^3$ |
|---|---|---|---|---|
| Quartz | $SiO_2$ | 2.654 | 2.650 | 2.648 |
| Calcite | $CaCO_3$ | 2.710 | 2.708 | 2.710 |
| Dolomite | $CaCO_3MgCO_3$ | 2.850 | 2.863 | 2.850 |
| Halite | NaCl | 2.165 | 2.074 | 2.032 |
| Gypsum | $CaSO_4 2H_2O$ | 2.320 | 2.372 | 2.351 |
| Anhydrite | $CaSO_4$ | 2.960 | 2.957 | 2.977 |
| Sylvite | KCl | 1.984 | 1.916 | 1.863 |
| Coal bituminous | | 1.200 | 1.272 | 1.173 |
| | | 1.500 | 1.590 | 1.514 |
| Coal anthracite | | 1.400 | 1.442 | 1.355 |
| | | 1.800 | 1.852 | 1.796 |
| Fresh water | $H_2O$ | 1.000 | 1.110 | 1.000 |
| Salt water | 200,000 ppm | 1.146 | 1.273 | 1.135 |
| Oil | $n(CH_2)$ | 0.850 | 0.970 | 0.850 |
| Methane | $CH_4$ | 0.000677 | 0.00084 | |
| Gas | $C_{1.1}H_{4.2}$ | 0.000773 | 0.00096 | |

*Density given on log = 1.0704 ($\rho e$) – 0.1883

**Table 9.3** Modern density tools.

*1. Density measurement*

| Name | Symbol | Company |
|---|---|---|
| Formation Density Compensated | FDC | Schlumberger |
| Compensated Densilog | CDL | Western Atlas, Halliburton |
| Compensated Density | CDS | BPB |

*2. Density and Photoelectric measurement*

| Name | Symbol | Company |
|---|---|---|
| Litho-Density Tool | LDT | Schlumberger |
| Compensated Z-Density | ZDL | Western Atlas |
| Photoelectric Density | PDS | BPB |
| Spectral Density Tool | HSDL | Halliburton |

far detector response enhance the formation effects (Figure 9.6). The most recent density tools (Table 9.3) use more efficient scintillation detectors which separate high (hard) and low (soft) gamma ray energy levels (Figure 9.3). This allows a better evaluation of borehole effects, so providing a more accurate density measurement as well as the additional photoelectric factor value (Section 9.7). Source and detectors are mounted on a plough-shaped pad which is pressed hard against the borehole wall during logging (Figure 9.4). Density-log readings therefore refer to only one sector on the borehole wall.

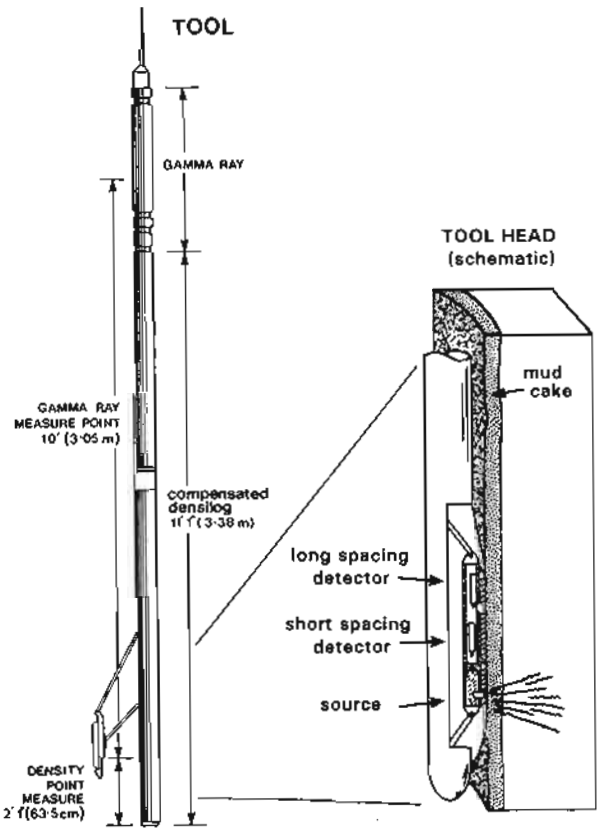


**Figure 9.4** A density tool (Densilog from Atlas Wireline) and a tool head (modified from Dresser Atlas, 1982 and Ellis, 1987).

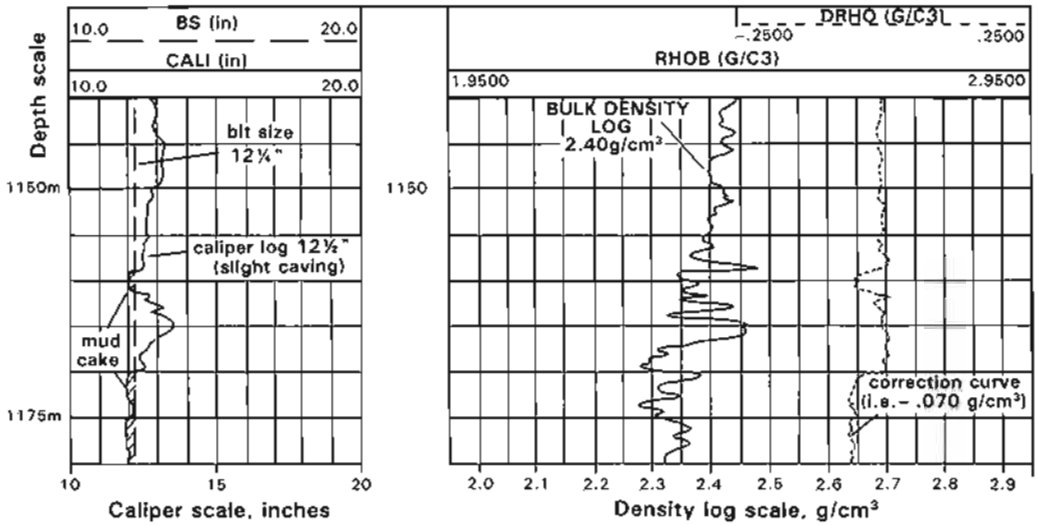


**Figure 9.5** Typical heading of a density log. The density log is over tracks 2 and 3: the scale is in g/cm³. Any mud weight correction is shown in log form (dashed) and is automatically applied. It is based, in this example, on a barite mud containing 272ppm barium and with a density of 1.84g/cm³.

### *Log presentation, scales and units*

The density log is normally plotted on a linear scale of bulk density (Figure 9.5). The log is run across tracks 2 and 3, most often with a scale between 1.95 and 2.95 g/cm³. The main log is accompanied by a curve indicating the borehole and mud-cake corrections that have been automatically applied. A record of cable tension may also be included, as the density tool tends to stick in poor holes.

The tool is run typically as a density-neutron combination along with a gamma ray tool and a caliper, e.g. CDL-GR-N (Western Atlas), FDC-CNL-GR or LDT-CNL-NGT (Schlumberger). The caliper is an essential accompaniment to the density log for reasons of quality control.

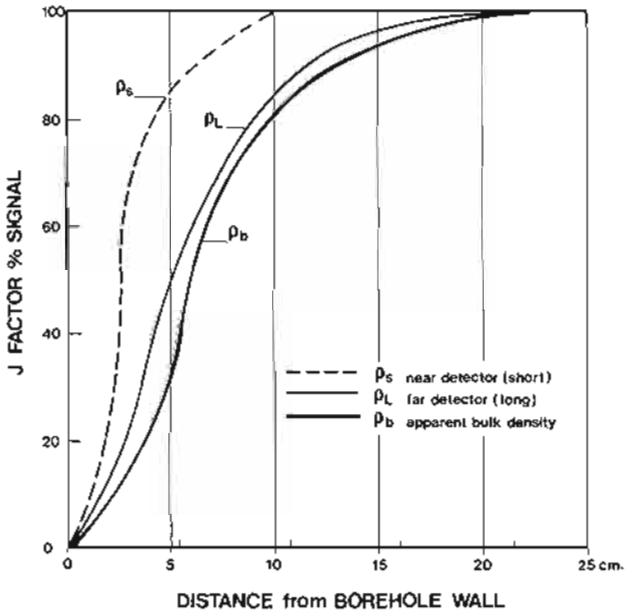


**Figure 9.6** The depth of investigation of the density tool is very shallow. The graphs show experimental results for a 35% porosity, water-filled sand. (Re-drawn from Sherman and Locke, 1975).

## 9.4 Log characteristics

### *Depth of investigation and bed resolution*

Research into the density tool's characteristics shows that its depth of investigation is very shallow. Figure 9.6 shows that 90% of the original Schlumberger FDC response probably originates from 13cm (5in) or less from the tool. These are experimental results using a sand with 35% porosity (Sherman and Locke, 1975). In normal logging, the investigation depth will probably be even less, especially for the more modern tools, around 10cm (4in) for average densities. Consequently the density tool is likely to be much affected by hole conditions. Moreover, in porous zones where the tool has its principal petrophysical use, it will be measuring the invaded zone. There is little chance of it detecting fluids, notably liquid hydrocarbons, in place.

While the depth of investigation of the density tool is small, the bed resolution is good. At average logging speeds (about 400m/h, 1300ft/h), true densities can be read in beds down to about 60cm (2ft). At lower logging speeds, higher sampling rates and selective processing, it may be possible to resolve beds down to 15cm (6") (Flaum *et al.*, 1987). Partial reaction from the density tool may be caused by very thin beds, especially if they have a very high or very low density. Calcareous nodules 5–10cm thick, for example, are seen as peaks on the density log.

Good bed resolution renders the density log useful for drawing bed boundaries.

### *Unwanted logging effects*

The most frequently encountered unwanted logging effects are shown in Table 9.4. The shallow depth of investigation of the density tool makes it very susceptible to hole conditions, despite compensation and automatic corrections. The density log should be interpreted along with its corresponding caliper log.

**Table 9.4** Unwanted environmental effects – density log.

| Factor | Effect on log | Severity* |
|---|---|---|
| Caved or rough hole | Decrease in formation density to approach a drilling mud density value | Frequent |
| Barite in the drilling mud | Automatically corrected in the tool– when mud-cake is thick, gives the cake density | (Rectified) |

*When the effect makes the log reading unusable. Ratings: frequent, common, present, rare.

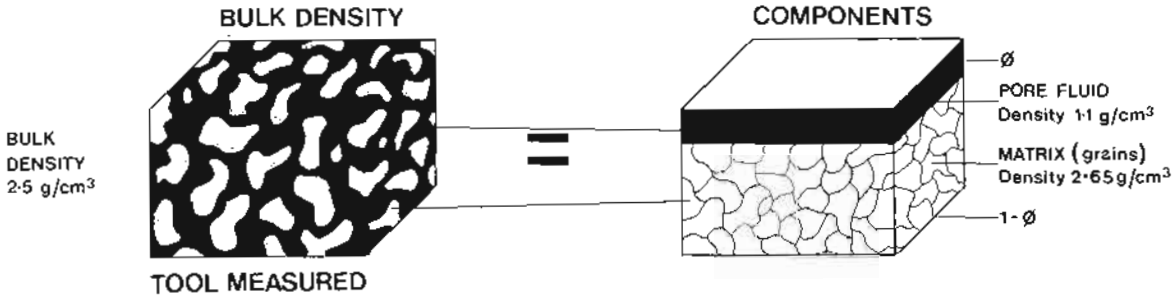


**Figure 9.7** Tool measured bulk density and a visualization of the derivation of the porosity component. The figures are for a sandstone with 10% porosity.

## 9.5 Quantitative uses

***Porosity calculation***

The density log is used to calculate porosity and it may also, with difficulty, be used to calculate hydrocarbon density. To calculate porosity from log-derived bulk density it is necessary to know the density of all the individual materials involved. The density tool sees global (bulk) density, the density both of the grains forming the rock and of the fluids enclosed in the interstitial pores (Figure 9.7). As an example, if the tool measures a bulk density of 2.5g/cm³ in a salt-water-bearing formation (fluid density 1.1g/cm³ [as seen by the tool]) we can interpret any of the following:

| *Lithology* | *Grain density* | *Porosity* |
|---|---|---|
| Sandstone | 2.65g/cm³ | 10% |
| Limestone | 2.71g/cm³ | 13% |
| Dolomite | 2.87g/cm³ | 21% |

Of course, if we know the grain (matrix) density and the fluid density we can solve the equation that gives porosity from the summation of fluid and matrix components (Figure 9.7). For example,

$$\text{bulk density } (\rho_b) = \text{porosity } (\phi) \times \text{fluid density } (\rho_f) + (1 - \phi) \times \text{matrix density } (\rho_{ma})$$

When solved for porosity this equation becomes:

$$\text{porosity } \phi = \frac{\rho_{ma} - \rho_b}{\rho_{ma} - \rho_f}$$

where $\rho_{ma}$ = matrix (or grain) density, $\rho_f$ = fluid density and $\rho_b$ = bulk density (as measured by the tool and hence includes porosity and grain density).

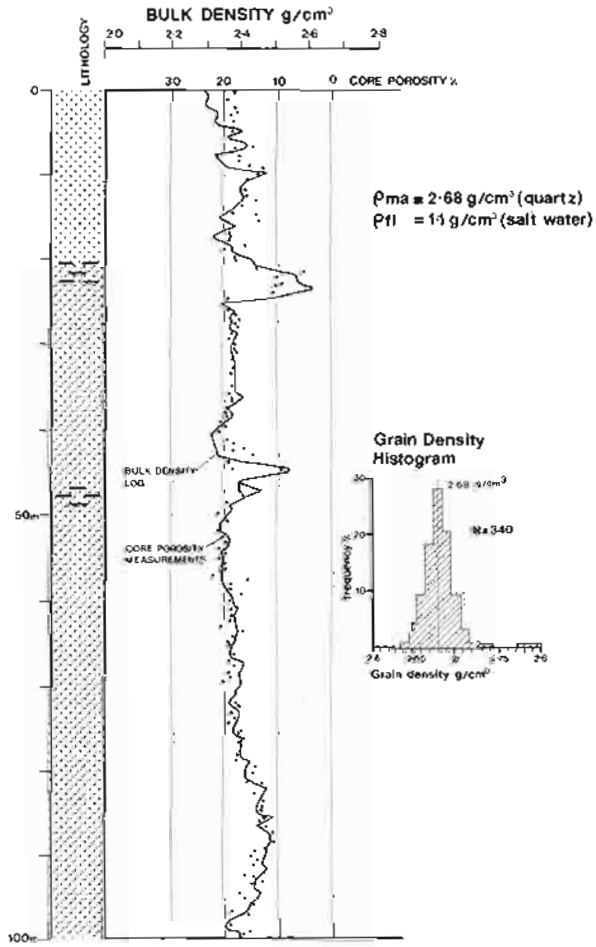


**Figure 9.8** Close correspondence between the bulk density log and core-measured porosity in an orthoquartzite. The bulk density can be converted to porosity using a matrix density of 2.68g/cm³, as indicated by the inset histogram.

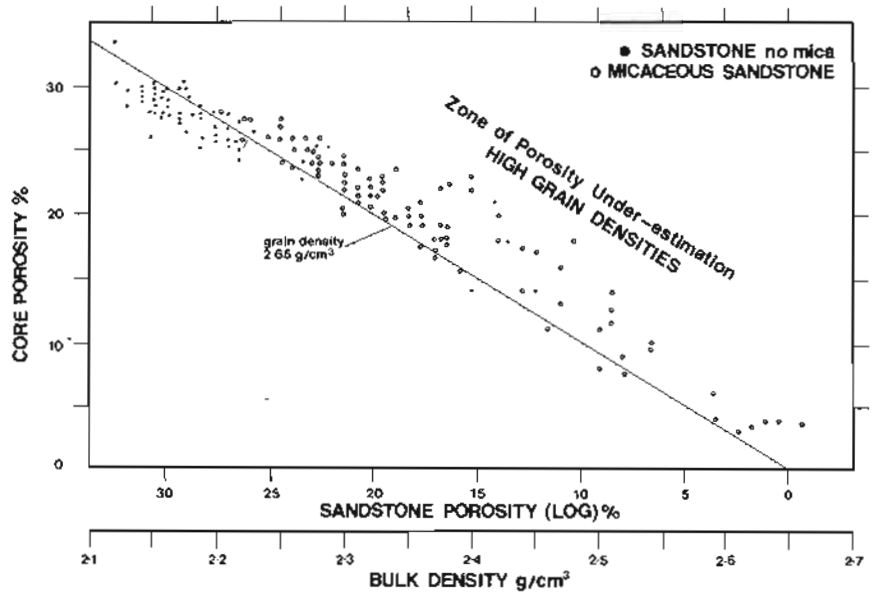


**Figure 9.9** The effect of mica on porosity values derived from the bulk density log. For the graph a matrix density of 2.65g/cm³ was used (giving the diagonal line). For the micaceous sands, core-measured porosities are consistently higher than those given by the log, because the grain density is too low at 2.65g/cm³. Mica has densities up to 3.10g/cm³. (Re-drawn from Hodson, 1975).

The relationship between the bulk density (as measured by the tool) and porosity can be extremely close when the grain density remains constant (Patchett and Coalson, 1979). The example shows a reservoir of orthoquartzite composition and a reasonably constant grain density of 2.68g/cm³ (Figure 9.8). The porosity derived from the bulk density log in this example corresponds well to the core porosity when a matrix density of 2.68g/cm³ and tool-registered fluid density of 1.1g/cm³ are applied.

If constant grain-density figures are applied to a formation and the grain density is not constant, the porosity calculated is inaccurate. An error in grain density of 0.01g/cm³ has been calculated to cause an error of 0.5% (Granberry *et al.*, 1968). Such errors can occur in the North Sea Jurassic sands, where up to 30% mica can increase the average grain density to 2.84g/cm³ (mica density is about 2.76–3.1g/cm³). When too low a grain density is used, the porosity is underestimated by the density log (Figure 9.9).

Erroneous porosities may also be calculated when the fluid density changes. This is the case when a rock is saturated with gaseous hydrocarbons. As shown above, the porosity equation is furnished with a grain density and a fluid density. The latter is 1.0g/cm³ for fresh water and 1.1g/cm³ for salt water (but may vary with temperature). In the presence of gas (typical density 0.0007g/cm³) the fluid density drops dramatically. As the example shows, the density log gives too high a porosity (Figure 9.10). If the porosity (and water saturation) can be calculated by other means, the density log can be used to calculate the hydrocarbon density.

When oil is present, the porosity given by the density log is essentially correct. This is because the density tool

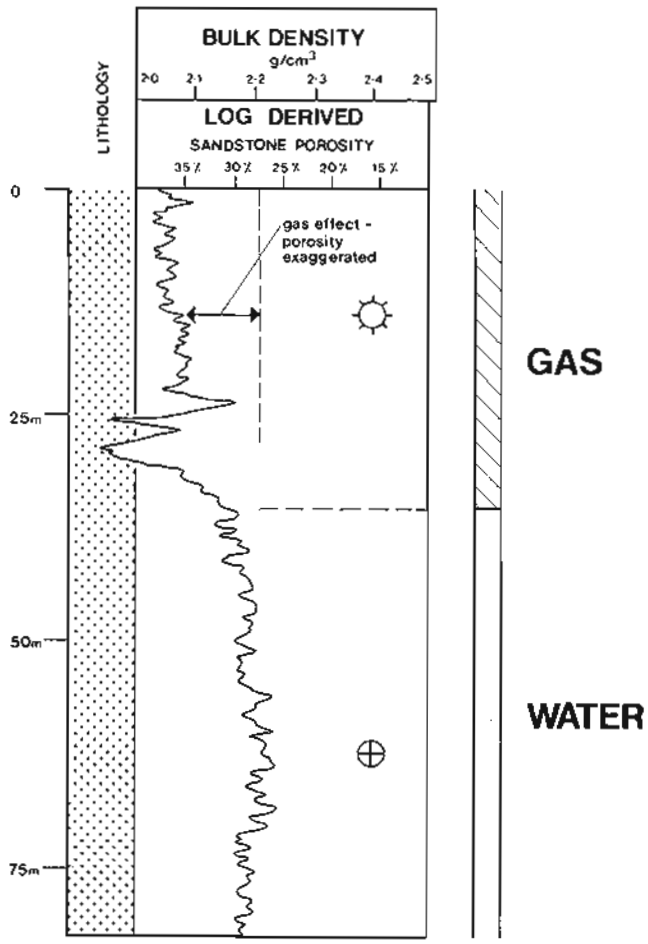


**Figure 9.10** The effect of gas on the density log. In this example the gas zone reads about 35% porosity: it should read 27% porosity.

investigates the flushed zone (*see* 'Depth of investigation', Section 9.4) where only a small volume of oil remains. Moreover, the density of oil is quite close to that of water (0.7g/cm$^3$ vs. 1.0g/cm$^3$). Gas, however, is more mobile and frequently occurs in the flushed zone where, because of the large density difference with water, it has the effect of diminishing the bulk density as described above.

***Acoustic impedance***

The density log is used in conjunction with the sonic log to calculate acoustic impedance. The subject is briefly described in Chapter 8 (*see* 'Seismic applications of the sonic log').

## 9.6 Qualitative uses

The density tool gives a continuous log of the formation's bulk density and it needs no interpretation as the character is given directly. The qualitative use of this log therefore depends on the geological significance of the density of a formation.

***Lithology identification***

The densities of the more common lithologies are rarely diagnostic since there is too much overlap and too much spread caused by differences in composition and texture. Shales, for example, may have densities ranging from 1.8g/cm$^3$ to 2.7g/cm$^3$: the density difference between a plastic clay and a compacted shale (Table 9.5). Overall, oilfield densities generally measure between 2.0g/cm$^3$ and 3.0g/cm$^3$, the common lithologies spanning the whole of this range (Figure 9.11).

**Table 9.5** Densities of common lithologies (*see also* Figure 9.11).

| Lithology | Range (g/cm$^3$) | Matrix (g/cm$^3$) |
|---|---|---|
| Clays–shales | 1.8–2.75 | Varies (av. 2.65–2.7) |
| Sandstones | 1.9–2.65 | 2.65 |
| Limestones | 2.2–2.71 | 2.71 |
| Dolomites | 2.3–2.87 | 2.87 |

Although the density log is itself a poor indicator of lithology, combined with the neutron log it becomes excellent. In fact the neutron-density log combination is probably the best qualitative indicator of general lithology especially in the presence of a valid PEF curve. The subject is described in Chapter 10 (*see* 'Neutron-density combination').

***The density log in shales: compaction, age and composition***

The compaction of shales with burial is a well-known phenomenon and it can be followed on the density log. Shale compaction involves a series of textural and compositional changes, resulting in a progressive increase in density (e.g. Burst, 1969). For example shallow, uncompacted clays have densities around 2.0g/cm$^3$, while at depth, this figure commonly rises to 2.6g/cm$^3$.

Changes due to compaction are gradual and, when seen in one well, occur over a considerable thickness of sediment (Figure 9.12). To see clay compaction changes, unless the shale series is very homogeneous, the density log should be re-plotted at a small vertical scale (say 1:5000). This method allows clay compaction to be examined even in shale-sand or shale-lime sequences.

***Shale age and unconformities***

Although it is by no means diagnostic, shale density is often indicative of age. In general, older shales are more dense. Palaeozoic clays are rare, as are Tertiary shales. The increase in shale density during compaction, although essentially due to a decrease in porosity, is accompanied by irreversible diagenetic changes (Shaw, 1980). Compaction trends therefore become 'fossilized'. This means that in the subsurface, a change in compaction trends will indicate a change in age, in other words an unconformity (Figure 9.13). Beyond this, if general compaction curves for a region can be established, the maximum depth of burial of a formation can be estimated. The methodology is similar to that described using the sonic log (*see* 'Compaction', Chapter 8). However, for compaction studies the density log must be used carefully.

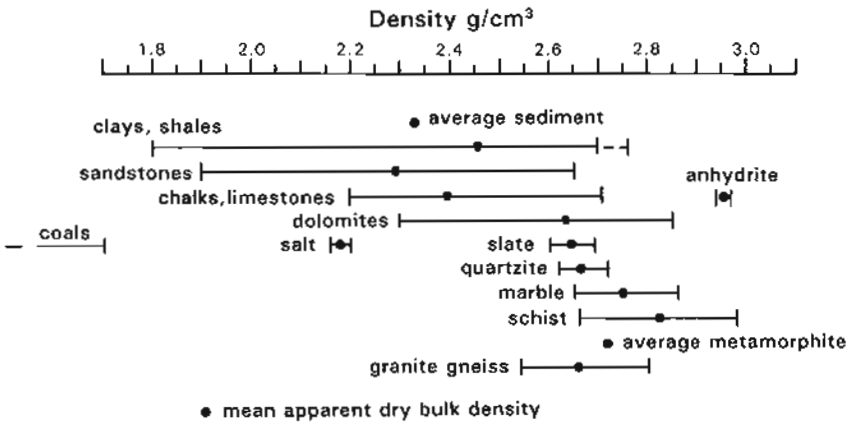


**Figure 9.11** Density ranges of some common lithologies. Note the similar ranges of clay/shale, sandstone and limestone (modified from Jackson and Talbot, 1986).

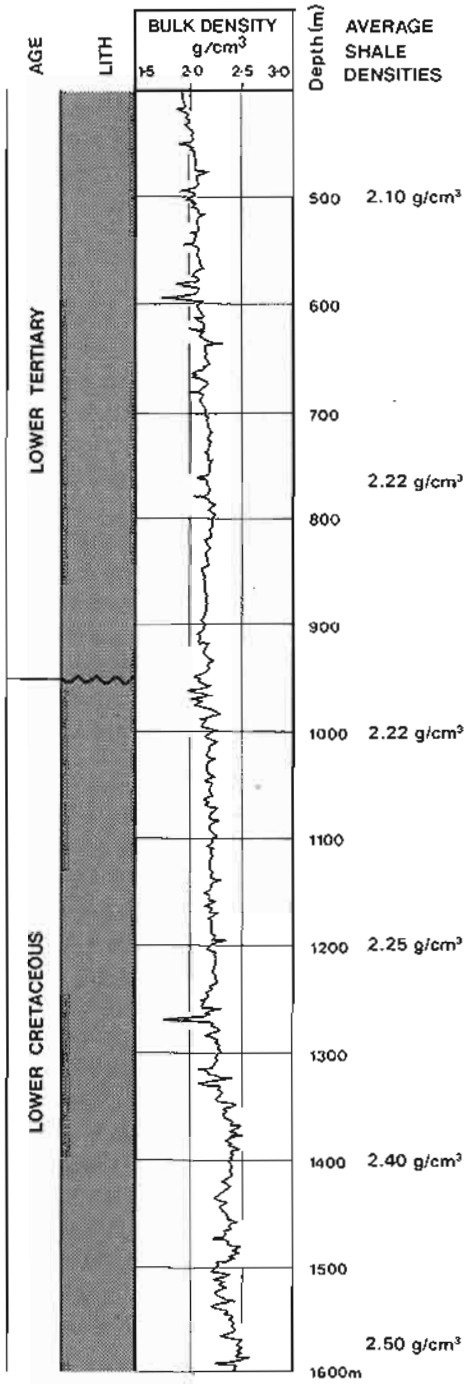


**Figure 9.12** Shale compaction with depth seen on a bulk density log plotted at a compressed (small) vertical scale.

It is very responsive to local lithological variations and a usable average is often hard to obtain.

### *Shale composition*

Shale density changes due to compaction are gradual, while small-order, local variations are more likely due to changes in shale composition. For example, an increase in carbonate content is generally accompanied by an increase in shale density (Figure 9.14). The increase in density is even more marked when iron carbonate

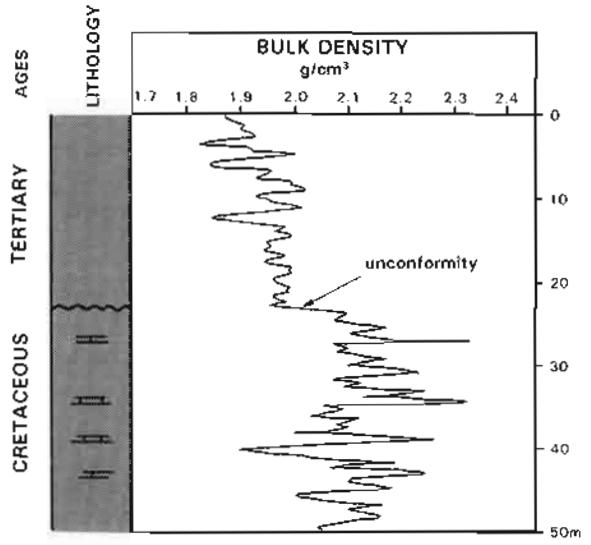


**Figure 9.13** Tertiary shales unconformably overlying dipping, eroded, Cretaceous shales. The abrupt change in density marks the unconformity.

(siderite) is involved (density when pure, 3.89g/cm³). When organic matter is present, the reverse occurs and the density diminishes, organic matter having a very low density (of around 1.2g/cm³; Figure 9.22). This relationship may be quantified (*see* 'Source rock evaluation' *below*).

### *The density log in sandstones – composition and diagenesis*

Bulk density variations in sandstone generally indicate porosity changes. However, as explained above, this is not true when there are changes in grain density. Pure quartz sands are considered to have a grain density of 2.65g/cm³, but in reality such sands are rare. Overall grain density will change depending on the non-quartz constituents. Sands are commonly mixed with feldspars (density 2.52–2.63g/cm³), micas (2.65–3.1g/cm³) lignite fragments (0.5–1.8g/cm³) and rock fragments (variable density). Heavy minerals may also be a constituent (2.7–5.0g/cm³). The well-known mica sands of the North Sea Jurassic reservoirs (as already discussed) contain up to 30% muscovite (Figure 9.9). The density of muscovite (2.76–3.10g/cm³) increases the average grain density from 2.65g/cm³ to *c.* 2.82g/cm³ and it varies with the mica content (Figure 9.15). In sands without shale, therefore, grain density can give some idea of sand composition.

Changes in grain density in sands are generally gradual and of a moderate order. Abrupt changes, especially in otherwise homogeneous beds, often indicate diagenetic or secondary changes. The example shows a sand with zones of secondary carbonate cement (Figure 9.16). In cores these zones are shown to have very abrupt limits. A similar phenomenon may also occur with secondary pyrite cement.

### *Mineral identification*

Density becomes a criterion for lithological identification when it is either abnormally high or abnormally low (the average for sedimentary rocks in oil wells being about

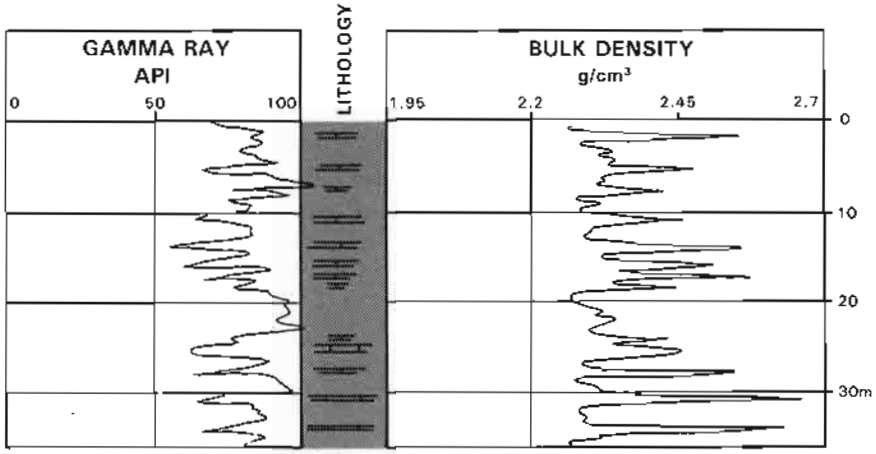


**Figure 9.14** Thin, carbonate/siderite cemented horizons in shale. The intervals may be thin continuous bands or irregular, nodular horizons.

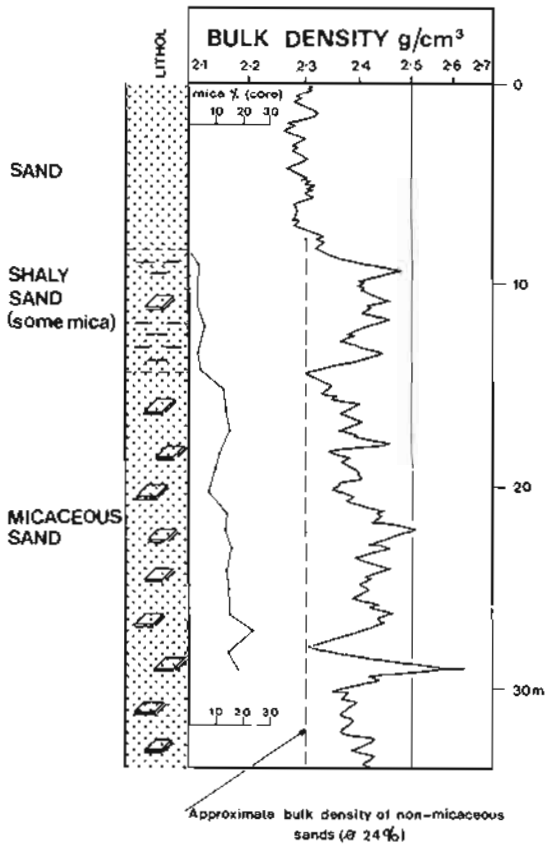


**Figure 9.15** The effect of muscovite (grain density 2.76 – 3.1 g/cm³) on the bulk density log in micaceous sands. The increase in density below 15m is due to the mica content. The percentage of mica indicated is based on thin-section analysis of core material.

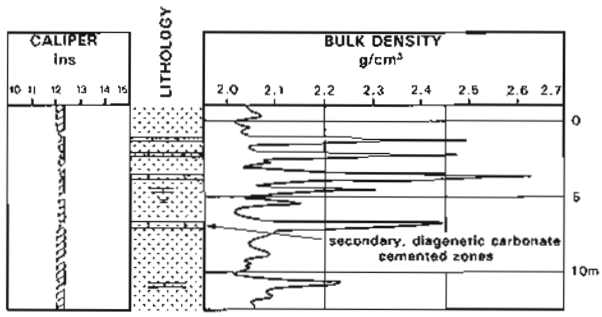


**Figure 9.16** Secondary calcareous cementation in sandstone. The density log shows thin, cemented intervals which have little or no porosity while the reservoir generally has 30% – 35% porosity.

**Table 9.6** Diagnostic mineral and lithological densities (from Serra, 1972, 1979; Gearhart, 1983; Dresser Atlas, 1983).

| | | (g/cm³) |
|---|---|---|
| Low | Lignite | 0.50–1.50 |
| | Coal | 1.15–1.70 |
| | Anthracite | 1.15–1.70 |
| | Organic shale | 1.80–2.40 |
| High | Pyrite | 4.80–5.17 |
| | Siderite | 3.0–3.89 |
| | Basalt | 2.70–3.20 |
| | Gneiss | 2.60–3.04 |

2.3g/cm³). Coals, for example, are identified by very low densities, between 1.2g/cm³ and 1.8g/cm³, and pyrite, conversely, by very high densities, between 4.8g/cm³ and 5.17g/cm³. The extreme values for these minerals may not be reached under natural conditions, but abnormally high and abnormally low peaks are still easily visible (Figure 9.17). The more common extreme and diagnostic densities are shown above (Table 9.6).

***Evaporite identification***

Chemical deposits, because of their purity, may at least be suspected if not positively identified by their densities (Table 9.7). Care must be taken, as evaporites may be impure and densities will be altered. However, most evaporites tend to give intervals of constant density with very little variation. When this occurs, along with densities near the pure mineral values, evaporites are probable (Figure 9.18).

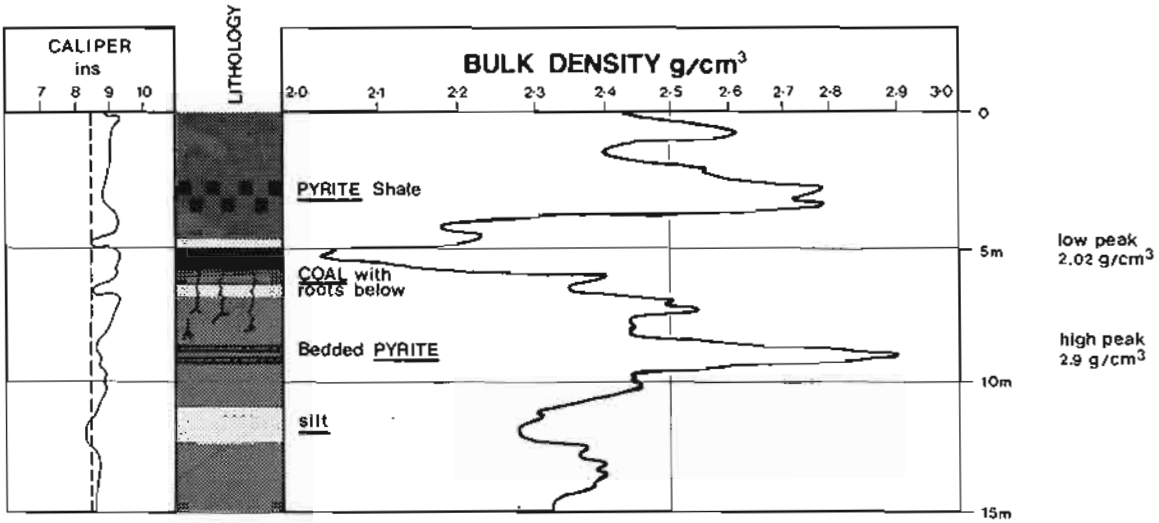


**Figure 9.17** The identification of coal, with low density and pyrite, with high density, on the bulk density log. Lithology from core analysis.

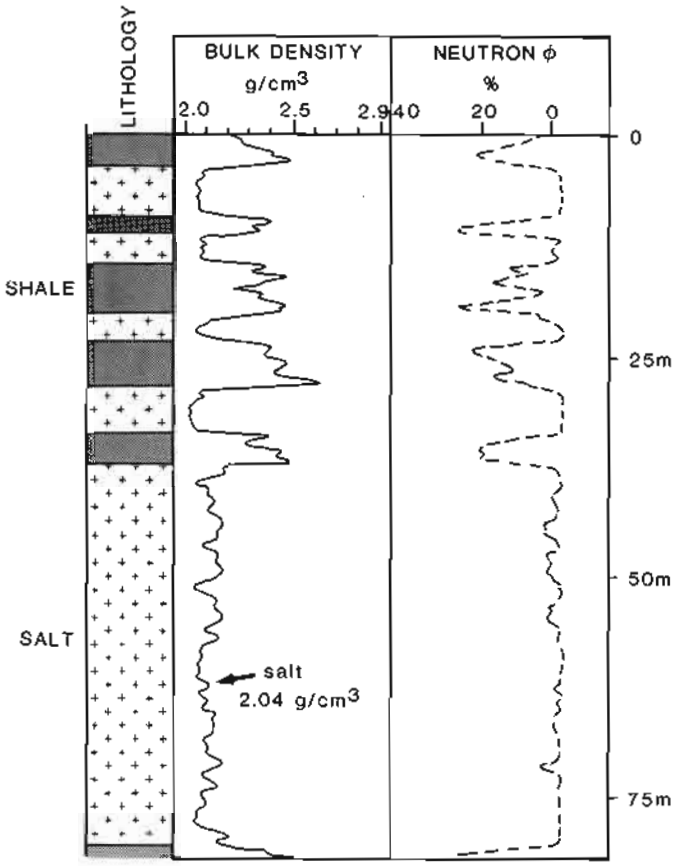


**Figure 9.18** Bulk density log over a salt-shale series. The density log over the evaporite intervals tends to give constant values. The neutron log assists in the identification of the evaporite intervals. ( $\phi N$ salt = -3).

### *Overpressure identification*

The general increase in shale density with depth of burial was described under the heading of compaction. The principal cause for this gradual increase is a diminution in shale porosity with increasing overburden. Mudstone porosities may be as high as 50% near the surface,

**Table 9.7** Evaporite densities. Typical values as seen on the density log (Schlumberger, 1989a).

| Evaporites | Density g/cm³ |
|---|---|
| Salt | 2.04 |
| Gypsum | 2.35 |
| Anhydrite | 2.98 |
| Carnalite | 1.57 |
| Sylvite | 1.86 |
| Ploythalite | 2.79 |

diminishing rapidly to below 20% from about 600m downwards (Figure 9.19) (Magara, 1978). The actual figures and gradients vary from one region to another (Table 9.8), although the normal trend of a progressive porosity loss is universal.

However, porosity may increase with depth and when it occurs there is overpressure. The general decrease in shale porosity is accompanied by an expulsion of both pore-water and interstitial water (Burst, 1969). The fluids are gradually squeezed out during burial. If the fluids cannot escape, once trapped they inevitably become overpressured: they begin to support some of the overburden pressure (*see* Chapter 2). This has the effect of preserving porosity. It is this preservation which causes a break in the compaction trend which is registered by the density log. The density break therefore identifies zones of abnormal pressure (e.g. Fertl, 1980) (Figure 9.20).

### *Fracture recognition*

Numerous methods have been proposed for the identification of fractures (Schafer, 1980). One of these involves the comparison of density-log porosity with sonic-log porosity. The density tool records bulk density, and as such will include both intergranular porosity and fracture porosity. For the sonic measurement, however, the sound waves will take the quickest path from emitter to receiver. This

path should avoid the fractures. The sonic velocity will therefore give only intergranular porosity. When the density-derived porosity is much more than the sonic porosity, the difference is due to the fracture porosity (Schafer, 1980). The example shows this effect in a compact, upper Carboniferous sandstone and shale sequence (Figure 9.21).

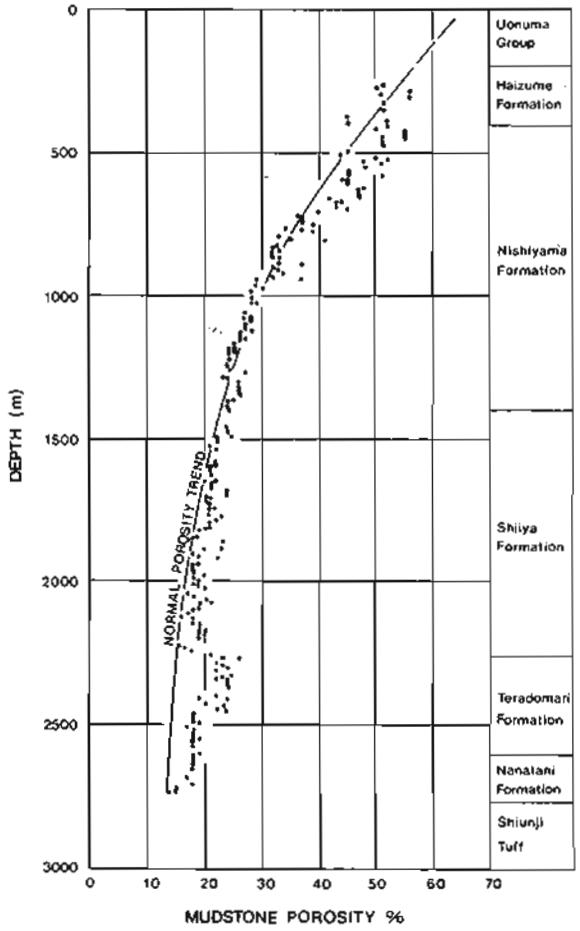


**Figure 9.19** Diminution of mudstone porosity with depth. Neogene, Japan. (Re-drawn from Magara, 1968).

In practical terms, the two logs should be normalized to permit a proper comparison. This may be done with the logs themselves or by cross-plotting core-verified values to define 'fracture fields' (Et yre, 1981).

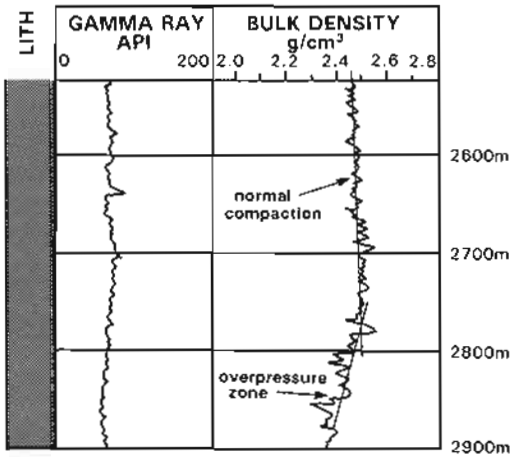


**Figure 9.20** Overpressure seen by a bulk density drop and break in the normal compaction curve. The gamma ray shows the interval is shale.

**Table 9.8** Some shale porosity values (1, 3, 4, from ref. 2).

| | Approximate shale porosity | | | |
|---|---|---|---|---|
| **Area** | **500m** | **1000m** | **2000m** | **5000m** |
| 1. Gulf Coast | 45% | 28% | 22% | 13% |
| 2. Nagaoka Plain Japan | 45% | 29% | 17% | – |
| 3. Venezuela | 30% | 24% | 12% | – |
| 4. Oklahoma | 23% | 13% | 4% | (0) |

1. Dickinson (1953) 2. Magara (1968)
3. Hedberg (1963) 4. Athy (1930)

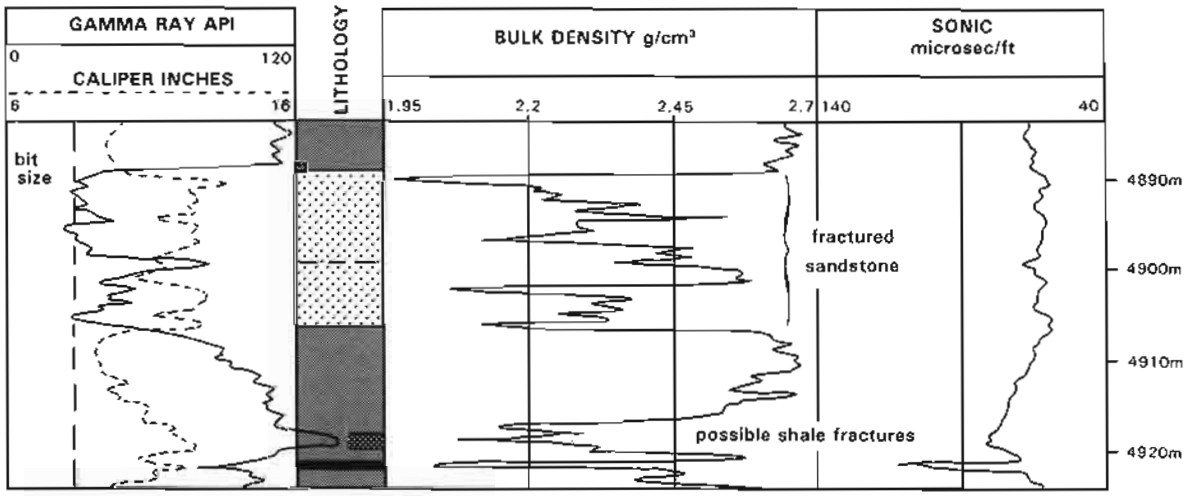


**Figure 9.21** The contrasting effect of fractures on the density log and sonic log. The density log shows very low values over the fractured sandstone interval while the sonic is not affected. The shale interval may also show a similar effect. The caliper is from the density tool.

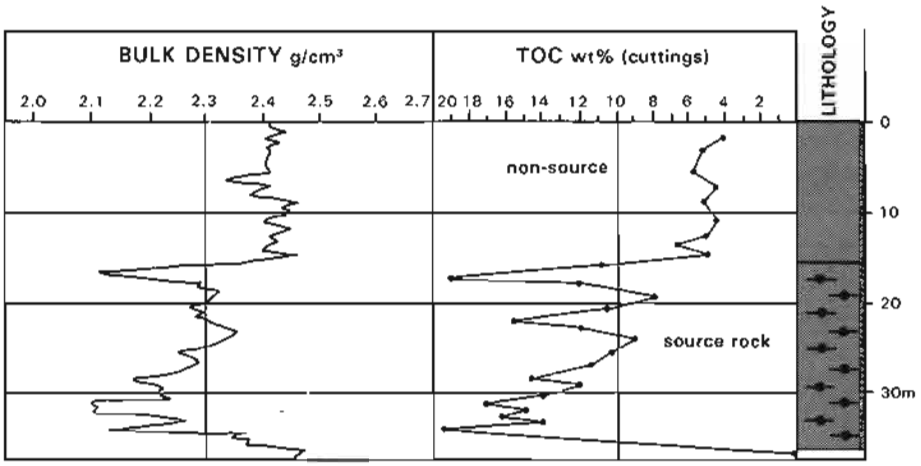


**Figure 9.22** The effect of organic matter on the density log. The relationship may be quantified, the greater the amount of organic matter, the lower the density (*see text*).

### *Source rock evaluation*

The presence of organic matter in shales lowers their density. The normal average matrix density of a mixture of clay minerals is about 2.7g/cm³ (Table 9.9), while organic matter has densities between 0.50g/cm³ – 1.80g/cm³ (Table 9.6). The presence of organic matter therefore has a marked effect on the overall shale bulk density (Figure 9.22).

This organic matter effect on the density log can be quantified, as was very early recognized (Tixier and Alger, 1967), so that the log can be used to evaluate source rocks. Traditionally, to do this the relationship between organic matter content and the density log is normalised using sample analyses (Schmoker and Hester, 1983) (Figure 9.23). The normalized density log can then be used to interpolate between analysed points. More importantly, in the same basin, a normalized log can also be used in wells where no analyses are available. Difficulties arise when the organic matter is mixed with a high density mineral such as pyrite (density 4.8–5.17g/cm³, Table 9.6) since the high density of the pyrite masks the effect of the low density organic matter. Compaction must also be taken into account. This has led some workers to abandon the density log for source rock studies (Passey *et al.*, 1990).

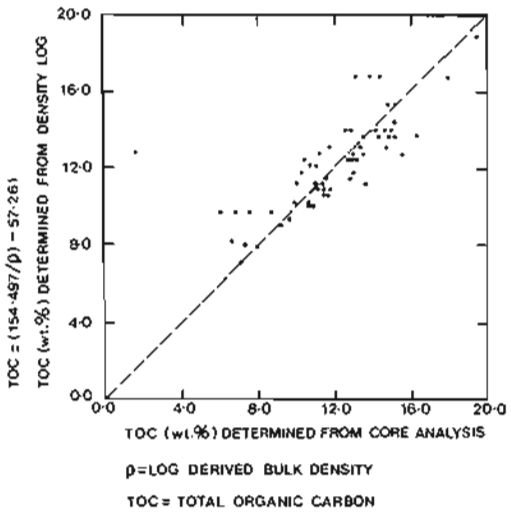


**Figure 9.23** Comparison of the organic content derived from the density logs and from core analysis, Bakken Formation, Williston Basin. Dashed line shows ideal agreement. (Re-drawn from Schmoker and Hester, 1983).

**Table 9.9** Clay and clay-mineral densities (from Fertl, 1977; Johnson and Linke, 1978; Patchett and Coalson, 1982).

| Species | | Density (g/cm³) |
|---|---|---|
| Smectite | | 2.00–3.00 |
| Kaolinite | | 2.40–2.69 |
| Chlorite | | 2.60–3.22 |
| Illites | Muscovite | 2.76–3.10 |
| | Biotite | 2.65–3.10 |
| Average shale matrix | | 2.65–2.70 |

However, the density log has long been used in coal logging as an indicator of the ash content of the coal beds, to the end that log based calculations obviate the need for coring (Lavers and Smits, 1977). Properly used, the density log is an excellent indicator of the amount of shale in coal and vice versa. For example, a robust and simple method for using the density log to estimate organic carbon content has recently been proposed. It avoids the initial need for lengthy normalization and allows TOC (Total Organic Carbon) values to be quickly derived (Myers and Jenkyns, 1992).

The method is based on the proposition that non-source shale intervals are identical to source intervals apart from the organic matter content. To derive the quantitative organic matter effect on the logs over a source interval, it is sufficient simply to subtract the log values of a contiguous non-source interval. For instance, in Figure 9.22, the average density of the shales from 0m to 13m can be used to evaluate the source rock richness from 13m to 35m. The effect can then be converted to TOC%. In this way, depth and in general, compositional

effects will be automatically accounted for, the principal unknown being the density of the organic matter (kerogen). The method is presented below.

The following assumptions are made (for details *see* Myers and Jenkyns, 1992):

1) The source rock is composed of mudrock (matrix density = 2.70g/cm³), water filled porosity (density = 1.05g/cm³) and kerogen (density = 1.1 or 1.2g/cm³).
2) The non-source interval has the same mudrock matrix density, water density and water filled porosity as the source interval (Figure 9.24).

$$\phi_{fl} = \frac{\rho_{ns} - \rho_{ma}}{\rho_{fl} - \rho_{ma}} \quad (1)$$

$$\phi_{ker} = \frac{\rho_{s} - \rho_{ns}}{\rho_{ker} - \rho_{ma}} \quad (2)$$

$$TOC\% = \frac{0.85 \times \rho_{ker} \times \phi_{ker}}{\rho_{ker}(\phi_{ker}) + \rho_{ma}(1 - \phi_{fl} - \phi_{ker})} \quad (3)$$

Where:
$\rho_{ns}$ = density non-source interval (average from log)
$\rho_{s}$ = density source interval (from log)
$\rho_{ma}$ = 2.70g/cm³, assumed mudrock density
$\phi_{fl}$ = water filled porosity, derived with equation (1)
$\phi_{ker}$ = kerogen filled porosity, derived with equation (2)
$\rho_{ker}$ = 1.1 or 1.2g/cm³, kerogen density
$\rho_{fl}$ = 1.05g/cm³, density water
TOC% = 0.85 × wt.% kerogen

The water filled porosity of the contiguous non-source interval is given by equation (1). The volume (porosity) filled with kerogen of a given density is given by equation (2). The conversion of kerogen volume to weight and then TOC% using a weight % kerogen equivalence to weight % carbon of 0.85, is given by equation (3).

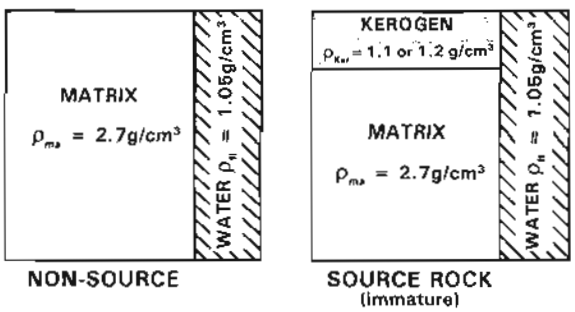


**Figure 9.24** Schematic basis for using the density log quantitatively to derive total organic carbon, TOC. The matrix and water content characteristics are assumed identical in both the source and non-source. Kerogen is an additional part of the total volume in a source rock.

# THE PHOTOELECTRIC FACTOR LOG (or Litho-Density)

## 9.7 Generalities

***The log***

The Photoelectric Factor (or PEF) log (the Litho-Density log of Schlumberger) is a continuous record of the effective *photoelectric absorption cross section index* or Pe of a formation. The photoelectric absorption index is strongly dependent on the average atomic number, Z, (i.e. atomic complexity) of the constituents of the formation, which implies the composition and by inference, the lithology: the effects of porosity are kept to a minimum (Figure 9.25). For instance, the photoelectric absorption index of a sandstone (quartz matrix) at 0% porosity is Pe 1.81 while at 35% fresh water filled porosity it is Pe 1.54. For limestone (calcium carbonate matrix) the figures are, at 0% porosity (i.e. matrix) Pe 5.08 and at 35% porosity Pe 4.23 (Figure 9.26) (Gardner and Dumanoir, 1980). That is, the difference between the Pe values of the two matrix types (i.e. 3.27 units) is more significant than the variations within each individual matrix type caused by porosity changes (i.e. 0.27 and 0.85 respectively) (Figure 9.26).

***Principal uses***

The photoelectric absorption index is used principally in a quantitative manner as a matrix indicator, either alone or, especially when cross-multiplied with the corresponding density log value, to produce the value $U$ (Table 9.10). Qualitatively, in the correct borehole environment, it can be used to indicate lithology and certain, mainly diagenetic minerals.

The use of the litho-density log is severely restricted by the fact that it is ineffective in holes with barite weighted mud, since the photoelectric absorption index for barite is nearly 150 times that of most of the common minerals and when present will dominate the log response. If the log is to be used effectively, the drilling mud must not contain barite.

The litho-density log is sometimes, misleadingly, called the lithology log. It is not: it is a log of the effective photoelectric absorption index. Its response is no closer to the lithology than that of any other log.

**Table 9.10** Principal uses of the photoelectric factor (PEF) log.

| | Dicipline | Used for | Knowing |
|---|---|---|---|
| Quantitative | Petrophysics | Matrix identification | $\rho_{maa}$, Ø |
| | | $U_{maa}$ | $U_{ma}$, $U_{fl}$ |
| Qualitative | Geology | Matrix type | mineral values |
| | | Diagenetic minerals | elemental values |

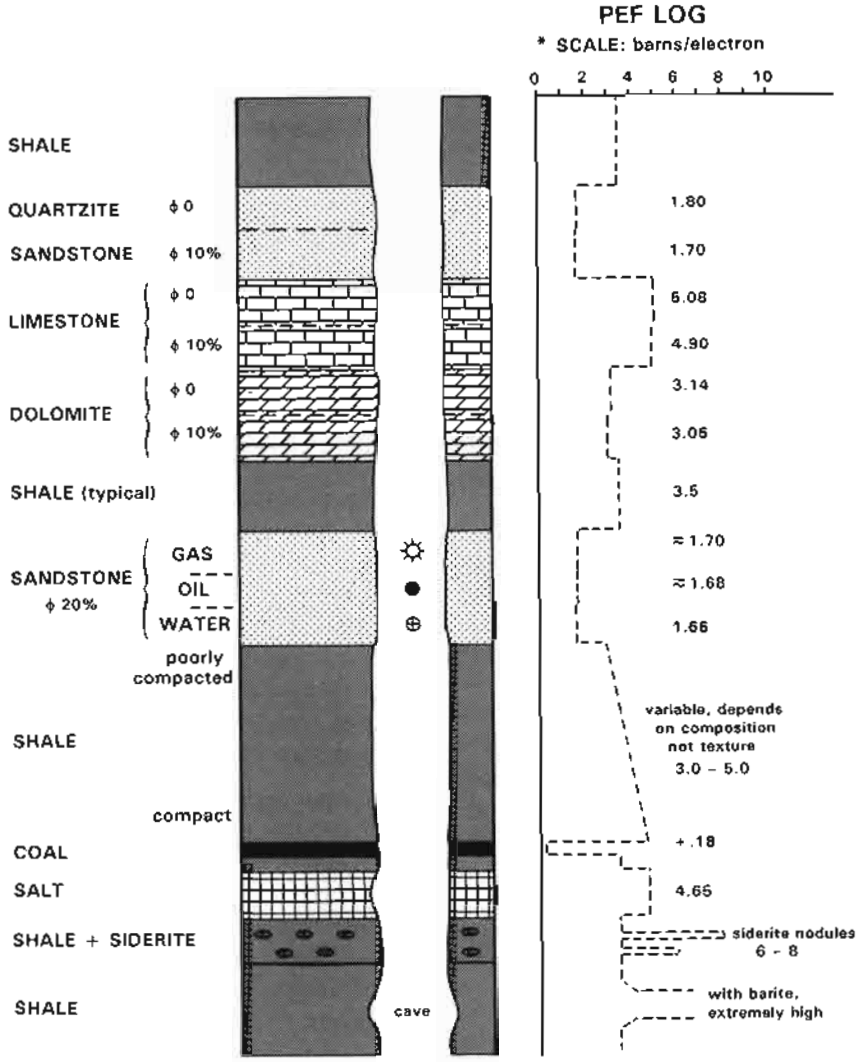


**Figure 9.25** The PEF or Photoelectric Factor log. The log is a measure of the combined atomic complexity of the formation so that porosity effects are minimal. The lithologies are comparable to those used in Figures 9.1 and 10.1.
* a Barn is $10^{-24}cm^2$.

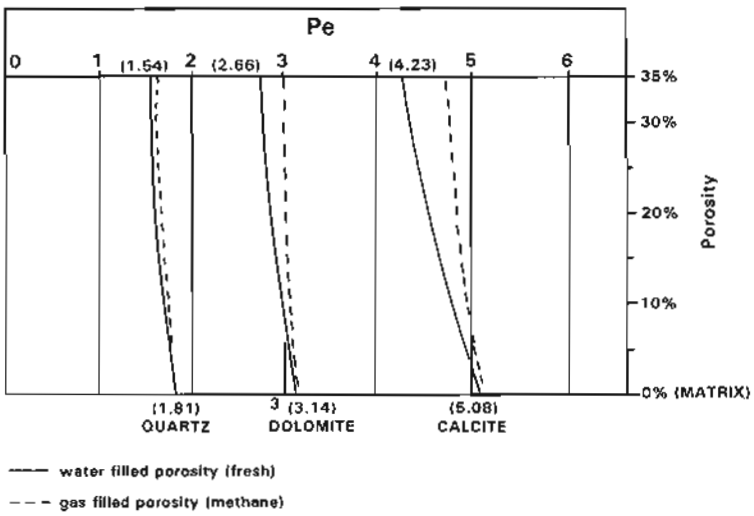


**Figure 9.26** PEF values of quartz, dolomite and calcite over the porosity range from 0 to 35%. Porosity generally has only a subsidiary effect on the PEF value: matrix type is more important. (Modified from Gardner and Dumanoir, 1980).

## 9.8 Principles of Measurement

When gamma rays pass through matter, at most energies they degrade through collision or Compton scattering (para 9.2). In addition, at low energies, below about 100 keV, the phenomenon known as photoelectric absorption takes effect. Photoelectric absorption occurs when gamma rays have lost sufficient energy to be captured and absorbed by electrons electrically bound to atoms. The capturing electron acquires energy, leaves its atomic orbit and becomes ionised (Figure 9.3). The degree of absorption depends on both the atomic number ($Z$) and the electron density ($\rho_e$) of the atoms, effectively their atomic complexity. In geological terms, this is related to chemical composition and indirectly to lithology.

A *Pe* measurement is made by most of the modern generation of density tools, the LDT or litho-density of Schlumberger, the Z-Density of Western Atlas and the Photo Density of BPB. These tools are similar to the two detector density tools described previously (Section 9.2) in that they have a high energy gamma ray source, generally of 662keV, and a near and far detector. However, the modern tools have more efficient scintillation detectors with more complex energy gates which detect both high (hard) and low (soft) gamma radiations. Thus, the detectors register counts in both the high energy area, dominated by Compton scattering, and the low energy area where the photoelectric effect is important (Figure 9.3). Both an improved energy value and a photoelectric factor are measured (Section 9.3). The photoelectric factor *Pe*, plotted on the log, is based on corrected counting rates in the low energy area, principally from the far detector.

In reality, the count rate in the low energy area is a combined result of the electron density effect of Compton scattering and the photoelectric absorption effect of the formation. That is, in the low energy area a quantity called $U$ (photoelectric absorption cross section per unit volume) is registered which is the product of the electron density, $\rho_e$ and the photoelectric factor, *Pe* (Gardner & Dumanoir 1980). Pe, the photoelectric factor, is therefore the ratio of the two:–

$$Pe = \frac{U}{\rho_e}$$

Where:
$U$ = photoelectric absorption cross section, per unit volume (low energy window count of tool),
$\rho_e$ = electron density index, per unit volume (high energy window count), and
*Pe* = photoelectric absorption factor, per unit weight.

This means in effect that *Pe*, the photoelectric factor plotted as the log, is derived by stripping the electron density effect of the high energy window from the overall effect in the low energy window (Figure 9.3).

It is worth noting that $\rho_e$ is in electrons/cm$^3$, *Pe* is in barns/electron and $U$ is in barns/cm$^3$, the effective photoelectric absorption cross section index per unit volume.

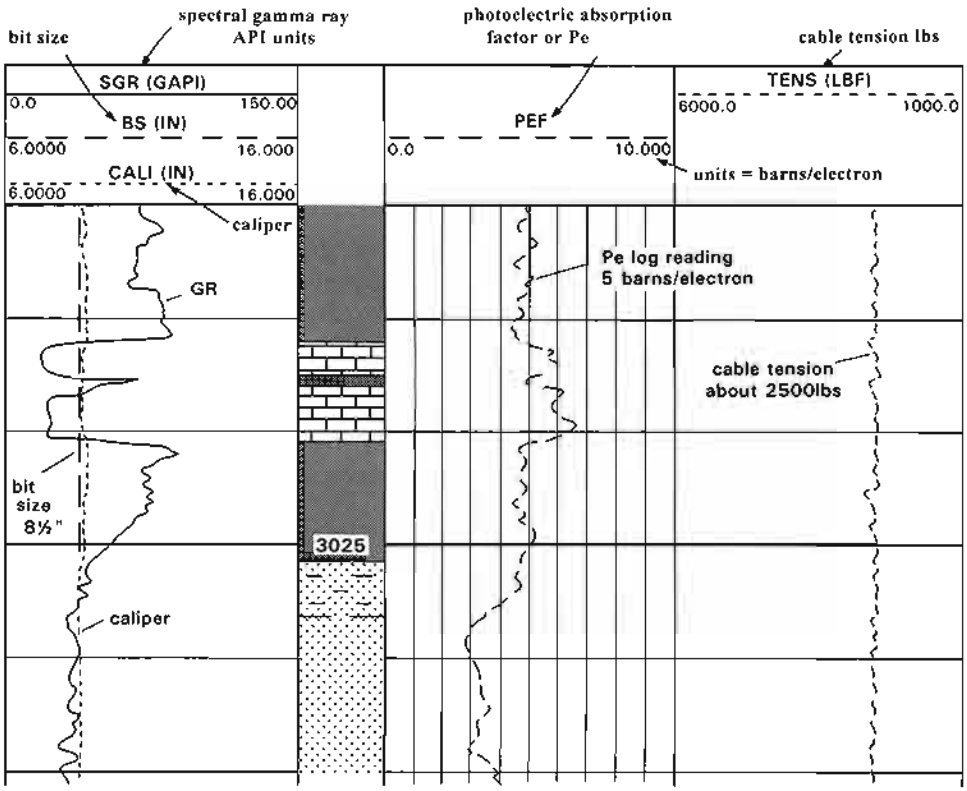


**Figure 9.27** A typical PEF log through shale, limestone and sandstone. Note the similar gamma ray value of sandstone and limestone but very different PEF values.

Table 9.11 Common photoelectric factor and related log values (from Suau and Spurlin, 1982; Ellis, 1987; Schlumberger, 1989a).

| Name | Formula | *Pe | $+U_{ma}$ | $\#\rho_{ma}$ |
|---|---|---|---|---|
| Quartz | $SiO_2$ | 1.81 | 4.79 | 2.65 |
| Calcite | $CaCO_3$ | 5.08 | 13.77 | 2.71 |
| Dolomite | $CaMg(CO_3)_2$ | 3.14 | 9.00 | 2.86 |
| Barite | $BaSO_4$ | 266.8 | 1074.0 | |
| Shale (av) | | 3.42 | 9.05 | 2.65 |
| Shaly sand | | 2.70 | 6.52 | 2.41 |
| Feldspar (K) | | 2.86 | 7.51 | 2.62 |
| Muscovite | | 2.40 | 7.90 | 3.29 |
| Biotite | | 6.30 | 21.03 | 3.34 |
| Glauconite (wet) | | 5.32 | 21.00 | 3.95 |
| Siderite $FeCO_3$ | | 14.69 | 56.00 | 3.81 |
| Pyrite $FeS_2$ | | 16.97 | 82.00 | 5.00 |
| Limonite | | 13.00 | 46.67 | 3.59 |
| Halite | NaCl | 4.65 | 9.65 | 2.07 |
| Gypsum | $CaSO_4.H_2O$ | 3.42 | 8.11 | 2.37 |
| Anhydrite | $CaSO_4$ | 5.06 | 14.95 | 2.96 |
| Coal bituminous | | 0.18 | 0.26 | 1.47 |
| Coal anthracite | | 0.16 | 0.28 | 1.75 |
| Water | | 0.36 | 0.40 | 1.11 |
| Salt water (120.000ppm) | | 0.81 | 0.96 | 1.19 |
| Oil $CH_2$ (variable) | | 0.13 | 0.12 | 0.97 |
| Gas $CH_4$ | | 0.095 | 0.119.ρgas | 1.25.ρgas |

*log Pef, $+U_{ma} = Pe.\rho_e$, # tool density ($\rho_e$) cf Table 9.2

***Log presentation, scales and units***

The photoelectric factor log is generally called the PEF log (i.e. PhotoElectric Factor). The scale used is barns per electron being a measure of the capture cross-section or capture efficiency. A barn is $10^{-24}cm^2$.

The PEF curve is normally plotted combined with the density and neutron logs in tracks 3 and 4, the scale being from 0–20 or 0–15 barns, most of the common minerals having values below 6 (Figure 9.27, Table 9.11). This means that the PEF curve is plotted close to the 0 or left hand side of the scale. However, it frequently interferes with the neutron and density and makes all three difficult to read. If colour is used it is easier but as a rule the PEF curve should be plotted on its own.

## 9.9 Log Characteristics

***Depth of Investigation***

The PEF curve has a slightly better resolution than the bulk density curve, the latter having a vertical resolution of 50–60cm from the modern litho-density tools (Schlumberger, 1989a). With modern processing, however, this vertical resolution can be reduced to 15 cm (Flaum *et al.*, 1989). From previous discussion of the derivation of the PEF value (Section 9.8), it is clear that the PEF is as dependent on the far spacing detector (i.e. 50–60cm vertical resolution) as it is on the near spacing detector (vertical resolution 7cm)(Smith, 1990). This means that the depth of investigation is especially dependent on the far detector configuration and signal processing while adverse borehole effects will be more a result of the near detector configuration (cf. Figure 9.6).

***Unwanted log effects***

The photoelectric factor log has been in service for a number of years but is still not used routinely. The principal reason is that the log is unusable when barite muds are in the borehole. The *Pe* value for barite is 267 barns/electron while most common minerals have a *Pe* value of less than 6 (Table 9.11). The presence of barite swamps the true response (Figure 9.28).

## 9.10 Quantitative uses

***Matrix identification – lithology***

When only two matrix minerals (and porosity) are present, the photoelectric factor log values may be used to derive the volumetric fractions of each, the *Pe* value being plotted against the bulk density value (Gardner and Dumanoir, 1980)(Figure 9.29).

The most effective use, however, is when three minerals are present (and porosity), the *Pe* value being used in combination with the density log value. The two are

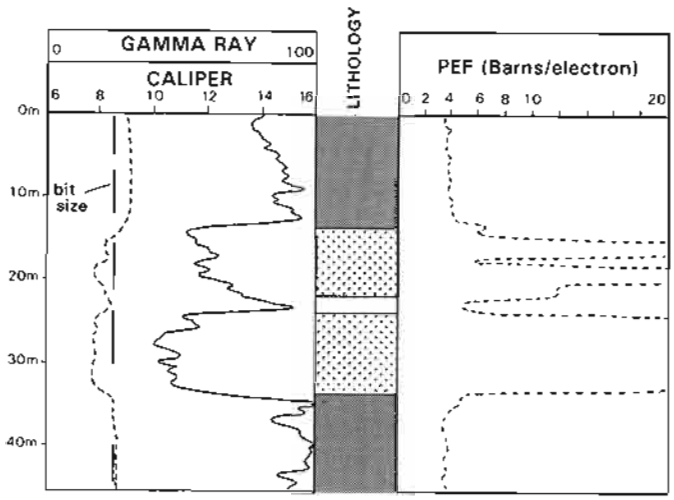


**Figure 9.28** The effect of barite on the PEF log. The barite in the mud cake causes very high PEF values and does not allow the log to be used for lithology identification.

cross-multiplied to produce the factor $U$, the volumetric photoelectric absorption index (Gardner and Dumanoir, 1980) also discussed above (Section 9.7). The reasoning is that the *Pe* value is not volume but mass related and hence both the density and $U$ are volume related. The *Pe* value and density value combined will therefore reflect both the lithology *per se* and the porosity effects which are lithology controlled. The methodology is generally found to be useful in areas of complex carbonate-evaporite lithology where porosity is lithology dependent especially in the presence of gas which does not affect the *Pe* value (McCall and Gardner, 1982). In sand-shale sequences the effect is less evident.

In practical terms, over the zone of interest, the $\rho_{maa}$ (matrix density apparent) and porosity ($\phi$) are found from a density-neutron cross plot (Figure 10.26), while the $U_{maa}$ (matrix volumetric absorption index .apparent) is found from a nomogram (Schlumberger, 1989a) relating *Pe*, $\rho_b$ and porosity ($\phi$) to $U_{ma}$ or the following equation:

$$U_{maa} = (1 - \phi_a)U_{ma} + \phi_a.U_{fl}$$

$U_{fl} = 0.5$ (salt water)

Plots of $U_{maa}$ against $\rho_{maa}$ are considered to be indicative of lithology (Gardner and Dumanoir, 1980). However, like most log calculations, it is seriously disturbed by shale.

## 9.11 Qualitative uses

### *Lithology*

In the same way as the log is used quantitatively to identify matrix type, it can help identify lithology qualitatively, in that *Pe* values are matrix specific and unaffected by porosity variations (Figure 9.26). Usefully, the log can be used to separate clean sand from clean limestone (Figure 9.27). However, shale presence makes the identification of shaly formations (calcareous or siliceous) difficult.

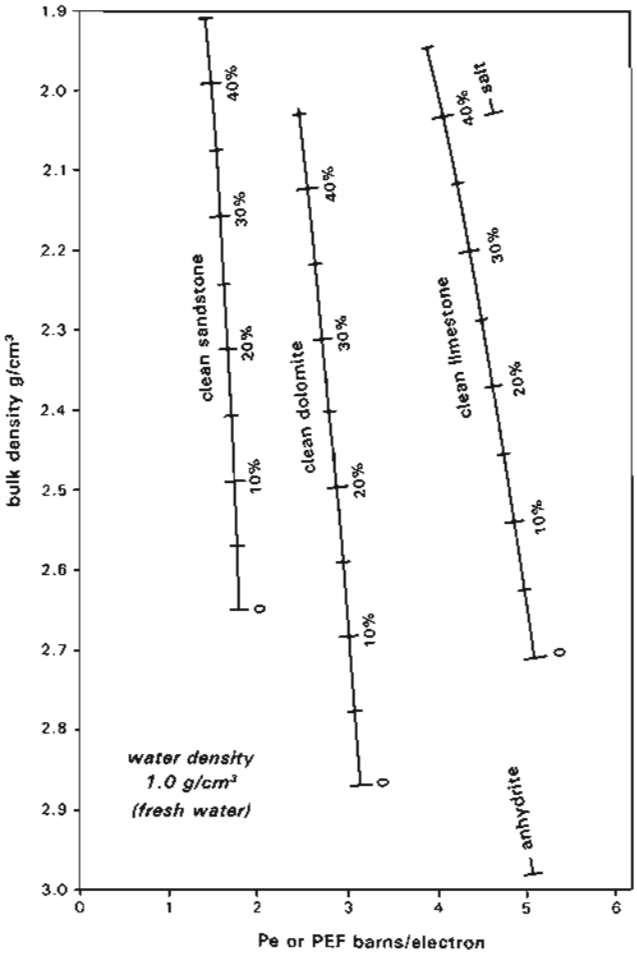


**Figure 9.29** Matrix identification using the PEF and bulk density log values. Porosity values are indicated along the matrix lines. (From Schlumberger, 1989a).

### *Diagenetic and other minerals*

One of the more interesting uses of the PEF log is in the identification of certain, mainly diagenetic minerals which contain an element, such as iron, with a high $Z$ number (Fe, $Z = 26$). Mineralization may occur in thin zones, difficult to sample and too thin for good definition by other logs. For example, siderite ($Fe_2CO_3$) mineralization frequently occurs in thin, nodular beds in many sandstones and shales. The PEF value for siderite is high (14.69, Table 9.11) but significantly the Uma value, the volume related effective photoelectric absorption cross section, is very high (56.0, Table 9.11), so even small quantities have a marked effect on the log (Humphreys and Lott, 1990) (Figure 9.30). Other iron minerals such as pyrite and haematite will have a similar marked effect (Suau and Spurlin, 1982). In reasonable abundance, between 5–10% by volume, biotite and glauconite may also be detected (Humphreys and Lott, 1990).

It has been suggested that cross-plotting *Pe* against potassium or the Th/K ratio of the spectral gamma ray log, can help to indicate clay minerals and micas. The plots have very little experimental backing and are best used with caution (to say the least).

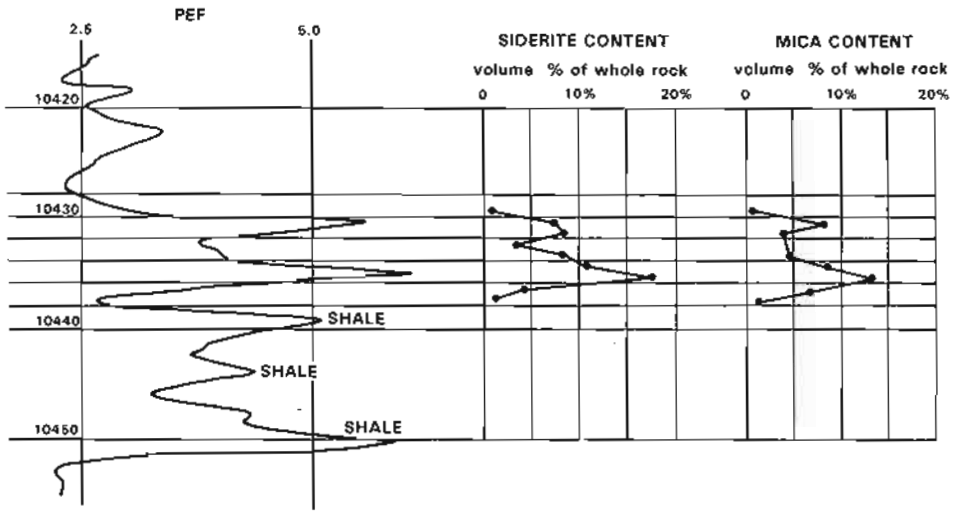


**Figure 9.30** The effect of siderite on the PEF log. High peaks on the log are caused by even small quantities of siderite, which has a large, effective photoelectric absorption per unit volume, Uma (Table 9.11). (From Humphreys and Lott, 1990).

# 10
# THE NEUTRON LOG

## 10.1 Generalities

***The log***

The neutron log provides a continuous record of a formation's reaction to fast neutron bombardment. It is quoted in terms of *neutron porosity units*, which are related to a formation's *hydrogen index*, an indication of its richness in hydrogen.

Formations modify neutrons rapidly when they contain abundant hydrogen nuclei, which in the geological context are supplied by water ($H_2O$). The log is therefore principally a measure of a formation's water content, be it bound water, water of crystallization or free pore-water. This hydrogen richness is called the hydrogen index (*HI*) which is defined as the weight % hydrogen in the formation/wt % hydrogen in water, where *HI* water = 1 (Table 10.8). However, the oilfield interest in water is as a pore fluid filler and porosity indicator so that the neutron log response is given directly in *neutron porosity units*. Neutron porosity is real porosity in clean limestones, but other lithologies require conversion factors. Since it is calibrated to limestones, the log is sometimes called the Limestone Curve (Figure 10.1).

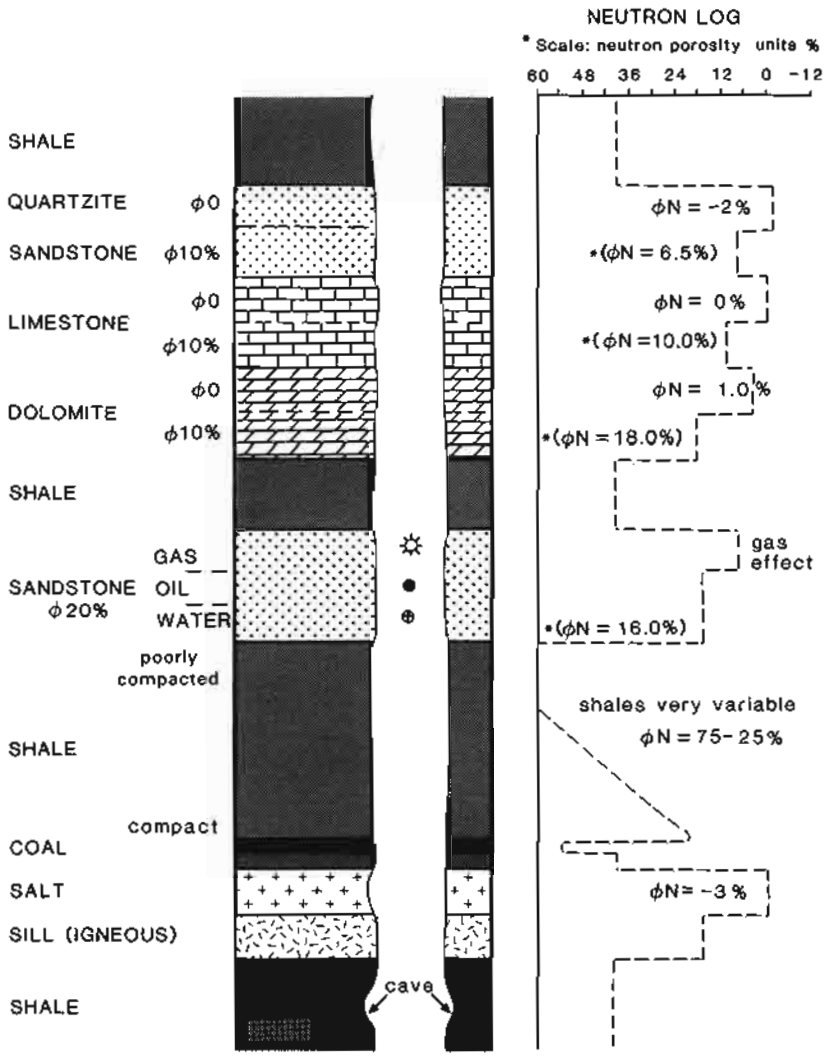


**Figure 10.1** The neutron log: some typical responses. The neutron log shows *hydrogen index* which is converted to *neutron porosity units*.
* Porosity with fresh water and the Schlumberger CNL tool (cf. Figure 9.1 which is on a compatible scale of porosity).

**Table 10.1** The principal uses of the neutron log.

| | Discipline | Used for | Knowing |
|---|---|---|---|
| Quantitative | Petrophysics | Porosity | Matrix<br>Hydrogen index |
| Qualitative | Petrophysics | Identification of gas | Lithology |
| | Geology | Lithology – shales | Gross lithology |
| | | Evaporites | Neutron evaporite values |
| | | Hydrated minerals | |
| | | Volcanic and intrusive rocks | Calibration |
| | | General lithology | Combined with density* |

*using neutron log combined with density log on compatible scales.

***Principal uses***

Quantitatively, the neutron log is used to measure porosity. Qualitatively, it is an excellent discriminator between gas and oil. It can be used geologically to identify gross lithology, evaporites, hydrated minerals and volcanic rocks. When combined with the density log on compatible scales, it is one of the best subsurface lithology indicators available (Table 10.1).

## 10.2 Principles of measurement

Neutrons are subatomic particles which have no electrical charge but whose mass is essentially equivalent to that of a hydrogen nucleus. They interact with matter in two principal ways, by collision and absorption: collisions are mainly at higher energy states, absorption occurs at lower energy.

The lifetime of a free neutron is one of losing energy and can therefore be usefully described in terms of energy state, namely fast, epithermic and thermic in order of decreasing energy (Figure 10.2). The energy loss from fast neutron energy levels through epithermic to the limit of thermic energy, is generally thought of as a loss of velocity which occurs especially through *elastic scattering*, that is collisions with particles having the same mass as neutrons. For logging purposes this is mainly hydrogen nuclei. Collision with other, heavier particles, called *inelastic scattering*, does not result in significant energy loss (Table 10.2). These two moderating reactions are considered to cause the velocity loss over a certain trajectory called the *slowing-down length*. The slowing-down length is proportional to the root mean-square distance from the point of emission of high energy neutrons to the point at which they reach the lower limit of epithermal energy levels. This distance can be calculated from a knowledge of the combined capture cross-sections of the constituent elements of the material traversed. In a hydrogen rich medium, slowing-down

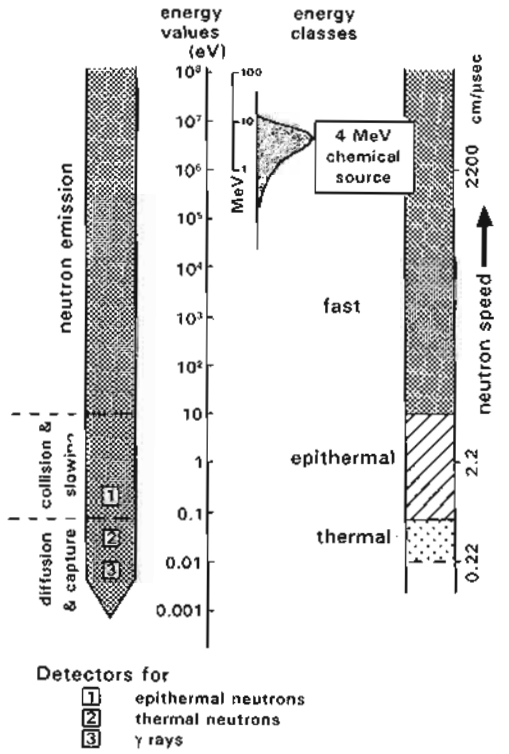


**Figure 10.2** Schematic diagram of a neutron life, showing the energy degradation after emission and the neutron tool detector levels. (From Serra, 1979; Tittle, 1961; Owen, 1960).

length will be short compared to that in a hydrogen free environment (Figure 10.3, Table 10.2). Slowing-down length is an important concept in logging as it is used to place detectors at an optimum distance from the tool's neutron source.

Most logging tools use a chemical source producing *fast neutrons*. These have an initial energy of around 4 MeV (see Tools), which means that they have an initial velocity of approximately 2800 cm/μsec (Figure 10.2). With this energy and velocity, the neutrons have considerable

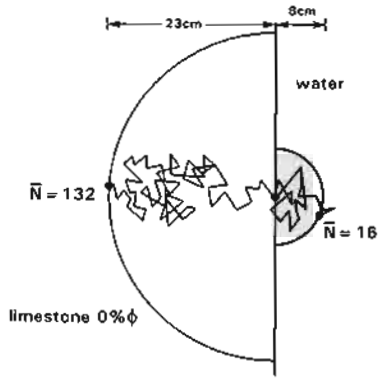


**Figure 10.3** Schematic trajectories of a neutron in a limestone with no porosity and pure water. The slowing down length in the limestone is far greater than in water (modified from Ellis, 1987).

**Table 10.2** Neutron slowing-down parameters (*number of collisions involved during change from 4.2 Mev to 1 eV). (from Ellis 1987).

| Moderator | *no. of collisions |
|---|---|
| H | 14.5 |
| C | 91.3 |
| O | 121 |
| Ca | 305 |
| $H_2O$ | 15.8 |
| Limestone 20% ϕ | 29.7 |
| Limestone 0% ϕ | 132 |

penetration capabilities but after a few microseconds and successive collisions (100 or so), the original fast neutrons have slowed down through epithermic to thermic levels with about 0.25 eV of energy and a velocity of around 0.22 cm/μsec (Figure 10.2). To reduce a neutron from 2 MeV (2200 cm/μsec) to 0.025 eV (0.22 cm/μsec) requires 18 (elastic) collisions with hydrogen nuclei but 257 (non-elastic) collisions with silicon and 368 with calcium nuclei (Serra, 1979). Expressed in another way, elastic collision with hydrogen can take all a neutron's energy but in non-elastic collisions with heavier elements, the energy reduction is typically around 10% to 25%: the effect of hydrogen is seen as dominant (Table 10.2).

At the lower energy, thermic levels, the neutron is thought of as diffusing, rather than having a velocity. For example, in a vacuum, a thermal neutron will diffuse randomly for 13 minutes, but in earth materials the time varies: 5 μsec in rock salt, 450 μsec in a limestone without porosity and 900 μsec in a quartzite (Serra, 1979). The period of diffusion comes to an end as the neutrons undergo *absorption* interactions. That is, they are captured by other nuclei which then change energy state and, mostly, become unstable. For example, some nuclei, on capturing a neutron, spontaneously de-excite and emit gamma rays of capture, the so-called n,γ capture radiation (an effect used in pulsed neutron logging) (Figure 10.2). The rapidity of neutron absorption depends on the *capture cross-section* of the absorbing nuclei of the formation, which is a measure of how effective it is at capturing neutrons. Gadolinium and boron have large thermal neutron cross-sections but are quite rare: chlorine, common in saline formation fluids, has a moderate cross-section (Table 10.3).

**Table 10.3** Thermal neutron capture cross-sections of some elements, (note the values for H and Cl as well as B and Gd).

| Element | Capture cross-section, barns | *cross-section* atomic weight |
|---|---|---|
| H | 0.33 | 0.33 |
| C | 0.0034 | 0.00028 |
| O | 0.00027 | 0.000017 |
| Na | 0.53 | 0.023 |
| Mg | 0.063 | 0.0027 |
| Al | .23 | 0.0085 |
| Si | .16 | 0.0057 |
| Cl | 33.2 | 0.94 |
| K | 2.10 | 0.054 |
| Ca | 0.43 | 0.011 |
| B | 759 | 70.3 |
| Gd | 49,000 | 312 |
| Cd (shield material) | 2,450 | 21.9 |

– cross-section/atomic weight gives a guide to the effect of a thermal absorber relative to the volume of formation it occupies.
– Cadmium is separated on the list as it is rarely encountered naturally but is used in tool construction as a thermal absorber.
from Dunlap and Coates, 1988.

As far as logging is concerned, the dominant effect on neutrons during the collision and scattering phase, is the mass of the (formation) nuclei, hydrogen dominating: the dominant effect during the absorption phase is the capture cross-section of the thermal neutron absorbers, the effect of hydrogen being much less marked (Table 10.3).

## 10.3 Tools

The neutron tool today generally consists of a fast neutron source and two detectors (Figure 10.4). The source bombards the formation with neutrons and the detectors measure their loss of energy as they pass through it.

Tool sources are mostly chemical, such as plutonium-beryllium (PuBe) or americum-beryllium (AmBe), which produce fast neutrons with a peak energy level around 4 Mev. These are the most common. Infrequently, high energy neutrons at up to 14 MeV are produced using accelerometers, in which the neutrons are created by bombarding a target with charged particles.

Historically, the first neutron tools consisted of a source and just a single detector but these were quite affected by borehole environment and most tools now

have two detectors, a near and far (Figure 10.4). Neutron detection is not simple and consists of a two-step process. First, the neutrons react with a material to produce charged, energetic particles; these, in turn, are detected through their ionising ability. Thus a detector will consist of a target material and a proportional counter. The most common tool detectors are based on the 3He *n,p* ( i.e. neutron, proton) reaction in which 3He is used as both a target and proportional gas in a counter.

The efficiency of these counters varies inversely with the square root of the neutron energy. They therefore respond primarily to thermal neutrons (lower energy). If epithermal neutrons are to be sensed the same detectors can be used but covered by a cadmium sheath which effectively absorbs the thermal neutrons (Table 10.2), leaving only the epithermal neutrons to pass. The most commonly used tools now use thermal-epithermal neutron detection but tools also exist for epithermal detection or even gamma rays of capture (Table 10.4).

In the tool, both source and detectors are placed on a skid pressed against the borehole wall (Figure 10.4). The two detectors are placed along the skid, away from the source, at a distance calculated from the slowing down length (*see* Section 10.2) so that they are mainly in the area of thermal neutron energy in typical formations. The tool results are given by a ratio of the near detector/far detector counts, thereby eliminating borehole effects as much as possible. This is because the far detector readings, which contain both hole and formation effects, are 'corrected' by the near detector readings which have mainly hole effects, leaving only the effects of the formation. The ratio results are presented on the log as neutron porosity units after empirical calibration (*see* Units of measurement *below*).

Today, the neutron sonde is usually combined in one tool with the density, gamma ray and caliper as in the FDC-CNL and LDL-CNL of Schlumberger or the CDL

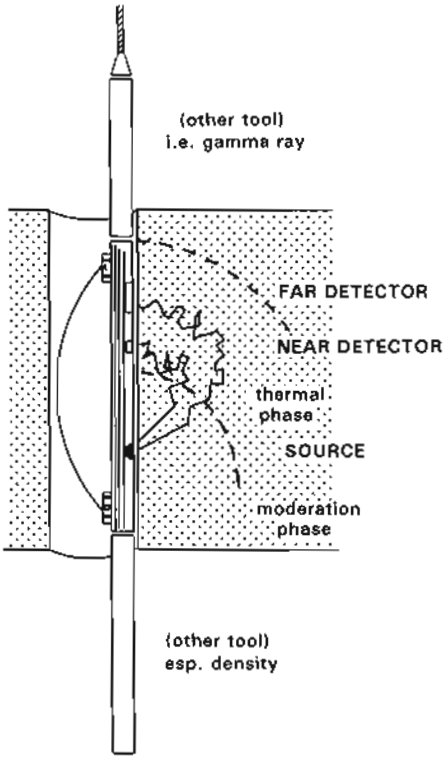


**Figure 10.4** A compensated neutron tool – schematic. The source and detectors are held pressed against the borehole wall.

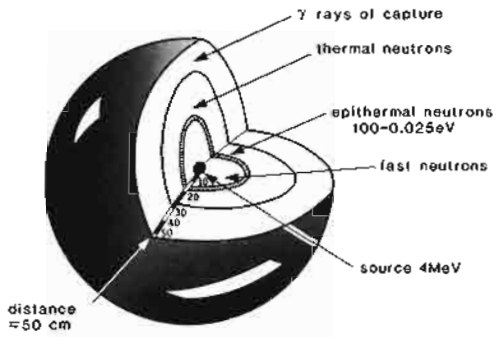


**Figure 10.5** Spatial distribution of neutrons and disintegration products around a fast neutron source as used in logging tools. (Modified from Serra, 1979).

**Table 10.4** Neutron logging tools.

| Name | Symbol | Company | Detectors |
|---|---|---|---|
| *Compensated Neutron Log | CNL | Schlumberger | T |
| Dual Neutron Log | DNL (CNT–G) | Schlumberger | T + E separately |
| Sidewall Neutron Porosity | SNP | Schlumberger | E |
| *Compensated Neutron | CN | Western Atlas | T |
| Sidewall Epithermal Neutron | SWN | Western Atlas | E |
| *Compensated Neutron Tool | HDSEN | Halliburton | T |
| Epithermal Neutron | DSEN, SNL | Halliburton | E |
| *Compensated Neutron Sonde | CNS | BPB | T |
| Epithermal Neutron Sonde | ENS | BPB | E |

(tools with gamma ray detectors such as the GNT (Schlumberger) or NG (Western) are generally no longer used).
Detectors: T = thermal neutron, E = epithermal neutron
*the most commonly used tools, combined especially with the density.

and ZDL of Western Atlas (Table 10.4). In these combination tools, the neutron sonde is positioned above the density sonde, thus logging the formation first, since the gamma bombardment used by the density tool (Chapter 9) could affect the neutron readings.

***Units of measurement***

Most neutron logs are now plotted on a standardized arithmetic scale of neutron (or limestone) porosity units. Previously, each logging company used different units for its own neutron tool, but it was shown (Archie, 1950) that there is a consistent relationship between neutron-tool values and porosity in clean limestones (Figure 10.6). This value represents real porosity only under standard conditions in clean limestones, but to find the real porosity in other lithologies, the neutron-log value can be converted by using tables or empirical calibrations (*see* Quantitative uses *below*).

An API standard unit does exist for neutron tools and is defined, as it is for the other nuclear tools, in the test pit in the grounds of the University of Houston, Texas. This pit contains a 6 ft zone of Indiana limestone with a porosity of 19% and it is fresh-water wet (Figure 10.7). One neutron API unit is 1/1000 of the difference between the instrument zero with no radiation and the log deflection opposite the limestone. Three other zones are included in the pit, one of pure water, one of Austin Chalk (porosity 26%) and one of Carthage Marble (porosity 1.9%) (Belknap *et al.*, 1959). These standards enable neutron tools to be calibrated and the neutron log readings standardized. However, recent evaluations of the test pit (Butler and Clayton, 1984) suggest that it is open to errors and that a series of synthetic formations would offer a more reliable calibration standard than complex natural ones.

***Log format***

The neutron log is generally plotted across tracks 2 and 3 (Figure 10.8). The units, as discussed above, are *neutron porosity units* from empirical calibration. That is, neutron porosity units represent *real porosity* in clean limestones but *only* in clean limestones. The most common scale is from 45% (to the left) to –15% neutron porosity units. A ratio may be used instead of a % making these figures .45 to –.15 neutron porosity units.

Since the neutron is generally run combined with the density in one tool, a combined neutron-density log heading has become standard. This generally shows the scales for both the neutron and the density standardised for clean limestone matrix (*see* Section 10.7 Neutron-

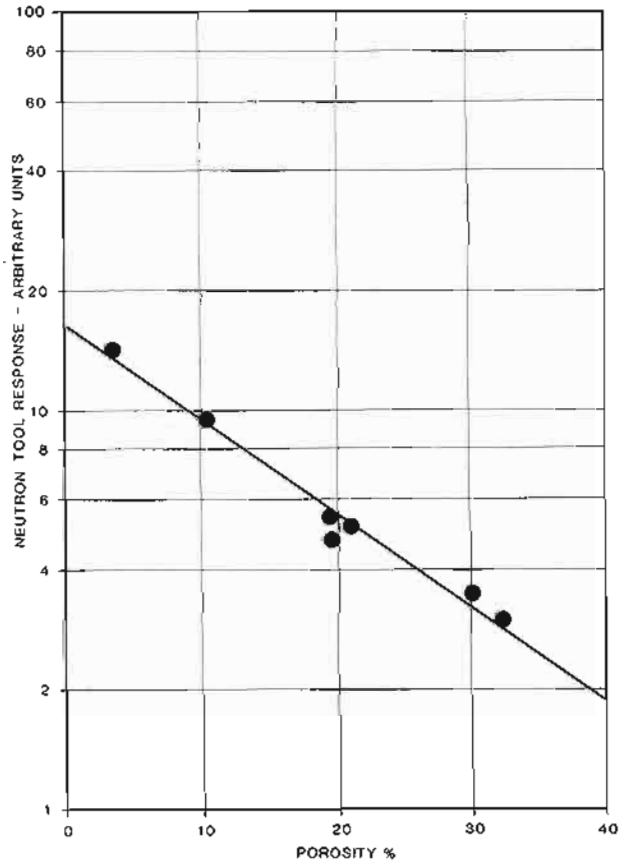


**Figure 10.6** Graph showing the consistent relationship between neutron tool response and total limestone porosity: Devonian, Crossett Limestone, Texas. (Re-drawn from Archie, 1950).

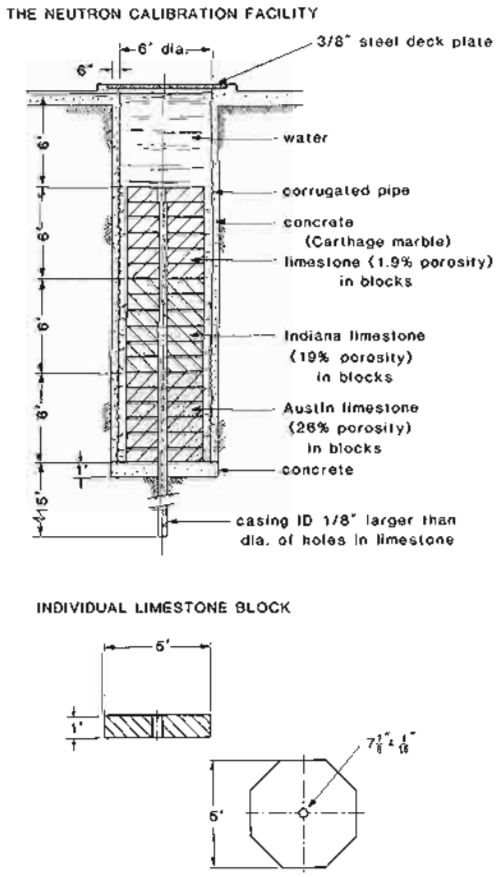


**Figure 10.7** The API nuclear log calibration facility at the University of Houston, Texas, USA. (From Belknap *et al.*, 1959).

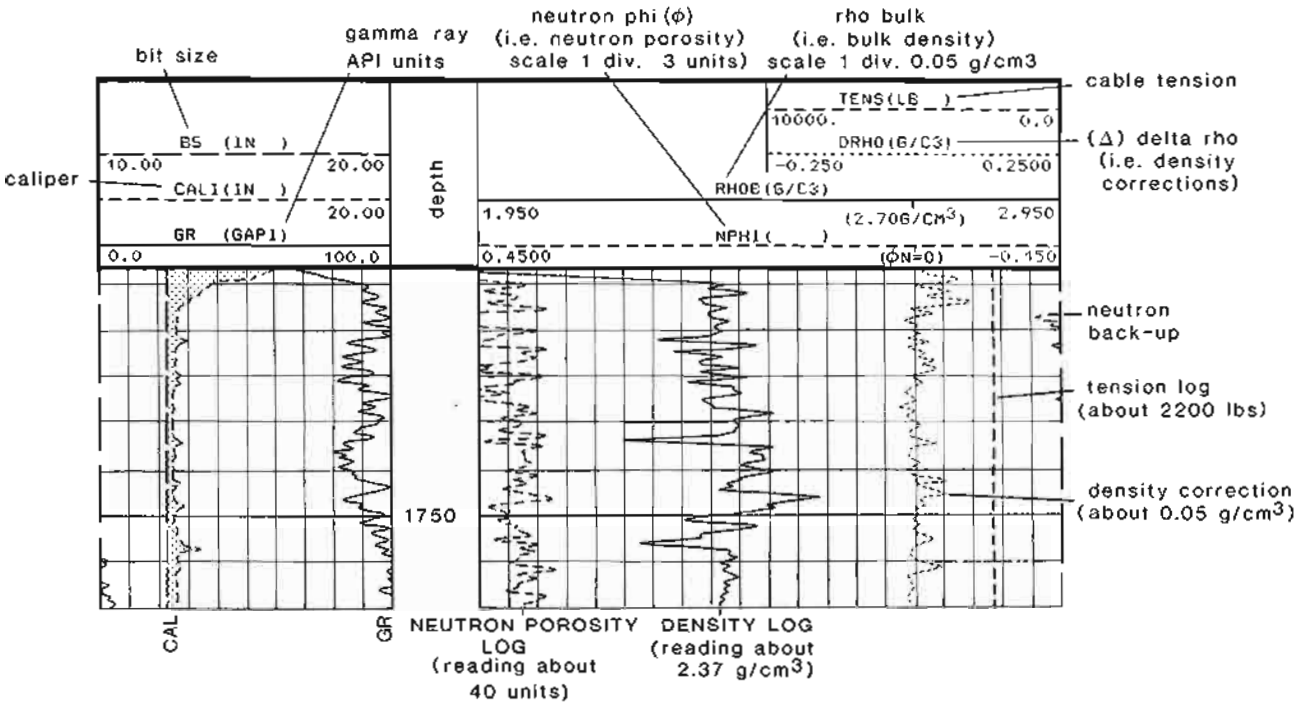


**Figure 10.8** Typical log heading for a neutron-density tool combination. This heading is of the type produced by the Schlumberger CSU unit. The neutron and density log scales are compatible for a clean limestone φN, 0% = 2.70g/cm³.

density combination). On this format the density log is a solid line, the neutron log a dashed line (Figure 10.8).

## 10.4 Log characteristics

***Depth of investigation***

The depth of investigation of the neutron tool is generally small. In most normal logging it is of the order of 15–25 cm (6"–10") (Figure 10.9). It varies with each tool but also varies as a function of the hydrogen index and therefore porosity. Maximum investigation is in low-porosity materials (Table 10.5). As the table shows, the maximum penetration in a tight formation with a low hydrogen index is between 50–60 cm (20"–24").

***Bed resolution***

The relatively shallow depth of investigation of the neutron tool is accompanied by good bed resolution. True formation values may be obtained on the log in beds down to about 60 cm (24 in) with the SNP or 40 cm (15 in) with the more modern CNL and CN. However, with average logging speeds it is best to consider the minimum resolution to be 1 metre (3 ft). The neutron log has a slightly lower resolution than the density log but is still a good bed boundary indicator.

**Table 10.5** Depth of investigation of the neutron tools as a function of porosity (from Serra, 1979, after Schlumberger).

| Porosity % | 90% of signal |
|---|---|
| 0 | 60 cm |
| 10 | 34cm |
| 20 | 23cm |
| 30 | 16.5cm |

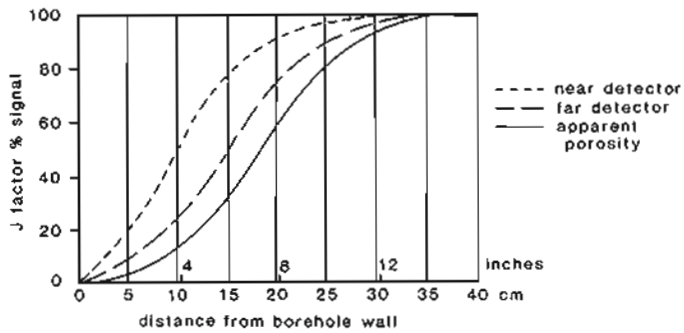


**Figure 10.9** The moderate depth of investigation of the neutron tool illustrated by experimentally-derived J-factor curves. These are for a thermal type, two-detector neutron tool and a 35% porosity water-filled sand. (From Sherman and Locke, 1975).

***Unwanted logging effects***

The common unwanted environmental effects which influence the neutron log are shown in Table 10.6. None is unduly annoying.

## 10.5 Quantitative uses

***Porosity***

The neutron log is used to derive porosity. The tool, as indicated above, measures hydrogen abundance or hydrogen index. In clean, water-bearing formations, the only

**Table 10.6** Unwanted environmental effects – neutron log.

| Factor | Effect on log | *Severity |
|---|---|---|
| Hole rugosity and caving | Increase (normally) in $\phi$ neutron–to read mud | Common |
| Mud salinity | Automatically corrected – most effect on thermal neutron detectors | Rare |
| Temperature and pressure | Automatically corrected in each individual run | Rare |

*When the effect makes the log reading unusable.
Ratings: frequent, common present, rare.

hydrogen present is in the formation water ($H_2O$). The neutron tool therefore responds to the volume of water-filled pore space, and gives a measure of the porosity. Expressed mathematically,

$$\log_{10} \phi = aN + B$$

where $\phi$ is the true porosity, $a$, $B$ are constants, and $N$ is the neutron-tool reading.

However, calibration is necessary for the above calculation as matrix materials have differing effects on the neutron log which change with porosity. A water-filled sandstone with 20% porosity gives a different neutron-log reading to water-filled limestone with 20% porosity (Figure 10.10). Alternatively, if very accurate results are required, for example in a field study, the neutron log porosities can be compared to measured core porosities (Figure 10.11). The empirical calibration allows zones not cored to be accurately and confidently interpreted.

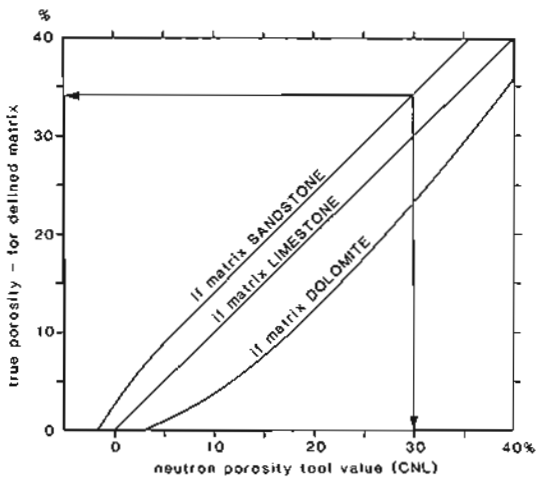


**Figure 10.10** Graph for deriving the true porosity from a Schlumberger CNL tool values for defined sandstone, limestone and dolomite matrices. Note that only the limestone matrix gives a 1/1 relationship. Example: tool neutron porosity = 30%, true porosity for sandstone matrix = 34%. (From Schlumberger, 1972).

This latter method is especially useful in limestones and dolomites.

***Hydrocarbon effects on neutron porosity***

The rules governing the relationship between neutron-log porosity and the true porosity in clean formations are valid when either water or oil fill the pores (the two fluids have essentially the same hydrogen index). However, gas having a very low density, has a very low hydrogen index compared to water. The presence of gas makes the neutron log give too low a porosity (Figure 10.12). Corrections for gas content can be made (Gaymard and Poupon, 1968) but the best use of this phenomenon is qualitative. Moreover, on the neutron-density combination (*see below*) gas stands out very distinctly, giving a large negative separation (Figure 10.12).

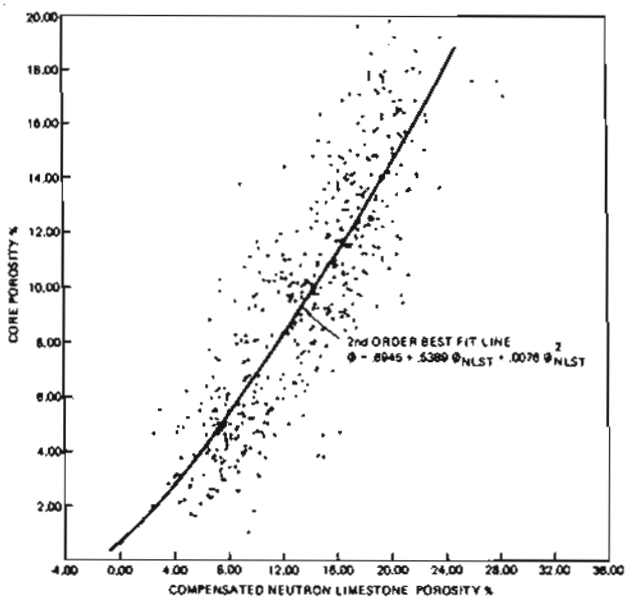


**Figure 10.11** Compensated neutron log values plotted against core porosity values (points with grain densities between 2.84 – 2.88g/cm$^3$). 18, West Pembina D-2 Reef wells: $N$ = 475. (From McFadzean, 1983).

***Shale effects on neutron porosity***

Since the neutron log is sensitive to all hydrogen nuclei, it is sensitive to both free and bound water. The former is formation water, the latter occurs in clays either within the molecule or adsorbed between clay mineral layers (*see* Neutron log in shales, Section 10.6).

Slight admixtures of shale with reservoir matrix material therefore disrupt neutron porosity values, and the true porosity cannot be calculated without corrections. The example (Figure 10.13) shows that the neutron porosity stays constant while the true porosity varies considerably.

A study of shaly sandstones showed that in quartz-clay mixtures the hydrogen indexes of wet clay and formation

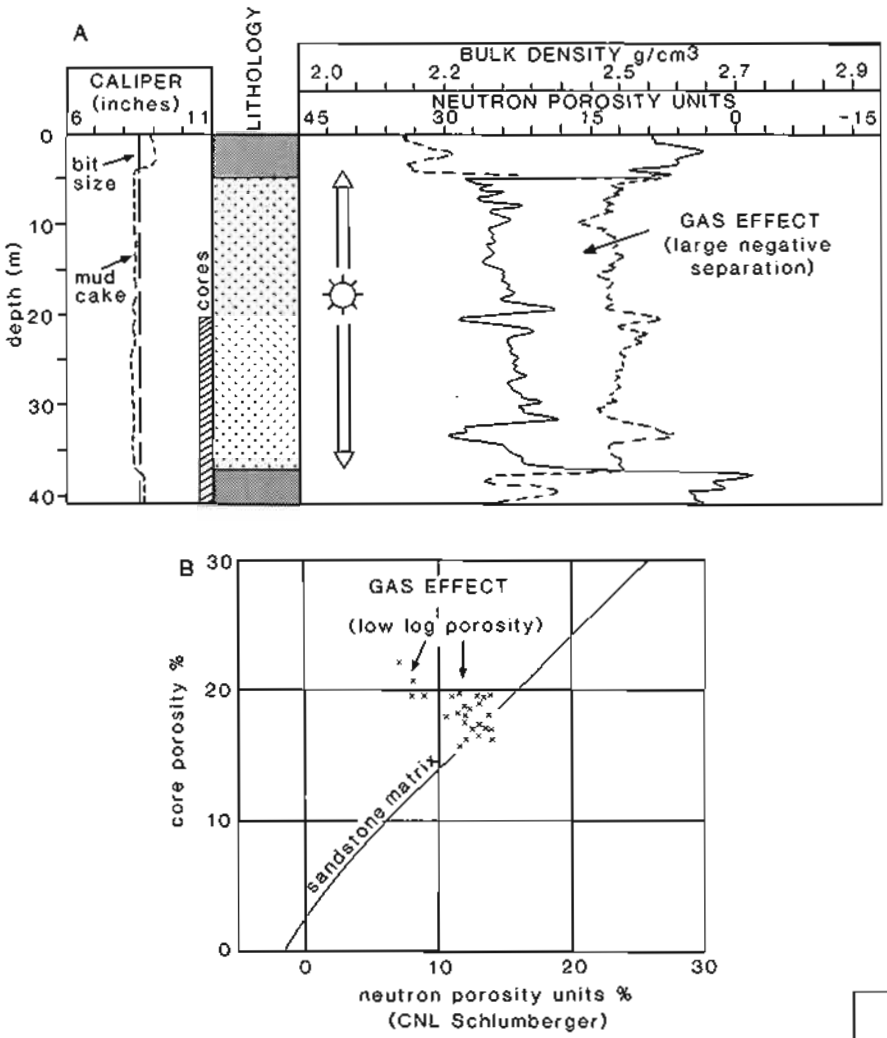


**Figure 10.12** Logs (A) and cross-plot (B) showing the effect of gas on the neutron (and density) logs. The neutron values from A are used in the cross-plot B. The neutron shows too low a porosity in gas zones.

water are very similar (Heslop, 1974). In other words, the neutron is incapable of separating wet clay from water. Cross-plotting gamma ray values (as a clay indicator) against neutron log values illustrates this. The gamma ray log shows diminishing clay volume and the neutron maintains a constant value (Figure 10.14). The neutron-derived porosity is therefore erroneous and the neutron cannot be used to derive a clay volume. In shaly sandstones, therefore, the neutron porosity value should not be used.

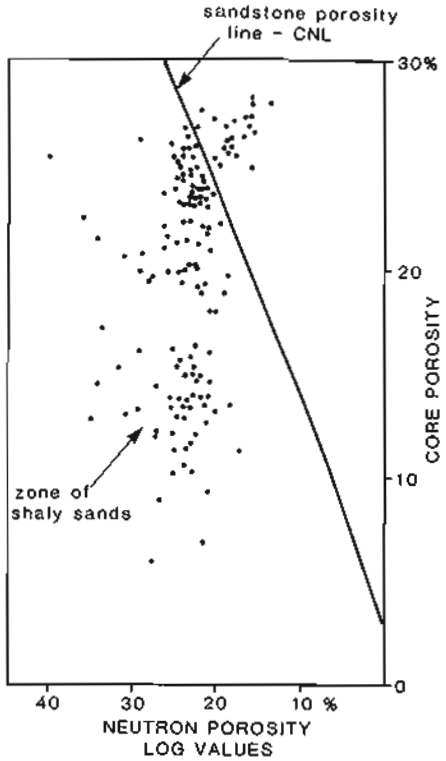


**Figure 10.13** The effect of shale on neutron porosity values. The neutron log registers shale as porosity (water). The true porosities should fall along the diagonal line (compare Figure 10.14).

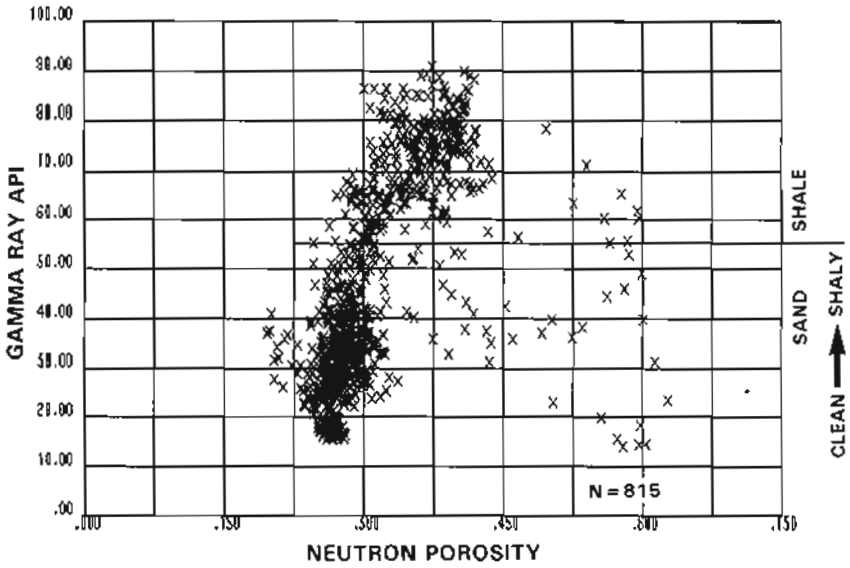


**Figure 10.14** Neutron log values cross-plotted with gamma ray values in a shaly sand formation. The neutron log indicates the same porosity in shaly sands, with gamma ray values between 40–55 API, as in the clean sands with gamma ray values below 40 API. This is not the case, porosities are lower in the shaly sands (compare with Figure 10.13).

## 10.6 Qualitative uses

***Lithology identification***

The use of the neutron log to identify lithologies depends on an understanding of the distribution of the hydrogen index in natural materials.

The hydrogen detected by the neutron tool occurs in two principal chemical combinations, one between hydrogen and carbon (the hydrocarbons), and one between hydrogen and oxygen (simply water). Hydrocarbons occur as gases (methane, etc.), as liquids (oil, bitumen, etc.) or as solids (coal, organic matter). Water occurs as free water (in pores), as adsorbed ions (as in clay interlayer zones), as water of crystallization (as in evaporites), or as combined water (as in igneous rocks).

The lithologies in which these various forms of combined hydrogen are found have hydrogen indexes which cover almost the entire scale between 1 and 0 (Tables 10.7, 10.8). Probably only pure water can be recognized categorically by its hydrogen index, which is 1. However, the neutron log gives an extremely sensitive reflection of lithological characteristics and changes, and combined with other log responses the hydrogen index becomes diagnostic. This is examined below.

***Neutron log in shales: porosity and compaction***

The neutron log shows abnormally high 'porosities' in shale or clay intervals. Values vary between 75% $\phi N$ and 25% $\phi N$, but a typical shale has values around 40–50% $\phi N$ (Figure 10.15). The neutron log will therefore indicate probable shales (40–50% $\phi N$) as opposed to sandstones (0–30% $\phi N$) or limestone (0–35% $\phi N$). The values in brackets are only 'typical', not exact. A shale with a neutron porosity value of 50% does not have a real

**Table 10.7** Neutron log values of some common lithologies (from Serra, 1979; Edmundson and Raymer, 1979).

| | Limestone porosity units CNL | Hydrogen index† |
|---|---|---|
| Water, fresh | 100 | 1.00 |
| Water, salt | 60 + | 0.90 |
| Quartz | –2 | 0.01 |
| Sandstones* | –2 to 25 | |
| Calcite | –1 | – |
| Limestones* | –1 to 30 | |
| Dolomite | 1 | – |
| Dolomites* | 1 to 30 | |
| Shales | 25 to 75 | 0.09 to 0.37 |
| Coal, lignite | 52 | 0.66 |
| Coal, anthracite | 38 | 0.40 |
| Methane | (20 to 50) | 0.49 |

*Approximate ranges up to 30% porosity
†200° F, 7000 psi

**Table 10.8** Combined water in clays.

| Clay type | % water* (av.) | Hydrogen index* | Neutron porosity value (CNL) |
|---|---|---|---|
| Illite | 8 | 0.09 | 30 |
| Kaolinite | 13 | 0.37 | 37 |
| Chlorite | 14 | 0.32 | 52 |
| Smectite | 18–22 | 0.17 | 44 |

*Weaver *et al.* (1973) *Serra (1979)

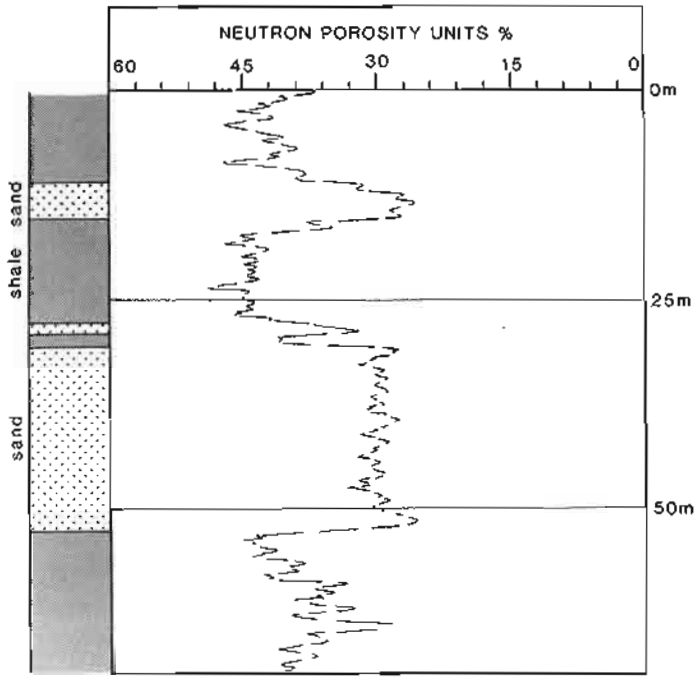


**Figure 10.15** Typical neutron log response in a sand-shale sequence. Shale gives high values N 40–45%: sands give lower values $\phi N$ 28-30%. $\phi N$ in shales is due to free, adsorbed and interlayer water, and does not give real porosity.

porosity of this value. The hydrogen index is high because of the presence of both free and bound water.

When a clay is deposited, up to 70% or more of its volume may be water. This diminishes very rapidly, and over shallow geological depths typical of oil wells, is generally between 10% and 25% depending on the degree of compaction (cf. Figure 9.11).

Clay water is divided into free pore-water, adsorbed water clinging to the clay but also in the pores, and lattice-water which forms part of the clay mineral structure. Clays with no lattice-water show a gradual elimination of both pore and adsorbed water by compaction. A residuum of about 10% usually remains. Interstitial water is an important element of the smectites (Table 10.8) and complicates compaction since it is more or less stable up to an abrupt dehydration point. This point is largely temperature-controlled, but in oilfield work is often related to depth. A clay rich in smectite above the dehydration point may contain up to 20–25% interlayer water: below it is rapidly eliminated. In depth terms this can be anywhere between 1500 m and 5000 m but is usually at about 2000 m (Shaw, 1980).

An attempt has been made to study the behaviour of the various clay waters using neutron-density cross-plot techniques (Honda and Magara, 1982). Adsorbed and free water will be detected as porosity by both the density and the neutron tools. Interlayer water will, however, only be detected by the neutron. The line of equal density-neutron porosity indicates the limit of the interlayer water (Figure 10.16).

This theoretical behaviour of water in clay formations (Figure 10.16) is difficult to see on the neutron logs. In a typical well of 3000 m there is a gradual diminution of the average neutron shale value (Figure 10.17). This is presumably the compaction effect yet it is surprisingly small when the theoretical diminution of water content with depth is considered. Frequently, when compaction is indicated on other logs (for example the sonic) the neutron log value remains constant (Figure 10.18). A verified explanation of these phenomena has yet to be found, but they suggest that the bulk water content of a clay, as seen by the neutron, remains constant, while its distribution between pore-water, adsorbed water and interlayer water changes. Pore-water should diminish with compaction.

### *Neutron log in shales: composition*

Even though there are differences in the amounts of combined water and neutron log value between the different clay mineral species (Table 10.8), variations in the proportions of these in natural shales seem to have little effect on the neutron log. Variations in non-clay minerals are much more noticeable and they dominate the neutron response.

Rapid or short-amplitude changes of the neutron log values in shales mostly result from two causes: changes in admixed quartz content and changes in organic-matter content.

Typical quartz-clay changes are seen on the neutron log in an example of a coarsening-up deltaic sequence (Figure 10.19). The upwards addition of increasing amounts of quartz, with a hydrogen index of 0.01, to clays with a high hydrogen index, acts as a effective dilutant, persistently lowering the neutron value (Heslop,

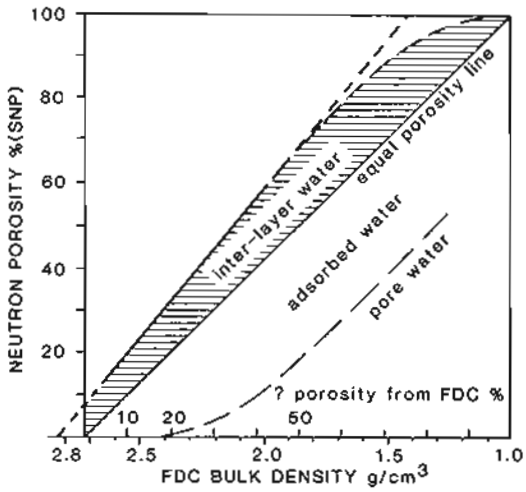


**Figure 10.16** Indication of clay-water types on a density-neutron cross-plot. The outside (heavy) line has a slope of $\phi SNP = 7.65 + 1.14\ \phi FCD$. (Re-drawn from Magara, 1982).

1974). The same result is obtained on the admixture of any material with a very low hydrogen index with clays. This may be quartz as above, limestone, dolomite or certain evaporites: the lower the clay volume the lower the neutron log value.

Entirely the reverse effect is caused by the admixture of organic matter with clays: it causes an increase in the hydrogen index. This is because organic matter has a higher hydrogen abundance per unit volume (hydrogen index around 0.66) than clay (Table 10.8) (Figure 10.20). The increase in neutron log values with organic matter is notable, especially when combined with the attendant decrease in bulk density (*see* Figure 9.18).

One aspect in the evaluation of shales with neutron tools which does not seem to have been evaluated sufficiently, is the effect of thermal neutron absorbers. Capture and absorption in pore space liquids are mainly due to hydrogen and chlorine (NaCl) which are corrected for in tool response. Capture in the solid matrix is negligible unless it contains elements with unusually high capture cross-sections, such as boron or gadolinium (Table 10.3). Boron content has been examined in the Gulf Coast and is said have a noticeable effect in certain shales and shaly sands (Dunlap and Coates, 1988). The geological significance of this and of the distribution of boron and gadolinium is not known.

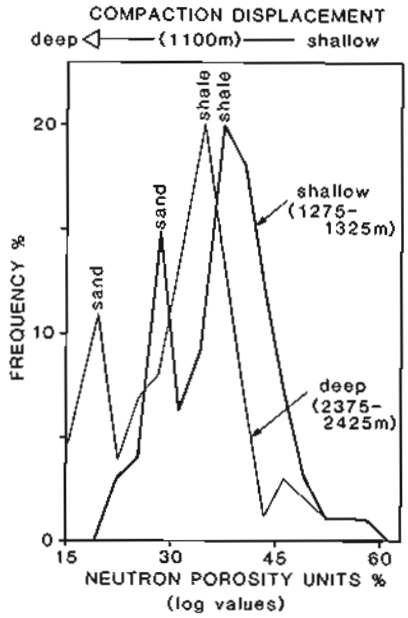


**Figure 10.17** The effects of shale compaction on neutron log values in a sand-shale sequence. Histograms of the log values show the diminution in sand porosity, but only a small change in the shales.

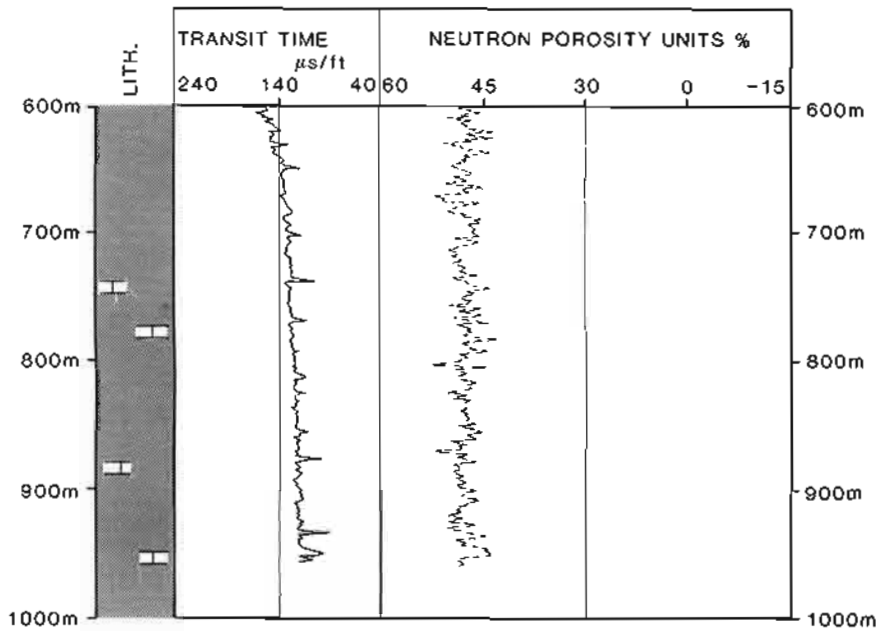


**Figure 10.18** Compaction in a shale sequence shown by a decrease in interval transit time (increase in velocity) while the neutron log shows constant values.

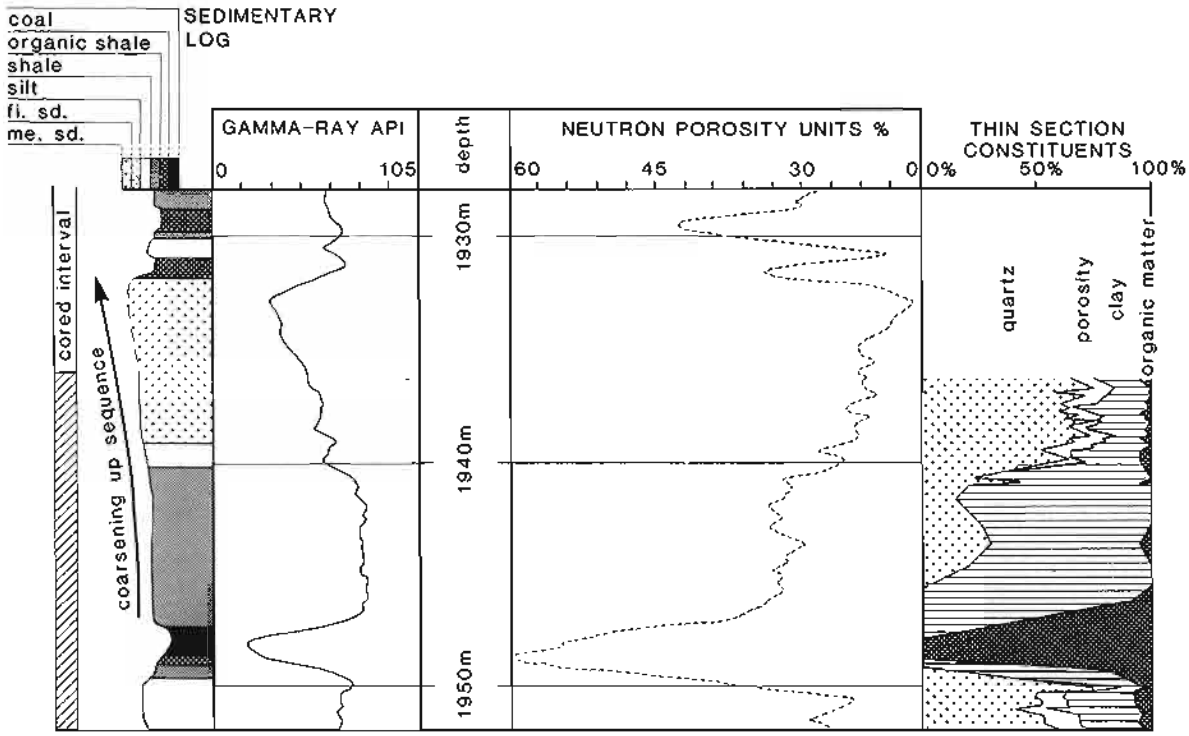


**Figure 10.19** Changes in the neutron log correlatable with changes in quartz admixture. The higher the quartz content, the lower the neutron value.

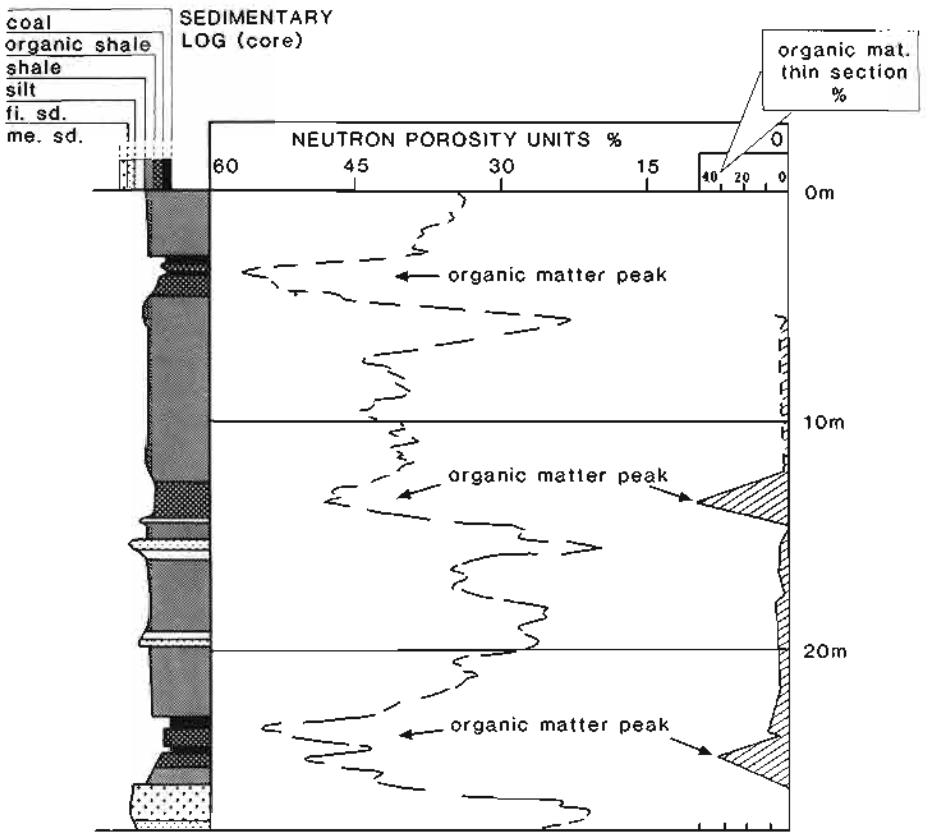


**Figure 10.20** The effect of organic matter on the neutron log. Organic matter has a high hydrogen index and causes a moderate increase in the neutron log values.

### *Evaporites*

The neutron log can be used to distinguish between evaporites on the basis of water of crystallization (Table 10.9). Of the evaporites with water of crystallization, gypsum ($CaSO_4.2H_2O$) is the most common. However, carnallite, polyhalite and kainite also contain the water radical (Table 10.9). All these minerals have a high neutron-log value which differentiates them from other evaporites such as salt (NaCl) or anhydrite ($CaSO_4$), which contain no water and hence have a log value of zero (Figure 10.21).

### *Identification of hydrated minerals*

Hydrated minerals (excluding evaporites) are not common. However, hydrated iron compounds may be sufficiently abundant to affect the logs. Thus a zone of

**Table 10.9** Neutron log values of some evaporites (from Schlumberger, 1985).

| Mineral | Composition | Neutron log Value† | |
|---|---|---|---|
| Carnallite | $KClMgCl_2.6H_2O$ | 60† | High |
| Gypsum | $CaSO_4.2H_2O$ | 60† | |
| Kainite | $MgSO_4KCl.3H_2O$ | 60† | |
| Polyhalite | $K_2SO_4MgSO_4$ $2CaSO_4.2H_2O$ | 25 | |
| Halite | NaCl | –3 | Low |
| Anhydrite | $CaSO_4$ | –2 | |
| Sylvite | KCl | –3 | |

† $\phi$CNL – apparent limestone porosity

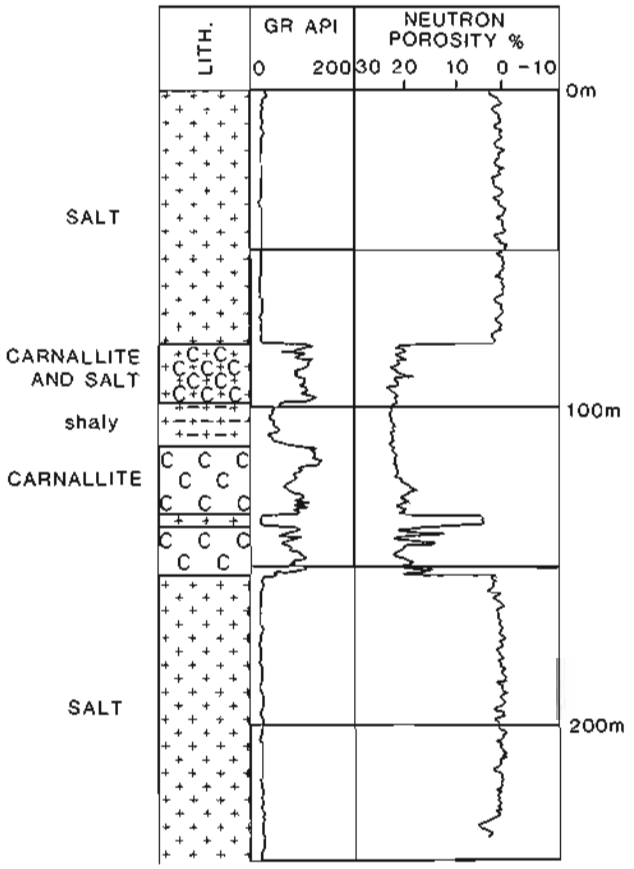


**Figure 10.21** The hydrated evaporite carnallite ($KClMgCl_2.6H_2O$) identified on the neutron log. The halite which accompanies the carnallite has a neutron value near zero.

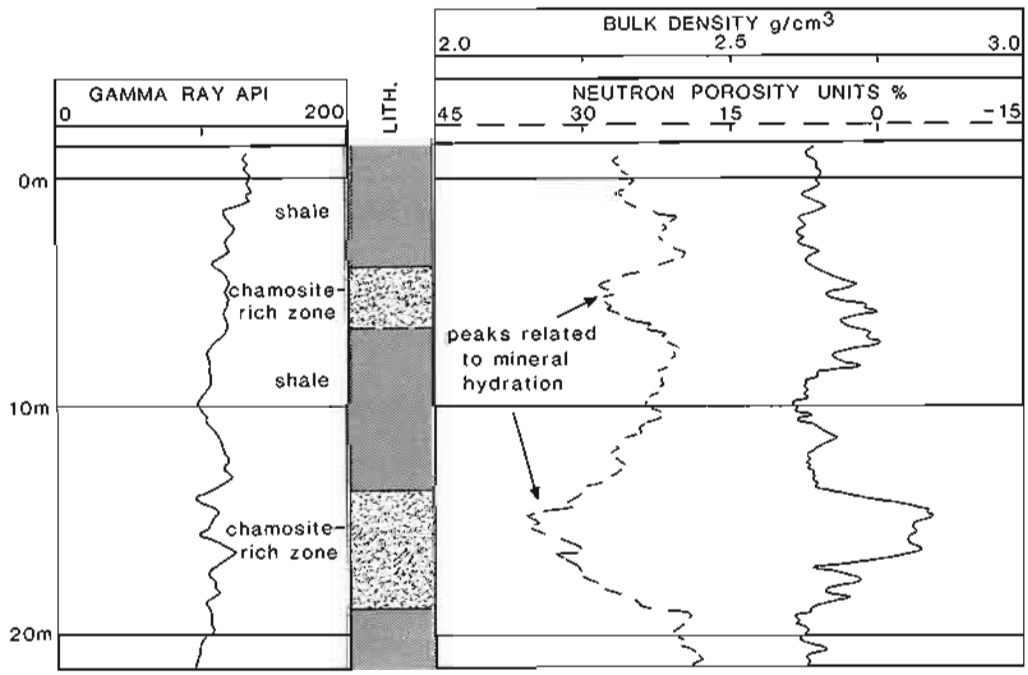


**Figure 10.22** Chamosite, a hydrated iron mineral of formula $2SiO_2.Al_2O_3.3FeO.nH_2O$, causing high neutron values. Note the high density of the chamosite zone. Liassic, North Sea.

chamosite ($2SiO_2Al_2O_3 3FeO nH_2O$) in the Liassic shales of the North Sea is sufficiently rich to be seen on the neutron log (Figure 10.22). The zone is characterized by an increase in the neutron log value associated with a corresponding increase in the bulk density (*see also* Section 10.7, Neutron-density combination).

### *Volcanic and intrusive rocks*

The neutron log is especially useful in the recognition of intrusive and volcanic rocks: most of these show high neutron log values and high densities (as in many shales) but associated with low gamma ray values (unlike shales).

The high neutron-log values in igneous rocks are due to their high content of chemically-bound water. The bound water may be original or associated with alteration products, mainly clay minerals, which result from the reaction of hydrothermal fluids with the original intruded rock.

An example is shown of an altered diabase with no porosity (Figure 10.23). The neutron log is seen to be responding entirely to the bound water (between 1–4% by weight). The alteration products in this example are biotite, sericite, kaolinite, montmorillonite and chlorite, all of which themselves have varying amounts of water (Table 10.8) (Nelson and Glenn, 1975).

A series of basalt flows from the Middle Jurassic of the North Sea also show high neutron values, here diagnostically associated with low gamma ray readings and high densities (Figure 10.24). A characteristic profile of increasing values upwards is developed in the neutron log in each individual lava flow (Figure 10.24). The response appears to be typical of subaerial flows and is also seen in the Deccan traps of India (Buckley and Oliver, 1990). Two proposals exist for this neutron response. The first suggests that it is related to alteration products, such as chlorite, which occur progressively towards the tops of the flows and formed during soil development and weathering. The second suggests that the increase in vesicles upwards is the cause, either enclosing water or water rich chemicals such as zeolites.

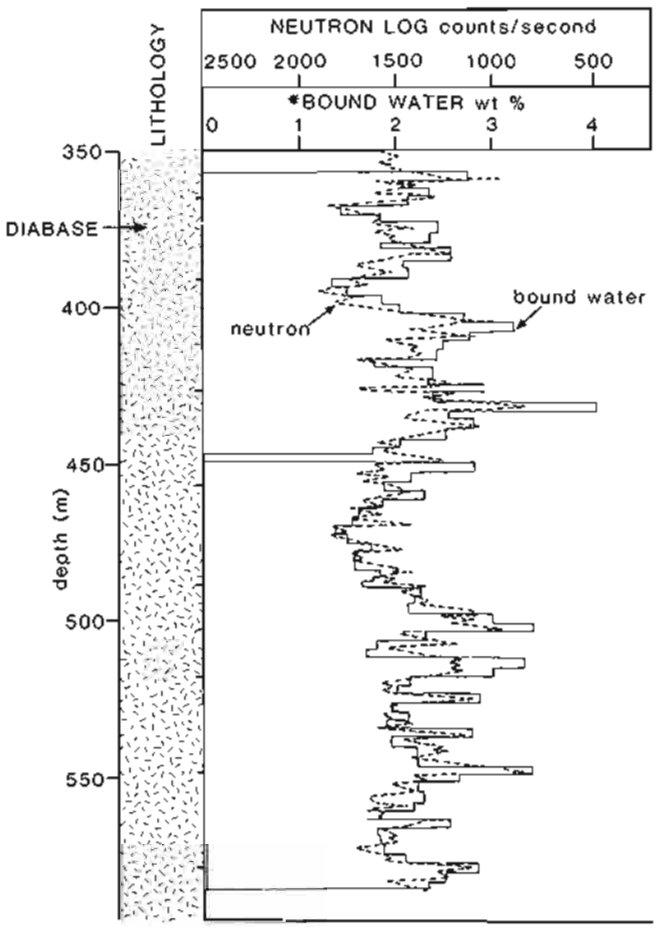


**Figure 10.23** Neutron response to volcanic rocks with bound water: the example is of a diabase with 1–2% of sulphide mineralization. It has no porosity. *Bound water values from analyses of 10ft (3m) composites on pulp. (Re-drawn from Nelson and Glenn, 1975).

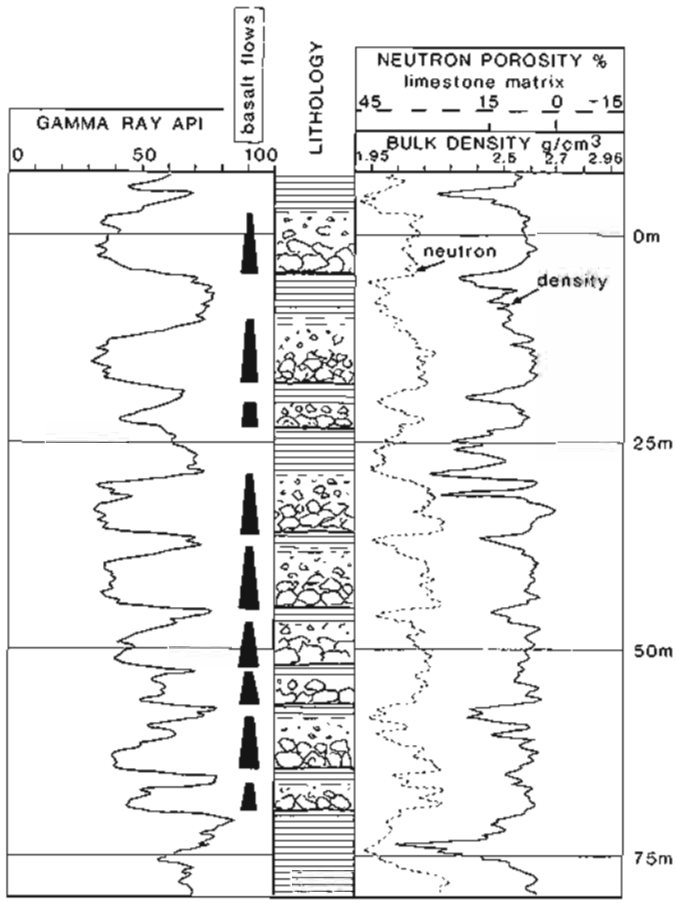


**Figure 10.24** Neutron log response to basalt flows. The Jurassic age flows from the North Sea show low gamma ray values and high neutron log values. The flows are interbedded with iron-rich, clay soil.

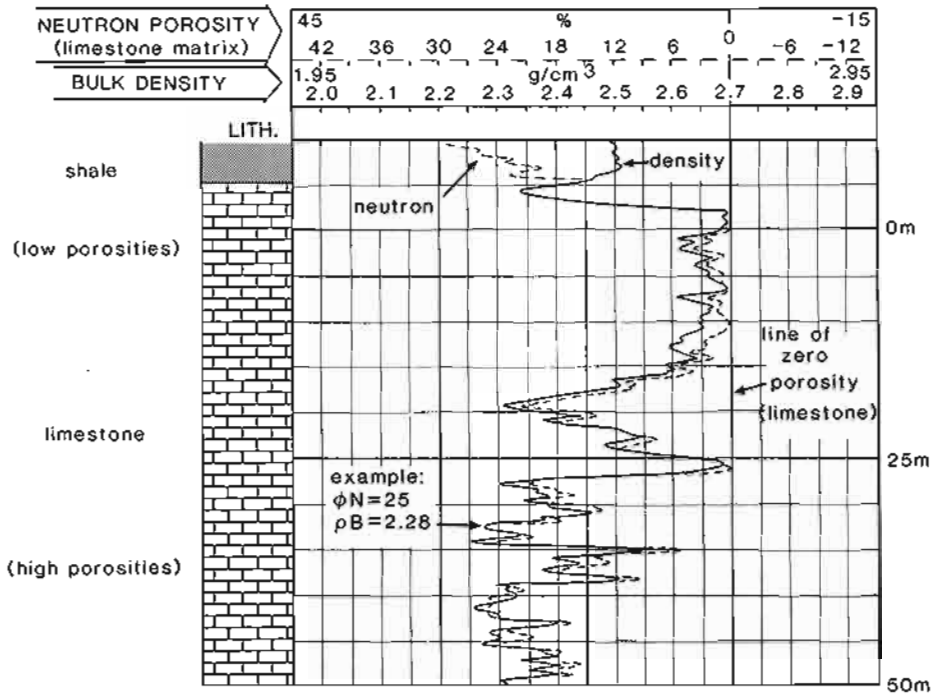


**Figure 10.25** Neutron porosity log and bulk density log plotted on compatible scales. The neutron porosity is displayed with a scale for a limestone matrix: the density for a matrix of 2.70g/cm³ (= zero porosity). The two logs follow each other closely over the limestone interval. Example: φN = 25%. Bulk density = 2.28g/cm³. *See* Figure 10.26 for cross-plot position.

## 10.7 Neutron-density combination: lithology identification

*Clean formations*

By themselves, both the neutron and the density log are difficult to use for gross lithology identification. However, once combined, they become probably the best available indicator for the reasons given below.

Both the neutron log and the density log should be showing the same formation parameter – porosity. Plotted on compatible porosity scales, they should give identical values and it should be possible to superimpose the two logs (Figure 10.25). In practice, this is only the case in clean, water-filled limestones which give almost perfectly superimposable logs, as shown in Figure 10.25.

The explanations can be taken in two stages. Firstly, the scales of the two logs are made compatible (normally) on a clean-limestone scale. A neutron-log value of zero (no porosity, 100% matrix) corresponds to a bulk density of 2.70 g/cm³ (the density of pure calcite is 2.71 g/cm³), and so on to a neutron value of 100 (100% fluid) and a density of 1.0 g/cm³ (the density of fresh water) (Figure 10.26). A cross-plot of density-log values against neutron-log values will show a straight-line relationship, a point on the line corresponding to a particular porosity (Figure 10.26). This is the 'clean-limestone' line.

The second stage of the explanation is that the straight-line relationship *only* holds good for clean limestones because matrix material has variable effects on both logs.

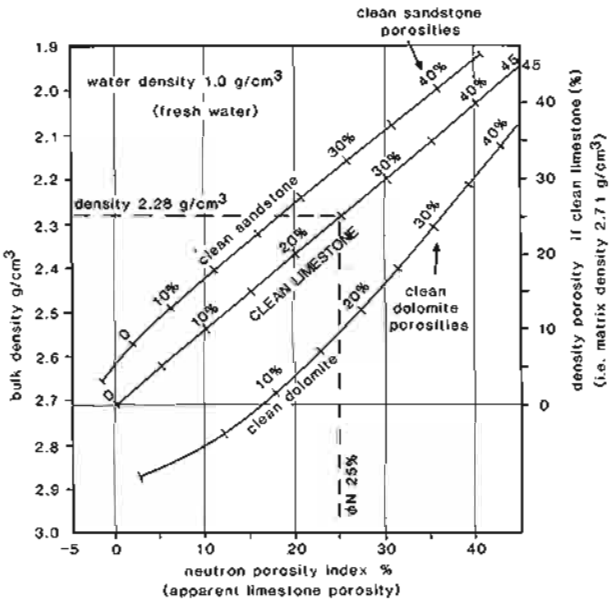


**Figure 10.26** The density-neutron cross-plot. The plot is necessary to find real, clean formation porosities because of the differing effects of matrix type on the two logs (*see* text). Example: density 2.28g/cm³, φN = 25%: real porosity 25%, lithology clean limestone - (cf. Figure 10.25). (Cross-plot for Schlumberger FDC-CNL logs in fresh water-filled sandstone. Plot from Schlumberger, 1979).

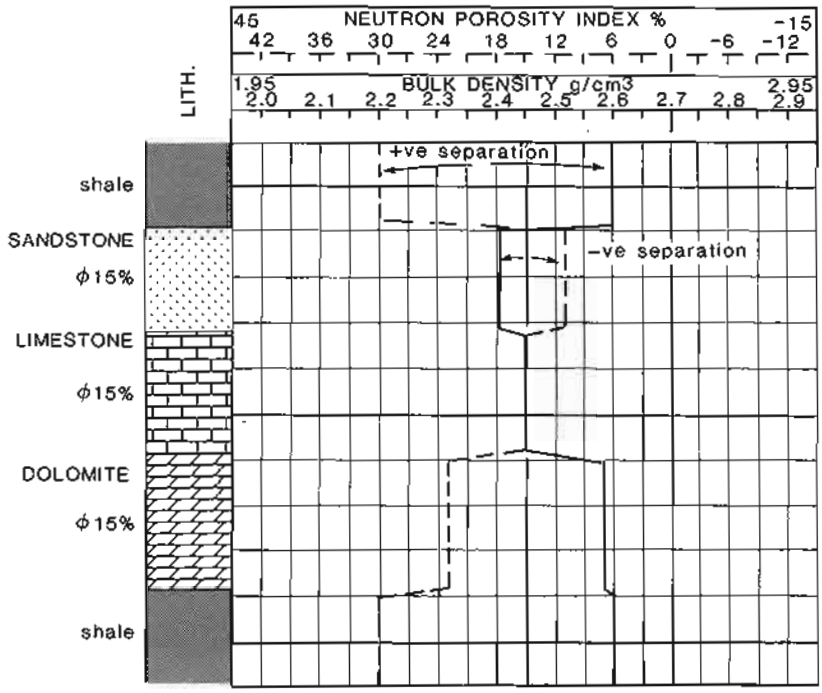


**Figure 10.27** Idealized neutron-density log combination responses. The figure shows clean sandstone, limestone and dolomite, all with 15% water-filled porosity.

A sandstone is seen differently from a limestone by the density log because of a different matrix density (*see* Chapter 9) and by the neutron log because of the different matrix effect (Figure 10.26). On the cross-plot of density-log values against neutron-log values, the clean-sandstone line plots as shown on Figure 10.26. Again, a point on this line corresponds to a clean sandstone with a particular porosity. In the same way a 'clean-dolomite line' may also be constructed (Figure 10.26).

For logs plotted on compatible scales, the variations in matrix are translated into a separation of the curves and it is this that is used for lithology identification. A clean limestone shows no separation, while for a clean sandstone the separation is slightly negative and for a clean dolomite moderately positive (Figure 10.27). For a constant matrix the absolute values will change with variations in porosity, but the separation will remain more or less constant (e.g. Figure 10.25).

***Shale and shaly formations***

Clean formations and the ideal reactions described above form the minority of cases. Shale is usually present.

Pure shale is recognized on the neutron-density combination when the neutron value is high relative to the density value. It gives a large positive separation to the logs, the neutron well to the left of the density. This separation is typical and diagnostic (Figure 10.27) and is due to the high hydrogen index of shale matrix material (*see* Neutron log in shales, *above*).

If shale becomes diluted by matrix grains such as quartz or calcite with low hydrogen indexes (Table 10.7), the neutron-log value decreases rapidly. Such a change is not seen so markedly on the density log since the matrix density of shales (2.65–2.7 g/cm3) is similar to that of quartz and calcite (2.65–2.71 g/cm3). On the log combination, the result is a decrease in the neutron-log value and a decrease in the log separation. The decreases continue until clean formation values are reached (Figure 10.28).

Ideally, the changes from pure shale to clean formation are progressive on both logs as the volume of shale decreases. The relationship can be considered as roughly linear. A 50% shale mixture should thus show 50% of the change from pure shale to clean formation. Qualitatively large or small separations can be considered to indicate more or less shale (Figure 10.28). In practice, small separations i.e., slightly shaly formations, tend to be related to low neutron values, while pure shales show large positive separation and high neutron values.

Used properly, the neutron-density combination is the best log indicator of shale. It allows a more reliable indication than the gamma ray log and, at least qualitatively, can be used to evaluate the degree of shaliness (Figure 10.28). Used thus, as a shale indicator and with typical known separations in clean formations, the neutron-density combination can give a good idea of lithology in almost all normal formations.

***Distinctive lithologies and minerals***

Certain minerals and some less common lithologies have very distinctive neutron and density values and show unusual neutron-density separations. Some of these are shown graphically on the neutron-density cross-plot grid (Figure 10.29). This figure shows clearly that on log plots some of these responses will be very distinctive and can be diagnostic. Coals, for example, are easily recognised from their very distinctive neutron-density response of

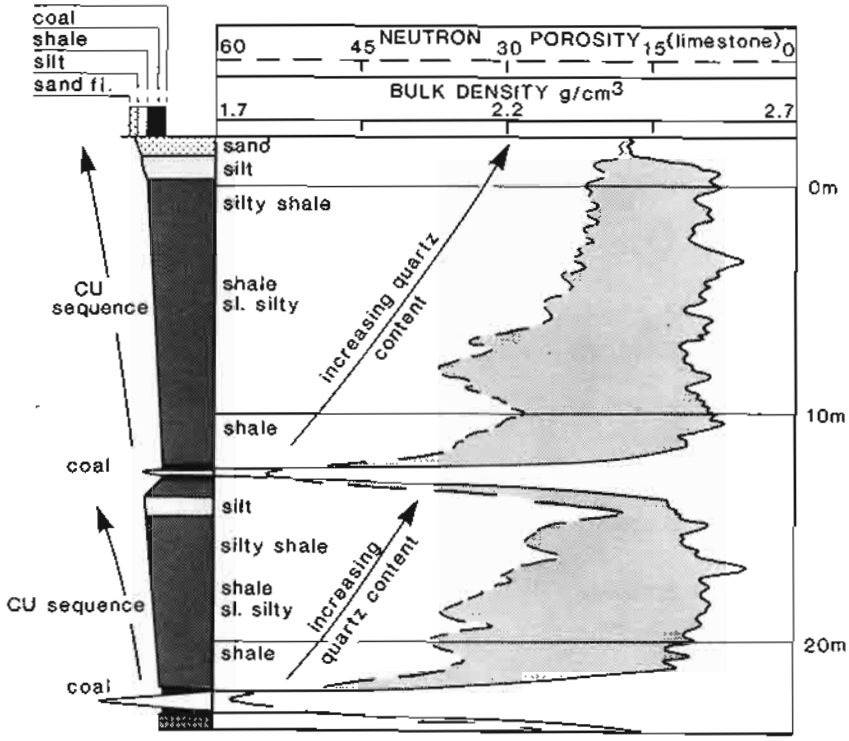


**Figure 10.28** Changes in the neutron-density combination separation due to changes in quartz-clay admixture. In the two coarsening-up, deltaic sequences shown, the quartz content increases upwards relative to the shale. The separation changes are due mainly to the changes in neutron value (compare Figure 10.19).

unusually low density combined with unusually high neutron values (Figure 10.28). Pyrite, haematite and to some extent siderite, are recognised by having very high density values with zero neutron response.

A further, interesting example underlines the use of the combined neutron-density response in identifying unusual lithologies and minerals. On log plots, both the density and the neutron-log generally 'move together', a higher density corresponding to a lower neutron-log value. When a very high density value corresponds to an even higher neutron-log value, a simple lithological explanation is not possible. This is exactly the case of the chamosite beds common in the Liassic of the northern North Sea (Figure 10.22). The high neutron-log values are caused by the chemically-bound water in the chamosite (an hydrated iron mineral), while the mineral itself has a high density (3.03 g/cm$^3$). The large positive separation, even larger than the surrounding shales, is very typical of the chamosite (Figure 10.22). On any other log the chamosite beds are not diagnostic.

### *Evaporites*

Evaporites are also distinctive. Since their densities (*see* Section 9.6, Mineral identification) and also their hydrogen indexes (*see above*, Evaporites) may be diagnostic, evaporites become very distinct by the combination of

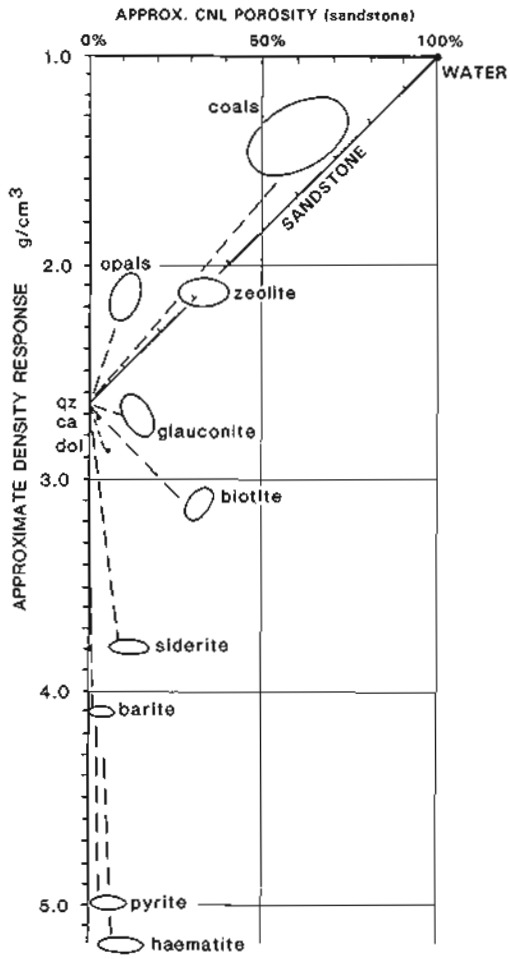


**Figure 10.29** Neutron-density cross-plot with tentative locations of some zero-porosity, non-quartz materials (modified from Ransom, 1977).

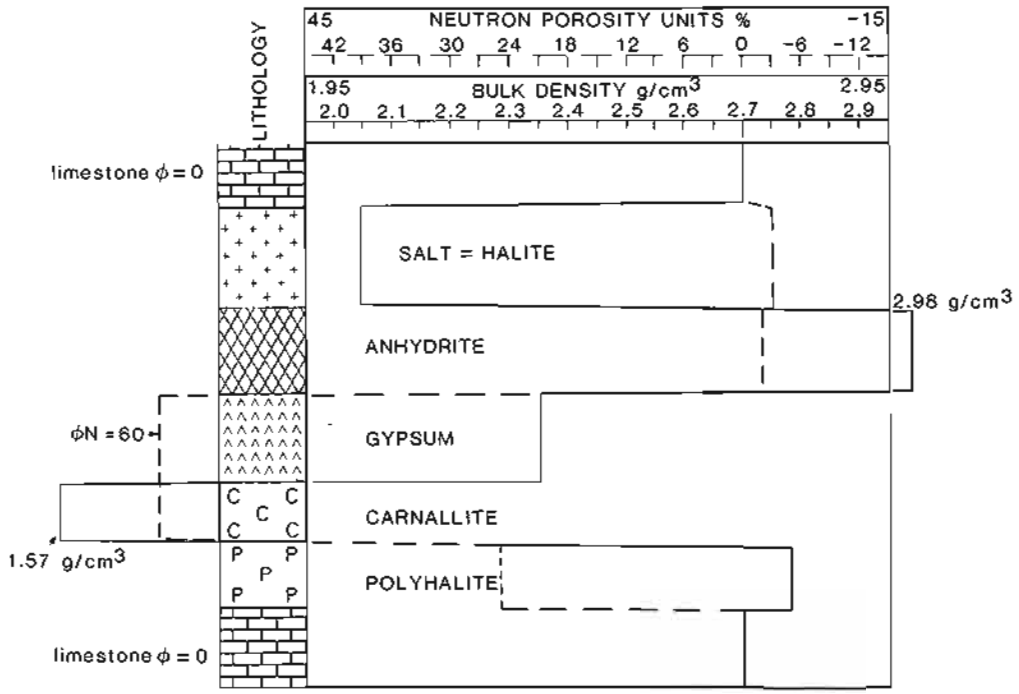


**Figure 10.30** Idealized neutron-density log, combination responses in a series of pure evaporites. (For FDC-CNL Schlumberger, figures from Edmundson and Raymer, 1979).

both logs. The absolute values of both logs and the log separation (Figure 10.30) are all indicative.

### *Conclusions*

The neutron-density combination is the best lithology indicator for most formations. Shales and shaliness and evaporites can be identified, clean formations and even matrix type can be suggested, and unusual minerals located with the possibility of identification.

Neutron and density values can also be used quantitatively for lithology identification. The method is described in Chapter 11 (*see* Cross-plotting compatible logs, Section 11.6).

# 11
# LITHOLOGY RECONSTRUCTION FROM LOGS

## 11.1 Introduction

There are two independent sources of lithology data available from oil wells, one set of data coming directly from the drilling and one set from the wireline logging.

The drilling data consist of cuttings, cores and all the recorded drilling parameters (and, of course, the MWD/LWD logs, although not discussed here). The logging data consist of the wireline, geophysical log suite and sidewall cores. For a reliable lithological reconstruction, both sets of data are essential. As a result of the great sophistication of wireline logs, the drilling data are often forgotten. This should never be the case since the only continuous sample of formation lithology comes from drill cuttings.

This chapter describes the methods for interpreting lithology by the manual method using log and drill data, semi-automatic methods using mainly logs and fully automatic methods using only a computer and logs.

## 11.2 Lithology from drill data – the mud log

The mud log and the way in which it is made is described briefly so that the data it represents can be used properly in log interpretation. Drill-derived data and log-derived data often appear to be in conflict. Which can be believed? This book describes how logs can be used and this section describes how drilling data can be used, their reliability, and some pitfalls in their use.

The mud log (a misnomer that has somehow stuck) is the geologist's record of the drilling of a well. Before wireline logging was invented, it was the only record that existed. On this log is recorded the lithology, the drilling rate, bit changes, gas record, calcimetry, dates and events (Figure 11.1). The lithology is based on an examination of cuttings – small chips broken off the formation as the drill advances. They are washed away in the stream of

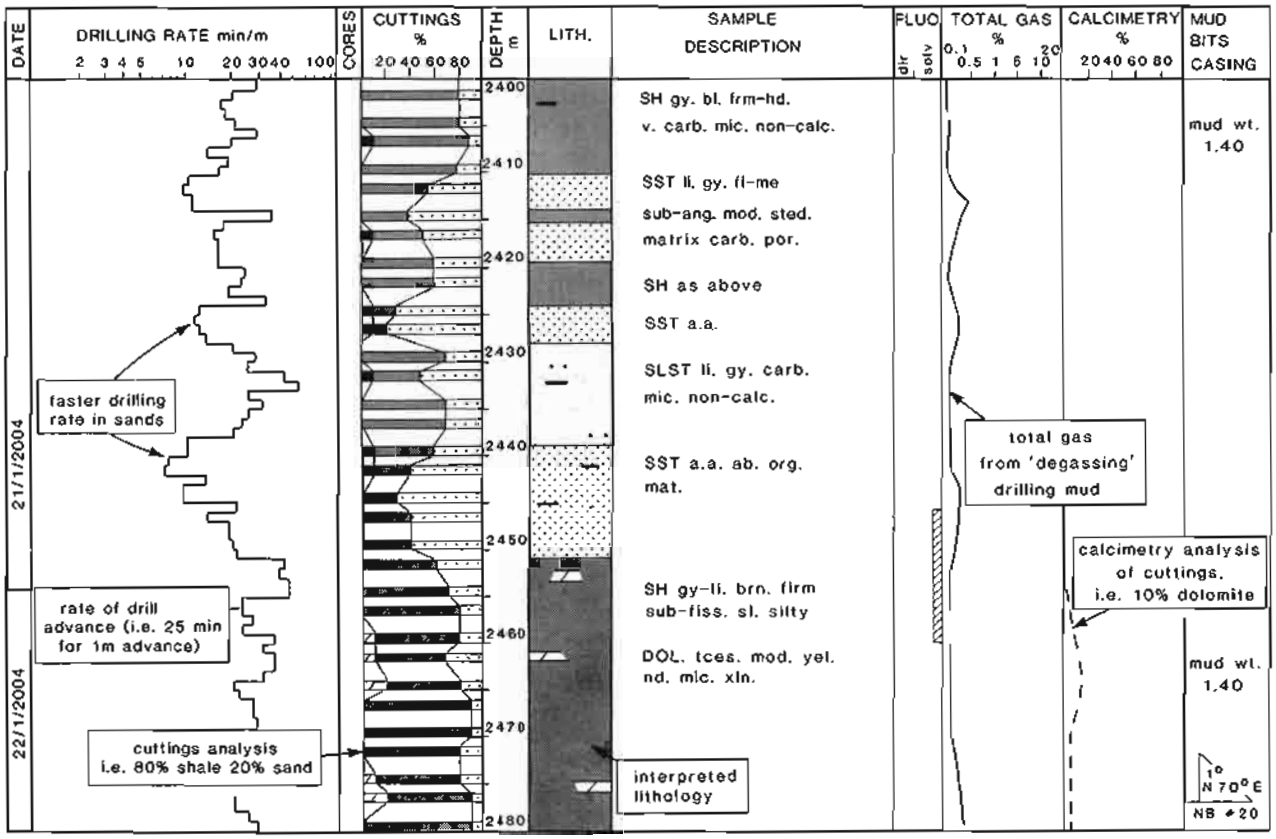


**Figure 11.1** A typical mud log. The log is the well-site record of lithology (cuttings) and some drilling parameters. In this example cutting samples were taken every 2–3m.

drilling mud and brought to the surface. They do not usually 'float' in the mud, but are pushed upwards by friction and drag. At the surface, the drilling mud is passed through a large metal sieve, the 'shale shaker', and the cuttings are recovered. It is from the shale shaker that the geological cuttings sample is taken.

On the mud log, lithology is usually recorded in percentage of cuttings types in a particular sample, say 10% sand and 90% brown shale. New samples are taken every 2 to 20 metres, depending on the rate of drilling. Fast drilling rates of perhaps 1 minute per metre at the top of the hole allow only one sample to be taken every 20–25 m drilled (i.e. 1 sample per 20-25 minutes). At greater depths, rates of 30 minutes to drill 1 metre of formation are common, and a sample can be taken every 2 metres (i.e. 1 sample per hour) or even closer.

To reconstruct the mud log, the time it takes a sample to reach the surface after being cut, the *lag time*, must be calculated. A sample drilled at 3000 m will take perhaps 1 hour and 10 minutes to reach the surface. It will be travelling at 43 metres per minute up the hole (about 2.6 km/h), the exact rate depending on the rate at which the mud is 'circulated', that is pumped through the mud system. The drilling rate is used as the basic curve for the mud log (Figure 11.1) and is presented as real depth. A metre drilled is instantly recorded, but the cuttings sample is tied to the drilling-rate log, so the lithology corresponding to the depth 3000m–3002m will only be recovered at the surface 1 hour and 10 minutes after it has been drilled.

The same principle of lag time is applied to gas readings and to shows as to cuttings.

On most mud logs the geologist has recorded not only an analysis of the percentages of the cutting types present, but also what this means in terms of real subsurface lithology. For instance, if a sand-shale-coal sequence is being drilled, all these lithologies become 'smeared' while travelling to the surface. In the cuttings sample will be seen 50% shale, 40% sandstone and 10% coal. The geologist will then make a 'guess' at the real lithological column using the drilling rate, knowing that shales will drill slowly, sandstones faster (Figure 11.1).

There are occasions when the drilling rate can be compared to a sonic log or a gamma ray log (Figure 11.2) and a good interpretation of bed boundaries has been made from it. However, in general, the drilling rate involves too many variables, such as weight on the bit, bit wear, pump rates and so on, for it to be an accurate boundary indicator. The mud-log interpretation of lithology should not be used to interpret boundaries on the well logs.

It is important, therefore, to use the cuttings percentages in the right manner. As described previously, a rock cutting from 3000 m takes over one hour to reach the surface. During this time it becomes mixed with other cuttings taken at shallower depths and moving more slowly up the hole. It also becomes mixed with chips washed from the well walls, higher up the hole, so-called 'cavings'. By the time they reach the surface, samples are therefore considerably mixed and heterogeneous. An experienced rig geologist will usually recognize cavings and eliminate them from his count. The mixture of cuttings, however, from the various lithologies is the reason why percentages are recorded. All lithological boundaries have become very blurred.

When interpreting the cuttings logs, it is the arrival of a new lithology which is significant. During drilling from a thick shale into a thick sandstone, when the bed is actually penetrated only a small percentage of the cuttings will be sandstone. This increases, but there will be 80% sandstone only several metres lower (Figure 11.2). The drilling rate however will correlate with major lithological changes – the so-called 'drilling break'. Gas levels are also likely to change.

Clearly, the difficulties in interpreting the mud log and the need for immediate, accurate information, were behind the requirement for LWD logs, or logs made while drilling. If these are available, the techniques described below for lithology interpretation from logs (Section 11.4), can be used while drilling continues, rather than after drilling, as is the case with the wireline logs.

***Some pitfalls***

Certain lithologies are notorious for appearing on wireline logs, but not in the cuttings samples. Such is the case for loose sands, silts and soluble evaporites (e.g. salt).

The mesh of the sieving 'shale shakers' is such that loose grains of sand or silt, even coarse sand, pass through the mesh. If this is suspected, the mud may be diverted through de-sanders, where all small grains are extracted. However, de-sanding is not routine and there are many cases where unconsolidated sand reservoirs have been drilled and shale has been recorded on the mud log! Salt is a very similar case. Unless the drilling mud is salt-saturated, no cuttings will be found on surface. Shale, mostly cavings, will be recorded. An experienced rig geologist, however, will note mud salinity changes along with drilling-rate indications which suggest the presence of salt.

The exact opposite exists where lithologies which seem to appear on the mud log do not actually occur in the formation. A typical cause is the use of lignosulphonate, a mud additive which reduces water loss. It resembles lignite and has very often been interpreted as such on mud logs, but this interpretation is suspect if it implies the presence of coals in pure shale intervals: real coals mostly occur in zones of both sand and shale.

Despite these various anomalies, the mud log is essential to the lithological interpretation of wireline logs. As previously indicated, it represents the only continuous record of real lithologies (except where cores exist: *see below*). However, because of the way in which the samples are collected, lithologies have become mixed and bed-boundaries smeared. Wireline logs can be used to separate the mixed elements and define the bed boundaries.

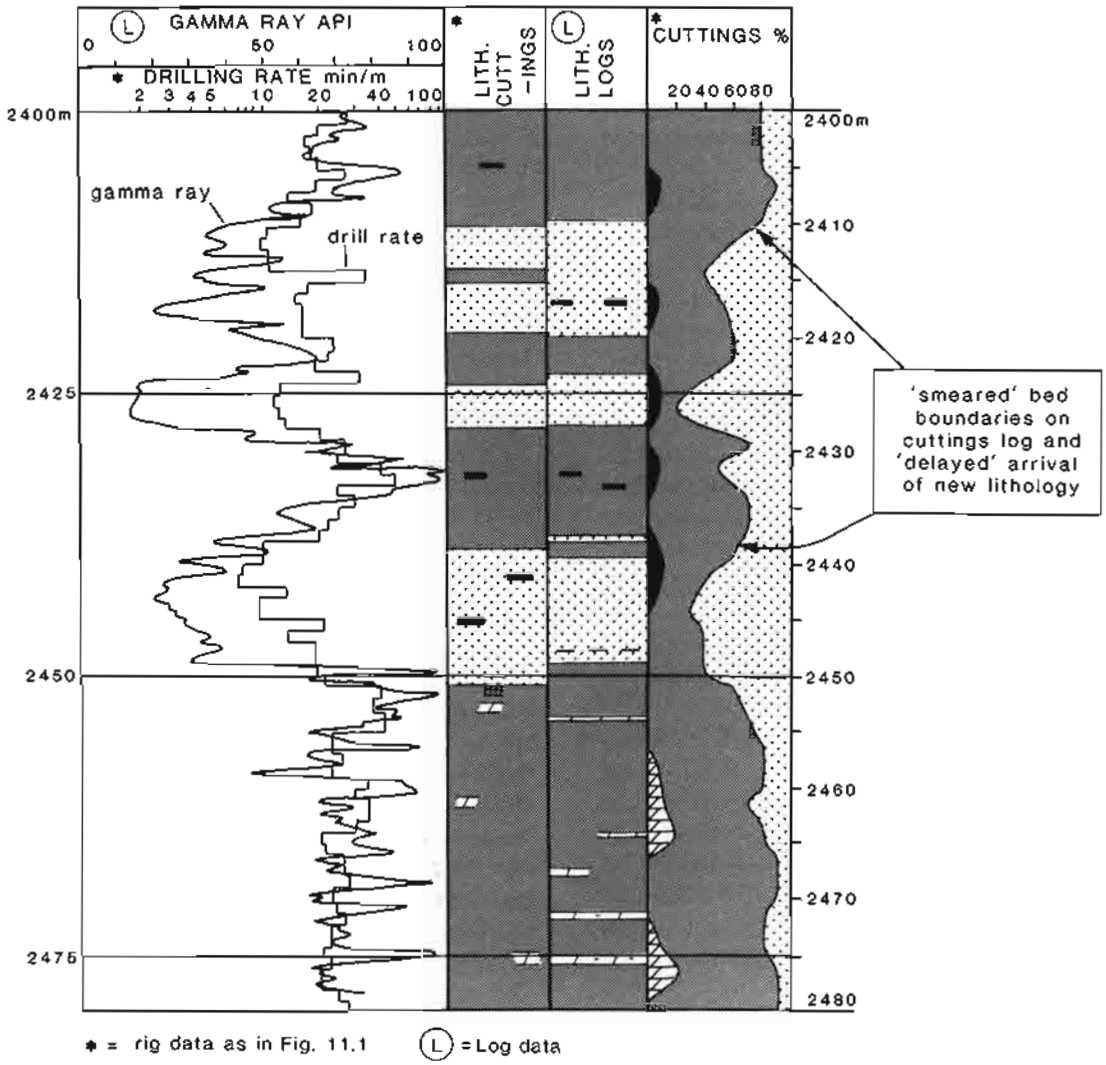


**Figure 11.2** Comparison between rig-derived lithology interpretation and subsequent log interpretation. Note the effect of the arrival of a new lithology on the cuttings percentages. The rig bed boundaries are only 'good guess.'

## 11.3 Lithology from cores – direct physical sampling

Cores may be cut during drilling, when a continuous, cylindrical sample of the formation is recovered, or they may be taken after drilling, when small, punctual samples may be taken from the borehole wall.

### *Cores cut during drilling*

During drilling and before logging, when a complete record of lithology is required (for example in a reservoir), a continuous sample is taken by coring. The drill bit is replaced by a core barrel. The retrieved core, depending on the preceding hole size, will be a cylinder of rock 2–15 centimetres in diameter and up to 60 metres long (Blackbourn, 1990). It is a direct physical sample of the formation.

Being a real physical sample of the formation lithology, a core appears to need no interpretation. In fact the reverse is true; cores should be used as a reference to calibrate the logs from a lithological point of view and to compare with the lithology interpreted from the wireline logs. Indeed, such comparisons are used frequently through this book: they are essential to a proper understanding of the capabilities of wireline logs. Cores provide the geologist with the only record of real subsurface lithology.

Cores do in fact need interpretation and processing before they can be compared to logs. The principal problem is one of depth. Cores are cut during drilling so that their depth limits are calculated by adding all the lengths of drill string together. Mistakes often occur, and frequently these depths do not agree with the depths shown on the well logs. The logs are taken as the reference: for detail the reference may be just one log, frequently the sonic or the density log. The drill depths for a core must therefore be adjusted to log depths. The changes are usually about ±5m but may be as much as ±15m. Moreover, because of recovery problems, the depth changes between contiguous cores are frequently different. When working with the more detailed logs, such as the dipmeter (Chapter 12) or the image logs

(Chapter 13), minor depth miscalibrations are seen within single cores. These can be due either to the core itself, where there may be losses in friable or broken zones or to the tool, where minor sticking and cable stretch can cause depth errors. A perfect match at fine scales is often not achieved.

Even with the core depths perfectly matched to the log depth, inconsistencies between the two may arise. It is at this point that the capabilities of the logs emerge. The problems of bed definition (*see* Chapter 2) become clear, as do those of depth of investigation (*also* Chapter 2) and what this implies in terms of the volume of rock sampled by a log. In extremely heterogeneous formations, the directional tools such as the density-log tool may be difficult to calibrate because of changes across the small distance between the core and the borehole wall. These particular problems are discussed in the chapters on individual tools.

The level of detail at which cores can be compared to logs is an important aspect of core utilization. A core-derived sedimentological log should already bring the natural detail of a core to a manageable level for comparison with the logs, at a scale of 1:200 (Figure 11.3) or if necessary 1:50. Reservoir, sedimentological and calibration studies can all be kept at these scales. However, for general stratigraphical work, the 1:500 scale completion log (*see below*) is used and much less detail is desirable: 20 m of core is represented by only 4cm on the log, so that considerable lithological generalization is usually necessary (Figure 11.3). Generalization is a skill learned through experience and it must give clear and concise, but accurate results. The natural lithological detail of a core is not 'mimicked' by a sedimentological log. The latter should be a stylized representation of a core, an implied interpretation having been made. This sedimentological detail remains on a 1:200 scale log even though there has been a 200% decrease in scale. For general work this detail is usually lost, and at a working 1:500 scale the only difference over a cored interval is a slightly more precise and accurate lithology (Figure 11.3) (Blackbourn, 1990).

### *Cores cut after drilling*

Several methods are available for core sampling once a hole has been drilled and logged. All of them involve cutting into the borehole wall.

The most frequent method is sidewall coring. A sidewall 'gun' is lowered into the hole on the logging cable: it consists of a series of hollow cylindrical 'bullets' 1.8 cm in diameter and 2.0–3.0 cm long (Figure 11.4). The 'bullets' are arranged in series along the sidewall tool and attached to it by retainer wires. The tool is run to total depth, depth-calibrated with a gamma ray tool on the gun, and then pulled up the hole. The sampling points are decided in advance and are based on an inspection of the logs already run. When a sampling point is reached, the sidewall tool is stopped exactly at the depth chosen and a 'bullet' is fired. A small directional charge shoots the hollow steel sidewall bullet into the formation wall which it penetrates by force. As the tool is moved upwards to the next location, the retaining wires pull the bullet out of the formation. The sample that the sidewall gun recovers is, as indicated, about 1.8 cm in diameter and up to 3 cm long. This sample is a reliable indicator of lithology (depending on the accuracy of the depth calibration), but because of the sampling method the rock is frequently

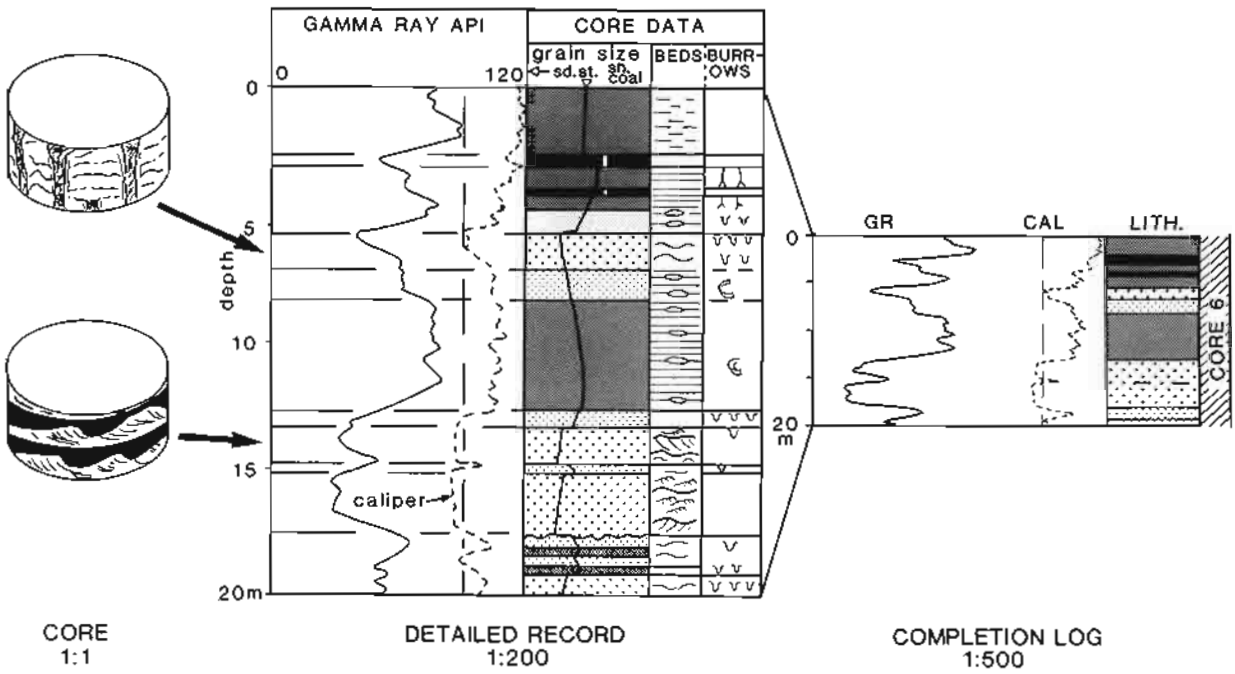


**Figure 11.3** Record of cores cut while drilling. The natural detail of a core is 'generalized' on the sedimentological log at 1:200 scale. The sedimentological detail is generalized to lithology only at the 1:500 scale.

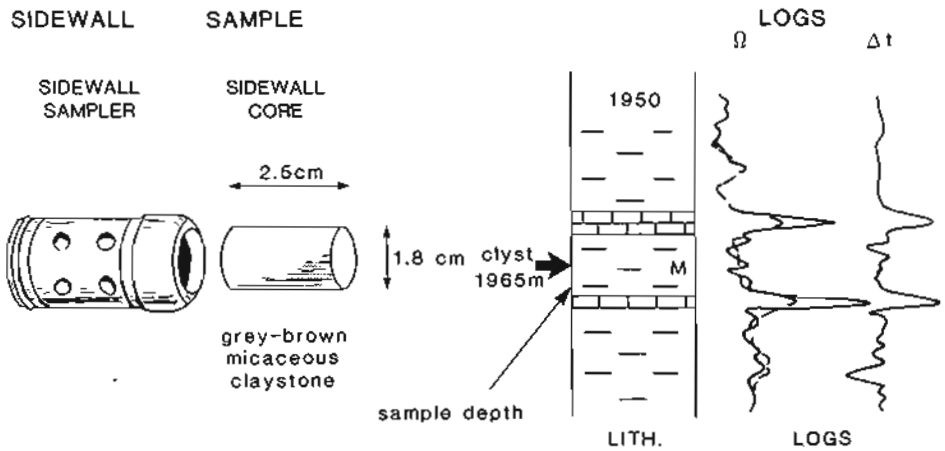


**Figure 11.4** Sidewall core sample. Schematic illustration of a sidewall sampler, sidewall core and its record on a lithological log.

shattered, so that the petrological characteristics are destroyed. Porosity measurements, for example, should not be made on these cores, as the grains are usually shattered. A tool does exist which actually drills out the sidewall sample downhole. It can be effective in hard formations and presumably gives reasonable porosity measurements, but is not frequently used.

Sidewall coring as a method of lithology sampling should be used essentially for verification. As the sample is so small, interpretation problems can arise, and sidewall core results should be used with care. In sands with shale laminae, for example, a sidewall may fall in a shale lamina and it will not be representative of the zone as a whole. For this reason, in reservoirs, a closely-set series of samples is taken. The obvious advantage of a sidewall core is that its depth is known and it can be taken in a specific, chosen lithology.

## 11.4 Lithology interpretation from wireline logs – manual method

The manual interpretation of lithology from well logs should be undertaken only using all the logs registered. Using digital log records, all the runs from a well can be re-plotted by computer to give one composite plot (Figure 11.5). This is an essential document. The final lithological interpretation may appear on this composite plot or, to avoid over-cluttering, may be transferred to a document with only the logs usually used for correlation. This is often the gamma-ray (or SP) and a resistivity log, or the gamma ray and a sonic log (Figure 11.9). The original lithological interpretation, however, must be made on the composite document showing all the logs.

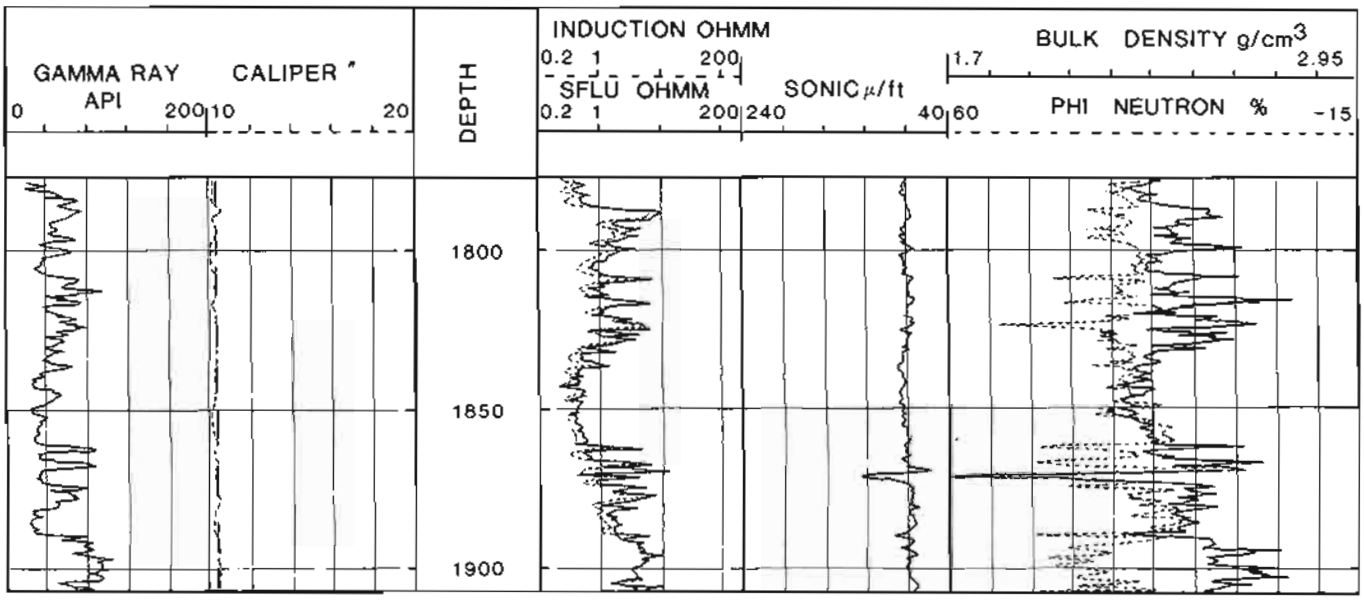


**Figure 11.5** Well-log composite. All logs run over the same interval are replotted together. The composite forms the basic document for a manual interpretation of lithology.

*Horizontal routine*

There are no simple rules for the quick manual interpretation of lithology from logs – if there were, this account would be superfluous. This book outlines the capabilities and characteristics of each of the openhole tools. To interpret lithology, these capabilities and characteristics must be known and used. A systematic approach is best. Thus, the gross lithology is suggested by the mud log, this can then be corroborated and compared at the same depth, horizontally, to a simple log such as the gamma ray or the SP (Figure 11.6,2). The interpretation is then continued, again horizontally, through the other logs – resistivity, sonic and density-neutron. If all corroborate the same interpretation, the lithology can be noted and then compared to sidewall cores or other samples (Figure 11.6,*3*). If the lithology is not corroborated, then there must be a 'feedback' from one log to the next. The first aspect to check is that of log quality. The hole may be very caved, one or more of the logs may be badly recorded, and hence the readings are anomalous. These aspects are considered in the chapters on the individual tools. However, the anomaly may be within the lithology itself.

For example, in a sand-shale sequence, there may be 40% sand and 60% shale marked on the mud log. The gamma ray log may read persistently high, so that only shale is suspected. The resistivity log and the sonic log are not diagnostic, but the density-neutron combination shows that it is either sandstone, limestone or dolomite: sandstone is indicated from the mud log. The sandstones are then marked on the lithology log and compared to the mud log or sidewall samples. A check with the SP shows that the neutron-density indicated sand intervals correspond to permeable zones, and that in turn these have mud-cake indicated by the caliper. The anomalous log, therefore, is the gamma-ray. From the interpretation it can be concluded that the sandstones have a high gamma ray count because of included feldspars, micas or other non-shale radioactive elements. The manual interpretation should find a compatible explanation for the reactions of all the logs.

*Vertical routine*

Although the horizontal routine is the basis for any lithological interpretation, individual logs should also be examined vertically for trends, baselines or, absolute values. For the gamma ray log, for instance, and also the SP, a shale baseline can be drawn but also a minimum, clean sand? limestone? etc., line for the gamma ray and a maximum deflection (SSP) for the SP – (*see* Chapter 6 for the gamma ray and Chapter 5 for the SP) (Figure 11.7).

Instead of a line, colour may be used. The caliper may be coloured to give caves and mud-cake zones. The density-neutron combination, if the logs are plotted on compatible scales (Chapter 10), can be coloured to underline curve separations (Figure 11.7). The latter is an excellent lithology indicator, as has been described in Chapters 9 and 10. Thus, a certain amount of preparation of the composite plot in the vertical sense can aid in the horizontal routines.

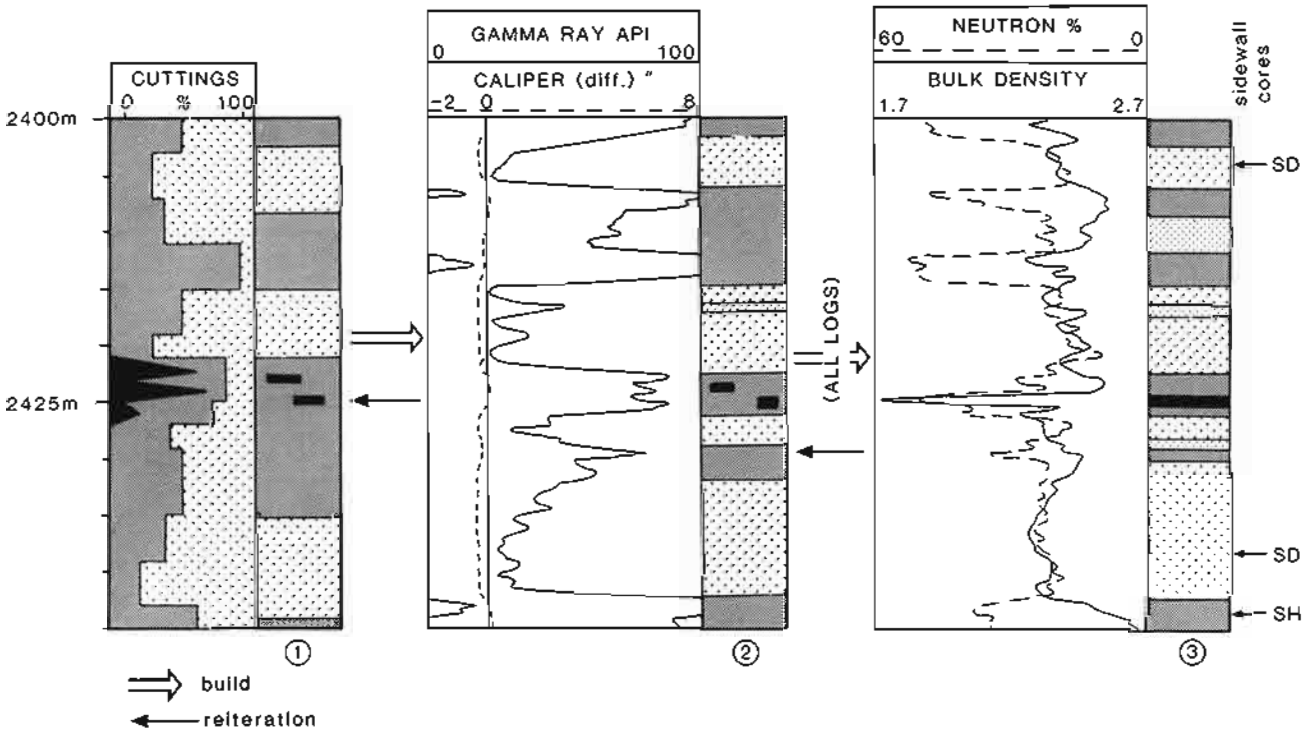


**Figure 11.6** Horizontal routine, manual method. The stages for building up lithology: 1, rig data; 2, simple wireline log; 3, all logs and well samples (only neutron-density shown). The lithology is built up from 1 to 2 to 3, but with iteration. Note the increasing detail and precision.

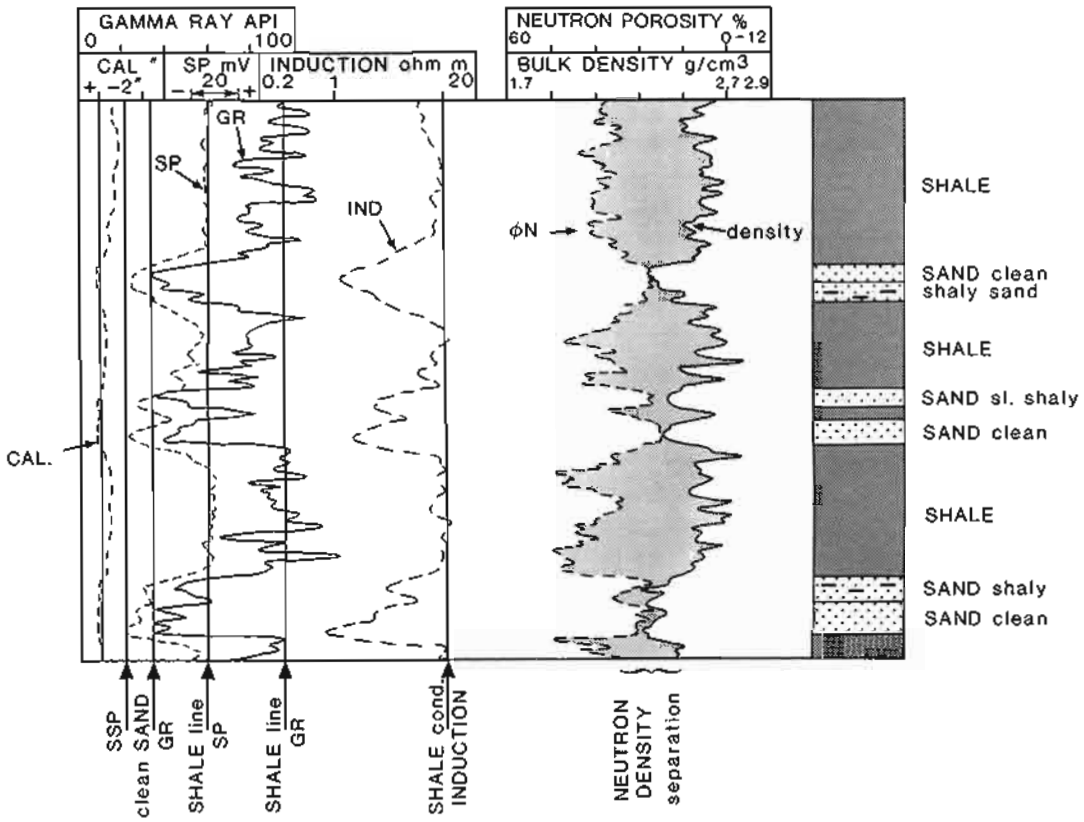


**Figure 11.7** Vertical routine, manual method. Base lines and curve separations are used for the vertical analysis in this sand-shale sequence.

### *Absolute values and lithology*

For some of the more difficult, uncommon lithologies and for beds with very high or very low readings, absolute value tables can be useful. For example, evaporites are generally pure enough in the subsurface to have distinct densities and velocities – this is certainly the case with salt (Chapters 8, 9). Abrupt peaks, which may be important in stratigraphical interpretations or diagnostic of a particular interval, are often best interpreted using absolute-value tables. Coals, for example, will be distinct on logs, as will be pyrite and other mineralizations (cf. Figure 9.18).

Table 11.1 gives a résumé of some of the more useful absolute log values for lithology interpretation. Tables in the individual chapters should also be consulted.

### *Bed boundaries*

Bed boundaries should be drawn concisely. Moreover, the correct log should be chosen to position a limit. The best geophysical logs for bed boundary definition are those with a moderate depth of investigation (Chapter 2), in general the SFL (Chapter 7) and density logs (Chapter 9). The shoulder, where a log is responding to two different lithologies simultaneously (Chapter 2), is generally broader in logs with greater depth of investigation but thinner in shallow investigating logs (Figure 11.8). When mud cake is present, an accurate limit may be taken from the caliper (Chapter 4) because it gives a mechanical response and has no shoulder effects (Figure 11.8).

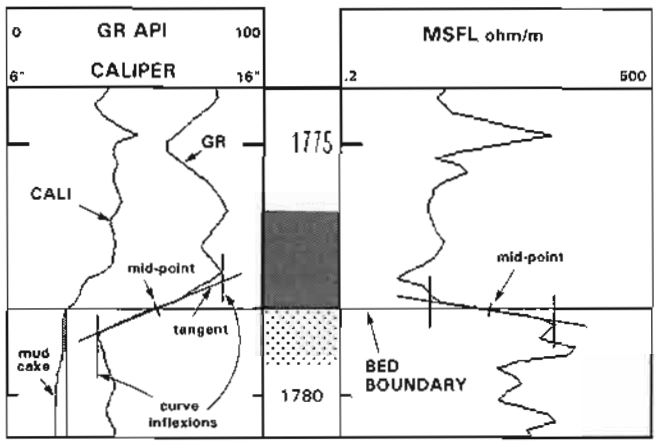


**Figure 11.8** Positioning a bed boundary. The mid-point of the tangent to the log curve between inflection points (i.e. the shoulder interval) is taken. Note this is thinner on the MSFL compared to the gamma ray log, but the mid-point is the same. The caliper, being mechanical, shows an instantaneous response, in this case to mud cake limit.

As a general rule, a bed boundary should be drawn in the mid-point of the tangent to a shoulder (Figure 11.8). This may not always be the real position as anisotropy affects log responses (Chapter 2), but it is an identifiable method which can be applied consistently and corrected subsequently if necessary.

**Table 11.1** Logging-tool response values. All values are shown so that they cover the ranges found in the various sources, i.e. none of the sources has values outside those listed. From Serra (1972, 1979), Dresser Atlas (1983), Gearhart (1983), Schlumberger (1985, 1989a).

| | Material | Resistivity (ohm $m^2/m$) | Gamma ray API[1] | Δtma (μs/ft)[2] | Density log [4] ($g/cm^3$) (ma) | Neutron porosity units[3] |
|---|---|---|---|---|---|---|
| Common lithologies[6] | Sandstones | up to 1000 | 18–160 | 53–100 | 2.59–2.84 | 0–45 |
| | Limestones | $80–6 \times 10^3$ | 18–100 | 47.6–53 | 2.66–2.74 | 0–30 |
| | Dolomites | $1–7 \times 10^3$ | 12–100 | 38.5–45 | 2.8–2.99 | 0–30 |
| | Shales | 0.5–1000 | 24–1000 | 60–170 | 2.65–2.7 | 25–75 |
| Matrix minerals | Quartz | $10^4–10^{12}$ | 0 | 51.2–56 | 2.64–2.66 | –2 |
| | Calcite | $10^7–10^{12}$ | 0 | 45.5–49 | 2.71 | –1 |
| | Dolomite | $1–7 \times 10^3$ | 0 | 38.5–45 | 2.85–2.88 | 1 |
| Clay minerals | Illite | | 250–300 | | 2.52–3.0 | 30 |
| | Chlorite | | 180–250 | | 2.6–3.22 | 52 |
| | Kaolinite | | 80–130 | | 2.4–2.69 | 37 |
| | Smectite | | 150–200 | | 2.0–3.0 | 44 |
| Micas | Glauconite | | 75–90 | | 2.2–2.8 | 38 |
| | Muscovite | $10^{11}–10^{12}$ | 140–270 | 49 | 2.76–3.1 | 20 |
| | Biotite | $10^{14}–10^{15}$ | 90–275 | 50.8–51 | 2.65–3.1 | 21 |
| Fsp | Microline | | 220–280 | 45 | 2.53–2.57 | –3 |
| | Orthoclase | | 220–280 | 69 | 2.52–2.63 | –3 |
| Coals | Anthracite | $10^{-3}–5$ | 0 | 90–120 | 1.32–180 | 38 |
| | Bituminous coal | $10–10^6$ | 0-18 | 100–140 | 1.15–1.7 | 60 |
| | Lignite | $4 \times 10^3$ | 6–24 | 140–180 | 0.5–1.5 | 52 |
| Fluids / Gas | Gas (av.) | α | 0 | | .000886 | |
| | Methane | α | 0 | 626 | .00076 | |
| | Oil (40° API) | $10^9–10^{16}$ | 0.12–0.40 | 238 | .85–.97 | 60 |
| | Water (80°F) | | | | | |
| | pure | α | 0 | 189–207 | 1.00 | 100 |
| | salt (33,000 ppm) | 0.031 (var) | 0 | 180 | 1.19 | 60 |
| Metallic minerals | Pyrite | $10^{-1}–10^{-4}$ | | 39.2–39 | 4.8–5.17 | –3 |
| | Siderite | $10^4–1000$ | 0 | 47 | 3.0–3.89 | 12 |
| Evaporites | Halite | $<10^4–10^{14}$ | 0 | 66.7–67 | 2.03–2.08 | –3 |
| | Anhydrite | $10^4–10^{10}$ | 0–12 | 50 | 2.89–3.05 | –2 |
| | Gypsum | 1000 | 0 | 52–53 | 2.33–2.4 | 60 |
| | Sylvite | $10^{14}–10^{15}$ | 500 | 74 | 1.86–1.99 | –3 |
| | Polyhalite | | 200 | 57.5–58 | 2.79 | 25 |
| Crystalline rocks | Basalt | $8 \times 10^2–10^5$ | 12–24 | 45–57.5[5] | 2.7–3.2 | |
| | Granite | $10^6$ | 24–96 | 46.8–53.5 | 2.52–2.8 | |
| | Gneiss | $10^2–10^4$ | 24–48 | 48.8–51.6 | 2.6–3.04 | |

(1) No hole conditions specified: will therefore vary.
(2) Values for the matrix material, compressional wave.
(3) For the CNL tool of Schlumberger
Fsp = Feldspars ma = matrix
(4) Calibrated
(5) Pressure 1 kbar.
(6) All values variable.

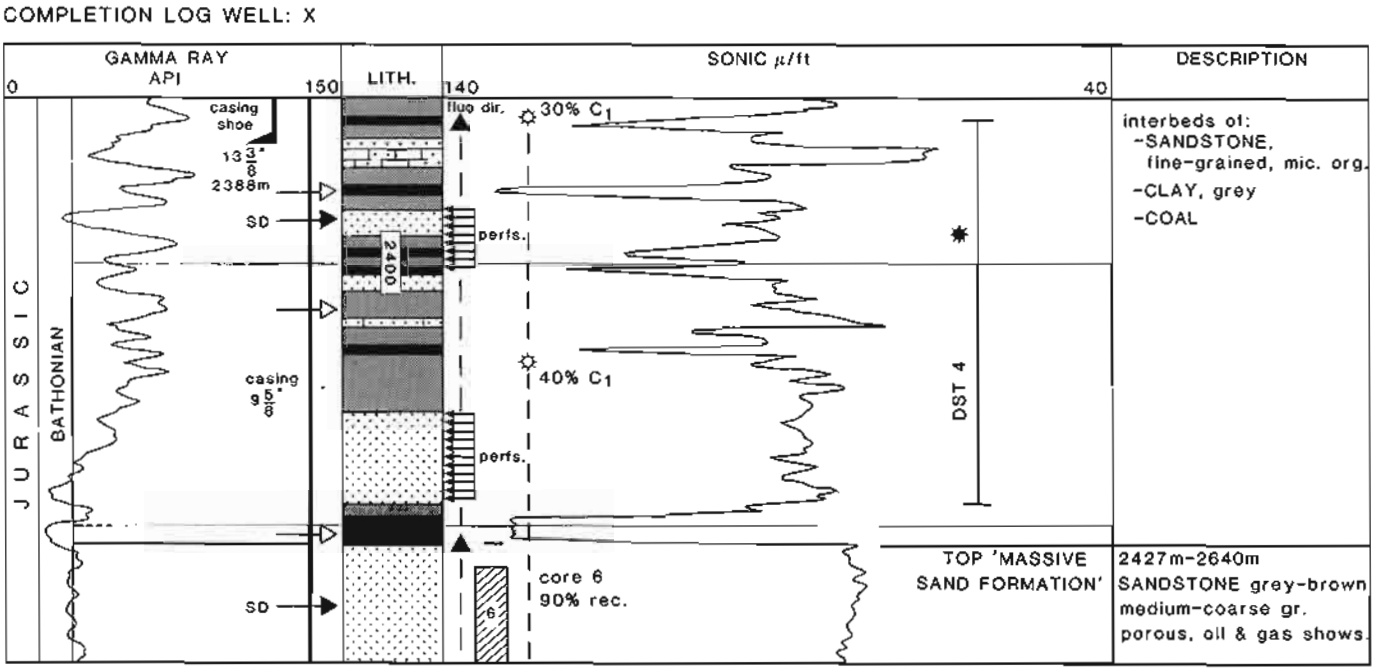


**Figure 11.9** The completion log. An example of the log with interpreted lithology, stratigraphy, hydrocarbon shows, tests and drill data. It is the geologist's 'basic record' of a well. The lithology comes from an interpretation of the log composite plot, cores and drill data.

A bed boundary will inevitably be represented on an interpreted log by a line and hence appear as sharp. It may or may not be sharp in reality and the interpretation is a simplification. However, this is justified since any significant change in log parameters is caused by a significant change in formation characteristics which, at log plot scales, is effectively sharp.

***Presentation***

The final lithological interpretation should be clear and concise. Accepted and stylized symbols for lithology and bed boundaries should be used (*see also* Chapter 14). Inevitably, the interpretation will lose some of the details seen on the well logs. Nonetheless, it is the interpreter who is the last to have all the data for the interpretation at his disposal, and who must decide the level of detail necessary. The resultant lithology should not be over-cluttered. It is this interpretation which will be used for the Well Completion Log, the document used to summarize drilling and geological data when a well is completed (variously called Final Log, Completion Log, Composite Log etc.) (Figure 11.9). The interpretation will also be used as a database for stratigraphy, correlation and for making small scale, résumé logs. Too much detail is a disadvantage. The scheme followed through this book is an illustration of the use of simplified symbols for lithology.

## 11.5 Computer aids to lithology interpretation

A well log curve represents a series of quantitative values, each value derived from the formation. The formation, and hence the lithology, can be quantified. However, for quantification to be an aid to, or the tool for interpretation there must be a *grouping*. That is, a particular set of values must be shown to represent a particular lithology. The lithology will be defined numerically, rather than by its subjective appearance to the geologist through cores and cuttings.

This quantification may be made at several levels of sophistication: one-log, two-log or multi-log. The most sophisticated multi-log quantifications can give an entirely computer-derived interpretation. Over the years the 'computerization' of lithology, lithology at the push of a button, has become somewhat of a 'Holy Grail': the objective is clear but does not exist in reality.

***Histograms – one-log quantifications***

The simplest way of grouping well-log values is by using a histogram, where the log value is plotted against frequency (Figure 11.10). The histogram has various uses. It can be used to define populations or average values. For example, the 'shale' and 'sand' values of a gamma ray log may be presented in this manner (Figure 11.10). A second example shows a gamma ray histogram in a series of volcanic rocks with values forming distinct populations (Sanyal *et al.*, 1980) (Figure 11.11). Used in this way, the histogram helps to define the log limits of lithology and average log values (Walters, 1968).

A second use is in the normalization of particular logs. This is done by selecting a consistent stratigraphic interval and comparing the log responses by comparing histograms of the log values (Figure 11.12) (Kowalchuk *et al.*, 1974). This is done as much for petrophysical as

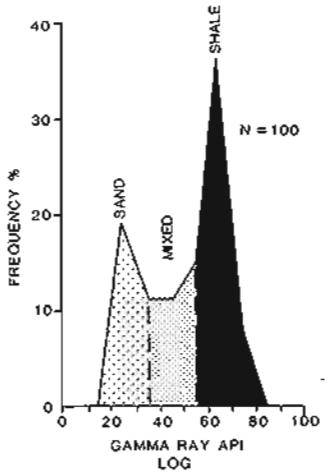


**Figure 11.10** Histogram of log values. This histogram is of gamma ray values over 100m of formation. The sand and shale populations are indicated. Between them is the zone of shaly sands and sandy shales.

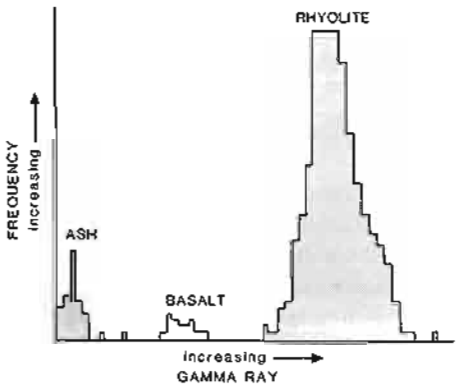


**Figure 11.11** Histograms of gamma ray log values. Gamma ray values from a volcanic sequence showing distinct populations for various lithologies. (Re-drawn from Sanyal *et al.*, 1980).

for geological reasons. In this same manner, histograms of log values may be compared to histograms of laboratory values when the same character is being measured (*see* Chapter 9). In the petrophysical usage, logs and laboratory values are made consistent for reservoir calculations. In the geological usage, slight lithological changes may indicate facies trends (*see* Chapter 14).

Finally, histograms have been used to make stratigraphic correlations when curve comparisons were inconclusive (Walters, 1968). The method is difficult to apply, but does bring out the idea that a formation can have a certain set of data ranges which are stratigraphically or lithologically diagnostic.

### *Cross-plots – two-log quantification*

When any two values are cross-plotted, the resulting series of points may be used either to define the relationship between the two variables, or to define fields, using both $x$ and $y$ axis values, giving the upper and lower limits of both variables.

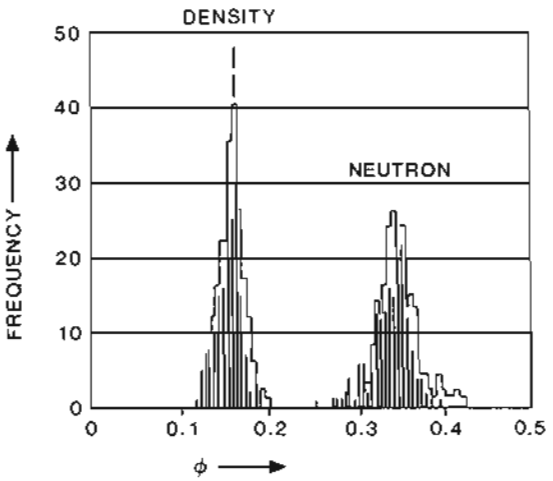


**Figure 11.12** Comparison to a master histogram. Neutron and density log value histograms of one well compared to master histograms (continuous line) of six wells from the First White Speckled Shale, Upper Cretaceous, Alberta, Canada. (Re-drawn from Kowalchuk *et al.*, 1974).

Both the above outputs are used in cross-plotting well logs.

Three types of well log cross-plot exist:

1. Cross-plots of compatible logs, that is those measuring the same parameter, for example porosity logs;
2. Cross-plots of incompatible logs, for example a plot of gamma ray v. neutron values – the logs do not measure the same parameter;
3. Cross-plots of laboratory or sample values against log values, for example porosity core values against neutron porosity values.

### *Cross-plotting compatible logs*

Typical and illustrative of this type is the neutron-density cross-plot: the plot of neutron porosity values against density porosity values. The method has been explained previously (*see* Chapter 10, Neutron-density combination). It was shown that cross-plotting neutron and density values can be used to identify pure matrix and/or the related porosity. This is impossible using only the value from one of the logs. For example, a neutron log value of 25% may be a dolomite with 17% porosity, a limestone with 25% porosity or a sandstone with 29% porosity (Figure 10.26), but when associated with a density of 2.28 g/cm$^3$ it has a unique attribution, a limestone with 25% porosity.

When there are only two variables, such as porosity and one matrix type (lithology) and no hydrocarbons, the neutron-density cross-plot allows an automatic identification of lithology (actually matrix density). This is done essentially by applying algebraic solutions to cross-plot type datasets (Doveton, 1986). However, when there is a third variable, a second type of matrix or more usually shale, there are no longer unique solutions and new end-

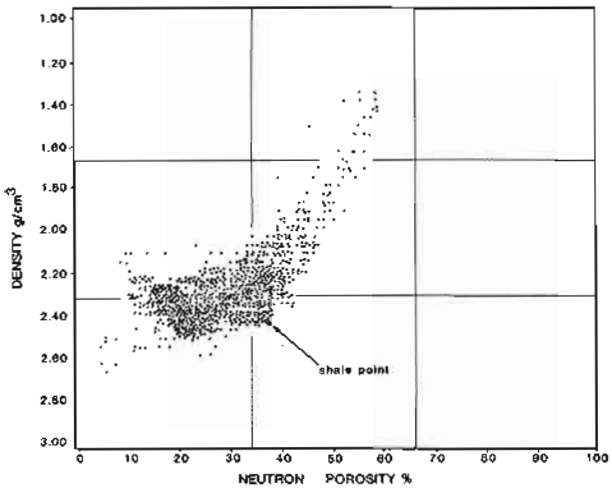


**Figure 11.13** Shale point defined on a neutron-density cross-plot. Values from 200m of a sand- shale formation. Note the arbitrary choice of one 'point' to represent shale.

member values must be defined. For example, to find a solution for any point when shale is present, a shale end-member with density and neutron values must be defined. Typically, this 'shale point' is defined empirically. A great many lithologically unidentified points are plotted and the 'shale point' is chosen to correspond to the extreme value but within the supposed shale field (Figure 11.13). Once the 'shale point' is defined, the cross-plot can be divided into a compositional triangle, the end-members being shale 100% (shale point), porosity 100% (fluid point, i.e. neutron porosity 100%, bulk density 1.0g/cm$^3$) and matrix 100% (matrix point, i.e. for limestone, neutron porosity 0%, bulk density 2.7 g/cm$^3$). Any point on the plot now has a precise value of the three variables.

This 'shale point' cross-plot has many drawbacks. Firstly, only one matrix can be considered at a time. A zone will be interpreted as only shaly sandstone or only shaly limestone – never both. But more importantly, it mixes definable with undefinable values. Shale is inevitably very variable, and the shale point therefore very imprecise (Figure 11.13) yet the matrix and liquid points are both quite precise (Doveton, 1994). This mixing of precise and imprecise is a general criticism of most cross-plot use.

A more realistic approach from a geological point of view is to define fields of values on this plot in which a particular lithology is likely to be plotted. The approach is empirical and the log limits of each lithological field will vary from well to well, and even within one well with depth (Figure 11.14). This is best achieved today by using software (i.e. TerraStation) which allows the interactive exploration between logs and their cross-plot, both of which are displayed simultaneously on the screen. That is, intervals selected on the log traces may be inter-actively matched to points on the cross-plot (i.e. calcareous shale, Figure 11.15) or a set of points on the cross-plot identified in their position on the log traces (i.e. gas sand, Figure 11.15). Core data may be integrated. This approach allows for a rigorous graphical use of cross-plots and an effectively quantitative identification of lithology. An extremely useful tool.

A sophistication of the cross-plot method of lithological quantification is to cross-plot cross-plots. This is the basis of the Schlumberger *M–N* plot (Burke *et al.*, 1969).

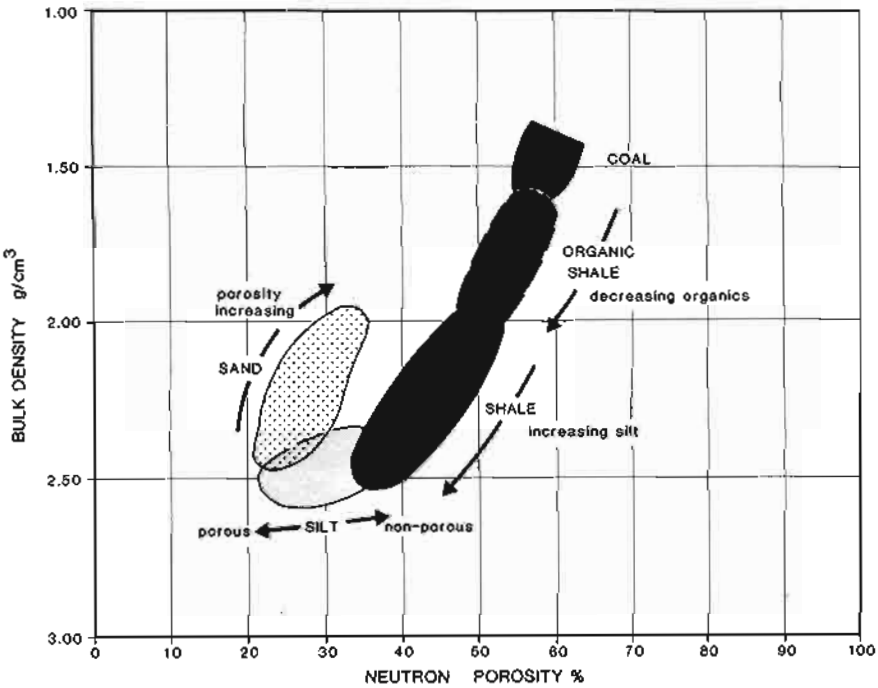


**Figure 11.14** Lithological fields defined on a neutron-density cross-plot. Based on the values from a 500m interval in one well.

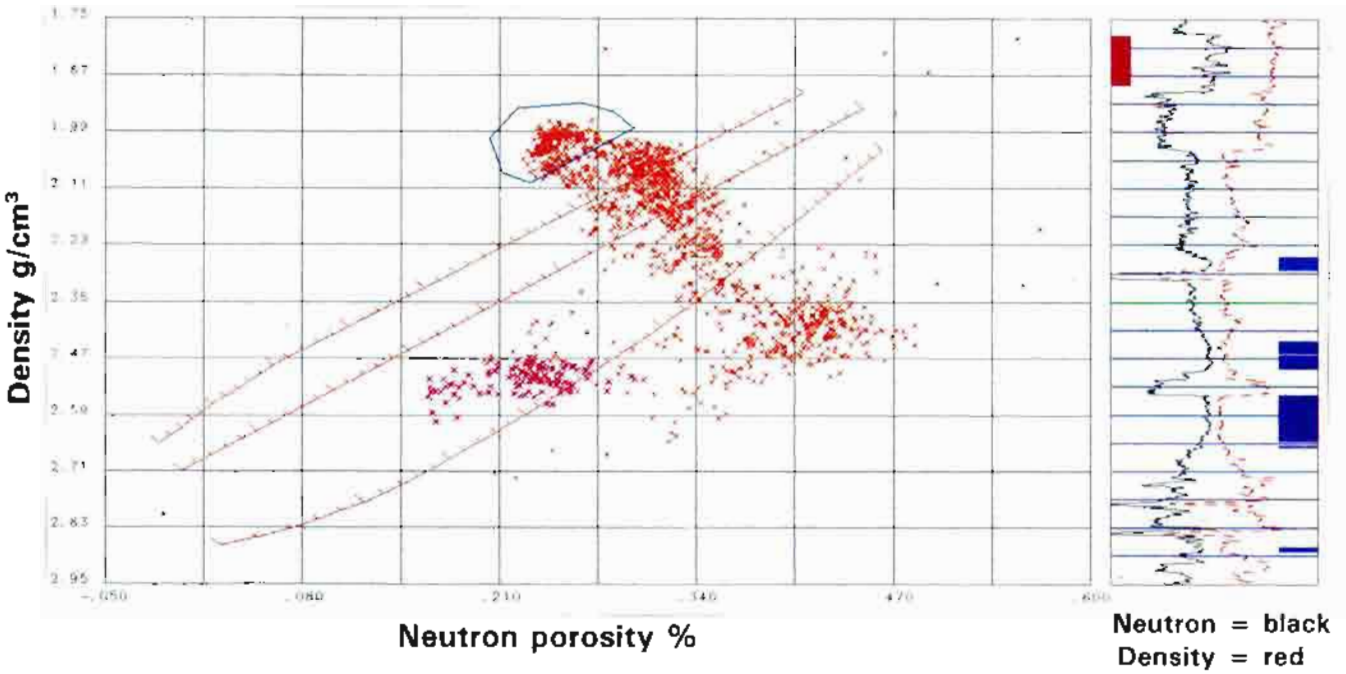


**Figure 11.15** Interactive investigation of a neutron-density cross-plot in order to define lithology empirically but quantitatively.
1. Magenta: interval interactively selected on the logs (bar on left margin of log track), plots as magenta coloured points on the cross-plot. The lithology is calcareous shale.
2. Blue: points in the area outlined on the cross-plot come from the log intervals indicated by blue bars on the right-hand margin of the log track. The lithology is clean, porous sand (with gas). (TerraStation Software)

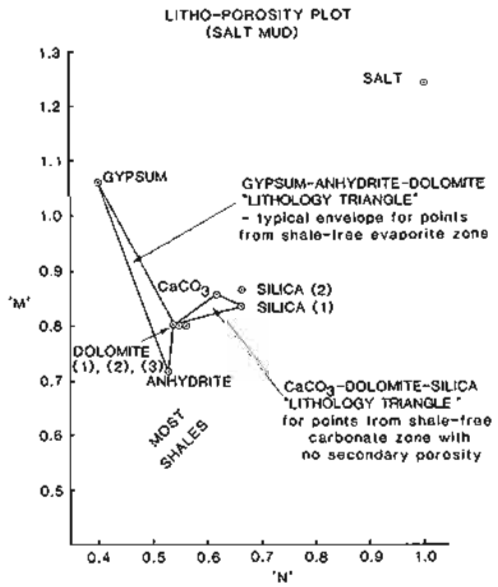


**Figure 11.16** Cross-plot of cross-plots. The M and N plot from Schlumberger. (From Burke *et al.*, 1969).

*N* is defined by a density-neutron cross-plot, *M* is defined by a density-sonic cross plot, and *M* is plotted against *N* (Figure 11.16). Theoretically, minerals and shale become separated into fields, and porosity is eliminated. However, the geological value of the logs is lost and a mineral identification more reliably done using mud log and simple cross-plots. In fact there is a tendency to rather obscure cross-plotting in the vain hope of finding a unique 'shale point' or 'mineral point'. These points rarely exist in nature. Rather than use complex numbers to cross-plot, the variables can be kept simple but the cross-plot itself made more sophisticated. For example, a third dimension can be added to produce the so called z-plot, such as a gamma ray added to a neutron-density plot. This third axis is best manipulated with the computer when, on screen, values may be indicated using a colour scale or when plotted, number values added to the points. Alternatively, the plot may be represented in three dimensions as some form of isometric presentation (Figure 11.17) or a 3-D surface projection made of an envelope of the points. These plots are generally visually impressive but not always easy to use.

### *Cross-plotting incompatible logs*

The cross-plotting of incompatible logs is usually done to quantify lithology. Incompatible logs are those which do not, in the first instance, measure or indicate the same parameter. Resistivity and gamma ray logs are incompatible, one gives the resistivity, the other natural radioactivity and, by inference, shale volume. However on cross-plotting, compatibility will become evident (there usually is compatibility). The resistivity logs, for instance, will show a consistent set of values in shales, as will the gamma ray log; this will become evident on cross-plotting (Figure 11.18). In fact in almost all cross-plots, it is rare not to find a consistent relationship of some sort (cf. Heslop, 1974).

Often empirical relationships become evident which otherwise would remain hidden.

Plotting the gamma ray log values against the neutron log values, for example (Figure 11.19) brings out several relationships (Rider *et al.*, 1979). There is a consistent, straight-line relationship between the two where both the gamma ray and the neutron logs are reacting to a shale-sandstone mixture. Each log is showing the volume of shale in its own way. Through this straight-line region, changes in porosity typically involve changes in shale content (possibly related to grain size changes). However, in the very clean sandstones there are variations in porosity which do not involve shale and the relationship between the two logs changes. In the example (Figure 11.19) the sands are gas filled and the changes in porosity affect the neutron considerably, diminishing it as porosity increases. On the gamma ray alone these changes are not seen: when the logs are plotted together the relationship becomes evident (cf. Heslop, 1974).

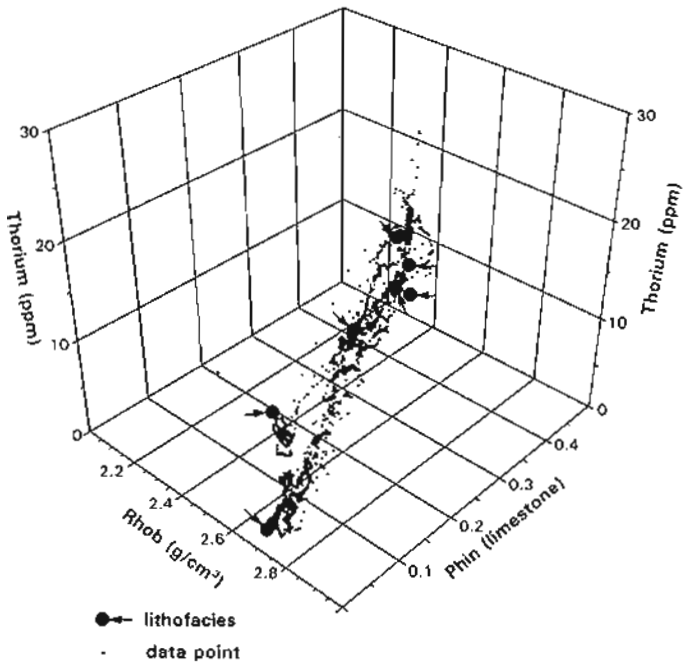


**Figure 11.17** 3D cross plot density-neutron-thorium, attempts to show the inter-relationships between the three components. Selected lithofacies points are indicated. (From Baldwin, 1990).

On this same plot (Figure 11.19), at higher gamma ray and neutron values there is also a relationship break. It is due to organic matter. Since the neutron tool reacts to all hydrogen present (Chapter 10), it reacts to the hydrogen combined with carbon in organic matter (a solid hydrocarbon). In the example, the organic matter is mostly coal and lignite grains with low radioactivity. Thus, while the gamma ray values diminish as the organic matter replaces the shale, the neutron values increase or remain high (Rider *et al.*, 1979).

This neutron-gamma ray plot, in fact, is very useful for analysing shale changes in general. Condensed sequences with a high uranium content (Chapter 7) for example, will fall outside the straight line field: the gamma ray will be affected (increasing) but the neutron log unaffected (or increasing). Textural and well as compositional differences can be brought out: the neutron log increasing in higher shale porosities, the gamma ray being insensitive. As suggested, plotting incompatible logs brings out relationships which are often geologically significant.

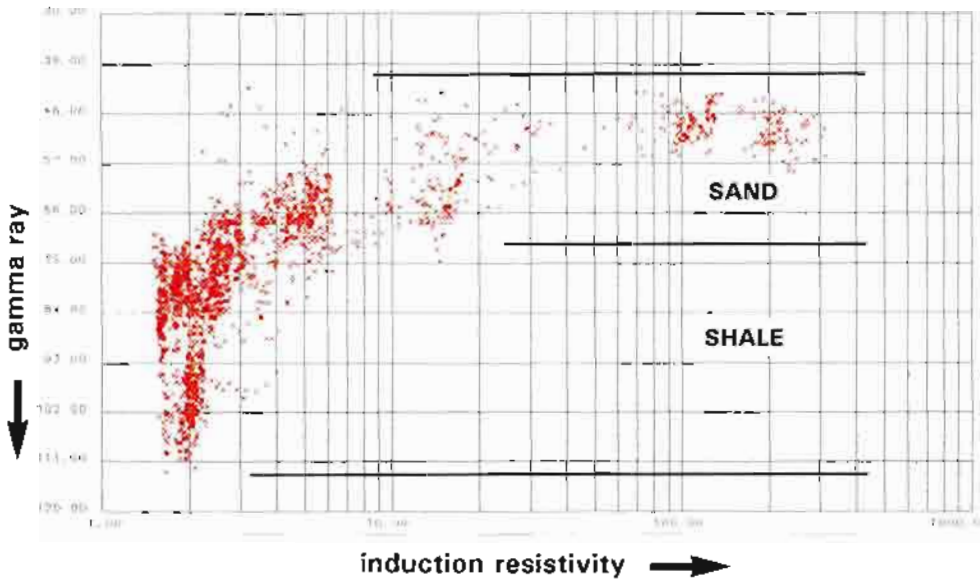


**Figure 11.18** Cross-plot of 'incompatible' logs. Gamma ray and resistivity values cross-plotted to define lithology fields. Shales are seen with gamma ray values ranging from 70–112 API but consistent resistivity values below 2.5 ohm/m. Sands show high resistivities (hydrocarbons) up to approximately 300 ohm/m and with low gamma ray values between 40–70 API. A clear change is seen on the cross-plot at 70 API, where the increase in resistivity indicates the beginning of effective porosity and change in pore fluids.

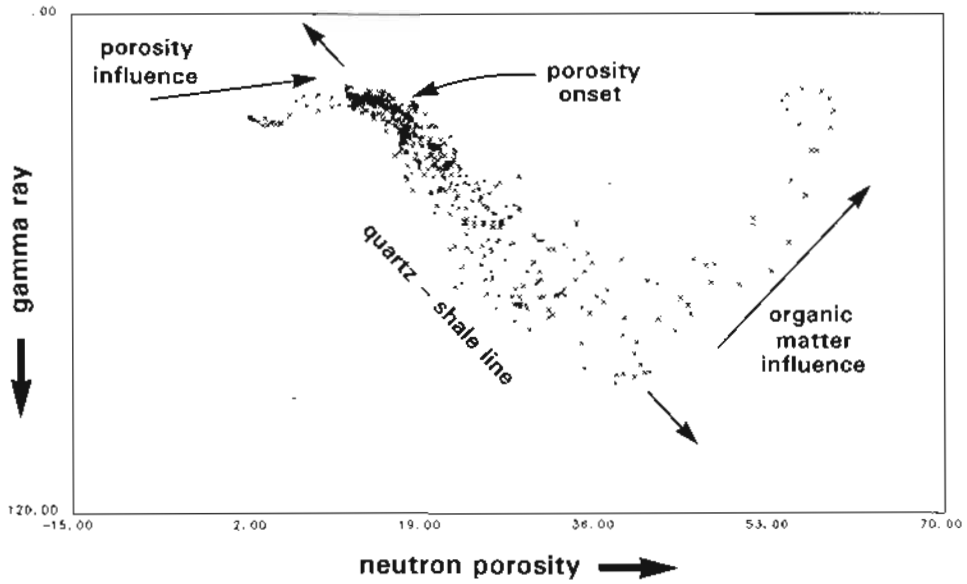


**Figure 11.19** Cross-plot of gamma ray against neutron porosity. A constant relationship is seen over a wide range of values when only quartz and shale are involved (quartz-shale line). Where porosity begins, an inflection is seen. Where organic matter becomes abundant, an opposite inflection is seen.

***Cross-plotting log values against sample values***

The first use of this technique was to verify log calculated values of porosity against those from the laboratory (Figure 11.20). This, obviously, can only be done over cored intervals. The cored zone is then used to calibrate the logs, and the normalized log values applied more confidently to zones without cores. The technique is essential to log interpretation. However, when it is applied it must always be remembered that measured values and log values are not *a priori* identical. Core porosities are measured in a small plug about 10 $cm^3$ in volume, porosity logs measure between 1000 $cm^3$ and 10,000 $cm^3$ of formation (i.e. up to over 1000 times the plug volume). Core porosities are measured under atmospheric conditions, log porosities under reservoir conditions, notably of pressure and temperature. A persistent difference between log and core porosities of 1 or 2% will often indicate a difference in physical conditions, rather than badly-calibrated logs (Dahlberg and Fitz, 1988).

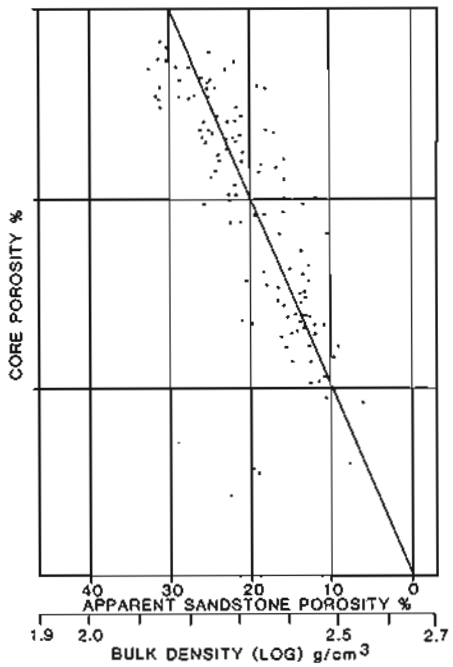


**Figure 11.20** Cross-plot of log values (density porosity) against sample values (core porosity). The plot shows the limits of accuracy to be expected from log values.

Sample calibration may also extend to lithologies. For example, the validity of the gamma ray log as a shale indicator can be checked against laboratory measurements of clay percentages (Heslop, 1975) (Figure 11.21). The amount of ash in a coal can be compared to its bulk density as measured by logs (Lavers and Smits, 1977). This technique of calibration for lithology is not used enough for geological purposes.

Cross-plotting log reading against laboratory value means that the depth position of the various points used is lost. This is a statistical comparison, which is the advantage of the method: it compares averages. In order to re-introduce individual depth readings, depth identified points from a core can be plotted on a cross-plot with log values. For example, in order to identify lithological fields on a neutron-density cross-plot, points with defined neutron-density co-ordinates and lithology defined from core, can be plotted and labelled on the cross-plot grid (cf Fig 11.14). This is easily done with the interactive software described above (cross-plotting compatible logs, Figure 11.15). This is a process once removed from plotting the laboratory values on a depth scale and comparing with the logs themselves.

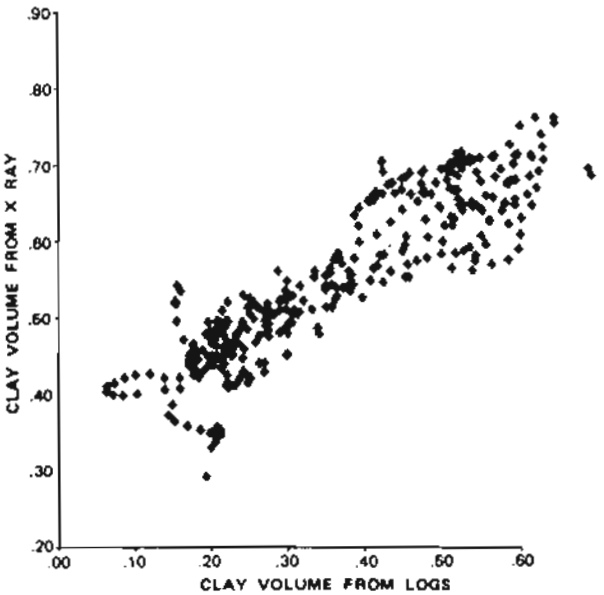


**Figure 11.21** Cross-plot of laboratory values (of clay volume) against log values (of clay volume). The plot is a partial verification of the log derivation of shale volume. (From Heslop, 1975).

## 11.6 Multi-log quantification of lithology

Two typical methods for the multi-log treatment of logs will be briefly described below. Many methods exist, so that mention here is only by way of illustration. The first method described is used essentially by the petrophysicist: it is designed to quantify hydrocarbon volume, and lithology is a secondary consideration. The second method is principally designed to indicate lithology.

***Petrophysical multi-log analysis***

On the way to quantifying oil volume, the petrophysicist must derive a lithology in order to isolate the rock effects on the logs as opposed to the effects of fluids, especially hydrocarbons.

Multi-log, petrophysical quantification for lithology begins with the numerical definition of all the variables; of the pure end-members of matrix, minerals, fluids and so on (*see below*). As discussed above (cross-plotting compatible logs) some end members are real, others fuzzy. Quartz (sandstone matrix) has relatively narrow properties in terms of log values and can be reasonably defined: shale has no such natural limits but none the less must be assigned fixed values. Difficulties obviously arise, but the interpretation methods can be designed with these in mind.

The mathematical process used to derive lithology as part of a petrophysical investigation, is essentially one of solving a number of linked, simultaneous equations, for unknown volumes of chosen minerals or matrices defined by pure, end member (hypothetical) log responses. That is, an 'inverse' method in which components are defined in advance. The methods used (i.e. Doveton, 1986; 1994) effectively imitate the graphical methods discussed previously (Figure 11.15). Pure end members (variables) of matrix, fluid etc. are defined for each log: to identify $n$ components (variables), $n$-1 logs are required, where $n$ is perhaps 3 or 4 and possibly up to 6. With pure end members such as limestone, dolomite and evaporites the method can work well as responses are generally linear. In the presence of shale, however, relationships are unpredictable and results are less satisfactory. Improvements can be made by user intervention and iteration. There is also the possibility of using several models simultaneously (Quirein *et al.*, 1986). However, perhaps it is best to use simple models in which user intervention can be more obviously applied (Marett and Kimminau, 1990). The output of these methods is always in volume per cent of the defined components such as clay, silt, sand and porosity: or clay, feldspar, mica, quartz and porosity. A log of this type is frequently referred to as a CPI (computer processed interpretation) (Figure 11.22).

This sort of output can be criticized from a geological point of view as being dependent on artificially-defined absolutes which have little relation to lithology in the usual sense. A sandstone is not defined by its quartz percentage: it has a compositional and textural definition. The output of these computer-defined 'lithologies' in percentage of constituents does not, therefore, represent geological lithologies.

***Statistical multi-log analysis***

An entirely different way to interpret for lithology is to use deductive statistical methods. The general approach is to combine all the log responses at one depth into a single, multi-dimensional set ($n$-dimensional space), and subject this to a statistical analysis, in fact to do classic multivariate analysis. Sets can be grouped into populations of numbers, which show some internal statistical similarity and can be statistically differentiated from other populations. The attempt then is to relate the statistically defined populations to particular lithologies or lithofacies. (The term 'electrofacies', has been used as a name for such statistically defined populations (i.e. Doveton, 1994), but in its original usage (Serra and Abbott, 1980), electrofacies was applied in a much broader sense and not purely in a mathematical one. The broader sense is used in this book – *see* Chapter 14. The qualifier 'statistical electrofacies' is used for the purely mathematical sense here.) A statistical electrofacies, then, is just numbers and to gain geological significance is assigned to, or shown to characterise, a particular lithology or lithofacies.

Such a statistical approach passes through several phases before the final result is achieved. First the data are formatted to allow for the use of statistics, next they are partitioned into the statistically definable populations

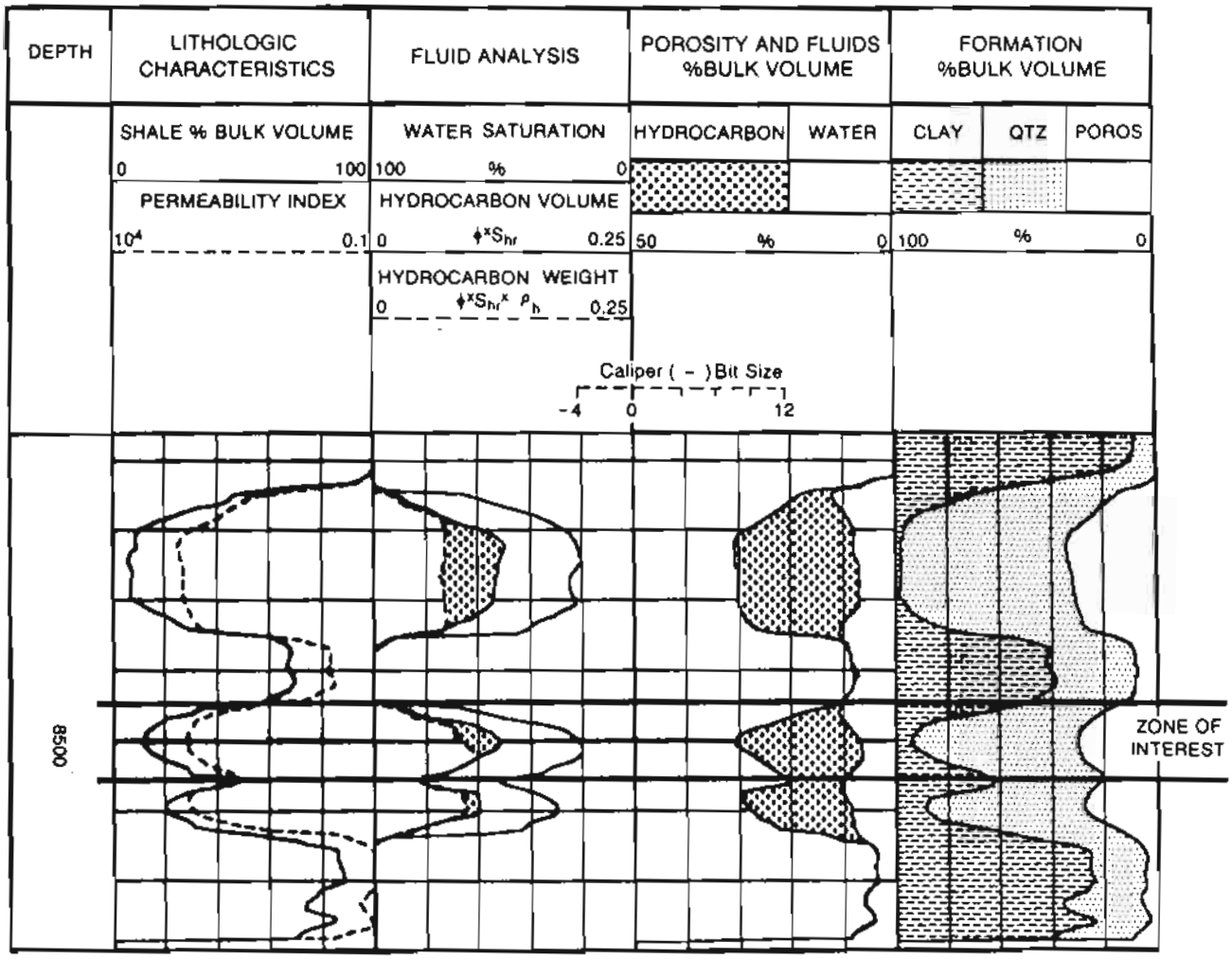


**Figure 11.22** Typical computer processed interpretation (CPI) output. The lithology is in volume % of end members. The log is mainly for hydrocarbon indication. (From Dresser Atlas, 1982).

and then, finally, each population is related to the external grouping of lithology (Anxionnaz *et al.*, 1990). The approach was well described by Serra and Abbott (1980) and recently reviewed by Doveton (1994). A brief description is given below.

Logs are first environmentally corrected and given consistent (15 cm) curve sampling rates. Log squaring or zoning (Serra and Abbott, 1980), is then applied to eliminate noise, diminish shoulder effects and in general diminish the spread of data and harmonise sensitivities so that a log such as the MSFL is made compatible with a log such as the gamma ray (Figure 11.23). A further harmonisation is necessary to give the logs numerically compatible scales. Neutron log values range from 0–80 while the resistivity values are from 0.1–2000. Re-scaling using the standard deviation of a log's data spread, reduces the variations to the same order.

Using the prepared database, the next stage is to apply a statistical grouping or clustering. The Schlumberger 'Faciolog' can be used to illustrate one approach (Wolff and Pelissier-Combescure, 1982). Prior to clustering, the edited data are re-scaled and reduced using principal component analysis. For log data, the first principal component axis of the dataset is in the direction of maximum variation, probably accounting for 80% of the variation. The second axis contains the next amount of variation and so on: all the axes are ordered. Principal component logs can be derived by projecting the normalised logs on the principal component axes (Figure 11.24). High order component variations are generally unimportant and are dropped. Clustering for faciolog is now applied using this reduced data and produces a series of small clusters or local modes and about 10 original data points have been reduced to one new one. However, the local modes are still too small to be interpretable in terms of lithology: there are perhaps 150 local modes but less than 20 statistical electrofacies required.

In order to decide on the level of statistical grouping, external data may now be consulted. For statistical electrofacies to have a geological meaning they must be calibrated to a lithology or lithofacies. The type of decisions required can be nicely illustrated by a dendrogram

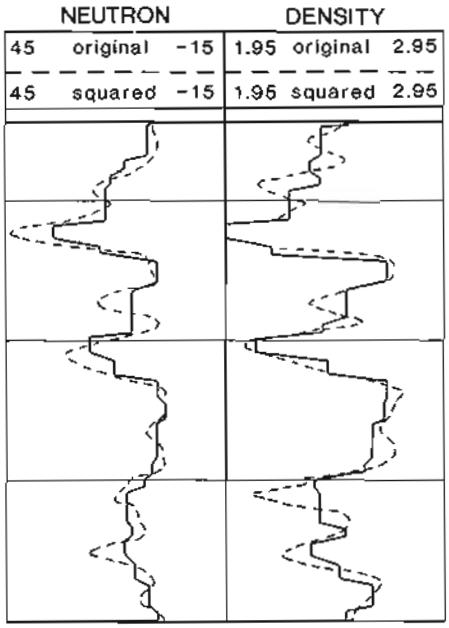


**Figure 11.23** Squared logs made from statistical clustering. The example shows the effect of plotting clustered values alongside the original values for a neutron log and a density log. (Re-drawn from Schlumberger, 1982).

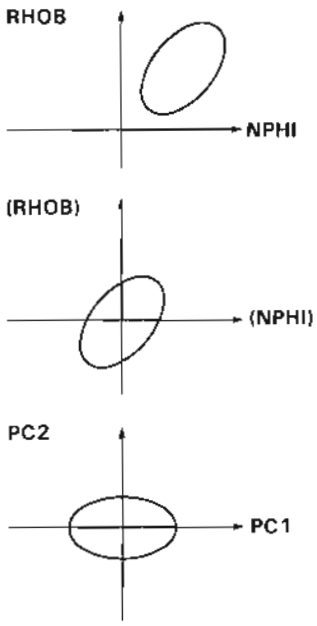


**Figure 11.24** Schematic representation of the derivation of principal component axes. PC1 = 1st principal component axis (the most important); PC2 = 2nd principal component axis (the next most important). There can be n axes.

(Moline *et al.*, 1992) (Figure 11.25). The dendrogram may be cut horizontally at any level to create more or less groups. Groups from the dendrogram may be compared to core data and the most appropriate grouping level chosen. The output can now be in terms of a lithology familiar to a geologist (Figure 11.26).

A number of clustering techniques have been applied to lithological log analysis. The problem is clearly one of multivariate analysis. Methods applied include gene typing (Griffiths and Bakke, 1988), a neural network approach (Baldwin *et al.*, 1990), dendrogram analysis (Moline *et al.*, 1992), and a kernel method of density probability estimation (Mwenifumbo, 1993). Knowledge based systems also try to solve the problems (Hoffman *et al.*, 1988). These groupings all attempt to produce statistical electrofacies as defined above. They should more properly be called geophysical lithofacies or electrolithofacies: they are of the same order as lithology or lithofacies, not facies *sensu stricto* (Figure 11.26). There is still a large distance between statistical electrofacies and facies as understood by the geologist.

The advantage of statistical methods is that natural variability is accounted for. The geological recognition of a lithology can then be reduced to the classification of a series of geophysical numbers: it is conceptually a simple operation (albeit complex mathematically). A geologist's lithology, formerly only a concept, becomes numbers, more easy to manipulate and more consistent.

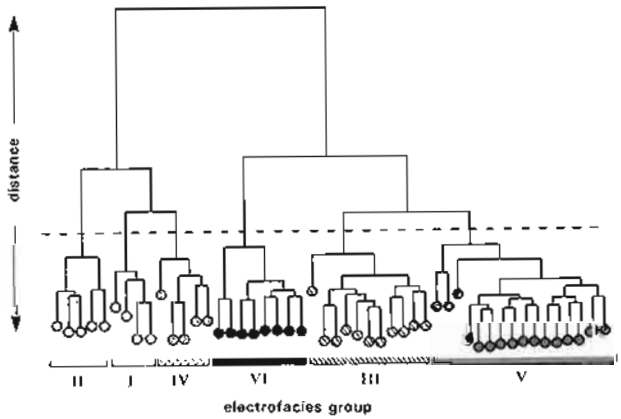


**Figure 11.25** Dendogram used to define electrofacies groupings. These groupings can change depending on the level (i.e. distance) of cut-off. (From Moline *et al.*, 1992).

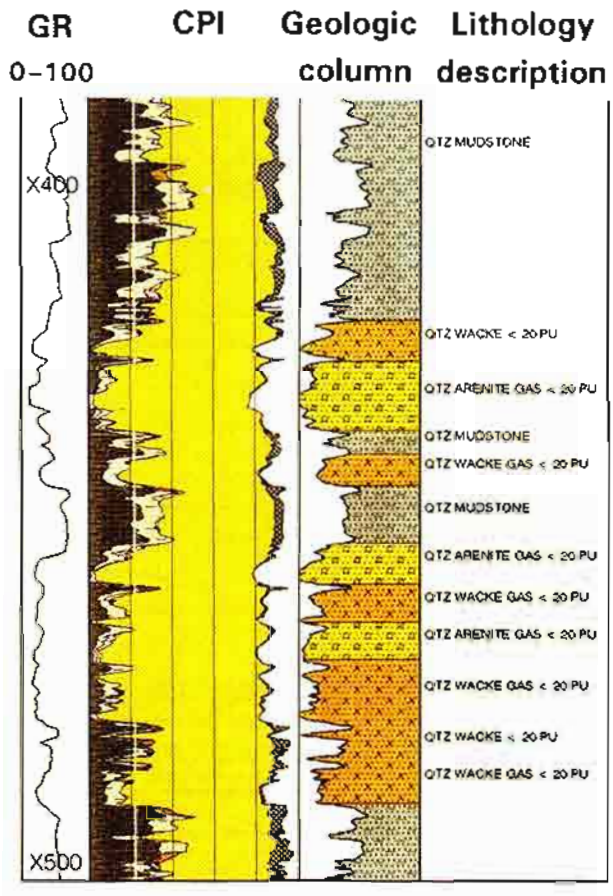


**Figure 11.26** Lithology derived from computer analysis. CPI (computer-processed interpretation) provides mineral, porosity and fluid volumes. The geologic column is more related to 'geological' lithology (modified from Darling *et al.*, 1991).

# 12
# THE DIPMETER

## 12.1 Generalities

*The log*

The dipmeter log provides a continuous record of formation dip and direction of dip or *azimuth. It comes from a two stage process: acquisition of the data followed by data processing. The tool acquires, typically, four microresistivity curves from orthogonal positions around the borehole: the first stage. By comparing the differences in depth between the curves across the borehole, the computer can provide a dip and an azimuth: the second stage (Figure 12.1).

Modern dipmeter tools have become very sophisticated: they consist not only of the logging sonde for the microresistivity curves, but also a positioning sonde so that tool orientation, inclination and speed are known, all essential to the computation of the dip and azimuth. Moreover, the dipmeter microresistivity curves are sampled 30 to 60 times more densely than ordinary logs (Figure 12.4).

Over the past few years, dipmeter processing has passed from being exclusively in the hands of the logging companies, to being available to all users. What previously required a mainframe or workstation can now be done satisfactorily on a personal computer, even a laptop. This has changed attitudes and practices: processing is now an interpretation tool. A tool, moreover, using interactive software.

*Azimuth is used to mean the direction, relative to true north, of dip or any other orientation measurement.

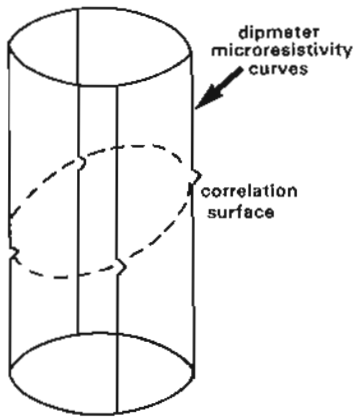


**Figure 12.1** The principle of the dipmeter. Detailed resistivity curves are measured from (typically) orthogonal positions around the borehole and then correlated to give a surface which has dip and azimuth. It is a two-stage process (from Cameron *et al.*, 1993).

*Principal uses*

Clearly, the principal use of the dipmeter is to provide dips! But there is more to the meaning of dip than is implied in the preceding sentence. The dipmeter provides data for two rather different domains: structural geology and sedimentary geology (Table 12.1). In structural geology it provides information on structural dip, unconformities, faults and folds. Structural dips from the dipmeter can be compared to dips on seismic sections or used in log correlation. In sedimentary geology, the dipmeter can provide facies information, bedform

**Table 12.1** Uses of the dipmeter log.

| Discipline | Feature | Comments |
|---|---|---|
| General | Hole position | gives continuous deviation and TVD |
| | Hole size and shape | gives shape with orientation |
| | Breakouts | derive stress field orientation |
| Sedimentary Geology | Sedimentary structure (bedform) orientation | from foresets, dunes, HCS, etc |
| | Palaeocurrent analysis | using statistical analysis |
| | Reservoir (sand-body) orientation | from compaction drapes, slumps etc |
| | Facies characterisation | thin bed analysis possible |
| Structural Geology | Structural dip | seismic overlays used |
| | Unconformities | vector analysis plots used |
| | Faults | stereographic analysis used |
| | Folds | graphic analysis used |
| | Fractures | (images now mostly used) |

orientation and palaeocurrent directions. Indeed the dipmeter is the only standard tool that can supply internal reservoir orientation information (image logs are not yet standard, Chapter 13).

Prior to 1967, a dipmeter tool could be expected to provide one dip and azimuth per 2 m. Between 1967 and 1984 this increased to 3–4 dips per metre: an eight-fold increase. But modern tools can provide 40 times more information than the original tools, that is up to 20 dips per metre: this means that there may be 20,000 individual dip points measured over 1000 m of logged open hole. This is a huge mass of data to interpret – and understandably discourages and confuses most geologists. Dip is a familiar geological concept and yet the data from the dipmeter are unfamiliar. Clearly, this is a fundamental problem that must be tackled.

***About this chapter***

In the past (and even now), too many expensive dipmeter logs have simply been put in a geologist's drawer and forgotten about. The high sampling rate of the raw dipmeter data has meant that in the past it was not integrated with the other open hole logs in computer software. Also, that it needs processing and that its presentation is unique, add more barriers. However, the dipmeter has and is still suffering from poor credibility, not because of tool design or reliability, or even processing – all excellent, but very poor interpretation.

Historically, dipmeter interpretation has been based on the recognition of dip patterns. Three patterns are standard: red = decreasing dip upwards, blue = increasing dip upwards and *green* = constant dip (Gilreath *et al.*, 1969). These patterns are given meaning: blue = foreset beds, red = channel fill, *green* = structural dip. The associations between the dip patterns and directional features have been expanded and enshrined since their original inception. The technique being that if a blue pattern or a red pattern can be identified, then an interpretation is assured. This methodology has been misrepresented over the years and has blocked creative thinking about the dipmeter. *It will not be mentioned again let alone used.*

In this chapter, a strong bias will be put on the author's own views on dipmeter interpretation. It will be shown how processing and interpretation interact and how outcrop models can (and must) help interpretation. Dipmeter logs have a great potential which is only even now being slowly realised.

Many of the ideas in the chapter owe a great deal to the work of colleagues.

## 12.2 Dipmeter tools

***Generalities***

As indicated, the dipmeter tool measures dip by comparing the displacements of microresistivity curves from opposing sides of the borehole wall (Figure 12.1). Typically four pads are used, but tools exist with 3, 4, and 6 pads (three being the minimum number of points to define a planar surface) (Table 12.2). Moreover, although a single electrode on each pad is usual, the SHDT of Schlumberger has two on each pad (Figure 12.5).

Since the electrodes of the dipmeter tools register resistivity or conductivity, it is necessary for the borehole mud to be water based, allowing an electrical contact between the tool and the formation. In oil based muds this is not possible, and specialist tools using induction principles are run (Table 12.2). Alternatively, in some cases, a compromise in oil based muds is to use a standard resistivity dipmeter tool with 'scratcher blades', upstanding blade-like electrodes attached to the pads to give a direct contact with the formation. The results using this configuration are variable.

***Tool mechanics***

The standard four arm dipmeter tool has four pads held at 90°, generally configured as two pairs, so that opposite pads move the same amount and the tool is automatically centred (Figure 12.2). The arms can be so engineered that as hole size varies, the pad pairs move in a plane normal to the tool axis but they generally move in a shallow arc

**Table 12.2** Dipmeter logging tools.

| Company | Tool | Names | Pads | Electrodes/pad | Comments |
|---|---|---|---|---|---|
| Schlumberger | HDT | High Resolution Dipmeter Tool | 4 | 1 | older tool |
| | SHDT | Stratigraphic High Resolution Dipmeter | 4 | 2 | 2.5mm samples |
| | OBDT | Oil Based Dipmeter Tool | 4 | 1 | oil base mud tool |
| Atlas Wireline | Diplog | Diplog | 4 | 1 | 5mm samples |
| | HDIP | Hexdip Log | 6 | 1 | independent arms |
| Halliburton | HEDT | High Resolution Dipmeter Tool | 4 | 1 | |
| | SED | Six Arm Dipmeter | 6 | 1 | independent arms |
| BPB | PSD | Precision Strata Dipmeter | 3–4 | 1 | 10.5 or 2mm |
| | MBD | MultiButton Dipmeter | 4 | 3 | samples |

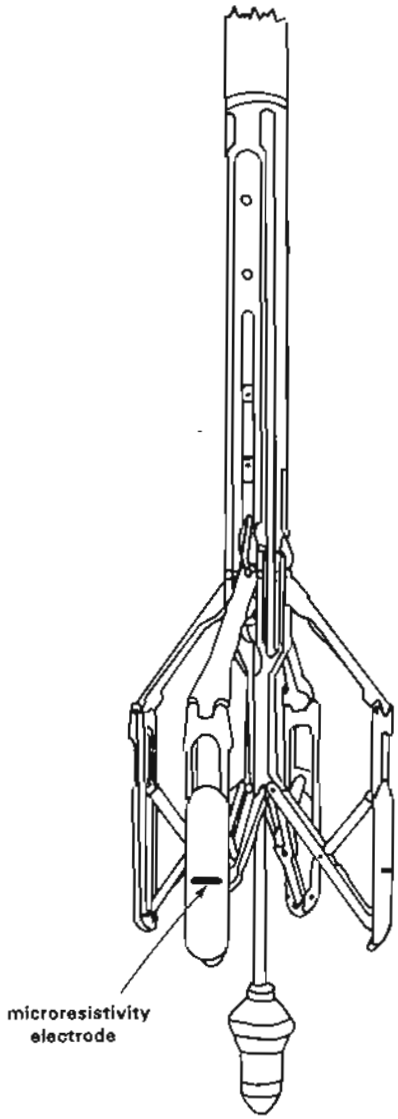


**Figure 12.2** A typical dipmeter tool: the HDT (high resolution dipmeter) of Schlumberger. The four arms are at 90° and acquire four, micro-resistivity curves (modified from Bell, 1990).

and in six arm dipmeters, each arm moves independently and also in an arc. The pads are held against the borehole wall hydraulically. In deviated boreholes this is a difficulty as the weight of the tool presses on the down-directed pad and the top pad 'floats' or becomes disconnected from the formation. The weight of the tool on the pads may be reduced using a flexi-joint and stand-offs (guards to keep the tool away from the borehole wall). Tools can function in holes from about 20" to 6" (50 cm–15 cm) in diameter but are best in holes in the 12"–8" (30 cm–20 cm) range.

***Resistivity curve characteristics***

A dipmeter tool measures a microresistivity curve (or curves) from each pad (Figure 12.3). The essential for these curves is to register small *variations* in resistivity or conductivity, and not absolute values. Consequently, a tool will typically use a 'floating zero'. The

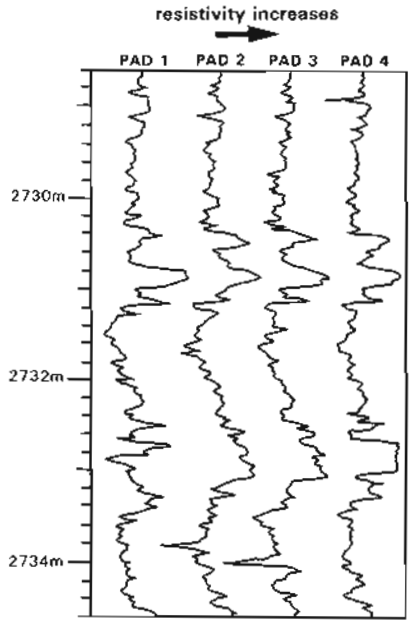


**Figure 12.3** Raw dipmeter data from a Western Atlas Diplog, sampled every 5mm (0.2").

Schlumberger SHDT dipmeter, for example, emits a current from the entire lower section of the tool (the Emex current). The pads themselves are conductive but only a small part of the overall current actually flows through the measuring button electrodes, the major part being used to focus the current from the buttons. Buttons, pads and sonde body are kept at the same potential, so that button *current* will vary with the conductivity of the formation in front of it. Since the Emex current is constantly varied, depending on the average formation resistivity, button resistivity (conductivity) variations are recorded in both generally high resistivity and low resistivity formations. For example, in both hydrocarbon and salt water zones (Figure 12.4). The dipmeter microresistivity curves do not, therefore, give a standard resistivity: this can only be calculated by accounting for the base current variations.

The dipmeter microresistivity curves are sampled very densely, every 5 mm (64 per foot) in the Western Atlas Diplog and at twice this rate, every 2.5 mm (0.1") in the Schlumberger SHDT, as oposed to the usual 15 cm (6") in other open hole logs (Figure 12.6). Dipmeter microresistivity data are handled in the so-called 'fast channel' while the navigation data and calipers are handled in the 'slow channels'. The high dipmeter curve sampling rate is associated with very small pad electrode, or button (i.e. small electrode) size, in the region of 1 cm, so that features as small as 1 cm–2 cm (0.4"–0.8") are registered and depth of penetration varies around 2 cm (0.9") (which must be added to the hole size to calculate dip). The SHDT for example, has two electrodes 1 cm in diameter 3 cm apart (Figure 12.5). The microresistivity pads themselves vary between tools but tend to be short and wide (5–6 cm) to maximise formation contact and avoid sticking (Bigelow, 1985).

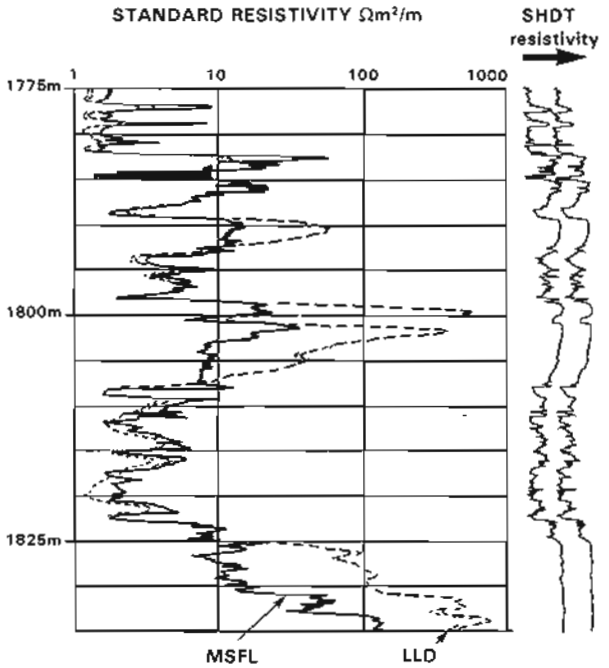


**Figure 12.4** Standard resistivity logs compared to SHDT dipmeter resistivity curves. The SHDT curves are sampled every 0.25cm (0.1") and are very detailed while the standard logs are sampled every 15cm (6"). However, the SHDT curves give only relative resistivity values, as base resistivity (EMEX) varies depending on formation resistivity. In this way, detail is measured in both the absolute low and high resistivity intervals (hydrocarbon bearing in this example). SHDT = Stratigraphic High Resolution Dipmeter of Schlumberger.

***Orientation and other measurements***

To calculate the resistivity curve displacement across the borehole, clearly, the borehole size must be known. To this end, the two pairs of arms measure two independent calipers, giving two orthogonal hole size measurements. This allows a dip to be calculated from the displacement. However, for this plane to represent the true dip, in other words not just any plane but referenced to north, other orientations must be measured by the tool. These are: the orientation of the tool in relation to north (pad 1 acts as the tool reference = pad 1 azimuth): the deviation of the axis of the tool from the vertical (= the deviation of the borehole): the direction of this deviation relative to north (= azimuth of hole deviation, sometimes called drift). The latter orientation is calculated, not measured, from the 'relative bearing', which is the clockwise angle between pad 1 azimuth and the high side of the tool (this is the same as the hole deviation azimuth orientation). Pad 1 azimuth minus relative bearing azimuth (+360°) = hole deviation azimuth. Speed variations may also be measured. This can be done directly by using accelerometers or by using a speed electrode. The latter is a duplicate electrode on one or two of the pads, several centimetres vertically above the main electrode, which should duplicate the main measurement. When there are large speed differences the speed electrode and main electrode readings will differ and corrections can be made.

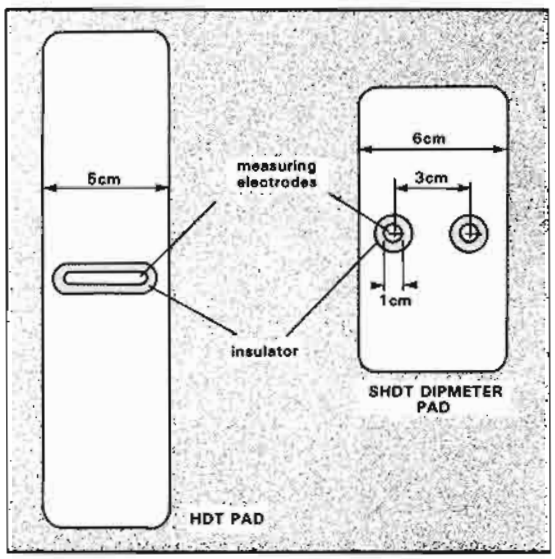


**Figure 12.5** Dipmeter pads. The single electrode HDT (High Resolution Dipmeter) pre-1985 and the two electrode SHDT (Stratigraphic High Resolution Dipmeter) with a shorter pad for better formation contact. (re-drawn from Schlumberger, 1986).

***Field log presentation***

Two types of dipmeter log are produced. The first is a field log, a plot of the raw data acquisition curves; the second presents the processed data – the actual dips derived by the computer. The field logs will be described in this paragraph, the logs showing dips are described in section 12.4.

A typical dipmeter field log will show not only the raw microresistivity curves, but also most of the orientation and caliper data. The example chosen is from a Western Atlas, 4-arm (pad) Diplog (Figure 12.6). In track 1 are the deviation of the borehole from the vertical (DEV) and azimuth (DAZ), the azimuth (AZ) of the reference pad (pad 1) and a gamma ray curve from a sonde attached to the dipmeter tool. The gamma ray allows the dipmeter to be matched to the standard log runs (note the great difference in detail between the gamma ray and the dipmeter curves). In tracks 2 and 3 are the raw acquisition curves, the tension and the two calipers. The tension curve is useful in identifying zones of tool sticking although these are usually evident on the caliper and the raw curves themselves. The format of the raw dipmeter data varies between companies although the basic information included is similar. The logs are plotted at a 1:200 scale.

## 12.3 Dipmeter processing

***Generalities***

To derive a dip direction and azimuth from the raw, tool produced resistivity curves, needs computer processing. The requirement is to correlate the curves around the borehole so as to identify the various displacements,

which then define a surface across the hole. There are two principal methods: *fixed interval correlation* and *feature recognition*. Fixed interval correlation is the most common method used and simplest for the computer but feature recognition imitates the way the human eye works. Processing is normally done automatically by the computer, but a modern development is the possibility of correlating the curves and producing dips interactively on the computer screen (Figure 12.7). Interactive methods are only for detailed work.

It is essential to understand the general principles of dipmeter processing; proper interpretation depends on it. This will be demonstrated subsequently. It is not necessary to know the details of the computer programmes, which vary between companies, but the basic, consistently used principles must be understood. The essentials of the two methods (fixed interval and feature recognition) will be described separately below.

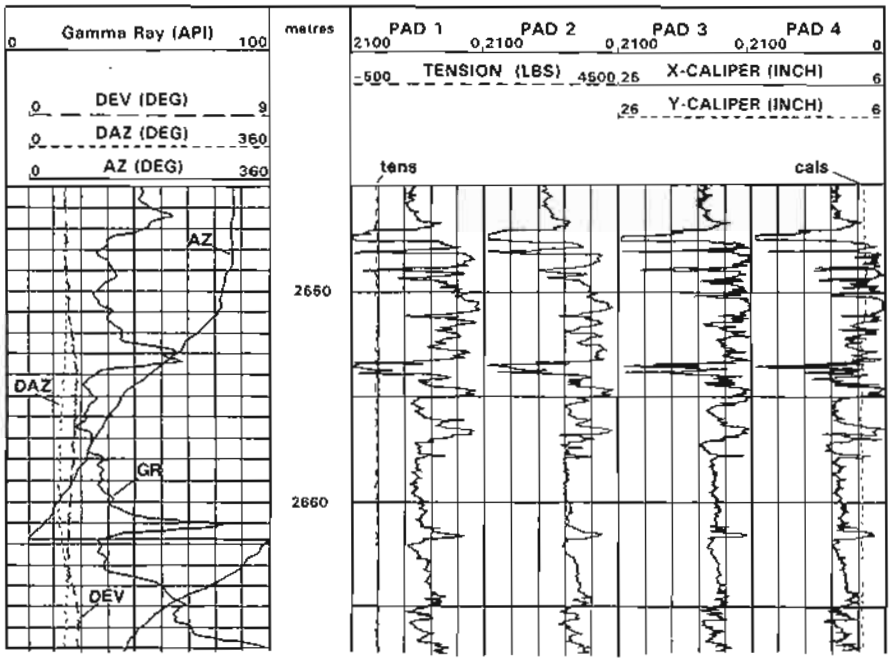


**Figure 12.6** Standard log presentation of raw dipmeter data. The dipmeter curves are sampled every 0.5cm (0.2") while the standard logs are sampled every 15cm (6") (Western Atlas Diplog). DEV = hole deviation from the vertical. DAZ = azimuth of hole deviation. AZ = azimuth of pad 1. Pad 1–4 = pad conductivity curves.

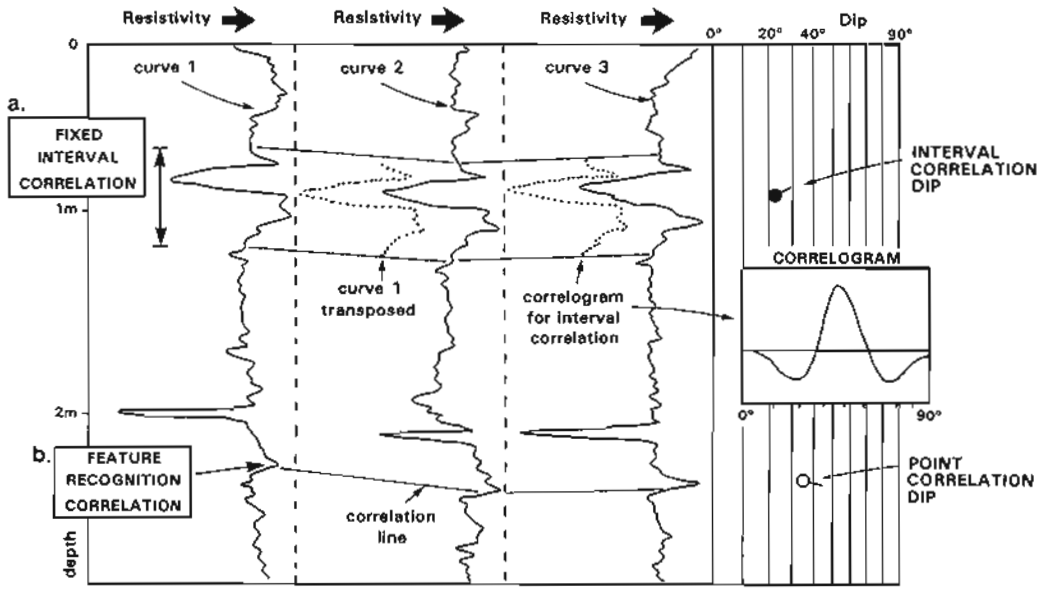


**Figure 12.7** Correlation methods for deriving dip and azimuth from dipmeter resistivity curves. a) Fixed interval correlation: one dip is produced representing the entire selected interval; b) feature recognition correlation: a dip is produced representing the correlation of a recognizable feature. Fixed interval correlation methods are the most common: feature recognition imitates the way the eye correlates. Example taken from interactive screen routines in QLOG.

***Fixed interval correlation methods***

Fixed interval correlation methods are the most commonly used. Dip computation is based on a comparison and correlation of the microresistivity curves over short, fixed vertical intervals or depths (Figure 12.7). The calculated correlation gives a curve displacement from which, with a minimum of three displacements around the borehole, a dip and azimuth can be derived. Several parameters are varied by the computer operator and are chosen depending on the perceived interpretation requirements. The three principal parameters to choose are the *correlation interval*, the *search angle* and the *step distance* (Figure 12.8). The correlation interval is the fixed depth interval, or more properly the length of microresistivity curve used for correlation, usually between 0.1 m (10 cm) and 2 m. The search angle defines the length of curve over which a correlation is searched for on a second curve, typically sufficient to give up to 70° of dip in the borehole's frame of reference. (Schlumberger often quote a search angle of 35° × 2, which means that the computer will search up to 35° on the first pass but if it really finds nothing, will eventually search another 35°. This is a technique to save computer time). The third parameter, the step distance, is the length of curve moved between one level of correlation and the next above (computation is always from the bottom upwards). Typically this amount is half (50%) of the correlation interval or a step ratio of 0.5 (Figure 12.8).

In more detail, the fixed interval method works as follows. The length of microresistivity curve *one* to be used is defined by the correlation interval, say 1 metre. This length of curve *one* is compared to microresistivity curve *two*, using cross-multiplication (*see below*) by moving curve *one* in increments along curve *two*. The length of curve *two* which is used is defined by the search angle.

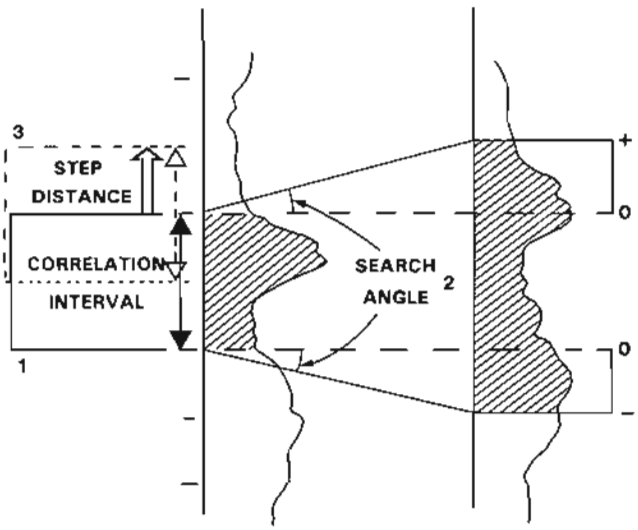


**Figure 12.8** The features which must be defined for a fixed interval correlation processing. 1. correlation interval = length of curve used; 2. search angle = length of new curve to be searched, defined in terms of dip angle; 3. step distance = depth increment change for next correlation (always above).

For instance, if a search angle of 50° is chosen, curve *two* will be searched along a length sufficient to give 50° dips and no higher (the actual length varies with size of borehole). Such correlations are made on all possible combinations, being 6 with 4 microresistivity curves, 15 with 6 curves, 28 with 8 curves. The displacements derived from the correlations are then used to define a plane – the dip. The entire process is begun again in the interval above according to the step distance. Typically this next interval will re-use the top 50% of the previous correlation interval. That is, if the correlation interval is 1 metre, the step distance will be 50 cm and the overlap will be 50% (Figure 12.8).

It is helpful to general understanding to examine the actual process of curve correlation. The system is one of cross-multiplication. A graphic representation of this, called a *correlogram*, shows that when the two curves are most similar, there is a maximum cross-multiplication product (Figure 12.9). That is, when the two curves are most similar, the correlogram has a marked peak, which is the correlation point and is taken as the curve displacement for dip calculation. When there is no peak, the two curves show no similarity. Mathematical tests for the quality of the computed dip can be made, for example by using the shape of the correlogram. Most dipmeter programmes give a quality rating scale to each dip and azimuth value of say 0–1 or 1–10. A simplified quality is usually indicated on the final dip and azimuth plots or else quality cut-offs are applied, below which the computed dips are simply not plotted (Section 12.5).

***Standard processing parameter variation***

The result of a fixed interval correlation programme is a *regular* series of dip and azimuth readings with a depth at the centre point of every correlation interval and separated vertically by the step distance increment. However, with a single set of raw dipmeter data, a whole series of processed dipmeter logs can be produced, by varying the processing parameters.

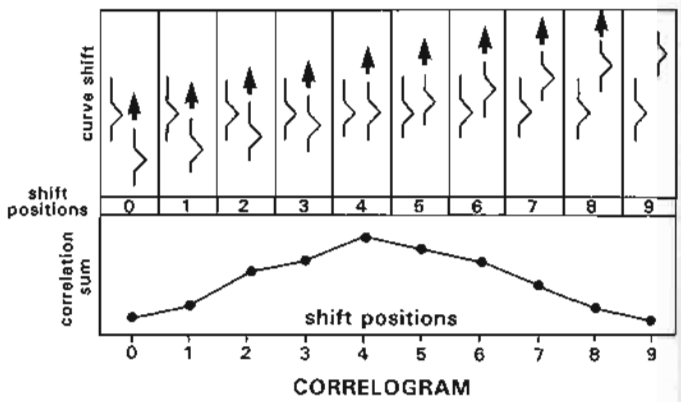


**Figure 12.9** Schematic representation of the construction of a correlogram used in automatic, fixed interval correlation routines (from Cameron *et al.*, 1993) (*see also* Figure 12.7).

For example, correlation interval, step distance and search angle must all be defined by the operator and therefore can be varied at will. A typical set of parameters will be 1.0 m correlation interval, 0.5 m step distance (4' correlation, 2' step are the foot equivalents) and a 50° search angle. A dip and azimuth value will be given every 50 cm (the step distance) but representing a 1 m interval. This is a relatively coarse set of parameters and is used for defining 'structural' dip (section 12.7): fine features will not be measured. The correlation interval may be set, however, at a much smaller value, even down to 10 cm (4") on very good quality SHDT logs, which means using only 40 microresistivity curve sample values (i.e. made every 2.5 mm) for each correlation. An example of a single set of raw dipmeter data processed with gradually varying parameters is shown in Figure 12.18 and discussed in Section 12.6.

***Feature recognition methods***

Microresistivity curve correlation by feature recognition tries to imitate the way the eye correlates. When correlating, the eye picks out a remarkable feature and searches for a similar feature on the curves to be compared. For instance the peak at 2.3 m (Figure 12.7) is picked out easily on all the curves and leads to a visual correlation. Programmes for feature recognition imitate this method. Geodip, a Schlumberger programme, mathematically defines a number of curve features such as large peaks, small peaks, large troughs, etc, and then correlates to similar features in the other curves (Vincent *et al.*, 1977). Interactive correlation programmes now allow this to be done by eye on the screen (Figure 12.7).

Feature correlation is made at a defined level, an identifiable curve feature is being used. This gives an *irregular* series of dip and azimuth results; where curve features are good, results are dense: where curves are featureless there are no results. This clearly has geological implications as will be discussed below (Section 12.7). But feature correlation methods are not often used and are certainly not standard.

## 12.4 Processed log presentations

Although the 'tadpole plot' *(see below)* is standard for the processed dipmeter log, a number of additional presentations are also available, especially as more dipmeter processing software programmes become available. Some presentations are general, others unique to one service company or one software programme. Some of these are shown below but the list is not exhaustive.

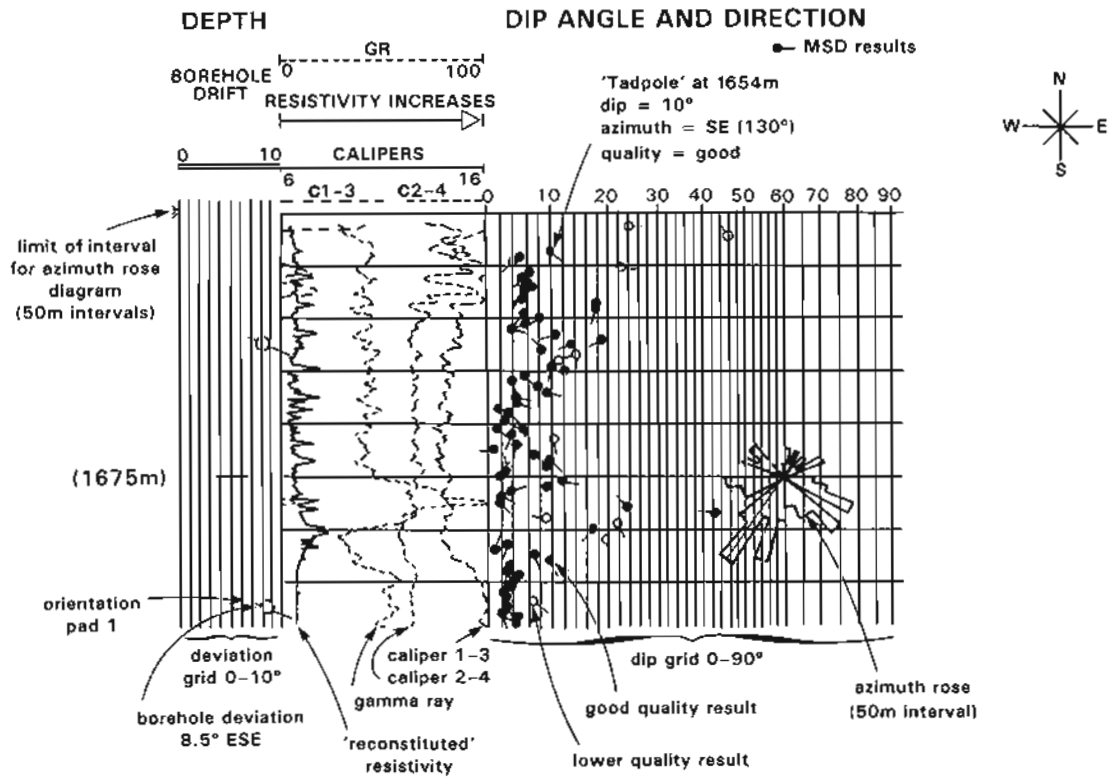


**Figure 12.10** A standard, processed dipmeter tadpole plot and log header. The example is of an MSD (Mean Square Dip, a fixed interval method) processing from a Schlumberger SHDT tool (*see text* for explanations).

***Simple standard presentation: the 'tadpole plot'***

The standard dipmeter presentation is a 'tadpole plot' (Figure 12.10). The basis for the plot is a standard grid in which the vertical scale is depth and the horizontal, variably spaced scale, is dip from 0°–90°. On this grid, the dip is plotted as a large black dot (the tadpole head) whose position has the co-ordinates of depth (from the vertical scale) and dip (from the horizontal scale). The azimuth is then given by a small, straight line (the tadpole tail) plotted from the centre of the dot with an orientation relative to the vertical grid lines which represent true north. On the example log (Figure 12.10), the 'tadpole' at 1654 m (arrowed) has a dip of 10° with an azimuth to the SE of 130°. The tadpole is often varied from the standard black dot. Square or triangular shapes may be used and sizes varied. Quality, discussed below (Section 12.5) is frequently indicated by infilled or open shapes, good quality infilled (i.e. solid tadpole 'head'), poor quality left open. When colour is used, dip types may be classified or a range of qualities indicated by different colours. The use of the various symbols or colours should be indicated on each log head.

***Accompanying log data***

On standard dipmeter logs processed by service companies, other information from the tool is plotted besides the dip grid with dip and azimuth values. Typically, this will include the two caliper results, a plot of hole azimuth and drift and a reference log such as a gamma ray or resistivity which allows correlation to the other open hole logs. These latter, however, are derived from the dipmeter tool itself, the gamma ray, for example, being from the gamma ray unit fixed to the dipmeter tool (Section 12.2, Figures 12.6, 12.10). Unfortunately, logging service companies seldom present dipmeter results along with the standard open hole logs. This is symptomatic of the 'isolation' of dipmeter data. Integration with the standard open hole logs is essential for proper interpretation; an integration from the level of computer format upwards.

***Acquisition curves***

It is a common and useful practice to plot the dipmeter microresistivity curves alongside the dipmeter grid and processed results. The plotted curves are usually edited and simplified from the raw data but are excellent for quality control, to indicate textural characteristics and for facies identification (Figures 12.24, 12.29).

The acquisition curves are normally plotted on feature recognition processed results logs, such as Geodip and Locdip from Schlumberger, so that the level of each correlation from which a dip is derived may be shown. A quick glance at a Geodip log shows that it has an important geological content, especially useful in examining sedimentary features (Delhomme and Serra, 1984).

## Additional plots on standard presentations

*– Azimuth rose plot*

Frequently on standard dipmeter tadpole plots, azimuth data are grouped over certain intervals. Typically, on a 1:500 scale dipmeter log, azimuth data are grouped over 50 m intervals and plotted as a frequency rose diagram (Figure 12.10). The azimuth rose is useful in indicating unconformities, structural dip direction and faulting. Plotting azimuth roses on pre-determined intervals (i.e. each 50 m) however, should be refined by plotting over intervals with meaningful stratigraphic or sedimentary limits (Figure 12.11). Standard azimuth plots often fail to show important surfaces such as unconformities or faults, which have different azimuths, because the pre-determined zone straddles the feature (Cameron, 1992).

*– Dip histogram*

A useful addition to the rose diagram is a dip histogram plot in which dip angle, on the X axis, is plotted against frequency on the Y axis. A histogram is integral to some software programmes (Figure 12.11). The plot is useful in showing a separation of structural and sedimentary dip and in showing high angle noise dips (Section 12.5).

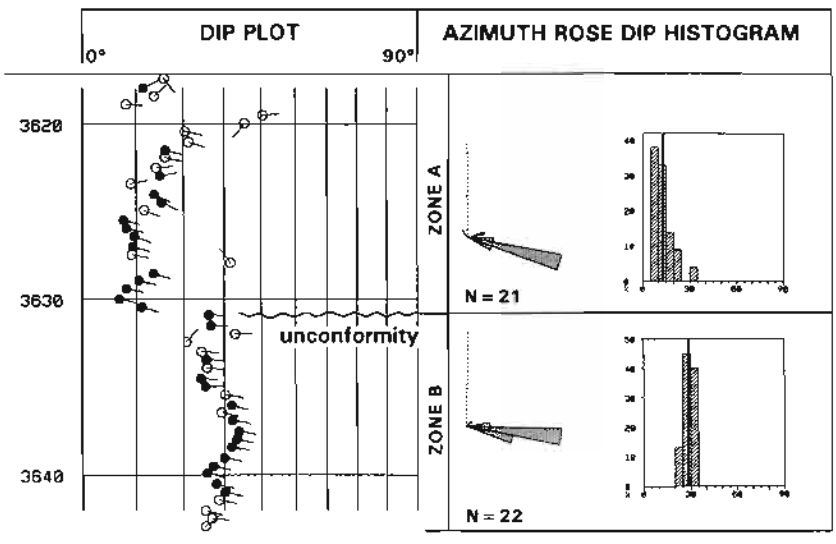


**Figure 12.11** Standard tadpole plot with associated azimuth rose diagram and dip histogram presentations of zoned data. The zones are above and below an unconformity. Such data zoning allows the overall dip and azimuth characteristics of intervals to be quickly assessed.

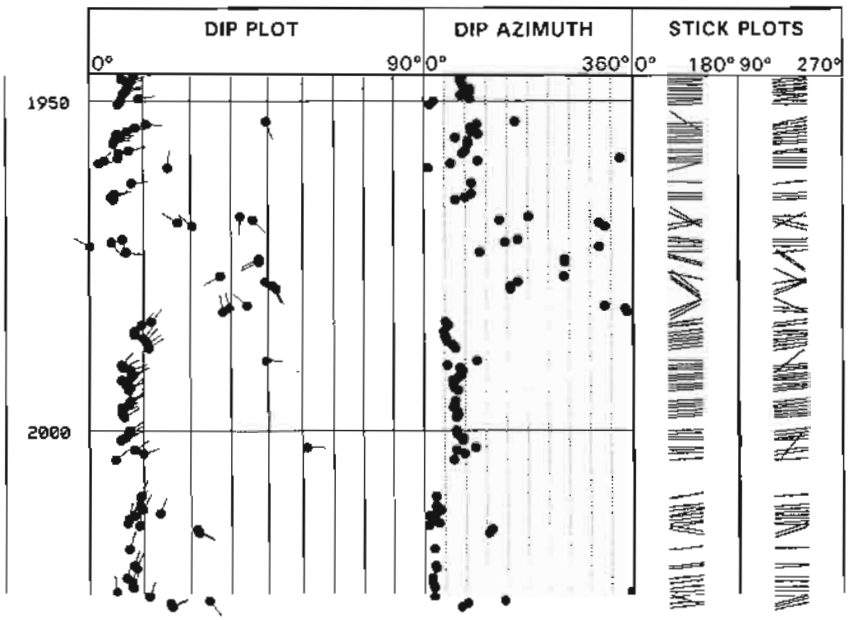


**Figure 12.12** Standard dipmeter tadpole plot (left) with corresponding dip azimuth against depth plot (centre) and two, orthogonal orientations of stick plot (right). The azimuth plot is especially useful in structural analysis. The stick plot is used on correlation cross-sections and for seismic comparisons.

*– Separate azimuth plot*

By using a standard dip grid and a 360° grid side by side, dip may be plotted on the first, and azimuth values alone, as dots, on the second. The second grid brings out the variations in azimuth which are generally masked on the standard plot (Fig 12.12). The separated azimuth plot is a powerful aid in structural dip interpretation.

A specialised structural interpretation technique called SCAT (Bengtson, 1981; 1982) uses a variation of this plot. It will be discussed under structural dip interpretation (Section 12.8).

## Some stand alone plots and manipulations

*– Stereographic polar plot*

Much used by structural geologists to analyse complex geometry, stereographic polar plots are also a useful tool in dipmeter analysis, especially for structural geometry. Special polar grids (Wulff net or Schmidt net) are used on which planes are ploted as their poles (normal axis) and three dimensional geometry can be analysed graphically (cf Figure 12.14). Stereographic plots of dipmeter data are generally made for selected intervals and for specific, usually structural problems. They require careful analysis. This is not the place to describe the use of stereograms, the classic text of Phillips should be consulted (Phillips, 1971).

*– Stick plot*

A stick plot represents dip as a line. Because no azimuth can be indicated, stick plots are usually presented in two (sometimes more) sections, one at 90° to the other: typically a north-south and an east-west set. The sticks represent the apparent dip in the orientation indicated (Figure 12.12). The plots are most effective using broad interval averages and small vertical scales to illustrate an entire well. Stick plots can be useful added to correlation diagrams.

The conversion of dipmeter records to a time scale (as opposed to depth) is a very useful development. Time scale data are normally presented in the form of a stick plot, so as to be exactly compatible with seismic sections. This presentation is especially useful for structural interpretation (Fig 12.32).

*– Azimuth vector plot*

Azimuth vector plots are constructed by plotting dip azimuth values sequentially in their true orientation but without any depth scale. Thus, a sequence with a dip to the west will create an east-west line: one to the northwest, a line to the northwest and so on (Figure 12.13). At an unconformity, where dip azimuth changes, the line orientation will change. Faults will also cause orientation changes but they will be more variable than at unconformities.

This plot is useful where small azimuth changes occur, such as at disconformities. Azimuth vector plot data must be combined with the standard open hole logs to be interpreted. Variations to this type of plot have been proposed (Hurley, 1994).

*– Structural dip rotation*

An essential routine in dipmeter work is to be able to change the structural dip (*see* Section 12.8 for a definition of structural dip). When, for example, palaeocurrent directions are obtained from sedimentary cross-bed orientations, if there is structural dip, the palaeocurrent orientation will be structurally distorted. To obtain the true palaeocurrent direction the structural dip must be 'rotated out'. In other words the structural dip must be returned to zero (Figure 12.14). Very little effect is seen in dips below 5°, but as the dip increases so the rotation effect increases, as would be expected.

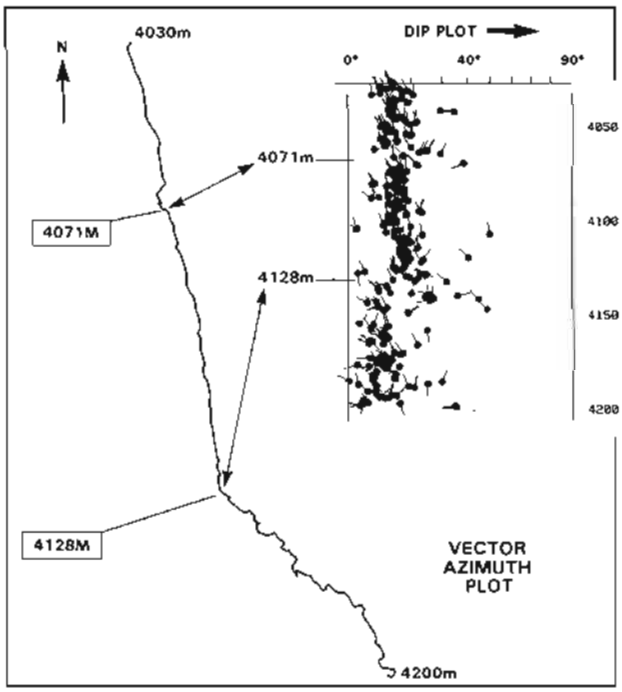


**Figure 12.13** An azimuth vector plot and the corresponding standard tadpole plot of the same interval. The azimuth vector plot shows the nature of the structural break at 4128m much more clearly than the tadpole plot. The plot is used in the analysis of unconformities and faults.

Structural dip rotation should be available both as a bulk facility and as a zone facility. The sedimentary effect described above only requires the zone with cross-beds to be rotated. If an unconformity comes in the middle of a well and the well is structurally tilted, it is useful to be able to rotate out the structural dips above and below the unconformity separately. Or to be able to structurally rotate separate fault blocks. That is, it should be possible to rotate one dip and azimuth value from an entire well, or one small zone.

*– Summary scale logs*

An extremely useful facility in dipmeter analysis, indeed the analysis of any log, is to be able to change scales. Compressed scale, summary dipmeter logs of 1:2000 to 1:5000 do two things. Firstly they allow a bulky document at standard 1:500 or 1:200 scales to be presented on one A4 page, and secondly, they bring out large scale structural trends.

Frequently, structural dip varies gradually but consistently through a well (Figure 12.30). For example, a typical normal fault block shows slowly increasing dips over several hundred metres, as the fault is approached. Drape of shale sequences over reefs or fault blocks will equally show only gradual changes. Such changes are brought out clearly in summary scale logs. Indeed, a structural interpretation indicated on a summary scale dipmeter log should be a standard document in any well file: it will ensure that the dipmeter is used and that it contributes to routine analysis.

## 12.5 Dipmeter quality assessment

The assessment of the quality of a processed dipmeter log is essential: it affects the possibilities but especially the credibility of an interpretation. In very poor datasets, there is often a high noise content. Noise dips have no meaning and are a result of the computation method (Cameron, 1992). Even on properly processed and filtered logs, core to log comparisons show that noise dips are still present. However, interpretation routines are designed to accommodate this and along with careful raw data examination, noise effects on a final interpretation can be minimised. Quality assessment is essential.

Borehole conditions, data acquisition and data processing should all be assessed for quality: all affect an interpretation and are considered below.

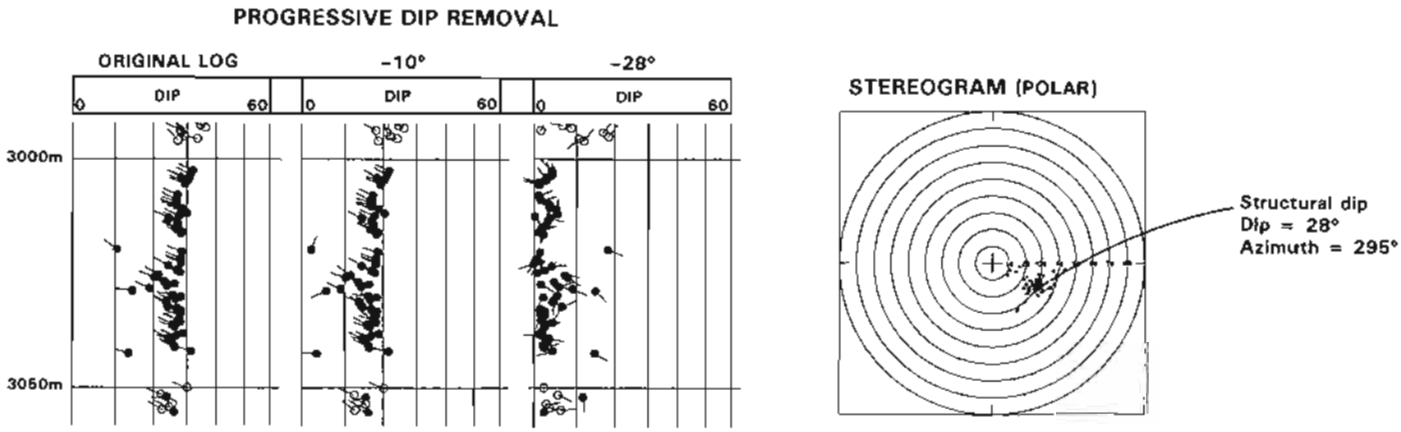


**Figure 12.14** The effect of structural dip rotation. The original dipmeter log shows a structural dip of 28°, azimuth 295°, seen on the stereographic representation. Subtracting this dip and azimuth from the original log removes all structural dip (log on the right) while subtracting only 10° at 295° still leaves a substantial structural element. This routine is used, for example, in sedimentary palaeocurrent analysis.

*Borehole quality*

Poor borehole conditions affect the dipmeter probably more than the other standard open hole tools. Hole ovality causes pads to 'float', especially in deviated wells. A floating pad loses contact with the formation and shorts out into the mud. Caving may also cause pads to float and is often the cause of a tool sticking.

A good method of judging hole quality is to plot compressed scale dipmeter calipers (e.g. 1:5000), along with the dipmeter tool orientation data. When this is done, intervals where data may be poor are quickly seen (Figure 12.15). Frequently borehole wear can be seen on these plots, the nearer the hole to TD the better the condition, the lower parts having been less exposed to drilling wear. Alternatively, detailed 1:20 or 1:50 scale plots are found to be useful in indicating where dipmeter curves mimic the calipers, as occurs in small scale riffling (R.Trice, pers. comm.). Although calipers are normally plotted with the processed dipmeter results, prior examination helps the processing itself.

*Data acquisition*

Quality assessment at the acquisition stage concerns tool performance during logging and tool calibration. Tool rotation, sticking and curve activity are indicative of performance. A tool should not rotate more frequently than one turn per 15 m (50'), as this can affect processing (Waid, 1987) and dips can be seen to vary with rotation. Orientation data are averaged over a correlation interval in fixed interval routines (section 12.3), so that rapid tool rotation affects especially high dips and logs processed with broader parameters rather than small ones (it does not affect manual picking). Tool rotation is quickly judged from the compressed scale logs (Figure 12.15).

Sticking in poor borehole is serious for the dipmeter. Although the tool contains accelerometers and speed changes can be accounted for, serious sticking generally does not allow valid data to be collected. A tool which sticks (stops moving) while the cable runs several metres and then jerks free, will be noticed on both the tension and the featureless curves gained during the stuck period (Figure 12.16). Speed correction will attempt to discount the data when the tool is stuck and expand the data collected as the tool jerks free. However, when sticking is serious, there will be no valid data.

As a check on the orientation calibration of the dipmeter tool, which can cause problems, it is useful to compare dipmeter derived hole deviation with the quite independent directional surveys measured during drilling.

*Processing quality*

Most processing software has built-in quality indicators. That is, tadpoles are plotted with filled or open heads representing good or bad data. This assessment is generally statistical. However, the limit between good and bad data, as printed on the log, can generally be varied at will.

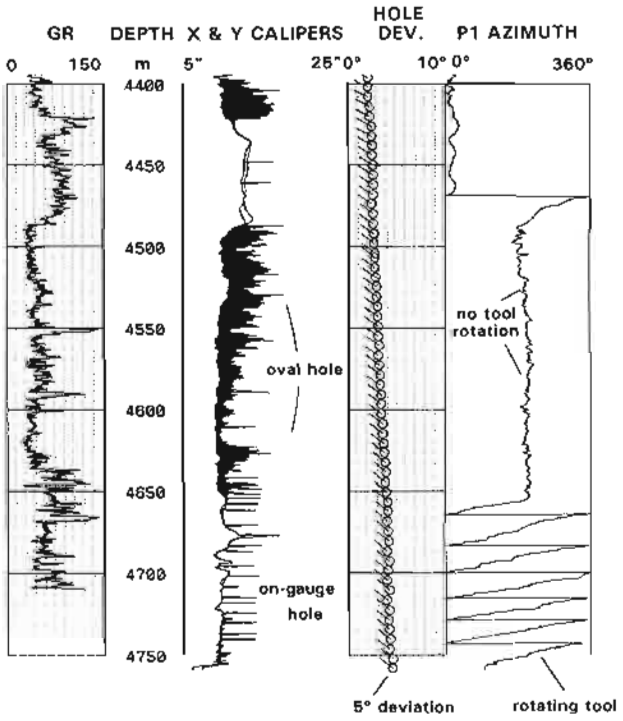


**Figure 12.15** Compressed scale logs of factors which affect dipmeter acquisition. From logs such as these the quality of a processed dipmeter can be assessed. Note the tool rotation (indicated by pad 1 azimuth) over the interval of on-gauge hole. Over the section of oval hole there is no tool rotation as one set of calipers becomes fixed in the long axis of the hole, which in this case has a constant orientation.

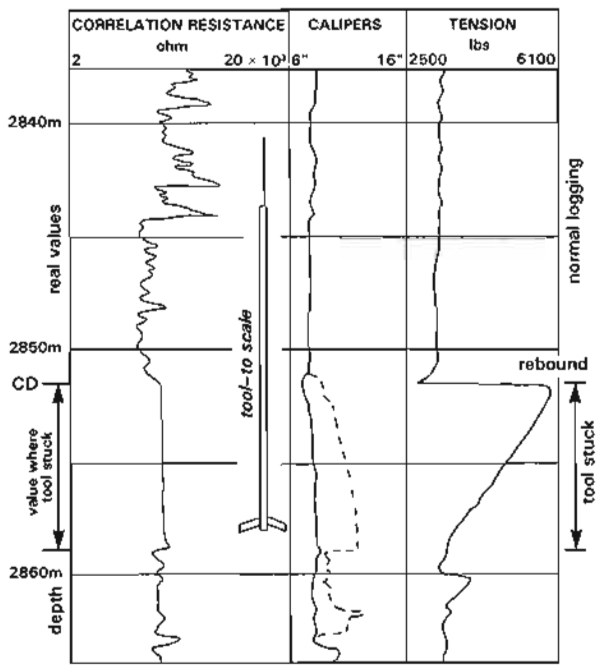


**Figure 12.16** The effect of a dipmeter tool sticking. The cable continues to be reeled in, even though the tool is stuck. The cable tension increases continually until the tool breaks free (it may then rebound or yo-yo as in this example). When the tool breaks free a 'flat' set of data are produced.
CD = compressed data

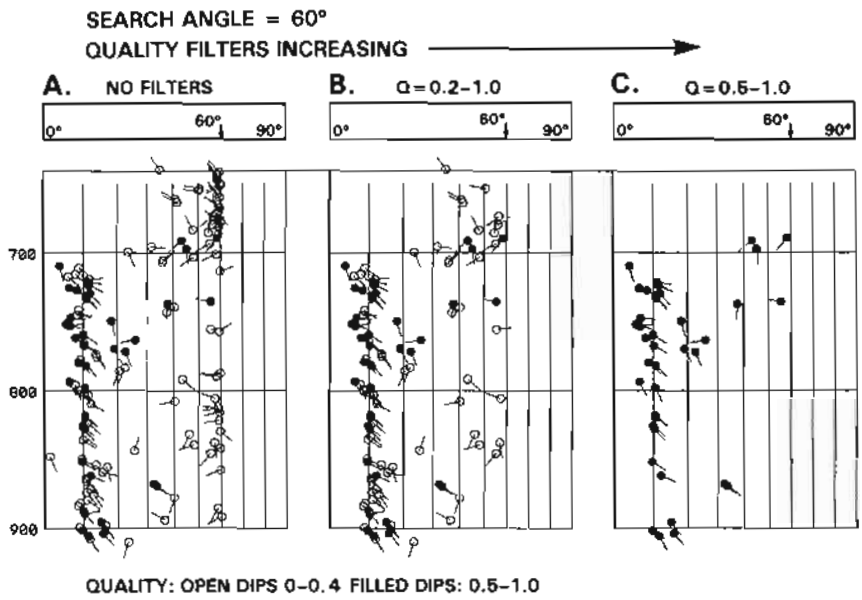


**Figure 12.17** Dip correlation quality characteristics. Dip quality is based on the statistical values of the correlation which in this example have a scale of 0–1.0 (0 = poor, 1.0 = excellent: open dips = 0–0.4, filled dips 0.5–1.0). The poorest dips tend to plot at the correlation angle (log *a*) and are removed by not plotting qualities below $Q = 0.2$ (log *b*). Only plotting quality above $Q = 0.5$ (log *c*) gives a much 'cleaner' looking result.

The example shows the effect of quality rating with a dataset using a scale of 0–1 (0 = poorest, 1 = best) and a cut-off from open dips to closed dips at 0.5 (Figure 12.17). With all the data, two lines of dip are evident, at 10° and at 60°. The search angle for this data is 60° and the poorest data are concentrated at about the search angle, that is the high angle line of dips. If the data with 0 to 0.2 quality rating are discarded, most of the data at the search angle disappear, but there is still a considerable scatter. With only data with a quality rating between 0.5 and 1.0, that is only the filled-in dips, the log has a much 'cleaner' look and is much more interpretable. The quality filters are based entirely on correlation statistics.

Processing quality can depend very much on choosing the right parameters, especially correlation interval, to suit the data. Very good quality logs may be processed with small correlation intervals but with too small parameters, many logs will become meaningless. Comparisons with core show that datasets can be processed with 10 cm–15 cm (4"–6") correlation intervals and still retain meaningful results. When a dataset breaks down, noise dips and poor data will appear close to the search angle as described (Figure 12.17).

When borehole conditions are very bad, noise on the dipmeter traces will tend to cause anomalous spikes simultaneously on all the curves. These will be in a plane perpendicular to the hole axis (i.e. tool axis) and all at the same depth. On the processed log they will be seen as dips of apparently good quality, but will have a dip angle equal to the borehole deviation (i.e. tool tilt) and with an azimuth exactly opposite. These are historically termed mirror image dips.

## 12.6 Dipmeter interpretation: the basic principles

***The problem***

A correctly processed dipmeter log is not immediately intelligible; it requires a great deal of interpretation. To most geologists who have tried to use dipmeter logs, this is a truism, and the preceding sentence is quite unnecessary! But to persist. The reason it requires interpretation is that the dipmeter log presents a data set quite unlike any which a geologist working at outcrop will collect. It is beyond normal geological experience. When dip and azimuth or palaeocurrent data are required, a geologist chooses where he will make a measurement: his data points have been very strongly selected. Dipmeter results show no selectivity: everything is mechanically measured. Herein lies the philosophical problem. The dipmeter is like a radio receiver that accepts all wavebands simultaneously and produces a nonsensical cacophany. The data must be filtered, must be selected. The difference between the geologist at outcrop and the dipmeter in the subsurface is:

outcrop
*geologist – choice – dips*
subsurface
*dipmeter – dips – choice*

This is a simple concept but important (Cameron, 1992). It shows that the dipmeter interpretation problem is one of how to 'choose' dip data.

***The solution***

More than with the other open hole logs, the dipmeter requires manipulation (in effect computer manipulation), before interpretation is possible. The manipulation is effectively a progressive series of choices which, in themselves, are already part of the interpretation process. Three principal choices are invloved: choice of *processing parameters*: choice of *post-processing data grouping*: choice of *processed data format*. What these choices imply is briefly explained immediately below while their effect on the data is illustrated in the examples through the text.

The division of dipmeter interpretation into the sedimentary and structural fields has been mentioned. The choice of *processing parameters* underlines this division. A sedimentary interpretation requires a detailed, small scale processing, while structural interpretation, using the same raw data, needs a broader scale (Figure 12.18). In other words, it must be known whether a structural or a sedimentary interpretation is required before processing parameters are chosen. A 'structural' processing cannot replace a 'sedimentary' processing and vice versa. For the dipmeter interpreter, this choice is similar to the selection, by a field geologist, of a site for dip measurement: it gives an intentional bias to the data.

The choice of *processed data format* can also be regarded as an interpretation tool. The children's game of joining numbered points to make a picture involves a choice of format: simply adding a line makes the data understandable. Similarly, with dipmeter data, varying the format or the way in which the data are presented helps interpretation. The reason for this is that, for most people, a series of 'tadpoles' on a dipmeter grid does not suggest the geometric form that created them. A fold or fault is not recognisable from a line of dips. Choice of format includes the scale of display, the separation of dip and azimuth and the choice of a format that attempts to actually reconstruct the geometry of the feature measured by the dipmeter.

*Post-processing data grouping* is carried out on logs already processed and provides a means of enhancing useful data. As discussed, comparison with cores shows that poor dipmeter logs contain noise. Individual noise dips cannot be identified or eliminated in a subsurface data set, but their effects may be significantly lessened by grouping processed results: it allows valid data to dominate (Cameron, 1986; 1992). For instance, for a structural interpretation, all data over a 200 m interval may be grouped to give a dip and azimuth mean, which, if there is data scatter will not be clear on a standard plot. In a sedimentary analysis, grouping data from a single channel allows palaeocurrent data to be extracted. Clearly, the choice of data to group together must be geologically biased.

The results of using these three choices on dipmeter data are illustrated in the examples below.

## 12.7 Sedimentary dipmeter interpretation

***Sedimentary dip: definition and processing***

By *sedimentary dip*, in the dipmeter context, is intended *the dip of any sedimentary structure which is inherited during deposition, or soon after*. It is a loose definition

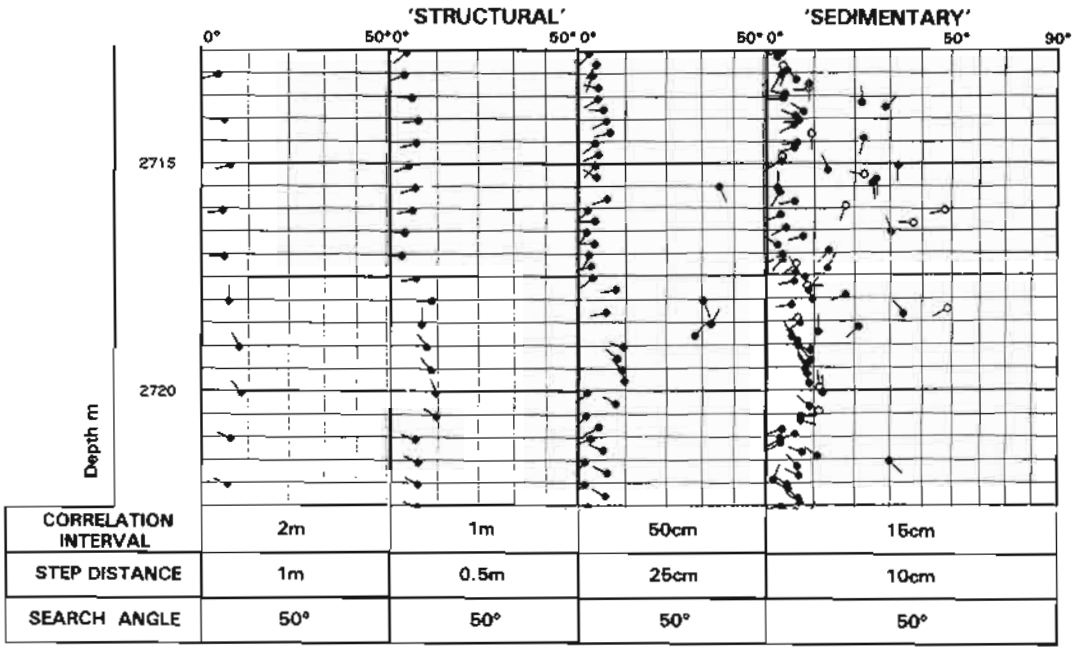


**Figure 12.18** The effect of varying fixed interval processing parameters using the *same* raw, dipmeter data. The logs processed with broader correlation intervals such as 2m or 1m are used for structural interpretations. Processing with small scale correlation intervals such as 15cm, produce logs used for sedimentary structure analysis and palaeocurrent interpretation.

and includes sedimentary structures such as laminations, cross-beds, bioturbations, slumps and drapes. The principal objective of sedimentary dipmeter interpretation is to find the orientation of reservoirs and reservoir parameters. This can be based on the orientation of internal features such as cross-beds and hence palaeocurrents, or external features such as compaction drapes. The characterisation of facies is another objective (Table 12.1). For some unknown reason, some service companies refer to this use of dipmeter as 'stratigraphic'.

Dipmeter data must be specifically processed for sedimentary interpretation. The effects of changing the correlation interval in fixed interval correlation processing have already been illustrated (Figure 12.18). Smaller correlation intervals are necessary for sedimentary studies. If the dip of the internal laminae of sedimentary structures is being looked for, then the length of the correlation interval is critical. For example, the typical thickness of cross-bedded structures is less than 1 m (Höcker *et al.*, 1990). If the raw data are processed with a correlation interval of 1 m, no internal lamination dips will be measured (Figure 12.19*a*). This is because the set boundaries have the greatest textural contrast and cause the largest resistivity peak. This peak will be preferentially correlated (Rider, 1978). It is only when small correlation intervals are used that the internal features stand the chance of being measured (Figure 12.19*b*). Typically, the dipmeter processed for a sedimentary interpretation will have a correlation interval of 15 cm–20 cm (6"–10") and a step distance of 7 cm–10 cm (3"–5"). However, these parameters will depend on the size of the sedimentary features being looked for and the quality of the data. Interpretation begins with the choice of processing parameters (*see especially* cross-beds *and* palaeocurrents *below*).

### *Scale*

When the dipmeter is used as a sedimentological tool, as described above, the question of scale arises immediately. What is the optimum size of sedimentary feature 'seen' by the dipmeter (i.e. the dip measured) and what is the minimum size? The minimum resolution of the dipmeter tool sensors is between 1.0 cm–0.5 cm (0.4"–0.2"): a bed of this approximate thickness will cause dipmeter curve variation. A bed of 1.3 cm (0.5") will be fully resolved (Sallee and Wood, 1984). Tool resolution is not the limiting factor.

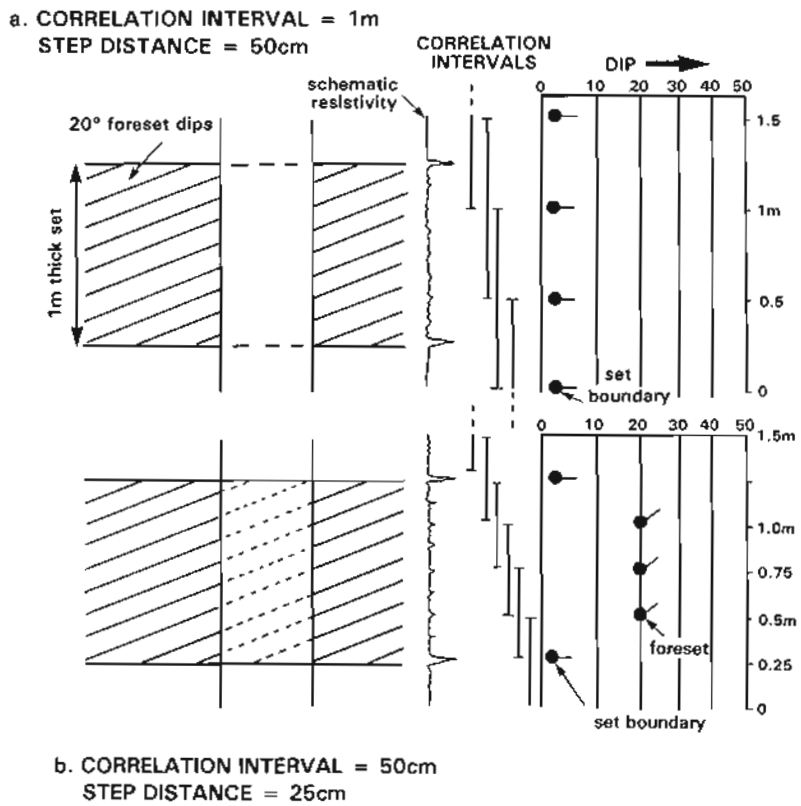


**Figure 12.19** Fixed interval dipmeter processing parameters in relation to size (thickness) of sediment structure. With a cross-bed set 1m thick, a dipmeter log processed using a correlation interval of 1m (example a), will not show the dips of the cross-bed laminae. A dipmeter log processed with a 50cm correlation interval (example b), can show several cross-bed lamina dips from one set. The choice of processing parameters is therefore crucial for cross-bed interpretation.

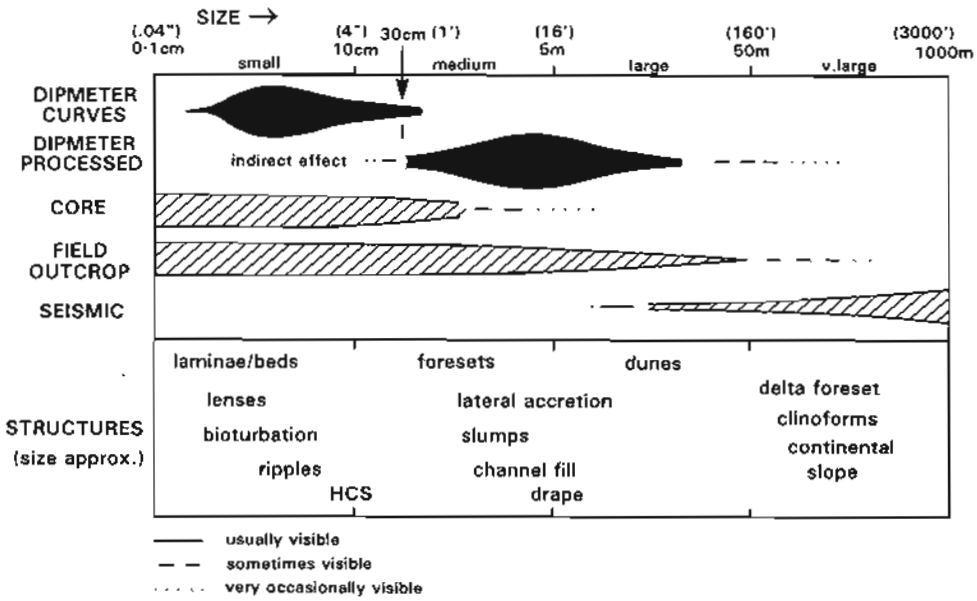


**Figure 12.20** Dipmeter resolution of sedimentary structures. Very small scale features can be detected (not identified) by the dipmeter curves. Processed dipmeter logs are quite different. Sedimentary structures with vertical thicknesses from about 30cm – 50m can be measured and recognized. The minimum depends on processing parameters, the maximum on presentation format. (HCS = hummocky cross-stratification).

The minimum size of sedimentary structure with internal dips which can be resolved by the dipmeter is in the region of 30 cm (1ft). Ripples, for example, will not be seen (Figure 12.20). *The limiting factor is processing resolution.* To show how the dipmeter derives its dip, take this book to any outcrop with sedimentary structures and lay it on the rock surface. Now interpret the structure with the part behind the book covered. This is what the dipmeter does. It assumes that if there is a correlation in the curves, it is due to a planar surface crossing the entire borehole (Figure 12.19).

To have the potential for being resolved, a structure must be present, and consistent along bedding, for at least the across-hole displacement of internally dipping surfaces. For foresets, the cross-bedding structure must be quite large (i.e. thick in dipmeter terms). A foreset with a 25° dip (bedding horizontal) has an across borehole displacement of 10 cm in an 8.5" borehole and 14.5 cm in a 12.25" borehole (Table 12.3). For the foreset laminae to be measurable, they must be present over the vertical thickness required for at least two separate, processed measurements (fixed interval processing). For example, a minimum thickness of 40 cm (16") with a 20 cm (8") correlation interval (10 cm (4") step) is required (Table 12.3). From theoretical considerations and empirical observations, cross-bed foreset structures (subaqueous only) exist with heights between 10 cm and 10 m (aeolian go up to 100 m) with typical values being (subaqueous) between 10 cm (4") and 2 m (6'). At the smaller scale, the structures will not generally be seen (Figure 12.20).

If the minimum size of structure resolved is dictated by processing, the maximum size is dictated by the structure itself. Generally structures which have a vertical thickness of around 50 m (160') (provided they cause a recognisable anomaly), are clear on the logs. Partly this is a question of display format. Compressed scale logs (Figure 12.30) can show much larger scale structures than normal 1:500 scale logs. However, in most large scale structures, such as drapes and sedimentary depositional slopes, the angles involved are very small, 2°–4°, and

**Table 12.3** Across hole displacements of dipping surfaces.

| Hole size | 6" | 8.5" | 12.25" | 17.5" |
|---|---|---|---|---|
| Dip 10° | 2.7cm (1.1") | 3.8cm (1.5") | 5.5cm (2.2") | 7.8cm (3.1") |
| Dip 20° | 5.5cm (2.2") | 7.9cm (3.1") | 11.3cm (4.5") | 16.2cm (6.4") |
| Dip 30° | 8.8cm (3.5") | 12.4cm (4.9") | 18.0cm (7.1") | 25.7cm (10.1") |
| Dip 40° | 12.8cm (5.0") | 18.1cm (7.1") | 26.1cm (10.3") | 37.3cm (14.7") |

will not be differentiated from random, background spread, which is typically around 5°. As a rule of thumb, the optimum size of sedimentary structure resolvable by the dipmeter (including internal structures), assuming a correct and appropriate processing, is 30 cm to 50 m (1ft–160ft) (Figure 12.20). There are exceptions.

### *Cross-beds and palaeocurrents*

Dipmeter response to cross-bedding is central to sedimentary dipmeter interpretation. All the basic principles are involved. Response depends on textural (electrical) contrast, size of structure and processing parameters. Moreover, interpretation of cross-beds requires a knowledge of the sedimentology of bed-forms and an understanding of the manipulation of grouped dip and azimuth data. These principles will be illustrated using dipmeter-type logs (dip-logs) measured at outcrop as well as subsurface examples.

The outcrop example (Figure 12.21) is from a deltaic sequence in which both tabular and trough cross-bedded structures are present (Cameron *et al.*, 1993). Bed-set thicknesses are generally 1 m (3') or less. That is, one bedform with a consistent set of cross-beds is normally less than 1 m in thickness. This is a typical size (thickness) and has implications for the choice of processing parameters as discussed above. Only logs with small correlation intervals, in this example 20 cm (simulated), will contain foreset data. When the correlation interval is too large, the set boundaries, which have a high textural contrast and hence create a strong resistivity anomaly, will dominate the correlations (Figure 12.19). A correlation interval of *no more than half the bedform thickness* is needed to bring out the internal structure.

With a correct correlation interval, the outcrop work demonstrates that a typical cross-bedded interval shows dip groupings or 'clumps' related to the cross-bed dips

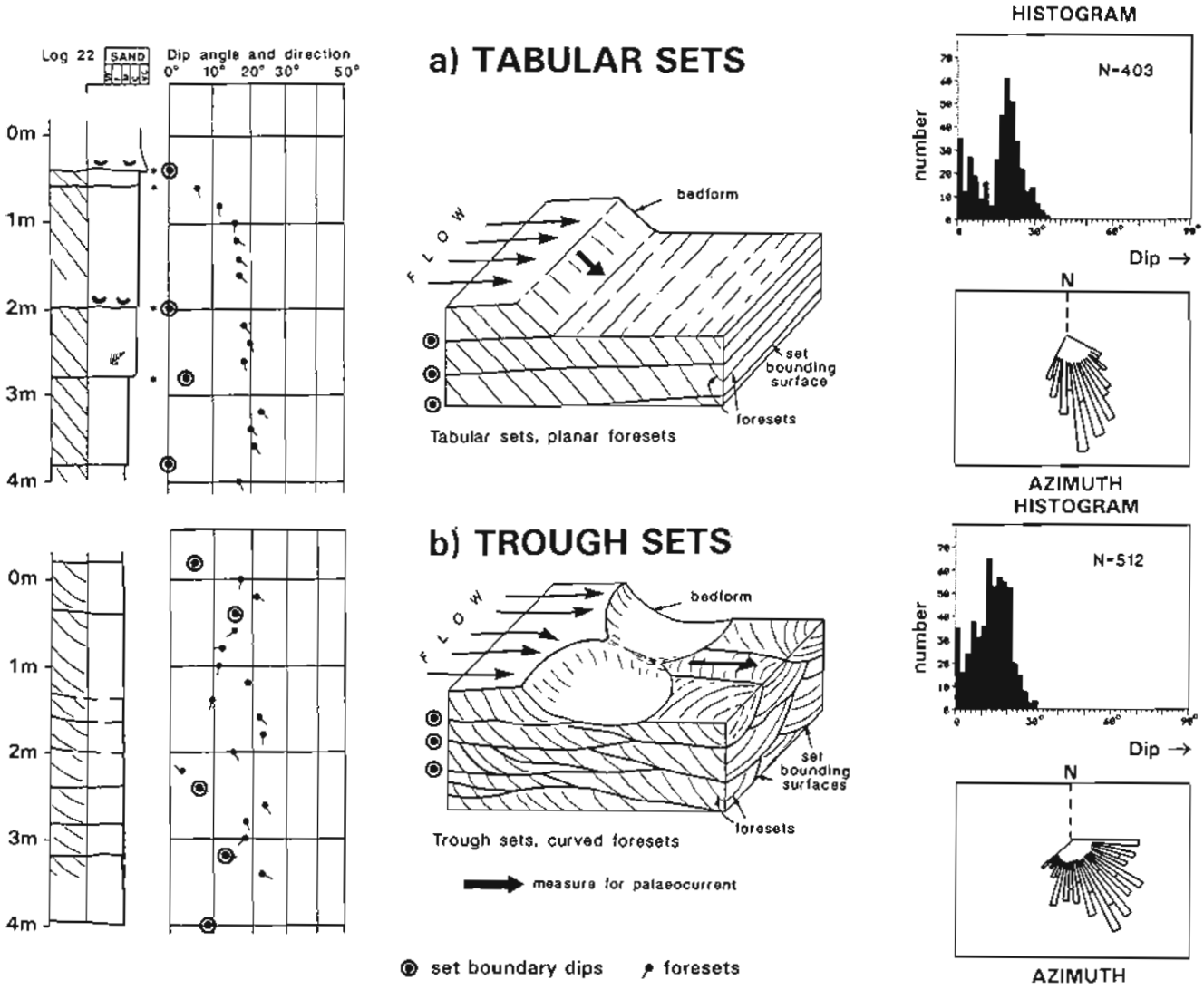


**Figure 12.21** Dipmeter cross-bed characteristics illustrated by outcrop measured diplogs. a) Tabular sets show a bi-modal dip histogram (set boundaries and cross-beds) and tight azimuth rose; b) trough sets show a uni-modal dip histogram (set boundaries and cross-beds combined) and a broad azimuth rose. Simulated 20cm correlation interval (from Cameron *et al.*, 1993).

(Figure 12.21). The actual style of the clumps depends on the bed form: tabular sets give regular clumps with low angle set boundary dips, trough sets give less regular dips with higher angle set boundaries (Figure 12.21). Each of the two bedforms gives a distinctive dip histogram and azimuth rose diagram. The tabular sets give a tight azimuth rose and two populations of dip, a higher angle one between 10°–30°, which are the foresets and a very low angle one, which are the bed-set boundary dips (Figure 12.21*a*). The trough-set bedform gives a more variable rose azimuth diagram and a single dip population with a maximum around 15°–20°. In trough sets, the set bounding surfaces themselves are dipping, albeit at a wide angle to the cross-beds, but set-boundary and cross-bed dips are indistinguishable (Figure 12.21*b*).

To derive a palaeocurrent from such dipmeter data it is essential to try to eliminate the effects of set boundaries as much as possible (Williams and Soek, *in press*). This is especially true if trough cross-beds are involved. These, as shown above, have set boundary dips at high angles to the palaeocurrent (Figure 12.21*b*). The outcrop example shows that dominant cross-bed dips are between 10°–30° (Cameron *et al.*, 1993). Thus, if only dips in this range are accepted as possible foreset indicators, set boundary effects will be minimised. Filtering the data in the outcrop example in this way yielded palaeocurrent directions essentially identical to directions previously measured by classical means (Bristow and Myers, 1989).

The techniques learned from outcrop can be applied to the subsurface. The example (Figure 12.22) shows that the degree of data filtering leading to the interpretation is considerable. Firstly, the dipmeter is plotted with, at very minimum a gamma ray log, so as to be sure of lithology: in this case a sand interval. The consistent azimuth and high dip angles through the sands, suggest foresets: such dips are limited to the sands. With this diagnosis, the low angle dips are discarded and an azimuth rose constructed using only the dips between 15°–30°. These data indicate the palaeocurrent orientation (Figure 12.22).

The next stage in the study of orientations is to analyse a number of wells through the same sandbody and prepare a palaeocurrent map. This may be presented either using the azimuth rose diagrams (Figure 12.23*a*) or the orientations may be analysed statistically. There are a

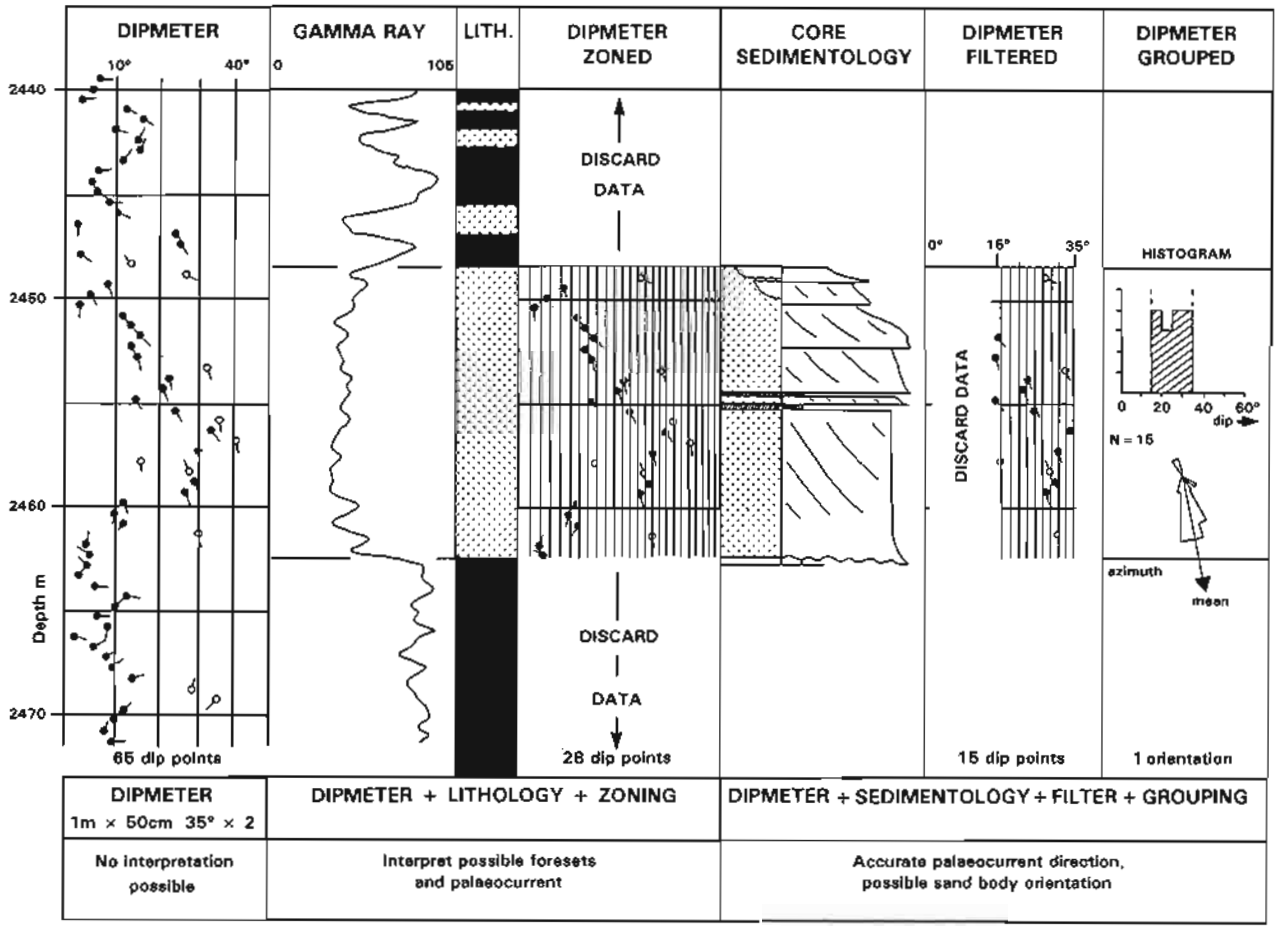


**Figure 12.22** Analysing a subsurface interval for cross-bed orientations. The dipmeter data are strongly filtered for lithology and dip characteristics to reduce the 65 dip data points to 1 measurement of mean azimuth. The mean azimuth can be interpreted in terms of palaeocurrent (*see text*).
(NB structural dip =<1°)

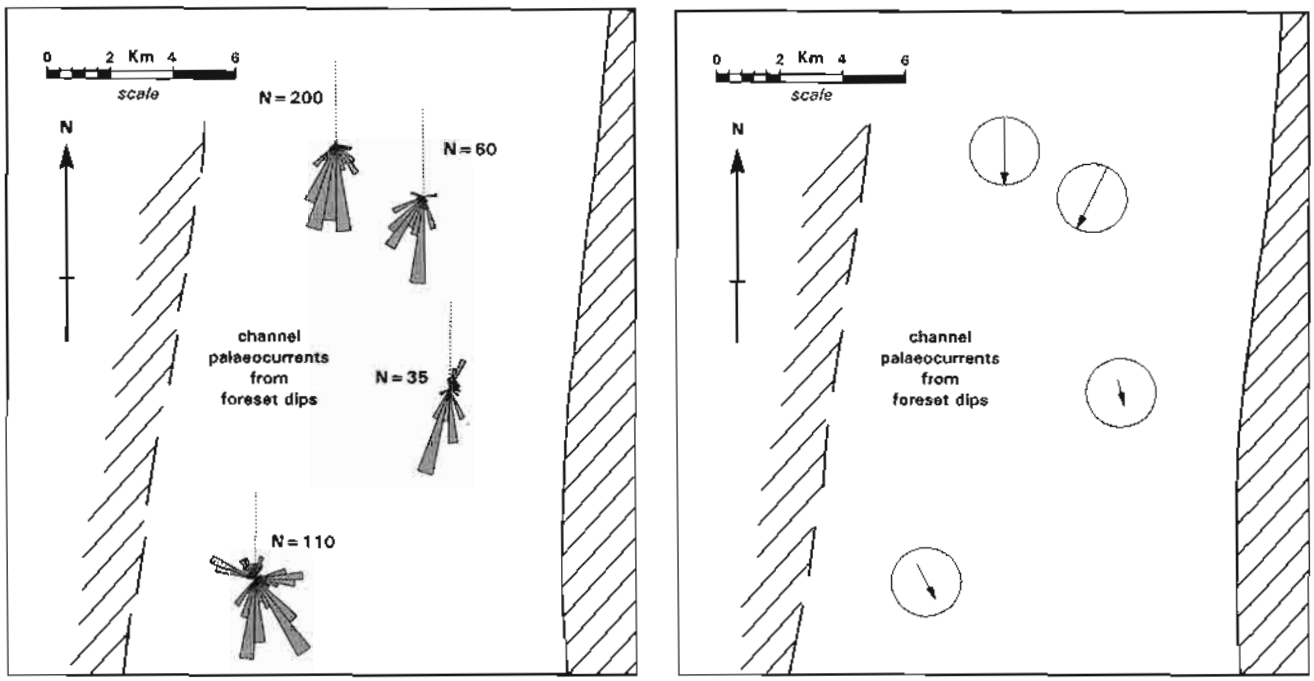


**a. azimuth rose diagrams** **b. vector mean azimuths**

**Figure 12.23** Palaeocurrent analysis from subsurface dipmeter. Carefully filtered dipmeter logs give an indication of cross-bed orientations and palaeocurrents. Only dips in sands and with dip values from 15°–40° have been retained. Map a) shows the data plotted as azimuth roses; map b) shows the mean azimuth orientations of the same data, the length of the arrow being related to the Rayleigh test value (*see text*).

limited number of ways of analysing circular data. The vector mean azimuth simply gives the mean orientation, but the resultant length, with a value between 0 and 1 gives an indication of the narrowness of the population about the vector mean. The higher the value the narrower the population. However, these tests are designed for uni-modal distributions. Generally in sedimentary dipmeter work there is a large spread of data. An additional statistic, the Rayleigh test, may be applied to rate the significance of a preferred orientation (Davis, 1986). That is, it gives a measure of the probability that a given azimuth sample comes from a uniform (i.e. random) population. The smaller the test value the more likely it is that the sample comes from a population with a clear uni-modal distribution. It can be used as a measure of the value of the vector mean azimuth. In this way a large dataset of dipmeter results can be distilled to a single azimuth with a value rating (Figure 12.23*b*).

Occasionally the interpretation of foresets from the dipmeter is possible without the filtering just discussed. When structures are very large and very consistent, such as in aeolian dunes or tidal sandwaves, dipmeter patterns are self-obvious, and even toe-sets are seen (Figure 12.24). But it should be stressed that these cases are not frequent and the structures involved are unusually large.

A geologically meaningful grouping of data is generally the key to interpreting cross-beds and palaeocurrents from dipmeter. The complex routines used in the example (Figure 12.22) were quite simply carried out with interactive software. One complication which has not been brought up here is that of structural dip rotation. When sedimentary, especially palaeocurrent information is required, all structural dip must be 'rotated out' before applying filters as discussed above. That is, the structural dip must be put back to zero first. Only when this is done will the sedimentary dips have their true, original orientation and magnitude (Figure 12.14).

### *Depositional surface dips*

The dip of most depositional surfaces is very close to the horizontal. For instance, in deltaic mouth-bar areas, or in alluvial levées, depositional surfaces have dips of less than 2°. Since dipmeter dip accuracy is within this amount, dipmeter studies cannot indicate the dip of depositional surfaces – despite many authors who have proposed models to the contrary. Also, depositional surfaces seen on the seismic, such as clinoforms, have very low absolute dips and are only seen because the horizontal scale of the seismic sections is very compressed. The vertical exaggeration is some 13–30 times and real dips are in the region of 2–6° (slumping begins at 4°). It is unlikely that these would be recognised on a typical dipmeter log: local, small scale variations dominate.

The dip characteristics of depositional surfaces which do have significant dips, other than those associated with cross-beds and dunes, are not well-known. Accretion surfaces which infill channels, show lower angles of repose than typical cross-beds and, importantly, their dip azimuth is at 90° to the depositing current and channel orientation (Figure 12.25) (Herweijer *et al.*,

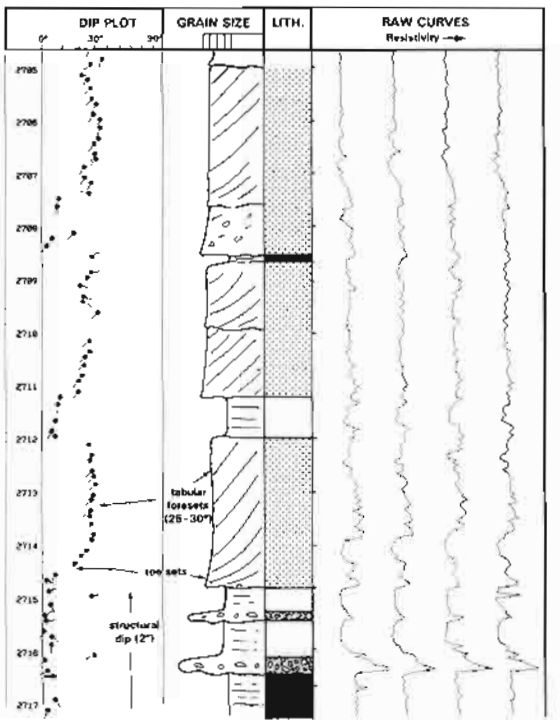


**Figure 12.24** Very large, shallow marine cross-bed structures (sand waves) and characteristic dipmeter plot. The consistently oriented dips at 30° indicate cross-bed orientation. Tangential laminae (toe-sets) are seen between 2714m – 2715m. Structural dip is below 3°. The acquisition curves are plotted to help refine correlation to core. Such large scale sedimentary structures and clear dipmeter patterns are not common.

1990). 'Classic' channel fill with compaction drape which features in many dipmeter manuals is reserved for the very large scale and is rare (*see* Figure 12.27). More typical, in fact, are compaction features above or below channels, although the orientation of these in respect to the channel axis is generally difficult to be certain of.

### *Some other structures*

Many features detected by the dipmeter which are shown to have a marked preferred orientation, have no sedimentological model applicable to dipmeter interpretation. For example, HCS (hummocky cross-stratification) often gives good, slightly irregular dip with vertically consistent orientations (Figure 12.26). HCS is generally not thought of as showing a depositional orientation: the dipmeter suggests otherwise. Recently, it has been suggested that in rare cases, preferred orientations may exist (Duke, *et al.*, 1995). The dipmeter suggests that in fact it is quite common. However, whether this orientation is parallel to the coastline, facing the offshore or the onshore (most probable) is not yet known (cf. Williams and Soek, 1992).

The dipmeter characteristics of turbidite sequences are generally uncertain. One example, however, shows some characteristics which may be expected. In this example (Figure 12.27) a large (30 m × 1 km), previously eroded channel is filled essentially by shale but with several episodes of turbidite sand channels (Phillips, 1987). The western margin of the channel is picked out on the dipmeter as a result of draping from the covering sediments

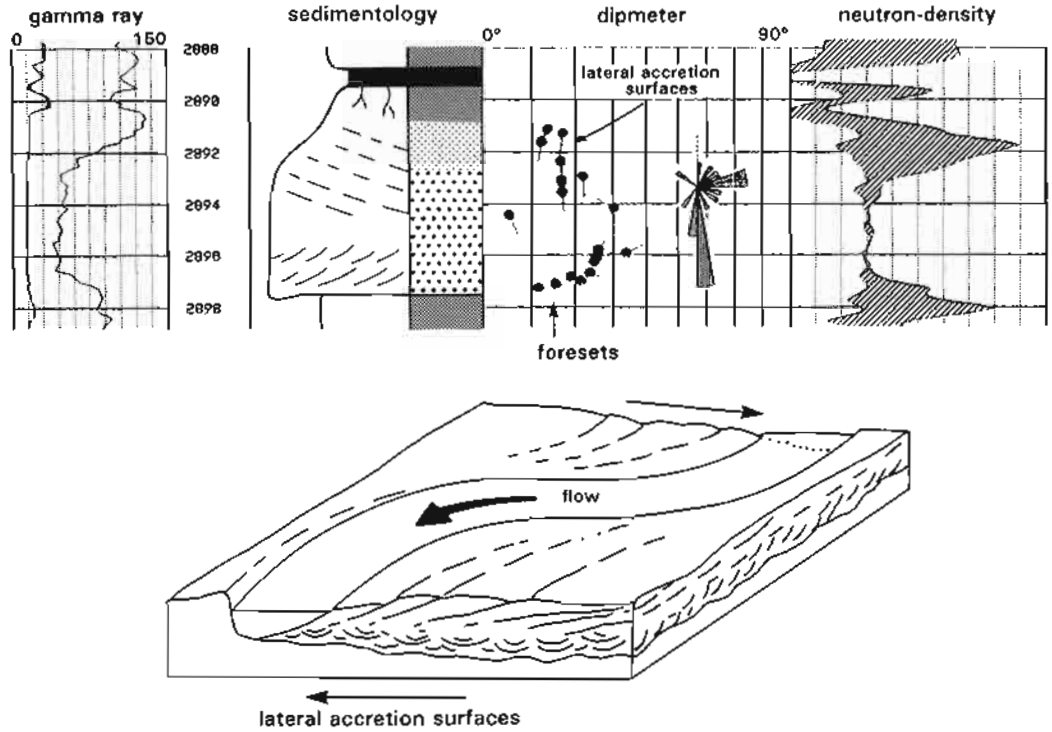


**Figure 12.25** Complex dipmeter from a deltaic channel. The lower interval shows higher angle dips to the east (cross-beds). The upper interval shows lower dips to the south – which are lateral accretion surfaces. Cored interval.

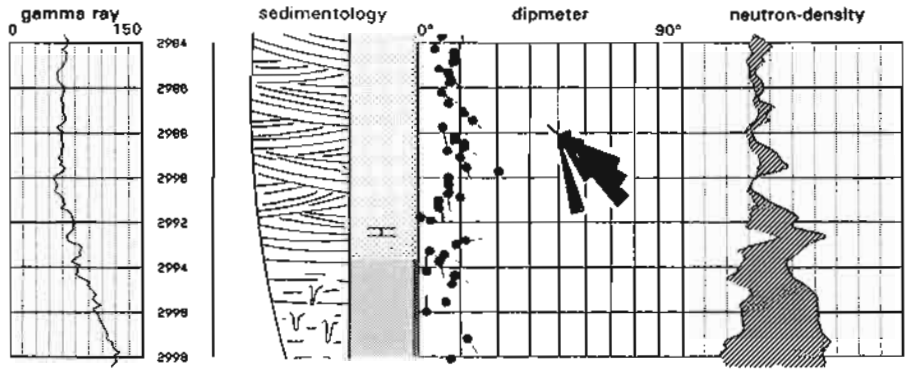


**Figure 12.26** Dipmeter characteristics of HCS (hummocky cross-stratification) in a coarsening-up, marine sequence. Low angle dips with consistent orientations occur in HCS quite frequently. Cored interval.

(Figure 12.27, AU19). Slumping is also interpreted, essentially as small normal faults (Figure 12.27, AU23). As far as the turbidite sands themselves are concerned they show no internal dipmeter characteristics and are considered massive. Their orientation, however, is indicated by drape (Figure 12.27, AU15), generally assumed to be normal to the depositing currents.

These seem in fact to be the more typical features of turbidite sequences. Within sand intervals, high, irregular dips are generally measured (Figure 12.28) which are from bed boundaries and generally show a random orientation. Regular dips however, occur in the thicker shale intervals, but these change from one shale section to the next, the overlying shales giving drape orientations (Fig 12.28). Whether these are channel margin or lobe margin orientations depends on the type of turbidites present. In the example (Figure 12.28) a lobe deposition is suggested, and sand thickness is predicted to increase to the southwest.

### *Texture and facies*

Dipmeter microresistivity curves are acquired to bring out small scale resistivity variations and are therefore sensitive to small scale variations in lithology and texture (Figure 12.19). In the simplest case, the curves can be used to identify thin beds, beds down to 1 cm rather than 15 cm typical of the standard logs (cf Serra *et al.*, 1993). However, from a geological perspective, the fine scale of the dipmeter curves may be used as facies indicators (Cameron, 1992). Three typical siliciclastic facies are illustrated along with schematic dipmeter microresistivity curves (Figure 12.29*a–c*). Each facies shows distinct microresistivity curve characteristics illustrated by the real, core controlled, subsurface examples alongside

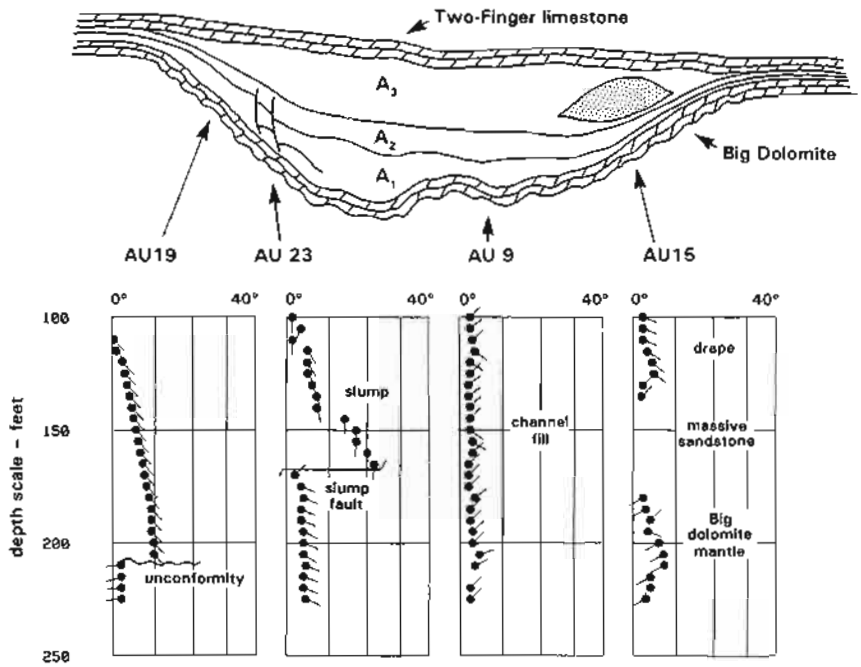


**Figure 12.27** Dipmeter characteristics of a valley-fill sequence. The previously eroded channel was filled by shales and some turbidite sands. On the dipmeter the sands are featureless but the shales show compaction (AU19), slumping (AU23) and draping over sand-bodies (AU15). (Re- drawn and plotted after Phillips, 1987).

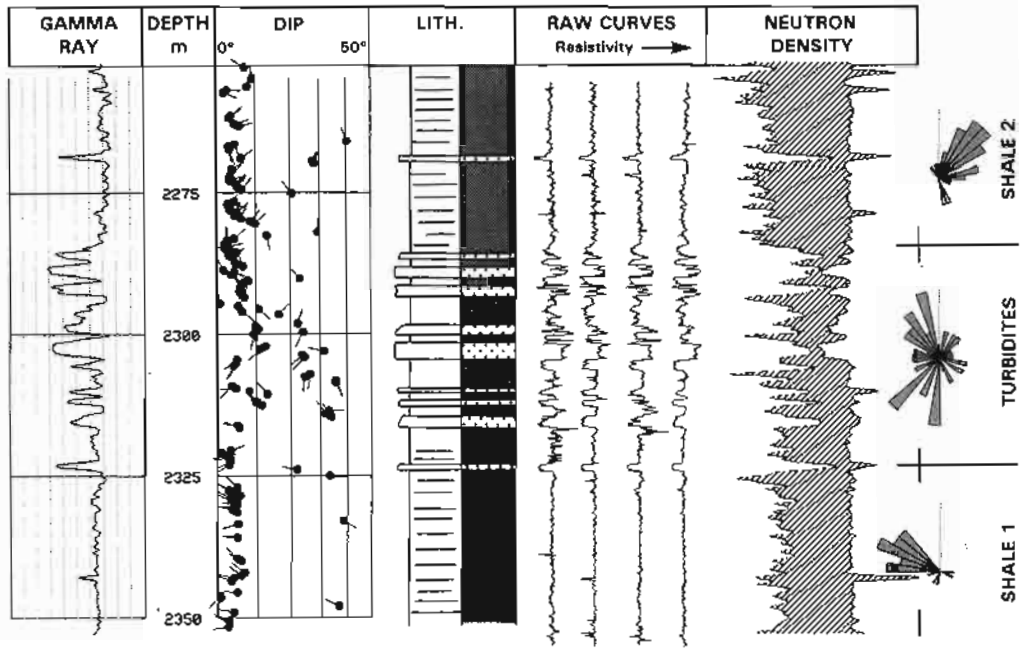


**Figure 12.28** Typical dipmeter response in a turbidite sequence. The turbidite sands show scattered dips with no preferred orientation. The shale sections show regional dip (shale 1) and drape over very subdued submarine topography, in this case a lobe (shale 2). The acquisition curves are essential to fine lithological interpretations in such (thin-bed) sequences.

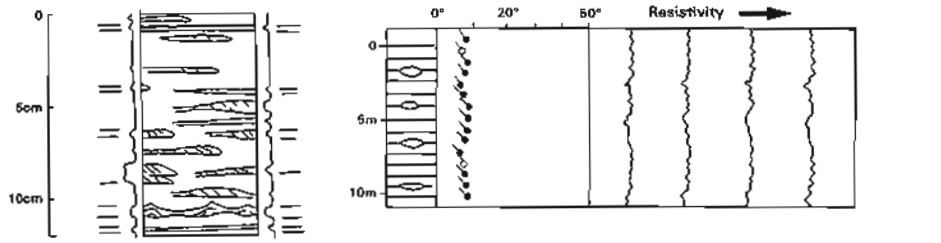


A. LAMINATED silty shale

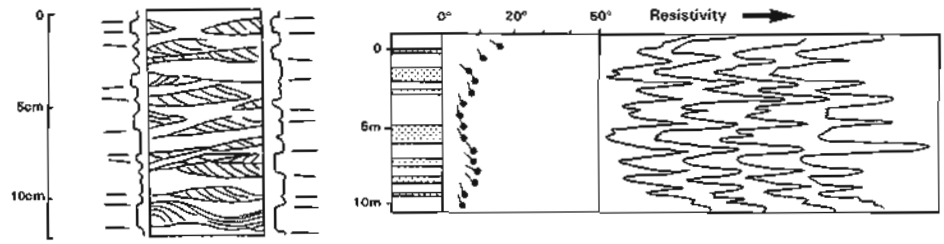


B. FLASER-LINSEN sands and shales

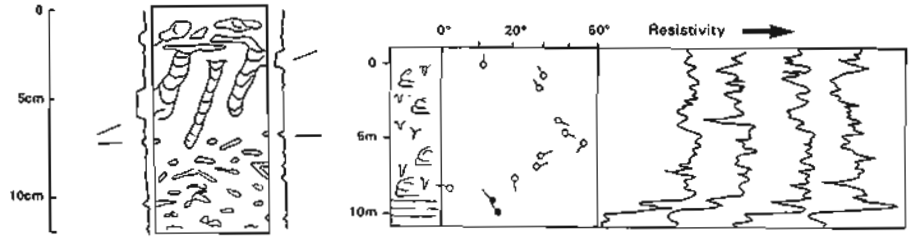


C. BIOTURBATED sandy shale

**Figure 12.29** Texture and facies indicated by dipmeter acquisition curves and dipmeter plots. A. Laminated silty shales give regular dips but little acquisition curve character; B. flaser and linsen give excellent curve character but irregular, variable dips; C. bioturbation can give good curve character which is, however, irregular and produces poor quality, scattered dips (the so-called bag-of-nails).

(Figure 12.29). For example, facies *b*, flaser and linsen, shows strong electrical contrast between the discrete, clean sand and clean shale layers. In facies *a*, laminated shale, electrical contrasts are much less pronounced.

Although it is principally the microresistivity curve characteristics that bring out facies information, the processed dipmeter results themselves are indirectly affected. For example, although a bioturbated sandy shale may show good electrical contrasts in the curves, there is no curve similarity and the processed dips are poor, inconsistent and scattered (Figure 12.29*c*). Equally, the other two facies illustrated show the effects that the curve characteristics have on the computed results, although it is only when the curves are plotted alongside the results that it is possible to make a facies interpretation.

## 12.8 Structural dipmeter interpretation

### *Structural dip: definition, processing and identification*

By *structural dip* is intended the '*general attitude of beds*'. It is the dip that would be measured at outcrop. It is usually the dip seen on seismic reflectors, themselves a generalisation. It avoids any sedimentary structures of any size and is generally considered to represent the depositional surface which also is considered to be horizontal. There are of course many exceptions where the depositional surface is not horizontal (Figure 15.23).

A dipmeter log is processed for structural dip with a relatively broad correlation interval, typically 1 m (3' or 4') (Figure 12.18) (Bigelow, 1985). Step distance,

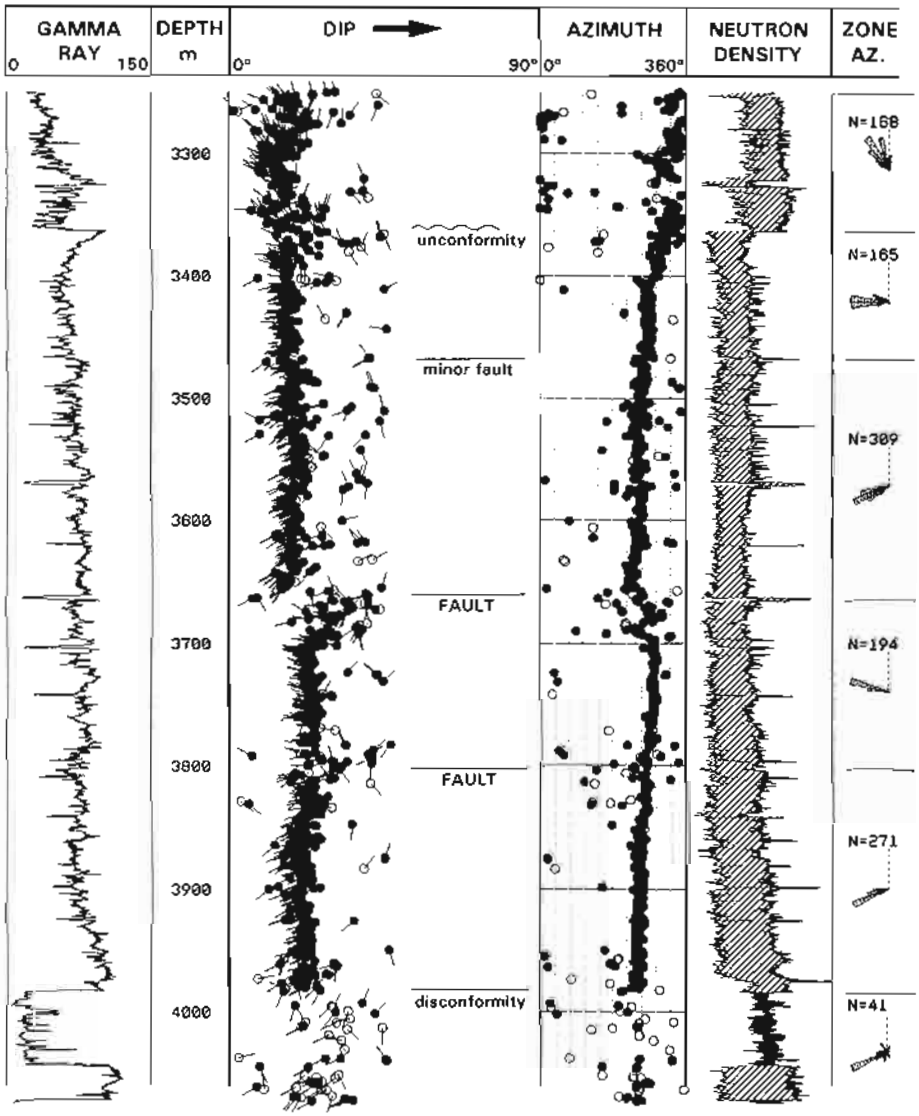


**Figure 12.30** Structural dip seen on a summary scale dipmeter log. Dips are generally to the west at between 10°– 15° through this essentially shale section, but as the zoned azimuth plot and the azimuth log indicate, there are subtle variations caused by faulting and unconformities. Such changes are not picked out effectively on standard scale plots.

expressed as a percentage, is normally 50%, although 25% sometimes gives better results. The search angle may be set reasonably low if the general dip is known. Programmes that generalise and 'clean up' dipmeter logs can be used for structural work. Cluster, a Schlumberger programme (Hepp and Dumestre, 1975), attempts to diminish inconsistent dips so bringing out structural trends in the more consistent data. However, programmes which group and do not modify the original data are probably better (*see* next section).

On the log itself, structural dip should be measured over fine grained (shale) intervals where bedding is more likely to be planar and regular (Figure 12.30). Thick shale intervals are clearly best since thinner shales in sand-shale sequences often show distortion inherited during compaction. Structural dip may be measured either on the log itself when it is relatively constant and there is little scatter, or from a stereographic polar plot, where it will be chosen as the most common orientation (Figure 12.14). Statistical tests may also be applied to derive a value. In the case of structure, simple two dimensional statistics are usually not acceptable and it is necessary to apply eigen vector analysis (Davis, 1986).

A reliable identification of structural dip is essential, as most recognisable structural features are a distortion of it. The structural interpretation of dipmeter data, like structural geology, is about geometry and geometrical consistency or inconsistency.

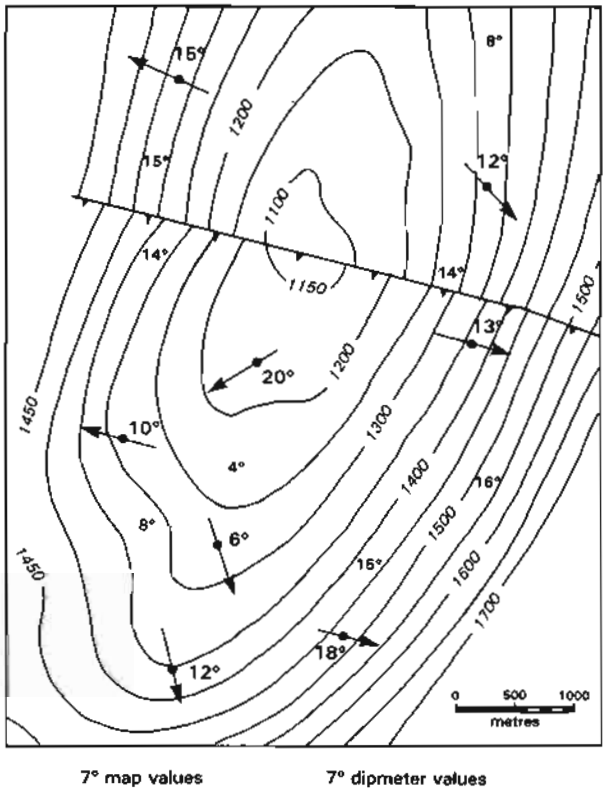


**Figure 12.31** Structural dipmeter results plotted on an isobath map produced from the seismic. Dip angles derived from the map are shown: the azimuth is indicated by the map contours. Dipmeter and map data should correspond.

### *Structural dip: correlation, mapping and seismic sections*

The most straightforward use of the structural dipmeter is in simple structural situations. For example, on structural cross-sections or correlation sections which are drawn to scale, dipmeter stick plots in the line of the section (i.e. show the apparent dip in the line of the section) can be very helpful. Secondly, seismic maps can be checked against the dipmeter. The contours of a typical, depth converted (isobath) seismic map contain an implied amount of dip and orientation. Map and dipmeter can be checked one against the other (Figure 12.31).

An extremely practical and useful aid to structural dipmeter interpretation is to be able to directly compare dipmeter results with seismic sections. This involves quite complex conversions such as plotting the dipmeter

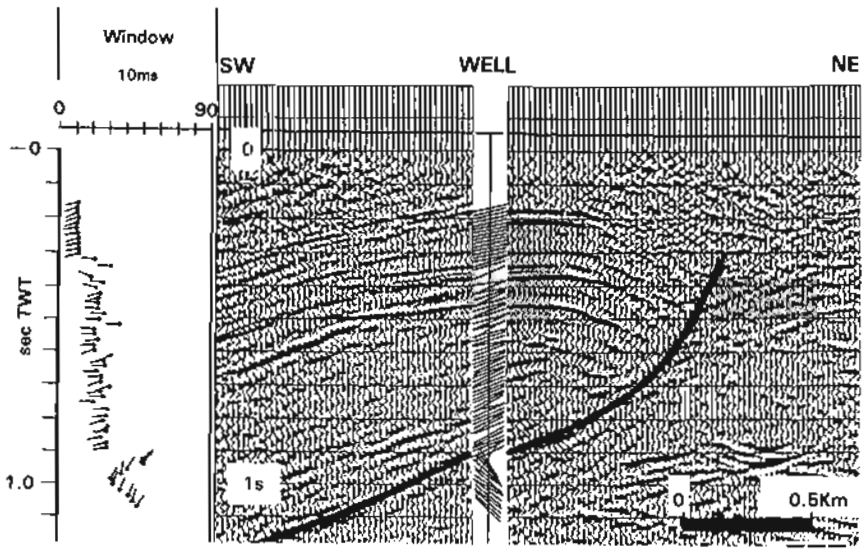


**Figure 12.32** Dipmeter data plotted on a time scale and converted to the scales and orientation of a seismic line for direct overlay. A stick plot is used for this. The example shows a listric fault with rollover (from Werner *et al.*, 1987).

on a time scale rather than depth scale, correcting for interval velocity, plotting the dip results in the plane of the seismic section (i.e. with apparent dip) and with a compressed horizontal scale. The results are best presented in the form of a stick plot. Necessarily, this conversion is achieved by computer. The example (Figure 12.32) shows a listric fault, with a marked rollover, crossing the well just above TD (Werner *et al.*, 1987). The fact that it is a listric fault is clear on the seismic but not on the dipmeter; but the location of the fault is clear on the dipmeter, difficult to pick on the seismic. The integration of both sets of data, dipmeter and seismic, gives confidence in an interpretation beyond either set individually. In areas for example, of difficult multiples, side-swipe or complex tectonics, the seismic dipmeter plots are very useful.

### *Unconformities and disconformities*

One of the most frequently perceived uses of the structural dipmeter is in the identification of unconformities. However, for an unconformity to be seen on the dipmeter it must be angular: disconformities or paraconformities will not be seen. The first example (Figure 12.33) shows a strong, angular unconformity; the beds above being nearly horizontal, those below dipping at approximately 22° to the west. The example also shows, which is very typical, that the dipmeter cannot be used to pinpoint the actual unconformity level; the dips are too scattered due to burrowing, weathering or diagenesis. Using the neutron-density logs allows the precise level to be located at a probable hardground (Figure 12.33), but it is only the dipmeter that indicates the angularity of the break. The second example (Figure 12.34) shows a more typical unconformity, where the angular change is very small and the break indicated by a moderate azimuth change, not a dip change. For such subtle breaks to be brought out, it is necessary to use a compressed scale log (1:2000 to 1:5000) and to zone the dipmeter data carefully, the actual break being selected on the standard logs rather than the dipmeter itself. The necessity for combining the dipmeter with other open hole logs is clear.

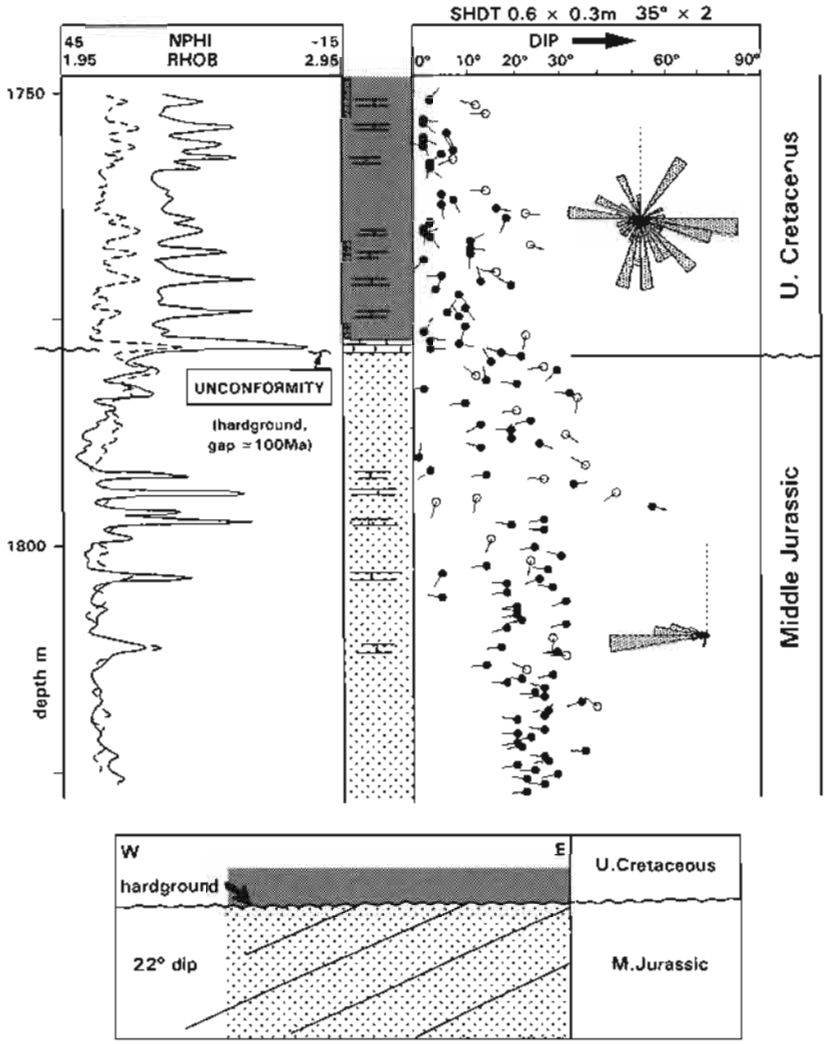


**Figure 12.33** An angular unconformity on the dipmeter. Jurassic sands dip at approximately 22° to the west and are overlain by horizontal, Upper Cretaceous shales. The unconformity is picked from the standard logs and a hardground is interpreted from the density log at the unconformity level. It is the dipmeter, however, that shows that the unconformity is angular.

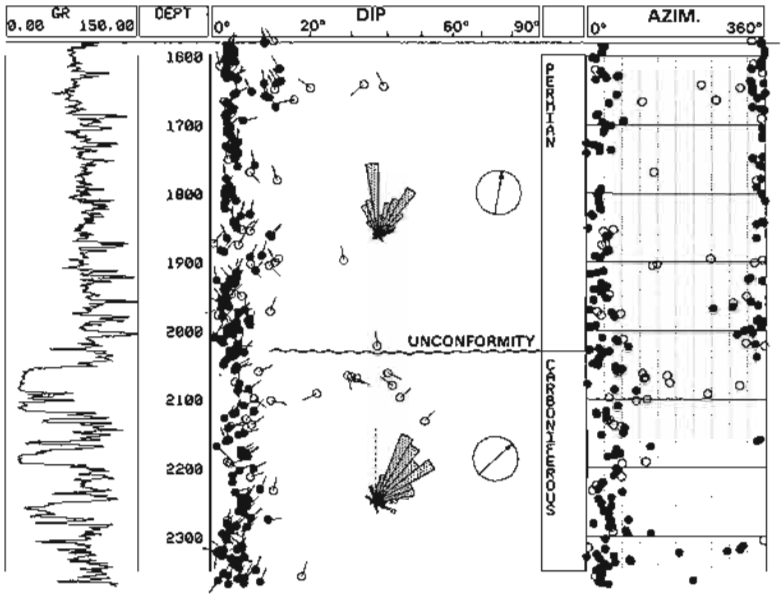


**Figure 12.34** A slight angular unconformity indicated by zoned dipmeter data. Only when the unconformity is picked on the standard logs and the dipmeter data are zoned, do the differences in azimuth become apparent. This type of unconformity is typical.

### *Faults*

Faults are identified on the dipmeter through geometrical distortion: that is changes of dip or changes of azimuth, or both (Figure 12.30). If there is no distortion, no fault will be seen. In reality, there are two types of distortion with a potential to be identified on the dipmeter: distortion about the fault plane itself and distortion, or geometrical change from one fault block to another. Interpreters often confuse the two, but the scale is quite different as illustrated below.

A second confusion is that the dipmeter can seldom give a conclusive indication of fault plane dip, or of whether the fault is normal or reversed. If distortion about a fault is cylindrical, a fault plane strike can be given but not the dip of the fault plane. The following examples show this.

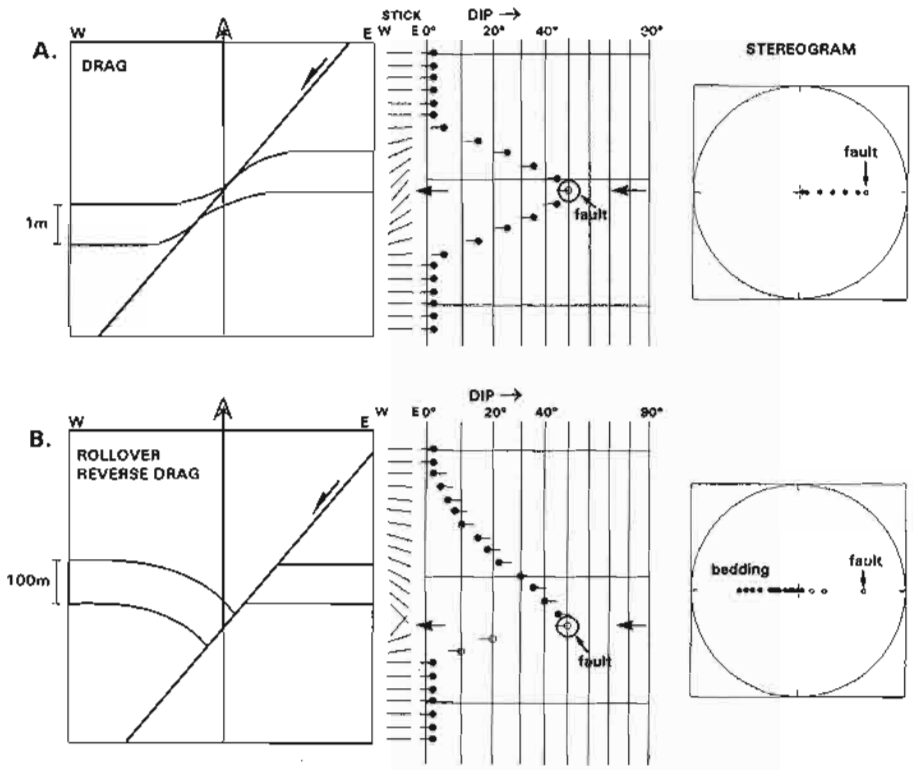


**Figure 12.35** Fault characteristics on the dipmeter illustrated by a sketch, log and stereogram (Schmidt). A. drag, typically at a small scale around the fault plane itself. The stereogram shows cylindrical distortion with the highest dip close to the dip and orientation of the fault plane. B. rollover or reverse drag, a large scale effect. The stereogram shows cylindrical distortion with the dip of the fault plane opposite to bedding dip.

*– distortion at the fault plane, fault drag*

It is generally assumed that faults can be recognised on the dipmeter by *tectonic drag*. Drag forms as beds are pulled along a fault zone like a wet rag, as movement progresses (Figure 12.35*a*). This movement is considered cylindrical, so that beds are rotated (dragged) progressively into the plane of the fault as the fault itself is approached. A dipmeter through a zone of drag will show a cusp pattern on the log (Figure 12.35*a*) while the dips in the cusp, when plotted on a stereogram, will fall on a great circle (i.e. form a cylinder). There are cases when this is true, but personal field experience suggests that drag zones are very limited and often not seen on a structurally processed log or the style of drag is not the classical cylinder (Figure 12.37).

It is sometimes suggested that drag, when it occurs, can indicate the amount of throw on a fault. That is, the vertical extent of the drag zone corresponds to the amount of throw. It is possible to use the drag zone as a minimum, but not as an absolute indication of the throw. An interesting case described recently suggests that drag characteristics may be indicative of whether a fault seals or not (Berg and Avery, 1995).

*– distortion between fault blocks, tectonic rollover and reverse drag*

Frequently, what is considered as, or at least called drag, is in fact *tectonic rollover or reverse drag*. Rollover and reverse drag occur on a much larger scale than drag and are related to the distorting effects that faulting has on the entire rock mass, not the distortion just around the fault itself. Moreover, rollover and reverse drag cause beds to dip *into* a fault, not to parallel it (Figure 12.35*b*). (Although rollover is shown in the example (Figure 12.35*b*) as restricted to the hanging wall, this is not always the case. It *is* the case in listric faults – *see below*). If a cusp pattern is identified on the dipmeter, it is essential to know whether it is drag and parallel to the fault, or rollover/reverse drag and contrary to the fault. This dilemma is beautifully expressed by an example from Nigeria (Adams *et al.*, 1992). An obvious tectonic cusp pattern is seen in the dipmeter over 200 feet (60 m) of borehole, the dip consistently increasing downwards from 10° to 50°, then dropping back to 10° (Figure 12.36). A computer programme was used to model this dip pattern. Three equally valid cases satisfy the dipmeter results: a normal fault with drag, a normal fault with reverse drag and a listric fault with rollover. The computer programme very effectively provides a model for the eye that a line of dips cannot (cf. Etchecopar and Dubas, 1992). Indications from the seismic suggest that it is a normal fault with drag. However, the example illustrates perfectly the difficulties in interpreting faults from the dipmeter and that even though a fault may be identified from the dipmeter alone, it is generally not possible to interpret the type of fault or the direction of displacement on it. The fault strike is however generally clear, being orthogonal to the distorted bedding dip.

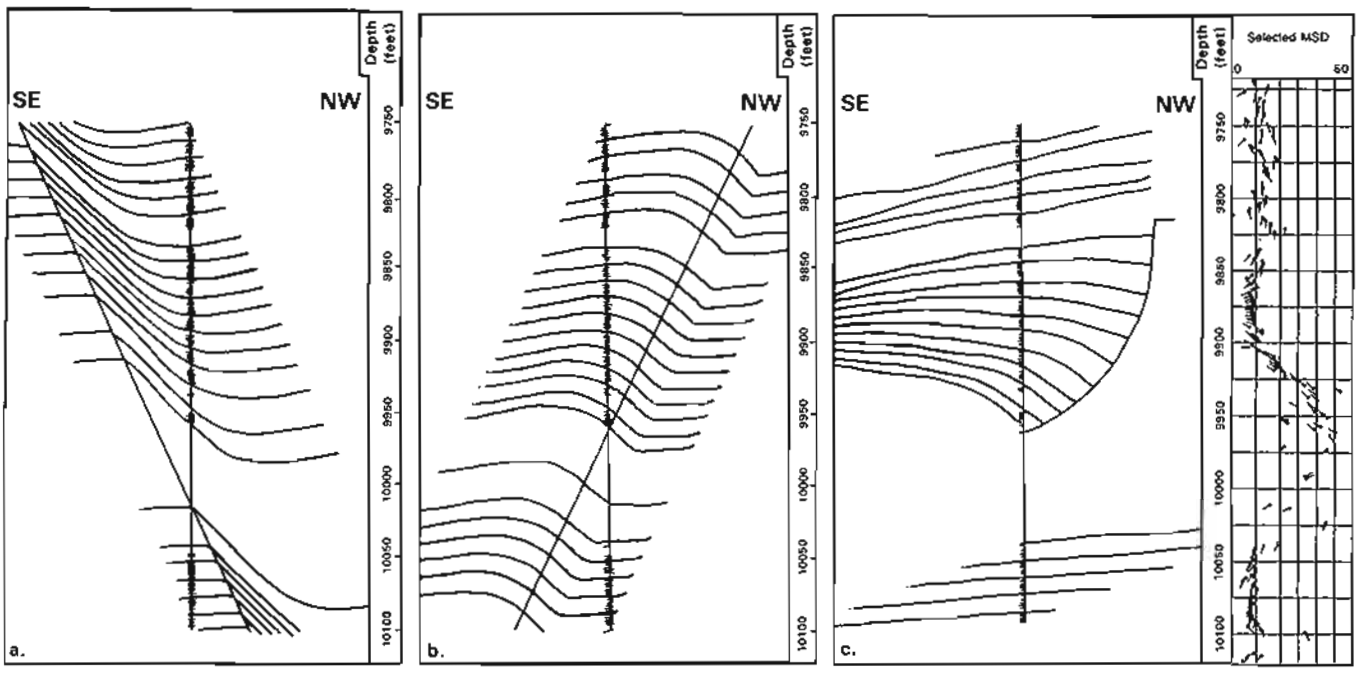


**Figure 12.36** Fault geometry interpreted from the dipmeter. Three interpretations are possible from the one dipmeter dataset (shown on the right): a) normal fault with drag (correct interpretation); b) reverse fault with drag; c) listric fault. Computer generated profiles (from Adams *et al.*, 1992).

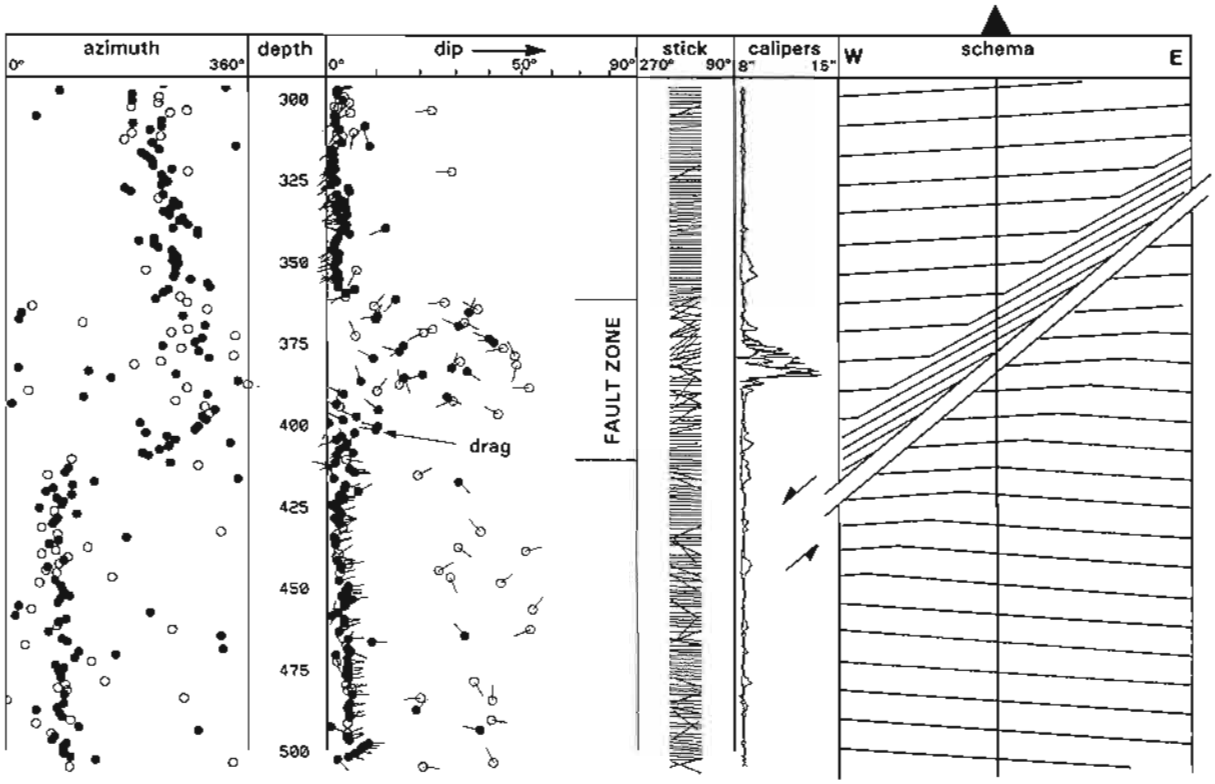


**Figure 12.37** Dipmeter example of a large normal fault (300m throw, seismically visible, westerly dipping). There is no clear dip change and the fault is best recognized from the azimuth plot (far left): dip azimuth is east below the fault, west above. There is no typical drag but a zone of about 50m has high dips which parallel the fault dip. The position of the fault plane (if there is just one) can be proposed at the site of caving indicated on the calipers. The entire section is shale.

*– subsurface example*

The reality of fault identification using the dipmeter is more prosaic and practical than most dipmeter handbooks would suggest. The first necessity is to identify a break as a fault. The next necessity is to describe the geometry. Usually the dipmeter responses are not classical in the least. The example (Figure 12.37) shows the dipmeter response to a large normal fault through a shale sequence. The presence of a fault is obvious. The upper section (300 m–360 m) dips at low angles to the west: the lower section (390 m–500 m) at low angles to the east. There is a distinct azimuth change although no change in dip angle, a feature common in subsurface faults. Between the two sections is a zone of high, poor quality, confused dips which is the fault zone. In this case, a normal fault has been identified on the seismic dipping to the west. The dipmeter then shows the exact location of the fault, that the dominant dips in the fault zone are westerly and parallel to the fault plane. There is very minor drag just below the fault seen as a dip reversal. Clearly, there is an absolute need for combining the carefully analysed dipmeter with seismic interpretation. This can be refined by using the time scale dipmeter plots in direct overlays as illustrated previously (Figure 12.32).

*– outcrop example*

The final example is of field measured diplog profiles across a small fault which outcrops over a wide, wave-cut platform and through an associated vertical cliff. The illustration shows the fault as it is seen in the cliff, dipping to the north (Figure 12.38a). The two diplog profiles are measured at different points on this fault as it crosses the wave-cut platform. The first diplog, 130 m from the cliff, shows the fault more or less as it is in the cliff section (Figure 12.38b). The diplog registers the fault as a change in azimuth and not a change in dip, which tends to be a more diagnostic feature for the eye in vertical slices through faults. The second profile (Figure 12.38c) 230 m from the cliff, crosses the same fault where there is neither a dip nor an azimuth change; no fault would be identified in the subsurface. There is clear character change along fault strike.

This example is used to stress two things: the dipmeter is just one more tool in fault identification to be used in conjunction with others and that there is a great need for outcrop study of fault detail in terms of dipmeter response.

### *Folds*

Folds are not often seen in hydrocarbon wells in their entirety. Slump folds are the obvious exception. However, it is instructive to look at dipmeter patterns of small scale folds to illustrate the problems of interpretation of large scale folds as they are encountered in wells.

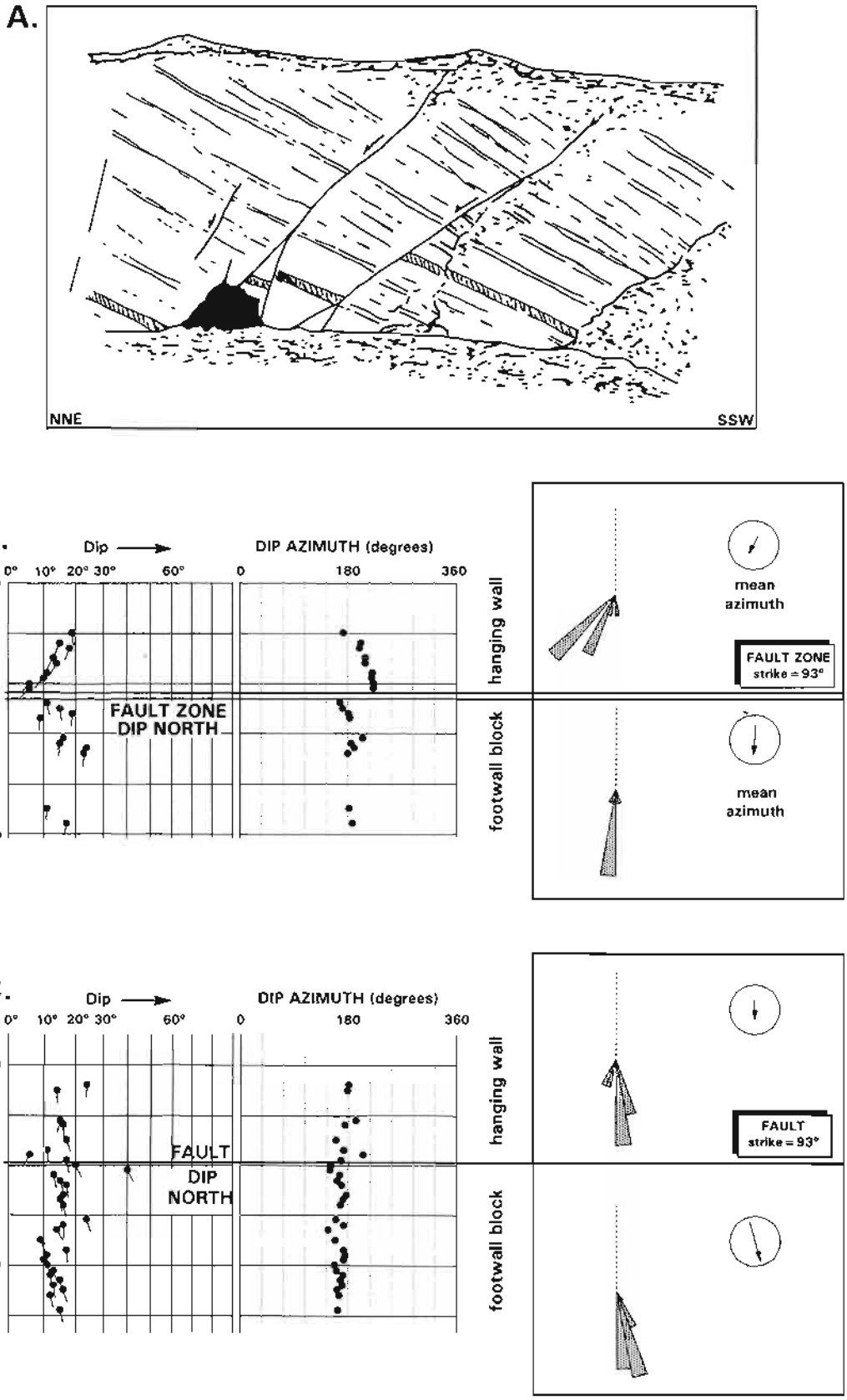


**Figure 12.38** Outcrop example of a small normal fault. A. cliff profile. The diplogs were measured through the fault across a wave-cut platform in front of the cliff. B. 130m from the cliff, showing a well-defined fault and azimuth change. C. 230m from the cliff showing no dipmeter changes across the fault. The example illustrates that character may change along the same fault and that a fault may not be detected by the dipmeter when there is no geometrical change (measurements by C. Townsend and R. Sutherland).

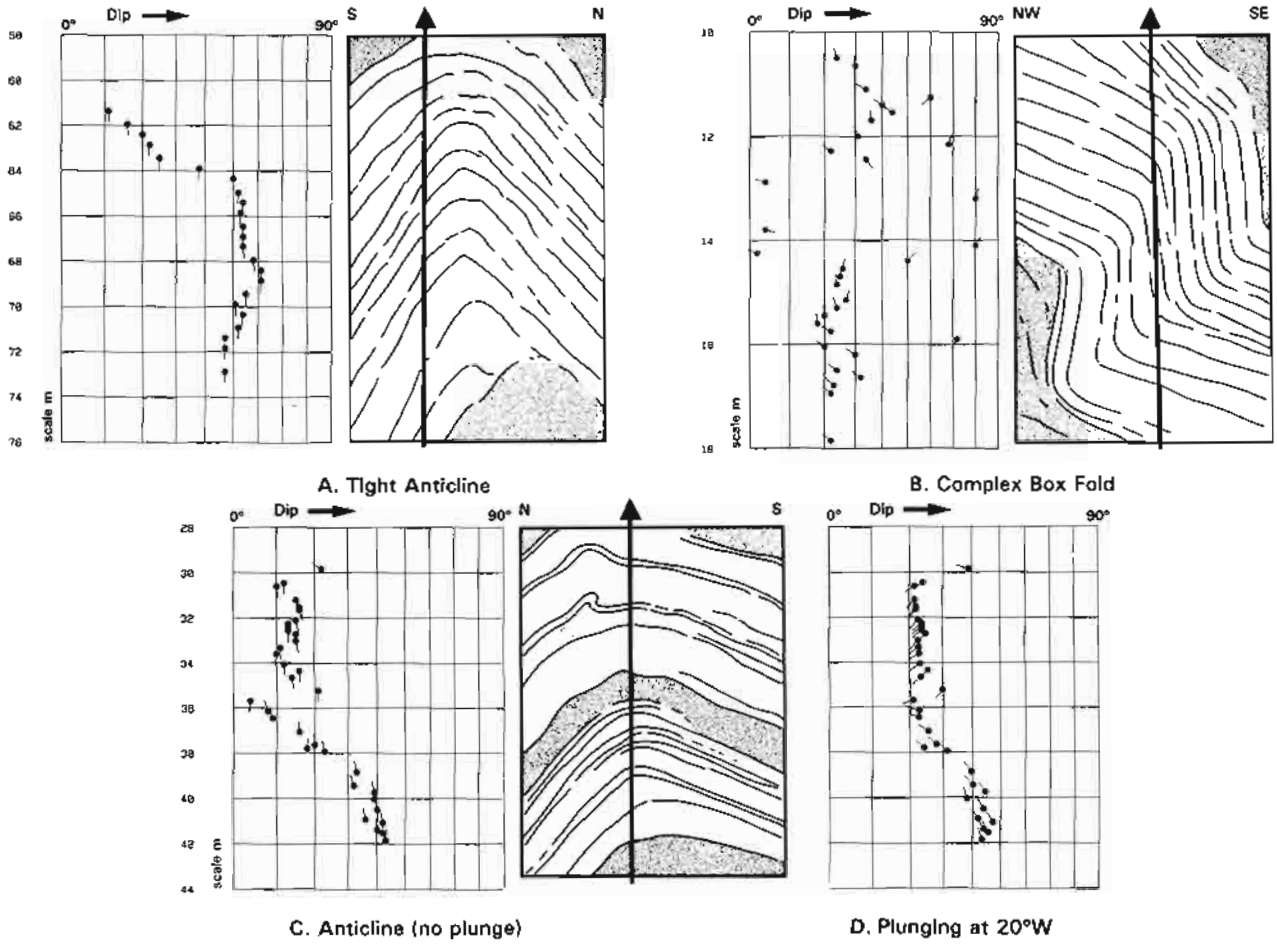


**Figure 12.39** Folds on the dipmeter. Outcrop measured diplogs with line diagrams of the corresponding fold. The well symbol indicates the line of measurement. a) tight anticline, one limb measured; b) complex box fold; c) anticline with well crossing the fold axis (dip section, oriented N–S); d) same with a 20° plunge to the west (measurements by G. Cameron).

The figures (Figure 12.39), are all taken from photos rendered as line drawings. The dipmeter profiles alongside the drawings are measured partly in the field, partly from the photos and are therefore somewhat schematic. Case A is a tight anticline sampled from one limb. The picture is relatively simple. Case B is a box fold with vertical beds in one limb. The dipmeter in this case would be extremely difficult to interpret and may be confused with a fault or simply missed. The last case, C, is of a simple anticline with the well passing across the crest. The line of the section is north-south so that as the fold crest is crossed, dips swing abruptly from south to north across a low dipping section. The dipmeter profile is reasonably interpretable, especially if a sterographic projection is used. If, however, the fold plunges, the dip pattern becomes more complex and interpretation more difficult. In this case stereographic analysis is obligatory. The obvious feature of these examples is the extreme difficulty in recognising the fold geometry from the dipmeter profile. To analyse and identify fold geometry, stereograms may be used as in classical structural geology (Ramsey, 1967) but this destroys the depth information in the original dipmeter data. A more effective solution is to present the dip and azimuth data separately or as SCAT plots (Bengtston, 1980; 1981; 1982).

Details of the SCAT (Statistical Curvature Analysis Technique) plot technique cannot be given here, but it allows folds to be identified and also the level at which the well crosses certain unique positions such as the fold axis and axial plane. An effective description of the structure being drilled can be made. In some exploration areas, even today, seismic is very poor and wells are drilled on surface outcrop structure just as they were in early days. SCAT techniques allow the integration of the surface data and the well data. The example shows the fold of figure 12.39*c* in SCAT format (Figure 12.40).

### *Fractures*

Fracture identification with the dipmeter is notoriously difficult. Dip tadpoles themselves will not normally indicate fractures since they have dips much higher than the associated bedding. When a dip is calculated, the lowest angle of dip is taken and two dips cannot be calculated at the same level. Hence, even when marked fractures are present, the dipmeter dip will be that of the bedding. This is nicely illustrated by an image log analysis of the

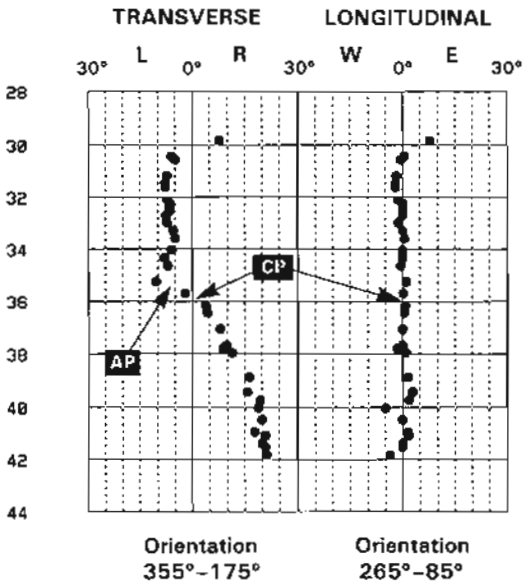


**Figure 12.40** SCAT (Statistical Curvature Analysis Techniques) plot of the fold of Figure 39, C. The transverse plot shows the amount of dip in the dip (or transverse) orientation while the longitudinal plot shows the amount of dip in the strike (or longitudinal) orientation. Special points are the CP or crestal plane (the present structural top) and the AP or axial plane, which is the point of maximum dip change. Such plots are used to identify geometry, especially of folds, from dipmeter plots.

Monterey Formation of California. Manual image log analysis identifies high dipping fractures and low dipping bedding planes while dipmeter processing of the same data shows only the bedding planes (Sullivan and Schepel, 1995).

The technique for fracture identification which has been marketed uses the dipmeter curves, not the processed dip results. When an open fracture is present it will be seen on a dipmeter microresistivity curve as a conductive anomaly, caused by the invasion of the drilling mud. Normally, this anomaly will only be seen on one (at most two) of the curves. Thus, comparing the normal resistivity at any level allows conductive anomalies to be detected. These are attributed to fractures and may be given an orientation since the dipmeter pad bearings are known. Although this was an interesting idea, its application was full of problems from floating pads, poor hole etc and the results never certain. Borehole imaging tools now offer an excellent way of detecting fractures (Chapter 13).

## 12.8 Conclusion

This chapter on dipmeter interpretation requires a conclusion. The dipmeter, an expensive tool to run, is still not being used to its full extent. Interpretation is to blame.

Dipmeter interpretation is heavily dependent on the computer, for processing, formatting and manipulation. Each step involves geologically biased choices, so it must be a geologist who uses the computer.

The dipmeter should never be interpreted alone. Dipmeter 'experts' have a tendency to 'over interpret' the data, generally in isolation. The log is just another tool: provides just another set of data and must be integrated with the standard logs, with sedimentology and the seismic, at the very minimum. The recently arrived image logs (next Chapter) are considered to replace the dipmeter. This is not so. The dipmeter complements the image logs and is used alongside them. Moreover, some of the problems of image log interpretation are identical to the problems encountered in dipmeter interpretation.

The great lack in dipmeter work is that there are so few outcrop analogues and models of orientation data collected in such a way as to be usable by the dipmeter interpreter. This applies as much to sedimentological dipmeter interpretation as to structural dipmeter interpretation. The advent of the image logs is exacerbating the problem.

# 13
# IMAGE LOGS

## 13.1 Generalities

***Description***

A fundamental new concept has been introduced into logging with the advent of the modern imaging tools. The formation is no longer sampled by a single sensor to create a single log, it is sampled many times horizontally and at a high rate vertically, to form a dense matrix of measurements from which is created an image. This is not a picture like a core photo made in visible light, it is a computer created image based on geophysical measurements of acoustic reflectivity or of electrical conductivity. The images represent formation response at the borehole wall and give a continuous vertical record of the entire borehole circumference (or as much as possible in the case of the electrical images). Standard interpretation techniques no longer apply. With the new tools, there are new attitudes.

Since the mid-eighties there has been an explosive development in imaging technology, principally in terms of tools but also in terms of producing the image. The progress has been linked with the availability of downhole digitisation of signals and the possibility of transmitting large data volumes in real time. Where the standard logs are sampled every 15 cm (6"), image logs may sample every 0.25 cm (0.1"): where the standard logs have one measurement per depth point, image logs may have 250. This makes for very large data volumes, for some tools in the region of 200 kilobits per second transmitted up the cable to achieve a collection rate of 60,000 samples per metre of borehole. Imaging technology is still evolving rapidly and is affecting the entire logging field.

**Table 13.1** Imaging tools.

**Electrical Imaging Tools:** water-based only, ratio of resistivities mud/formation less than 20,000 ohm/m, mud maximum resistivity 50 ohm/m, not too conductive: partial borehole coverage only: vertical sampling rate 0.1" (2.5mm) for Schlumberger tools.

| Company | Symbol | Name | Description |
|---|---|---|---|
| Schlumberger | FMI | Fullbore Formation MicroImager (current tool 1996) | 4 pads + flaps<br>192 (4 × 48) electrodes |
| Schlumberger | FMS | Formation MicroScanner (older tools, pre-1991) | 2 or 4 pads<br>54 (2 × 27) electrodes<br>64 (4 × 16) electrodes |
| Halliburton | EMI | Electrical MicroImaging | 6 independent pads<br>150 (6 × 25) electrodes |
| Western Atlas | *STAR | Simultaneous Acoustic & Resistivity Borehole Imager | 6 independent pads<br>144 (6 × 24) electrodes |

*the STAR tool consists of a 6 arm resistivity tool combined with the CBIL tool

**Acoustic ImagingTools:** used in any fluid including oil-based mud, density range of mud up to 1.8 g/cm$^3$ (15 lbs/gal) (cf. Table 13.6): full borehole coverage: vertical sampling depends on logging speed.

| Company | Symbol | Name | Description |
|---|---|---|---|
| | BHTV | Borehole Televiewer | general name |
| Western Atlas | *CBIL | Circumferential Borehole Imaging Tool | 6 revolutions/sec<br>250 samples/rev. |
| Schlumberger | UBI | Ultrasonic Borehole Imager | 7.5 revolutions/sec<br>180 samples/rev |
| Halliburton | CAST | Circumferential Acoustic Scanning Tool | 12 revolutions/sec<br>200 samples/rev |
| BPB | AST | Acoustic Scanning Tool | 4 revolutions/sec<br>200 samples/rev |

*combinable in the STAR tool with a 6 arm electrical imaging device

This chapter is written with two objectives in mind: to describe the way in which the imaging tools work and to show something of the practicalities and results from image interpretation. It is intended for generalists who will look at logs interpreted by specialists, and not the specialists themselves. It is an introduction to a very active field.

### *Types of imaging tool*

Two imaging tools will be considered in this chapter, one which creates an acoustic image and one which creates an electrical image (Table 13.1).

The acoustic imaging tool, generally called the borehole televiewer or BHTV, uses the detailed acoustic response of the formation at the borehole wall to create an image. A transducer on the logging sonde is turned rapidly, like a radar scanner, while sending and receiving ultrasonic pulses to and from the borehole wall. It sweeps the entire borehole circumference several times a second, making over 200 paired measurements of amplitude and travel time during each revolution. A very dense dataset is created which is used to build the acoustic images. Acoustic imaging tools provide a full coverage around the borehole and function in holes filled with any type of liquid, fresh water, water-based barite mud and oil-based mud (Table 13.1). Acoustic imaging is described in Sections 13.7–13.10.

The electrical imaging tools use the detailed electrical response of a formation to create their image. These tools evolved from dipmeter technology and now consist of a device with four or more pads similar to the dipmeter, but instead of one electrode per pad there is a large array of very small, button electrodes. The fine resistivity responses of all of the electrodes are processed together, as a matrix, into an image. Necessarily, the electrical images are only measured immediately in front of each pad: between the pads is a gap. The present electrical imaging tools give excellent, high resolution images but the gaps between pads remain and they only operate in water-based muds (Table 13.1). Electric imaging is described in Sections 13.2–13.6.

### *Creating an image*

To create an image from a set of data it is simply necessary to define a grey scale or a colour by a particular range of values. For example, 0–10 may be green, 10–20 light green, 20–30 light yellow and so on. With this technique a single curve can be plotted in a one dimensional colour image, in effect a colour bar code (Figure 13.1*a*).

A different technique is used for the image logging tools. These tools provide multiple readings at any one depth. The FMI, for example, provides 192 electrical readings at any one depth: there are 192 logs, not just one. To create an image from such a dataset, all the logs are sampled with a vertical increment which is the same as the spacing between the curves (being 2.5mm, 0.1", for the FMI). When the borehole is divided like this into regular vertical and horizontal intervals, a patchwork is created with vertical and horizontal co-ordinates: in other words a pixel (picture element) matrix. Each pixel has a false colour coded from the associated log value. If the pixels are small enough, an image will be perceived (Figure 13.1*b*).

### *Image presentation*

The standard presentation for image logs is the 'unwrapped borehole' format. The cylindrical borehole surface image is unzipped at the north azimuth and unrolled to a flat strip (Figure 13.2). The compass points form the horizontal, X co-ordinates, the vertical Y axis, is depth. In this way, a continuous representation can be made of the borehole either on a screen or as a hard copy log plot. Other, especially 3-D formats exist for on-screen display but the unwrapped borehole presentation has become the standard.

With the unwrapped borehole format, like any projection of a curved surface on a flat one, there is inevitable

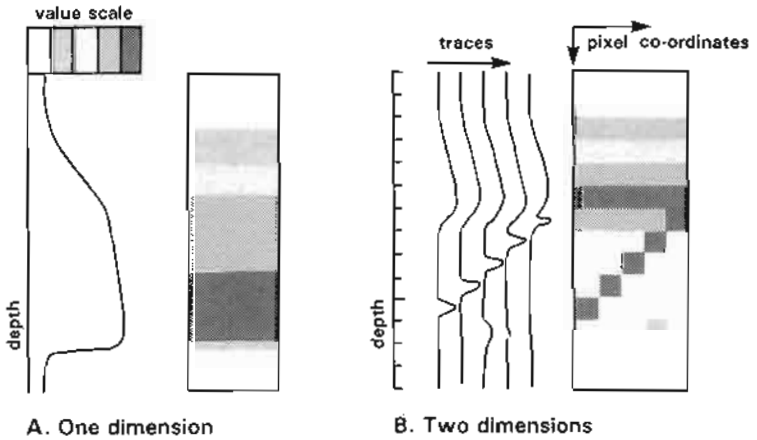


**Figure 13.1** Producing an image from log responses. A. One dimensional method in which a defined range of log values is represented by a particular grey shade or colour. A banded column is produced. B. Two dimensional method used with multiple log traces. Each trace is sampled at regular vertical increments so that, with multiple logs, a pixel matrix is achieved. False colours or grey scales still represent defined ranges of log values.

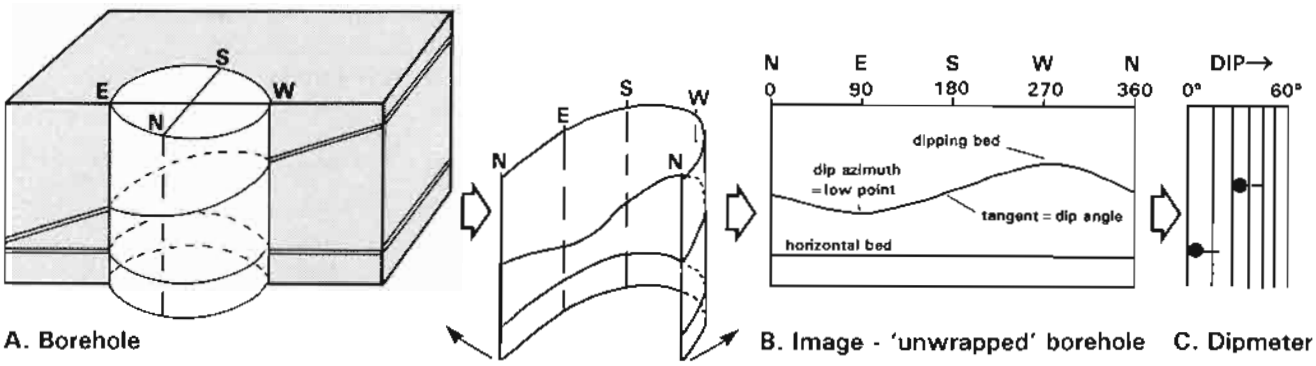


**Figure 13.2** Representation of borehole wall images on a flat surface. The images derived from the cylindrical borehole (A) are presented on a flat surface (screen or hard copy log plot) by 'unwrapping' onto a vertical depth grid and horizontal grid of compass bearings. (B) In this format, horizontal and vertical surfaces are unchanged but dipping surfaces become represented by a sinusoid. (C) Such dip and azimuth may be represented on a dipmeter tadpole plot.

distortion. Real horizontal features will simply be seen on the image log format as horizontal: real vertical features as vertical. But real dipping surfaces will be represented on the plot (log) by a sine wave (Figure 13.2*b*), the steeper the dip the greater the wave amplitude. The actual dip of a bed can be accurately measured from the sine wave. The crest of the curve is the high point of the surface as is crosses the borehole, the tangent to the slope is the dip angle and the trough, the low point of the surface crossing the borehole, gives the dip azimuth (Figure 13.2). Typically today, the sine signature of a dipping bed on the image can be matched by an ideal, computer derived sine curve which automatically provides a dip and azimuth (Figure 13.2*c*). This is described in more detail below (Section 13.3, The workstation).

## 13.2 Electrical imaging, the FMS and FMI

### *The tools*

At present (1996) electrical imaging is dominated by Schlumberger, although new tools are being actively introduced by the other service companies. In the mid-1980s, Schlumberger introduced their first electrical imaging tool, the Formation MicroScanner (FMS), as an evolution of their SHDT dipmeter (Chapter 12). The first tools only provided an image of 20% of an 8.5" borehole, using just two pads. Since then there has been steady progress in borehole coverage (Bourke, 1992) and tool technology. The present tool, the Fullbore Formation MicroImager (FMI) provides nearly 80% coverage in an 8.5" diameter borehole of high quality images (Table 13.2). Since this is the most recent Schlumberger tool it will be used for description (information from Schlumberger 1994, unless otherwise indicated).

The Schlumberger FMI consists of four pads on two orthogonal arms like the dipmeter (Figure 13.3), but in the imaging tool, the four pads each have a hinged flap so as to extend the area of electrical contact (Figure 13.4). Pad faces are curved to match borehole curvature and are approximately 8 cm (3.2") wide and 18 cm (7") long; flaps are 8 cm (3.2") wide but only 6 cm (2.5") long. Both pad and flap have arrays of 24 button electrodes

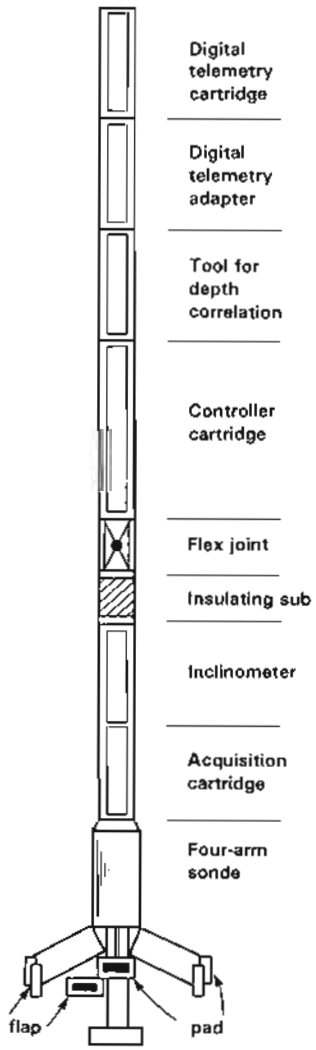


**Figure 13.3** The FMI (Fullbore Formation MicroImager) tool of Schlumberger (re-drawn from Schlumberger, 1994).

**Table 13.2** Borehole circumference coverage of the Schlumberger electrical imaging tools in approximate percentages.

| Tool | No. of electrodes | Logging speed | Hole diameter 6" | 8½" | 12¼" |
|---|---|---|---|---|---|
| FMI 4 pad + flaps | 192 | 550m/h (1800'/h) | 90% | 80% | 50% |
| FMI 4 pad | 96 | 1100m/h (3600'/h) | 50% | 40% | 25% |
| FMS 4 pad | 64 | 500m/h (1600'/h) | 50% | 40% | 25% |
| FMS 2 pad | 54 | 500m/h (1600'/h) | 25% | 20% | 12% |
| SHDT dipmeter | (8) | 1650m/h (5400'/h) | | | |

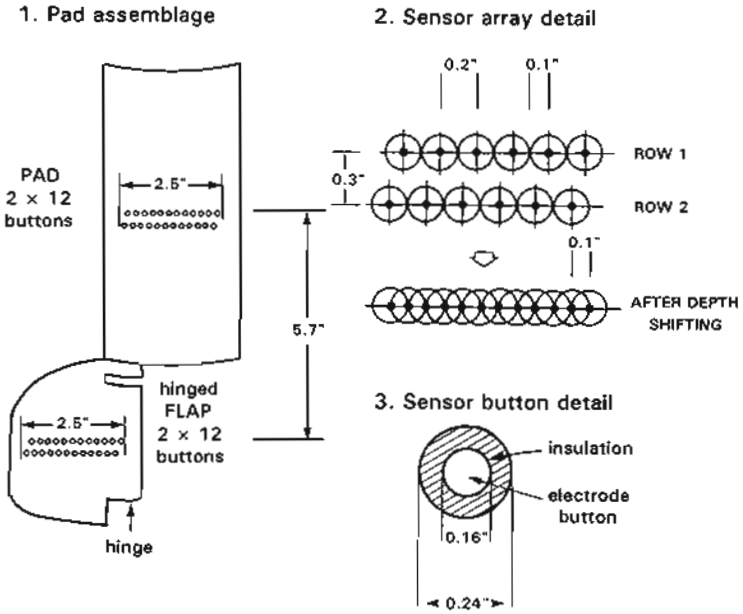


**Figure 13.4** Pad assemblage and sensor detail from the Schlumberger FMI tool (re-drawn from Ekstrom *et al.*, 1987 and Schlumberger, 1994).

(described below). In order that the pads and flaps maintain contact with the formation, they are free to tilt independently of the tool body. Thus, when the tool is not parallel to the borehole wall, as frequently occurs in horizontal and highly deviated wells, the pads still remain in contact. In addition, the tool uses hydraulic self-centreing to improve pad contact, especially in horizontal wells, where the usual pad leaf springs are not adequate.

As well as the tool circuitry, the body of the FMI tool houses the inclinometry (as in the dipmeter), and a digital telemetry sub (Figure 13.3). The upper part of the tool is insulated from the lower part and acts as a return electrode (see *below*). A gamma ray sonde can be added into the string and the entire tool may be nearly 15 m (50 ft) long.

The unique design elements of the FMI are the pad and flap and electrode array. Pad and flap are both conductive and have inset, 24 individually insulated button electrodes, arranged in two rows of 12 (Figure 13.4). Individual buttons are 0.5 cm (0.2") apart and the two rows are separated by 0.75 cm (0.3") (Figure 13.4). The buttons of one row are offset 0.25 cm (0.1") vertically compared to the other. The top row of buttons on the pad is 14.5 cm (5.7") above the top row of buttons on the flap. When the tool is used with the flaps, 192 (8 × 24) button samples are recorded at every depth sample point around the borehole. The tool may also be run in four-pad mode when 96 (4 × 24) button samples will be recorded.

Button electrodes are 0.4 cm (0.16") in diameter but with surrounding insulation this increases to 0.6 cm (0.24") (Figure 13.4). With this arrangement, it is considered that the electrodes have a resolution of 0.5 cm (0.2"). However, because the electrodes are offset vertically, the formation is sampled horizontally across the electrode array at half this distance, that is every 0.25 cm (0.1") (Figure 13.4). At logging speeds of 1800 ft/hr button currents are sampled vertically every 0.25 cm (0.1"). The tool, therefore, acquires a data matrix of 0.1" both vertically and horizontally in front of the pads and flaps (calipers, magnetometers and accelerometers are sampled every 3.8 cm (1.5")).

In terms of electrical circuitry, the imaging tools are similar to the dipmeter tool in that a slowly varying, 'low

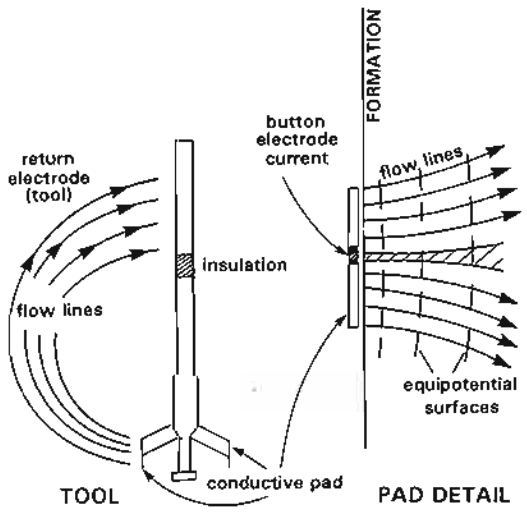


**Figure 13.5** Electrical flow characteristics of an electrical imaging tool (based on the FMI of Schlumberger) (re-drawn and modified from Ekstrom *et al.*, 1987 and Schlumberger, 1994).

frequency' EMEX signal, which is modulated for formation resistivity changes, is used to focus a rapidly changing, 'high frequency' signal from the pads themselves (Figure 13.5). In practice, each conductive pad face is an equipotential surface, held at a constant potential relative to the return electrode, which is the upper section of the tool (Ekstrom *et al.*, 1987). The pad injects current into the formation and the current density across the pad is sampled by the button array (Figure 13.5). Changes in current density across the pads are caused by local formation resistivity variations. Button array resolution is discussed below (Section 13.3).

***Electrical image processing***

The raw data acquired by an electrical imaging tool is a series of microresistivity curves. For the FMI there are 192. These form the matrix which is processed into an image.

The first necessity of electrical image data processing is to correct for variations in EMEX and to equalise the curves to the same gain and offset (Table 13.3) (Harker *et al.*, 1990). That is, the curves must be equalised to give them all the same sensitivity range (Ekstrom *et al.*, 1987).

**Table 13.3** Electrical image (FMS/FMI) processing steps (modified from Harker *et al.*, 1990).

| | |
|---|---|
| 1. Data restoration: | –EMEX correction<br>–equalisation for offset and gain<br>–depth correction, speed corection |
| 2. Image generation | –choice of colour palette<br>–choice of colour ranges |
| 3. Image enhancement | –static normalisation<br>–dynamic normalisation<br>–image refinements (image processing) |

They will normally be acquired in this format but subsequent refinement may be necessary. Secondly, depth differences must be corrected. The resistivities are acquired at different depths, a 0.75 cm (0.3") difference for the two button rows on one pad and a 14.5 cm (5.7") and 15 cm (6") difference between the pads and flaps. These different acquisition depths are simple to correct if the tool speed is constant at no more than 550 m/hr (1800 ft/hr) (Figure 13.6). However, if the tool does not run smoothly a simple depth correction leaves differences, especially between pad and flap measurements (Figure 13.6), and a speed correction is necessary to make a proper depth correction using the accelerometers included in the tool.

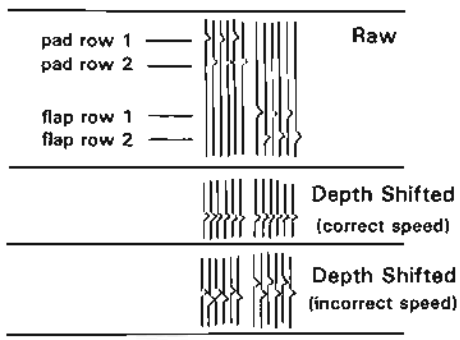


**Figure 13.6** The effect of depth shift and speed correction on the raw image traces (modified from Serra, 1989; Schlumberger, 1994).

With the equalised, depth corrected dataset, images may be produced. As discussed previously (Section 13.1, Creating an image), vertical increment co-ordinates are set equal to the horizontal spacing of the curves. That is, each log is sampled at a regular vertical distance which is the same as the horizontal spacing between the curves. With the FMI, the spacing between curves (i.e. between electrode buttons) is 2.5mm (0.1"). This therefore gives a datapoint every 2.5mm (0.1"), both vertically and horizontally: a single log measurement represents a 2.5mm square pixel. Individual log values are colour coded by assigning certain ranges to chosen false colours (or grey scales). The defined ranges of log values may be chosen using equal value increments or, more usefully, equal volumes of data (i.e. the same number of datapoints for each colour, Figure 13.7). Having set the scales, each pixel can now be represented by a false colour and a matrix of coloured boxes 2.5mm square at natural scale is created (Figure 13.1). When scaled down horizontally and vertically, generally to 1:5 if equal vertical and horizontal scales are needed, or 1:10, an interpretable image is created.

Two types of image colour designation are possible, one in which the colour range covers a population representing the entire log dataset, called *static normalisation*, and one in which the sampled population is a screenful (or similar limited quantity) of data values, when it is

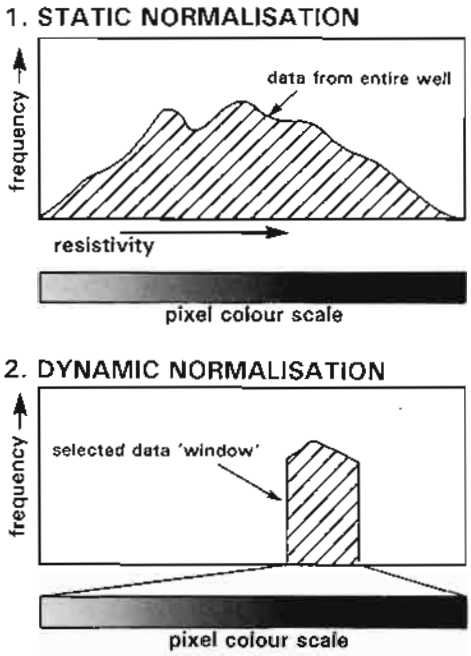


**Figure 13.7** The principle of static and dynamic normalisation. Static normalisation can be used to compare images over an entire well. Dynamic normalisation is used to bring out local detail. The full colour scale is used for a limited data range or 'window' which can be from any chosen interval such as a bed of interest, a screenful or a pre-set, small depth range.

called *dynamic normalisation* (Figure 13.7). Using static normalisation, intervals (formations) with similar electrical properties will be relatively similar throughout the log. However, much detail will be lost, especially in zones of very high values such as may be found in hydrocarbon bearing reservoirs. The detail may be recovered by using dynamic normalisation. Even at overall high values, small variations will be sufficient to cause a colour code change since the entire population sample itself has high values (Figure 13.7). However, with a dynamic normalisation, similar lithologies may appear different through the one log. The two processings are complementary (Section 13.4). Dynamic normalisation is generally best for detailed workstation interpretation, static normalisation is conveniently used for whole well analysis, and whole well hard copy, especially at compressed vertical scales when detail is inevitably lost.

Processed data will normally be examined on the workstation in the 'unwrapped' format previously described (Figure 13.2). It is possible at this stage to refine the processing in terms of speed correction and button correction on screen, to 'sharpen up' and 'tidy up' the images. These refinements are not always necessary or useful. Logs which indicate image acquisition quality, such as the calipers and tension data should be included on the basic workstation screen format. Standard open hole logs must also be included and not just the gamma ray which may be part of the tool string. Additional screen space may be taken up with a dipmeter grid or core photograph images as is felt necessary.

## 13.3 Electrical image interpretation, some generalities

***The workstation, dip and azimuth measurement***

Interpretation of the electrical images (and acoustic) is today accomplished on a workstation and not on paper copy as previously. Initially, workstation facilities for interactive image interpretation were not widely available, but are now reasonably commonplace and routines sufficiently simple to be undertaken on a PC. Necessarily, image manipulation facilities are linked to overall processing. But although the processing stage and the interpretation stage have a fuzzy boundary, their objectives are different and hence routines are different.

The first objective of workstation interpretation is the dip and azimuth measurement of planar features. The image data are displayed on screen in the unwrapped borehole format (Figure 13.2). As explained, with this format, horizontal surfaces appear flat but dipping surfaces appear as a sine wave, the amplitude indicating the dip, the position of the low point of the wave, the dip azimuth (Figure 13.2). Using the workstation, a computer sine wave can be fitted to an imaged surface and the dip and azimuth automatically given. The fitting may be either by choosing interactively, three or more points along the surface and letting the computer choose the sine wave that fits best, or by using a preset, but interactively adjustable sine wave which is permanently on the screen and is fitted by eye to the surface to be measured (cf. Figure 13.23). These interactive measuring routines are simple and accurate but take considerable time.

For the dip and azimuth measurements to be effective in subsequent analysis, every measured surface should be classified according to the feature it represents. For example, if fractures are being measured, interpretation should allow coding of the several types able to be identified; open fractures, cemented fractures, drilling induced fractures and so on. If sedimentary features are being analysed, the classification may include foreset laminae, shale bedding, concretions, in fact any feature necessary. Sine curve fitting to features provides excellent orientation information, but when the data set has been fully measured, it is necessary to be able to extract selected information for analysis and display. For example, open fractures and cemented fractures may come from quite differently oriented populations and must be analysed separately: foreset orientations must be extracted from all other measurements to study palaeocurrent directions.

The quantitative measurement of orientation is ideal for the computer. The workstation can also be used for qualitative analysis, most effectively when core is available as described below.

***Core to image comparison***

It is quickly discovered that image logs do not replace cores: the two datasets are complementary. The imaged electrical response of a formation provides much information but does not give anything like the detail of a

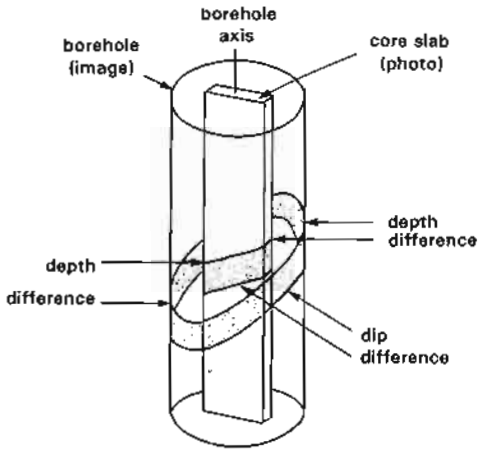


**Figure 13.8** Illustration of the difficulties of matching core photos to borehole images.

visual response, and moreover must be interpreted like any resistivity log in terms of formation electrical characteristics.

Comparison between core and image is inevitable and necessary but image and core will not be similar. It is like comparing an X-ray of a body to the body itself: like are not being compared. At best, the log response to individual features such as fractures or foresets can be directly observed. The features are recognisably resolved. But many features are not fully resolved (*see below*, log resolution), and an 'image facies' technique is used to infer them. For example, bioturbation is usually not resolved as recognisable, separate features on the images, but does cause a typical 'look' on the log responses. These are sufficiently distinctive to be able to be recognised over useful intervals of log. That is, they can be recognised as an 'image facies' which is similar both over cored intervals and beyond, and can be used to make a quasi-sedimentological interpretation.

Recognising image facies is best undertaken using the workstation and requires the use of core photos (which may be put on the screen, *see below*), sedimentological logs and the standard logs at a minimum. Care needs to be taken since similar image responses may have different causes: a cemented sand may be confused with a carbonate. Or similar lithologies may show different responses: a hydrocarbon bearing sand will appear different from the same sand with salt water. And of course, dynamic normalisation causes images to vary. However, once calibrated from core, an image facies, combined with the standard logs and linked to a visual core facies, can be used as a template for interpretation.

Comparing image to core involves coping with physical differences of depth, spacial position and distortion of the projection. Working with cores it becomes quickly clear that there are real depth calibration difficulties at the centimetre scale of the image logs. The logging cable stretches or core pieces are missing. Modern workstations attempt to aid core to image comparisons by allowing core photos to be displayed on the screen and moved at will to a position over the appropriate image site. However, even this is often difficult, as the photo is of a slab from the centre of the borehole, while the image is from around the borehole wall thus causing depth mismatches (Figure 13.8). Moreover, the orientation of the core slab is quite likely to change from core piece to core piece.

***Image resolution and identification***

The resolution of individual FMI buttons is indicated at 0.2" (0.5 cm) which is also the effective electrode size (Schlumberger, 1994). Signal penetration is around 1.4 cm (Bourke, 1993) but varies. However, in terms of the images produced, because of tool design and log sampling rate, the formation is sampled horizontally and vertically every 0.1" (0.25 cm) (Section 13.2, Figure 13.4). Pixels of 0.1" × 0.1" (0.25 cm × 0.25 cm) are used for image creation, that is, half the individual electrode resolution. Features the size of a pixel will not be resolved, i.e. will not be separated. Features smaller than a pixel will appear pixel sized. When considering the images themselves (not the individual electrodes) it is the ability to be able to recognise an object which is important. How small an object can be recognised on the images? This is difficult to define scientifically and it is essentially through use that we find out.

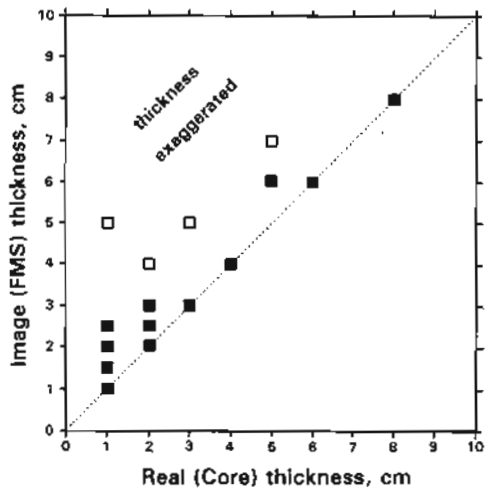


**Figure 13.9** Comparison of real thin bed thickness from core and estimated bed thickness from electrical images. Sands were relatively more resistive than shales (after Trouiller *et al.*, 1989).

Some notion of the practical possibilities of log use can be gained from work on bed resolution. This shows that shoulder effects (Chapter 2) are important. Schlumberger (Trouiller *et al.*, 1989) found that the FMS tool would resolve the thickness of sand beds (resistive) in a sand/shale turbidite sequence, down to 5 cm accurately. For sand beds thinner than this, interpretation of the electrical image gave an exaggerated thickness (Figure 13.9) and a corresponding under-estimate of (conductive)

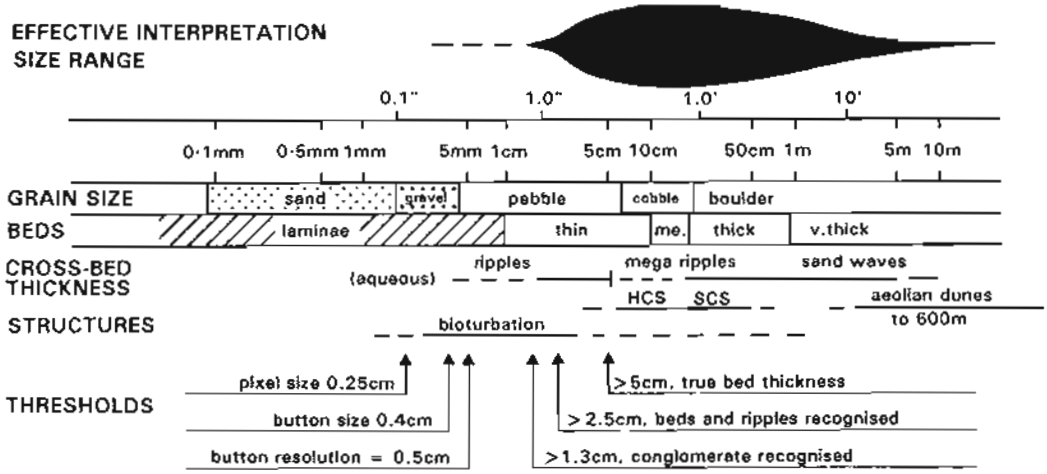


**Figure 13.10** Recognition and resolution of electrical images in relation to grain size, bedding and common sedimentary structures.

shale bed thickness. However, thin turbidite sands have been recognised down to 2.5 cm (Pezzard *et al.*, 1992). At an even finer scale, below tool and image resolution, fine lamination can be recognised but in a general sense rather than each lamina being identified. This is the case in the example of HCS (hummocky cross-stratification) (Figure 13.11).

For irregular features, at very small scales, shoulder effects are likely to merge and dominate and render identification difficult or impossible. For example, individual bioturbations are not often identifiable, although they affect the log in that they have a different texture and permeability from the surrounding formation. A blotchy type image is produced which appears almost random at certain intensities of bioturbation (Figure 13.12). For more regular structures such as ripples (Figure 13.13), these are too small to be resolved from internal features, although some authors have been able to identify and measure them from external shape (Pezzard *et al.*, 1992). At a distinctly larger scale, most foreset bedding will be resolved (Figure 13.15), although dip and azimuth consistency are generally used to confirm the identification.

The eventual identification of features near the limit of image resolution will depend on their geometry. Linear features will most likey be identified (of any orientation), while irregular features of limited extent are very difficult to identify. The smallest irregular objects to be identified are probably conglomerate or breccia pebbles (Figure 13.14). The electrical contrast of the feature being examined will contribute to the identification and objects down to 1.3cm (0.5") have been recognised (Harker *et al.*, 1990).

In effect, electrical images are sufficiently sharp to provide interpretable information down to 2cm–3cm (0.75"–1.2"). Although there are some examples at even smaller scales, confidence is low (Figure 13.10). Generally, it is the small scale limit of detection which preoccupies interpreters. There is, however, an upper limit also. This is hard to define but, depending on the interpretation techniques used, is around 2m–3 m (6'–10') and almost certainly below 10m (30') (Figure 13.10).

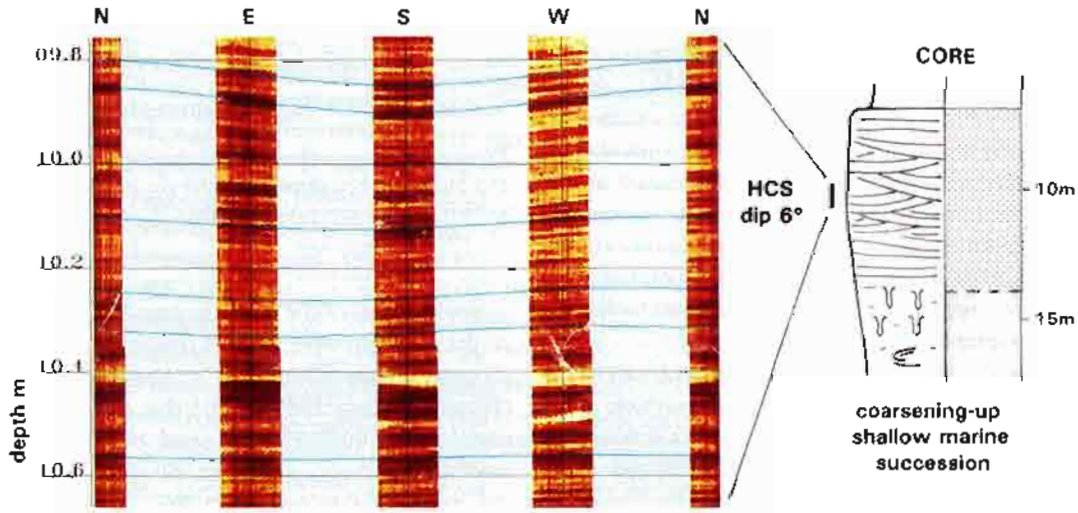


**Figure 13.11** Electrical image of HCS (hummocky cross-stratification). HCS shows excellent, regular laminae with low angle dips (5° – 10°) in fine grained sands (cored section, high resistivity is dark, Schlumberger FMS tool).

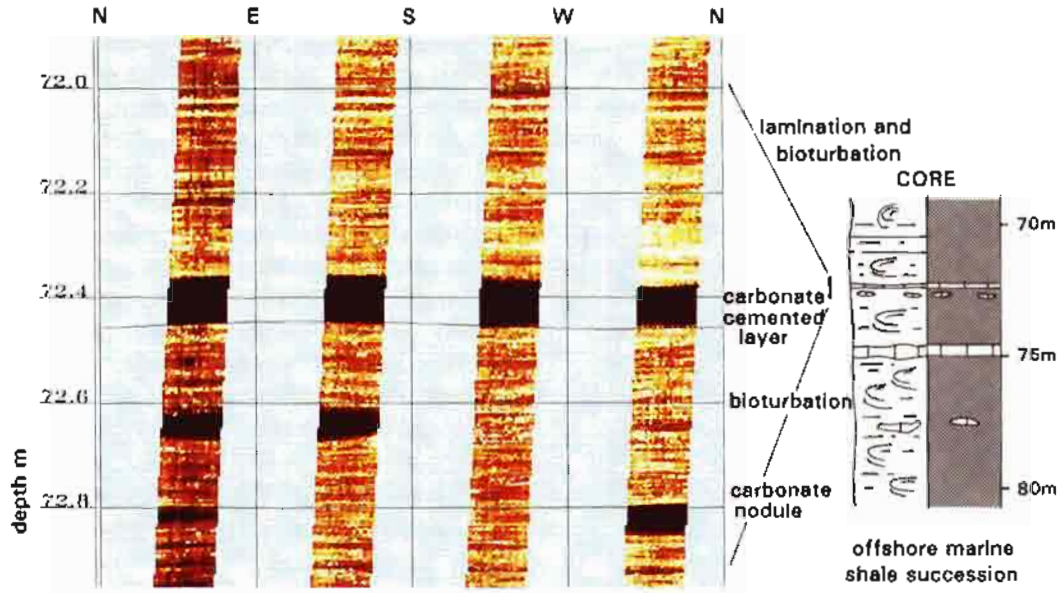


**Figure 13.12** Electrical image of bioturbation in shallow, marine shale. Bioturbation typically creates a speckled image. Carbonate beds and concretions appear as dark, well-defined bands (cored section, high resistivity is dark, Schlumberger FMS tool).

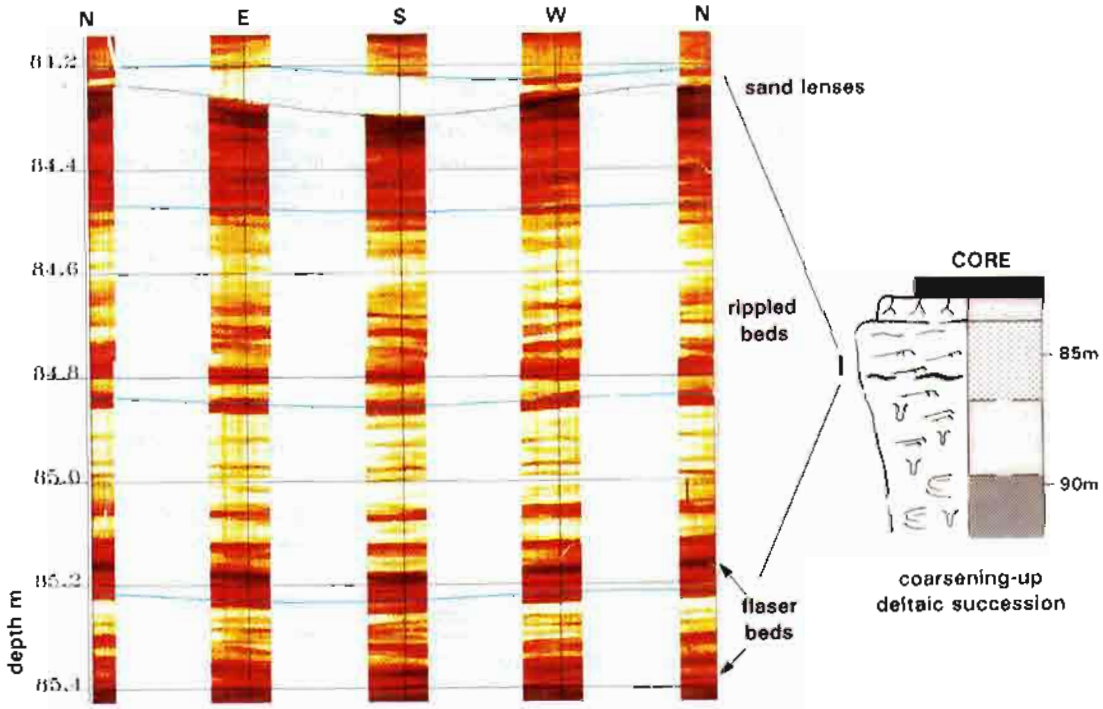


**Figure 13.13** Electrical image of flaser and linsen. Electrical contrast is good but the laminae are irregular. No internal features are recognisable in the linsen (cored section, high resistivity is dark. Schlumberger FMI tool).

*Artifacts and log quality*

The electrical image logs are susceptible to quality difficulties more obviously than the standard logs. The quality is affected at the acquisition stage, by the borehole condition and the functions of the logging tool; at the processing stage, where parameter manipulation is important; and during interpretation, where artifacts may be confused with real features.

Mud conditions are important for good acquisition. The mud to formation resistivity ratio should be less than 20,000 and the maximum mud resistivity 50 ohm/m (Schlumberger, 1994). Borehole rugosity and caving, clearly, have a great effect since the electrical image log is produced by a pad tool and images are essentially of the borehole wall. As a minimum, in caved formations, pads (some or all) will 'float', that is loose contact with the formation, and a flat series of low, mud values will be recorded. In the worst case, the tool will stick and a flat series of values will be recorded on all curves as the cable continues to be reeled in but the tool is stationary (cf.

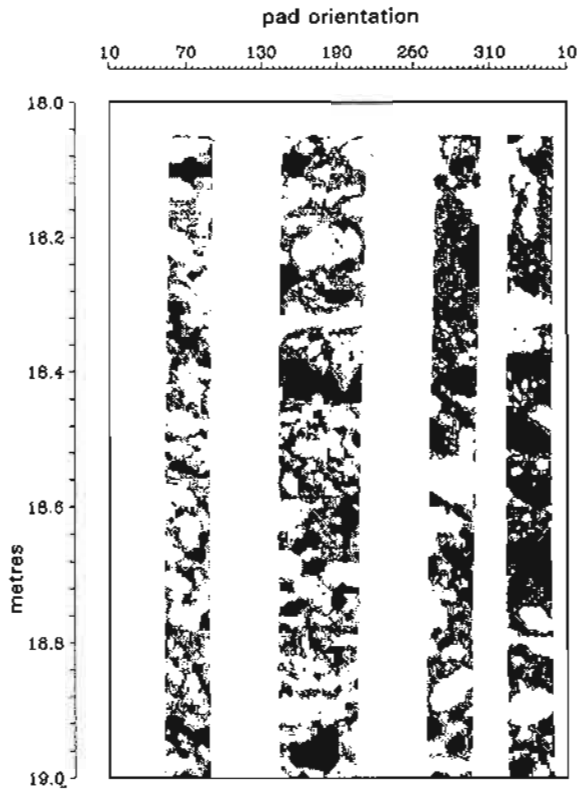


**Figure 13.14** Electrical image of a grain supported conglomerate. Dark areas indicate pebbles that have been plucked out of the borehole wall during drilling (high resistivity is light, Serra *et al.*, 1993).

Figure 12.29). Very poor acquisition parameters will be recognised on the logs but slight sticking and speed variation may not. This is when speed correction is necessary. Malfunctioning of buttons also occurs during acquisition. Selective electrodes may become clogged and fall dead: a straight vertical trace being left on the log where no data are acquired. The effect is easily recognisable and although some processing packages interpolate for the dead button, it is not always necessary. More difficult to cope with are pads that collect cuttings or lumps of detatched formation and drag them along while logging (Bourke, 1989). Fuzzy images and poor data zones running more or less vertically up the image are created.

Less obvious are those log artifacts which are a result of the way that the images are acquired. For example, in intervals where mud cake is thick (over 1.2cm), images may come from the mudcake or irregularities in the mudcake. This is especially true where a previous tool has left pad traces in the cake or logging cable rub has made a groove. Generally, these features will be recognised as they continue vertically for some distance or spiral up the images. Detailed discussions of artifacts are found in published literature (i.e. Bourke, 1989; Serra, 1989).

## 13.4 Electrical image sedimentary interpretation, some concepts and examples

From a sedimentary and sedimentological point of view, electrical images are used to identify sedimentary structures and features, measure sedimentary orientation and give detailed information on lithology, texture and sedimentary facies and sequences.

The sedimentary interpretation of electrical image logs tends to follow routines similar to those used in a purely sedimentological analysis, building up through lithology, texture and sedimentary structures to facies and eventually sequences. With the image logs this tends to consist of: feature identification: dip and azimuth measurement with classification: refinements to lithological interpretations: recognition of image facies and sequences. These aspects are broadly described below.

*– feature identification and dip and azimuth measurement*
In sedimentary image log interpretation, some images are instantly identifiable, some require additional log information and some require calibration with core to be recognised (Table 13.4) (Serra, 1989; Salimullah and

**Table 13.4** Grades of image in interpretation (modified from Serra, 1989; Salimulla and Stow, 1992).

| | Tectonic | Sedimentary | Diagenetic |
|---|---|---|---|
| **Grade 1**<br>self evident | structural dip<br>fractures<br>folds | bedding surfaces, laminations<br>cross-bedding, grading<br>erosional surfaces,<br>deformation features i.e. slumps<br>lithology changes | stylolites<br>(high amplitude peaks) |
| **Grade 2**<br>ambiguous | faults | cobbles, pebbles, breccia<br>detrital shale,<br>ripples, bioturbation<br>grain size textures | nodular concretions<br>chert<br>vugs, caverns<br>sulphide/sulphate crystals |
| **Grade 3**<br>needs core | small fractures<br>horizontal fractures | bioturbation, thin lamination<br>limestone textures | stylolites<br>(low amplitude peaks) |

Stowe, 1992). For example, foresets can usually be recognised from image characteristics alone, they show fine but faint lamination and variable dip angles (Figure 13.15). The internal structures of ripples, however, are generally beyond the resolution of the tool (Figure 13.10) but ripple bedded facies once calibrated to core, may be recognised outside cored intervals (Figure 13.13). Finally, without cores it has been found impossible to differentiate between pebbles, mud clasts, concretions and bioturbations (Salimullah and Stowe, 1992). Core calibration is an important aspect of feature identification.

Beyond simple identification, the image logs allow the measurement of sedimentary structure orientation using the workstation, as described above (Section 3.3). For these dip and azimuth data to be of most use, the feature measured must be identified as foreset, sand bed, shale lamina, concretion, and so on. The classification will be used for subsequent filtering and, for example, foresets will be extracted to provide palaeocurrent directions. The identification of the causal features is, of course, subject to the difficulties outlined in the previous paragraph, so that any classification must be sufficiently robust to account for surfaces positively recognised, such as foresets, to those vaguely recognised such as ripple bedding and also unrecognised features (cf. Bourke, 1992). A numerical quality rating may be included from certain to doubtful.

As work progressses on an image log, so a more and more detailed picture is built up. For example, orientation data may allow an interval to be identified as deposited in lateral accretion surfaces: mottled images identified as debris flows and so on. This progressive building is implied in the following sections.

*– lithology*

Lithological information will be needed at an early stage of image interpretation outside cored intervals. Many sedimentary features have lithological associations and electrical logs are not primary lithology indicators (Chapter 6). Lithological information must come from other sources, such as the neutron-density, gamma ray logs and drill cuttings. However, the image logs provide very detailed textural information, can show thin beds and give accurate bed boundaries and so can be used to

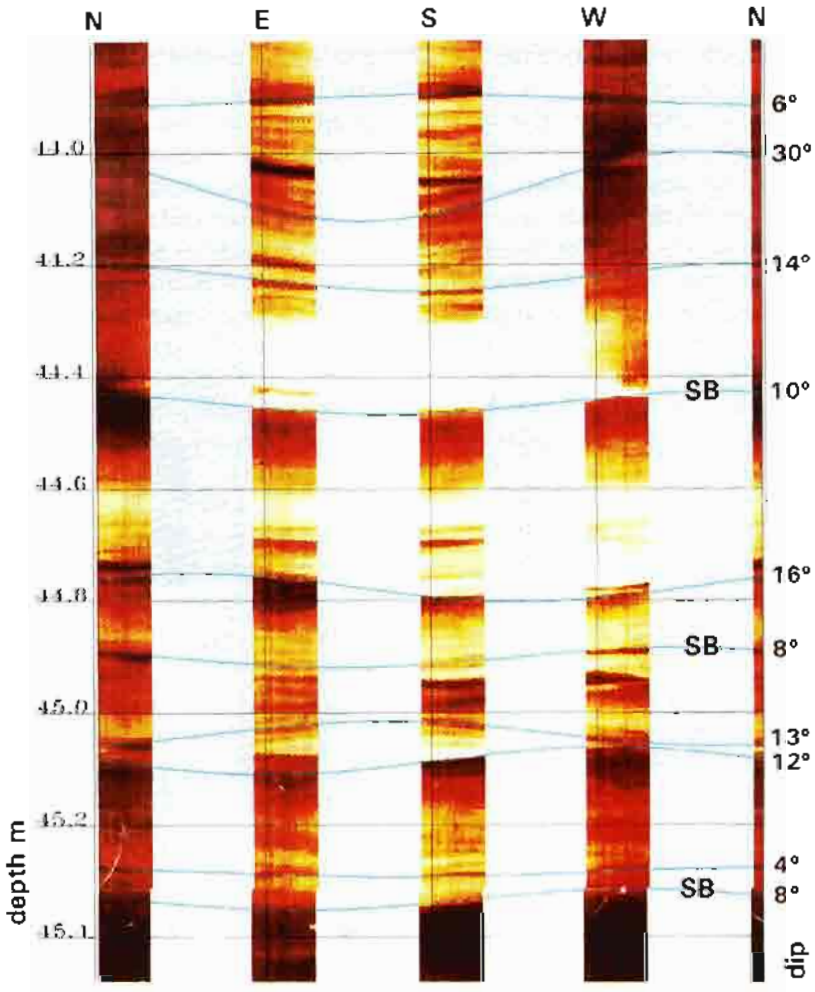


**Figure 13.15** Cross-bedding in electrical images. Good, slightly irregular bedding with moderate dip angles (15° – 35°) in sandstone are typical. From a deltaic channel shown in Figure 13.17. SB = set boundary (high resistivity is dark, Schlumberger FMI tool).

refine a routine lithological interpretation. For example, a sand interval may be recognised on the standard logs. Using the images a basal erosion surface can be identified and the fact that the upper interval is interbedded sands and shales rather than gradational (Figure 13.16).

The ability of the image logs to detect much thinner beds than the standard logs is a very significant contribution to lithological analysis. Flaser bedding for example, the fine centimetric interlamination of clean sand and clean shale, is not detectable on the standard logs but is well characterised on the image logs (Figure 13.13). In a series of deep sea turbidites, beds down to 2.5cm (1") were individually recognised and analysed (Pezard *et al.*, 1992) (although *see* Resolution *above*, Figure 13.10).

For work on lithology, statically normalised images can be used along with the standard open hole logs (and core). The image information can be extracted and transferred to a standard log scale, say 1:200, or a standard log plot for reservoir description at a 1:50 scale (Figure 13.17). The detail is best presented in the quasi-sedimentological format described below (*see* Output).

*– image facies and sequences*

Electrical image logs provide lithological and textural information in two dimensions. With such characteristics, they can be used to recognise 'image facies'.

An image facies can be considered as an image with sufficient characteristics to be able to be recognised in itself and to be able to be separated from other image facies. For these to have geological significance, they must generally be calibrated to core (*see* Core to image comparison *above*). With core comparisons, ripple bedded sands may become evident, limestones with vugs and stylolites, laminated shales and so on. Some geological facies may not be electrically distinctive, others may be electrically distinctive but combining several geological facies. Definitions are necessarily qualitative and often dependent on the interpreter. Some image facies are often recognised, others are typical of one log or one field – in the same way as sedimentological facies in outcrop and core.

In order to recognise image facies effectively, the lithological information previously described is required. Fine scale laminations on a dynamically processed image look similar in shale, in sand and in carbonate: it is the local electrical contrasts which dominate. Moreover, many sedimentary structures are restricted to certain lithologies, such as foresets to sands. Thus, structures can be interpreted from their position in a sequence along with a typical image facies. For example, a sanding-up (coarsening-up) sequence may be identified from the standard logs. Laminations at the base of the sequence may be identified as shale, those above as sand. Because of their position, the sand laminae can reasonably be inferred to be hummocky cross-stratification (HCS) (Figures 13.11, 13.16).

With individual image facies recognised, it is possible to combine them into sequences much in the way that a sedimentological analysis will lead to a description in terms of facies and then sequences. Reference will be made to any core information and lithological information must be included. If a quasi-sedimentological presentation is used (Figure 13.17) the amount of detail interpretable from the images can be indicated in the sedimentary structure column.

Using the interpreted image facies and sequences, a

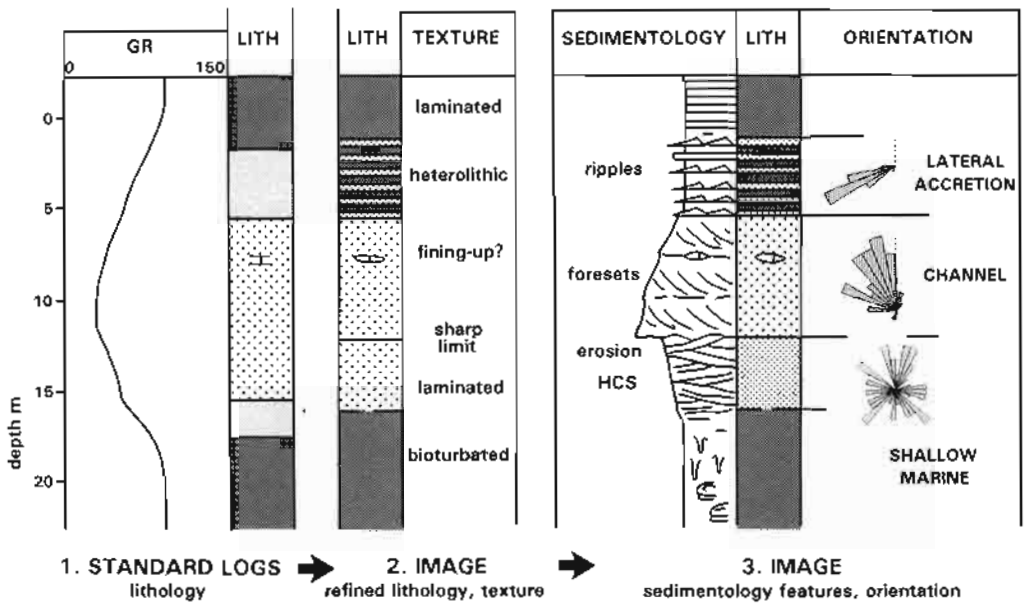


**Figure 13.16** Technique for interpreting an image derived grain size, sedimentology and orientation using both the standard logs and the electrical image logs. 1. Lithology interpreted from the standard logs. 2. Lithological boundaries and thin beds refined using the images. 3. Sedimentary structures interpreted from the image characteristics; notional grain size interpreted from the standard logs refined using the images; orientations from image picking.

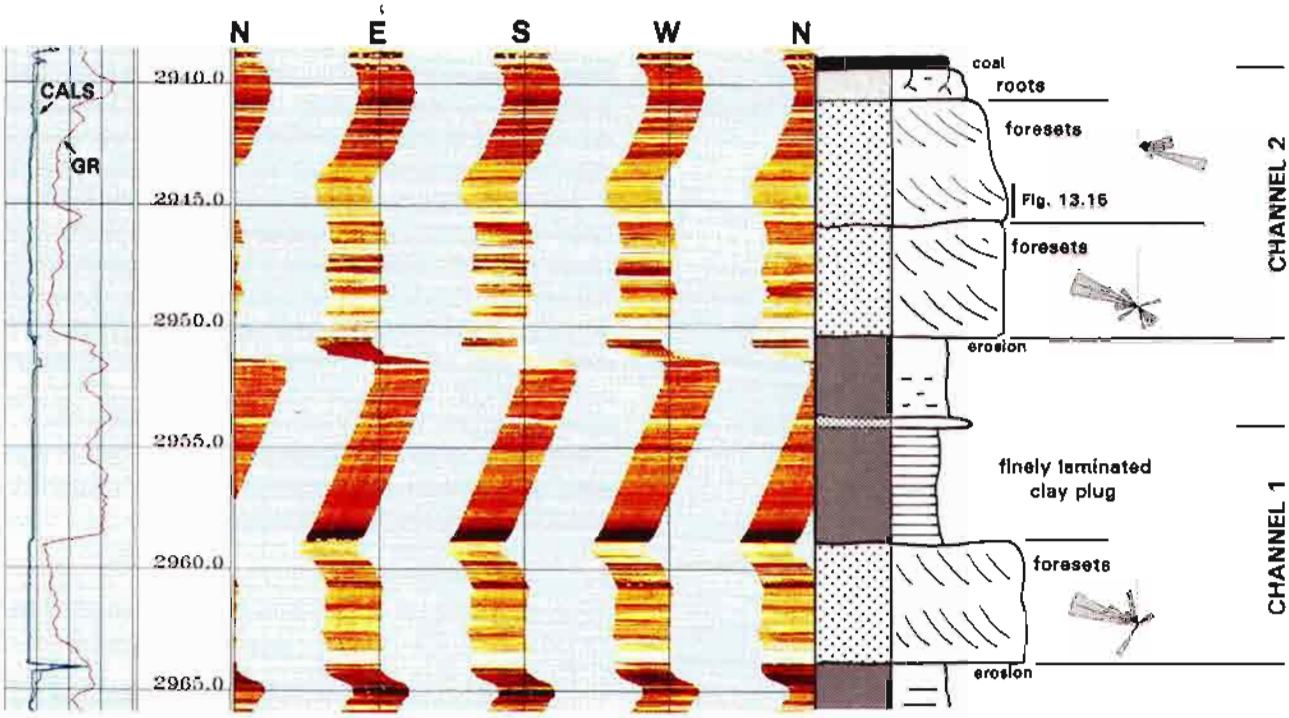


**Figure 13.17** Deltaic sandbodies defined using image interpretation. Channel 1 shows an erosional base, foresets and an overlying laminated clay interval interpreted as a plug. Channel 2 shows multistorey development with differently oriented foresets. Meandering is indicated with the overall transport being to the northeast. The detail of Figure 13.15 is from the upper channel (high resistivity dark, Schlumberger FMI tool).

new attempt can be made at the identification of sedimentary structures and the classification of orientation measurements discussed previously (feature identification). For example, measurements in laminae originally unidentified or simply classified as sand bedding, may now be classified as possible HCS lamination. A cemented layer may be recognised as a probable flooding surface and so on. At this stage, it is also possible to extract the orientation information for a statistical analysis. Foresets may be taken out of individual sand-bodies and grouped to give an azimuth rose and mean direction as a palaeocurrent indicator (Figure 13.17). Structural dip will be subtracted as necessary. Certain dominant orientations may become evident that were not previously seen and the distinctive characteristics of the orientation data may lead to the feature being recognised. This is frequently the case with SCS (swaley cross-stratification), lateral accretion surfaces and slumps or drapes.

Clearly, the final image interpretation will be built-up gradually. There is continuous interaction between feature recognition, lithology and texture definition, and facies and sequence interpretation (Figure 13.16).

*– orientation data, output and hardcopy plots*

The dip and azimuth data that are created from the image log analysis are normally extracted and treated simply as directional data in the same way as for dipmeter measurements. The statistical analysis of orientation data has been described in the chapter on dipmeter (Section 12.7). Image log data may be treated in exactly the same manner, but the quality of the information is that much better. For example, foreset orientation data are derived from directly observed foresets rather than inferred, as is the case with the dipmeter. Individual sets may be identified on the images and for example, multistorey sands separated into different bodies quite effectively. It is also possible to be more certain of information from features such as lateral accretion surfaces or drapes, where dips are much lower and greater measurement accuracy is required for their recognition. Although analysed separately, the orientation data are most effective when re-integrated with the overall sedimentary analysis (Figure 13.17).

In a final interpretation, the huge amount of data produced by the image logs must be reduced and synthesised for use in routine work by non-image specialists. The basic output is typically a hard copy colour plot at 1:5 or 1:10 vertical scale, the chosen sine wave measurements being annotated with the dip and azimuth figures and the interpreted or observed causal features noted (Figure 13.15). A 1:5 scale log may be made approximately 1:1, by choosing the correct plot width (it varies with hole size), but since there is geometric distortion in the type of projection used, a 1:1 scale for hard copy is not always necessary.

Beyond the detailed print-out, a summary log of the data is essential, at 1:200 scale or the same scale as is used to display reservoir detail. Image interpretation and recognition is impossible at this scale but if a statically normalised image log is used, annotated with both a

lithology column and a sedimentary structure column, the document is usable by non specialists and can include most of the features interpreted including sedimentary orientation (Figure 13.17).

## 13.5 Electrical image structural interpretation, some examples

The first, simple, basic objective in the structural analysis of images is to recognise and measure an accurate structural dip and recognise unconformities, even disconformities. But objectives normally go far beyond this and the recognition and measurement of fractures, faults and eventually slumps are attempted.

*– structural dip and unconformities*

Measurement of dip from image logs tends to give values which are very variable and influenced by sedimentary features. Not every possible feature will be measured but an interpreter will take quite a high density of readings especially where values vary. This will favour sedimentary dips (cf. Hurley, 1994) and features such as concretions, which stand out electrically but do not give a the structural dip and azimuth values.

To find a structural dip, orientation data are extracted from the image interpretation and zoned in the same way as for dipmeter data (Section 12.8). However, because of the dominant sedimentary influence, the data will show a very wide spread and often high dip angles (Figure 13.18). To reduce this, the image information must be filtered: only shale dips should be used for structural dip. However, such is the accuracy of the image dip and azimuth measurement that thin shale sections should be avoided as even these show a wide scatter, often as a result of dips from concretions and cemented layers. If thick shale intervals are chosen, a good structural dip can be obtained.

Another way of deriving structural dip is to use dipmeter style measurements taken from the raw image tool data. Curves are selected in the appropriate position from

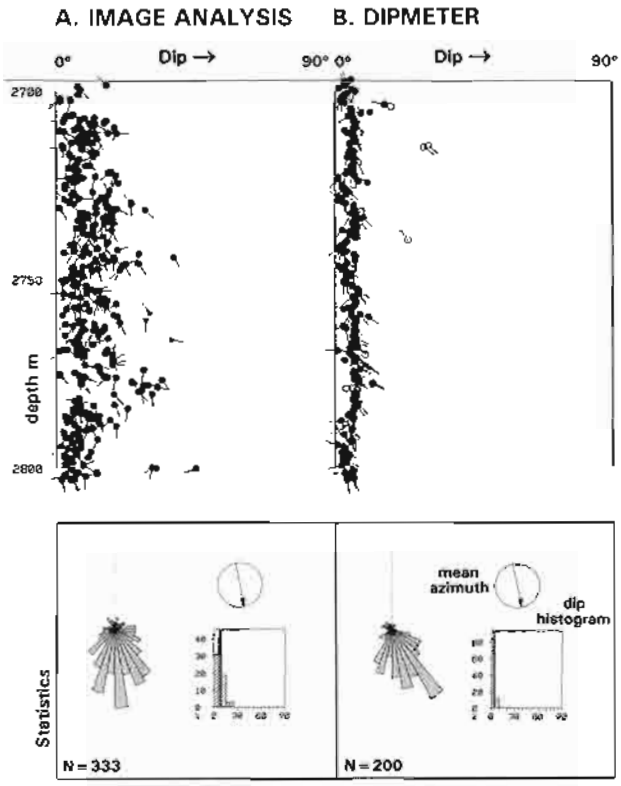


**Figure 13.18** Comparison of the orientation data derived from image interpretation (A) and a standard dipmeter processing (B). The image data show a wider spread reflecting greater detection of sedimentary features. Dipmeter processing parameters: 1.0m correlation interval, step 0.5m, search angle 60°. The dipmeter processing is used for structural analysis.

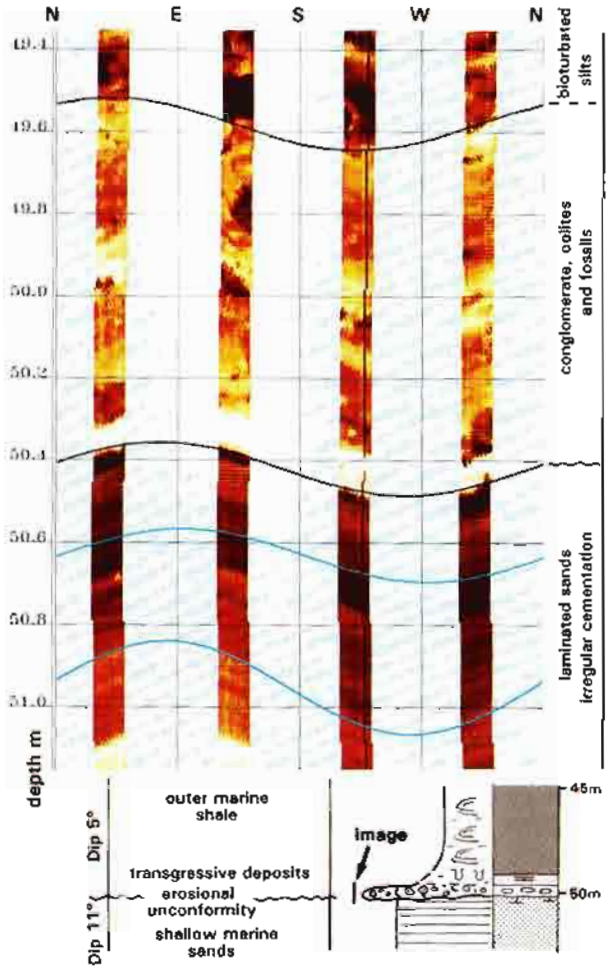


**Figure 13.19** Electrical image of an unconformity and covering transgressive lag. The unconformity is seen as a sharp surface on the image with cementation below. The transgressive lag gives a speckled image although permeability is suggested by the colour (cored interval, high resistivity is dark, Schlumberger FMI tool).

the image set to imitate the SHDT and, using the FMI orientation and caliper data, can be processed as a dipmeter. For structural use, typical structural parameters are chosen of 1.0 m correlation interval and 0.5 m step distance (Chapter 12). The resulting dipmeter provides a good structural dip and allows the interpreter to 'stand back' from the overwhelming and, for structural analysis, unnecessary detail of the image derived measurements (Figure 13.18). These dipmeter results can be used for structural rotation, unconformity recognition and fault location.

A unique element of the interpretation for unconformities and disconformities with the image logs, is that the surface itself can be examined. The actual level of an unconformity can be examined for diagenetic effects, abrupt changes in image facies and biological activity as well as the angular change (Figure 13.19). Such details are also helpful in sequence stratigraphic analysis, as image features around important stratigraphic surfaces are often very distinctive.

*– fractures and faults*

The detection of fractures and eventually faults is a fundamental objective of the image logs, traditionally more so for the acoustic images than for the electrical images. Fractures are never satisfactorily cored so that to be able to see them *in situ* using the image logs, and to measure their attitude accurately, is invaluable. However, frequently there is difficulty in recognising fractures and certainly in recognising faults (Table 13.4). The difficulty with fractures depends very much on the sequence and lithology. For example in sand-shale sequences, sedimentary responses tend to dominate while in carbonates, fractures are often more easily identified.

**Table 13.5** Some simple test parameters for fracture identification (after X. Li, pers. comm.).

| Surface characteristics | Image characteristics |
|---|---|
| Sharp surface at an angle to the sedimentary bedding | images different on either side of surface, visible shift of bedding across surface |
| Irregular, discontinuous surface at an angle to sedimentary bedding | images continuous or slightly displaced across the surface |
| Bedding parallel surface | images different either side of the surface (may be a structural change or sedimentary change) |
| **Natural fractures** | **Drilling induced fractures** |
| –cementation evident | –parallel to borehole axis |
| –shift in bedding | –parallel to axis in deviated hole |
| –same geometry in core and image | –one side of borehole only |
| | –strike normal to breakouts $Sh_{min}$, parallel to $Sh_{max}$ |

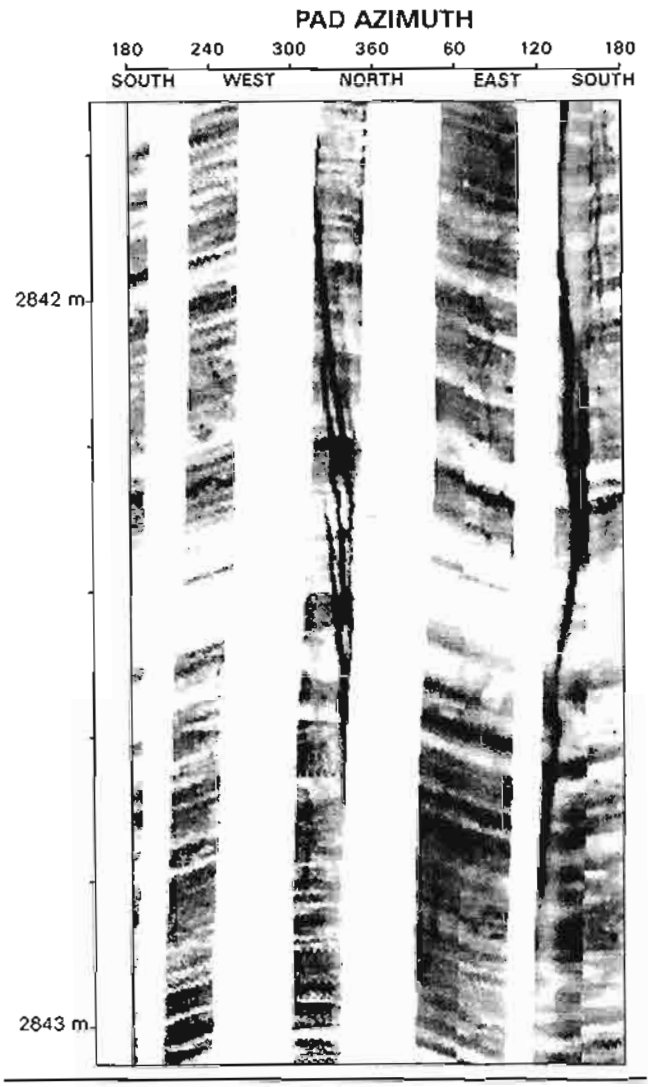


**Figure 13.20** Electrical image of a near vertical, open fracture (conductive) in a carbonate gainstone with foresets (high resistivity is light, 27 button, 2 pad, Schlumberger FMS tool; Lloyd *et al.*, 1986).

To be seen on the images, fractures must show some form of electrical contrast, that is be open and filled with mud (Figure 13.20), be cemented, or have associated displacement. Closed fractures will not be seen (Figure 13.21). Or show some geometrical relationship such as high dip in a sequence with low structural dip (i.e. Gonfalini and Anxionnaz, 1990). Clearly, measured fractures need to be classified: as cemented, induced and so on, so that they can be separated in subsequent orientation analysis. Most interpreters will provide themselves with a conscious or unconscious flow path for fracture recognition. As always, it is necessary to begin with cored intervals and fractures seen on cores may be explored on the images (Figure 13.21). However, drilling induced fractures are common in cores and although they have typical characteristics, separating them from natural fractures is not always easy (Kulander *et al.*, 1990). Beyond cores, a series of test parameters may be

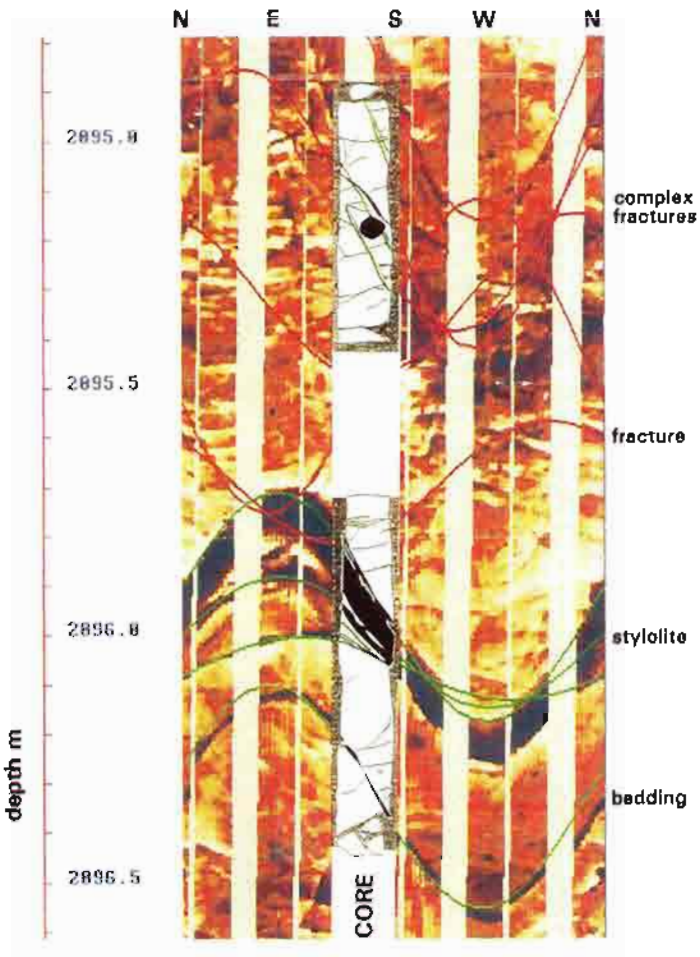


**Figure 13.21** Electrical image of extensively fractured chalk with stylolites (cored section, high resistivity light colours, Schlumberger FMS tool, two passes).

applied to identify fractures (Table 13.5) but care must be taken to account for the physical effects that drilling has on them (*see* Section 13.9).

Image logs are generally too detailed to allow the identification of faults on images alone, although cases do exist (Figure 13.22). Examination of any outcrop will soon show that actual fault planes are more chaotic the closer you get. Stand away from a fault and it is obvious: stand close to and order disappears. For fault identification, a dipmeter processed to bring out structural information is necessary. This will allow intervals where faulting is possible to be identified. These intervals may then be examined with the detail of the image log.

Details in fault zones are quite variable. Certain faults are associated with an increase in fracture intensity (cf. Koestler and Ehrmann, 1991) but frequently there is a change in texture (cf. Knott, 1994). Within faults with considerable throw, these textures tend towards shear fabrics or chaotic breccias (cf. Hurley 1994; Berg and Avery, 1995). Image logs tend to be very difficult to interpret in such zones especially if several lithologies are involved. Moreover, there is a tendency for fault zones to cave (cf. Figure 12.38) so that images are of poor quality.

*– slumps*

If definitions are to be followed strictly, then slumps are a sedimentary feature. However, following a definition for a definition's sake is an Anglo-Saxon failing. Slumps are considered here as illustrating fold aspects on the images and, indirectly, the aspect of non-linear features in general. Slumping involves both folds and faults at a small scale. A slump fold will be used here as a example. The image (Figure 13.23) is of a slumped chalk interval. Slumped chalks are common in the area but the image is taken from a bed which, on the standard logs, simply appears as a carbonate interval in a shale to marl section. Clearly the carbonate was not deposited in place and has slumped from a nearby source. The structure is a recumbent fold with an east to west fold axis and recumbent (i.e. closed) to the west (Figure 13.23), this being the direction of down-slope movement.

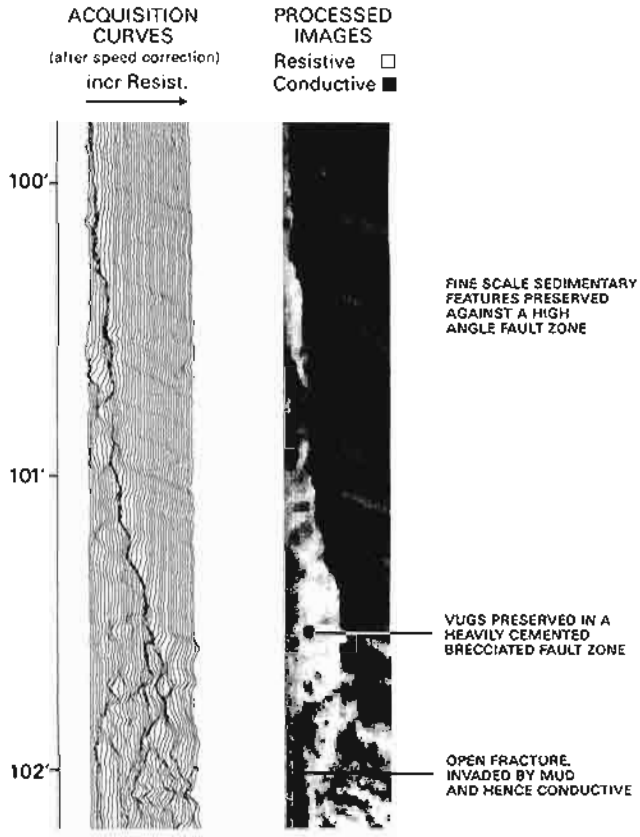


**Figure 13.22** Electrical image of a steeply dipping (minor?) fault. The sediments in the hanging wall show fine, slightly dipping laminations: those in the footwall or fault zone itself are fractured (high resistivity is light, 27 button, 2 pad, Schlumberger FMS tool; Lloyd *et al.*, 1986).

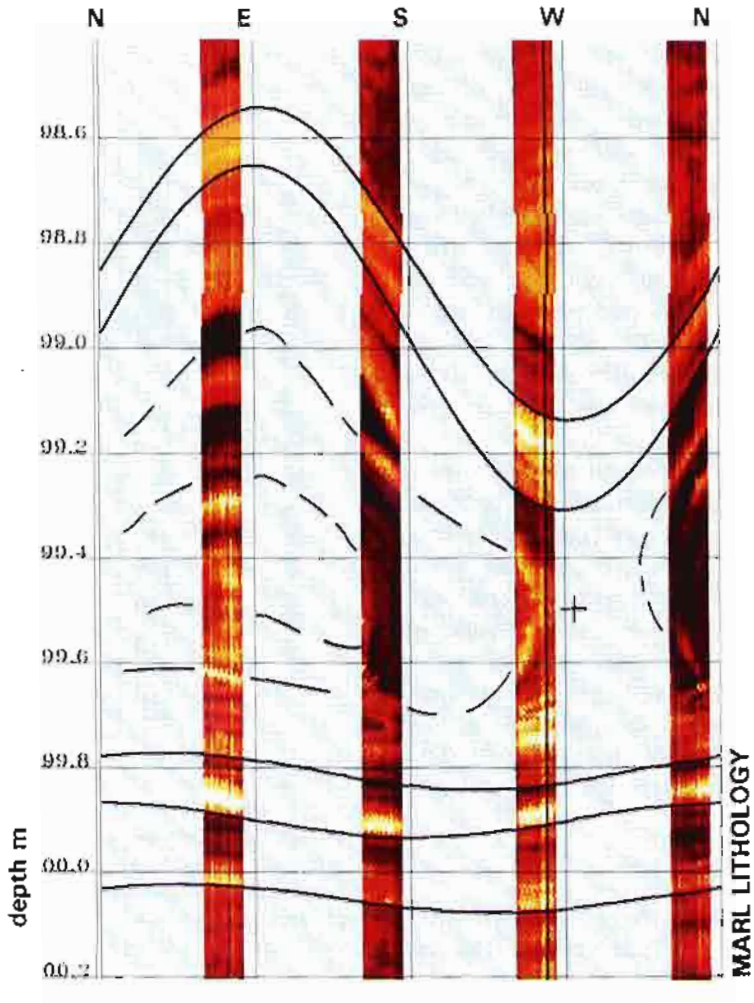


**Figure 13.23** Electrical image of a slump fold in marls. The fold is recumbent and rests on beds with very low dips. The laminae above the fold also have a very low dip suggesting infilling cover (high resistivity is dark, Schlumberger FMI tool).

## 13.6 Quantitative uses of electrical images

Much of the interpretation on image logs is qualitative. But there is a need and the possibility for quantitative methods (Serra *et al.*, 1993; Sullivan and Schepel, 1995). The quantitative analysis of images should use the two dimesional aspects of the logs and not simply be modifications of the one dimensional, standard log analysis. Some of the more interesting methods proposed so far with some rather limited examples are given below.

– *bed thickness*

Electrical images can be used to quantify thin beds (Trouiller *et al.*, 1989). The fine resolution of the electrical images (see resolution) allows beds down to at least 5cm (2") to be accurately evaluated. Beds down to 1.0 cm (0.4") can be detected but from about 2.5 cm (1"), bed thickness is apparently exaggerated (Pezard *et al.*, 1992). However, this evaluation is simply in terms of sand/shale and similar to the standard thin bed analysis using dipmeter curves (Anxionnaz *et al.*, 1990). It is a one dimensional analysis albeit at a scale finer than for the standard logs and images lend themselves to two dimensional analysis.

– *porosity and permeability*

A quantitative, two dimensional approach is used by Schlumberger in the analysis of carbonate textures (Delhomme, 1992). Carbonate textures lend themselves to electrical image analysis because pores and vugs can be large and have large electrical contrast to the matrix. The method proposed by Schlumberger is based on an analysis of the images themselves, either leading to new images of selected features or new summary data.

Without descending into details, images are analysed to identify individual vugs, to define their size and their shape from which a porosity can be inferred. That is, the large scale reservoir behaviour is built up by adding together individually observed features. The method may be used in cases where conductivity differences are large, such as in some conglomerates (the inverse case to vugs). This method of analysis is the antithesis of standard log analysis where elements are 'bulked' or an overall effect is analysed, not the individual contributions. The success of this form of image analysis method depends on formation characteristics and the size of the individual features (Delhomme, 1992). However, two dimensional analysis leading to predictions in three dimensions is the direction image quantification should take.

Permeability has yet to be derived quantitatively from images. However, empirical comparisons may be made in two ways and quantification may be possible. The first is by using the mini-permeameter. If sufficient mini-permeameter readings are taken, images can be produced of permeability distribution across core slabs (Bourke *et al.*, 1993). These can then be compared directly to the electrical images having relatively similar sampling densities. A different method of camparison is to use electrical images of core slabs (Jackson *et al.*, 1992). These images can be effectively explored under laboratory conditions.

*– fractures*

Fracture porosity and aperture have been evaluated quantitatively using the FMS by Schlumberger (Hornby *et al.*, 1990). The technique used was to model the FMS tool response to open fractures, that is open apertures filled with conductive mud, taking account of mud and formation conditions. Conductive anomalies were then statistically extracted from the image log and compared to the model to provide the fracture width. Output can be provided as an azimuthal plot (like the images themselves) with colour coded widths, a maximum fracture width and a fracture porosity (/inch or /ft). By comparison with other methods and with core analysis, the calculations showed some success.

Further studies by Schlumberger suggest that quantitative fracture measurements allow hydrocarbon to water contacts to be identified in fractured intervals (Standen *et al.*, 1993). Studies in the Monterey Formation of California show that fracture counts on images correlate well with temperature derived productivity (Figure 13.24) (Sullivan and Schepel, 1995).

Methods for the quantification of image log attributes are being actively developed. But to be effective, these methods must address the revolutionary way in which these logs sample the formation – in great detail and in two dimensions. Extensions or refinements of methods used in standard log analysis will not do justice to the data.

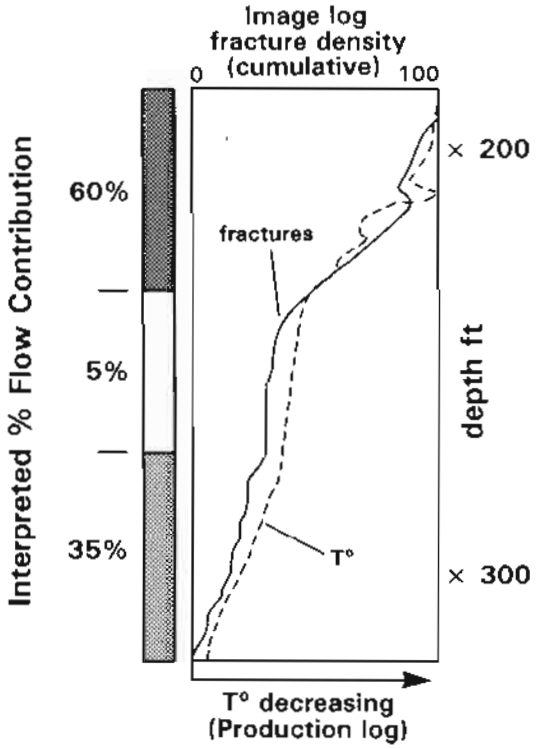


**Figure 13.24** Density of fractures interpreted from electrical images compared to a temperature log and production flow estimates, Monterey Formation, offshore California. (re-drawn from Sullivan and Schepel, 1995).

## 13.7 Acoustic imaging, the borehole televiewer

***The tools***

An acoustic imaging tool was first developed by Mobil in the 1960s (Zemanek *et al.*, 1969; 1970), was further developed and improved by the oil companies Amoco and Shell and later ARCO before eventually being taken on by the service companies in the late 80s (Broding 1982; Faraguna *et al.*, 1989). The tool uses a rotating rapidly pulsed sound source, a piezoelectric transducer, which both sends and receives the sound signal, that is, in pulse-echo mode (Figure 13.25). As the tool is pulled up the hole, with the transducer rotating, a very dense matrix of datapoints is collected from around the borehole wall, which is then processed into an image. Early versions of the tool used photos of oscilloscope output to create the image but today images are created by the computer using measurements which have been digitised downhole (Zemanek *et al.*, 1970; Pasternack and Goodwill, 1983). The modern service company tool will be illustrated by the Circumferential Borehole Imaging Tool (Log) (CBIL) of Western Atlas (Faraguna *et al.*, 1989; Atlas Wireline, 1992).

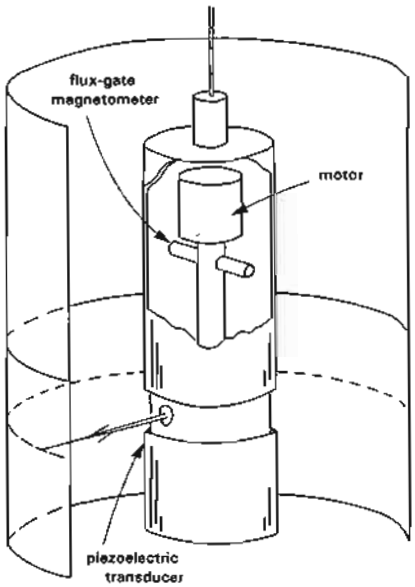


**Figure 13.25** The borehole televiewer tool (BHTV), schematic representation. A piezoelectric sonic transducer in transmit-receive mode, spins rapidly as the tool is pulled up the borehole (re-drawn from Zemanek, 1969).

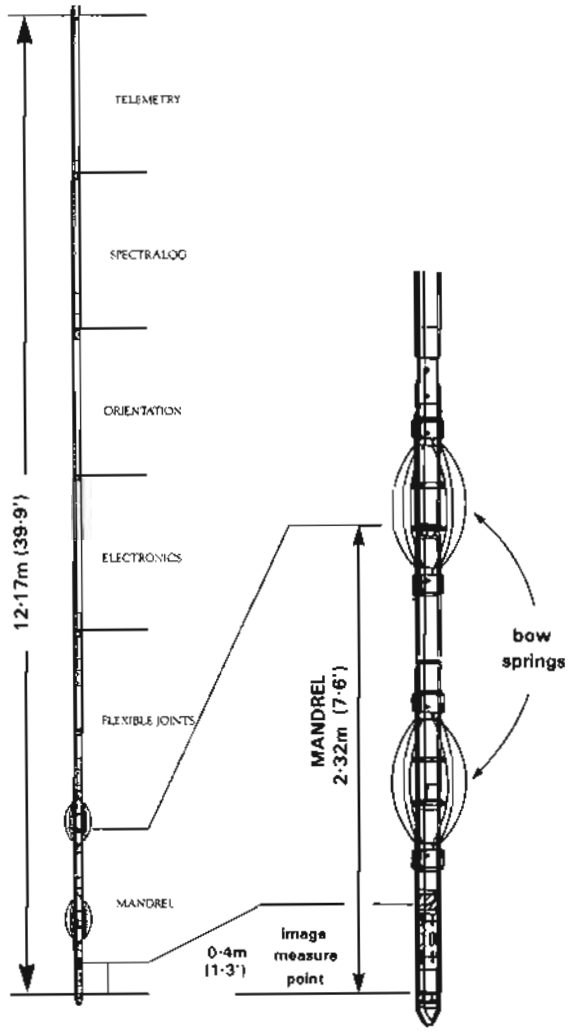


**Figure 13.26** Illustration of an acoustic imaging tool, the Western Atlas CBIL (Circumferential Borehole Imaging Log). (Modified from Atlas Wireline, 1992).

CBIL consists of a tool string typically approximately 12 m (40ft) long with the rotating transducer housed in a mandrel at the bottom (Figure 13.26). Bowsprings keep this part of the tool centred. Above this are the orientation and telemetry electronics and a spectral gamma ray sonde (Figure 13.26). When the tool is logging, the transducer, in pulse-echo mode, turns at 6 revolutions per second, taking 250, digitised samples on each revolution, or every 1.44°. It thus acquires a tight spiral of data points from around the entire borehole wall. When logged at a typical logging speed of 3 m (10ft) per minute, the tool makes 1 scan of the borehole circumference each 0.83 cm (0.33") of depth, thus acquiring a matrix of 30,000 sample points of paired data readings (30,000 readings of amplitude and 30,000 of travel time, as explained below) for each metre of borehole logged.

Transducers in the imaging tools are piezoelectric, that is, activated by an electric pulse. They are normally made from a thin circular disc 1"–2" in diameter. In CBIL, the transducer is hemispherical and has a concave surface facing outwards which has the effect of collimating (focusing) the sound pulse. Pulse beams can only hold an optimum focus over a short distance so that CBIL allows the choice of two different transducers with different diameters and different focal lengths, for use in different sized holes. One has a diameter of 3.8 cm (1.5") for small holes, the other a diameter of 5.1 cm (2") for use in larger holes. The smaller 1.5" transducer is focused to a 0.76 cm (0.3") diameter beam from 15 cm to 20 cm (6" to 8"); the larger 2" transducer has a similar beam from 20 cm to 30 cm (8" to 12") (Faraguna *et al.*, 1989).

The tool is considered suitable for use in holes between 5"–18" (13 cm–46 cm) in diameter (depending on mud weight). Piezoelectric materials can produce (or detect) a signal with very little 'ringing' and may therefore be pulsed very rapidly. In the CBIL tool, the transducer produces an ultrasonic pulse 1500 times per second with a frequency of 250 kHz giving it good penetration. The original Mobil design used 2 MHz signal, the Amoco design 1.3 MHz, so that CBIL has a distinct penetration advantage.

At each sample point, the acoustic tool acquires a measurement of the time of flight (or travel time) and

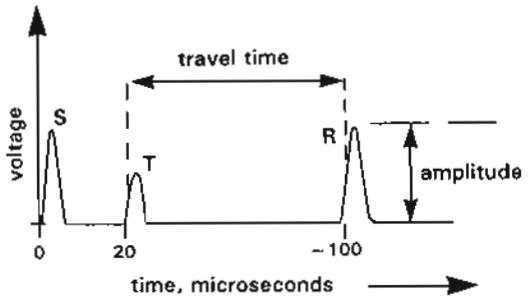


**Figure 13.27** Schematic televiewer waveform pulse characteristics. S = synchronise pulse, T = transmitted pulse, R = reflected pulse (amplified). The amplitude of the returned pulse is measured and also the travel time (time of flight). (Modified after Pasternack and Goodwill, 1983).

reflected amplitude (Figure 13.27). The time of flight is simply the time between emission, reflection off the borehole wall and detection back at the transducer: it varies with hole geometry. The reflected amplitude is the accumulated response over a predetermined time span. That is, the received reflected signal is converted by the transducer into an electrical signal, the strength of which is the reflected amplitude (simply called amplitude) (Figure 13.27). The amplitude varies with the acoustic impedance of the reflecting borehole wall, due both to lithology and physical features (*explained below*).

Acoustic imaging tools can function in a hole filled with any fluid; water, water-based mud or oil-based mud. But mud attenuates the signal. In effect, the tools can only be used in holes with lower density muds. CBIL uses a lower frequency signal which improves operating ranges, so that it can be used with mud densities upto 1.7–1.9 g/cm$^3$ (15–16 lbs/gal) (Table 13.6).

***Acoustic image processing***

Raw acoustic travel time and amplitude data are generally processed to a colour image presentation. Flight time data can also be displayed as a continuous acoustic caliper, either as logs or, more interestingly, in 2D or 3D plan view. The image type presentations will be discussed first.

The dense matrix of both amplitude and travel time data acquired by the acoustic imaging tools, covering the entire borehole wall, is processed into colour (or grey scale) images and presented in the unwrapped borehole log format described previously (Figure 13.2) (Pasternack and Goodwill, 1983). The two measurements are plotted as two image log strips, side by side, so that they can be compared (Figure 13.28). To make the image, each sample is represented by one pixel. The pixel matrix is built up from the 250 (or other) horizontal samples from around the borehole circumference and the very small regular depth sampling. The actual area of borehole wall represented by a pixel will depend on borehole size and the logging speed. In an 8.5" hole, logged at 3 m (10ft) per minute with 250 samples per revolution and 6 revolutions per second (CBIL), each sample will represent an area of approximately 1.46 cm (.58") on the X (horizontal) axis by 0.833 cm (0.33") on the Y (vertical, depth) axis. In a 12.25" borehole the equivalent area will be 3.04 cm (1.2") X axis by 0.833 cm (0.33") Y axis. Clearly, with the tool operating from the centre of the borehole there is sample variation as hole size varies.

Production of the colour or grey scale image is the major step in both amplitude and travel time image processing. However, because of a number of unwanted acquisition effects (*described below*), improvements are often made to the images themselves (of both measurements) by a second layer of processing. This includes filtering, equalisation, edge detection and other techniques of image processing (Wong *et al.*, 1989). The improvements can be operator applied to workstation displays.

The time of flight measurements which are used to produce one of the image sets, may also be presented as an acoustic caliper. That is, the time of flight can be converted into a distance by accounting for the mud velocity (which is monitored continuously by the tool in a special sensor). This produces 250 (or other) tool to borehole measurements around the full circumference of the borehole. These values may be used to produce standard log trace type caliper curves (Figure 13.28). However, they may also be displayed as a polar plot that is viewed looking down the hole (Figure 13.33). Some software packages produce a 'travelling polar plot' which allows the operator to observe the caliper changes on the screen, moving up the hole rather as the tool does. There are also more complex 3D formats for screen use.

***Resolution***

Feature resolution is controlled by transducer beam characteristics, which in turn are a function of transducer size and tool electronics (*see* The tools *above*) (Georgi, 1985). Using experimental models, under ideal conditions the Western Atlas CBIL acoustic tool is indicated to *detect* a fracture aperture with a width of 0.025 mm (0.001") (Lincecum, 1993), much smaller than the resolution of the transducer. Resolution is equal to the radius of the pulse beam (or the transducer size in unfocused beams). In this context, detection is the ability to recognise a single object while resolution is the ability to separate two objects. The experiments show clearly that the acoustic tools can detect features (fractures essentially) below their resolution, but that all features up to the resolution resemble each other.

Laboratory based figures are somewhat modified in subsurface practice. For example, an in-house tool used by Shell (Dudley, 1993) was able to detect in the subsurface, fractures 1 mm (0.04") or greater in width and to resolve fractures 8 mm (0.3") apart. Other studies have found that the BHTV could detect fractures only with apertures greater than 0.5 mm (0.02") (Laubach *et al.*,

1988). Clearly there are variations between tools and local conditions affect the operation.

In more general terms, CBIL is indicated to have a vertical resolution of approximately 1.3 cm (0.5") (Verdure, 1991). This figure is indicative of the resolution to expect when examining sedimentary features. However, figures indicative from subsurface analysis are often much larger than this and an early study found that features 15 cm (6") thick were not recognised (Laubach *et al.*, 1988). Experience shows that recognising especially smaller scale sedimentary structures using the present acoustic tools is difficult.

***Factors affecting acquisition***

There are a number of factors which affect acoustic tool acquisition in general and have an influence on quality and hence interpretation. These are briefly described below.

*– borehole geometry and tool position*

Because the transducer pulse is highly collimated (focused), it will only be reflected back to the transducer from a surface that is normal to the beam (Georgi, 1985). With angles even slightly away from 90°, little or no energy will be returned to the transducer. This means that hole ovality and tool tilt or non-centring will affect the sampling (Figure 13.29). The result will be dark or light stripes running up the image. Controls such as AGC (automatic gain control) help to diminish these effects in the more modern tools and they are generally (but not always) contained. This allows real geometric hole effects still to be seen, such as spiralling (Figure 13.28) and breakouts, especially in the time of flight plot (Figure 13.33).

*– mud weight*

Although acoustic imaging tools need a fluid in the borehole to function, mud causes attenuation (Table 13.6). The pulse energy is absorbed and scattered by the mud particles and the beam is spread. This means that the acoustic tools will not function in heavy muds. All mud causes some loss of signal and it is suggested that quality is poor in 8.5" holes with weights above 1.62 g/cm$^3$

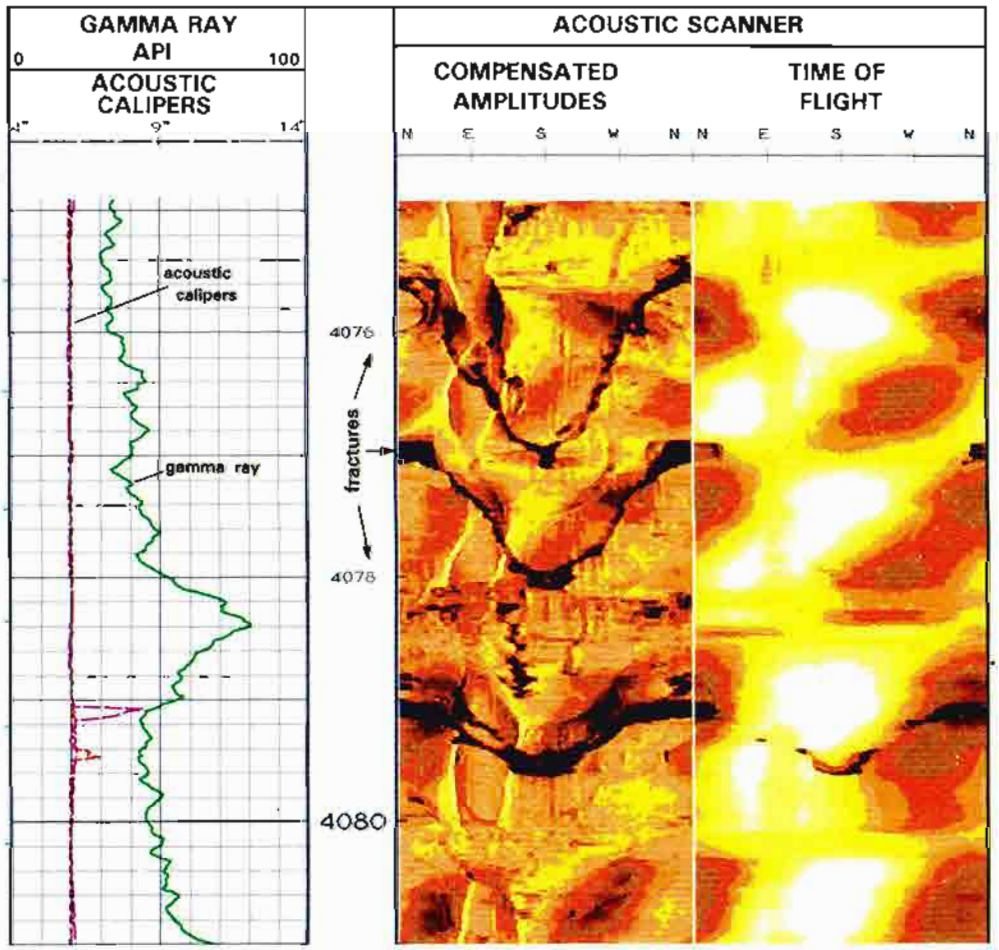


**Figure 13.28** Acoustic image presentation format. Track 1: acoustic calipers and standard gamma ray. Track 2: amplitude image (high = light). Track 3: time of flight image (long = light). The lithology consists of fractured carbonates. Note the caving between 4079.10m – 4079.5m related to fracturing (BPB Acoustic Scanning Tool).

(13.5 lbs/gal) and 1.25 gcm$^3$ (10.5 lbs/gal) in 12.25" holes. However, such strict limits are not indicative, as much depends on the acoustic impedance between the mud and the formation (see *below*). It is certain that the tool should generally not be used in mud weights above 1.7 gcm$^3$–1.9 gcm$^3$ (15–16 lbs/gal), even with CBIL which has lower operating frequencies.

*– acoustic impedance contrast*

For there to be a significant reflection of pulse energy at the borehole wall, there must be an acoustic impedance contrast between the mud and the formation. For this reason, the acoustic imaging tools are traditionally used in 'hard' formations such as limestones or older rocks (and crystalline rocks for the non-hydrocarbon industries). However, it is equally true that strong acoustic impedance between formations produces viable images. This is well illustrated by the use of the tools in the coal industry (Rübel *et al.*, 1986): coal has big impedance contrasts with other lithologies.

*– borehole surface*

In the same way that borehole geometry affects the strongly focused acoustic beam, so also does the reflectivity, the topography of the actual surface of the borehole wall. That is, good reflection will come from a smooth surface, any roughness will cause scatter and reduce the energy of the reflected signal. Thus, acoustic images show scratches left by the bit on the borehole wall, or zones of wall breakage (spalling). Such effects may dominate an image. However, usefully, fractures and other natural features such as breakouts will also be seen for the same reason (Section 13.9).

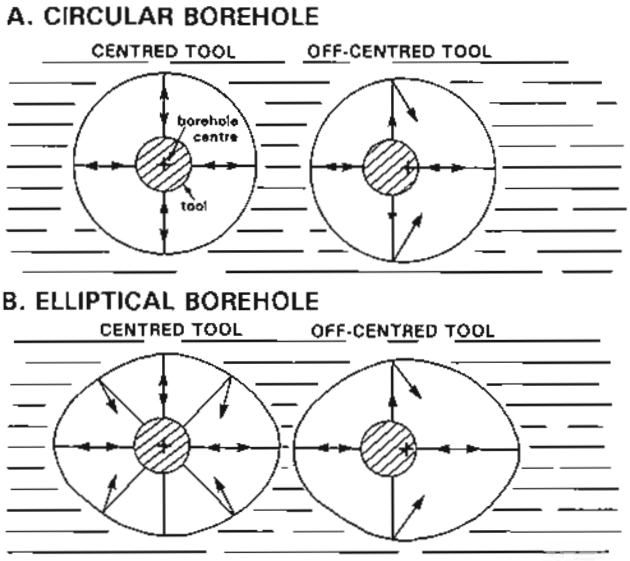


**Figure 13.29** Unwanted geometrical factors which can affect acoustic images (re-drawn from Georgi, 1985).

**Table 13.6** CBIL theoretical signal attenuation related to mud weight and hole size. Signal loss in decibels. Barite oil-base mud (after Faraguna *et al.*, 1989).

| Mud g/cm$^3$ | Weight lbs/gal | Hole Diameter 8½" | 12¼" | 17½" |
|---|---|---|---|---|
| 1.08 | 9.0 | *-7.5 | *-12.5 | *-20.0 |
| 1.44 | 12.0 | *-14.4 | *-25.6 | -40.6 |
| 1.80 | 15.0 | *-22.5 | -38.5 | -60.6 |

*acceptable signal. No star, signal not acceptable

## 13.8 Acoustic imaging tool interpretation, generalities

Acoustic imaging tools are used to provide high quality dip and azimuth measurements, to investigate fractures, to provide information on borehole breakouts and to some extent to give information on lithological boundaries, textures and some sedimentary features. By far the commonest use of the acoustic imaging tools to date, has been to investigate fractures.

*– display and manipulation*

The use of a workstation for acoustic log interpretation is standard. The two log processings, as described, are displayed side by side so that they may be compared. Typically, the amplitude scale uses the lighter colours or shades for large amplitudes and black for zero amplitude (Figure 13.28). The time of flight scale is from near reflection darker shades to far reflection or none at all (light). The polar caliper from the time of flight can be displayed simultaneously in a corner of the screen. Helpfully, the images will be displayed with standard logs and possibly caliper traces (Figure 13.28).

Acoustic image display software usually incorporates enhancing routines which can be used during interpretation as needed. These routines are helpful in taking out unwanted artifacts caused for the most part by hole geometry.

Sine wave fitting routines for measuring dip and azimuth are the same for the acoustic tools as for the electrical tools. Dip and azimuth are displayed on screen and features may be annotated. One development which seems more common with the acoustic logs, is software able to work through an entire log, picking image sine wave dip and azimuth measurements automatically (e.g. Torres *et al.*, 1990). Orientation classification and identification routines are as for the electrical images.

*– amplitude versus time of flight*

The juxtaposition of the two acoustic image logs, the reflected amplitude, or reflectance and the travel time to and from the borehole wall or the 'time of flight', is an aid to interpretation. Of the two readings, the amplitude is

generally the one that is the most sensitive and contains the most character (Figure 13.28). In comparisons, it is the amplitude image which is compared with the electrical image. The amplitude log is an indication of both acoustic impedance and borehole wall roughness. In this way it provides lithological information (Figure 13.34). For example, a dense carbonate presents a smooth borehole wall and returns a high amplitude signal while coals have low reflectance and return a low amplitude signal. The acoustic impedance variations of the borehole wall may be dampened somewhat by the acoustic impedance contrast between the mud and the borehole wall. Best signals come from intervals where this contrast is considerable.

Time of flight response is clearly quite different from the amplitude response. Time of flight records borehole geometry. It is therefore sensitive to hole ovality, a sensitivity which is used in the identification of breakouts (Section 13.9). However, it will also be affected by voids on the borehole wall such as open fractures, which will return no signal (Figure 13.28). Lithological effects will be minimal except where slight borehole size differences are caused by different lithologies.

The complementary nature of the two presentations helps in their mutual interpretation. For example, comparison between amplitude and time of flight logs can indicate whether a fracture is open or closed. An open fracture gives a response on the amplitude log through loss of signal, and also on the time of flight log as no signal is returned. A filled fracture will provide an image on the amplitude log (depending on acoustic impedances) but no image on the time of flight log (Taylor, 1991).

*– electrical images vs. acoustic images*

There is a tendency to compare the acoustic images with the electric images, not just because they are both images but also because of commercial competition. Of course the two should be compared, not in a competitive sense but to find out which tool to use for a particular set of circumstances.

There are two obvious differences between the tools. The acoustic tools can be used in any fluid including oil-based muds, the electrical tools cannot: the acoustic tools give a full 360° coverage, the electrical tools give partial coverage, from 20%–90% (Table 13.1). The claimed resolution and detection are similar for both tools although in practice, the electrical images can be interpreted at a much finer scale for many features than the acoustic images (*see* Resolution).

From experience it is found that the acoustic tools have a good sensitivity to fractures. The full 360° coverage is essential to study fractures which are often irregular, branching and non-planar (Laubach *et al.*, 1988). The acoustic logs are also good in the study of borehole geometry and breakouts. The acoustic caliper, along with the images are excellent for this (Figure 13.33). However, definition of sedimentary features and lithological boundaries is generally poor to moderate. Sedimentary structures, and image facies are more effectively analysed with the electrical images.

In summary, electrical images are favoured for sedimentary analyses where water-based muds are used, the BHTV for fracture and tectonic studies or where oil-based mud is used. However, the choice is often imposed by drilling conditions.

## 13.9 Some examples of acoustic imaging tool interpretation

*– structural dip*

Used in the simplest way, acoustic images provide a high quality dipmeter, the dip and azimuth taken from sine wave fitted to surfaces using the work station. This was indeed the early use to which the tool was put (Rambow, 1984). The data from such a process are generally much less scattered than the comparable data from the electrical images (Section 13.5) and can be effectively used as a structural dip.

*– fractures*

By far the most common use of the acoustic log is in the examination of fractures (Paillet *et al.*, 1990). This is as much the case in the hydrocarbon as in the non-hydrocarbon industries (water, geothermal etc.). The advantage for all is that the images allow the identification, measurement and recognition of fracture type in the subsurface.

In laboratory experiments, fractures have been detected down to a width of 0.025 mm (0.001") (*see* Resolution). In practice, detection in the subsurface is at around 0.5 mm (0.02") to 1 mm (0.04") while two fractures must be separated by about 8 mm (0.3") to be recognised (Dudley, 1993). In core to image comparisons, the logs are seen to detect perhaps only 25% of all fractures although possibly 50% of the larger, more important ones with apertures above 0.5 mm (0.02") (Dudley, 1993). In highly controlled cases, all the important fractures are seen on the acoustic images. The example shown previously is of fractures in a carbonate (Figure 13.28).

Although the detection of a fracture and its orientation measurement in the subsurface is a major step, 'Just to find a fracture is not enough' (Nelson, 1985). There is a need to identify the type of fracture and, as more image logs become available, it is clear that drilling induced fractures are far more common than was originally thought (Lincecum *et al.*, 1993).

One difficulty with the study of fractures is the damage that occurs to them during drilling, of spalling, chipping and erosion by circulating mud. For example, highly dipping surfaces are generally eroded away or broken at the high and low borehole crossing points (Figure 13.30) (Paillet *et al.*, 1985). Such breaks can be seen on the fractured carbonate example (Figure 13.28). In a similar

way, fracture infill may be plucked out during drilling in the immediate vicinity of the borehole and the walls of the fractures broken, so enlarging the aperture.

Separating drilling induced from natural fractures is notoriously difficult. On cores, distinctive geometry and surface features are used (Kulander *et al.*, 1990). In the subsurface, a combination of geometry and orientation can be used (Table 13.5, Figure 13.31) (Lincecum *et al.*, 1993). For example, most drilling induced fractures form parallel to the maximum horizontal stress direction $Sh_{max}$, which means that they are extensional fractures. The $Sh_{min}$ orientations are well identified from breakouts (*see below*) and may be used to define preferred fracture orientation (Figure 13.31). Apart from this, induced fractures, of course, are never mineralised and never cause bedding offset. For natural fracture classification, the important distinctions other than orientation are whether the feature is open or closed or mineralised. As described (Section 13.7) comparisons between amplitude and time of flight images can suggest whether a fracture is open or mineralised, open fractures having an image on both logs, mineralised fractures on only the amplitude image (Taylor, 1991).

Despite all the difficulties, fracture studies with acoustic images make a significant contribution to reservoir understanding. This is well illustrated by the USGS technique of combining image studies with high quality flowmeter measurements (Paillet *et al.*, 1987; Paillet, 1991). It is well known in aquifer studies that major flow is usually from only a few fractures. Using the BHTV allows major fractures to be located and their orientations measured. Adding flowmeter readings allows the flowing fractures to be separated from the non-flowing ones: essential information (Figure 13.32).

*– borehole breakouts*

Because of its sensitivity to borehole geometry, the BHTV is an excellent indicator of breakouts (Chapter 4). Breakouts are marked by hole enlargement in the direction of minimum horizontal stress, $Sh_{min}$. Enlargement is seen on the amplitude image log and the time of flight log as vertical strips indicating poor reflectivity and long travel time or lost signal (Figure 13.33) (Paillet and Kim, 1987). In addition to the images, the acoustic caliper derived from the time of flight measurements, can be used to indicate the hole circumference profile (Figure 13.33).

As discussed above, the use of breakouts to derive present day *in situ* stress orientations, is an important phase in the attempt to separate natural from drilling induced fractures. Although dipmeter calipers are traditionally used for breakout analysis (Chapter 4), when BHTV images are available they are far more effective and more precise.

*– texture, lithology & sedimentary features*

For lithological features to be seen on the acoustic images, there must be large acoustic impedance contrasts. The coal industry has long used the BHTV to localise coal seams and give accurate bed limits (e.g. Rübel *et al.*, 1986). However, coal seams are an exception in terms of lithology and more general lithological investigations

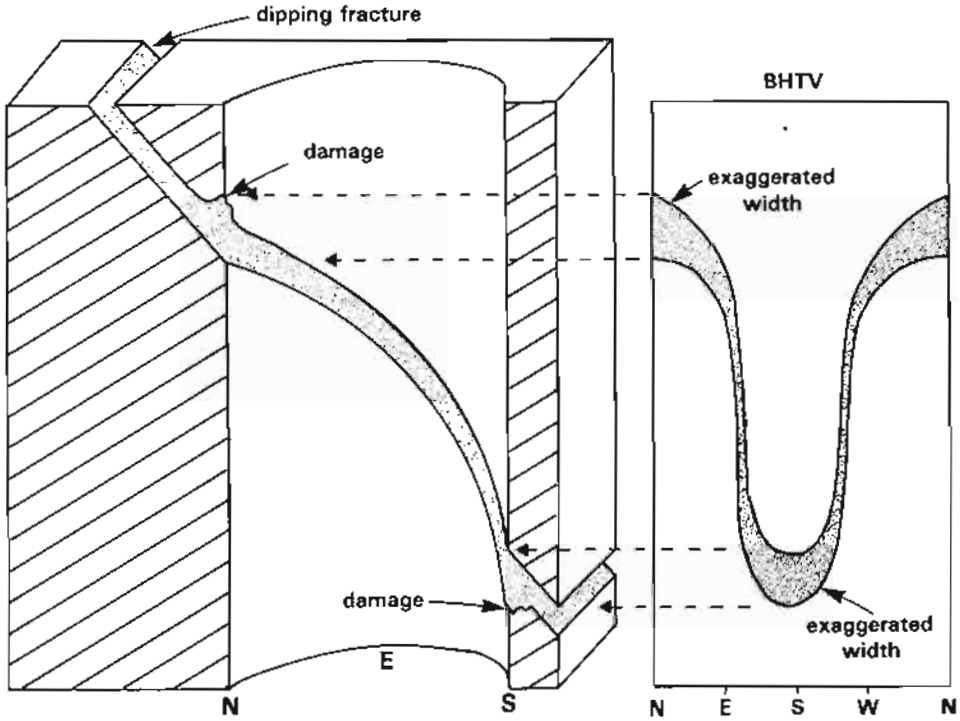


**Figure 13.30** Typical characteristics of an open fracture seen on an acoustic image log. The fracture width becomes exaggerated at certain points around the borehole wall as a result of drilling damage (re-drawn from Paillet *et al.*, 1985). Note this effect on the fractures of Figure 13.28.

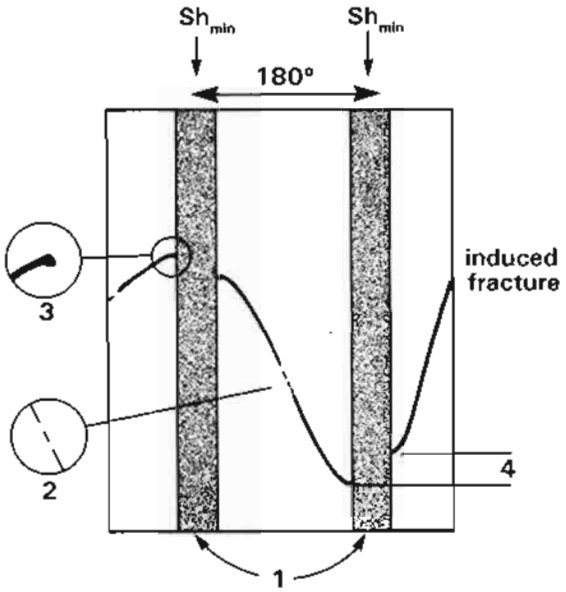


**Figure 13.31** Acoustic image chacteristics of induced fractures. The sinusoid is an open, induced fracture and the dark, vertical stripes are breakouts. 1, breakouts indicating the orientation of $Sh_{min}$. 2, fracture strike parallel to $Sh_{max}$. 3, spalling at breakout margin. 4, offset across breakout (modified from Lincecum *et al.*, 1993).

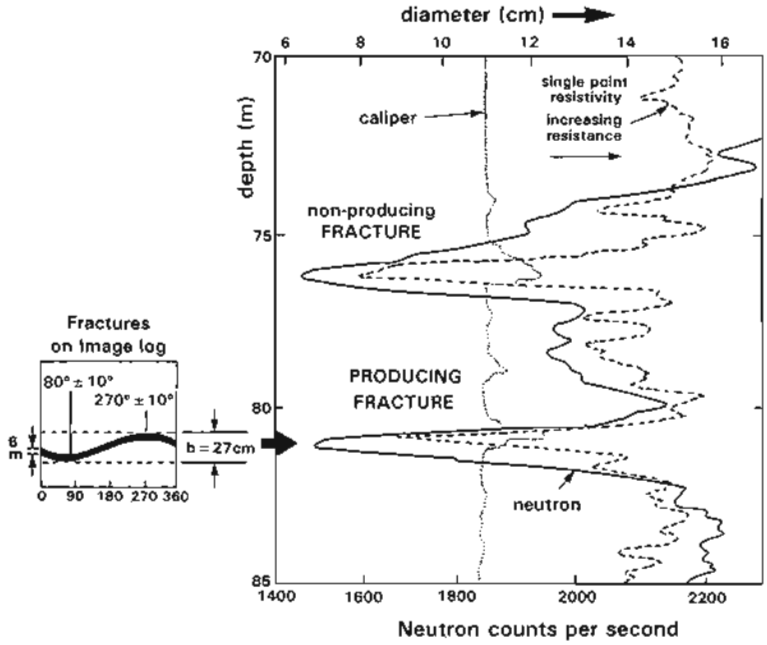


**Figure 13.32** Fluid flow from an open fracture identified on an acoustic image log. The neutron counts are high (high water content) and the resistivity is low (salt water) both indicating an open, water filled fracture. The caliper shows caving at the fracture level. The acoustic image shows a well-defined feature at the lower level (from Paillet *et al.*, 1987).

with acoustic images are only now beginning to be used (e.g. Verdur *et al.*, 1991) (Figure 13.34). One of the problems with acoustic images in sedimentary sequences is that the acoustic impedance contrasts between lithologies, beds or laminae is small. However, major bed boundaries are found to be imaged (cf. Rambow, 1984) and so are tight or cemented zones (cf. Hurst, 1995) (Figure 13.34).

In the same way that lithological investigations are difficult with acoustic logs, so too are investigations of sedimentary structures. Some success in this field is beginning to be seen (e.g. Verdur *et al.*, 1991 and Figure 13.34) but in general electrical images are far more effective for this task.

## 13.10 Quantitative interpretation of acoustic images

The only effective quantification using acoustic images is of fractures. These may be quantified in terms of aperture, effective porosity and frequency.

The simplest form of quantification from acoustic images is provided by fracture counts. Fractures are recognised and then converted into an individual count, total count or number of fractures per selected interval (i.e./m). Core studies suggest that BHTV fracture frequency is a lot less than core frequency (Dudley, 1993). However, fracture counts do not take into account fracture size and correlation with bulk seismic methods shows that this can be important (e.g. Barton and Moos, 1987).

Measuring fracture width on the acoustic logs does not always give a clear result (Paillet *et al.*, 1985). Two problems arise, one is of fracture enlargement during drilling, the other is of the limited resolution of the tool itself. Fracture enlargement by drilling mud erosion and breakage have been described above. Also, tool resolution indicates that below tool resolution, all fractures appear to have the same width. There is generally going to be an exaggeration of width. However, the fractures that are detected are the major ones, so that a fracture count is the most likely attribute to correlate with fracture permeability. Unhappily, in comparisons between image fracture counts and flow in closely spaced water wells (Paillet *et al.*, 1992), very few of the BHTV detected fractures actually flowed. This may be typical.

## 13.11 What next?

The reason for using the imaging tools, electrical or acoustic, is not just to provide pretty pictures of the formation (although they do!), it is to provide a detailed and accurate description of the reservoir. As always with new logging tools, interpretation lags behind tool technology. Certainly, the qualitative capabilities of the imaging tools are being used, although not fully. The quantitative aspects are in reality, to come.

It is certain that some hindrance to the wider use of image logs lies in their commercial side. To interpret the image logs satisfactorily, a workstation must be used. It is only when workstations are generally available and enough minds are put to the subject, that image log analysis and interpretation will become properly developed and properly used.

The active introduction of new imaging tools and refinements of tools already in service continues rapidly (*see* Chapter 16). At present, imaging tools are considered as 'specialist', and only occasionally requested. This will change. They will soon become if not routine, then at a minimum, essential.

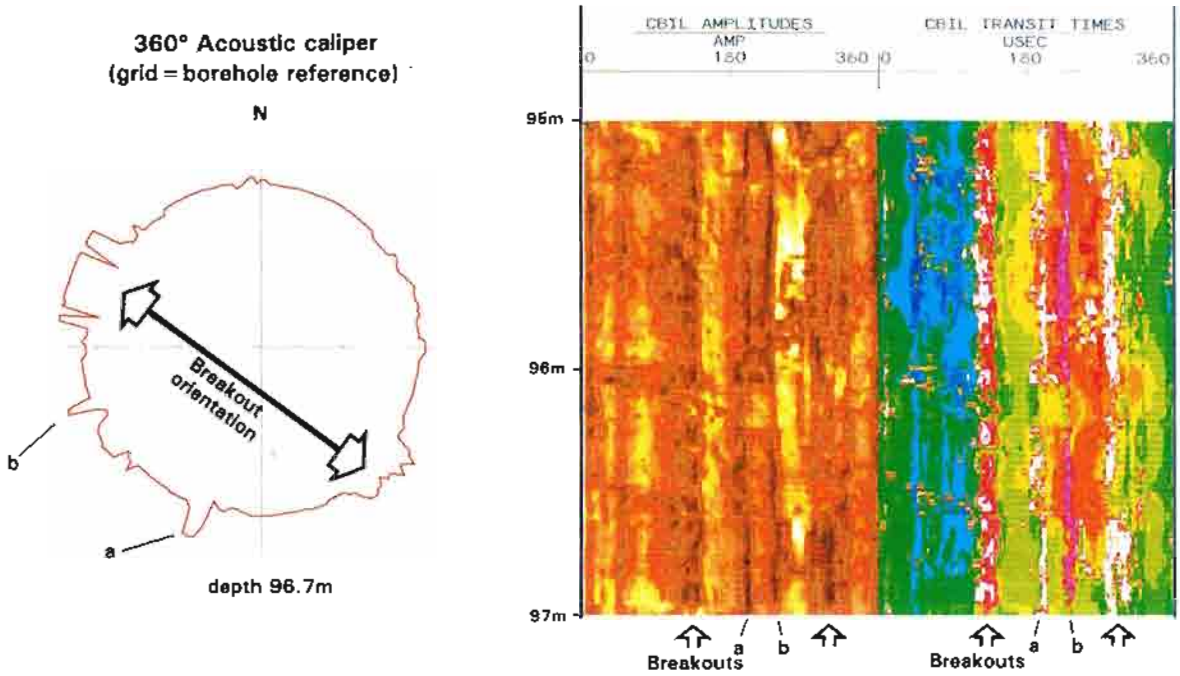


**Figure 13.33** Breakout indicated on acoustic images. The 360° caliper (from depth 96.7m) shows the breakouts oriented approximately NW-SE. The amplitude image shows the breakouts as dark, vertical strips (arrowed). The transit time image shows them as well-marked light stripes (arrowed). a and b are additional vertical features. Western Atlas CBIL, IMAGEPRO output.

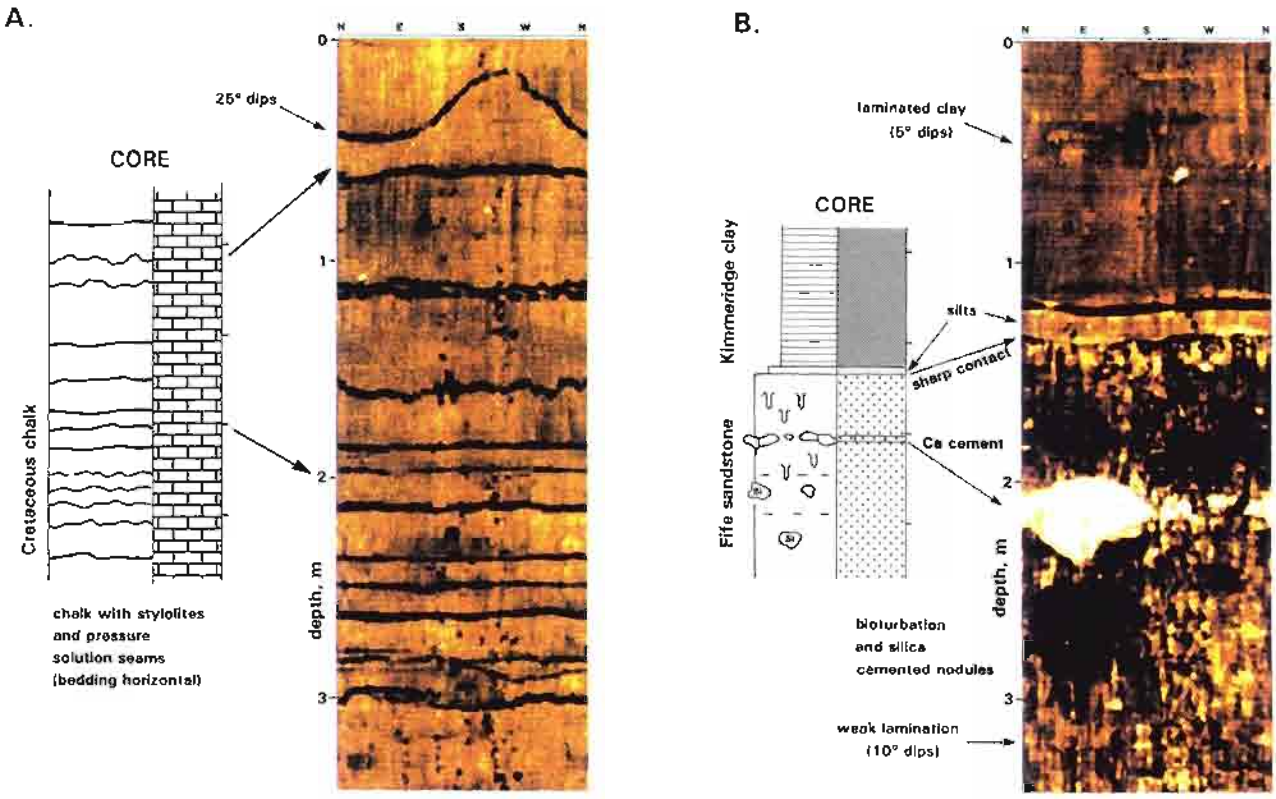


**Figure 13.34** Lithology and sedimentary features on acoustic images. A. Chalk with stylolites and pressure solution seams. B. Burrowed, fine grained Fife sands with carbonate layers and silica cemented nodules, abruptly overlain by laminated Kimmeridge clay. Normalised acoustic amplitude plots from Western Atlas CBIL, Western Atlas output, light = high amplitude. Core sedimentology from D. Mackertich Amerada. Data published by permission of Amerada Hess (UK) Ltd. and Western Atlas.

# 14
# FACIES, SEQUENCES AND DEPOSITIONAL ENVIRONMENTS FROM LOGS

## 14.1 Introduction

The use of well log analysis in geological disciplines is developing, but only slowly. Traditionally, logs are used to correlate: one well is compared to another and lines drawn between the two. This is a primitive approach, and logs have a far greater potential.

Chapter 11 describes the use of logs to construct lithology. This chapter takes geology a step further and describes how logs can be used for facies and sedimentological analyses. Modern subsurface geological analysis can and should employ a thorough and sophisticated analysis of well log data.

## 14.2 Facies

***Gamma ray log shapes***

A basic scheme to classify sand bodies in the Gulf Coast area of the USA, apparently developed by Shell (cf. Serra and Sulpice, 1975) was based on the shape of the SP log (Figure 14.1) along with its mirror image (sometimes) the resistivity log. The principal shapes observed were the bell, the funnel and the cylinder (Figure 14.1). The scheme was intended to give a classification of log shapes in order to aid correlation: it was essentially a geometrical approach. However, rather than just recognising and classifying shapes, an attempt should be made to understand why the shapes exist.

Although the SP was at the origin of the interest in log shapes, it is the gamma ray log that is generally used today; the curve gives greater variety of shapes, shows greater definition and has more 'character'. To explain a log shape, the log response itself must be understood. Since the gamma ray log is *frequently* an indicator of clay (shale) content (but by no means always – *see* Chapter 7, *and below*), gamma ray log shapes can be explained in terms of variations in clay (shale) content. A bell-shaped log (Figure 14.1), where the gamma ray value increases regularly upwards from a minimum value, should indicate increasing clay content: a funnel shape, with the log value decreasing regularly upwards, should show the

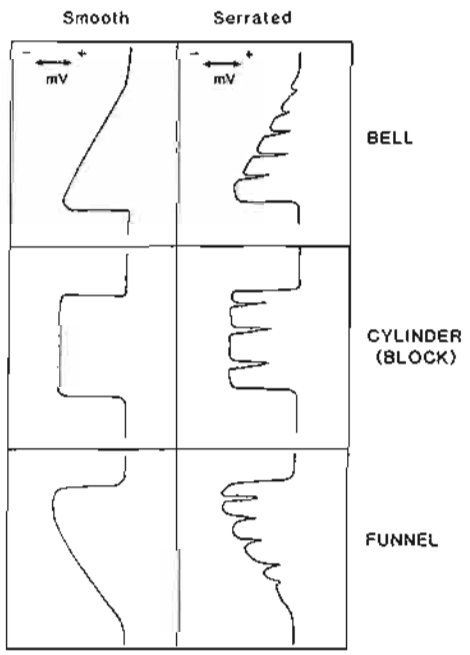


**Figure 14.1** Log shape classification. The basic geometrical shapes and description used to analyse SP and gamma ray log shapes.

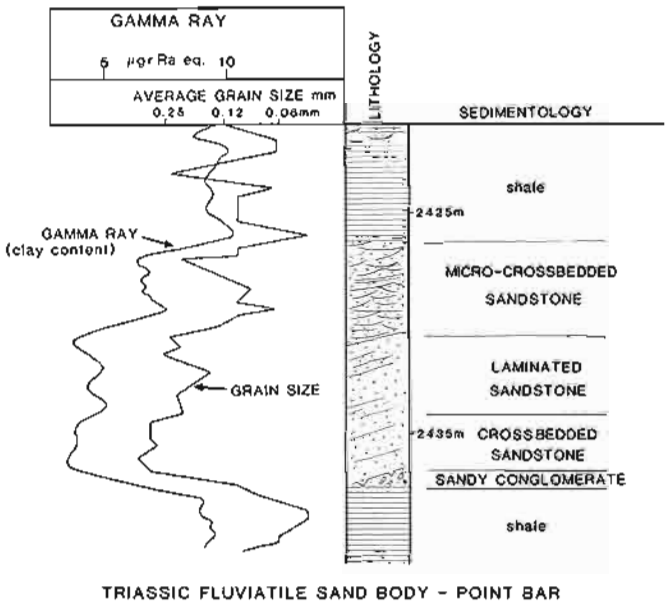


**Figure 14.2** Sedimentology of a bell shape. A core cut through a sand body with a typical bell shape on the gamma ray log shows it to be a fluviatile channel. Note the close correspondence between the gamma ray (giving clay content) and grain size. Triassic, Sahara. (re-drawn from Serra and Sulpice, 1975).

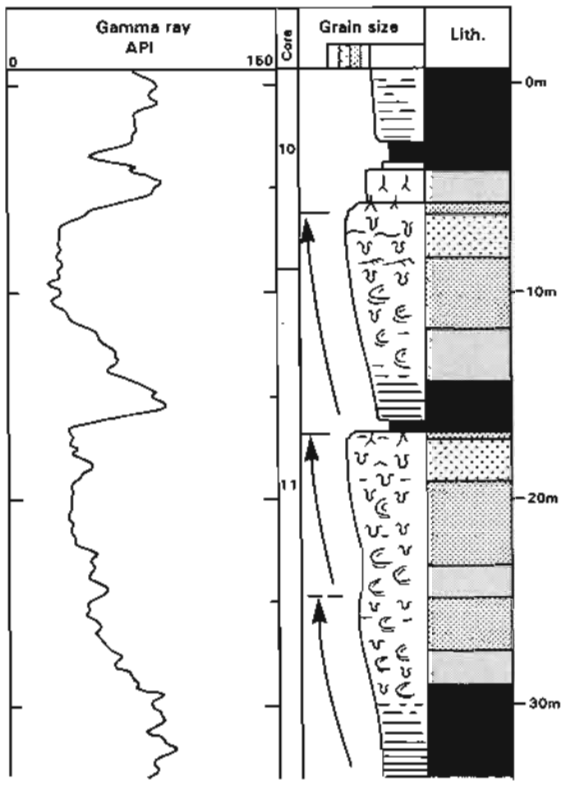


**Figure 14.3** Funnel shapes on the gamma ray log corresponding to coarsening-upwards sequences, interpreted to have been deposited in prograding, estuarine shorelines. The gamma ray shapes in this example are characteristic.

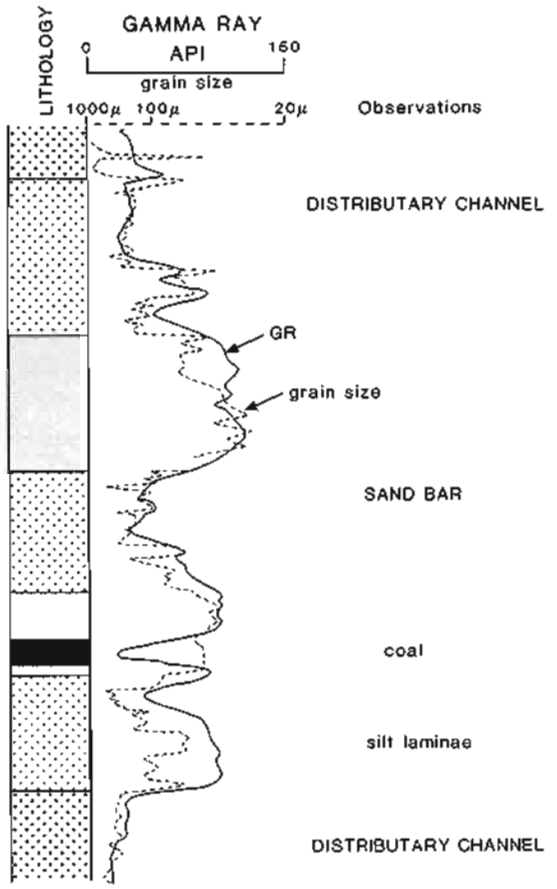


**Figure 14.4** Grain size – gamma ray correlation: a very close relationship is possible between the two. (Modified from Simon-Brygoo, 1980).

reverse, a decrease in clay content.

A core cut through a Triassic fluviatile sand body in the Sahara (Figure 14.2) shows a typical bell shape on the gamma ray log response (Serra and Sulpice, 1975). The increase in gamma radiation corresponds to an increase in clay content regularly upwards. The increase in clay content is correlated to a decrease in the sand-grain size. A sedimentological analysis of the core shows a set of sedimentary structures typical of fluviatile point bar deposits (Serra and Sulpice, 1975). The bell shape, therefore, can be interpreted as indicative of a fining-upwards, fluviatile, point bar sandstone (in this case). A second example shows gamma ray funnel shapes with the corresponding, core-derived sedimentology (Figure 14.3). Each funnel-shape represents a succession coarsening-upwards from bioturbated, offshore muds to silts to bioturbated, shallow marine sands capped by root beds and coals. The successions are interpreted to have been deposited in prograding, estuarine shorelines. The funnel shape is therefore indicative of coarsening-up, prograding estuarine shoreline successions (in this case).

These examples show the close relationship possible between the gamma ray log and sandstone grain size. Shapes on the gamma ray log can be interpreted as grain-size trends and, by sedimentological association, as facies successions. A decrease in gamma ray values will indicate an increase in grain size: small grain sizes will correspond to higher gamma ray values (Figure 14.4). The sedimentological implication of this relationship leads to a direct correlation between facies and log shape, not just for the bell shape and funnel shape as described above, but for a whole variety of shapes.

Numerous publications show the log shapes expected or found in various facies (Krueger, 1968; Galloway, 1968; Fisher, 1969; Fons, 1969; Pirson, 1970; Goetz *et al.*, 1977; Coleman and Prior, 1982; Galloway and Hobday, 1983; Vail and Wornardt 1990; Van Wagoner *et al.*, 1990; Cant, 1992). They all depend on the relationship between log shape and grain-size trends in sandstone bodies: A bell shape indicates a fining-up sequence which may be an alluvial/fluvial channel but also a transgressive shelf sand. A funnel shape is a coarsening-up succession which may be a deltaic progradation or a shallow marine progradation (Figure 14.5). The analogies may even be extended to deep sea deposits. In these cases the log shapes are those of overall successions rather than individual bodies (Parker, 1977). The shapes come from the diminution in bed thickness associated with diminution

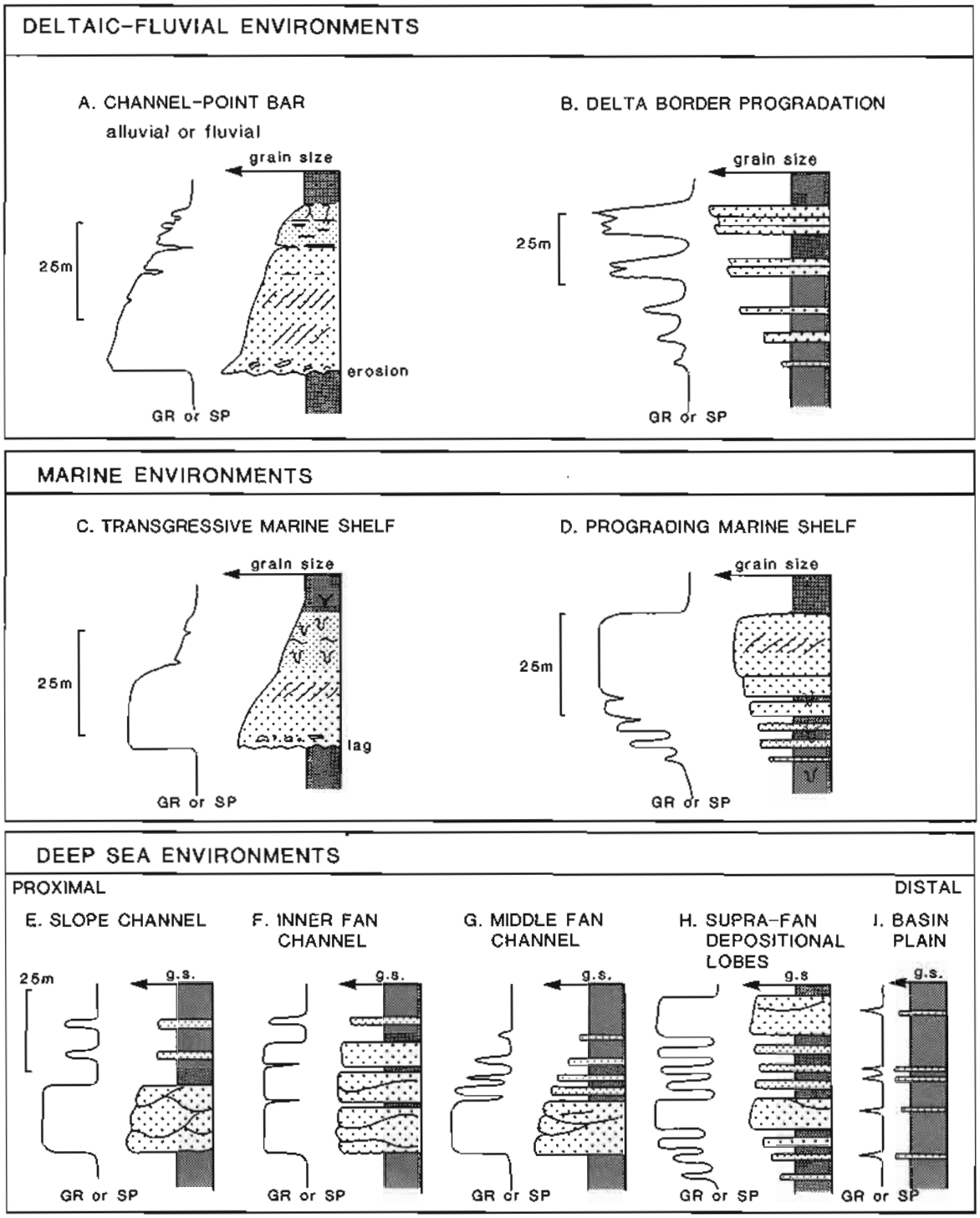


**Figure 14.5** Facies indications from gamma ray (or SP) log shapes. These are idealized examples both of log shape and sedimentologic facies. (Modified from Serra, 1972; Parker, 1977; Galloway and Hobday, 1983).

in grain size, rather than the direct change in grain size itself. However, the principles are similar (Figure 14.5).

Once established, the log shape system can be used in a number of ways. Maps made of the geographical distribution of log shapes, are effectively both facies distribution and palaeogeographic maps (Saitta and Visher, 1968; Doveton, 1986; Finley and Tyler, 1986; Cant, 1992). Once an interval is reliably identified, then the variations in log shape within that interval give an indication of facies variations and hence, an indication of palaeogeography (Figure 14.6). More recently, log shapes have been used as a tool for sequence stratigraphy (Van Wagoner *et al.*, 1990), with variations in log shape

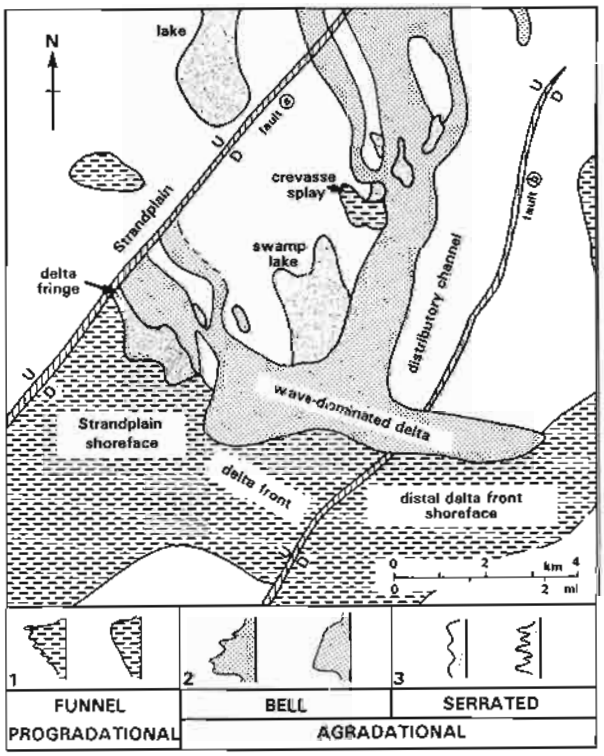


**Figure 14.6** A palaeogeographic reconstruction based on SP log shapes in a deltaic environment, the Cayce sandstone (modified from Finley and Tyler, 1986).

(generally gamma ray), indicating facies relationships within parasequences (Figure 14.7), parasequence stacking patterns or facies changes at sequence boundaries (Chapter 15). Indeed, often a heavy reliance is put upon log shapes. However, from a sedimentological viewpoint, relating a particular log shape to a particular facies should not be done (Cant, 1992), there are too many overlaps of different facies giving similar shapes. But the questions which arise from a logging view are more fundamental. Is there a consistent reason why log shapes exist? Do they signify what is claimed of them? The reliability of using log shapes to supply grain size, and ultimately, facies information is examined below.

### *The gamma ray - grain size relationship; a critical examination*

The gamma ray log does not vary because of changes in grain size; it varies (often) because of changes in clay content (the same is true for the SP). However, sedimentological interpretations based on gamma ray log shapes require the log to vary with grain size. This involves undeclared assumptions. 1: gamma ray variations are related to clay volume changes and, 2: clay volume changes are related to grain size differences. These two assumed relationships will be examined.

First of all the gamma ray relationship to clay volume. This has been discussed previously (Sections 7.6, 7.8). It was pointed out that care must be taken in using the gamma ray to indicate clay volume, because clay radioactivity is not constant (it depends on the clay mineral and mineral mix) and, more importantly, there are naturally radioactive minerals in the sand-sized grain fraction (Rider, 1990). For example, sands which contain potassium feldspars have a natural (potassium) radioactivity. Gamma ray log variations will therefore reflect the distribution of the feldspars, which may vary with grain size, and not clay. Other radioactive grains include micas, glauconite, heavy minerals and rock fragments in general, all of which will disturb gamma ray log shape interpretation. These grain type variations are normal and are the basis of the often used classification of sands devised by Folk (1954) which shows quartz (non-radioactive), feldspars (radioactive) and rock fragments (frequently radioactive) as the *compositional* elements which vary independently against clay content which gives the *textural* element (Figure 14.8).

Secondly, the relationship between clay volume and grain size. There is no doubt that a grain size/clay content relationship exists (i.e. Figures 14.2, 14.3). However, it is by no means a constant one. The textural analysis in the example (Figure 14.9) is of two sandstones, one an alluvial molasse showing a consistent relationship between grain size and clay content, and the other a well-winnowed, marine sandstone with no relationship at all (Pettijohn *et al.*, 1972). Using the gamma ray log itself and comparing it to grain size fractions over cored intervals, brings out similar relationships (Figure 14.10): in some sandstones where clay content varies with grain size, so do the gamma ray values (Figure 14.10*b*) in others there is no relationship (Figure 14.10*a*). Frequently, good relationships are seen in deltaic and fluvial environments, where deposition is largely controlled by flowing current energy. However, in many cases, the changes in grain size which are essential to the identification of sedimentary structures or sequences do not involve changes in clay content or at least changes sufficient to affect the gamma

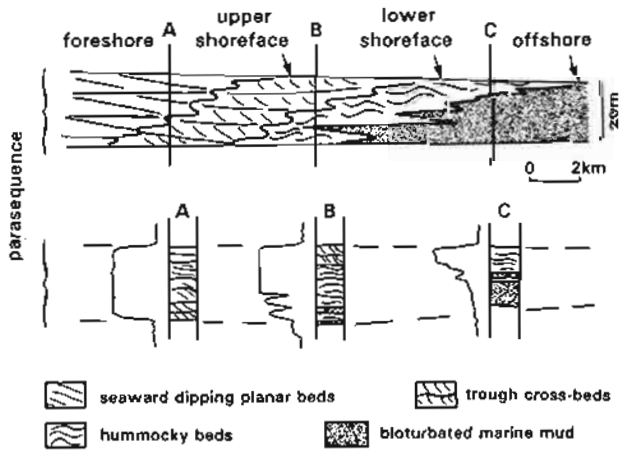


**Figure 14.7** The gamma ray log used to show facies differences in a sequence stratigraphic analysis (from Van Wagoner *et al.*, 1990).

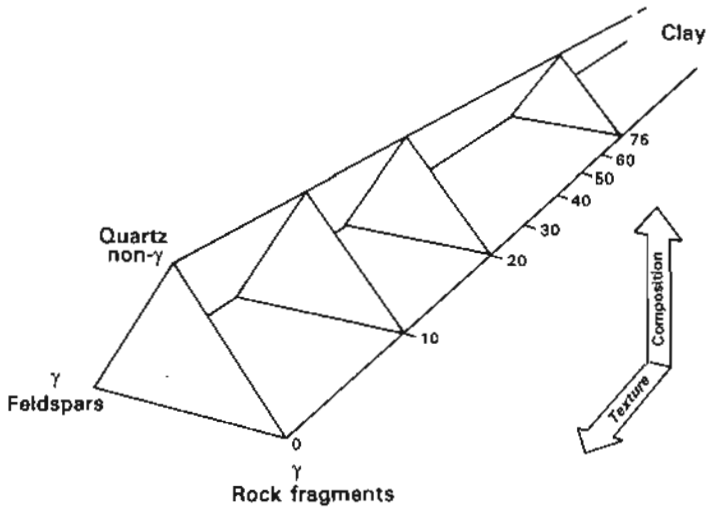


**Figure 14.8** The Folk classification of sedimentary rocks. It is based on separate variations in composition and texture. Composition is defined by quartz (non-radioactive), feldspar (radioactive) and rock fragments (often radioactive). Texture concerns the variation between the elements of composition and clay (after Folk, 1954).

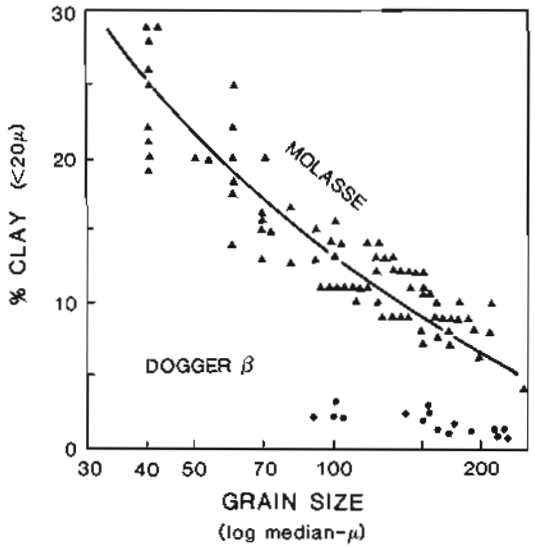


**Figure 14.9** Textural analysis of the clay – grain size relationship. Clay content compared to grain size for an alluvial sandstone (the Molasse) and a marine sandstone (Dogger β). (From Pettijohn *et al.*, 1972; modified from Fuchtbauer, 1964).

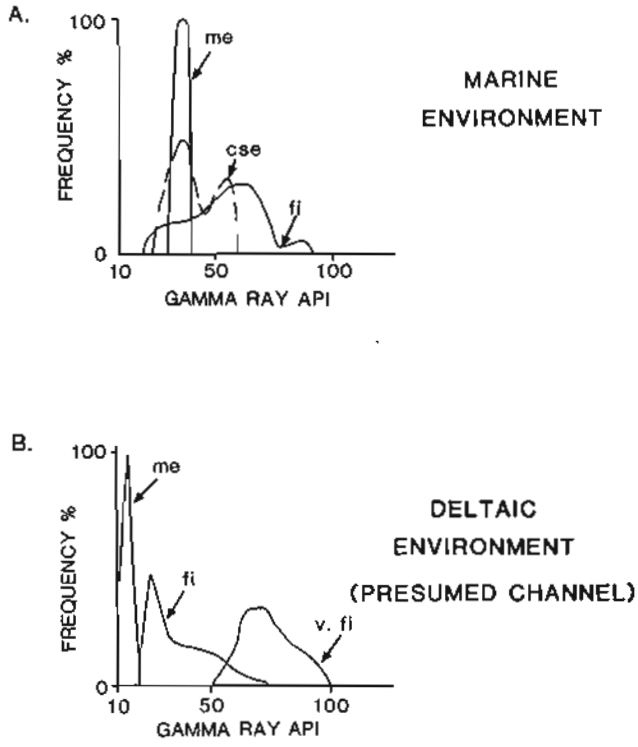


**Figure 14.10** Gamma ray value correlated with grain-size classes. A The marine sandstone shows similar gamma ray API values for different grain size classes, i.e. there is overlap. B The deltaic sandstone shows excellent separation of classes. Average grain sizes from thin sections: cse = coarse, me = medium, fi = fine, v.fi = very fine. (From Simon-Brygoo, 1980).

ray (Figure 14.11). In turbidites, grain size variations are seldom seen on the gamma ray (e.g. Shanmugam *et al.*, 1995), only bed thickness changes, and as beautifully demonstrated by Slatt in outcrop studies (Slatt *et al.*, 1992), interpreting the gamma ray response in terms of bed thickness/grain size trends can be very misleading (Figure 14.12). The clay volume-grain size relationship, therefore, is sufficiently common to be thought universal,

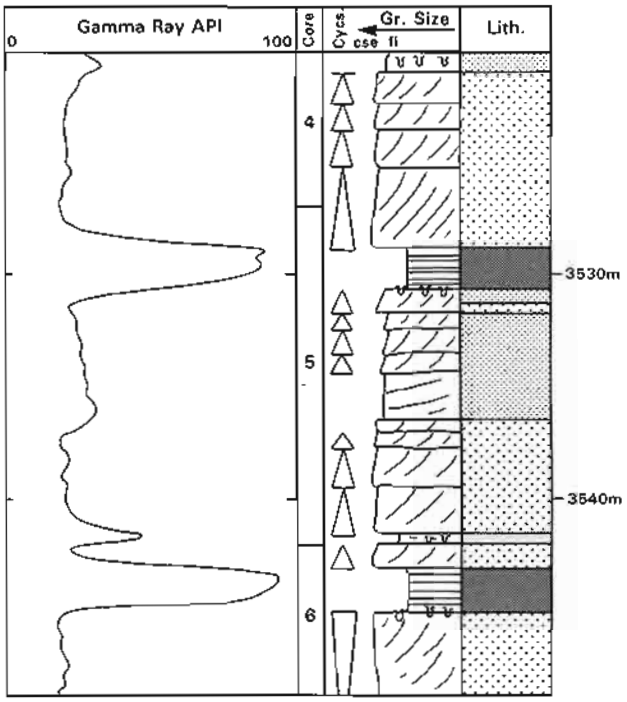


**Figure 14.11** Gamma ray *not* showing grain size variations. Core analysis shows considerable variation from fine to coarse grain sizes within the sands. Because clay is not involved, grain size changes do not involve the gamma ray.

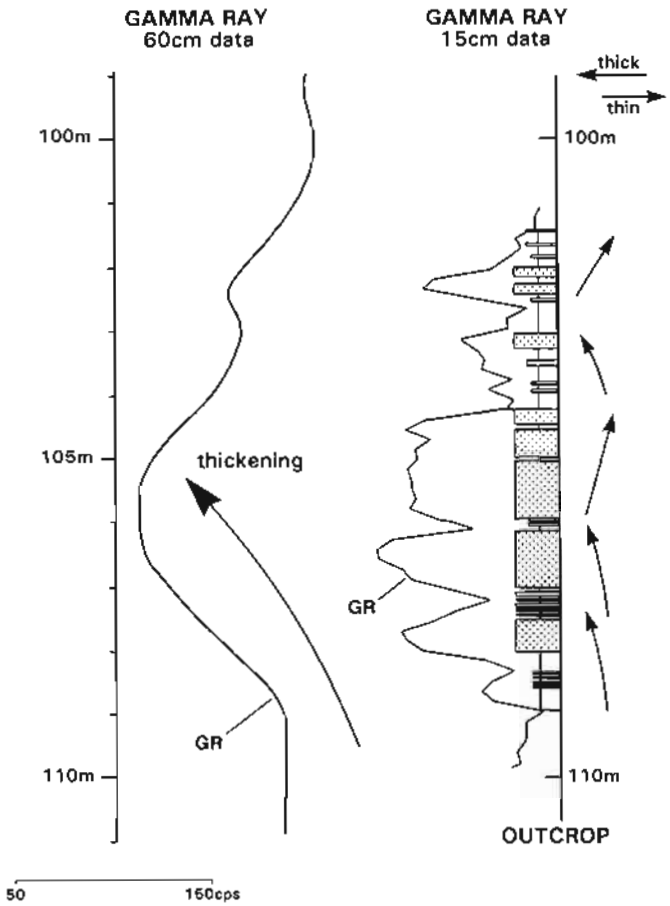


**Figure 14.12** Outcrop analysis showing errors that may be made by interpreting grain size trends using the gamma ray log. The thickening-up trend interpretable from the 60cm gamma ray data (typical of subsurface sensitivity) in reality corresponds to a complex series of smaller scale sequences, to some extent shown by the 15cm data (modified from Slatt *et al.*, 1992).

but when detailed data are available, evidence shows this is not the case.

In conclusion, the attractive idea that log shapes indicate sandstone depositional environments is too simplistic. Neither the relationship between gamma ray value and clay volume, nor the relationship between clay volume and grain size are consistent, as they should be if the shape of the gamma ray log is to be used as a universally applicable facies indicator. However, core to log comparisons indicate that these relationships are *frequently* consistent enough for log shapes to be useful facies indicators. But great care must be taken using them. The next section describes a quite different, more thoughtful and very effective way of geologically analysing logs.

## 14.3 'Electrosequence Analysis' – a tool for sedimentological and stratigraphic interpretation

***The concept***

This section describes a system for the identification and analysis of log-based sequences or electrosequences. Previously called 'sequential analysis' (Rider, 1986), it is now called 'Electrosequence Analysis', as the previous title could be confused with some aspect of sequence stratigraphy and not associated with log analysis. An electrosequence is: *an interval defined on wireline logs, through which there are consistent or consistently changing log responses and characteristics, sufficiently distinctive to separate it from other electrosequences.* It will typically be tens of metres thick and corresponds to the sedimentological succession of facies (i.e. a cycle). The objective of an electrosequence analysis is to extract from the logs as much geological information as possible, by identifying vertically continuous, depositional, stratigraphic and eventually sequence stratigraphic units.

The study of log shapes described in the previous section, has two major shortcomings: only one log is considered, and only sand bodies are involved. 'Electrosequence Analysis', by contrast, avoids these shortcomings and uses *all* the available logs, much other data, and covers *all* the well, not just the sand bodies and reservoirs. It is, above all, a *systematic* approach to log sequence interpretation and was developed by Elf in France (Serra, 1972; 1973; Serra and Sulpice, 1975). The present author has subsequently simplified the system and modified some of the sedimentological and

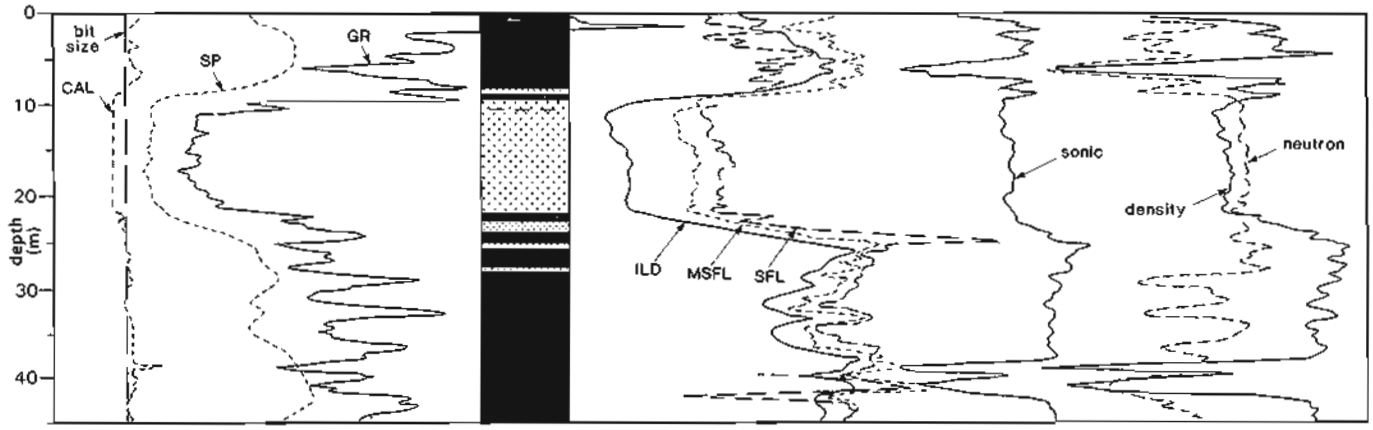


**Figure 14.13** The database for electrosequence analysis, a full set of logs through reservoir and non- reservoir. The fine-grained section shows a progradational sequence from coal to organic shale to shale with an increasing quartz content: the sand, on the other hand, shows no well-defined trends. Note the varying reactions of the individual logs.

stratigraphic principles to suit modern attitudes. These modifications have come out of both practice and discussions with oil industry colleagues during many industrial courses. Throughout, the system has shown itself to be simple to apply, adaptable and capable of bringing out a great deal of geologically significant information. It also forms a base for an eventual sequence stratigraphic analysis (Chapter 15).

The first principle of the system is that reservoirs and non-reservoirs are equally important: geology is not restricted to reservoirs. In a sand-shale sequence, for example, the environmental information contained in the fine-grained, non-reservoir intervals, equals or even exceeds that in the reservoir zones. The second principle is that no one log can characterize a formation: each logging tool examines the same formation but from different aspects, and all are equally characteristic (Figure 14.13).

The essential steps for a proper electrosequence analysis are laid out below in moderate detail. A house is built from the foundations upwards: the roof comes last. Electrosequence analysis must follow a route of construction; an interpretation for facies, depositional environment or sequence stratigraphy comes last, a lithological interpretation comes first (Figure 14.14).

***Step 1: Interpretation of lithology***

The electrosequence analysis is undertaken using a document on which all the well logs are plotted, depth-correlated and at the same scale. Since modern log acquisition is digital, a re-plot of all the logging runs in one well is a fairly simple affair and can be requested from the service company or made in-house. The re-plotted data should, however, be checked for computer (actually human!) errors in scale, depth matching and even log label. The 'merged data' document can then be completed with a detailed lithological interpretation, using the methods previously discussed in Chapter 11 (Figure 14.13). The lithological interpretation will come from an examination of both log- and drill-derived data (Figure 14.14). It is an essential and fundamental first step.

***Step 2: Electrofacies annotation***

Once the lithology is established, the logs can be examined for characteristics seen on the traces which may or may not have geological significance. These characteristics, *baselines, trends, shapes, abrupt breaks and anomalies* will be discussed individually below. Together, they make up what is called (in this book at least) an 'electrofacies', which can be defined as: *a suite of wireline log responses and characteristics sufficiently distinctive to be able to be separated from other electrofacies*. Facies in the usual geological sense, may not be identical to the electrofacies.

The principal objective of an electrofacies annotation is to prepare the log set for an ultimate interpretation for whatever geological information can be obtained, such as log sequence, depositional environment or facies. For example, an interval may be interpreted lithologically as entirely shale; an electrofacies annotation will bring out the fact that there are two distinct types of shale within this interval and that they are in fact separated by an unconformity. There is much more in the logs than just lithological information and the electrofacies annotation will show this.

The annotation should be done in a somewhat 'unthinking' manner. That is, an immediate explanation should not be sought for the annotations that are being marked; the explanation is intended to be extracted in the final interpretation when all the information has been amassed. Also, it is a job for coloured pencils; dashes, dots and symbols are not enough. Although this is a 'low tech' approach, it is highly effective. Chapter 15 describes sophisticated 'high tech' methods.

The annotations that should be marked on the logs are described below in a logical order of simple to more and more complex.

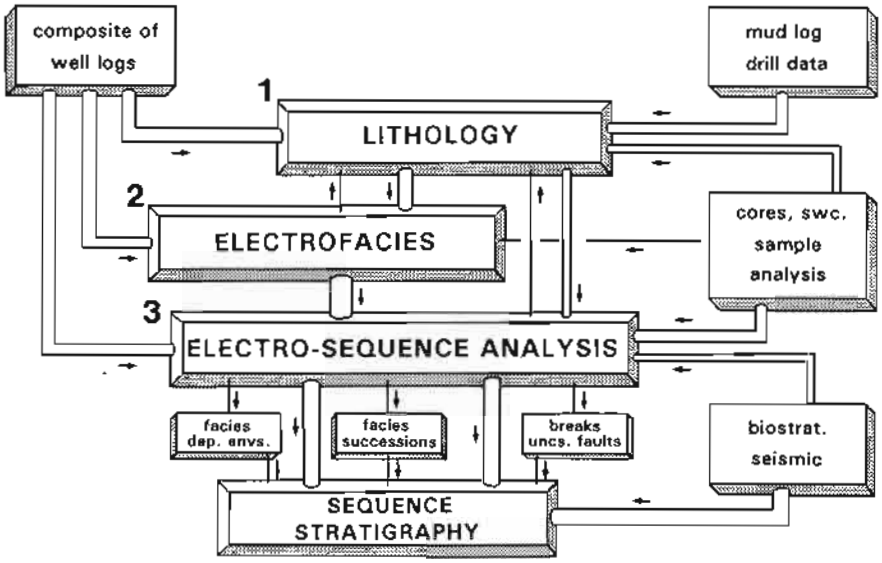


**Figure 14.14** Flow chart for an electrosequence analysis. Numbers refer to interpretation steps discussed in the text.

*Baselines.* A baseline is a vertically constant log value. It has both lithological and stratigraphic significance. The name may perhaps be misleading as baseline in the present context is considered rather as a 'base value' or even 'average' value, which is constant vertically for at least some tens of metres but possibly up to hundreds of metres. Gamma ray baselines are described in Chapter 7 as an aid to lithological interpretation (Figure 7.12), high average values (high baseline) indicating clean shale and low baseline values indicating clean sand (i.e. the sand and shale lines). However, this technique implies that neither the shales nor the sands change vertically, hence the consistent log responses, which in stratigraphic terms means that they are from the same formation. When the formation changes, baselines change.

Baselines, or base values can be used with all logs, not just the gamma ray (Figure 11.7), so that if any log shows vertically constant values, it suggests that either the lithologies are constant and/or there is no change of formation. The example shows sections of three shale intervals from one well, each over 50 m thick (Figure 14.15). Although some baselines are similar from one interval to the next, for instance the gamma ray baseline is similar in the top and middle intervals, the *combination* of baseline values for each interval is quite distinct. Each shale has a different composition and texture which may affect one log more than another. In short, each comes from a different stratigraphic formation: each has a different electrofacies.

A baseline is marked on a log with a ruler as a constant value – for as long as it *is* constant. In the analysis for log based sequences, it is the changes which become significant: they will require a geological explanation. Baselines are marked in green.

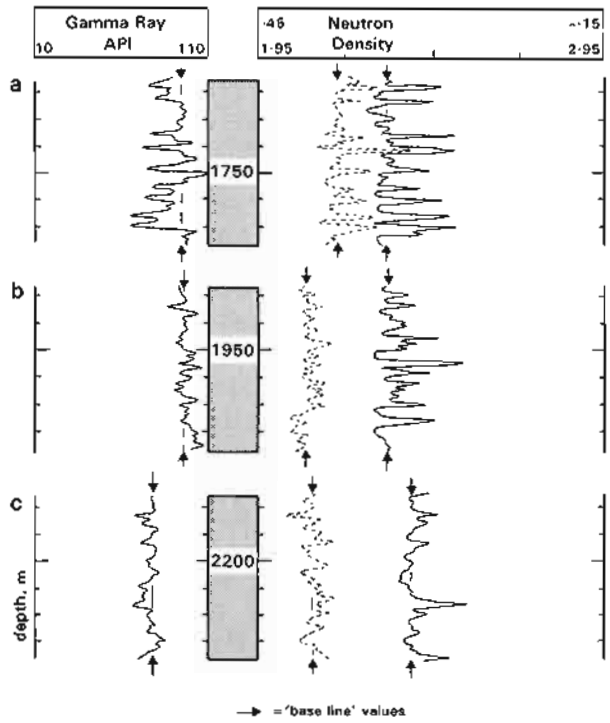


**Figure 14.15** Baselines on the gamma ray, neutron and density logs in three shale sections of the same well. The baseline values of each log are indicated by the arrows. Some values are similar between sections but in combination, the intervals are clearly different: the shales have different composition and texture.

*Trend lines.* A log trend is a persistent change in a log value over a certain thickness, either increase or decrease. Trends may be over one metre, when they are related to beds and bed junctions, tens of metres, when they are

most likely to be related to cycles or sequences, or over hundreds of metres when they are related to large structures or basin filling. Trends over small thicknesses may occur within longer trends as second order variations (Figure 14.16).

The trends that are chosen to be marked will vary in scale. Each change in log value over a few metres may be considered as a trend but there is generally no geological significance in them at this scale. Trends over greater thicknesses may, however, indicate persistent changes in sedimentation, such as coarsening-up or fining-up successions. It is these that should be brought out.

In most non-systematic analyses it is trends, the movement of values vertically, that catch the eye. It was, in effect, trends that were discussed in the previous section under gamma ray log shapes. Examining any log set, it is quickly very evident that trends are not limited to the gamma ray log and occur, with varying significance, on all the logs.

Trends should be marked on each log with separate colours indicating decrease or increase *upwards* (e.g. red = increase; blue = decrease). Do not use one colour for changes to the right or left of the log grid, this will cause confusion during interpretation. For example an increase in neutron values marked in red (indicating increase in shaliness?) deviates to the left, while an increase in gamma ray values marked in red (also indicating increase in shaliness?) deviates to the right.

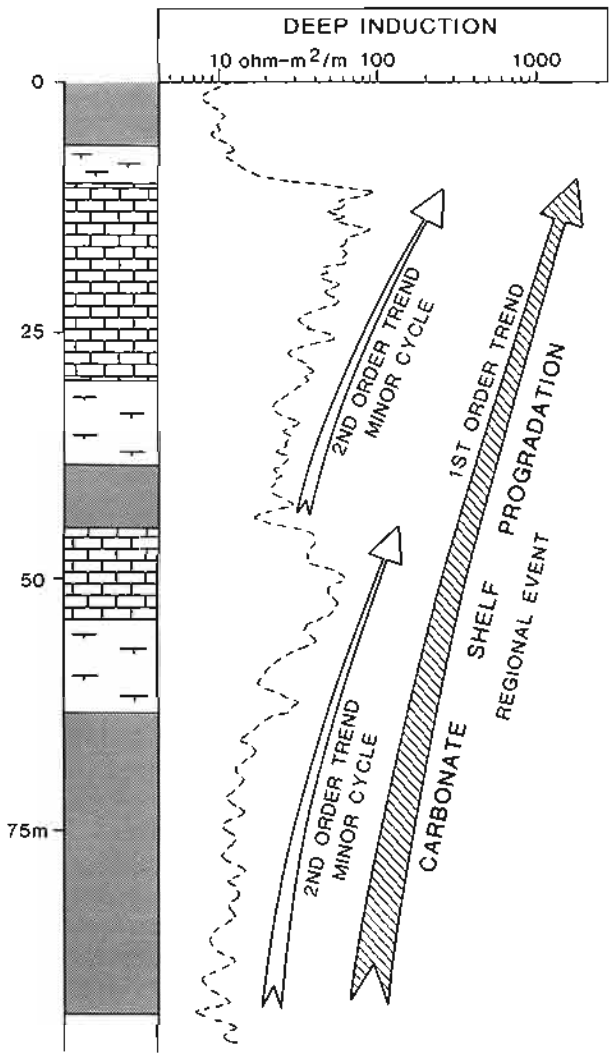


**Figure 14.16** Trend lines. Large-scale, first-order log trend (on a deep induction) enclosing smaller second-order trends in a prograding carbonate shelf complex. Lithology from log analysis and drill cuttings.

*Shapes*. A log shape is a recognisable, but complex log pattern. Log shapes in sandstones have already been discussed (Section 14.2); such as increasing gamma ray in a fining-up sequence. However, shapes may occur in any lithology, on any log, in any form and at many scales. The form, as it exists, should be marked on the log in a distinct colour (distinct from the baseline and trend colours – say purple). It is difficult to define what is and what is not a shape to be marked. This will possibly only become evident after examining a number of logs in the same area. Some shapes will simply be facies indicators, such as the bell and funnel shapes mentioned above. However, the target of the selection should be shapes which are not geometrically simple, probably occur in fine-grained intervals, could represent some distinct event and may have basin-wide significance. Their explanation may not be immediately evident. The example shows a complex shape on neutron logs, repeated in wells 50 km apart (Figure 14.17), which represents a set of distinctive basin filling events covering approximately 30 Ma.

*Abrupt breaks*. The recognition of abrupt breaks in a log sequence is very important. They can indicate changes in lithology, structural breaks, changes in fluids but, most importantly, they may indicate a break in 'depositional logic', that is a break in the vertical flow of (laterally) related facies. In this sense, abrupt breaks are especially important in sedimentological reconstructions and sequence stratigraphic analysis. In the analysis for electrosequences, abrupt break applies to any sudden and significant change in log values. Obviously, the suddenness or rate of change will vary between tools but will normally be within the diameter of the depth of investigation of the tool concerned (Serra and Sulpice, 1975). An abrupt change on the density log (depth of investigation 10–15cm) will be sharper than that of the gamma ray (depth of vertical investigation about 40 cm) (cf. Figure 2.10,*3*). A rapid baseline shift may also identify an abrupt break.

Abrupt breaks may fit logically into a lithological (and depositional) pattern, such as the erosional base of a sandstone bed over shale, or they may be entirely unrelated to the lithological sequence, such as a fault or an unconformity.

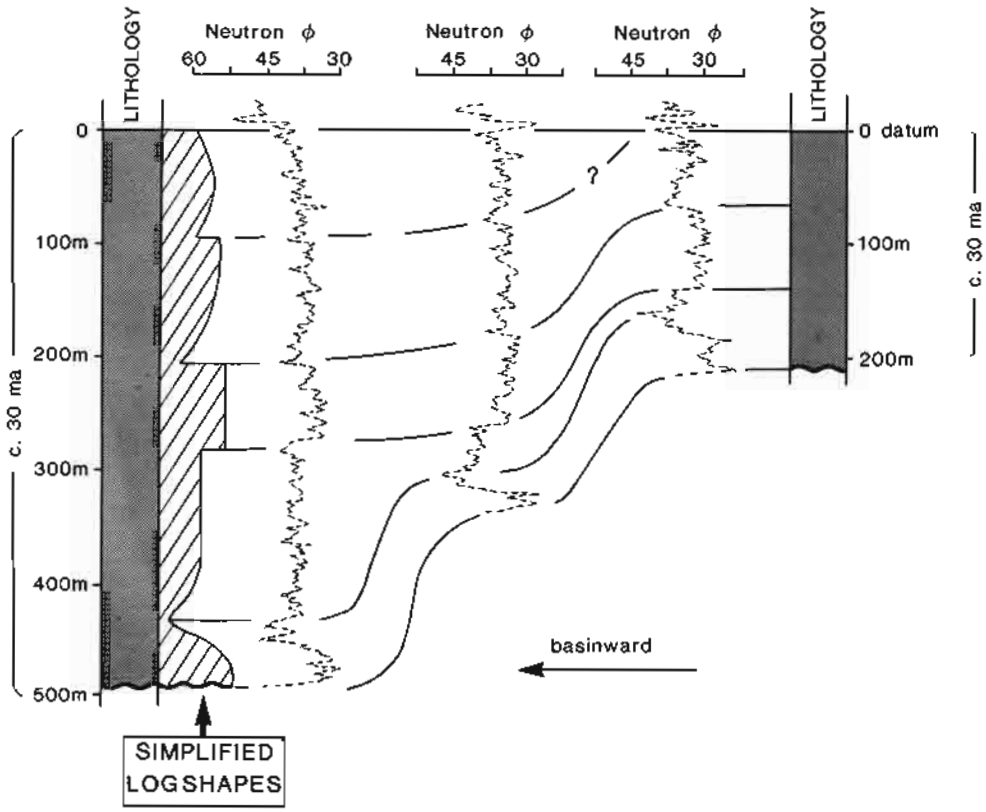


**Figure 14.17** Complex log shapes indicating depositional patterns. Log shapes in neutron logs are persistent over thick shale intervals which represent at least 30 Ma of deposition and basin filling. The shapes are caused principally by changes in quartz content, carbonate and organic matter: they indicate basin filling conditions. The two outside wells are over 50km apart.

The following abrupt breaks are identifiable:

| | | |
|---|---|---|
| 1) | Lithologically related breaks | **Erosion**<br>**Flooding**<br>(catastrophe) |
| 2) | Non-lithological breaks | **Unconformity**<br>**Fault**<br>(diagenetic change)<br>(fluids change) |

(The items in brackets should be eliminated from the analysis as soon as possible as they do not contribute directly to the eventual geological interpretation).

All abrupt breaks should be marked (in pencil) on the side of the lithological interpretation, initially by a thick horizontal line. Next, an attempt is made to annotate the break by examining it with a 'geological logic'. For instance, if the abrupt log break separates a sandstone above from a shale below, this may be an erosional contact and can be annotated as such on the log using the appropriate symbol (Figure 14.18*A*). If, on the contrary, the abrupt break shows a shale resting sharply on a sandstone, then erosion is unlikely and a flooding event can be proposed, again by inserting the appropriate symbol (Figure 14.18*B*). These are only *reasonable propositions* and will need to be substantiated subsequently using additional data. If the lithological interpretation shows that the abrupt break is entirely within a shale sequence, shale resting on shale, then neither erosion nor flooding is an appropriate initial proposition and a fault or unconformity can be suspected (Figure 14.18*C,D*). Clearly, more data are required to differentiate a fault from an unconformity; dipmeter and seismic possibly to substantiate the fault hypothesis, dipmeter, seismic and faunal dating to identify an unconformity. A symbol is used to indicate the possibility selected.

Many abrupt breaks will have a banal explanation and should be eliminated – simply rubbed out (hence the pencil). For instance, the limits of most coal beds are sharp, as are some diagenetic contacts. Other breaks may be more subtle and kept in for further thought as is the case with shale on shale contacts. During the interpretation phase, the important abrupt breaks will normally come to stand out. It should of course be added here that when a sequence stratigraphic interpretation is attempted, the breaks that have been marked will take on a new and quite specific significance (Chapter 15).

*Anomalies.* Anomalous log values are important – excessively high or excessively low peaks (values) may have great stratigraphic importance. The concentration of

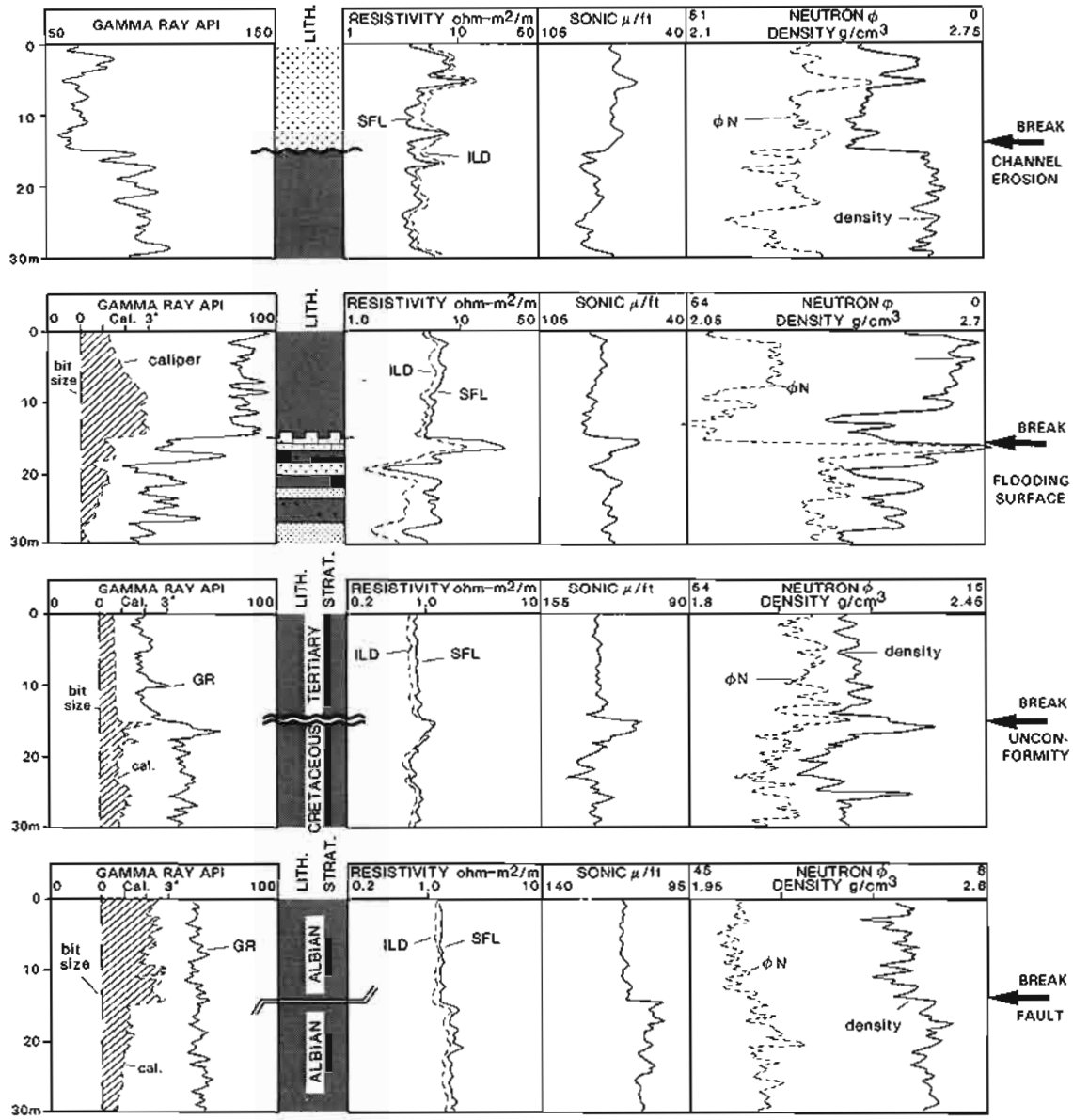


**Figure 14.18** Examples of abrupt breaks. A, channel erosion, sand overlying shale; B, flooding surface, shale overlying sand; C, unconformity, shale on shale; D, fault, shale on shale.

unusual minerals at unconformities or in hardgrounds, for instance, will often create a large gamma ray peak (Figure 14.19), a high density value and so on. Anomalous log values are often either ignored, not identified as anomalous or wrongly interpreted lithologically. They will contain unusual minerals, often in small quantities and indeed the lithology may be very complex, as is the case with most hardgrounds. The example (Figure 14.19) shows an unconformity which spans a gap of approximately 15 Ma marked by an anomalously high gamma ray peak. The mineralogical concentrations at the unconformity are not known but quite probably include a high concentration of uranium possibly associated with phosphatic nodules (Chapter 7).

Anomalies should be annotated with an asterisk by the side of the anomalous log response.

***Step 3: Electrosequence analysis for log-based sequences, facies and depositional environment***

Having established a lithology and built up an annotation of electrofacies, the only remaining preparation before undertaking the final, grand interpretation, is to add to the document all other relevant data such as stratigraphic ages, core sedimentology, thin section information, dipmeter interpretations and so on (Figure 14.14). Frequently, an enormous amount of data is available which is not exploited: all should be added to the composite, annotated document.

The entire suite – lithology interpretation, electrofacies annotation, sample analysis data, can now be subjected to the 'Electrosequence Analysis' from the base of the well upwards. All the data are used (Figure 14.20). In this step of the interpretation, the objective is to build the vertical

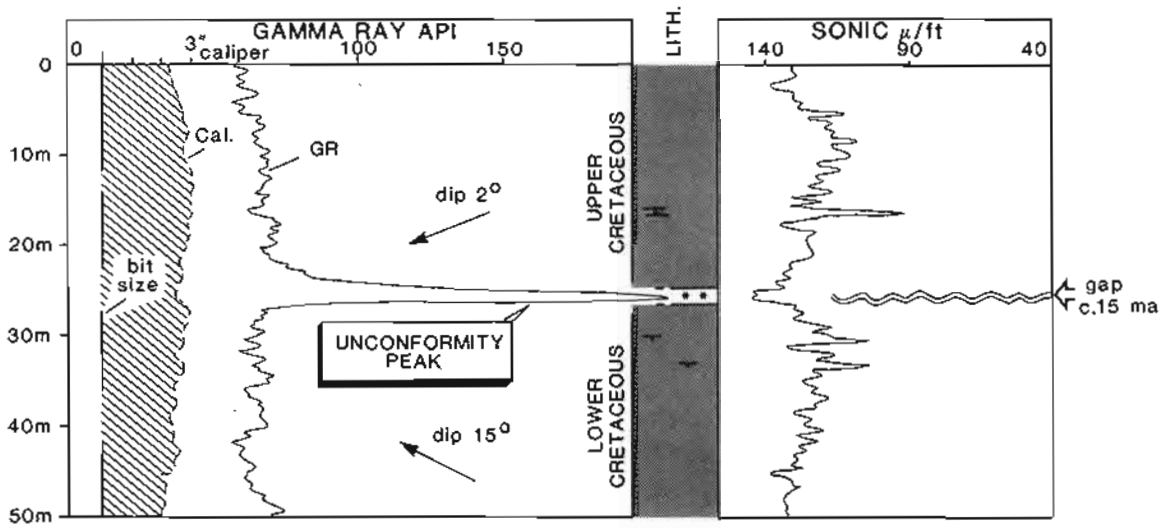


**Figure 14.19** Anomalous gamma ray peak at an unconformity. The peak corresponds to gap of 15 Ma: its stratigraphic importance is evident. The radioactivity is probably due to uranium concentrated in phosphatic nodules.

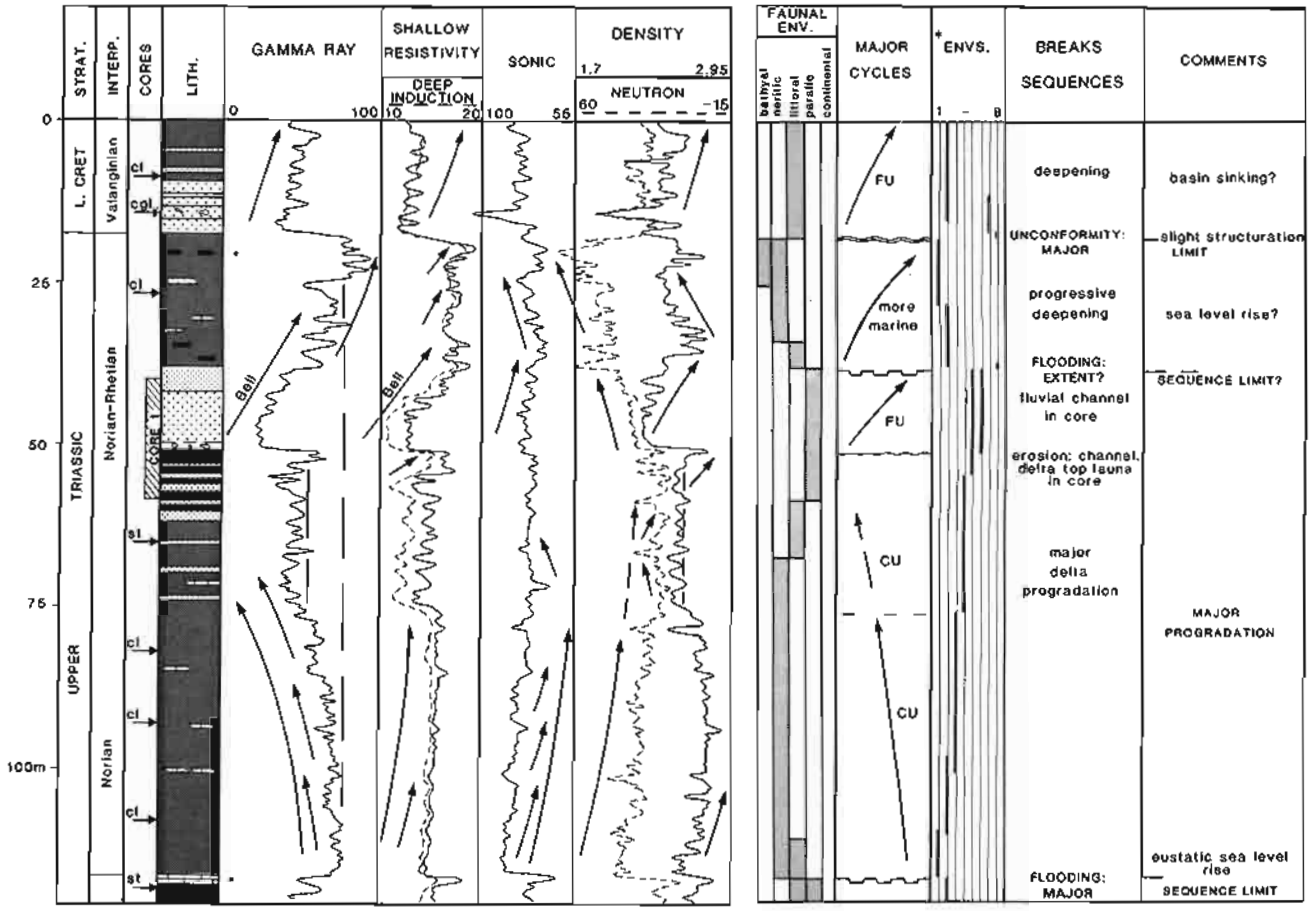


**Figure 14.20** A completed electrosequence analysis. Lithology, electrofacies and sample data are brought together to give a vertical sequence of depositional environments and an indication of the depositional sequences and major breaks.
*Environments: 1, deeper marine; 2, shallow marine; 3, prodelta; 4, delta front; 5, delta top; 6, channel; 7, beach-littoral; 8, continental; CU = coarsening up, FU = fining up.

succession of electrofacies into log-based electrosequences, which can be interpreted in terms of possible depositional environments, facies, facies successions and stratigraphic breaks, faults and unconformities. The evidence for the construction comes from each preceding step. For example, the lithology analysis indicates a moderately thick sand interval with thick shale intervals above and below. The electrofacies annotation indicates log trends which show the sand to have a gradational base and be part of a typical cleaning-up succession. The top of the sand is separated from the overlying shale by an abrupt break indicative of a flooding surface. The electrosequence therefore consists of a set of log trends indicating diminishing shale upwards into a clean sand which is capped by an abrupt break indicating flooding. Biostratigraphic analysis of sidewall cores in the shale section shows the presence of marine fauna. The dipmeter indicates good lamination throughout and no large sedimentary structures. The evidence for a shallow marine, prograding succession of facies and subsequent flooding is building up. Does this fit with the interpretation of the preceding and following electrosequences?

The final interpretation should be a sedimentologically logical succession of facies and depositional environments. The breaks recognised from the logs should be added to the environmental interpretations and the principal electrosequences marked. The environmental logic should only continue *between* the major breaks. This document will now show the distinctive log-based electrosequences, stratigraphic breaks (disconformities, unconformities) and structural breaks (faults) (Figure 14.20). It is impossible to give details of all the reasoning that goes into constructing a document of this sort. Many geological disciplines are involved. This section simply describes the system, here called electrosequence analysis, and how the body of data is built up to form the interpretation tool. To use the tool one needs not just the data from this book, but training and experience in all fields of oil geology.

Previously, the geological document produced from this anlaysis would have been the final one and used for understanding basin development, correlation and matching with the seismic. Today, it is not sufficient. The data must now be subjected to a sequence stratigraphic analysis. And this is the principal subject of the next chapter.

# 15
# SEQUENCE STRATIGRAPHY AND STRATIGRAPHY

## 15.1 Introduction

As a means of correlation, the use of wireline logs is obvious. As an aid to stratigraphic analysis, logs are invaluable. But as a tool in sequence stratigraphy, their use so far, is seriously underdeveloped. This chapter principally describes the use of logs in sequence stratigraphy, by building on the techniques laid down in Chapter 14, and developing them in terms of sequence stratigraphy. It also describes a more modern and thoughtful, computer-based methodology for such analyses. The chapter ends with a description of logs used in classical correlation and stratigraphy. These come last as the ideas of sequence stratigraphy have caused such a revolution that earlier ideas can never again be seen in the same light.

## 15.2 Well logs and high resolution siliciclastic sequence stratigraphy

***Principles and generalities***

Sequence stratigraphy is *'the study of genetically related facies within a framework of chronostratigraphically significant surfaces'* (Van Wagoner *et al.*, 1990). It was developed to a very high degree of sophistication by Exxon and is illustrated by the 'type' exposures of Book Cliffs in Utah and Colorado, USA (Van Wagoner *et al.*, 1990). It is a concept that explains the vertical and lateral variations of sedimentary successions in terms of relative sea level changes. The sequence (Figure 15.1) is the fundamental stratal unit of sequence stratigraphy and records between 0.5–3 Ma of sedimentation (Vail *et al.*,

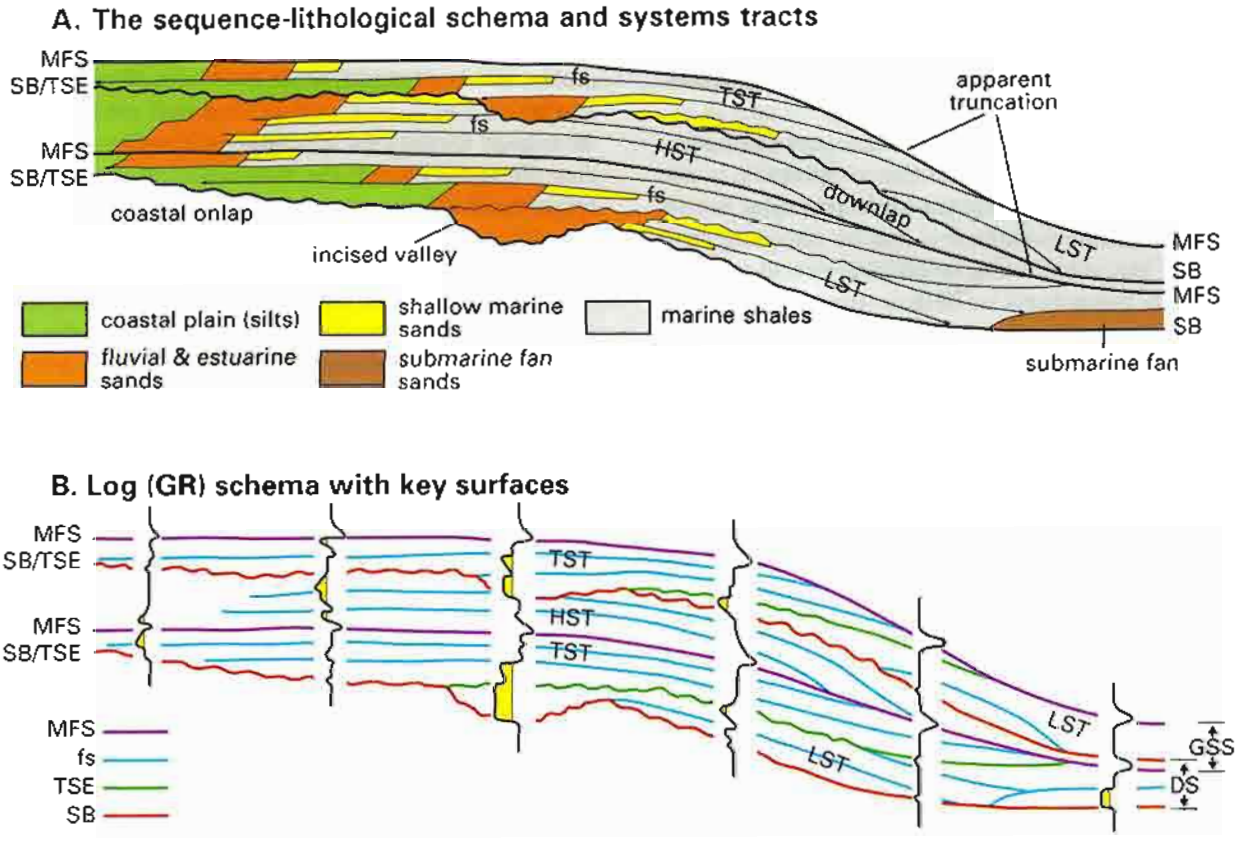


Figure 15.1 The depositional model of sequence stratigraphy defined for the DS, depositional sequence (after Exxon) and the GSS, genetic stratigraphic sequence (after Galloway). A. The sequence as a lithological schema with sequence tracts (forced regression is not included, the upper, incised valley was cut at lowstand, filled during later transgression). B. The same model with gamma ray log traces and key surfaces (from various sources including, Van Wagoner *et al.*, 1990, Mitchum & Van Wagoner 1991, Bhattacharya 1993). MFS = maximum flooding surface: TSE = transgressive surface of erosion: SB = sequence boundary: fs = flooding surface. LST, TST, HST, = Lowstand, Transgressive, Highstand Systems Tracts.

1977). By Exxon it is defined as an *unconformity* bounded succession of genetically related facies (SB to SB Figure 15.1). Other workers use different definitions (esp. Galloway, 1989a,b; *see* facies successions *below*). The bounding unconformities (and important internal surfaces) are all caused by relative sea level changes. In the purest sequence stratigraphic application, (contested by almost all except Exxon) all major sea level changes are eustatic (i.e. global) and therefore all the unconformities bounding sequences (sequence boundaries) have absolute geologic ages (dated using correlative conformity sections). This provides rules for correlation on a regional and global scale.

High resolution sequence stratigraphy is the application of sequence stratigraphic principles to outcrops, cores and well logs. It is obviously the well log applications which will be stressed in this section. However, most published work on high resolution sequence stratigraphy to date is based on outcrops and cores (e.g. Van Wagoner *et al.*, 1990; Posamentier *et al.*, 1993), although as initially proposed by Exxon it was a methodology for the interpretation of closely spaced well logs with core control (Van Wagoner *et al.*, 1990).

A word on the general approach presented here. Sequence stratigraphy as expounded by Exxon is heavily dependent on conceptual models and definitions of models. It is the Exxon technique. There is no point in repeating here all the models and definitions that they propose, their own texts do this better (Posamentier *et al.*, 1988; Van Wagoner *et al.*, 1990; Posamentier and James, 1993). Moreover, the rigorous Exxon approach is not used by many workers. But the basic principles are so fundamental and revolutionary, that in discussing and presenting the subject it is impossible not to refer to Exxon or to use rather a lot of their terminology. In this text, the sequence as presented by Exxon is used as a basis for description as it tends to be the more familiar. While most workers now accept that the influence on sedimentation of externally controlled sea level changes was badly underestimated prior to sequence stratigraphy, the belief that these sea level changes are all eustatic (i.e. global) is not accepted. An attempt will be made to present the subject from a well log point of view, using *real* (this is very important) examples, in such a way that the information can be used without prejudice. This is a book about well logs, not the semantics of sequence stratigraphy.

***Key surfaces***

A succession of sediments cannot be put into a sequence stratigraphic context without, first of all, identifying the key surfaces (Baum and Vail, 1988) (Figure 15.1). These fall into three main categories: surfaces with erosion, surfaces with drowning and surfaces and intervals of slow deposition. Some examples of these are given below with a description of their sequence stratigraphic significance.

**1) surfaces with erosion: channel base, sequence boundary, regressive surface**

*– channel base erosion*

The commonest example of an erosion surface is the sharp base to a coarse channel deposit cutting into the sediments below. On the logs, this type of erosion surface is characterised by an abrupt, upward change from shale or silt to sand and will be identified in the electro-sequence analysis (Figure 14.18*a*). That the overlying sequence is a channel deposit may be seen in the log trends showing shaling-up and decrease in porosity. The core calibrated log example (Figure 15.2), shows a series of thin, interbedded silts, sands and shales, abruptly overlain by a 12 m thick, fining-up sand with medium scale cross-beds. On the logs, erosion is indicated by the abrupt changes at the base of the sand. The fact that this is a local, channel-base erosion surface is suggested by its association with the shaling-up succession evident in the log trends.

This type of surface represents relatively local erosion and has no direct relationship to sea level changes. The currents which erode are also responsible for the transport of the sediments which immediately overlie the erosion surface. It is to be differentiated from surfaces showing erosion and truncation but on which the overlying sediments are not related to the principal erosion (*see below*).

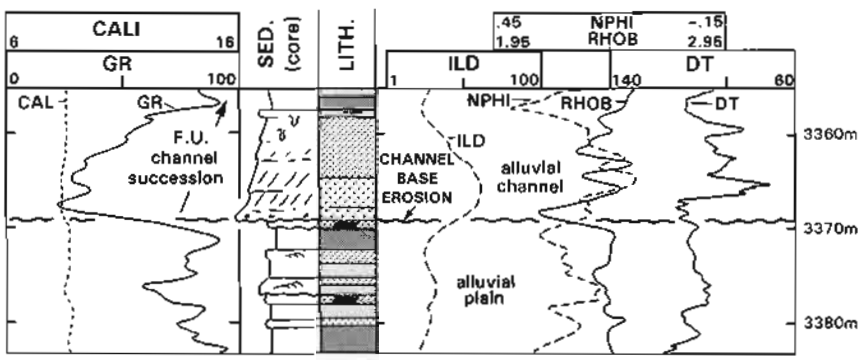


**Figure 15.2** Channel base erosion log example. The erosion occurs at the base of a fining-up sequence interpreted as an alluvial channel. The reservoir contains hydrocarbons.

*– sequence boundary (and regressive surface of erosion)*
The sequence boundary is an unconformity (or correlative conformity) surface on which there was subaerial erosional truncation and in some cases, submarine erosion (Exxon definition): it is the remaining evidence of a lowering of relative sea level. The vertical logic of facies successions, clearly, stops at such boundaries. Recognising a sequence boundary in outcrop is not easy, in cores difficult, and with logs alone the difficulties are considerable. A sequence boundary often resembles the channel base erosion surface described previously and in part, may be the same. On the logs, there is no set of diagnostic responses. However, there are clues.

The principal clue to sequence boundary identification is its position in the sedimentary succession. In outcrop and cores a major 'basinward shift in facies', caused by the lowering of sea level, is diagnostic: a facies with a depositional environment much shallower than would be expected is found resting on sediments from a deeper environment across a sharp boundary. For example, tidal-channel sands resting on outer shelf shales. The log example of a sequence boundary shows an abrupt change upwards from clean, distal marine shales to very coarse, nearshore marine sands (Figure 15.3) (the North Sea, Middle Jurassic Oseberg Formation resting on Lower Jurassic shales). The sands have large scale bedforms (Graue *et al.*, 1987) and a coarse lag at the base is full of heavy minerals, the cause of the high gamma ray spikes (Figure 15.3). This surface, the mid-Cimmerian unconformity, covers a large area and represents a significant downward shift in relative sea level (Underhill and Partington, 1993, 1994). Although erosion is strongly suggested by the logs in the one well, it is only correlation on a basin-wide scale that makes evident both the extent of the surface and the truncation associated with it. Core information is clearly significant.

A complication in using the 'basinward shift in facies' as an indication of a sequence boundary is that a similar effect can be created during the lowering phase of sea level, when it is accompanied by progradation and deposition. The sediments involved are typically deposited in coarsening-up, prograding shoreline successions of the so-called forced regression (Posamentier *et al.*, 1992). These coarsening-up deposits rest on an erosion surface and firm ground, the regressive surface of erosion or forced regression surface, which was formed as water became shallower (Plint, 1988). The log example (Figure 15.4) shows an abrupt upward change from a pure shale to very silty shale across a thin horizon with unusual neutron-density values (the gamma ray response is not diagnostic). This thin bed contains reworked chamosite oolites (hence the neutron-density response cf. Figure 10.22) and small phosphate pebbles, the base is sharp and the bed is very widespread. It is interpreted as a regressive surface of erosion (Plint, 1988). The underlying shales are distal marine shelf and above the boundary is the prograding, forced regression, coarsening-up shoreline sequence. The sequence boundary is above the shoreline deposits.

Sequence boundaries are not always at clear log defined erosional limits, although there is generally a notable change in log responses. For instance, an abrupt change of log response within a sand interval can signal an abrupt change of environment, as will occur at a sequence boundary. One sand may be cleaner, have a different mineralogical mix or simply a different texture: this will be seen on the logs. In shale sections, a sequence boundary may be marked by a change in shale type and this will be seen in the log responses.

Beyond recognising a sequence boundary directly, it can be indirectly recognised by its position in the succession. It is a matter of technique. In general, condensed sequences are more convincingly recognised than sequence boundaries (Galloway, 1989; Vail and Wornardt, 1990; Partington *et al.*, 1992a; Posamentier and James, 1993). This is true on cores, on the seismic (where it corresponds to a downlap surface, i.e. Figure 15.1) and on the logs (*see* item 3 *below*). Hence, if two condensed sequences are found, sequence stratigraphy predicts (Exxon, *see* Figure 5.1) that a sequence boundary exists

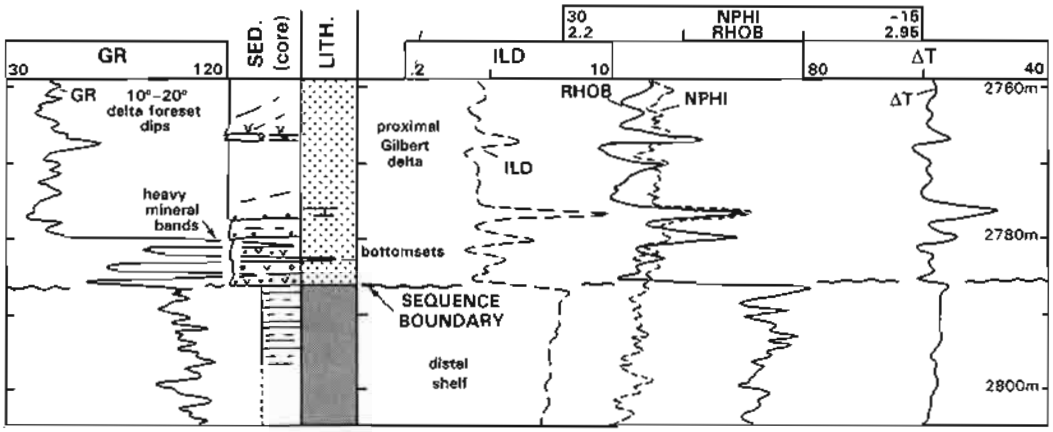


**Figure 15.3** Sequence boundary log example. The boundary is abrupt and known to be erosional. A Gilbert type delta with coarse sands overlies distal shelf shale. The basinward facies shift is very marked (*see* text).

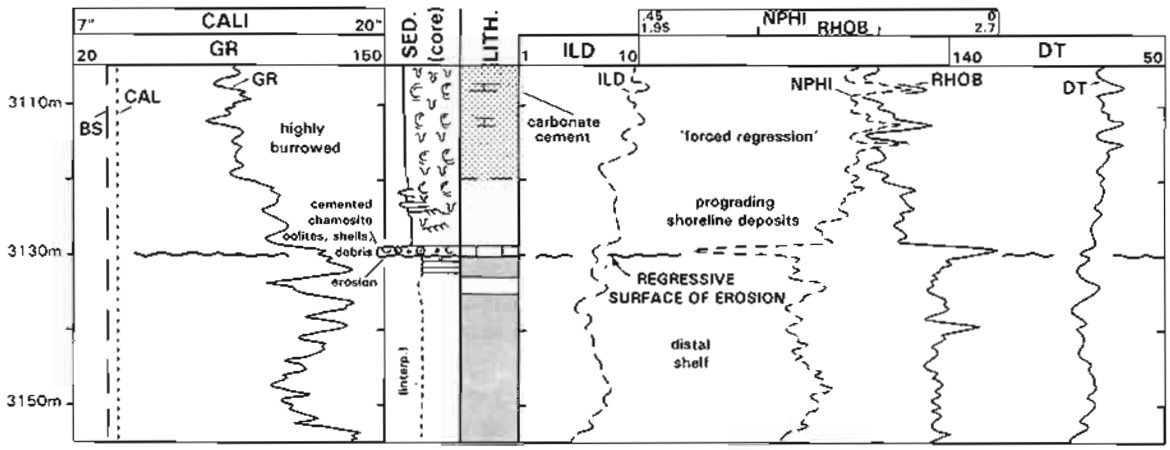


**Figure 15.4** Regressive surface of erosion log example. The interpreted environments of prograding shoreline deposits overlying distal shelf shales, indicate a 'basinward shift of facies' and shallowing water. However, the erosion surface is succeeded by progradation, indicating a forced regression. The surface itself is covered by chamosite oolites, the chamosite being indicated on the neutron-density response.

between them. Such inferred, 'model driven' interpretations are considered downright unscientific by critics.

### 2) surfaces with drowning: marine flooding surface, transgressive surface (ravinement surface)

Facies successions are frequently bounded by surfaces which record a rapid deepening of the depositional environment with little incoming sediment. These are considered in sequence stratigraphy to result from a rapid, relative rise in sea level (i.e. rapidly deepening water). The general term for these is marine flooding surface. The transgressive surface, also described in this section, is a special flooding surface in terms of both its sequence stratigraphic position and its sedimentological characteristics.

*– marine flooding surface*

In an electrosequence analysis, a marine flooding surface will be picked out, as described in Chapter 14, as an abrupt break between sand below and shale above (Figure 14.18*b*). Such surfaces typically terminate coarsening-up facies successions. The example (Figure 15.5), shows the coarsest, topmost part of a shallow marine, coarsening-up succession followed rapidly by a shale with deep water characteristics. Between the sand and the shale is a 2.5 m thick interval of highly bioturbated silty sand with scattered, coarse sand grains, separated from the sand below by a sharp surface: a marine flooding surface. The bioturbated interval shows as a subdued high on the density log (low porosity), but a high neutron value indicating a high shale content and, in this case, common chamosite oolites (Chapter 10). The gamma ray shows a rapid (but not abrupt) upwards increase through the bioturbated bed into the shale. Most flooding surfaces are associated with a similar intensely bioturbated interval (transgressive deposits) and the typical log responses of this example tend to be diagnostic (*see also* Figures 15.7 and 15.14).

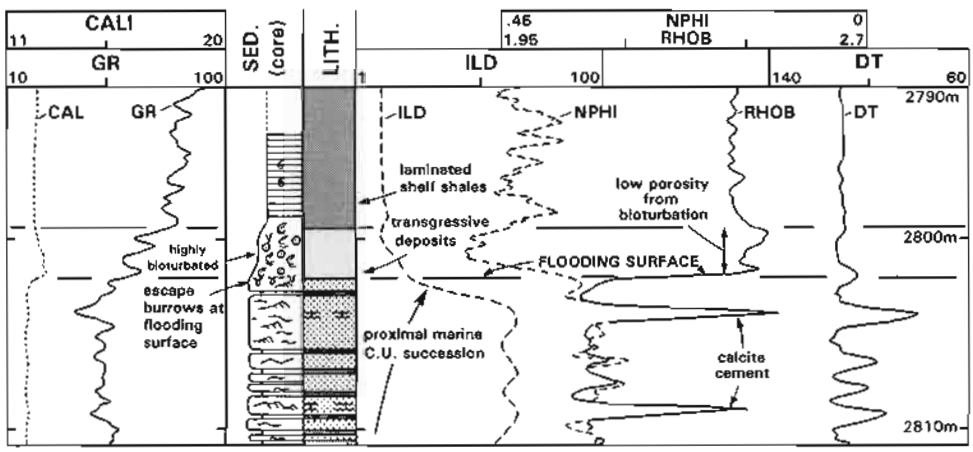


**Figure 15.5** Log example of a flooding surface and transgressive deposits. The coarsening-up, sandy, proximal marine succession is covered by a highly bioturbated silty, transgressive deposit giving characteristic responses on the neutron and density logs. The base of the transgressive deposits is sharp, shows escape burrows and represents the flooding event. There is no evident erosion. The calcite cement in the marine sands is secondary but possibly early.

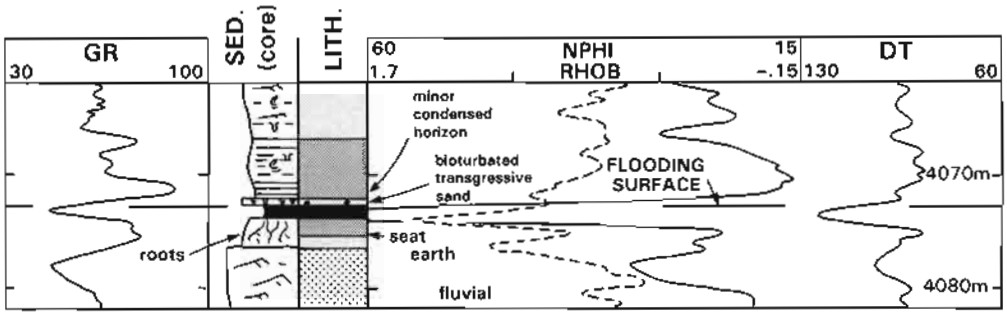


**Figure 15.6** Coal followed by a flooding surface. There appears to be no erosion associated with the flooding event (marked by a very thin, bioturbated, heterogeneous sand, too thin to be seen on the logs). Open marine, deeper water, organic rich shales of a minor condensed sequence follow the flooding.

The second example (Figure 15.6) shows another expression of a marine flooding surface, this time immediately following coal deposition. Coal represents slow accumulation at sea level with little detrital sediment input which, in this example, the core shows to have a seat earth and so be *in situ*. It is commonly associated with retrogradational episodes, that is coastal retreat (Milton *et al.*, 1990). Over the coal is 30 cm of dark, organic-rich, laminated shale with pyrite: a significant deepening of the environment of deposition is evident. On the logs this succession is seen as an obvious coal (low density, high neutron cf. Figure 10.28), followed abruptly by a shale with high gamma ray and very high neutron responses, (indicating the high organic content, cf. Figure 10.20) interpreted as a minor condensed sequence. This grades upwards to shales with a normal log response which the core shows to be bioturbated shale and silty shale.

The detail of the core shows that, in fact, immediately over the coal is a 20 cm burrowed, transgressive sand, not resolved by the logs (masked by the coal), which has a few scattered, very coarse sand grains and coal fragments: at its base is the flooding surface. As far as the logs are concerned and in the absence of core, it is the high gamma ray and high neutron responses (condensed sequence) immediately following the coal, which are very typical and suggestive of the marine flooding event. This example demonstrates the need for fine detail when examining key surfaces, satisfied in this case, by core. Image logs can also supply fine detail and, in the absence of core, can give invaluable information (Figure 13.19). This is true not just for a flooding surface, but any of the key surfaces described in this chapter. The use of the image logs in this area is developing rapidly (Chapter 13).

*– transgressive surface (ravinement surface)*

In the two previous examples there is no evidence for significant erosion and certainly no truncation at the level of the flooding surface. This is normally the case. There are, however, flooding surfaces across which there is evidence of considerable erosion, such as the presence of a lag, mineral, especially galuconite concentrations and cementation of the underlying surface (Baum and Vail, 1988). Such surfaces mark the passage from non-marine to marine sedimentation. The sequence stratigraphic interpretation of this erosion just before or during flooding is that it represents a transgression and sea level deepening (Nummedal and Swift, 1987). In Exxon terms this will be the case with the first marine flooding surface following maximum regression and in shallower areas of the shelf, where it is associated with erosion, it is variously called the ravinement surface or the transgressive surface of erosion (Nummedal and Swift, 1987; Baum and Vail, 1988).

On the logs, a transgressive surface will show similarities to a flooding surface but the log responses will tend to be more abrupt. The example (Figure 15.7) shows a medium grained sandstone deposited in cross-beds, with thin carbonate cemented zones and no bioturbation. On the core, the topmost surface appears to truncate a bedform and is very abruptly covered by a 20 cm, intensely bioturbated bed: there is also bioturbation at the junction. On the logs, the abrupt upper surface of the sandstone is evident and the bioturbated bed shows in the high density and low interval transit time (high velocity) responses, as described above (Figure 15.7). Clean, laminated and slightly organic-rich shale rapidly follows the bioturbated bed. At the base, where organic richness is at a maximum, there is a gamma ray high, a neutron high, density low and sonic high (velocity low). The sonic response is as much caused by the fine shale laminations as by the organic matter content (Chapter 8). As detrital input increases so the logs trend towards a normal shale response (Figure 15.7). These log trends are diagnostic (Creaney and Passey, 1993) and generally, where organic content is highest, assumed to represent an anoxic, condensed section (*see* surfaces and intervals of slow deposition *below*). The log responses in this example are typical.

The identification of this as a transgressive surface rather than a flooding surface depends on two things: the abrupt log responses and the position in the vertical sequence. The abruptness, clearly, is suggestive of an erosional break. However, it is the position which gives the most significant clues. Most flooding surfaces occur at the top of prograding, coarsening-up successions. Transgressive surfaces may not. They will cut into valley

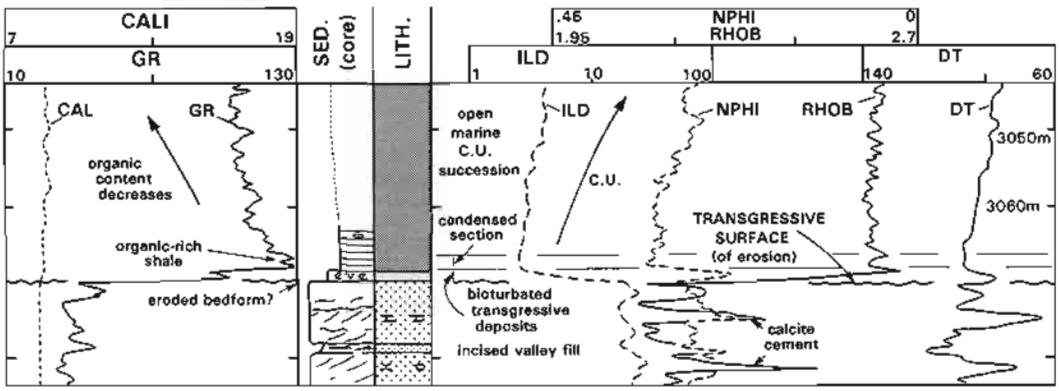


**Figure 15.7** Log example of a transgressive surface of erosion. The underlying sand sequence of probable estuarine deposits, shows eroded bedforms at the top. The erosion surface is covered by thin, bioturbated shaly sands; transgressive deposits. These are followed by well laminated, open marine, organic rich shales of a condensed section which form the base of a shallow marine, coarsening-up, prograding sequence.

fill sediments and cut with a lag into the interfluves (i.e. ravinement). The example (Figure 15.7) being a case of erosion into valley fill.

With logs alone, the transgressive surface is difficult to identify as it shows considerable variety. Where coarse valley fill is present it will be evident as the sands are followed by shales (e.g. Figure 15.7). Where the transgressive surface and the subaerial erosion surface (sequence boundary) are coincident (Figure 5.1), the only record of the transgressive surface may be a coarse lag, a centimetre or two thick, beyond log recognition (except image logs).

### 3) surfaces and intervals of slow deposition: condensed sequence, maximum flooding surface, downlap surface, hardground

A condensed sequence represents a long period of time during which land derived detrital input is small and most of the sediment deposited comes from a hemipelagic or pelagic source and represents deeper water conditions. Such a sequence is typically rich in pelagic fauna and microfauna, is finely laminated, has a low quartz content and is enriched in marine organic matter and exotic elements such as sulphides, pelletised glauconite, phosphates, and iridium. It may have a stable isotope fingerprint (Loutit *et al.*, 1988) (Figure 15.8). However, considerable variation exists in the characteristics of condensed sequences, strong bioturbation and mineralisation also occur so that they may be confused with subaerial erosion surfaces. In sequence stratigraphic theory, the maximum flooding surface (equally called the downlap surface when prograded over by highstand clinoforms) falls within a condensed section. Condensation lasts longer in the offshore but at its inland limit, lasts for a shorter time and therefore is the maximum flooding surface (Figure 15.1). The condensed section may in fact

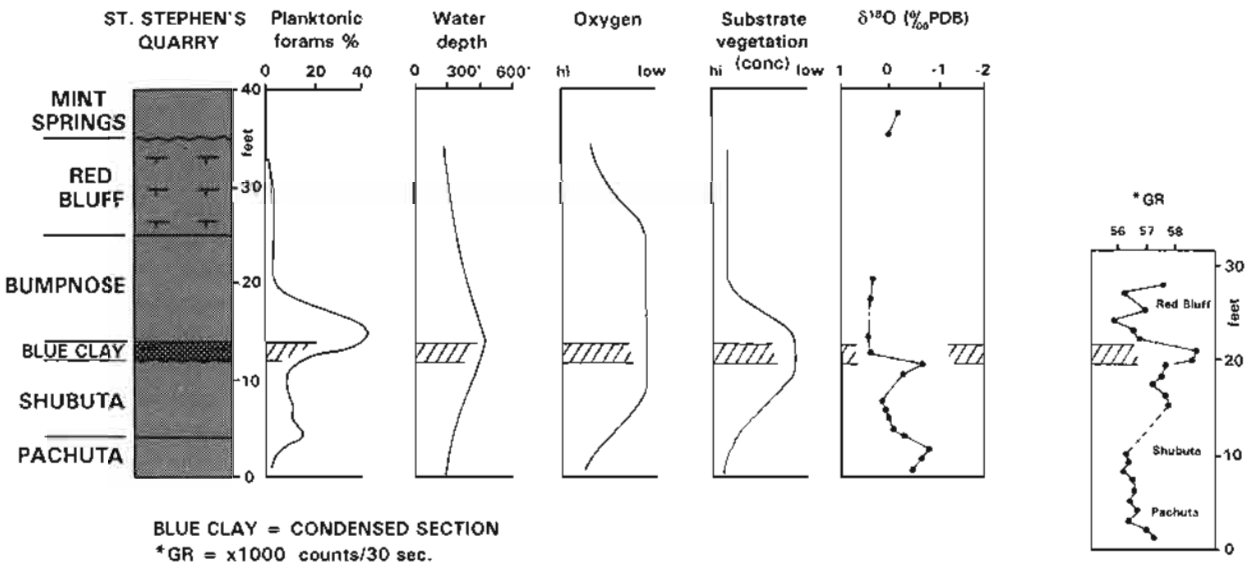


**Figure 15.8** Characteristics of a condensed section, the Blue Clay, showing faunal, chemical, water depth and gamma ray signatures (re-drawn from Loutit *et al.*, 1988).

be in two parts separated by the maximum flooding surface which is actually a bored, cemented starvation surface or hardground (Baum and Vail, 1988).

The log identification of condensed sedimentation depends mostly on its high organic matter content (Creaney and Passey, 1993) and its texture. Marine organic matter is associated with uranium (Chapter 7) so that condensed sediments have a high gamma ray value. A gamma ray 'spike' has now become the diagnostic feature for a condensed sequence and is often considered synonymous with the maximum flooding surface. This may (or may not) be so. Obviously, if a gamma spike is to be caused by uranium enrichment, it should be identified on the spectral gamma ray as such (Figure 7.31). Regrettably this log is not often available. However, as the first log example of a condensed section from shallow shelf detrital deposits shows (Figure 15.9), organic richness is also registered by high neutron values (Chapter 10) and a low density (Chapter 9). The fine laminations, a frequent feature of these slowly accumulating shales, amplify the high interval transit times (low velocity) and generally low resistivity (Chapter 6) already caused by the organic content (Creaney and Passey, 1993). In fact, most of the log responses will be such that in the electrosequence analysis (Chapter 14), condensed sections will be picked out as 'anomalous' (Figure 14.19). An organic rich condensed sequence therefore, has a whole suite of log responses (Figure 15.9) which are generally more diagnostic and reliable than the simple gamma ray 'spike', although not all condensed sequences are maximum flooding surfaces.

The second example (Figure 15.10) from the Lower Cretaceous of the Danish North Sea, shows that organic-rich condensed sections can equally be present in basinal carbonate environments. In detail, these intervals in the example have very fine alternating laminations of carbonaceous rich and nanofossil rich layers, lack bioturbation and contain glauconite and pyrite and are continuous over large areas (Ineson, 1993). On the logs, the gamma signature is evident but so also is the high neutron response. The lower interval shows a low density.

In shallow environments, condensed sequences often follow flooding surfaces and indeed, are a continuation of the same deepening process (cf. Galloway, 1989a,b). Two examples already given (Figures 15.6, 15.7) show this clearly. Black, laminated, organic-rich shales overlie thin, bioturbated, transgressive sand deposits. On the logs, the high density-low neutron of the transgressive sands are followed by the high gamma ray, high neutron, low density and high sonic (low velocity) of the organic-rich, condensed shales. The gradual return to normal sedimentation in these examples is shown in the log trends or electrosequences. Such organic-rich layers and to some extent the attendant electrosequences, can be followed into the offshore where there are no sands (Figures 15.14, 15.15). However, in certain, especially proximal environments, the traces remaining of transgression and condensed accumulation are more subtle. The example (Figure 15.11) shows high depositional energy, shoreface sands, in which there is an interval of finer grained, highly bioturbated sand which is interpreted, both from the core sedimentology and from correlation with other wells, as a low depositional energy, condensed sequence and maximum flooding surface. The shale mixed with the fine sand causes the high gamma ray: the other logs do not give notable responses. Clearly, in this case, core is essential for a proper interpretation.

The identification of condensed sections is fundamental in any sequence stratigraphic analysis, regardless of the theoretical system (models) preferred. In the deeper marine environment and even some shallow, near coastal environments, the increased organic content and laminated texture of the sections, gives a distinctive set of log responses which will generally be identified in an elec-

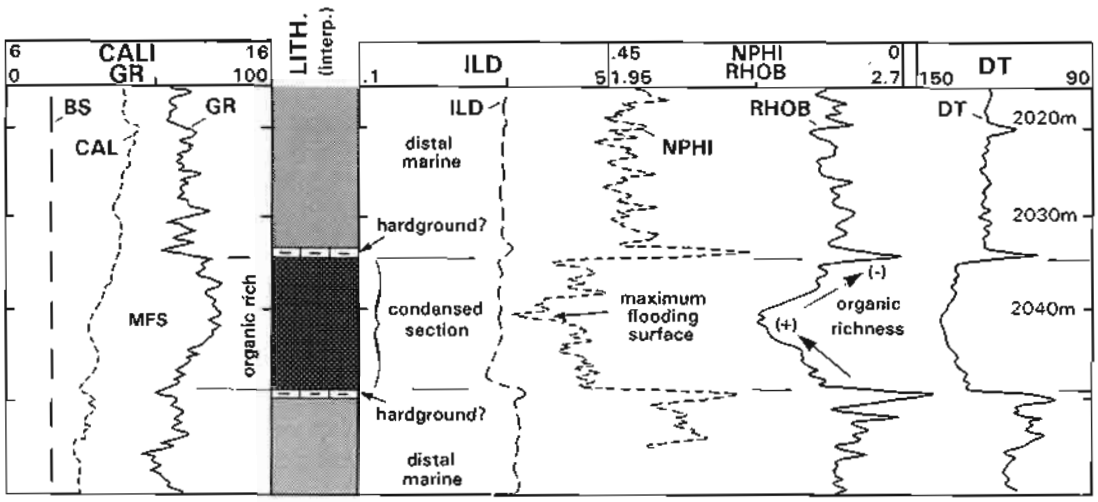


**Figure 15.9** Log example of a maximum flooding surface (MFS). The MFS is interpreted within a broader condensed section characterized by high gamma ray and neutron values, low density and low velocity. The MFS itself is interpreted where the neutron log is highest and the density lowest. The thin carbonate rich bands may be hardgrounds or a later diagenetic effect.

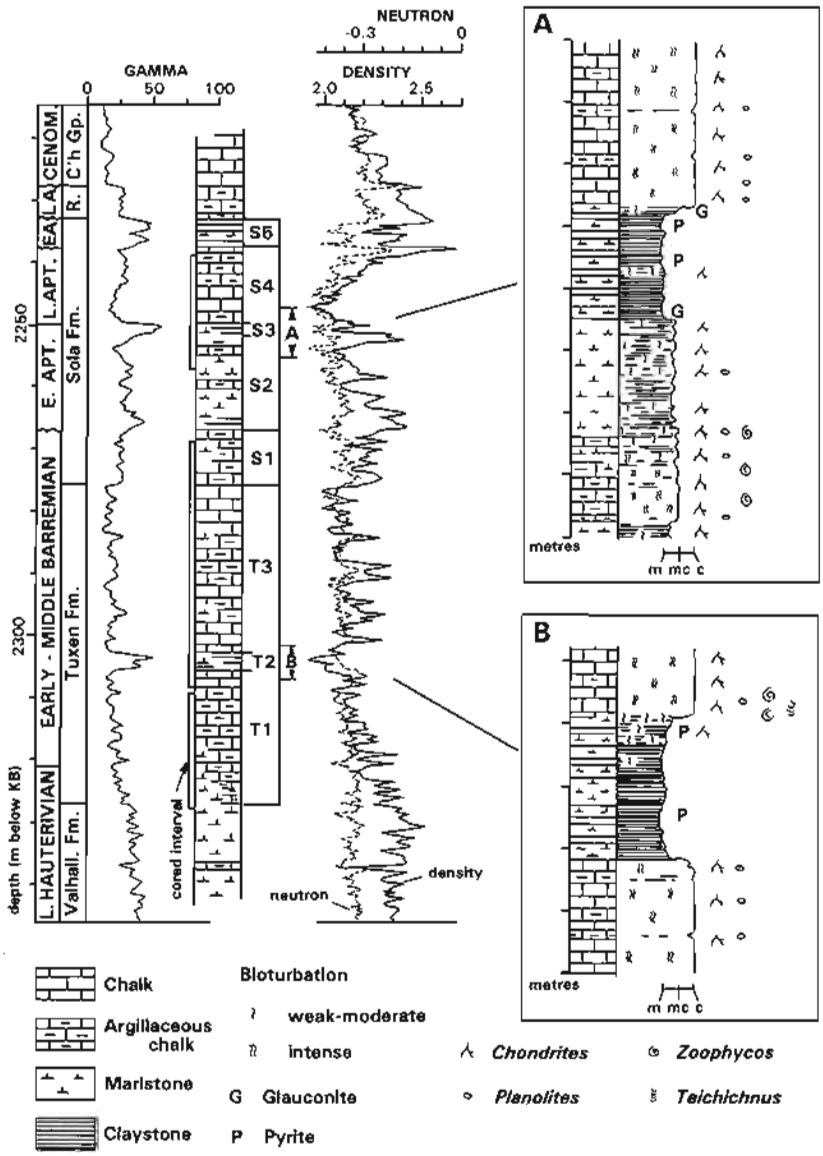


**Figure 15.10** Organic rich condensed sequences from a carbonate succession. Lower Cretaceous, Danish North Sea (from Ineson, 1993).

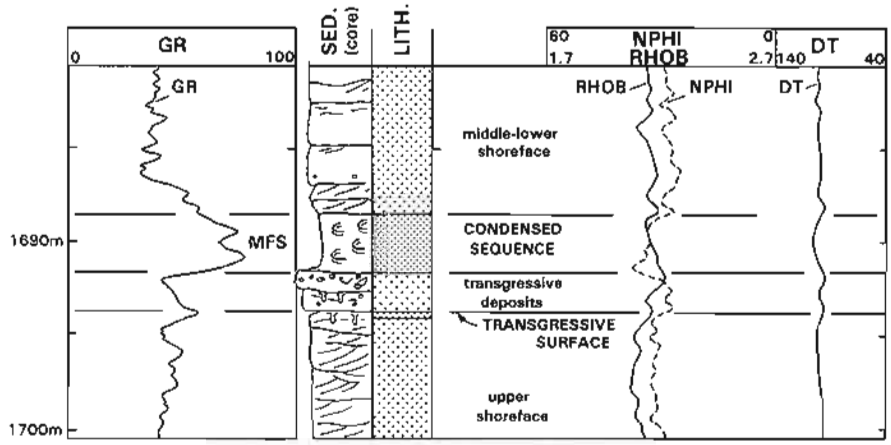


**Figure 15.11** A maximum flooding surface (MFS) in a shoreline (proximal) environment. High energy in general, even during maximum flooding, makes for subdued log responses. Without core, such an interpretation would be extremely difficult.

trosequence analysis as anomalous. They can be used to correlate from the deeper to shallower depositional environments and can also be used to divide the section up into sedimentologically distinct electrosequences (facies successions). Moreover, their nature as condensed can be confirmed by microbiological investigation as they contain increased numbers of pelagic fauna: this may also lead to a dated event. The more important condensed sequences are chronostratigraphic markers. However, not all condensed sequences are enriched in organic matter (Figure 15.11) and not all intervals enriched in organic matter should be assumed to be condensed sequences.

***Facies successions: parasequence & parasequence set, systems tract, genetic stratigraphic sequence and electrosequence.***

The building blocks of sequence stratigraphy are hierarchical (Figure 15.1*a*) and the key surfaces described above allow each block to be recognised (and defined). The lowest order of the hierarchy to be considered in this text is the *parasequence* which (for Exxon) is bounded by flooding surfaces. A parasequence and the older term sedimentary cycle are almost the same. However, to avoid confusion, the term cycle has been replaced in this text by 'succession of facies' (Walker, 1992) to indicate a sequence in purely sedimentological terms (i.e. not sequence stratigraphic). In the Exxon scheme, several parasequences build up to form a *parasequence set* which, together form a *systems tract* deposited during a particular stage in the cycle of sea-level rise and fall. At the equivalent hierarchichal level to the systems tract, but differently defined, is the *genetic stratigraphic sequence* (Galloway, 1989a, b) (Figure 15.1). A genetic stratigraphic sequence is a package of sediment recording a significant depositional episode of basin margin outbuilding and basin filling, bounded by sediments representing periods of widespread basin margin flooding (i.e. condensed sequences). A genetic stratigraphic sequence comprises regressive followed by transgressive sedimentary successions, bounded by the isochronous marine flooding surfaces or condensed sections, otherwise termed maximum flooding surfaces (Partington *et al.*, 1993 *a, b*).

Linked depositional systems are being identified at this scale and are recognised as bounded by major, key surfaces such as the transgressive surface, maximum flooding surface or sequence boundary. These will be illustrated, with discussion, by real examples. At this scale, large datasets are involved but are difficult to illustrate in book form so that very reduced example sets are used.

To identify a parasequence on the logs, both the facies succession and the bounding marine flooding surfaces must be diagnosed. A facies succession (cycle) is normally seen as an electrosequence, and will be identified as such in the electrosequence analysis (Chapter 14) as the persistent, upward change in log parameters, both in the fine grained shale and coarser grained, sand intervals, on all the logs. The core used in the example (Figure 15.12) shows three coarsening-up facies successions

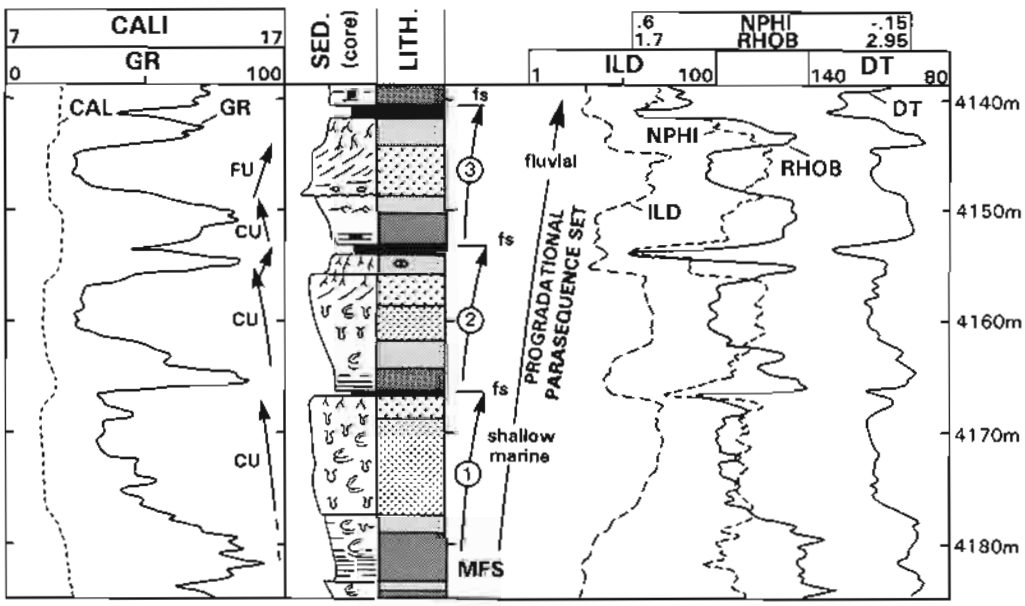


**Figure 15.12** Example of a progradational, parasequence set. Upwards the sands become coarser grained and with higher energy structures, the coals become thicker and the parasequences become thinner progressively upwards (rate of accommodation less than rate of sedimentation). A maximum flooding event is interpreted at the base of the parasequence set, indicating that these are highstand deposits.

bounded by coals and flooding surfaces. These are parasequences. They are equivalent to the three electrosequences evident on the logs and the flooding surfaces are seen as high gamma ray, high neutron responses immediately above the coals, although the responses are masked to some extent by the coals themselves.

In Exxon terminology, these three parasequences form a parasequence set. That is, they show progressively changing characteristics which, in this case are: they get progressively thinner upwards, the sands get cleaner and more porous (shown by the neutron-density separation), their depositional environment gets shallower, with both the seat earths and coals getting thicker and the fining-up successions get more important. The environment seems to have been shallowing by steps, each parasequence being deposited closer to the shoreline. This is a *prograding parasequence set* (Van Wagoner *et al.*, 1990) and the progressive thinning of each set suggests that deposition was faster than accommodation.

In the Exxon sequence stratigraphic scheme, the next in the hierarchy above the parasequence set is the *systems tract*, a *'linkage of contemporaneous depositional systems'* (Posamentier *et al.*, 1988), where depositional systems are three dimensional successions of facies. There are essentially three systems tracts, lowstand, transgressive and highstand. A combination of systems tracts forms the Exxon sequence (Figure 15.1) and is deposited during one major rise and fall of sea level, typically 0.5–3 Ma (Vail *et al.*, 1977). The schematic SP or gamma ray log characteristics of each of these systems tracts are shown as published (Vail and Wornardt, 1990)(Figure 15.13). A sequence may be made up of all three tracts or some combination, especially a transgressive followed by a highstand systems tract. In the preceding log example (Figure 15.12), the prograding parasequence set is bounded at the base by a condensed sequence and maximum flooding surface: it therefore makes up a highstand systems tract (cf. Figure 15.13). The key surface at the top should theoretically be a sequence boundary, but it has not been identified. This

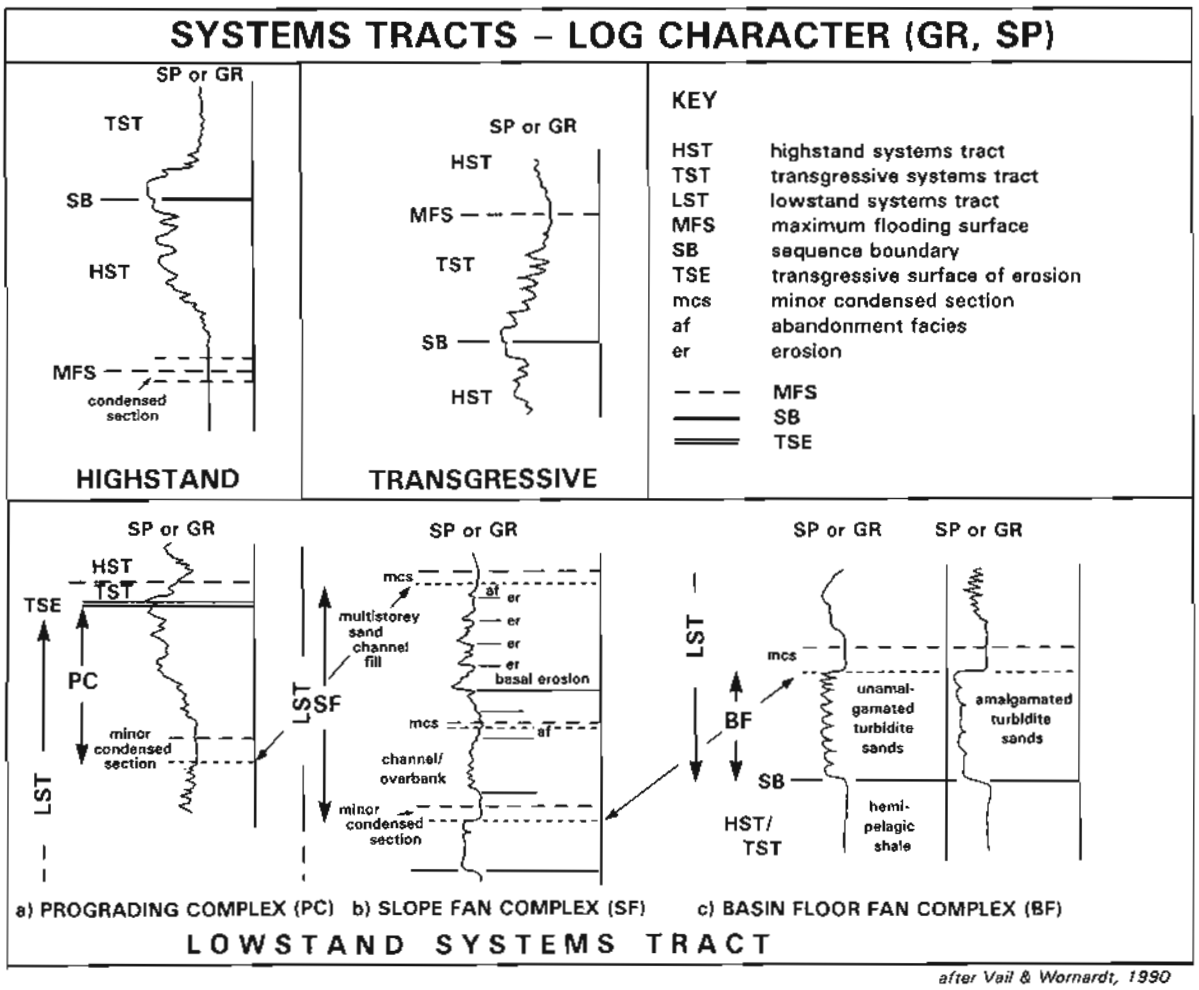


**Figure 15.13** Model log patterns of sequence tracts, including deep water deposits (from Vail and Wornardt, 1990).

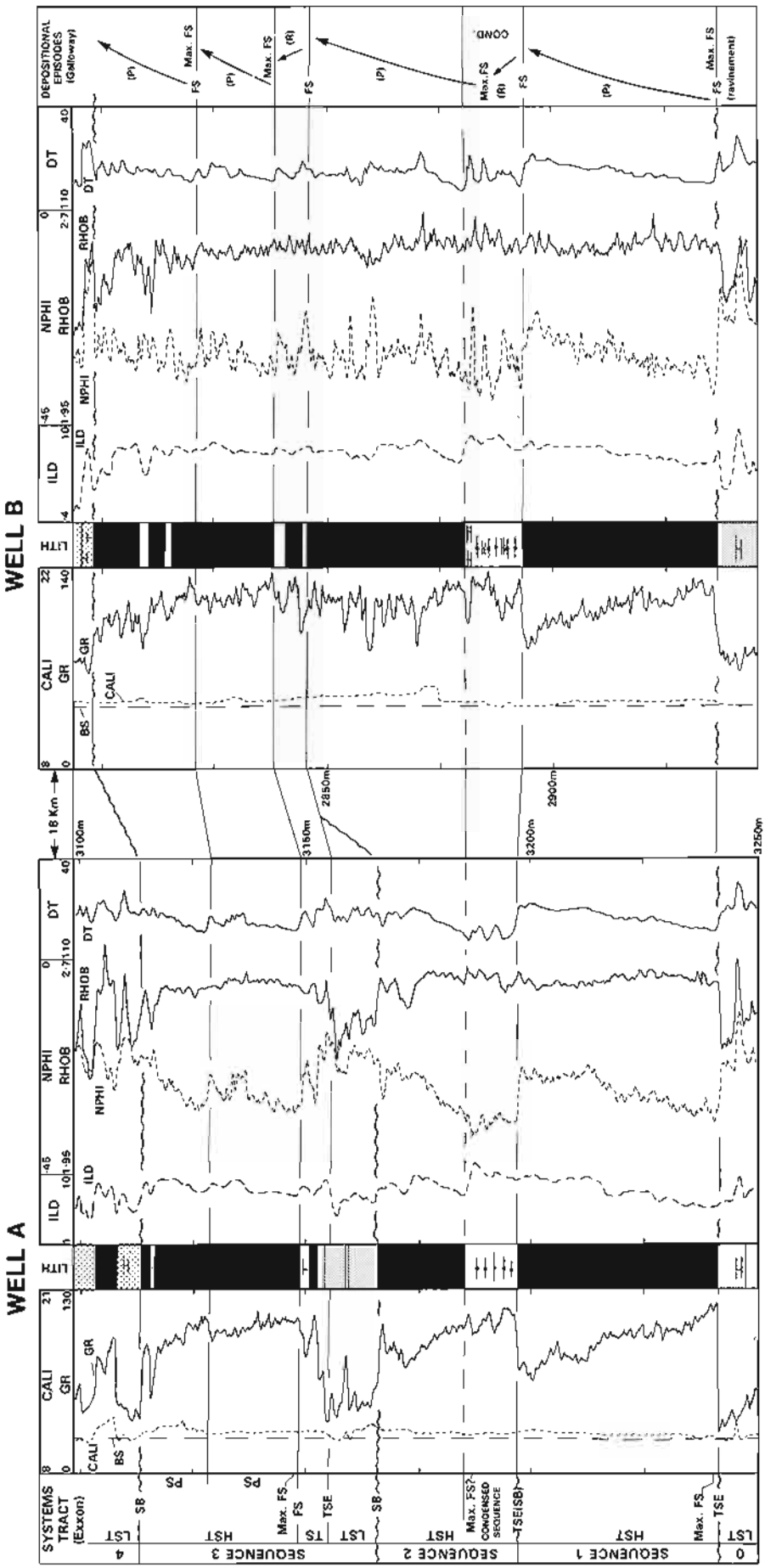


**Figure 15.14** Subdivision and correlation using sequence stratigraphic principles in shallow marine sediments. Exxon systems tracts and sequences on the left, Galloway genetic stratigraphic sequences on the right. *See text* for discussion. Systems tracts:- HST = highstand, TS = transgressive, LST = lowstand. TSE = transgressive surface of erosion: (Max) FS = (maximum) flooding surface: SB = sequence boundary: PS = parasequence: (P) = progradational: (R) = retrogradational.

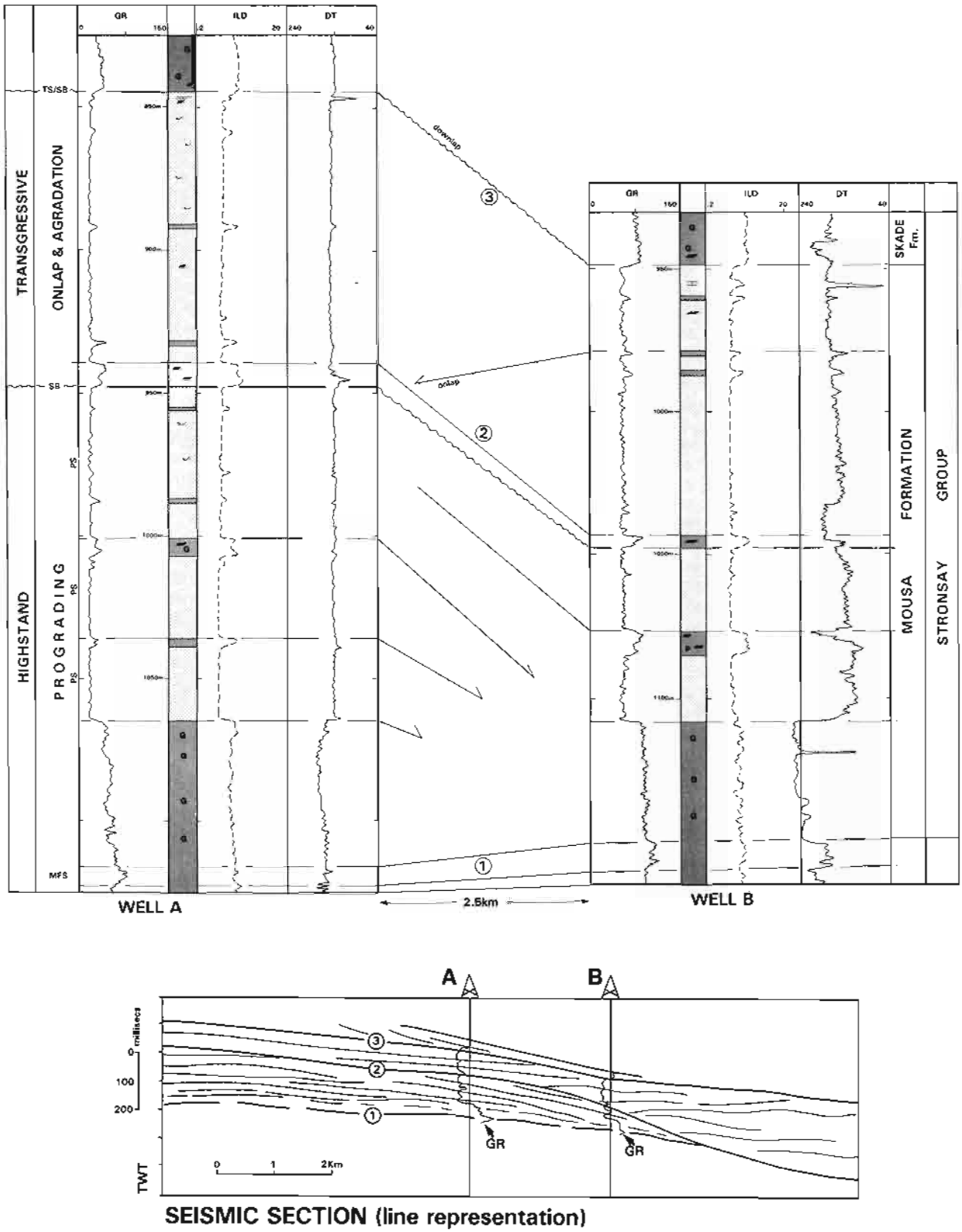


**Figure 15.15** Subdivision and correlation using seismic reflectors and sequence stratigraphic principles in deep water turbidite sediments. Without the seismic between the two wells, the correlation indicated would not have been possible. *See text* for discussion. PS = parasequence: SB = sequence boundary: MFS = maximum flooding surface: TS = transgressive surface. Palaeogene, North Sea.

type of highstand parasequence set appears to be the most common or perhaps easiest to identify (the automatic attribution of such sets to the highstand sea level phase has been questioned recently, as similar depositional patterns develop during the lowering of sea level in forced regression, Nummedal *et al.*, 1995). However, there is a tendency among many workers using sequence stratigraphy to simply identify the key surfaces and not add in the detail of systems tracts (cf. Walker, 1992), especially as the systems tracts are essentially used by Exxon.

Two examples attempt to show in detail the application of a sequence stratigraphic analysis on real log data, rather than dealing in models. The first example is in shallow marine to shelf sediments (Figure 15.14). The individual elements in the two selected wells are very distinct: a series of cleaning-up electrosequences with, at their base, organic-rich condensed sequences overlying thin, burrowed transgressive deposits. The top of the example section is a well marked, widespread erosional break (sequence boundary sensu Exxon); the base is interpreted as an erosional, transgressive surface. The sediments represent some 7–8 Ma. From the study of over 100 wells covering 23,000 km$^2$ it is known that these electro sequences can be correlated and to some extent, dated. There are obviously changes, but the principal framework is made up of the flooding surfaces/condensed sequences and closely preceding transgressive deposits. Good sands tend to be very localised. In the two example wells, when the section is broken down using the Exxon approach (Figure 15.14, left side), three sequences are interpreted and the marked base of a fourth cuts off the section at the top. Highstand systems tracts dominate, the transgressive tracts are mostly very thin and a lowstand systems tract is only interpreted in sequence 3. The boundary between sequence 1 and 2 is unsatisfactory although the very marked condensed sequence is undoubted. Besides the highstand systems tracts (which are clearly progradational), the identification of other systems tracts is more dictated by what is required by the model than by a positive identification or distinctive features. With the genetic stratigraphic sequence approach (Figure 15.14, right side) four transgressive-regressive sequences are very satisfactorily interpreted. However, the presence of sand in well A and not well B is not well brought out and the status of the surface at the top of the section is not clear.

The second example (Figure 15.15) is from a Palaeogene shelf edge area in the North Sea, for which good quality seismic is available. The two wells are 2.5 km apart. A shale section occurs at both the bottom and at the top of the selected interval. The well logs do not show distinctive depositional patterns (as seen in the previous example) and the principal feature is a thick sand section with more or less prominent, but thin shale intervals. The wells appear reasonably similar. An established lithostratigraphy (Knox and Cordey, 1992) can be applied to both (Figure 15.15, right). However, the line diagram of the seismic shows that the apparent correlations are false and the true correlations between the two wells are very complex. The sequence stratigraphic analysis (Figure 15.15, left) would not be possible without the seismic, but once in place can explain the complexities. The base of the sand near the bottom of the section is clearly downlapping on the seismic: it is diachronous. The shale interval (horizon 2) correlated between the two wells on seismic evidence is over an erosional sequence boundary and subsequently transgressed: a maximum flooding surface is proposed. Above this, the section is markedly onlapping and there is no direct correlation between the wells. Finally another sequence boundary (horizon 3) ends the section, with erosion indicated on the seismic and explaining the thickness difference in the upper section. A transgression and flooding surface follow this sequence boundary. From this example it is seen that the lithostratigraphy cannot contend with depositional complexity, that the well logs should not be correlated without the seismic and that tracing key surfaces is a natural result of integrating the logs with the seismic.

Sequence stratigraphy is very much an evolving subject at the time of writing this book. Modifications to the Exxon models are frequently being proposed or new explanations attempted. As a journalist would say 'the jury is still out', an ugly expression but effective.

***Computer techniques in sequence stratigraphy***

The concepts of sequence stratigraphy are very sophisticated and based on a huge amount of observation and experience. It is inconceivable that such concepts should not make use of the modern technology available for the manipulation of logs. This section describes the author's attempts at using interactive computer techniques for a sequence stratigraphic analysis.

The programme used is TerraStation, (from Terra Sciences). The principal routines discussed are the single log histogram, the interactive cross-plot and the interactive z-plot. The interactive cross-plot consists of a screen on which both the cross-plot is displayed and also the log traces themselves. Any two logs may be displayed, at any scale over any selected interval. The cross-plot is interactively linked to the log curve display so that groups of points on the cross-plot outlined by a mouse driven rubber band are immediately identified on the logs: conversely intervals identified by a mouse defined box on the log curves are highlighted as values on the cross-plot. In other words, points on the cross-plot can be identified on the curves and intervals on the curves can be identified on the cross-plot. The z-plot has the same facilities but the third dimension is added to the plot field.

The use of these capabilities will be illustrated using real examples.

The first step in dividing a well into sequence stratigrahic units is to identify the key surfaces. As far as the logs are concerned, as has been described, key surfaces tend to have extreme or even anomalous log responses.

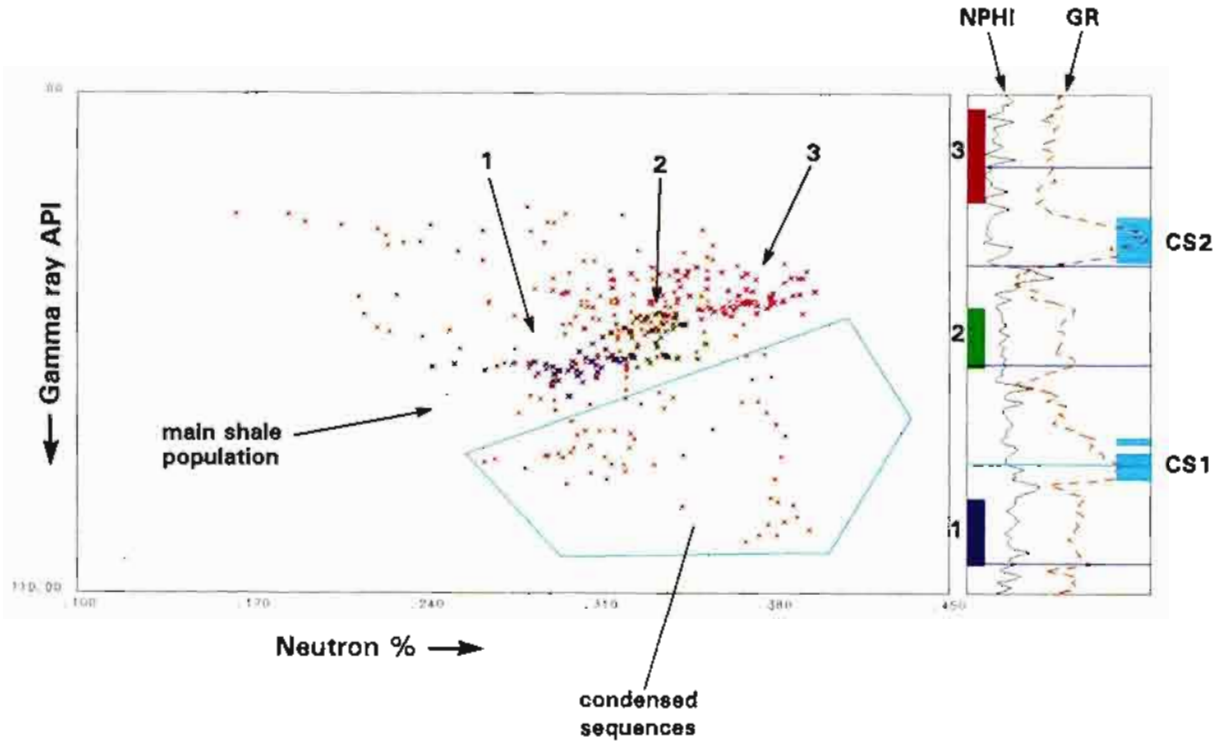


**Figure 15.16** Deep water shale sequences explored on an interactive gamma ray - neutron log cross-plot. The data points from the condensed sequences CS1 and CS2, show anomalous (unusual) log responses and are outlined on the cross-plot in blue outside the normal shale population. The two condensed sequences separate three shale populations: 1 (blue), 2 (green) and 3 (magenta). Each shale is seen as a different population on the cross-plot, indicating that the condensed sequences separate shales of different electrofacies (TerraStation software).

For example, condensed sequences have higher than normal gamma ray values, lower than normal densities and so on. The first technique is therefore to isolate these abnormal or excessive responses. A gamma ray, density or other histogram may be analysed and the high or low ends, extracted and identified in terms of log values. With TerraStation, this may be done using a simple histogram plot but is more effectively done on a cross-plot screen using gamma ray plotted against the neutron, the density, the sonic or a shallow resistivity log. Condensed sections will appear as the few points with high gamma ray values and low density, high neutron, low sonic or low resistivity (Figure 15.16). The plots can be cycled and the various levels with the highlighted responses noted.

As a next step, still searching for key surfaces, the various cross-plots can be explored for any other extreme log responses. That is, clusters of points, usually only a few, which are detached from the main cloud of points. The neutron-density, gamma ray-neutron and sonic-resistivity cross-plots are the best for this routine. The extracted intervals, identified on the screen log curves, should be reported to paper log plots. Such highlighted zones will frequently be key surfaces. The example (Figure 15.16) shows a gamma ray-neutron cross-plot of a deep water shale sequence with two condensed sequences (CS1, CS2). On the cross-plot, the condensed sequences plot within the field outlined in light blue, the points within this field being indicated on the log curve grid by light blue decoration on the right margin. The points within this field have anomalously high gamma ray values for the corresponding neutron value. Across each of the condensed sequences the shale composition changes, shale intervals 1 (blue), 2 (green) and 3 (magenta) marked on the left margin of the log column plotting as distinctly different populations on the cross-plot identified by their corresponding colours. Change of electrofacies across condensed sequences is both typical and diagnostic. If sequence stratigraphic models are consulted, environments before and after important condensed sequences (e.g. maximum flooding surface) are different. This is indicated in the log responses.

Electrosequences are best identified on paper plots of the logs as explained in Chapter 14. However, the analysis of the sequences, once identified (or postulated) is more effectively carried out with interactive cross-plots. For example, parasequence sets identified on the logs may be analysed for persistent trends. An example was shown of a prograding parasequence set (Figure 15.12). Analysed on the interactive, neutron-density cross-plot, persistent upward changes become clear (Figure 15.17). The sands of each parasequence clearly move across the plot, towards the cleaner, more porous texture of the highest parasequence. Also on this plot, the minor flooding surfaces and the maximum flooding

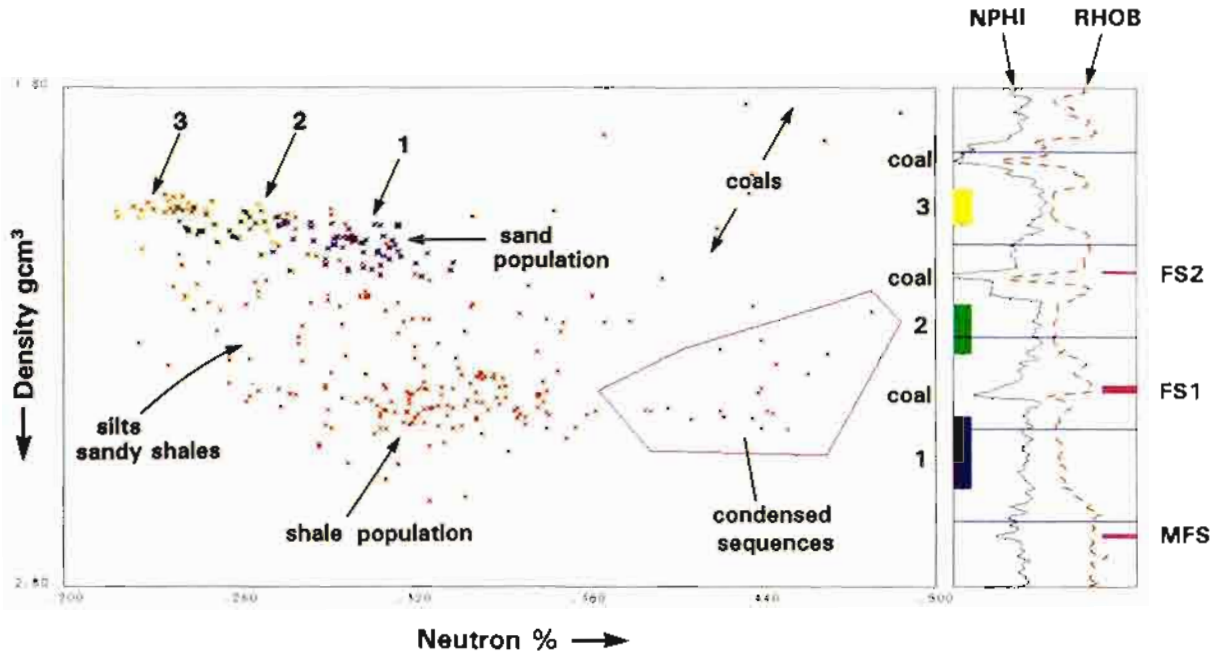


**Figure 15.17** The prograding, parasequence set of Figure 15.12 explored on an interactive neutron-density cross-plot. The sand intervals 1 (blue), 2 (green) and 3 (yellow) plot as contiguous but progressively changing (shallowing environment?) populations. The condensed sections MFS (maximum flooding surface), FS1 and FS2 (flooding surfaces), are distinct on the extremes of the general shale population and are outlined on the cross-plot in magenta (TerraStation software).

surface are picked out quite distinctly on the fringe of the shale population.

Obviously, the potential for showing the workings of an interactive computer technique in a book are very limited. Any cross-plot or z-plot can be explored and, when selected intervals such as one electrosequence are used, it is rare that a number of populations or relationships do not become evident. Shale composition changes become clear, changes in sand texture and composition identified, gradational sand to shale changes defined and anomalous log responses highlighted. In a book it is impossible to describe more.

## 15.3 Lithostratigraphy

***Type subsurface stratigraphy***

It must be remembered that sequence stratigraphy, exciting as it may be, like humans, had humble beginnings. And these beginnings are as important as the present evolutionary state. The simplest use of well logs, and still very important, is in the identification of lithostratigraphic units. Such units allow a well to be divided up into intervals, which all (regardless of theoretical sympathies) can identify, both in other wells and even at outcrop.

The best use of the lithostratigraphic unit in the subsurface is to define type sections. Just as type stratigraphic sections exist at outcrop, so type wells can be designated in the subsurface for particular lithostratigraphic formations. Well logs form the basis for these definitions. The various lithological units for the North Sea, for example, have been defined by government agencies of the countries concerned (Rhys, 1975; Deegan and Scull, 1977; NAM/RGD, 1980; Vollset and Doré, 1984; Knox and Cordey, 1992). Each lithological unit has been designated a type well which can be used as a reference for both lithological and log characteristics (Figure 15.18).

On a different scale, the stratigraphy of a particular field may be described using a type well and well logs illustrating each lithostratigraphic interval (e.g. Jamison *et al.*, 1980). Names in fields are frequently specific to the operating company. The illustration of the named intervals using well logs enables them to be identified outside the field and by other companies. It avoids annoying name confusion.

The modern North American tendency is to prefer allostratigraphy to lithostratigraphy in defining formal units (NACSN, 1983). Allostratigraphy uses the bounding limits of a sediment interval to define it, the contrary to lithostratigraphy which defines what the interval is. In terms of well logs, it is far easier to define the response of the interval itself, knowing the shortcomings this method has, than to define a limiting surface which may be impossible to detect. This was, and still is, the basis of our stratigraphic column and which none contest (e.g. Rudwick, 1985).

# NORWEGIAN WELL 7/9-1

OPERATOR: CONOCO
CO-ORDINATES: 57°20'37"N 02°51'21"E
SPUDDED: 22/4/71 DRILLING COMPLETED 19/5/71
KBE: 31m (101ft) WATER DEPTH: 70m(229ft)

SCALE: 1:2000

**Reference Well: GASSUM FORMATION, FJERRITSLEV FORMATION, HALDAGER FORMATION AND BØRGLUM MEMBER (BREAM FORMATION)**

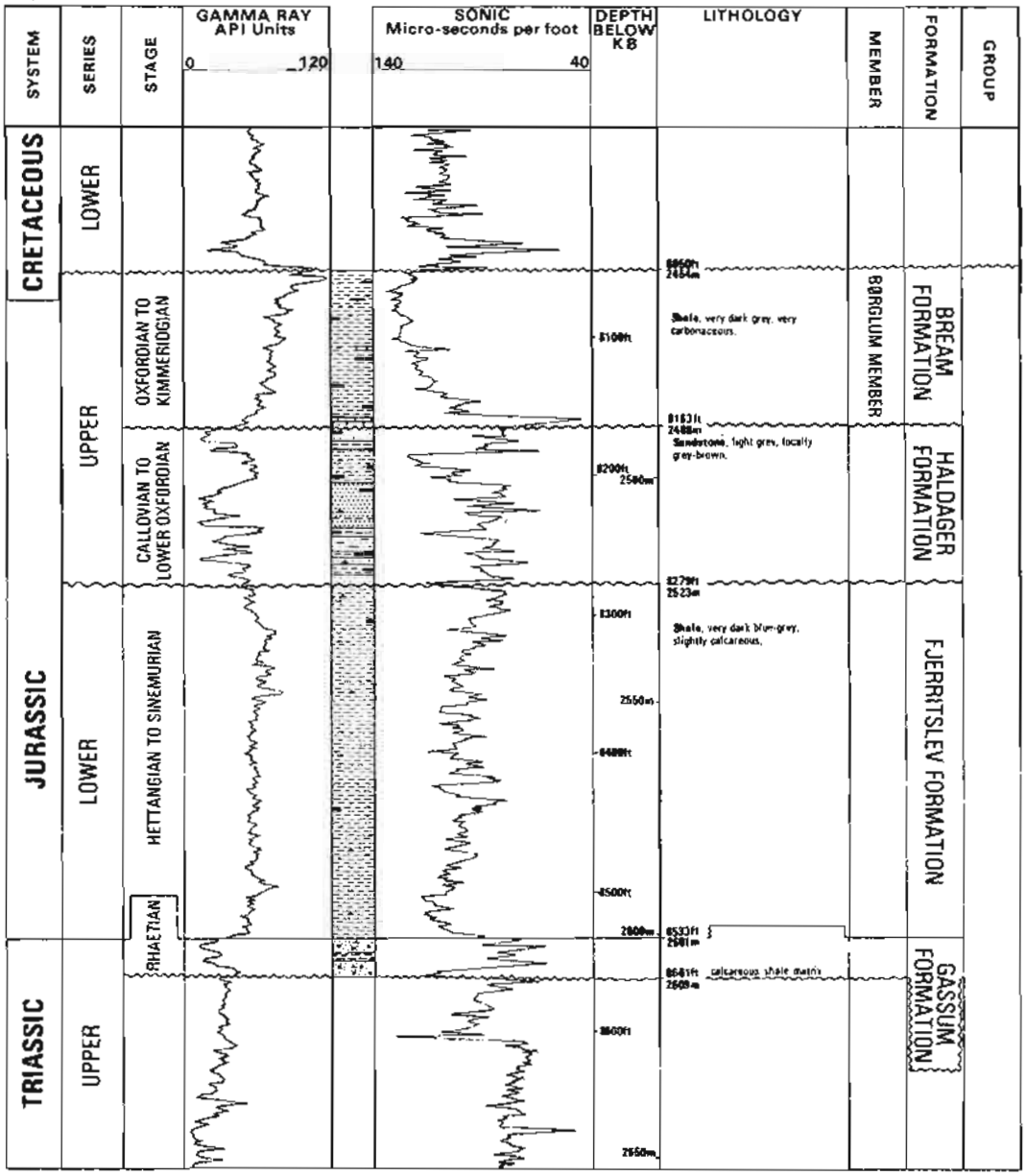


**Figure 15.18** Type section of an offshore formation illustrated by well logs. (Re-drawn from Rhys, 1975).

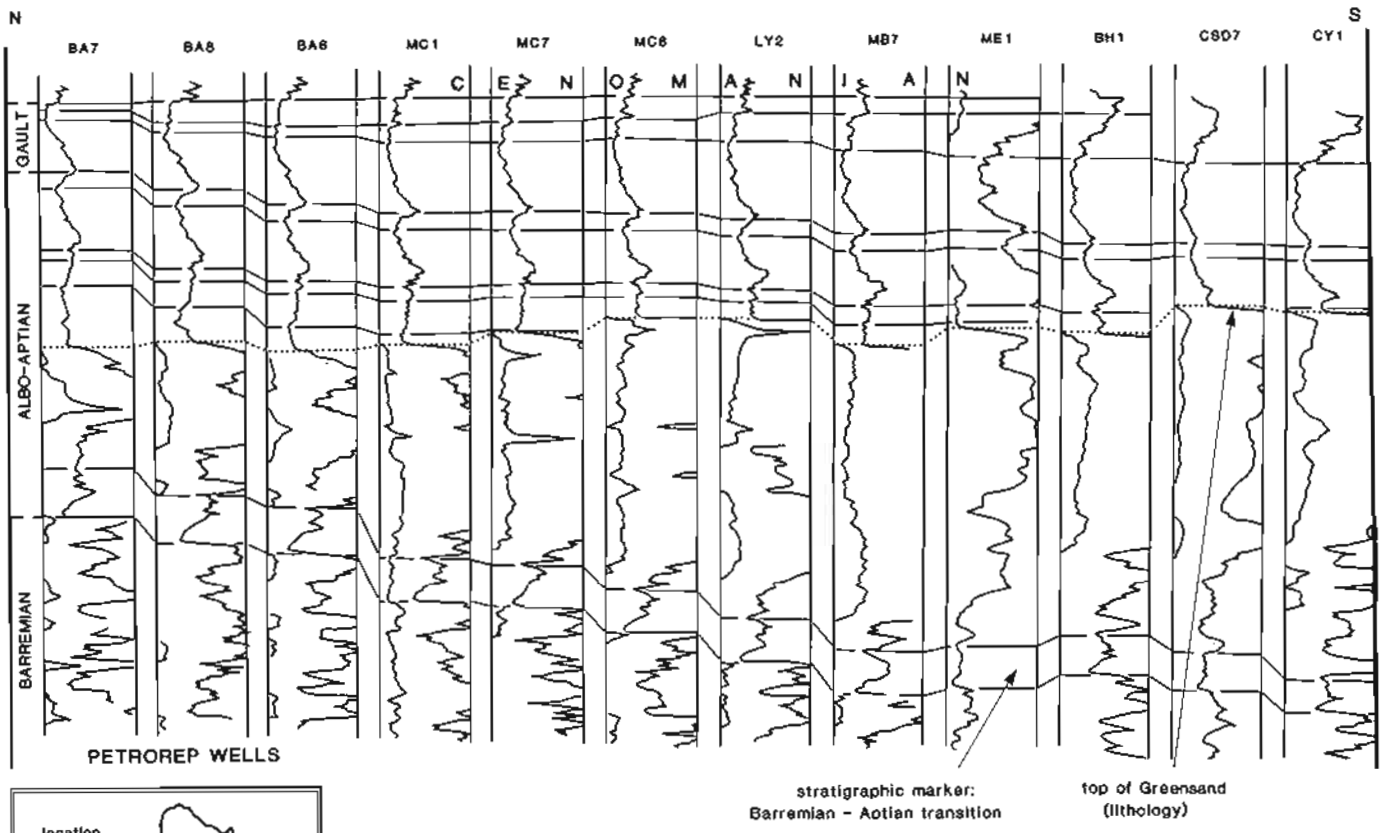


**Figure 15.19** Detailed correlation of log markers across the Paris Basin, France. This traditional way of correlating logs is now tied to detailed biostratigraphy: some markers are time transgressive. (From Serra, 1972).

## 15.4 Traditional correlation methods

### *Marker horizons*

The simplest and most evident form of log correlation uses log markers. This marker may be a distinctive peak, a distinctive shape or a distinctive lithology with unique log responses (this obviously has connotations in sequence stratigraphy). The Lower Cretaceous of the Paris Basin, for example, shows the behaviour of marker shapes over a stable intra-cratonic basin and illustrates traditional correlation (Figure 15.19). Today, such correlations are still usual, but associated with a detailed biostratigraphy and an explanation is now required as to why they exist, usually in sequence stratigraphic terms (Section 15.2). It is far better to know what causes a particular log marker, peak or trough, than to correlate uniquely on appearances.

### *False correlations – facies*

In sand-shale sequences, correlations often become extremely complex. It is exceedingly easy to correlate two similar-looking sand bodies between two wells, only to find that the liquids that they contain are incompatible for the structure, and that, in reality, they are not related. The correlation was of like facies. It is essential to take account of the facies being correlated. In sand-shale sequences, although sand bodies are the reservoirs and therefore important, they should, nonetheless, *not* form the basis for correlation.

In the example (Figure 15.20), correlation was based essentially on coals and electrosequences. From their position and log shape, the sandstone bodies appear to correlate, but in fact do not, as proved by fluid incompatibilities (Figure 15.20). The sands were deposited in channels and the similarities in log shape only indicate similar facies. This is an area of active deltaic deposition with channels forming and being abandoned; individual channel reservoir correlation is extremely complex but the channel facies is frequently repeated.

The rules for correlating only certain facies is universal, as has been demonstrated in the discussion of sequence stratigraphy (Section 15.2).

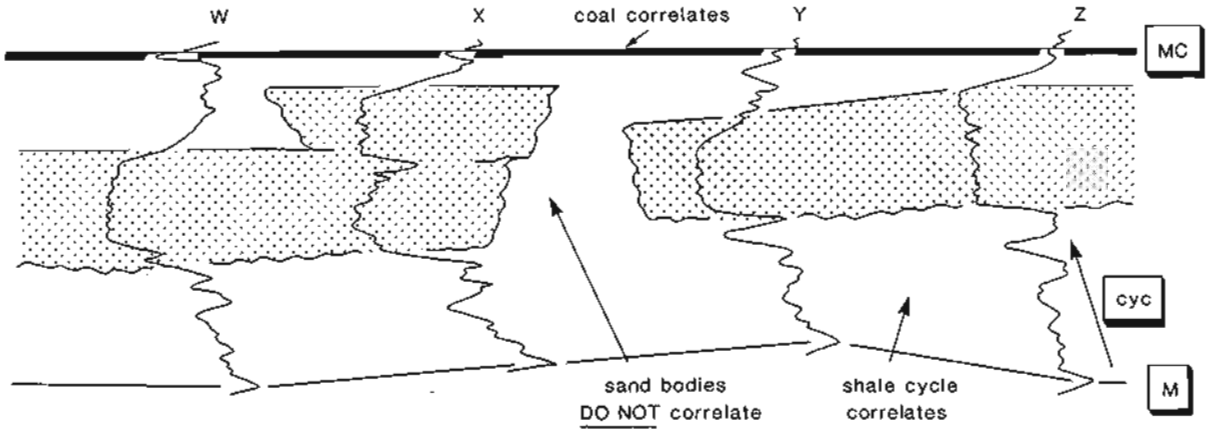


**Figure 15.20** Correlation of log shapes in a deltaic complex. From log shapes, the sand-body appears to be continuous but the shapes only indicate similar facies. Incompatible fluids show that two separated sand-bodies exist. Persistent correlations are based on coals and fine-grained facies. MC = marker coal, M = marker, CYC = marker cycle. W to Z is 3.5km.

***Palaeontologically controlled correlations***

Palaeontological control in correlation is essential in sequence stratigraphy but was not sufficiently stressed above (Section 15.2). This was done deliberately to emphasise the contribution of the logs. But any log study must be integrated with 'event stratigraphy' for reliable correlation. That is, correlations are based on various biological events such as blooms or extinctions as well as the traditional appearances and disappearances of species (e.g. Mitchener *et al.*, 1992). Some events are considered to be isochronous (as far as the individual basin is concerned) and therefore correlatable, others are facies controlled. Because of sampling difficulties in the subsurface, biostratigraphic events may not always be identified in a well or be precise. The combined use of event stratigraphy and well logs is therefore essential.

Every specialist considers that his 'discipline' is the most reliable and its results unassailable. The man who has spent his lifetime examining dinoflagellates, will argue their value to the denigration of any other information. The man who has spent his lifetime analysing well logs will do the same for the logs! Of course, the essential is to combine information using the strong points of each discipline. Frequently, specialists are unaware of (or unwilling to admit to themselves) the weaknesses in their own speciality.

This is simply to argue that much micro-biological information has limitations in accuracy where correlation is concerned. Well logs are, for the greater part, lithostratigraphic records. When the two are combined, there is often a tendency to say that a particular horizon is diachronous because microfauna occur at different levels. This is always a possibility, but distance between wells must be considered. Wells a few kilometres apart are unlikely to have the same facies with different ages. A careful balance in using the data must be achieved.

The example illustrated shows such a balance between log correlation and biostratigraphy, nicely achieved (Figure 15.21). Middle Cretaceous rocks cover a small pod-like horst (the Buchan Horst) in the central North Sea (Burnhill and Ramsay, 1981). The lithostratigraphy shows some continuity but also inexplicable discontinuities. The datings, fine enough for correlation, add sufficient information to explain the discontinuities and to corroborate the continuous log correlations. The combined log and palaeontological correlations show a mid-Cretaceous, early Turonian unconformity over the horst itself with a later Turonian onlap. By correlating the unconformity with a regional Turonian regressive phase which occurred throughout north-west Europe and North America, the authors show that the erosion was not a result of local movement on the horst, but the result of a global change in sea level (Burnhill and Ramsay, 1981). The succeeding onlap had a similar cause. Clearly, this sort of reasoning is not possible with undated log correlations.

***Correlations at outcrop***

Before a field is developed, the widely spaced exploration wells are correlated in detail over the reservoir interval and predictions made for the infill producer wells about to be drilled. As all geologists know, there are always surprises during the infill drilling. Some intervals show unattended continuity, others have unexpected variations. Work at outcrop tends to put a rather sober note on the possibilities for subsurface correlation, at least in some facies.

The illustration chosen is of one very evocative piece of work in which gamma ray profiles were logged at intervals along a quarry face by a gamma ray tool and a logging truck! (Slatt *et al.*, 1992). The correlations suggested by the log profiles can be compared with the actual correlations seen and drawn from the outcrop (Figure 15.22). The confidence which would justifiably exist after correlating the logs alone is misplaced, and perhaps explains why development infill wells produce surprises. The logs tend to simplify lithological responses, which in some instances is an advantage, in others it leads to errors. There is little that can be done about this except to be aware of it.

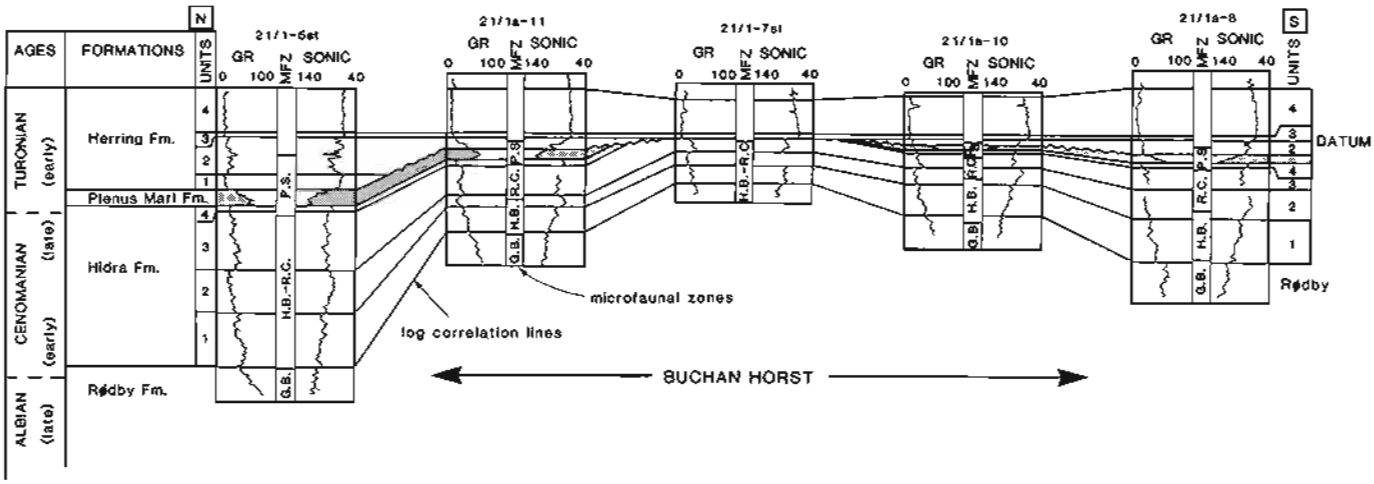


**Figure 15.21** Palaeontologically-controlled correlation. The mid-Cretaceous across the Buchan Horst, North Sea. Outside wells 6km apart. GR = gamma ray API units. Sonic = Δt microseconds per foot. MFZ = microfaunal zone. PS = *Praeglobotruncana stephani* biozone. RC = *Rotalipora cushmani* biozone. HB = *Hedbergella brittonensis* biozone. GB = *Globigerinelloides bentonensis* biozone. (From Burnhill and Ramsay, 1981).

### *Correlation and depositional or erosional topography*

The topography of the present day surfaces of sediment deposition must be similar to those that existed in the past. The environments of shelf, slope and basin existed in past geological time, as now. Long distance correlations should reflect these topographic elements.

The Pennsylvanian to Permian deposits of West Texas were apparently laid down close to the shelf edge (Van Siclen, 1958). Correlations over 10 km in these beds across the palaeo-shelf edge show the depositional topography as it then was (Figure 15.23). The topography is associated with changes in lithology and, in this case, limestone and reef development. Limestones develop on the platform, reefs on the platform edge and shales in the basin off the shelf slope.

Equally important as depositional topography, is erosional topography. Much importance is put in sequence stratigraphy on identifying 'valley fills' (Section 15.2). These are valleys cut during a relative fall in sea level and filled subsequently when sea level rises again. The modern example is the erosional valley beneath the present day Mississippi (Fisk and McFarlan, 1955), filled with the present day river deposits. In ancient sediments these deposits can be made evident in well correlations (Figure 15.24) if the correct datum is chosen, normally a key surface (Section 15.2).

To show depositional and erosional topography the choice of datum is obviously critical. In the example (Figure 15.23), the datum used is near structural and still allows the palaeotopography to be seen. However, this may not be the case and the chosen datum must correspond to a facies recognised as most likely to have

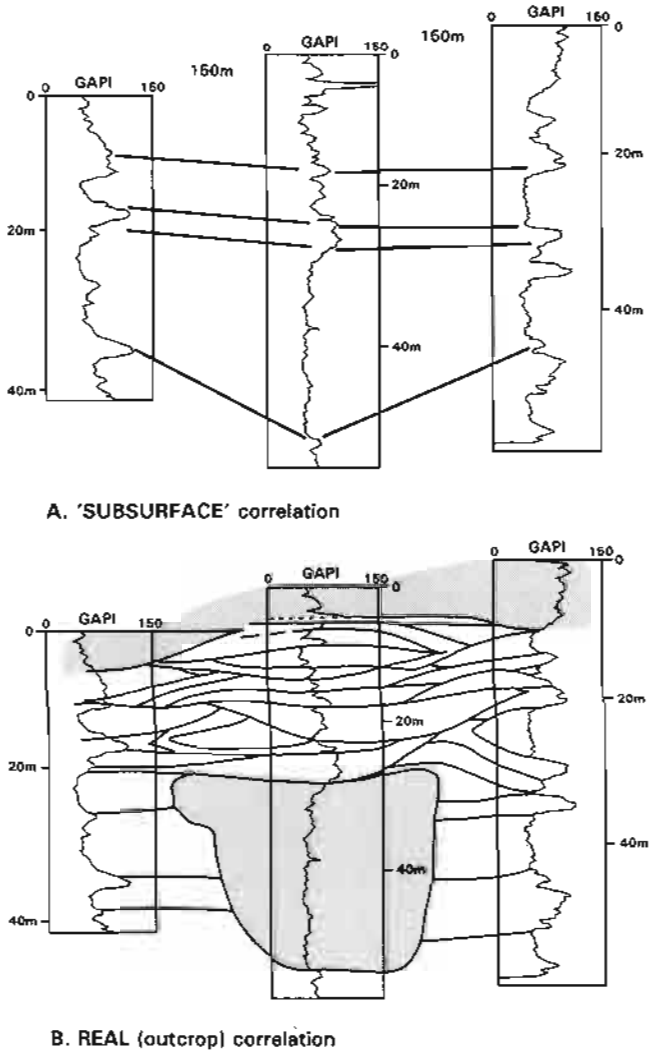


**Figure 15.22** The limitations of subsurface correlation illustrated by gamma ray profiles measured in sands and shales along a quarry wall. A. expected correlations from using gamma ray curves alone. B. The real correlations based on actually following beds along the outcrop (from Slatt *et al.*, 1992).

been horizontal at the time of deposition. Coals, for example are originally flat, so generally are transgressive surfaces: condensed sequences and flooding surfaces may not be. The ultimate choice is probably a matter of trial and error (*see also* Section 15.2).

### *Correlation and seismic*

Why is there a need to say that the seismic should be used in well correlations whenever possible? Even now, even with all the seismic available, it must still be said: seismic should be used in well correlation. The geophysicist cannot do his work without using the logs to 'tie' the picked horizons. The same is not true for the geologist. He will not automatically be asked about the seismic control for his correlation: he should be. In fact, log correlation and seismic mapping should be undertaken together; the approach must be iterative. Examining the mapped seismic horizons before completing a correlation will indicate whether such a correlation is compatible with the mapping or not. The example illustrated previously (Figure 15.15) is excellent and speaks for itself.

### *Computer aided correlation*

Considerable effort over the years has been devoted to finding a method to allow logs to be correlated automatically by computer (*see* Doveton, 1994 for review). The results have generally not produced helpful tools. Correlation inevitably involves gaps and breaks, changes in thickness and changes in facies. Correlation techniques used in dipmeter processing (Chapter 12), are based on the expectation of finding an exactly similar match, and are therefore unsatisfactory for stratigraphic correlation.

A more rewarding approach is found in sequence matching, in which a well is divided into a number of units manually or by computer, and the well to be correlated is checked to see if such a unit is present and its degree of matching (Fang *et al.*, 1992). With such a method the similarities of a number of logs or attributes may be checked, absence is a possibility and thickness similarity becomes only one of the attributes, not the dominant one (Figure 15.25). Thus, values can be given to a correlation which then becomes objective (within the limits of the method or the software).

Conceptually, a method in which computer decisions can be evaluated is more attractive than a computer correlation which is 'take it or leave it'. This chapter describes how thoughtful correlation must be in terms of, for instance, sequence stratigraphy, interactive log response exploration and biostratigraphy. Without being able to include such ideas, computer correlation will be, as is the case at present, disregarded. However, if a programme allows the similarities of two intervals to be compared, interest will be re kindled. If, moreover, this facility can be applied on the screen while a correlation panel is being prepared, it will be very useful.

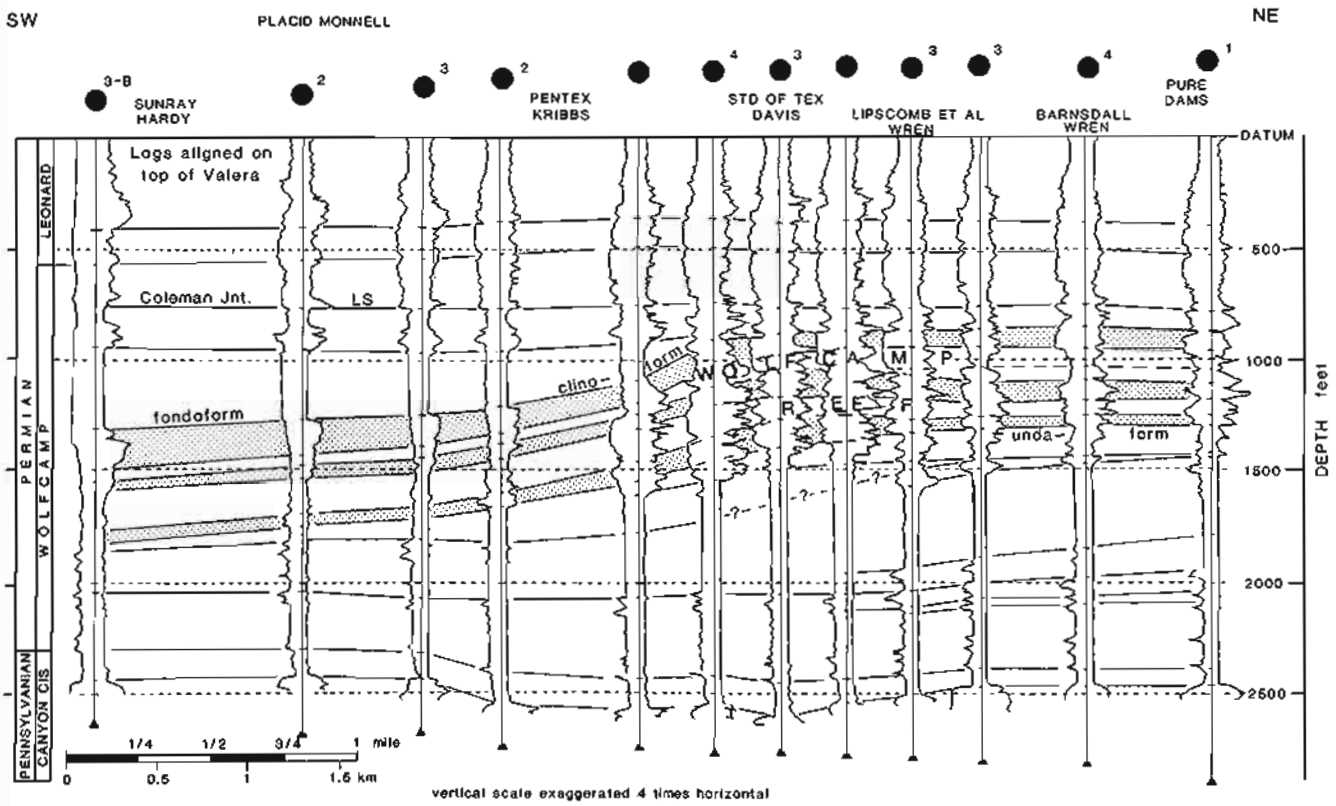


**Figure 15.23** Correlation and palaeotopography in the Permian of West Texas. Logs – SP to the left, electrical survey to the right. (Re-drawn from Van Siclen, 1958).

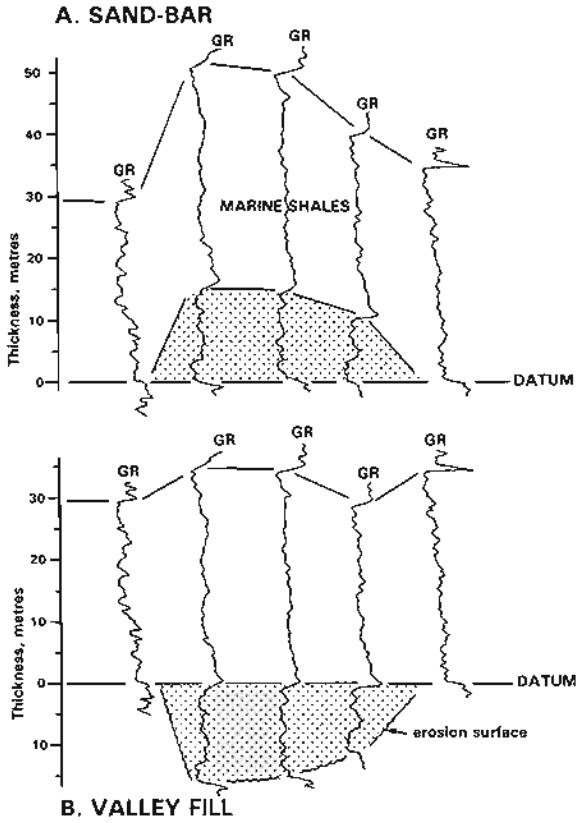


**Figure 15.24** The importance of choice of datum. If the base of the sand is taken as a datum, A., a sand bar is interpreted (unlikely). If the flooding surface at the top of the sand is taken, B., valley-fill is interpreted and the covering sequence shows a constant thickness.

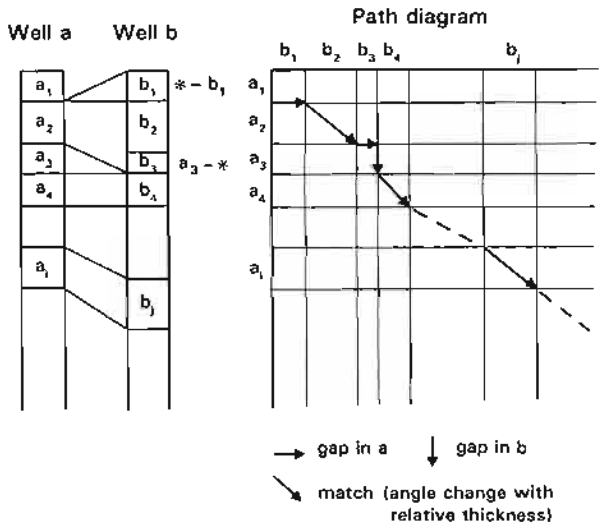


**Figure 15.25** Computer correlation. Schematic illustration of the sequence matching technique (re-drawn from Fang *et al.*, 1992).

An entirely different approach is to use the computer, not for the actual correlation procedure, but to create a new format which is more easily correlated. Modern software allows standard single curve logs to be plotted as a colour image or rather, a colour 'bar code' (Figure 13.1). With such a presentation, the eye has a much greater facility for comparison. The example shows gamma ray logs from eight closely spaced wells in a producing field, formatted as colour images rather than typical curves (Figure 15.26). The eye is able to follow a greater amount of detail than is possible with only the curves.

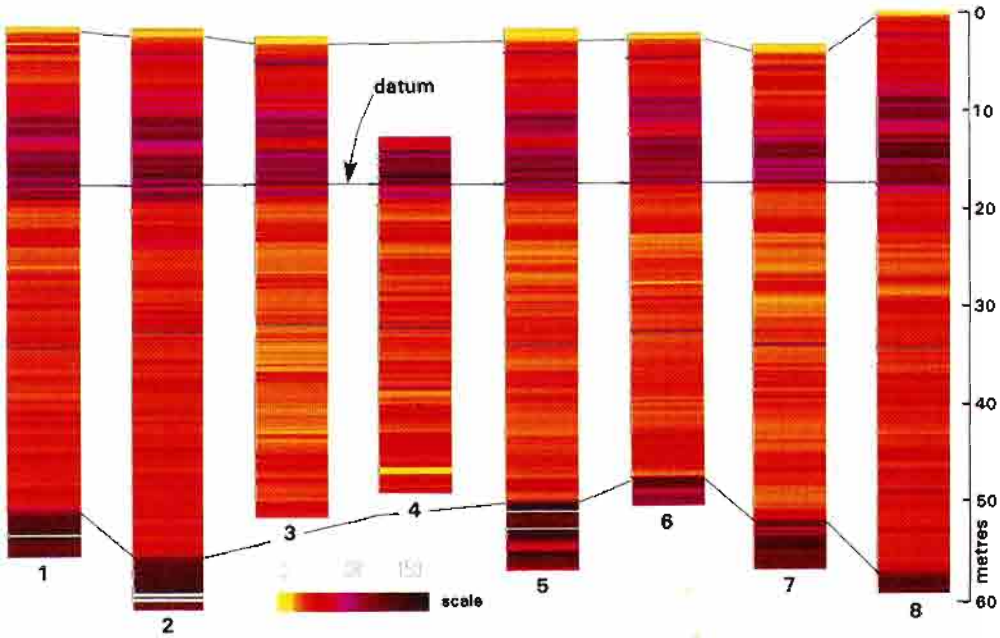


**Figure 15.26** Gamma ray logs plotted as colour images allowing a better visual correlation. The gamma ray scale has been normalised and the 8 wells are closely spaced (imaging routine from GeoScene software).

But of course careful normalisation and preparation are required, especially with gamma ray logs. The curves themselves may also be added to this format if required.

## 15.5 Conclusions

The subject of sequence stratigraphy dominates this chapter. It is only correct. Now that stratigraphy, sedimentology and the seismic are so closely linked, big advances are being made in each dis cipline in separate ways. As far as the logs are concerned, the chapter has tried to show their role as the common database. More than just a tool for other specialists, the logs form a geological dataset in their own right: that is important. More important still is the possibility of using modern computer methods in their analysis, a possibility not yet properly exploited.

# 16
# CONCLUDING REMARKS

## 16.1 The book of revelations

Sentences end with a full stop: scientific books end with a conclusion. But a book on wireline logging can have no conclusion. The technique is dramatically active and rapidly evolving. There are, nevertheless, strands to be pulled together and comments to be made. As an author's privilege, this last chapter is personal and idiosyncratic. In it are comments on what is happening at present and some ideas on what may happen in the near future. It is good to know where you are going but it is essential to know, in the first place, where you are!

I have just returned from the 36th annual SPWLA (Society of Professional Well Log Analysts) logging symposium in Paris. It was very pleasant. However, the conference keynote speaker complained that while most oilfield costs were dropping, logging costs were climbing, to reach even 20% of total well budget. Does this mean that we should cut down on logging? Any article bought should be assessed from two viewpoints: is it needed and is it worth the money? Are logs needed? Certainly, yes. Are they really worth the money? The answer must be no. They cost too much for *the way in which they are presently used.* We should not cut down on the logs run, we should use them better, and demonstrably so. Many times I find that the geological use of the formidable amount of data that logs provide is not properly employing new technology. It is falling further and further behind other disciplines. The data are not being used, the techniques are not being used. The water of progress is rushing past the geologist to make its own, confident course. This is a disappointment.

This final chapter is not written to express disappointment. Quite the reverse. It is written with the active future in mind. How to harness the new technologies: how to use all this formidable data. Those old ideas, those dusty shelves of old books, those inherited habits, must be by-passed. Discoveries lie in the new technologies. Let me illustrate in practice what I mean by looking at four things: how we look at outcrops; how new tools are changing ideas; how image logs are developing; and the software glut.

## 16.2 Outcrop bound

As the sophistication of logging tools and software advances, we are having more and more difficulty relating what the tools detect with what we observe in core and at outcrop. We have always assumed that the outcrop was the norm, the standard to which we refer: that the way a geologist defines lithology in the field was the correct way and that any work should be referred to it. But the new logging tools describe formations, albeit differently, in far greater detail and with more precision than a geologist is able to do with traditional outcrop descriptions. New detection methods must surely push the outcrop-bound geologist into thinking, not in terms of eye and touch, but in terms of the senses extended by technology. In many sciences this is a conscious move. It will become more and more the necessity for oilfield outcrop analogues.

Using portable gamma ray detectors to collect outcrop information comparable to subsurface data is a beginning to this process. The technique has been illustrated for lithological use and lithostatigraphic correlation of outcrop to the subsurface (Chapters 7 and 15). The example illustrated here is more subtle (Davies and Elliott, 1996). It shows spectral gamma ray logs acquired specifically to recognise important (key) sequence stratigraphic surfaces (Figure 16.1). There is an implicit realisation that geophysical sensing must be used to extend the unaided senses. Geologists are often amazed to find that distinctive subsurface log markers, and this includes gamma ray spikes, are not immediately identifiable when seen in cores. The same occurs at outcrop: the eye alone is not sufficient.

Taking a subsurface tool to measure the outcrop is the first step. What must also be done is to make geologically significant analyses, chemical, geochemical, physical, petrophysical, and compare these to the geophysical log measurements. Such direct sample analysis is routine with core. What can be done with core can be done at outcrop: and better. But, as the case below illustrates, the best examples of this are still with core data.

Detailed analyses of carbon isotope ratios ($\delta^{13}C$), made routinely in DSDP/ODP cores from very widely spread, deep oceanic sites, show remarkable similarities over the Palaeocene-Eocene boundary interval, between 50Ma–65Ma (Corfield and Norris, 1996) (Figure 16.2). These and other isotope changes can be interpreted as indicating long term, world-wide, oceanic water temperature changes. Superimposed on the slower changes, is a well documented, very short term $\delta^{13}C$ effect which, it is suggested, indicates that surface water temperatures rose by up to 4°– 6°, and then cooled, over a period of only thousands of years (<50 kyr) (especially in mid-high latitudes). This excursion is associated with a very unusual extinction of deep sea benthic foraminifera (Thomas and Shackleton, 1996).

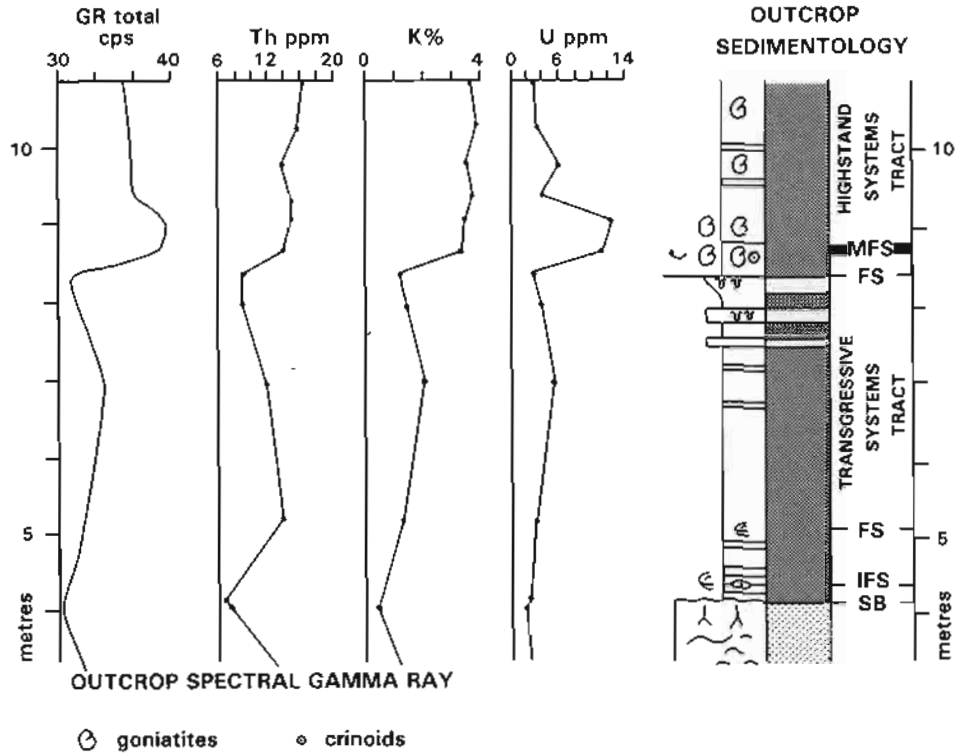


**Figure 16.1** Outcrop spectral gamma ray profile of key sequence stratigraphic surfaces including an important maximum flooding surface (MFS). Carboniferous (Namurian), Western Ireland. SB = sequence boundary. IFS = initial flooding surface. FS = flooding surface (data from S .Davies, modified from Davies and Elliott, 1996).

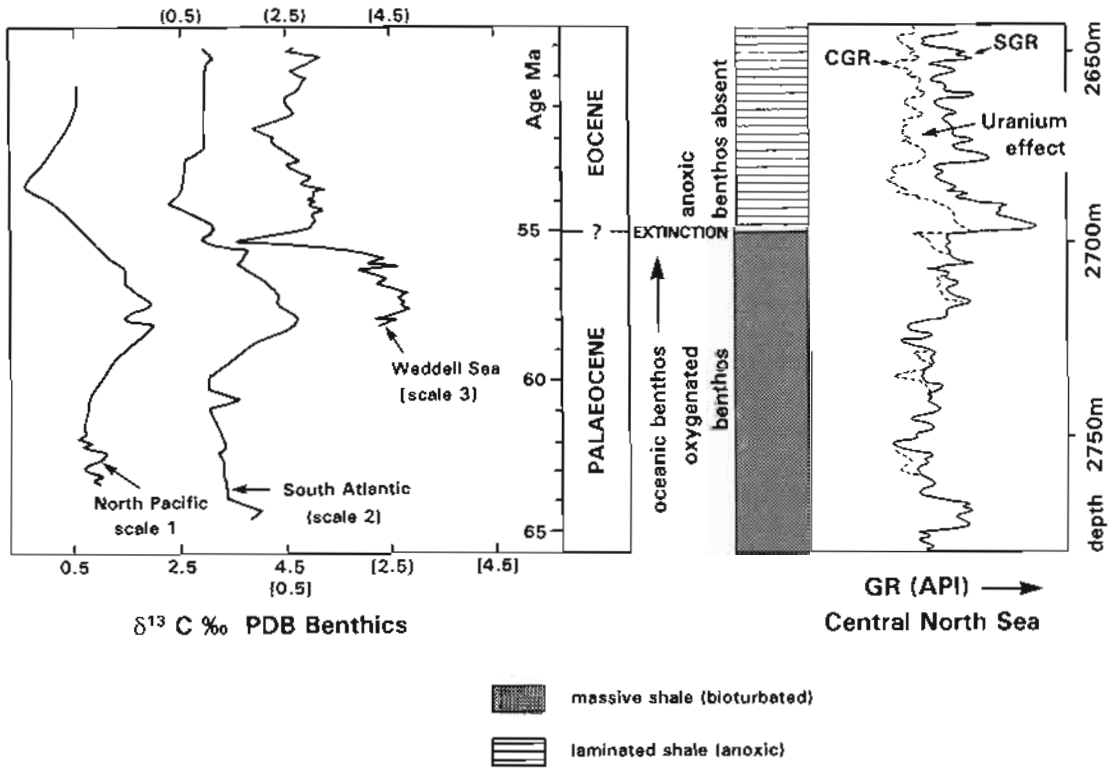


**Figure 16.2** The Palaeocene-Eocene boundary: carbon isotope values in deep ocean cores of the North Pacific (Shatsky Rise), South Atlantic (Walvis Ridge) and Weddell Sea (Maude Rise) compared to gamma ray logs from a well in the Central North Sea basin. *See text* for discussion (modified from Corfield and Norris, 1996 for isotopes and O'Connor and Walker, 1993 for well logs).

Well logs measured in deep water shales over the same late Palaeocene to Early Eocene interval in the North Sea show some remarkable changes in the uranium content measured by the spectral gamma ray logs (NGT) (Figure 16.2). Benthic fauna and bioturbation are abundant in the lower shale formation (Palaeocene) which has essentially no uranium indicated on the NGT. The overlying shales (Eocene?) have no benthos and no bioturbation (anoxic), are well laminated and contain significant uranium. Their base is abrupt and marked by a distinct gamma ray and uranium peak (O'Connor and Walker, 1993; Knox, 1996). Is this the oceanic event? Are the logs giving us, albeit indirectly, information of global ocean temperatures?

Clearly, to reply to the question, the sections with $\delta^{13}C$ isotope analyses must be measured for uranium response. But with the $\delta^{13}C$ analyses and the geophysical logs, interpretation can be extended beyond the possibilities of visual analysis alone. That outcrop may be tied into the now huge subsurface well database on equal terms, is tremendous.

## 16.3 Petrophysics is dead, long live petrophysics!

Wireline logs are not run for geological reasons: they are run on the instructions of the petrophysicist. They are run to be able to detect and to quantify the volume of hydrocarbons in a well, from which investment returns can be calculated. All the geologist can do is pick up the logging crumbs from the petrophysicist's table. However, there is no reason why the petrophysicist's goals and the geologist's should always be different, and indeed, because of the new logging tools, the two are approaching each other. Geological models must serve a quantitative purpose: petrophysical calculations need a geological basis.

Petrophysics depends on compromise. The amount of hydrocarbons in a formation, the quantity required, is not *directly* given by any log measurement, so that the petrophysicist must make use of 'best guess' formulae. However, new tools are getting much closer to the required measurement. As this happens, the measured parameters become more and more geological and the petrophysicist needs geological concepts to best use them. The data from the new generation of *NMR (nuclear magnetic resonance) tools are an example.

The new NMR tool measures the effect that an oscillating radio-frequency, working in a large, induced static magnetic field, has on the spin of hydrogen nuclei (Coates *et al.*, 1993). The measurement produces a pulse-echo relaxation spectrum, T2, which is influenced only by the hydrogen nuclei in free water (or hydrocarbons) in the formation: hydrogen nuclei combined in the matrix, shale or in bound water, are not detected. The tool measurements do not produce a directly interpretable log, but the pulse-echo spectrum of relaxation times can be successfully modelled and analysed to give a number of key petrophysical parameters. At present these include the total liquid filled porosity (from the magnitude of the NMR response), the pore size distribution (from the relaxation spectrum shape), the moveable fluids or FFI (free fluid index) (from cut-offs applied to the relaxation spectrum) and the permeability (from the FFI and pore distribution data).

Example NMR results are illustrated by a set of measurements made on carbonate plug samples in the laboratory (Chang *et al.*, 1994) (Figure 16.3). The laboratory tools and techniques are similar to those used in the subsurface NMR. The carbonates show a mixture of vuggy porosity and intergranular or matrix porosity. Vugs are large but generally unconnected or only partially connected. Matrix and intergranular pores are connected but mostly of small volume. This difference is well seen in the comparison between sample 43, with fine grained but connected matrix porosity, and sample 44 with a similar porosity, but principally unconnected in vugs (Figure 16.3). The vuggy sample has a much lower permeability. The picture is continued when sample 22, a vuggy limestone with slightly higher porosity but low permeability, is contrasted to sample 39, which is a grainstone, which has slightly higher porosity but very much greater permeability. The pores in the grainstone are quite large (the long T2 peak showing large intergranular pores and not vugs), and clearly interconnecting (Figure 16.3).

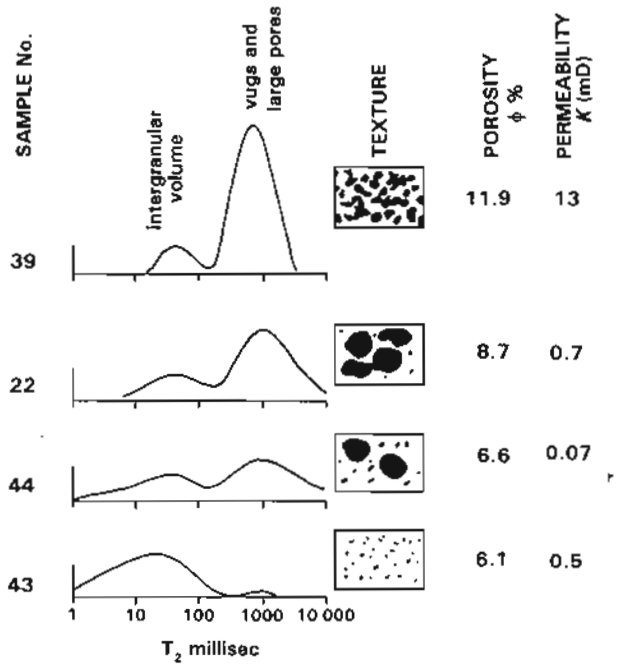


**Figure 16.3** Nuclear magnetic resonance (NMR) T2 relaxation spectrum responses in carbonates, showing the response relationship to pore volume distribution, porosity and permeability. Data from laboratory studies on West Texas carbonates (modified from Chang *et al.*, 1994).

*NMR is now called MRIL (Magnetic Resonance Imaging Logging) by Numar, who revolutionised the logging technique, to avoid using nuclear which 'sounds' radioactive.

This directly measured textural information is essential to the petrophysicist, but so are the geological associations. The tool identifies pore size distributions which can be interpreted in terms of porosity and permeability: it is geological analysis that recognises grainstones as opposed to vuggy limestones, facies effects as opposed to diagenetic effects. The data set becomes common ground for both the petrophysicist and the geologist, to the mutual benefit of both. 'Best guess' petrophysical formulae will not be required once direct measurements, such as these from the NMR, become available. The directly measured characteristics will, importantly, require a geological context.

## 16.4 An image of the future

Image logging technology is in its infancy. But even so the information that the logs contain is amazing. The first reaction of oil industry users has stopped at the amazement. But the service company developers are pushing ahead with both new tools and new software. They seem to have a clear idea of what they want; much more so than users. First some comments on the tools themselves.

One important aspect of the present imaging tools is that most of them make measurements on the immediate borehole wall (Chapter 13). Such tools are strongly influenced by borehole damage, some more than others, but all receive signals from the potentially drill modified zone. Shallow, drilling induced fractures, for example, when imaged at the borehole wall surface, are difficult to differentiate from fully penetrating natural fractures (Chapter 13). Imaging tools do now exist, however, in which the measured signals are received from deeper in the formation. The ARI (azimuthal resistivity imager) of Schlumberger is such a tool, having 12 electrodes spaced around the circumference of the sonde and with a depth of investigation similar to that of the deep laterolog. The 12 resistivity measurements can be processed into an image in the same way as for other imaging logs, although the pixels are much coarser. The signal however, is from beyond drilling damage, potentially, for example, beyond drilling induced fractures.

The implications of this tool for imaging logs in general are indeed interesting. Recent logging developments have seen two branches: the imaging branch, in which multiple sensors give a flat, but oriented set of readings from around the borehole and the other branch, also imaged, in which multiple sensors have different depths of investigation but are not oriented. Combining these two branches will give us full borehole coverage with multiple depths of investigation. We shall then be able to investigate a 'virtual' volume around the borehole. Indeed with the advent of tools such as the ARI and considering the present expertise in software, such images are not too far distant (Figure 16.4). The achievements are remarkable.

The standard, generally used techniques for image log interpretation are described in Chapter 13. From this it is evident that qualitative techniques are more happily used

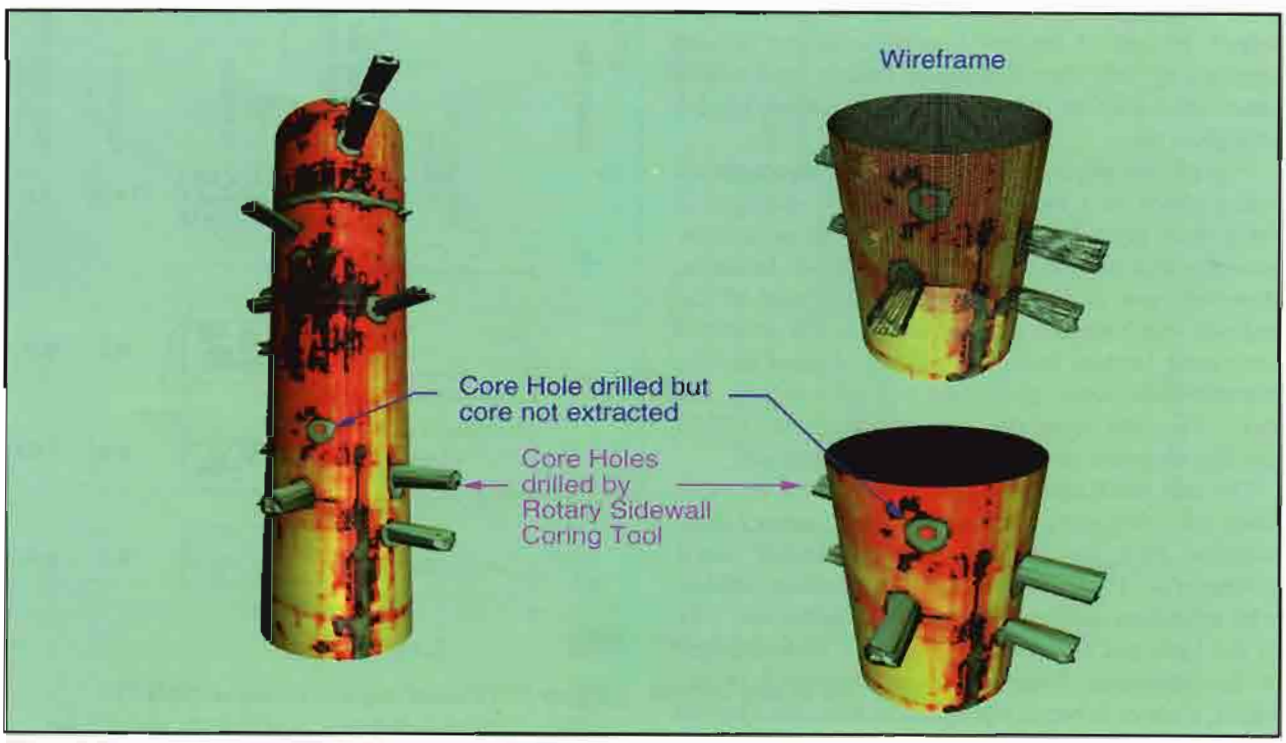


**Figure 16.4** Impressive 3-D images from a CAST (Halliburton) acoustic imaging tool of the borehole wall with holes cut in it by a rotary sidewall tool (data from D. Seiler, from Seiler, 1995).

at present than quantitative. This will necessarily change. The biological, astronomical and remote sensing sciences have long possessed imaging and have developed an array of image analysis techniques. These work on the images themselves. They enhance, modify and extract certain attributes. In image log analysis this is just beginning. For example, extracting dip from images is familiar. But techniques for extracting attributes indicative of thin beds, of fractures and even grain size and permeability, are being tentatively tried (Sullivan and Schepel, 1995). There is no reason why more geological attributes should not be extracted: facies, structures, sequences, and these will be quantitative attributes: the software will be new.

## 16.5 A rainforest of software

No one wants the rainforests to be cut down: but it is happening. No one wants to throw away software: but they should. Software comes in many guises: indispensable, useful, infuriating, fancy, pretty, pretty useless and unnecessarily expensive. 5% for the first: 40%? for the second: certainly 80% for the last. Let's look at software. There are essentially two categories, the first is signal processing software, the second is interpretation software.

An example of the first category is the software used to produce the output from the NMR tool discussed above. Interpretable information is only produced from the processed raw tool responses: there is a software interface between the raw data and the interpretable information. As tools become more sophisticated, they become more dependent on such software for signal processing. Indeed, this has been demonstrated with the dipmeter (Chapter 12), where the raw data (the microresistivity curves) are uninterpretable until processed into dip tadpoles. The dipmeter also shows that it is necessary to be familiar with at least some aspects of the signal processing in order to make a proper interpretation of the software produced results. The use to which the results will be put should influence the processing, whether this be for geological or petrophysical purposes. The current problem for both geologist and log analyst alike is to keep up with developments.

The second category is software which aids interpretation. While the influence of geological purpose on signal processing software is small, the influence can be dominant in interpretation software (should be dominant). This point was made, again, with dipmeter interpretation: dipmeter manipulation software should be designed with geological ends in mind (Chapter 12). The problem at present is that much geological software is written by software writers and undirected by geological needs. There are many 'feature rich' packages in which the routines dreamed up by the software writers are very impressive, but in practical terms, useless. Many simple routines which would be useful have not been written.

An exception, and notable for that, is time series analysis of log traces. This type of analysis treats a log as a geological record, containing therefore, a time element

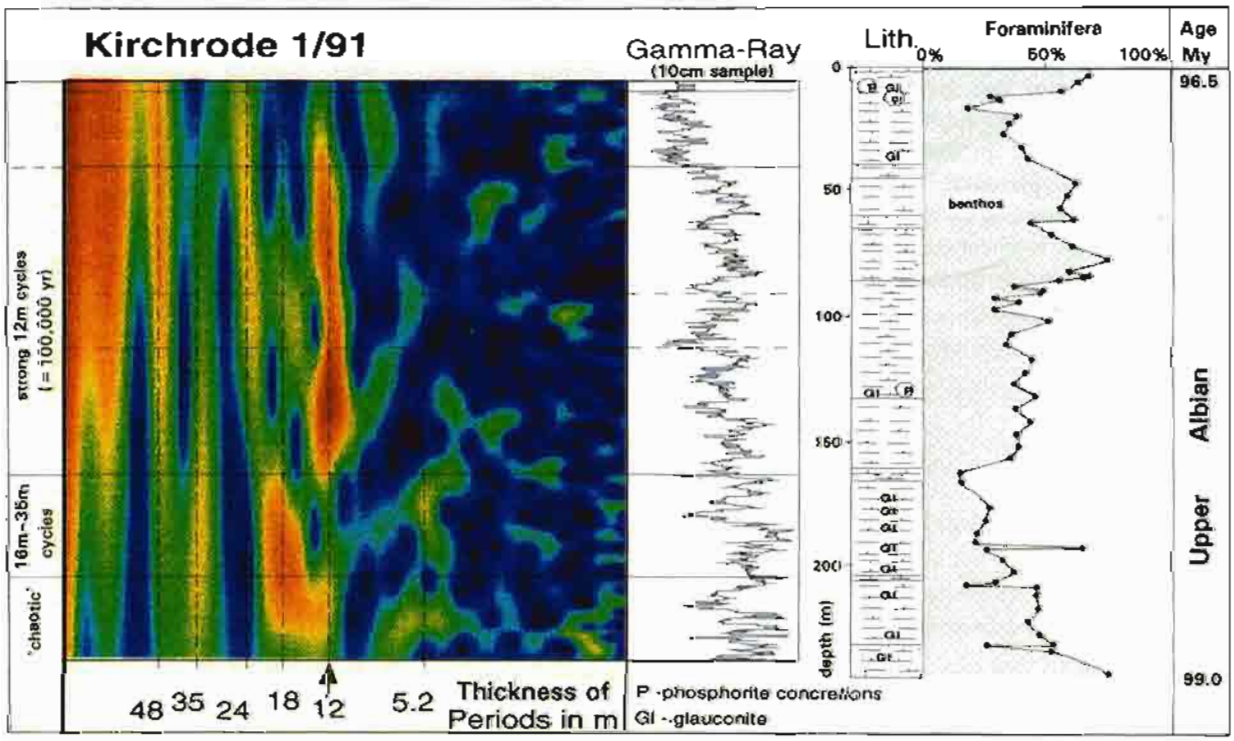


**Figure 16.5** Wavelet-spectrogram representation of a gamma ray log processed using a wavelet-transform method to bring out cyclicity. The section from 35m-163m shows well developed 12m thick cycles associated with a 100,000 year eccentricity period. Upper Albian marls, North Germany. Sedimentation rate from biostratigraphy, about 10cm/1000yrs (gamma ray data from J. Thurow, biostratigraphy from BCCP Group, 1994).

(for a good description of time series analysis *see* Doveton, 1994). By using spectral analysis techniques on a log trace, an attempt is made to mathematically extract the dominant scales of time dependent cyclicity, which are generally in the Milankovitch frequency band of 10,000–100,000 years (Moline and Ogg, 1990). The methods are especially suited, for the moment, to fine grained detrital sediments deposited in environments where the sediment record is essentially complete and sedimentation rates constant. The example shown is of an interval of Cretaceous (upper Albian) marl from a cored, shallow borehole in northern Germany (Kirchrode 1/91) with quite fast sedimentation rates (10cm/1000yrs) and representing 2.5 million years (from biostratigraphic dating, BCCP Group, 1994). The gamma ray log of the interval has been processed by wavelet-transform using variable 'windows' (Prokoph and Thurow, 1995) and re-displayed as a wavelet-scalogram (Figure 16.5). The plot makes identifiable the thickness (wave-length) of evident cycles which, if the sedimentation rate is known, can be given a time score. For example, the strong, 12m thick period seen between 35m–163m can be equated with a 100,000 year eccentricity cycle (based on sedimentation rates of 10cm/1000yrs). This strongly cyclic section is interpreted from biostratigraphic work to have been deposited during a sea level highstand (indicated by the foraminiferal analyses) when global rather than local influences were dominant (BCCP Group, 1994). Clearly, such a quantitative analysis of a log trace leads to far greater and more reliable interpretation possibilities than a simple, casual, qualitative inspection.

Despite this example, software which treats the purely geological aspects of logs is being left behind by the considerable advances in software designed to improve tool response, signal processing and petrophysical modelling and interpretation. What a geologist can do with his log data depends on the software that he has at his disposal. At the moment this is limited. There is a lot of progress to be made in the right direction, but the possibilities are enormous.

## 16.6 But is it geology?

At that same SPWLA meeting in Paris mentioned at the beginning of this chapter, there was an old French lady, quite tall, sprightly and speaking perfect English. She remembered as a little girl going with her father to the basement of the École des Mines in Paris to see some of his strange machines, all wires and coils and tubes. As the younger daughter of Conrad Schlumberger, she could never have imagined that her father would create within her lifetime, with his brother Marcel and friend Henri Doll, the company that is Schlumberger and the now very sophisticated technique of well logging. Predicting the future it seems, is of significantly less use than having confidence in the present.

The genius of the Schlumberger brothers and Henri Doll was involved in a field of its own making. Now the field has many workers, many contributors. But that does not mean that it has developed beyond invention. Charting the introduction of new logging tools year by year shows an interesting picture. From the early days in the 1920s to about the late 1970s there was a progressively steepening climb with many new inventions. A plateau occurred from the late 70s to the mid 80s with little that was new. The oil crisis intervened. Then there was another steep rise, so that at present, the rate of introduction of new tools is bewildering.

Again that SPWLA meeting. In the exhibition halls, most of the large computer screens belonging to the service companies had log generated images on them. Geological images. But how many *geologists* were there to see? Too few. And yet here is a huge bank of subsurface geological data, in detail never dreamed of by the Schlumberger brothers: and from a range of sensors they could only have hoped for. But of course it all needs interpreting, and this demands computers, applicable software, new ideas and a brave mind. The geological hammer is past: it isn't necessary to hit things anymore to understand them. A geologist today is only as good as his software.

But it *is* still geology.

# APPENDIX

## Logging Tool Mnemonics (only some!)

(*) Western Atlas mnemonics are only given where they are different from Schlumberger mnemonics or the tool is different.

| TYPE | SCHLUMBERGER | | WESTERN ATLAS (*) | |
|---|---|---|---|---|
| **RESISTIVITY LOGGING** | DIL | Dual Induction Log | DIFL | Dual Induction Focused Log |
| | DLL | Dual Laterolog | | |
| | SFL | Spherically Focused Log | | |
| | ISF | Induction Spherically Focused | | |
| | IES | Induction Electrical Survey | IEL | Induction Electrolog |
| | DIT-E | Phasor Induction | DPIL | Dual Phasor Induction |
| | AIT | Array Induction Log Imager | | |
| | ARI | Azimuthal Resistivity Imager | | |
| | | | TBRT | Thin Bed Resistivity Tool |
| **MICRO RESISTIVITY LOGGING** | ML | Microlog | ML | Minilog |
| | MLL | Microlaterolog | | |
| | PML | Proximity Log | PROX | Proximity Log |
| | MSFL | Micro Sperically Focused Log | | |
| | EPT | Electromagnetic Propagation Time Log | | |
| **ELECTRICAL** | SP | Self Potential (not company specific) | | |
| **SONIC LOGGING** | BHC | Borehole Compensated Sonic | AC | Acoustilog Borehole Compensated |
| | LSS | Long Spaced Sonic | ACL | Acoustilog Long Spaced |
| | ASL | Array Sonic | DAC | Digital Array Acoustilog |
| | DSI | Dipole Sonic Imager | MAC | Multipole Acoustic Tool |
| **NUCLEAR** | GR | Gamma Ray | | |
| | NGS = (NGT) | Natural Gamma Ray Spectroscopy (tool) | SL | Spectralog |
| | FDC | Formation Density Compensated | CDL | Compensated Densilog |
| | LDL (LDT) | Litho-Density Log (tool) | ZDL | Compensated Z-Densilog |
| | CNL | Compensated Neutron Log | CN | Compensated Neutron |
| | SNP | Sidewall Neutron Porosity | N-EN | Sidewall Epithermal Neutron |
| **MAGNETIC** | NMR | Nuclear Magnetic Resonance (not company specific) | | |
| | MRIL | Magnetic Resonance Imaging Log (Numar name for NMR) | | |

| TYPE | SCHLUMBERGER | | WESTERN ATLAS (*) | |
|---|---|---|---|---|
| **CALIPER & DIRECTIONAL** | CAL | Caliper | | |
| | BGL | Borehole Geometry | 4CAL | Dual Caliper |
| **DIPMETER** | HDT | High Resolution Dipmeter Tool | DIP | 4-Arm Dipmeter (Diplog) |
| | SHDT | Stratigraphic High Resolution Dipmeter Tool | | |
| | OBDT | Oil-Based Dipmeter Tool | | |
| | | | HDIP | 6-Arm Dipmeter (Hex dip) |
| **BOREHOLE IMAGING** | | | | |
| **ELECTRICAL** | FMS | Formation Micro-Scanner | | |
| | FMI | Fullbore Formation MicroImager | | |
| **ACOUSTIC** | BHTV | Borehole Televiewer (general term not company specific) | | |
| | UBI | Ultrasonic Borehole Imager | CBIL | Circumferential Borehole Imaging Log |
| **COMBINED** | | | STAR | Simultaneous Acoustic & Resistivity Borehole Imager (CBIL + HDIP) |

**MISCELLANEOUS MNEMONICS**

| | |
|---|---|
| BS | Bit Size |
| TD | Total Depth |
| MSL | Mean Sea Level |
| TVD | True Vertical Depth |
| MD | Measured Depth |
| RT | Rotary Table |
| KB | Kelly Bushing |
| BHT | Bottom Hole Temperature |
| MWD | Measurement While Drilling |
| LWD | Logging While Drilling |
| TTI (ITT) | Integrated Travel Time |
| PEF | Photoelectric Factor |
| HI | Hydrogen Index |
| API | American Petroleum Institute (*also* API unit for GR) |

# REFERENCES


Adams, J.A. and Weaver, C.E. (1958) Thorium-uranium ratios as indicators of sedimentary processes: example of concept of geochemical facies, *Bull. Am. Assoc. Petrol. Geol.* **42**(2), 387-430.

Adams, J.T., Ayodele, J.K., Bedford, J., Kaars-Sijpesteijn, C.H. and Watts, N.L. (1992) Application of dipmeter data in structural interpretation, Niger Delta. In: *Geological applications of well logs II*, eds. Hurst, A., Griffiths, C.M. and Worthington, P.F. Geol. Soc. London Sp. Pub. **65**, 247-264.

Allaud, L. and Martin, M. (1976) *Schlumberger, histoire d'une technique*. Berger-Levrault, Paris.

Allen, D.F. and Jacobsen, S.J. (1987) Resistivity profiling with a multi-frequency induction sonde. *SPWLA 19th Ann. Symp. Trans.*, Paper F, 1-9.

Alm, P.G. (1992) The temperature decay log: a different approach to presenting a temperature survey. In: *Geological applications of well logs II*, eds. Hurst, A., Griffiths, C.M. and Worthington, P.F. Geol. Soc. London Sp. Pub. **65**, 339-348.

Anderson, B. and Chew, W.C. (1985) SFL interpretation using high speed synthetic computer generated logs. *SPWLA 26th Ann. Symp. Trans.*, Paper K, 1-17.

Anxionnaz, H., Delfiner, P. and Delhomme, J.P. (1990) Computer-generated corelike descriptions from open-hole logs. *Bull. Am. Assoc. Petrol. Geol.* **74** No. 4, 375-393.

Archie, C.E. (1950) Introduction to petrophysics of reservoir rocks. *Bull. Am. Assoc. Petrol. Geol.* **34**(5), 943-961.

Archie, G. (1942) The electrical resistivity log as an aid in determin ing some reservoir characteristics. *Trans. AIME*, **146**, 54-62.

Asquith, G. and Gibson, C. (1982) Basic well log analysis for geologists. Am. Assoc. Petrol. Geol., Tulsa, *Methods in Exploration Ser.* **216**.

Atlas Wireline Services (1992) Digital Circumferential Borehole Imaging Log (CBIL) *tool brochure*. Western Atlas International.

Baldwin, J.L., Bateman, R.M. and Wheatley, C.L. (1990) Application of a neural network to the problem of mineral identification from well logs. *Log Analyst*, **31** No. 5, 279-293.

Barton, C.A. and Moos, D. (1988) Analysis of macroscopic fractures in the Cajon Pass scientific drillhole over the interval 1829-2115 meters. *Geophys. Res. Let.* **15**, No. 9, 1013-1016.

Baum, G.R and Vail, P.R. (1988) Sequence stratigraphic concepts applied to Palaeogene outcrops, Gulf Atlantic basins In: *Sea-level changes: an integrated approach*. eds. Wilgus, C.K., Hastings, B.S., Kendall, C.G.St.C., Posamentier, H.W., Ross, C.A. and Van Wagoner, J.C. *S.E.P.M Sp. Pub.* **42**, 309-327.

BCCP-Group (1994) The upper Albian of northern Germany: results from the Kirchrode I/91 borehole, boreal Cretaceous cycles project (BCCP). *Zbl. Geol. Paläont. Teil I*, **H.7/8**, 809-822.

Belknap, W.B., Dewan, J.T., Kirkpatrick, C.V., Mott, W.E., Pearson, A.J. and Rabson, W.R. (1959) Calibration facility for nuclear logs. *Drill and Prod. Prac. API*, 289-317.

Bell, J.S. and Gough, D.I. (1979) Northeast-southwest compressive stress in Alberta – evidence from oil wells. *Earth and Planetary Science Letters* **45**, 475-482.

Bell, J.S. (1990) Investigating stress regimes in sedimentary basins using information from oil industry wireline logs and drilling records. In: *Geological applications of wireline logs.*, eds. Hurst, A., Lovell, M., Morton, A., *Geol. Soc. London Spec. Publ.* **48**, 305-325.

Bengtson, C.A. (1980) Structural uses of tangent diagrams. *Geology*, **8**, 599-602.

Bengtson, C.A. (1981) Statistical curvature analysis techniques for structural interpretation of dipmeter data. *Bull. Am. Assoc. Petrol. Geol.* **65**, 312-332.

Bengtson, C.A. (1982) Structural and stratigraphic use of dip profiles in petroleum exploration. In: *The deliberate search for the subtle trap. Bull. Am. Asoc. Petrol. Geol. Memoir* **32**, ed. Halbouty, M.T. 31-45.

Benoit, W.R., Sethi, D.K., Fertl, W.H. and Mathews, M. (1980) Geothermal well log analysis at Desert Peak, Nevada. *SPWLA 21st Ann. Symp. Trans.*, paper AA, 1-41.

Berg, R.R. and Avery, A.H. (1995) Sealing properties of Tertiary growth faults, Texas Gulf Coast. *Bull. Am. Assoc. Petrol. Geol.* **79**, No. 3, 375-393.

Bhattacharya, J.P. (1993) The expression and interpretation of marine flooding surfaces and erosional surfaces in core: examples from the Upper Cretaceous Dunvegan Formation, Alberta foreland basin, Canada. In: *Sequence stratigraphy and facies associations*, eds. Posamentier, H.W., Summerhays, C.P., Haq, B.U., Allen, G.P. *IAS Spec. Publ.* **18**, 125-160.

Bigelow, E.L. (1985) Making more intelligent use of log derived dip information. *Log Analyst*, **26**, Parts 1-5.

Bjørlykke, K., Dypvik, H. and Finstad, K.G. (1975) The Kimmeridge shale, its composition and radioactivity. *NFP Jurassic Northern N. Sea Symp., Stavanger*, Paper 12, 1-20.

Blackbourn, G.A. (1990) *Cores and Core Logging*. Whittles Publishing.

Blakeman, E.R. (1982) A case study of the effect of shale alteration on sonic transit times. *SPWLA 23rd Ann. Symp. Trans.*, paper II, 1-14.

Block, L.V., Cheng, C.H. and Duckworth, G.L. (1991) Velocity analysis of multi-receiver full waveform acoustic log data in open and cased holes. *Log Analyst* **32**, No. 3, 188-200.

Bourke, L.T. (1989) Recognising artefact images on the Formation MicroScanner. *SPWLA 30th Ann. Symp. Trans.*, Paper WW, 1-25.

Bourke, L.T. (1992) Sedimentological borehole image analysis in clastic rocks: a systematic approach to interpretation. In: *Geological applications of wireline logs II.*, eds. Hurst, A., Griffiths, C.M., and Worthington, P.F. *Geol. Soc. London Spec. Publ.* **65**, 31-42.

Bourke, L.T., Corbin, N., Buck, S.G. and Hudson, G. (1993) Permeability images: a new technique for enhanced reservoir characterisation. In: *Advances in reservoir geology*. Ed. Ashton, M., *Geol. Soc. London Sp. Pub.* **66**, 219-232.

Boyeldieu, C., Coblentz, A. and Pelissier-Combescure, J. (1984) Formation evaluation in oil base mud wells. *SPWLA 25th Ann.. Symp. Trans.*, Paper BB, 1-18.

Brereton, R. and McCann, D. (1990) A fresh look at predictive equations for compressional wave velocity – porosity. In: *European Core Analysis Symposium*, 270-298.

Bristow, C.S. and Myers, K.J. (1989) Detailed sedimentology and gamma-ray log characteristics of a Namurian delta succession. I: sedimentology and facies analysis. In: *Deltas: sites and traps for fossil fuels*. Eds. Whateley, M.K.G. and Pickering, K.T. *Geol. Soc. London Sp. Pub.* **41**, 75-80.

Broding, R.A. (1982) Volumetric scan well logging. *Log Analyst* **XXIII** (1); 14-19.

Broding, R.A. (1984) Application of the sonic volumetric scan log to cement evaluation. *SPWLA 25th Ann. Symp. Trans.*, paper JJ, 1-17.

Broggi, G. and Gerdil-Neuillet, F. (1983) Cluster method and log data can determine lithology. *Oil & Gas J.*, July 18, 139-140.

Buckley, D.K. and Oliver, D. (1990) Geophysical logging of water exploration boreholes in the Deccan Trap, Central India. In: *Geological applications of well logs*, eds. Hurst, A., Lovell, M.A.

and Morton, A.C. *Geol. Soc. Spec. Publ.* **48**, 153-161.

Budding, M.G. and Inglin, H.F. (1981) A reservoir geological model of the Brent Sands in Southern Cormorant. In: *Petroleum Geology of the Continental Shelf of N.W. Europe*, eds. Illing, L.V. and Hobson, G.D., Heyden, London, 326-334.

Bulat, J. and Stoker, S.J. (1987) Uplift determination from internal velocity studies, U.K. southern North Sea. In: *Petroleum Geology of Northwestern Europe*, eds. Brooks, J. and Glennie, K.W., Graham and Trottman, 293-305.

Bunch, A.W.H. and Dromgoole, P.W. (1995) Lithology and fluid prediction from seismic and well data. *Petroleum Geoscience*, **1**, No. 1, 49-57.

Burke, J.A., Campbell, R.L. and Schmidt, A.W. (1969) The lithoporosity cross plot. *SPWLA 10th Ann. Symp. Trans.*, 1-29.

Burnhill, T.J. and Ramsay, W.V. (1981) Mid-Cretaceous palaeontology and stratigraphy, central North Sea. In: *Petroleum Geology of the Continental Shelf of N.W. Europe*, eds. Illing, L.V. and Hobson, G.D., Heyden, London, 245-254.

Burst, J.F. (1969) Diagenesis of Gulf coast clayey sediments and its possible relation to petroleum migration. *Bull. Am. Assoc. Petrol Geol.* **53**(1); 73-93.

Bussian, A.E. (1982) A generalised Archie equation, *SPWLA 23rd Ann. Symp. Trans.*, paper E, 1-12.

Bussian, A.E. (1983) A comparison of shaly sand models. *SPWLA 24th Ann. Symp. Trans.*, paper E, 1-16.

Butler, J. and Clayton, C.G. (1984) A new philosophy for calibrating oil well logging tools based on neutron transport codes. *SPWLA 25th Ann. Symp. Trans.*, Paper FFF, 1-26.

Cameron, G.I.F. (1986) Confidence and the identification of foresets in stratigraphic dipmeter surveys. *SPWLA 10th European Form. Eval. Symp.* paper O, 1-16.

Cameron, G.I.F. (1992) Analysis of dipmeter data for sedimentary orientation. In: *Geological applications of well logs II*, eds. Hurst, A., Griffiths, C.M. and Worthington, P.F. *Geol. Soc. London Sp. Pub.* **65**, 141-156.

Cameron, G.I.F., Collinson, J.D., Rider, M.H. and Xu, L. (1993). Analogue dipmeter logs through a prograding deltaic sandbody. In: *Advances in reservoir geology*. Ed. Ashton, M. *Geol. Soc. London Sp. Pub.* **66**, 195-217.

Cant, D.J. (1992) Subsurface facies analysis. In: *Facies models, response to sea-level change*, eds. Walker, R.G. and James, N.P., Geological Soc. Canada, 27-45.

Chamberlain, A.K. (1984) Surface gamma-ray logs: a correlation tool for frontier areas. *Bull. Am. Assoc. Petrol.Geol.* **68**(8) 1040-1043.

Chang, D., Vinegar, H., Moriss, C. and Straley, S. (1994) Effective porosity, producible fluids and permeability in carbonates from NMR logging. *SPWLA 35th Ann. Symp. Trans.*, Paper A, 1-21.

Chapellier, D. (1992) *Well-logging in hydrogeology*. AA Balkema, Rotterdam, 175p.

Chemali, R., Gianzero, S. and Su, S.M. (1984) The depth of investigation of compressional wave logging for the standard and the long-spacing sonde. *SAID 9th International Formation Evaluation Transactions*, Paper 13, 1-10.

Chmelik, F.B., Bouma, A.H. and Rezak, R. (1969) Comparison of electrical logs and physical parameters of marine sediment cores. *Gulf Coast Assoc. Geol. Socs. Trans.* **XIX**, 63-70.

Clavier, C., Coates, G. and Dumanoir, J. (1977) The theoretical and experimental bases for the 'dual water' model for the interpretation of shaly sands. *52nd Ann. Conf. SPE of AIME*, **118**, SPE paper 6859.

Coats, G.R., Vinegar, H.J., Tutunjian, P.N. and Gardner, J.S. (1993) Restrictive diffusion from uniform gradient NMR well logging. *SPE* **26472**, 575-590.

Cobern, M.E. and Nuckols, E.B. (1985) Application of MWD resistivity relogs to evaluation of formation invasion. *SPWLA 26th Ann. Symp. Trans.*, Paper OO, 1-16.

Cody, R.D. (1971) Adsorption and the reliability of trace elements as environment indicators for shales. *J. Sed. Pet.* **41**(2) 461-471.

Coleman, J.M. and Prior, D.B. (1982) Deltaic environments. In: *Sandstone Depositional Environments*, eds. Scholle, P.A. and Spearing, D., *Am Assoc. Petrol. Geol. Mem.* 31, 139-178.

Cooper, B.S., Coleman, S.H., Barnard, P.C. and Butterworth, J.S. (1975) Paleotemperatures in the northern North Sea basin. In: *Petroleum and the Continental Shelf of N.W. Europe*, ed. Woodland, A.W., Applied Sci. Publ., Barking, 487-492.

Corfield, R.M. and Norris, R.D. (1996) Deep water circulation in the Paleocene ocean. In: *Correlation of the early Paleogene in northwest Europe*, eds. Knox, R.W.O'B., Corfield, R.M. and Dunay, R.E. *Geol. Soc. London Spec. Publ.* **101**, 443-456.

Cornford, C. (1984) Source rocks and hydrocarbons of the North Sea. In: *Introduction to the Petroleum Geology of the North Sea*, ed. Glennie, K.W., ch. 9, Blackwell, Oxford, 171-204.

Cox, J.W. (1983) Long axis orientation in elongated boreholes and its correlation with rock stress data. *SPWLA 24th Ann. Symp. Trans.*, paper J, 1-17.

Creaney, S. and Passey, Q.R. (1993) Recurring patterns of Total Organic Carbon and source rock quality within a sequence stratigraphic framework. *Bull. Am. Assoc. Petrol. Geol.* **77** No. 3, 386-401.

Cunningham, A.B., Jay, K. and Opstad, E. (1991) Applications of MWD technology in nonconventional wells, Prudhoe Bay, North Slope, Alaska. *Log Analyst* **32** No. 1, 13-23.

Dahlberg, K.E. and Fitz, P.E. (1988) Comparing log-derived and core-derived porosity and mineralogy in thinly bedded reservoirs: an integrated approach. *SPWLA 29th Ann. Symp. Trans.*, Paper W, 1-18.

Darling, H., Patten, D., Young, R.A. and Schwarze, L. (1991) Single-well data integration. *Oilfield Review*, **3**, No. 3, 29-35.

Dart, R.D. and Zoback, M.L. (1989) Well-bore breakout-stress analysis within the central and eastern continental United States. *Log Analyst*, **30**, No. 1, 12-24.

Davies, D.K. and Ethridge, F.G. (1975) Sandstone composition and depositional environment. *Bull. Am. Assoc. Petrol. Geol.* **59**(2) 239-264.

Davies, S. and Elliott, T. (1996) Spectral gamma ray characterisation of high resolution sequence stratigraphy: examples from Upper Carboniferous fluvio-deltaic systems, County Clare, Ireland. In: *High resolution sequence stratigraphy: innovations and applications*, eds. Howell, J.A. and Aitken, J.F. *Geol. Soc. London Spec. Publ.* **104**, 25-35.

Davis, J.C. (1986) Statistics in geology 2nd ed. John Wiley & Sons, 646p.

De'Ath, N.G. and Schuyleman, S.F. (1981) The geology of the Magnus oil field. In: *Petroleum Geology of the Continental Shelf of N.W. Europe*, eds. Illing, L.V. and Hobson, G.D., Heyden, London, 342-351.

Deegan, C.E. and Scull, B.J. (1977) A proposed standard lithostratigraphic nomenclature for the central and northern North Sea. *Rep. Inst. Geol. Sci. Ldn*, 77/25, and *Bull. Nor. Pet. Dir.* **1**, 35.

Delhomme, J-P. (1992) A quantitative characterisation of formation heterogeneities based on borehole image analysis. *SPWLA 33rd Ann. Symp. Trans.*, Paper T, 1-25.

Delhomme, J-P. and Serra, O. (1984) Dipmeter-derived logs for sedimentological analysis. *SPWLA Trans. 9th European Formation Evaluation Symposium Paper* **50**, 1-15.

Desbrandes, R. (1968) *Théorie et interprétation des diagraphies*. Technip, Paris.

Desbrandes, R. (1982).*Diagraphies dans les sondages*. Technip, Paris, p. 575.

Devilliers, M.C. and Werner, P.H., (1990), Example of fault identification using dipmeter data. In: *Geological applications of wireline logs*. eds. Hurst, A., Lovell, M.A. and Morton, A.C. *Geol. Soc. London Spec. Publ.* **48**, 287-295.

Dewan, J.T. (1983) *Essentials of Modern Open Hole Log Interpretation*. Penn Well, Tulsa. 361p.

Dickey, P.A. (1969) Increasing concentration of subsurface brines with depth. *Chem. Geol.* **4**, 361-370.

Donovan, W.S. and Hilchie, D.W. (1981) Natural gamma ray emissions in the Muddy J formation in eastern Wyoming. *Log Analyst* **XXII** (2); 17-22 (re-publication).

Donovan, A.D., Baum, G.R., Blechschmidt, G.L., Loutit, T.S., Pflum, C.E. and Vail, P.R. (1988) Sequence stratigraphic setting of the Cretaceous-Tertiary boundary in Central Alabama. In: *Sea-level changes: an integrated approach*, eds. Wilgus, C.K., Hastings,

B.S., Kendall, C.G.St.C., Posamentier, H.W., Ross, C.A. and Van Wagoner, J.C. *S.E.P.M Sp. Pub.* **42**, 299-307.

Doveton, J.D. (1991) Lithofacies and geochemical facies profiles from nuclear wireline logs: new subsurface templates for sedimentary modeling. In: *Sedimentary modeling-computer simulations and methods for improved parameter definition.* Eds. Franseen, E.K., Watney, W.L., Kendall, C.J. amd Ross, W. *Kansas Geol. Soc. Bull.* **233**, 101-110.

Doveton, J.D. (1994) Geologic log analysis using computer methods *Am. Assoc. Petrol. Geol. Computer applications in geology* **2**, p. 169.

Doveton, J.H. (1986) *Log analysis of subsurface geology: concepts and computer methods.* Wiley and Sons, 273p.

Doveton, J.H. and Prensky, S.E. (1992) Geological application of wireline logs – a synopsis of developments and trends. *Log Analyst* **33** No. 3, 286-303.

Dresser Atlas (1982) *Well logging and interpretation techniques. The course for home study.* Dresser Atlas Publication.

Dresser Atlas (1983) *Log interpretation charts.* Dresser Atlas Publication.

Dudley, J.W.II (1993) Quantitative fracture identification with the bore -hole televiewer. *SPWLA 34th Ann. Symp. Trans.*, Paper LL, 1-4.

Duke, W.L., Arnott, R.W.C. and Cheel, R.J. (1991) Shelf sandstones and hummocky cross stratification: new insight on a stormy debate. *Geol.* **19**, 625-628.

Dunlap, H.F. and Coats, G.R. (1988) Boron: tracking a trace element. *Log Analyst*, **29** No. 6, 410-417.

Durrance, E.M. (1986) *Radioactivity in geology: Principles and applications.* John Wiley, 441p.

Dyos, C.J. (1987) Inversion of induction log data by method of maximum entropy. *SPWLA 28th Ann. Symp. Trans.*, Paper T, 1-13.

Dypvik, H. and Eriksen, D.Ø. (1983) Natural radioactivity of clastic sediments and the contributions of U, Th and K. *J. Pet. Geol.* 5(4) 409-416.

Eberli, G.P. and Ginsberg, R.N. (1988) Progradation, NW Great Bahama Bank. In: *Reefs and adjacent areas.*, eds. Geldsetzer, H.H.J., James, N.P. and Tebbutt, G.E. *Canadian Society of Petroleum Geologists, Memoir* **13**.

Edmundson, H.N. and Raymer, L.L. (1979) Table of radioactive logging parameters of common minerals. *SPWLA 6th European Symp. Trans., Ldn.*, Paper BB, 1-6.

Edwards, J.M., Ottinger, N.H. and Haskell, R.E. (1967) Nuclear log evaluation of potash deposits. *SPWLA 8th Ann. Symp. Trans.*, Paper L, 1-12.

Ekstrom, M.P., Dahan, C.A., Chen, M.Y., Lloyd, P.M. and Rossi, D.J. (1987) Formation imaging with microelectrical scanning arrays. *Log Analyst*, **28**, No. 3, 294-306.

Elkington, P.A. (1995) An introduction to invasion profile imaging. BPB publication.

Ellis, D.V. (1987) *Well-logging for earth scientists.* Elsevier, 532p.

Etchecopar, A. and Dubas, M.O. (1992) Methods for geological interpretation of dips. *SPWLA 33rd Ann. Symp. Trans.*, Paper J, 1-21.

Etnyre, L. (1981) Fracture identification in the Panoma Field, Council Grove formation. *Log Analyst* **XXII**(6):3-6.

Evans, T.R. (1977) Thermal properties of North Sea rocks. *Log Analyst* **XVIII**(2); 3-12.

Fang, J.H., Chen, H.C., Shultz, A.W. and Mahmoud, W. (1992) Computer-aided well log correlation. *Bull. Am. Assoc. Petrol. Geol.* **76** No. 3, 307-317.

Faraguna, J.K., Chace, D.M. and Schmidt, M.G. (1989) An improved televiewer system: image acquisition, analysis and integration. *SPWLA 30th Ann. Symp. Trans.*, Paper UU, 1-11.

Felder, B. and Boyeldieu, C. (1974) The lithodensity log. *SAID 6th European Symposium Transactions*, Paper O, 20.

Fertl,W.H. (ed.)(1976) *Abnormal Formation Pressures Implications to Exploration, Drilling and Production of Oil and Gas Resources.* Elsevier, Amsterdam.

Fertl, W.H. (1977) Shale density studies and their application. In: *Developments in Petroleum Geology I*, ed. Hobson, G.D., Applied Science, Barking, 293-327.

Fertl, W.H. (1979) Gamma ray spectral data assists in complex formation evaluation *SPWLA 6th European Symp. Trans.* Ldn, Paper Q, 1-32.

Fertl, W.H. (1984) Advances in well logging interpretation. *Oil & Gas J.* April 16th, 85-91.

Fertl, W.H. (1985) Logs help approximate reservoir temperature. *Oil & Gas J.* April 29th, 89-96.

Fertl, W.H. and Rieke, H.H. (1980) Gamma ray spectral evaluation techniques identify fractured shale reservoirs and source rock characteristics. *J. Pet. Tech.* November, 2053-2062.

Fertl, W.H. and Timko, D.J. (1972) How downhole temperature pressures affect drilling. *World Oil*, **7382**(10 parts). June 1972-March 1973.

Fertl, W.H. and Wichmann, P.A. (1977) How to determine static BHT from well data. *World Oil*, January.

Finley, R.J and Tyler, N. (1986) Geological characterization of sandstone reservoirs. In: *Reservoir characterisation*, eds. Lake, L.W. and Caroll, H.B. Academic Press: pages 1-38.

Fisher, W.L. (1969) Facies characterization of Gulf Coast basin delta systems, with some Holocene analogues. *Gulf Coast Assoc. Geol. Socs. Trans.* **XIX**, 239-261.

Fisk, H.N. and McFarlan Jr., E. (1955) Late quaternary deltaic deposits of the Mississippi river – local sedimentation and basin tectonics. *Geol. Soc. Am. Spec. Pub. Crust of the Earth*, paper 62, 279.

Flaum, C., Galford, J.E. and Hastings, A. (1987) Enhanced vertical resolution processing of dual detector gamma-gamma density logs. *Log Analyst*, **30**(3), 139-149.

Folk, R.L. (1954) The distinction between grain size and mineral composition in sedimentary-rock nomenclature. *Journ. Geol.* **62**, 344-359.

Fons, L. (1969) Geological applications of well logs. *SPWLA 10th Ann. Symp. Trans.* Paper AA, 1-44.

Galloway, W.E. (1968) Depositional systems in the lower Wilcox group, North-Central Gulf Coast basin. *Gulf Coast Assoc. Geol. Socs. Trans.*, **XVIII**, 275-289.

Galloway, W.E. (1989a) Genetic stratigaphic sequences in basin analysis I: architecture and genesis of flooding-surface bounded depositional units. *Bull. Am. Assoc. Petrol Geol.* **73**, 125-142.

Galloway, W.E. (1989b) Genetic stratigraphic sequences in basin analysis II: application to northwest Gulf of Mexico Cenozoic basin. *Bull. Am. Assoc. Petrol. Geol.* **73**, 143-154.

Galloway, W.E. and Hobday, D.K. (1983) *Terrigenous Clastic Depositional Systems. Applications to Petroleum, Coal and Uranium Exploration.* Springer-Verlag, New York.

Gardener, J.S. and Dumanoir, J.L. (1980) Litho-density log interpretation. *SPWLA 21st Ann. Symp. Trans.*, Paper N, 1-23.

Gaymard, R. and Poupon, A. (1968) Response of neutron and formation density logs in hydrocarbon bearing formations. *Log Analyst* **IX**(5); 3-12.

Gearhart, Inc. (1983) *Formation Evaluation Data Handbook.* Gearhart Inc. Publication.

Georgi, D.T. (1985) Geometrical aspects of borehole televiewer images. *SPWLA 27th Ann. Symp. Trans.*, Paper C, 1-17.

Gilreath, J.A. (1966) Electric log characteristics of diapiric shale. In: *Diapirism and Diapirs*, eds. Braunstein, J. and O'Brien, G.D., *Am. Assoc. Petrol. Geol. Mem.* 8, 137-144.

Gilreath, J.A., Healy, J.S. and Yelverton, J.N. (1969) Depositional environments defined by dipmeter interpretations. *GCAGS Transactions* **19**, 101-111.

Goetz, J.F., Prins, W.J. and Logar, J.F. (1977) Reservoir delineation by wireline techniques. *6th Ann. Conv. Indonesian Pet. Assoc.*, 1-40.

Goetz, J.F., Dupal, L. and Bowler, J. (1979) An investigation into discrepancies between sonic log and seismic check shot velocities. *APEA*, 1-11.

Gondouin, M., Tixier, M.P. and Simard, G.L. (1957) An experimental study on the influence of the chemical composition of electrolytes on the SP curve. *Pet. Trans. AIME* **210**, 58-72.

Gonfalini, M. and Anxionnaz, H. (1990) A complete use of structural information from borehole imaging techniques – a case history for a deep carbonate reservoir. *SPWLA 31st Ann. Symp. Trans.*, Paper J, 1-25.

Granberry, R.J., Jenkins, R.E. and Bush, D.C. (1968) Grain density

values of cores from some Gulf Coast Formations and their importance in formation evaluation. *SPWLA 9th Ann. Symp. Trans.*, Paper N, 1-19.

Graue, E., Helland-Hansen, W., Johnson, J., Lomo, L., Nottvedt, A., Rønning, A. and Steel, R. (1987) Advance and retreat of the Brent Delta system, Norwegian North Sea. In: *Petroleum geology of North West Europe*. eds. Brooks, J. and Glennie, K.W. *Proc. 3rd Conf. Pet. Geol. N.W. Europe*. 915-938.

Griffiths, C.M. (1982) A proposed geologically consistent segmentation and reassignment algorithm for petrophysical borehole logs. In: *Quantitative Stratigraphic Correlation*, eds. Cubitt, J.M. and Reyment, R.A., 287-298.

Griffiths, C.M. and Bakke, S. (1988) Semi-automated well matching using gene-typing algorithms and a numerical lithology derived from wireline logs. *SPWLA 29th Ann. Symp. Trans.*, Paper GG, 1-24.

Hallenburg, J.K. (1978) Use of the spontaneous potential curve in a mineral mapping technique. *SPWLA 19th Ann. Symp. Trans.*, Paper U, 1-12.

Hallenburg, J.K. (1992) Nonhydrocarbon logging. *Log Analyst*, **33** No. 3, 259-269.

Harker, S.D., McGann, G.J., Bourke, L.T., and Adams, J.T. (1990) Methodology of Formation MicroScanner image interpretation in Claymore and Scappa fields (North Sea). In: *Geological applications of well logs*, eds. Hurst, A., Lovell, M.A. and Morton, A.C. *Geol. Soc. London Sp. Pub.* **48**, 11-25.

Hartmann, D.J. (1975) Effect of bed thickness and pore geometry on log response. *SPWLA 16th Ann. Symp. Trans.*, Paper Y, 1-14.

Hassan, M. (1973) Radioelements and diagenesis in shale and carbonate sediments. *SAID 2nd Ann. Symp. Trans.*, Paper 8, 1-7.

Hassan, M., Hossin, A. and Combaz, A. (1976) Fundamentals of the differential gamma ray log interpretation technique. *SPWLA 17th Ann. Symp. Trans.*, Paper H, 1-18.

Hawkins, P.J. (1972) Carboniferous sandstone oil reservoirs, East Midlands, England. PhD Thesis, Univ. London (unpublished).

Head, E., Cannon, D., Allen, D. and Colson, L. (1992) Quantitative invasion description. *SPWLA 33rd Ann. Symp. Trans.*, paper B, 1-20.

Hepp, V., Dumestre, A.C. (1975) Cluster: a method for selecting the most probable dip results from dipmeter surveys, *SPE* **5543**.

Hermanrud, C. and Shen, P.Y. (1989) Virgin rock temperatures from well logs – accuracy analysis for some advanced inversion models. *Marine and Petroleum Geology* **6** No. 4, 360-363.

Herring, E.A. (1973) Estimating abnormal pressures from log data in the North Sea. *Petroleum Engineer*, Nov. SPE 4301.

Herweijer, J.C., Höcker, C.F.W., Williams, H. and Eastwood, K.M. (1990) The relevance of dip profiles from outcrops as reference for the interpretation of SHDT dip. In: *Geological applications of well logs* eds. Hurst A., Lovell, M.A. and Morton, A.C., Geol. Soc. London Sp. Pub. **48**, 39-43.

Heslop, A. (1974) Gamma-ray log response of shaly sandstones. *SPWLA 15th Ann. Symp. Trans.*, Paper M, 1-11.

Heslop, A. (1975) Porosity in shaly-sands. *SPWLA 16th Ann. Symp Trans.*, Paper F, 1-12.

Hill, A.D. (1990) Temperature logging, Chapter 4. In: *Production logging, theoretical and interpretative elements*. SPE Memoir 14, 19-36.

Hillis, R.R. (1995) Quantification of Tertiary exhumation in the United Kingdom, southern North Sea using sonic velocity data. *Bull. Am. Assoc. Petrol Geol.*, **79**, No. 1, 130-152.

Hillis, R.R. and Williams, A.F. (1992) Borehole breakouts and stress analysis in the Timor Sea. In: *Geological applications of wireline logs II.*, eds. Hurst, A., Griffiths, C.M., and Worthington, P.F. *Geol. Soc. London Spec. Publ.* **65**, 157-168.

Hinz, K. and Schepers, R. (1983) SABIS, the digital version of the borehole televiewer. *SPWLA 8th European Symp. Trans.*, Ldn, Paper E, 1-20.

Höcker, C.F.W., Eastwood, K.M., Herweijer, J.C. and Adams J.T. (1990) Use of dipmeter data in clastic sedimentological studies. *Bull. Am. Assoc. Petrol. Geol.* **74**, No. 2, 105-118.

Hodson, G.M. (1975) Some aspects of the geology of the middle Jurassic in the northern North Sea with particular reference to electro-physical logs. *NPF Jurassic Northern N. Sea Symp., Stavanger*. Paper 16, 1-39.

Hoffman, L.J.B., Hoogerbrugge, P.J., and Lomas, A.T. (1988) LOGIX: a knowledge based system for petrophysical evaluation. *SPWLA 29th Ann. Symp. Trans.*, Paper R, 1-13.

Honda, H. and Magara, K. (1982) Estimation of irreducible water saturation and effective pore size of mudstones. *J. Pet. Geol*, 4(4) 407-418.

Hood, A., Gutjahr, C.C.M. and Heacock, R.L. (1975) Organic metamorphism and the generation of petroleum. *Bull. Am. Assoc. Petrol. Geol.* **59**, 986-996.

Hornby, B.E., Luthi, S.M. and Plumb, R.A. (1992) Comparison of fracture apertures computed from electrical borehole scans and reflected Stoneley waves: an integrated interpretation. *Log Analyst*, **33**, No. 1, 50-66.

Hottman, C.E. and Johnson, R.K. (1965) Estimation of formation pressures from log-derived shale properties. *J. Pet. Tech.*, June.

Hsu, K. and Chang, S.K. (1987) Multiple-shot processing of array sonic waveforms. *Geophysics* **52**, No. 10, 1376-1390.

Humphreys, B. and Lott, G.K. (1990) An investigation into nuclear log responses of North Sea Jurassic reservoirs using mineralogical analysis. In: *Geological applications of well logs*, eds. Hurst, A., Lovell, M.A. and Morton, A.C. *Geol. Soc. London Sp. Pub.* **48**, 223-240.

Hurley, N.F. (1994) Recognition of faults, unconformities and sequence boundaries using cumulative dip plots. *Bull. Am. Assoc. Petrol. Geol.* **78**, No. 8, 1173-1185.

Hurst, A. (1990) Natural gamma-ray spectroscopy in hydrocarbon bearing sandstones from the Norwegian continental shelf. In: *Geological applications of well logs*. eds. Hurst, A., Lovell, M. and Morton, A.C. *Geol. Soc. London Sp. Pub.* **48**, 211-222.

Hurst, A. (1995) Probe permeametry: re-emergence of an old technology. *First Break.* **13** No. 5, 185-192.

Hyndman, R.D. and Ade-Hall, J.M. (1972) Electrical resistivity of basalts from DSDP Leg 26. *Results from Deep Sea Drilling* **XXVI**, ch. 15, 505-508.

Ichara, M.J. and Avbovbo, A.A. (1985) Study identifies Niger Delta log parameter, VSP trends. *Oil & Gas J.* March 4th, 94-101.

Ineson, J.R. (1993) The Lower Cretaceous chalk play in the Danish Central Trough. In: *Petroleum Geology of Northwest Europe* ed. Parker, J.R. *Proc. 4th Conf.* 175-183.

Issler, D.R. (1992) A new approach to shale compaction and stratigraphic restoration, Beaufort-Mackenzie Basin and Mackenzie Corridor, Northern Canada. *Bull. Am. Assoc. Petrol. Geol.* **76** No. 8, 1170-1189.

Jackson, P.P., Taylor-Smith, D. and Stanford, P.N. (1978) Resistivity porosity particle shape relationships for marine sands. *Geophysics* **43** No. 6, 1250-1268.

Jackson, M.P.A. and Talbot, C.J. (1986) External shapes, strain rates and dynamics of salt structures. *BGSA*, **97**, 305-323.

Jackson, P.P., Lovell, M.A., Harvey, P.K., Ball, J.K., Williams, C., Ashu, P., Flint, R., Meldrum, P., Reece, G. and Zheng G. (1992) Electrical resistivity core imaging: theoretical and practical experiments as an aid to reservoir characterisation. *SPWLA 33rd Ann. Symp. Trans.*, Paper W, 1-13.

Jacqué, M. and Thouvenin, J. (1975) Lower Tertiary tuffs and volcanic activity in the North Sea. In: *Petroleum and the Continental Shelf of N.W. Europe*, ed. Woodland, A.W., Applied Sci. Publ., Barking, 455-465.

Jamison, H.C., Brockett, L.D. and McIntosh, R.A. (1980) Prudhoe Bay: A 10-year perspective. In: *Giant Oil and Gas Fields of the Decade: 1968-1978*, ed. Halbouty, M.T., *Am. Assoc. Petrol. Geol., Mem.* **30**, 289-314.

Johnson, W.L. and Linke, W.A. (1978) Some practical applications to improve formation evaluation of sandstones in the Mackenzie Delta. *SPWLA 19th Ann. Symp. Trans.*, Paper C, 1-33.

Kayal, J.R. and Christoffel, D.A. (1989) Coal quality from geophysical logs: Southland Lignite Region, New Zealand, *Log Analyst* **30** No. 5, 343-344.

Keith, B.D. and Pittman, E.D. (1983) Bimodal porosity in Oolitic reservoir effect on productivity and log response, Rodessa limestone (lower Cretaceous) East Texas basin. *Bull. Am. Assoc. Petrol.*

*Geol.* **67**(9); 1391-1399.

Kerzner, M.G. and Frost, E. (1984) Blocking, a new technique for well log interpretation. *J. Pet. Tech.* Feb., 267-275, SPE 11093.

Keys, W.S. (1979) Borehole geophysics in igneous and metamorphic rocks. *SPWLA 20th Ann. Symp. Trans.*, Paper OO, 1-26.

Knott, S.D. (1994) Fault zone thickness versus displacement in the Permo-Triassic sandstones of NW England. *Quart. Journ. Geol. Soc. London* **151**, Pt. 1, 17-26.

Knox, R.W.O'B. (1996) Correlation of the early Paleogene in northwest Europe: an overview. In: *Correlation of the early Paleogene in northwest Europe* eds., Knox, R.W.O'B., Corfield, R.M. and Dunay, R.E. *Geol. Soc. London Spec. Publ.* **101**, 1-11.

Knox, R.W.O'B and Cordey, W.G. (1992) Lithostratigraphic nomenclature of the UK North Sea. J. *Palaeogene of the Central and Northern North Sea,* eds. Knox, R.W.O'B. and Holloway, S. BGS Publication.

Knox, R.W.O'B. and Morton, A.C. (1983) Stratigraphical distribution of early Palaeogene pyroclastic deposits in the North Sea basin. *Proc. Yorks. Geol. Soc.* **44** Pt. 3, No. 25, 355-363.

Koczy, F.F. (1956) Geochemistry of the radioactive elements in the ocean. *Deep Sea Research* **3**, 93-103.

Koestler, A.G. and Ehrmann W.V. (1991) Description of brittle extensional features in chalk on the crest of a salt ridge (NW Germany). In: *Geometry of normal faults* eds. Roberts, A.M., Yielding, G. and Freeman, B. *Geol. Soc. London Sp. Pub* **56**, 113-123.

Kowalchuk, H., Coates, G. and Wells, L. (1974) The evaluation of very shaly formations in Canada using a systematic approach. *SPWLA 15th Ann. Symp. Trans.*, Paper H, 1-21.

Krueger, W.C. (1968) Depositional environments of sandstones as interpreted from electrical measurements, an introduction. *Gulf Coasts Assoc. Geol. Soc. Trans.* **XVIII**, 226-241.

Kulander, B.R., Dean, S.L. and Ward, B.J.Jr. (1990) Fractured core analysis. *Bull. Am. Assoc. Petrol Geol. Methods in Exploration Series*, **8**, 88p.

Landes, K.K. (1967) Eometamorphism and oil and gas in time and space. *Bull. Am. Soc. Petrol. Geol.* **51**(6); 828-841.

Lang, W.H. (1978) The determination of prior depth of burial (uplift and erosion) using interval transit time. *SPWLA 19th Ann. Symp. Trans.*, Paper B, 1-17.

Laubach, S.E., Baumgardner R.W., Monson, E.R., Hunt, E. and Meadoor, K.J. (1988) Fracture detection in low-permeability reservoir sandstone: a comparison of BHTV and FMS to logs and core. *SPE Paper 18119*, 129-139.

Lavenda, B.H. (1985) Brownian motion. *Scientific American* **252**(2); 56-67.

Lavers, B.A. and Smits, L.J.M. (1977) Recent developments in coal petrophysics. *Log Analyst* **XVIII** (1); 6-16.

Leslie, H.D. and Mons, F. (1982) Sonic waveform analysis applications. *SPWLA 23rd Ann. Symp. Trans.*, Paper GG, 1-25.

Levorsen, A.I. (1967) *Geology of Petroleum*, 2nd edn., W.H. Freeman & Co., San Francisco.

Lewis, C.R. and Rose, C.C. (1970) A theory relating high temperatures and overpressures. *J. Pet. Tech.*, **22**, 11-16.

Lincecum, T.A.Ma.V., Reinmiller R. and Mattner J. (1993) Natural and induced fracture classification using image analysis. *SPWLA 34th Ann. Symp. Trans.*, Paper J, 1-25.

Livberg, F., Mjös, R. (1989) The Cook formation, an offshore sand wedge in the Oseberg area, northern North Sea. In: *Correlation in Hydocarbon Exploration*, ed. Collinson, J.D., Norwegian Petroleum Soc., 299-312.

Loutit, T.S., Hardenbol, J., Vail, P.R., Baum, G.R. (1988) Condensed sections: the key to age determination and correlation of continental margin sequences. In: *Sea-level changes: an integrated approach*, eds. Wilgus, C.K., Hastings, B.S., Kendall, C.G.St.C., Posamentier, H.W., Ross, C.A. and Van Wagoner, J.C. *S.E.P.M Sp. Pub.* **42**, 183-213.

Luthi, S.M. (1990) Sedimentary structures of clastic rocks identified from electrical borehole images. In: *Geological applications of well logs*, eds. Hurst A., Lovell, M.A. & Morton, A.C., Geol. Soc London Sp. Pub. **48**, 3-10.

McCall, D.C. and Gardener, J.S. (1982) Litho-density log applications in the Michigan and Illinois basins. *SPWLA 23rd Ann. Symp. Trans.*, paper C, 1-21.

McCrossan, R.G. (1961) Resistivity mapping and petrophysical study of Upper Devonian inter-reef calcareous shales of central Alberta, Canada. *Bull. Am. Soc. Petrol. Geol.* **45**(4); 441-470.

McFadzean, T.B. (1973) Cross-plotting, a neglected technique in log analysis. *SPWLA 14th Ann. Symp. Trans.*, Paper Y, 1-18.

Macgregor, J.R. (1965) Quantitative determination of reservoir pressures from conductivity log. *Bull. Am. Soc. Petrol. Geol.* **49**(9); 1502-1511.

Magara, K. (1968) Compaction and migration of fluids in Miocene mudstones, Nagaoka Plain, Japan. *Bull. Am. Assoc. Petrol. Geol.* **52**(12); 2466-2501.

Magara, K. (1978) Compaction and fluid migration. *Dev. in Petrol. Sci.*, **9**. Elsevier, Amsterdam.

Magara, K. (1980) Comparison of porosity-depth relationships of shale and sandstone. *J. Pet. Geol.* **3**(2); 175-185.

Marett, G. and Kimminan, S. (1990) Logs, charts, and computers: the history of log interpretation modelling. *Log Analyst* **31** No. 6, 335-354.

Mari, J.-L., Coppens, F., Gavin, Ph. and Wicquart, E. (1994) *Full waveform acoustic data processing.* Édit. Technip, Paris. 126p.

Martin, D.W., Spencer, M.C. and Patel, H. (1984) The digital induction – a new approach to improving the response of the induction measurement. *SPWLA 25th Ann. Symp. Trans.*, Paper M, 1-11.

Maute, R.E. (1992) Electrical logging: state-of-the-art. *Log Analyst*, **33**, No. 3, 206-227.

Meyer, C. and Sibbit, A. (1981) GLOBAL: un outil général pour l'interprétation des diagraphies. *SAID 7th Ann. European Symp. Trans., Paris*, Comm. 5, 1-27.

Meyer-Gürr, A. (1976) Petroleum engineering. In: *Geology of Petroleum*, 3, ed. Beckman, H., Pitman, London.

Meyer, B.L. and Nederlof, M.H. (1984) Identification of source rocks on wireline logs by density/resistivity and sonic transit time/resistivity crossplots. *Bull. Am. Assoc. Petrol Geol.* **68**(2); 121-129.

Michelsen, O. (1989) Revision of the Jurassic lithostratigraphy of the Danish sub-basin. *Geological Survey of Denmark*, series A, **24**, 1-21.

Miesch, E.P. and Albright, J.C. (1967) A study of invasion diameter. *SPWLA 8th Ann. Symp. Trans.*, Paper 0, 1-14.

Milner, C.W.D. (1982) Geochemical analyses of sedimentary organic matter and interpretation of maturation and source potential. In: *How to Assess Maturation and Paleotemperatures*, SEPM Short Course No. 7, 217-252.

Milton, N.J., Bertram, G.T. and Vann, I.R. (1990) Early Paleogene sedimentation and tectonics in the Central North Sea. In: *Tectonic events responsible for Britain's oil and gas reserves. Geol. Soc. London Spec. Publ.* **55**, eds. Hardman, R.F.P. and Brooks, J., 339-351.

Misk, A., Mowat, G., Goetz, J. and Vivet, B. (1977) Effects of hole conditions on log measurements and formation evaluation. *SAID 5th Ann. European Symp. Trans., Paris*, Comm. 22, 1-16.

Mitchener, B.C., Lawrence, D.A., Partington, M.A., Bowman, M.B.J. and Gluyas, J. (1992) Brent Group:sequence stratigraphy and regional implications. In: *Geology of the Brent Group*, eds. Morton, A.C., Haszeldine, R.S., Giles, M.R. and Brown, S., *Geol. Soc. London Spec. Publ.* **61**, 45-80.

Mitchum, R.M. and Van Wagoner, J.C. (1990) High frequency sequences and eustatic cycles in the Gulf of Mexico Basin. In: *11th Ann. Research Conf. Gulf Coast Section Soc. Econ. Pal. & Min. Found.* Eds. Armentrout, J.M. and Perkins, R.F., 257-267.

Moline, G.R., Bahr, J.M., Drzewiecki, P.A. and Shepherd, L.D. (1992) Identification and characterisation of pressure seals through the use of wireline logs: a multivariate statistical approach. *Log Analyst* **33**, No. 4, 362-372.

Moran, J.H. and Attali, G. (1971) Wireline logging operations to 50,000 feet. *8th World Pet. Congress. Trans.*, 149-158.

Mwenifumbo, C.J. (1993) Kernel density estimation in the analysis and presentation of borehole geophysical data. *Log Analyst* **34** No. 5, 34-45.

Myers, K.J. (1987) Onshore-outcrop gamma ray spectrometry as a tool

in sedimentological studies. *Unpublished PhD Thesis University London.*

Myers, K.J. and Jenkyns, K.F. (1992) Determining total organic carbon contents from well logs: an intercomparison of GST data and a new density log method. In: *Geological applications of wire line logs II*, eds. Hurst, A., Griffiths, C.M., Worthington, P-F. *Geol. Soc. London Spec. Publ.* **65**, 369-376.

Myers, K.J. and Wignall, P.B. (1987) Understanding Jurassic organic-rich mudrocks – new concepts using gamma ray spectrometry and palaeoecology. In: *Marine and clastic sedimentology: new developments and concepts.* Ed. Leggett, J.K., Graham and Trotman, London.

NACSN (North American Commission on Stratigraphic Nomenclature) (1993) North American stratigraphic code, *Bull. Am. Assoc. Petrol. Geol.* **67**, 841-875.

Nederlandse Aardolie Maatschappij B.V. and Rijks Geol. Dienst (1980) *Stratigraphic Nomenclature of the Netherlands.* Verlag. K., Ned. Geol. Mijnb. Genoot., p.77.

Neinast, G.S. and Knox, C.C. (1973) Normalization of well log data. *SPWLA 14th Ann. Symp. Trans.* Paper I, 1-9.

Nelson, P.H. and Glenn, W.E. (1975) Influence of bound water on the neutron log in mineralized igneous rocks. *SPWLA 16th Ann. Symp. Trans.*, Paper M, 1-9.

Nelson, R.A. (1987) Fractured reservoirs, turning knowledge into practice. *JPT*, 407-414.

Nelson, R.J. and Mitchell, W.K. (1990) Improved vertical resolution of well logs by resolution matching. *SPWLA 31st Ann. Symp. Trans.*, Paper JJ, 1-25.

Nentwich, E.W. and Yole, R.W. (1982) Sedimentary petrology and stratigraphic analysis of the subsurface Reindeer Formation (Early Tertiary) Mackenzie Delta Beaufort Sea area, Canada. In: *Arctic Geology and Geophysics*, eds. Embry, A.F. and Balkwill, H.R., Canadian Society of Petroleum Geologists, Mem. 8, 5581.

Nummedal, D. and Swift, D.J.P. (1987) Transgressive stratigraphy at sequence-bounding unconformities: some principles derived from Holocene and Cretaceous examples. In: *Sea level fluctuations an coastal evolution.* Eds. Nummedal, D., Pilkey, O.H. and Howard, J.D. *Soc. Econ. Paleontol. Mineral.* Spec. Pub. **41**, 241-260.

Nummedal, D., Sanjeev, G., Plint, G.A. and Cole, R.D. (1995) The falling stage systems tract: definition, character and expression in several examples from the Cretaceous of the U.S. western interior. In: *Sedimentary responses to forced regression: recognition, interpretation and reservoir potential.* Geol. Soc. London 7-8 Sept. abstract, 45-46.

Nurmi, R.D. (1984) Geological evaluation of high resolution dipmeter data. *SPWLA 25th Ann. Symp. Trans.*, Paper YY, 1-24.

Nyberg, Ø., Lien, K., Lindberg, P.A. and Smistad, J.K. (1978) Mineral composition, an aid in classical log analysis used in Jurassic sand stones of the northern North Sea. *SPWLA 19th Ann. Symp. Trans.*, Paper M, 1-35.

O'Connor, S.J. and Walker, D. (1993) Palaeocene reservoirs of the Everest trend. In: *Petroleum geology of Northwest Europe*. ed. Parker, J.R., *Proc. 4th Conf. Geol. Soc. London* 145-160.

Olsen, J.R. (1990) A new calibration, wellsite verification, and log quality-control system for nuclear tools. *SPWLA 31st Ann. Symp. Trans.*, Paper PP, 1-25.

Owen J.D. (1966) A review of fundamental nuclear physics applied to gamma ray spectral logging. *Log Analyst*, Sept-Oct, 37-47.

Paillet, F.L. (1991) Acoustic full-waveform logs and fracture permeability. *Log Analyst* **32**, No. 3, 256-270.

Paillet, F.L. and Kim, K. (1987) Character and distribution of borehole breakouts and their relationship to in situ stresses in deep Columbia River basalts. *Journ. Geophys. Res.* **92** No. B7, 6223-6234.

Paillet, F.L., Cheng, C.H. and Pennington, W.D. (1992) Acoustic-waveform logging – advances in theory and application. *Log Analyst* **33** No. 3, 239-258.

Paillet, F.L., Keys, W.S. and Hess, A.E. (1985) Effects of lithology on televiewer log quality and fracture interpretation. *SPWLA 27th Ann. Symp. Trans.*, Paper JJ, 1-30.

Paillet, F.L., Novakowski, K. and Lapcevic, P. (1992) Analysis of transient flows in boreholes during pumping in fractured formations. *SPWLA 33rd Ann. Symp. Trans.*, Paper S, 1-22.

Paillet, F.L., Hess, A.E., Cheng, C.H. and Hardin, E. (1987) Characterization of fracture permeability with high-resolution vertical flow measurements during borehole pumping. *Journ. Ground Water* **25**, No. 1, 28-40.

Paillet, F.L., Barton, C., Luthi, S., Rambow, F. and Zemanek, J. (1990) Imaging and its application in well logging – an overview. In: *Borehole imaging*, eds. Paillet, F.L., Barton, C., Luthi, S., Rambow, F. and Zemanek, J. *SPWLA reprint volume.* 472p.

Parker, J.R. (1977) Deep sea sands. In: *Developments in Petroleum Geology*, 1, ed. Hobson, G.D., Applied Sci. Pub., Barking, 225-242.

Partington, M.A., Mitchener, B.C., Milton, N.J. and Fraser, A.J. (1993a) A genetic stratigraphic sequence stratigraphy for the North Sea late Jurassic and early Cretaceous: stratigraphic distribution and prediction of Kimmeridgian-late Ryazanian reservoirs in the Viking Graben and adjacent areas. In: *Petroleum geology of Northwest Europe*, ed. Parker, J.R. *Proc. 4th Conf. Geol. Soc. London*, 347-370.

Partington, M.A., Copestake, P., Mitchener, B.C. and Underhill, J.R. (1993b) A biostratigraphic calibration of the North Sea genetic stratigraphic sequences. In: *Petroleum geology of Northwest Europe*, ed. Parker, J.R. *Proc. 4th Conf. Geol. Soc. London*, 372-386.

Passey, Q.R., Creaney, S., Kulla, J.B., Moretti, F.J. and Stroud, J.D. (1990) A practical model for organic richness from porosity and resistivity logs. *Bull. Am. Assoc. Petrol Geol.* 74 No. 12, 1777-1794.

Pasternack, E.S. and Goodwill, W.P. (1983) Applications of digital borehole televiewer logging. *SPWLA 24th Ann. Symp. Trans.*, Paper X, 1-12.

Patchett, J.G. (1975) An investigation of shale conductivity. *SPWLA 16th Ann. Symp. Trans.*, Paper U, 1-41.

Patchett, J.G. and Coalson, E.B. (1979) The determination of porosity in sandstones and shaly sandstones. Part 1, Quality control. *SPWLA 20th Ann. Symp. Trans.*, Paper QQ, 1-17.

Patchett, J.G. and Coalson, E.B. (1982) The determination of porosity in sandstones and shaly sandstones, Part 2: Effects of complex mineralogy and hydrocarbons. *SPWLA 23rd Ann. Symp. Trans.*, Paper T, 1-50.

Pearson, R.A. and Batchelor, A.S. (1986) The logging results of viscous simulation in a hot dry rock geothermal well. *SPWLA 10th European Form. Eval. Symp.* Paper U, 1-9.

Pettijohn, F.J., Potter, P.E. and Siever, R. (1972) *Sand and Sandstone.* Springer-Verlag, New York.

Pezard, P.A. and Anderson, R.N. (1990) In situ measurements of electrical resisitvity, formation anisotropy and tectonic context. *SPWLA 31st Ann. Symp. Trans.*, Paper M., 1-24.

Pezard, P.A., Hiscott, R.N., Lovell, M.A., Collela, A. and Malinverno, A. (1992) Evolution of the Izu-Bonin intraoceanic forearc basin, Western Pacific, from cores and FMS images. In: *Geological applications of wireline logs II.*, eds. Hurst, A., Griffiths, C.M. and Worthington, P.F., *Geol. Soc. London Spec. Publ.* **65**, 43-69.

Phillips, S. (1987) Dipmeter interpretation of turbidite channel reservoir sandstones, Indian Draw field, New Mexico. In: *Reservoir sedimentology*, eds. Tillman, R.W. and Weber, K.J. *SEPM Sp. Pub.* **40**, 113-128.

Phillps, F.C. (1971) *The use of stereographic projection in structural geology*, 4th edition, Edward Arnold, London, 90p.

Pickett, G.R. (1963) Acoustic character logs in the evaluation of sandstone reservoirs. *Journal Petroleum Technology*, 15, 650-667.

Pied, B. and Poupon, A. (1966) SP base line shifts in Algeria. *SPWLA 7th Ann. Symp. Trans.*, Paper H, 1-12.

Pirson, S.J. (1963) *Handbook of Well Log Analysis.* Prentice Hall, Englewood Cliffs.

Pirson, S.J. (1970) *Geologic Well Log Analysis.* Gulf Publishing, Houston, pp. 370.

Plint, A.G. (1988) Sharp-based shoreface sequences and 'offshore bars' in the Cardium Formation of Alberta: their relationship to relative changes in sea level. In: *Sea-level changes: an integrated approach*, eds. Wilgus, C.K., Hastings, B.S., Kendall, C.G.St.C.,

Posamentier, H.W., Ross, C.A. and Van Wagoner, J.C. *SEPM Sp. Pub.* **42**, 357-370.

Plum, R.A. amd Hickman, S.H. (1985) Stress-induced borehole elongation – a comparison between the four-arm dipmeter tool and the borehole televiewer in the Auburn geothermal well. *Journ. Geophysical Research*, **90**, No. B7, 5513-5521.

Posamentier, H.W. and James, D.P. (1993) An overview of sequence-stratigraphic concepts: uses and abuses. In: *Sequence stratigraphy and facies associations*, eds. Posamentier, H.W., Summerhays, C.P., Haq, B.U. and Allen, G.P. *IAS Spec. Publ.* **18**, 3-18.

Posamentier, H.W. and Vail, P.R. (1988) Eustatic controls on clastic deposition II, sequence and systems tracts models. In: *Sea-level changes: an integrated approach*, eds. Wilgus, C.K., Hastings, B.S., Kendall, C.G.St.C., Posamentier, H.W., Ross, C.A. & Van Wagoner, J.C. *S.E.P.M. Sp. Pub.* **42**, 125-154.

Posamentier, H.W., Allen, G.P., James, D.P. and Tesson, M. (1992) Forced regressions in a sequence stratigraphic framework: concepts, examples and exploration significance. *Bull. Am. Assoc. Petrol. Geol.* **76**, 1687-1709.

Posamentier, H.W., Summerhays, C.P., Haq, B.U. and Allen, G.P. (eds.) (1993) Sequence stratigraphy and facies associations. *Int. Assoc. Sed. Sp. Pub.* **18**, 644p.

Poupon, A., Hoyle, W.R. and Schmidt, A.W. (1970) Log analysis in formations with complex lithologics. *J. Pet. Tech.*, Aug., 995-1005, SPE 2925.

Prensky, S. (1992a) Temperature measurements in boreholes – an overview of engineering and scientific applications. *Log Analyst* **33** No. 3, 313-333.

Prensky, S. (1992b) Borehole breakouts and in situ rock stress – a review. *Log Analyst*, **33**, No. 3, 304-312.

Prokoph, A. and Thurow, J. (1995) Sea level controlled preservation of singularities and cyclicity in sedimentary sequences. In: *Predictive high resolution sequence stratigraphy*, NPF conference Stavanger, Norway. (abstract).

Purdy, C.C. (1982) Enhancement of long-spaced sonic transit time data. *SPWLA 23rd Ann. Symp. Trans.*, Paper V, 114.

Quirein, J.A., Garden, J.S. and Watson, J.T. (1982) Combined natural gamma ray spectral/litho-density measurements applied to complex lithologies. SPE **11143**, 1-14.

Quirein, J.A., Kimmanau, S., Lavigne, J., Singer, J. and Wendel, F. (1986) A coherent framework for developing and applying multiple formation evaluation models. *SPWLA 27th Ann. Symp. Trans.*, Paper DD, 1-16.

Raiga-Clemenceau, J. (1988) Taking into account the conductivity contribution of shale laminations when evaluating closely interlaminated sand-shale hydrocarbon-bearing reservoirs. *SPWLA 29th Ann. Symp. Trans.*, Paper DD, 1-14.

Raiga-Clemenceau, J., Martin, J.P. and Nicoletis, S. (1988) The concept of acoustic formation factor for more accurate porosity determination from sonic log data. *Log Analyst* **29** No. 1, 54-60.

Rambow, F.H.K. (1984) The borehole televiewer: some field examples. *SPWLA 25th Ann. Symp. Trans.*, Paper C, 1-22.

Ramsbottom, W.H.C. (1977) Major cycles of transgression and regression (mesotherms) in the Namurian. *Proc. Yorks Geological Survey*, **41**, 261-291.

Ramsey, J.G. (1967) *Folding and fracturing in rocks*, McGraw Hill, New York. 586p.

Ransom, R.C. (1977) Methods based on density and neutron well logging responses to distinguish characteristics of shaly sandstone reservoir rock. *Log Analyst* **XVIII**(3); 47-63.

Rasmus, J. and Voisin, B. (1990) A framework to estimate pore pressures in real time. *MWD Symposium, LSU*, Baton Rouge 355-376.

Rawson, P.F. and Riley, L.A. (1982) Latest Jurassic early Cretaceous events and the 'Late Cimmerian Unconformity' in North Sea area. *Bull. Am. Soc. Petrol. Geol.* **66**(12); 2628-2648.

Raymer, L.L., Hunt, E.R. and Gardner, J.S. (1980) An impoved sonic transit time to porosity transform. *SPWLA 21st Ann. Symp. Trans.*, Paper P, 1-12.

Reiter, M., Mansure, A.J. and Peterson, B.K. (1980) Precision continuous temperature logging and comparison with other types of logs. *Geophysics*, **45**, No. 12, 1857-1868.

Rhodes, D.F. and Mott, W.E. (1966) Quantitative interpretation of *gamumma-ray spectral logs. Geophysics, 31, 4-10.*

Rhys, G.H. (1975) A proposed standard lithostratigraphic nomenclature for the southern North Sea. In: *Petroleum and the Continental Shelf of N.W. Europe*, ed. Woodland, A.W., Applied Sci. Pub., Barking. 151-163.

Rider, M.H. (1978) Dipmeter log analysis, an essay *SPWLA 19th Ann. Symp. Trans.*, paper G, 1-18.

Rider, M.H. (1986) Geological analysis of well logs. Blackie,Glasgow.

Rider, M.H. (1990) Gamma-ray log shapes used as a facies indicator: critical analysis of an oversimplified methodology. In: *Geological applications of well logs*, eds. Hurst, A., Lovell, M.A. and Morton, A.C. *Geol. Soc. London Sp. Pub.* **48**, 27-38.

Rider, M.H. and Laurier, D. (1979) Sedimentology using a computer treatment of well logs. *SPWLA 6th European Symp. Trans.*, Paper J, 1-12.

Rübel, H.J., Schepers, R. and Schmitz, D. (1986) High resolution televiewer logs from sedimentary formations. *SPWLA 10th European Formation Evaluation Symp.* Paper GG, 1-15.

Rudwick, M.J.L. (1985) The great Devonian controversy. University of Chicago Press, 494p.

Russel, W.L. (1941) Well logging by radioactivity. *Bull. Am. Soc. Petrol. Geol.* **25**(9); 1768-1788.

Saiha, S. and Visher, C.S. (1968) Subsurface study of the southern portion of the Bluejacket delta. *Oklahoma Geological Society Guidebook*, 33p.

Salimullah, A.R.M. and Stowe, D.A.V. (1992) Application of FMS images in poorly recovered coring intervals: examples from ODP leg 129. In: *Geological applications of wireline logs II.*, eds. Hurst, A., Griffiths, C.M., and Worthington, P.F., *Geol. Soc. London Spec. Publ.* **65**, 71-86.

Sallee, J.E. and Wood, B.R. (1984) Use of microresistivity from the dipmeter to improve formation evaluation in thin sands, Northeast Kalimantan, Indonesia. *J. Pet. Tech.*, 10, **36**, 1535-1544.

Sanyal, S.K., Juprasert, S. and Jusbasche, M. (1980) An evaluation of a rhyolite basalt volcanic ash sequence from well logs. *Log Analyst* **XXI**(1); 3-9.

Sarg, J.F. and Skjold, L.J. (1982) Stratigraphic traps in Paleocene sands in the Balder area, North Sea. In: *The Deliberate Search for the Subtle Trap*, ed. Halbouty, M.T., *Am. Assoc. Pet. Geol. Mem.* **32**, 197-206.

Sarmiento, R. (1961) Geological factors influencing porosity estimates from velocity logs. *Bull. Am. Soc. Petrol. Geol.* **45**(5) 633-644.

Schafer, J.N. (1980) A practical method of well evaluation and acreage development for the naturally fractured Austin chalk formation. *Log Analyst* **XXI**(1); 10-23.

Schenewerk, P.A., Sethi, D.K., Fertl, W.H. and Lochmann, M. (1980) Natural gamma ray spectral logging aids granite wash reservoir evaluation. *SPWLA 21st Ann. Symp. Trans.*, Paper BB, 1-23.

Scherer, F.C. (1980) Exploration in East Malaysia of the past decade. In: *Giant Oil Fields of the Decade 1968-1978*, ed. Halbouty, M.T., *Am. Assoc. Pet. Geol. Mem.* **30**, 423-440.

Schlumberger (1970) *Fundamentals of Dipmeter Interpretation.* Schlumberger Publication.

Schlumberger (1972) *Log Interpretation, I, Principles.* Schlumberger Publication.

Schlumberger (1972) *The Essentials of Log Interpretation Practice.* Schlumberger Publication.

Schlumberger (1974) *Log Interpretation, II, Applications.* Schlumberger Publication.

Schlumberger (1979) *Log Interpretation Charts. English-Metric.* Schlumberger Publication.

Schlumberger (1982) *Well Evaluation Developments, Continental Europe.* Schlumberger Publication.

Schlumberger (1985) *Log Interpretation Charts.* Schlumberger Publication.

Schlumberger (1986) *Dipmeter interpretation – Fundamentals.* Schlumberger Ltd. U.S.A., 76p.

Schlumberger (1989a) *Log interpretation, principles and applications.* Schlumberger Educational Services.

Schlumberger (1989b) *Log interpretation charts,* 151p.

Schlumberger (1994a) *DSI Dipole Shear Sonic Imager.* Schlumberger Educational Services, 42p.

*Schlumberger (1994b) FMI Fullbore Formation Microlmager.* Schlumberger Educational Services, 42p.

Schmidt, G.W. (1973) Interstitial water composition and geochemistry of deep Gulf Coast shales and sandstones. *Bull. Am. Assoc. Petrol Geol.* **57**(2); 321-337.

Schmoker, J.W. (1979) Determination of organic content of Appalachian Devonian shales from formation density logs. *Bull. Am. Assoc. Petrol. Geol.***63** (9); 1504-1509.

Schmoker, J.W. (1981) Determination of organic-matter content of Appalachian Devonian shales from gamma-ray logs. *Bull. Am. Assoc. Petrol. Geol.* **65**, 1285-1298.

Schmoker, J.W. And Hester, T.C. (1983) Organic carbon in Bakken formation, United States portion of Williston Basin. *Bull. Am. Assoc. Petrol Geol.* **67**(12); 2165-2174.

Seiler, D. (1995) Borehole visualization in 3-D. *SPWLA 36th Ann. Symp. Trans.*, Paper UUU, 1-12.

Selley, R.C. (1976) Subsurface environmental analysis of North Sea sediments. *Bull. Am. Assoc. Geol.* **60**(2); 184-195.

Serra, O. (1972) *Diagraphies et stratigraphie.* Mem. BRGM Fr., No. 77, 775-832.

Serra, O. (1973) Interprétation géologique des diagraphies différées en séries carbonatées. *Bull. Centre Rech. Pau. SNPA* **72**(1); 265-284.

Serra, O. (1974) Interprétation géologique des séries deltaiques à partir des diagraphies différées. Rev. Assoc. Fr. Techn. Pet. 227, 9-17.

Serra, O. (1979) Diagraphies différées. Bases de l'interprétation. Tome 1: Acquisition des données Diagraphiques. *Bull. Centre Rech. Expl.-Prod. Elf Aquitaine*, Mem. **1**, Technip, Paris, 328.

Serra, O. (1985) *Sedimentary environments from wireline logs.* Schlumberger publications, 211p.

Serra, O. (1989) *Formation MicroScanner Image Interpretation,* Schlumberger Educational Services, 117p.

Serra, O. and Abott, H.T.(1980) The contribution of logging data to sedimentology and stratigraphy. *55th Ann. Conf. Dallas*, 1-19. SP 9270.

Serra, O., Baldwin, J. and Quirein, J. (1980) *Theory, interpretation and practical applications of natural gamma ray spectroscopy.* Schlumberger, M. 83214.

Serra, O., Stowe, J. and Motet, D. (1993) True integrated interpretation. *SPWLA 34th Ann. Symp. Trans.*, Paper Z, 1-25.

Serra, O. and Sulpice, L. (1975) Sedimentological analysis of sand shale series from well logs. *SPWLA 16th Ann. Symp. Trans.*, Paper W, 1-23.

Shanmugam, G., Bloch, R.B., Mitchell, S.M., Beamish, G.W.J., Hodgkinson, R.J., Damuth, J.E., Straume., T., Syvertsen, S.E. and Shields, K.E. (1995) Basin-floor fans in the North Sea: sequence stratigraphic models vs. sedimentary facies. *Bull. Am. Assoc. Petrol. Geol.* **79** No. 4, 477-512.

Shaw, H.F. (1980) Clay minerals in sediments and sedimentary rock. In: *Developments in Petroleum Geology 2*, ed. Hobson, G.D., Applied Sci. Pub., Barking, 53-85.

Sherriff, R.E. (1980) *Seismic Stratigraphy.* Int. Human Resources Dev. Corp., Boston.

Sherman, H. and Locke, S. (1975) Depth of investigation of neutron and density sondes for 35 per cent porosity sand. *SPWLA 16th Ann. Symp. Trans.*, Paper Q, 1-14.

Shields, C. and Gahan, M.J. (1974) The dipmeter used to recognise depositional environments. *APEA.*, 181-188.

Siemers, C.T., Tilliman, R.W. and Williamson, C.R. (1981) Deep water clastic sediments: A core workshop. *SEPM Core Workshop 2*, 416p.

Simon-Brygoo, C. (1980) Analyse qualitative des diagraphies. Essai de méthodes d'interprétation. Thèse, Univ. Bordeaux, No. 1557 (unpublished).

Slatt, R.M., Jordan, D.W., D'Agostino, A.E. and Gillespie, R.H. (1992) Outcop geometry logging to improve understanding of subsurface well log correlation. In: *Geological applications of well logs II*, eds. Hurst, A., Griffiths, C.M. and Worthington, P.F. *Geol. Soc. London Sp. Pub.* **65** 3-20.

Sloss, L.L. (1984) Comparative anatomy of cratonic unconformities. In: *Interregional Unconformities and Hydrocarbon Accumulation,* ed. Schlee, J.S., *Am. Assoc. Pet. Geol. Mem.* **36**, 1-36.

Smith, M.P. (1990) Enhanced vertical resolution processing of dual-spaced neutron and density tools using standard shop calibration and borehole compensation procedures. *SPWLA 31st Ann. Symp. Trans.*, Paper SS, 1-22.

Smith, M.L., Sondergeld, C.H. and Norris, J.O. (1991) The Amoco Array Sonic Logger. *Log Analyst* **32**, No. 3, 201-214.

Smith, J.W., Thomas, H.E. and Trudell, L.G. (1968) Geologic factors affecting density logs in oil shale. *SPWLA 9th Ann. Symp. Trans.*, Paper P, 1-17.

Søllie, F. and Rodgers, G. (1994) Towards better measurements of logging depth. *SPWLA 35th Ann. Symp. Trans.*, Paper D, 1-15.

Sovich, J.P. and Newberry, B. (1993) Quantitative approach to bore hole imaging. *SPWLA 34th Ann. Symp. Trans.*, Paper FFF, 1-18.

SPWLA (1982) Shaly sand reprint volume, S.P.W.L.A. p. 809.

Standen, E., Nurmi, R., Elwazeer, F. and Ozkanli M. (1993) Quantitative applications of wellbore images to reservoir analysis. *SPWLA 34th Ann. Symp. Trans.*, Paper EEE, 1-15.

Suau, J. and Spurlin, J. (1982) Interpretation of micaceous sandstones in the North Sea. *SPWLA 23rd. Ann. Symp. Trans.* Paper G, 1-32.

Sullivan, K.B. and Schepel, K.J. (1995) Borehole image logs: applications in fractured and thinly bedded reservoirs. *SPWLA 36th Ann. Symp. Trans.*, Paper T, 1-12.

Taherian, M.R., Habashy, T.M., Schroeder, R.J., Mariani, D.R. and Chen, M.Y. (1992) Laboratory study of the spontaneous potential: Experimental and modelling results. *SPWLA 33rd Ann. Symp. Trans.*, Paper E, 1-25.

Taylor, T.J. (1983) Interpretation and application of borehole televiewer surveys. *SPWLA 24th Ann. Symp. Trans.*, Paper QQ, 1-19.

Taylor, T.J. (1991) A method for identifying fault related fracture systems using the borehole televiewer. *SPWLA 32nd Ann. Symp. Trans.*, Paper JJ, 1-19.

Theys, P.P. (1991) Log data acquisition and quality control. *Éditions Technip*, Paris, 330p.

Thomas, D.H. (1977) Seismic applications of sonic logs. *SPWLA 5th European Symp. Trans., Paris*, Paper 7, 1-24.

Thomas, E. and Shackleton, N.J. (1996) The Paleocene benthic foraminiferal extinction and stable isotope anomalies. In: *Correlation of the early Paleogene in northwest Europe*, eds., Knox, R.W.O'B., Corfield, R.M. and Dunay, R.E. *Geol. Soc. London Spec. Publ.* **101**, 401-441.

Threadgold, P. (1971) Some problems and uncertainties in log interpretation. *SPWLA 12th Ann. Symp. Trans.*, Paper W, 1-19.

Tissot, B.P. (1973) Vers l'evaluation quantitative du pétrole formé dans les basins sédimentaires. *Rev. Assoc. Fr. Tech. Pet.* **222**, 27-31.

Tissot, B.P. and Welte, D.H. (1978) *Petroleum Formation and Occurrence: a New Approach to Oil and Gas Exploration.* Springer-Verlag, Berlin.

Tittle, C.W. (1961) Theory of neutron logging. *Geophysics* **26**(1); 27-39.

Tittman, J. and Wahl, J.S. (1965) The physical foundations of formation density logging (gamma-gamma). *Geophysics* **30**(2); 284-294.

Tixier, M.P. and Alger, R.P. (1967) Log evaluation of non-metallic mineral deposits. *SPWLA 8th Ann. Symp. Trans.*, Paper R, 1-22.

Torres, D., Strickland, R. and Gianzero, M. (1990) A new approach to determining dip and strike using borehole images. *SPWLA 31st Ann. Symp. Trans.*, Paper K, 1-20.

Trouiller, J-C., Delhomme, J-P., Carlin, S. and Anxionnaz, H. (1989) Thin bed reservoir analysis from borehole electrical images. *SPE 19578*, 61-72.

Truman, R.B., Alger, R.P., Connell, J.G. and Smith, R.L. (1972) Progress report on interpretation of the dual-spacing neutron log (CNL) in the United States. *SPWLA 13th Ann. Symp. Trans.*, Paper U, 1-34.

Underhill, J.A. and Partington, M.A. (1993) Jurassic thermal doming and deflation in the North Sea: implications of the sequence stratigraphic evidence. In: *Petroleum Geology of Northwest Europe,* ed. Parker, J.R. *Proc. 4th Conf.* 337-346.

Underhill, J.A. and Partington, M.A. (1994) Use of genetic sequence stratigraphy in defining a regional tectonic control on the 'mid-Cimmerian unconformity': implications for North Sea basin development and the global sea-level chart. In: *Siliclastic sequence stratigraphy.* Eds. Weimer, P. and Posamentier, H.W. *Am. Assoc. Petrol. Geol. Memoir* **58**, 449-484.

Vail, P.R., Mitchum, R.M. and Thomson, S. III, (1977) Seismic stratigraphy and global changes in sea level, part 3: relative

changes of sea level from coastal onlap. In: *Seismic Stratigraphy-Applications to Hydrocarbon Exploration* ed. Payton, C.E. *Bull. Amer. Assoc. Pet. Geol.* Mem. **26**, 63-97.

Vail, P.R. and Wornardt, W.W. (1990) Well-log seismic sequence stratigraphy: an integrated tool for the 90s. *G.C.S. SEPM Foundation, 11th Annual Res. Conference, Program and Abstracts*, 379-389.

Van Siclen, De W.C. (1958) Depositional topography examples and theory. *Bull. Am. Assoc. Petrol. Geol.* **42**(8); 1897-1913.

Van Wagoner, J.C., Mitchum, R.M., Campion, K.M. and Rahmanian, V.D. (1990) Siliciclastic sequence stratigraphy in well logs, cores and outcrops. *AAPG Methods in exploration series*, **7**, 55p.

Verdur, H., Stinco, L. and Naides, C. (1991) Sedimentological analysis utilising the circumferential borehole acoustic log. *SPWLA 32nd Ann. Symp. Trans.*, Paper II, 1-19.

Vincent, Ph., Gartner, J.E. and Attali, G. (1977) Geodip: an approach to detailed dip determination using correlation by pattern recognition. *SPE* **6823**.

Vollset, J. and Doré, A.G. (1984) A revised Triassic and Jurassic lithostratigraphic nomenclature for the Norwegian North Sea, *NPD Bulletin* **3**, 53p.

Vorren, T.O., Richardsen, G. and Knutsen, S-M. (1991) Cenozoic erosion and sedimentation in the western Barents Sea. *Marine and Petroleum Geology*, **8** No. 3, 317-340.

Waid, C. C. (1987) Effect of Tool Rotation on the Computation of dip. *SPWLA 28th Ann. Symp. Trans.*, Paper Q, 1-22.

Wahl, J.S., Tittman, J., Johnstone, C.W. and Alger, R.P. (1964) The dual spacing formation density log. *J. Pet. Tech.*, December, 1411-1416.

Walker, R.G. (1992) Facies, facies models and modern stratigraphic concepts. In: *Facies models, response to sea level change*. Eds. Walker, R.G. and James, N.P. *Geol. Soc. Canada*, 1-14.

Wallace, W.E. (1968) Observations on the SP curve in general and offshore problems in particular. *SPWLA 9th Ann. Symp. Trans.*, Paper A, 1-14.

Walsgrove, T.R., Daneshzadeh, M. and Dusang, J.P. (1992) A case study of the interpretational and financial implications of wireline versus measurement while drilling in 'high risk' scenarios. *SPWLA 33rd Ann. Symp. Trans.*, Paper G, 1-25.

Walters, E.J. (1968) Statistical study of neutron logs for correlation studies. *SPWLA 9th Ann. Symp. Trans.*, Paper F, 1-15.

Waples, D.W. (1980) Time and temperature in petroleum formation: application of Lopatin's method to petroleum exploration. *Bull. Am. Assoc. Petrol. Geol.*, **64**(6); 916-926.

Waxman, M.H. and Smits, L.J.M. (1968) Electrical conductivities in oil-bearing shaly sand. *Soc. Pet. Eng. J.*, June, 107-122.

Weaver, C.E. and Pollard, L.D. (1973) *The Chemistry of Clay Minerals* (Developments in Sedimentology 15). Elsevier, Amsterdam.

Werner, P., Piazza, J-L. and Raiga-Clemenceau, J. (1987) Using dipmeter data for enhanced structural interpretation from the seismic. *SPWLA 28th Ann. Symp. Trans.*, paper II, 1-11.

Whittaker, A., Holliday, D.W and Penn I.E. (1985) Geophysical logs in British stratigraphy. *Geol. Soc. London, Special Report* **18**, 1-74.

Wiley, R. (1990) Borehole televiewer revisited. *SPWLA 21st Ann. Trans., Symp.* Paper HH, 1-16.

Williams, H. and Soek, H.F. (in press) Predicting reservoir sand-body orientation from dipmeter data: the use of sedimentary dip profiles from outcrop studies. In: *The geological modelling of hydrocarbon reservoirs*, IAS publication.

Winsauer, W.O. and McCardell, W.M. (1953) Ionic double-layer conductivity in reservoir rocks: *Trans AIME*, **198**, 129-134.

Wolff, M. and Pelissier-Combescure, J. (1982) Faciolog-automatic electrofacies determination. *SPWLA 23rd Ann. Symp. Trans.*, Paper FF, 1-23.

Wong, S.A., Startzmann, R.A. and Kuo, T-B. (1989) Enhancing borehole image data on a high-resolution PC. *SPE* **19124**, 37-48.

Wyllie, M.R.J. (1963) *The Fundamentals of Well Log Interpretation.* 3rd edn., Academic Press, New York.

Wyllie, M.R.J., Gregory, A.R. and Gardener, L.W. (1956) Elastic wave velocities in heterogeneous and porous media. *Geophysics*, **21**(1); 41-70.

Yassir, N.A. and Dusseault, M.B. (1992) Stress trajectory determination in southwestern Ontario from borehole logs. In: *Geological application of wireline logs II.*, eds. Hurst, A., Griffiths, C.M. and Worthington, P-F, *Geol. Soc. London Spec. Publ.* **65**, 169-178.

Zemanek, J. Caldwell, R.I., Glenn, E.E., Holcomb, S.V., Norton, L.J. and Strauss, A.J.D. (1969) The borehole televiewer – a new logging concept for fracture location and other types of borehole inspection. *JPT*, **21**, 762-774.

Zemanek, J., Glenn, E.E., Norton, L.J. and Caldwell, R.L. (1970) Formation inspection with the borehole televiewer. *Geophysics*, **35**, 254-269.

Zemanek, J., Williams, D.M. and Schmidt, D.P. (1991) Shear-wave logging using multipole sources. *Log Analyst*, **32**, No. 3, 233-241.

Zoback, M.L., Zoback, M.D., Adams, J., *et al* (1989) Global patterns of tectonic stress. *Nature*, **341**, September 28th, 291-298.

# INDEX

# THE GEOLOGICAL INTERPRETATION OF WELL LOGS

This second edition of a highly successful book describes, discusses and illustrates the interpretation of well logs for geological ends. The book is illustrated profusely with many real examples and combines the well established with new and exciting developments. The principal open hole logging tools are considered from theory to data acquisition and interpretation, and new versions of old tools are included. Many new logging developments are illustrated. The revolutionary techniques of image logging and dipmeter are described extensively and the use of log data in subsurface sequence stratigraphy is amplified.

The geological emphasis of the book, on lithology, facies, depositional environment, sequence stratigraphy, correlation and more, makes it ideal for the geologist or sedimentologist using logs, or anyone in industry or academia who requires an understanding of the basics of logs and recent advances in the technology.

The author: Malcolm Rider is a director of Rider-French Consulting Ltd. He has extensive experience in the oil industry over many years and continues to work throughout the world in petroleum development and exploration. He presents courses in industry and academia on the geological aspects of well logs and specialist dipmeter and image logs.

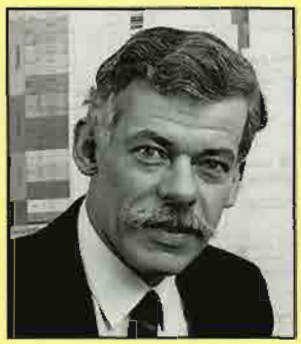

ISBN 0-9541906-0-2
9 780954 190606

RIDER FRENCH